Ultra-Cold Collisions of Identical Atoms

by

Joseph Noël Robin Côté

B.Sc., Université du Québec à Rimouski (1987)
M.Sc., Université Laval (1989)

Submitted to the Department of Physics
in the partial fulfillment of the requirements for the degree of

Doctor of Philosophy

at the

MASSACHUSETTS INSTITUTE OF TECHNOLOGY

February 1995

Author .....
Department of Physics
December 7, 1994

Certified by .....
Alexander Dalgarno
Professor of Astronomy, Harvard University
Thesis Supervisor

Certified by .....
Daniel Kleppner
Professor of Physics, MIT
Thesis Co-supervisor

Accepted by .....
George F. Koster
Chairman, MIT Departmental Graduate Committee

Ultra-Cold Collisions of Identical Atoms

by

Joseph Noël Robin Côté

submitted to the Department of Physics on December 7, 1994,
in partial fulfillment of the requirements for the degree of
Doctor of Philosophy

Abstract

Interaction potentials for the $X^1\Sigma_g^+$ and $a^3\Sigma_u^+$ states of Li_2 and Na_2 are constructed and used in the calculations of the elastic scattering of pairs of identical alkali atoms (^{7}Li,^{6}Li, and ^{23}Na) at ultralow temperatures. The extreme sensitivity of the cross sections to the details of the interaction potentials is demonstrated. The corrections due to retardation effects are explored (for ^{23}Na). The calculated elastic and spin-change cross sections are very large, of the order of $10^{-12} - 10^{-13}$ cm^2 at zero temperature. The predicted scattering lengths of ^{7}Li are positive for $X^1\Sigma_g^+$ ($36.9a_0$) and negative for $a^3\Sigma_u^+$ ($-17.2a_0$), and both are positive for ^{23}Na ($34.9a_0$ for $X^1\Sigma_g^+$ and $77.3a_0$ for $a^3\Sigma_u^+$). Pronounced shape resonances appear at temperatures as low as 10 mK, where higher partial wave contributions start to be important.

Studies of semi-classical approximations are reported, together with the construction of a zero-energy wave function. Quantum suppression as a function of the energy and of the distance is explored.

The probability of spontaneous and stimulated radiative transitions during ultracold collisions is investigated for both ^{6}Li and ^{7}Li isotopes. Experimental data show two series of peaks. Our calculations identify the strong one with the triplet transitions, and the weak one with the singlet transitions. A link between their intensities and the scattering length is made and compared with experimental values. High partial waves are shown to contribute at temperatures near 5 mK, with the effect of shape resonances then dominating. Computation of the line profiles and fitting to the experimental ones enable us to estimate the temperature of the experiment at 7 mK, and identify a possible shape resonance. Finally, studies of the bound-bound transitions indicate the possibility of creating translational cold molecules.

Thesis Supervisor: Alexander Dalgarno
Title: Professor of Astronomy, Harvard University

Thesis Co-supervisor: Daniel Kleppner
Title: Professor of Physics, MIT

Acknowledgments

This work would not have been possible without the help and support of the many exceptional people whom I met during my graduate studies at MIT and Harvard.

First of all, I want to express my sincere gratitude to my thesis advisor, Professor Alexander Dalgarno. His experience and insight in atomic and molecular physics were invaluable for the progress of my research. More generally, his great generosity, encouragement, patience and the enthusiasm he showed for my work, were greatly appreciated, especially at times when my progress was slow. His kindness went as far as not waking me up during a rare nap, by dropping softly a draft on the desk in front of me.

I would also like to thank my thesis co-supervisor, Professor Daniel Kleppner, for allowing me to come to the Center for Astrophysics and ITAMP, and offering me support and advice as my academic adviser. I owe special thanks to Prof. Wolfgang Ketterle, who responded to a last minute request and was able to read the manuscript in time for the thesis presentation. I also want to thank Prof. George Koster and Peggy Berkovitz of the graduate physics office for answering all my questions during these many years.

In addition to Alex Dalgarno, many others helped me at one stage or another in my research project at ITAMP, namely Eric Heller, Michael Jamieson, Ron Farren, Yan Sun, James Boyle, and soon to be Dr. Mircea Marinescu. As a new colleague, I would like to extend my thanks to all the members and the numerous visitors of ITAMP: I am grateful to them for creating a pleasant atmosphere to work in.

The support of all my close friends has been invaluable to me, especially from Alain Curodeau, Luis Cruz-Cruz, Hugues Malvos, and Roland Netz. Thanks to these friends and others too many to mentioned here, my stay in Boston has been a very enjoyable and memorable period of my life, that I will undoubtedly look back upon with a smile. My stay would have been less lively without the Plough & Stars Wednesday night and the Thursday night hockey games.

My family has always supported me and their continuing concern and care have played a decisive role. I want to express my deepest gratitude to my mother and father, Aline and Fernand, for encouraging me in this long quest. A special thankyou is due to Silvia Dorado for her support in the last miles: she kept me energized, and going ...

This thesis research was supported by doctoral fellowships from the Canadian government (NSERC) and the Québec government (FCAR), and by the Institute for Theoretical Atomic and Molecular Physics (ITAMP) at the Harvard-Smithsonian Center for Astrophysics. ITAMP is funded by the National Science Foundation (NSF).

Robin Côté
December 7, 1994

To my Parents

Contents

List of Figures

List of Tables

Introduction

In the last decade, both laser cooling [1, 2] and evaporation of trapped atoms [3] have made it possible to cool atoms to temperatures below 1 mK. This opened a window on new physical phenomena to be explored by experimental and theoretical studies, known as the cold and ultracold collisions.

Whenever a physical parameter is changed by many orders of magnitude, as it is the case here for the temperature, we can hope to observe qualitatively new phenomena. For example, the atom velocities range from m/s at 1 mK to mm/s at 1 nK, and during collisions occurring so slowly, the probability of stimulated and spontaneous radiative transitions can approach unity (Miller, Cline and Heinzen [4]). Such optical transitions play a crucial role in the associative ionization of ultracold atoms [5, 6]. In fact, for the sodium (Na) atom, Lett *et al.* [5] have observed a large increase in the ionization rate during the high-intensity ("trapping") periods of their laser trap when compared to the low-intensity ("cooling") periods. The cause of these differences can be traced back to the fact that ionization will only occur near the equilibrium point R_e of the Na_2^+ molecular ion potential curve, since many spontaneous emissions will take place otherwise (see Julienne and Heather [6]).

Another dramatic possibility, first discussed by Thorsheim, Weiner and Julienne [7], is that colliding ultracold atoms could display a resolved photoassociation spectrum. This is due to the fact that the energy spread of the initial collisional state is so small at low temperature (*e.g.*, $k_B T/h = 21$ MHz at $T = 1$ mK) that the free-bound absorption lines can have a sharpness comparable to those normally associated with spectroscopy between bound states. These spectra have been measured in the case of rubidium (Rb) by Miller, Cline and Heinzen [4], for sodium (Na) by Lett *et al.* [5], and more recently by McAlexander *et al.* [8] for lithium (Li). As is shown in the above studies, the photoassociation spectroscopy is a powerful technique for probing the excited molecular states. Since photoassociation involves free to bound transitions, it provides a way to explore the high-lying molecular vibrational levels that are usually hard to access. Moreover, the line shapes of high resolution photoassociation spectra could be used to evaluate the temperature of the trapped atom gas (see Napolitano *et al.* [9]). The photoassociative spectroscopy technique of ultracold trapped atoms can also be extended to probe the ground state molecular levels via a two-photon Raman process. Abraham *et al.* [10] have recently located the last bound level of the triplet ground state of $^7Li_2$. This in turn gives information in the long-range form of the molecular potentials, and could also lead to measurements of the effect of Casimir (or retardation) corrections to the long-range potentials.

The interest in ultracold collisions is also stimulated by the possible realization of Bose-Einstein condensation (BEC) and precise experiments such as the construction of an ultrastable cesium (Cs) clock. This comes from the fact that, although less easy

to manipulate than charged particles, atoms have the advantage that the number of particles dealt with simultaneously can be large without significant mutual perturbation. The study of elastic collisions for the atoms in their ground state is crucial to BEC. In fact, at ultra-low temperature, only the s-wave contributes (*e.g.*, see Côté, Dalgarno and Jamieson [11] for the case of ^{7}Li) and from it one defines the elastic scattering length $a = -\lim_{k\to 0} \delta_0(k)/k$, with δ_0 the s-wave phase shift. The sign of a seems to play a vital role in the stability of the Bose condensate (see Abrikosov, Gorkov and Dzyaloshinki [12]), although this has not been proved rigourously. If $a > 0$, the condensate would be stable, and a negative scattering length would imply an unstable condensate. Notice that one desires the elastic collision cross sections to be as large as possible, since they are required for evaporative cooling used to reach BEC transition temperature (see Moerdijk and Verhaar [13]). However, there are also inelastic processes occuring in those atom traps. One of them, the spin-flip collisions, are harmful because they allow the magnetically trapped atoms to escape. These spin flips are also a limitation to the accuracy one can expect to achieve in atomic clocks

Another very important domain of new physics is the evidence of quantum suppression in the case of collision of atoms with a surface. This has been measured for collision of hydrogen on liquid helium 4 by Ite *et al.* [14], who found that the sticking probability goes as $\sqrt{T}$ when the temperature tends to zero. Other manifestations and applications of ultracold collisions are more ambitious, for example realizing "optical" elements like atom cavities [15] or observing a CP violating electron electric dipole moment [13]. Even the possibility of producing translational low energy molecules in

their ground states does not seem out of reach (see §4.7 of the present work).

The main drive of this work comes from the recent experiments on photoassociative spectroscopy done on the two isotopes of lithium atoms, namely ^{6}Li and ^{7}Li, more precisely the measurements made by R. Hulet and his group at Rice University. Another key element to motivate this study arizes from the very accurate potential curves available for Li and Na molecular ground states. In fact, the scattering length, and elastic scattering in general, depends crucially on the position of the last bound state energy level. Hence, in order to make a meaningful exploration of the elastic and spin flip cross sections, only the most accurate potential curves can be used. Notice that such precise curves are now also available for potassium (K) atoms (see Stwalley and Zemke [16]). Moreover, such accurate potentials bear the possibility of studying the effect of the long-range form of the potentials, and the modifications due to retardation corrections.

Another reason for this study resides in the verification of the validity of certain semi-classical treatments to determine the scattering length and the number of bound states. This also gives the opportunity to look at the quantum suppression during ultracold collisions, and verify the temperature dependence of such phenomena.

Finally, the ratio of signal intensities between the different peaks in the spectroscopic data from Hulet requires a thorough investigation of the problem. The rapid decay of the peaks as the probe laser detuning increased, and the very different behaviour of the singlet and triplet signals, both constitute a challenge. Moreover. the structure within the individual peaks added to the mystery of the experiment. Fi-

nally, the possibility to assess the temperature from the experimental data also played a crucial role in choosing to tackle this problem.

Let us now describe briefly the content of the different chapters. At first, we will give a review of the theory relevant to this study, namely the potential scattering theory. Still in Chapter 1, we will elaborate on the method of partial waves, especially regarding the behaviour of the phase shifts as we lower the energy. Finally, we will give a short overview of the effect of shape resonances, to be completed with two more topics: the Levinson theorem and the effective range theory. These two last items link the number of bound states and the position of the last one to the value of the phase shifts as the energy tends to zero.

In Chapter 2, we will compute the different elastic and spin flip cross sections for both Li and Na. More precisely, we will show how to construct the potential curves used in this work, with emphasis on the long-range aspect of those interaction potentials (including the Casimir corrections). We will then look at the scattering results. First, we will compare the dissociation energies obtained with other published values, and then describe the zero-energy behaviour of our results (*i.e.* the $l = 0$ partial wave). Then, using our potentials, we will compare the bound state energy levels of the ground states with the available experimental values. The effect of higher partial waves and the possibility of shape resonance will then be addressed, and the total elastic and spin flip cross sections will be analysed. The effect of Casimir corrections will also be explored in detail. Finally, the temperature dependence of the cross sections, and especially the spin change rate coefficients, will be computed.

The number of bound states and their locations will be compared with values obtained from various semi-classical treatments in Chapter 3. We first will describe the LeRoy-Bernstein method for the molecular bound state energy levels, followed by the Gribakin-Flaubaum semi-claasical formulation for the number of bound states and the scattering length. We will compare our scattering length with the semi-classical ones, and then expand Gribakin-Flaubaum treatment to construct a zero-energy wave function to be used to evaluate the effective range. Finally, using all the previous analytical tools, we will explore the quantum suppression (when compared with semi-classical results) arizing from very low energies.

In the last chapter, we will compute the photo-absorption spectrum for both ^{6}Li and ^{7}Li at low temerature ($\sim$ 1 mK) and compare with the experimental results of Hulet and his group. At first, we will give a rapid summary of the theory involved, followed by description of the excited potential curves used, together with the dipole moment matrix elements (§4.2). Then, we will give the results from our calculations for the total spectrum (from 0 to $\sim$ -2000 GHz detunings) for both isotopes. We will make a link between the intensities of the peaks and the scattering length, and compare those predictions with experimental results. Then, we will explore the effect of higher partial waves on the structure of particular peaks, especially the influence of shape resonances in the ground state. After computing the natural width of particular levels, we will look at the their line shape and infer a temperature dependence. Moreover, we will estimate the temperature at which the experiment was performed. Finally, we will explore the possibility of creating cold translational molecules in

their ground states. This may open a new domain of exploration for the cold collision community.

Finally, we will make our concluding remarks and enumerate future work that this study made possible to address. Some topics were left out and a brief explanation of the reasons will also be given.

Let us now describe the theoretical framework of this study.

Chapter 1

General Theory

In this chapter, we will review the theoretical background necessary to understand the ultra-cold collision physics. Although more elements could be included here, we will limit ourselves to the domains directly needed for our calculations. We will begin by an overview of the potential scattering theory, followed by the method of partial waves. The effect of the interaction potential between atoms will be discussed in the section on resonances, together with the Levinson theorem. Finally, we will look at the effective range expansion for small kinetic energies.

1.1 Potential Scattering

We begin in this section our study of the simplest collision process: the non-relativistic scattering of two particles which interact through a potential $V(\mathbf{r})$ depending only on their relative coordinate. We shall first reduce our general problem of solving the Schrödinger equation, using the *time independent* method and the *Born-Oppenheimer approximation*, to a stationary state system. After separating the motion of the

center of mass, we will give the basic differential equation to be solved throughout this work. We will derive the expression of the scattering cross section and relate it to the forward differential cross section through the *optical theorem.* That will complete our introduction to the potential scattering problem.

1.1.1 The Born-Oppenheimer approximation

According to the principles of quantum mechanics, the dynamics of a given system is governed by the *time-dependent Schrödinger equation*

$$H\Psi(\mathbf{s},t) = i\hbar\frac{\partial}{\partial t}\Psi(\mathbf{s},t)\ , \tag{1.1}$$

where $\Psi(\mathbf{s},t)$ is the *wave function* and H is the Hamiltonian operator of the system. Here s represents the coordinates of all the particles.

We consider a system made of colliding atoms, *i.e.* an ensemble of nuclei and electrons interacting during a collision. Let us write down the Hamiltonian operator of the whole system of nuclei and electrons. Since we are interested in the collision of identical atoms only, we will consider the case where the nuclei have the same mass M and charge Q. The generalization to a less restrictive system is straightforward but the notation becomes rather lengthy (see Hirschfelder, Curtiss and Bird [17] for a more complete discussion). Let $\mathbf{u}_l$ represents the position of the l^{th} nucleus and $\mathbf{r}_i$ the position of the i^{th} electron. The total Hamiltonian is (*e.g.*, see ziman:solids)

$$H = -\sum_l \frac{\hbar^2}{2M}\nabla^2_{\mathbf{u}_l} - \sum_i \frac{\hbar^2}{2m}\nabla^2_{\mathbf{r}_i} + \sum_{i<j}\frac{e^2}{|\mathbf{r}_i - \mathbf{r}_j|} + V(\mathbf{u},\mathbf{r}) + G(\mathbf{u})\ . \tag{1.2}$$

The first two terms are the kinetic energy operators for the nuclei and the electrons.

The next term is the electron-electron interaction. Then we have the potential energy of the electrons in the field of the ions. Finally, $G(\mathbf{u})$ symbolizes the potential energy of any direct forces between the nuclei.

Since the Hamiltonian is *time-independent*, we may directly separate out the time dependence of the wave function. Indeed, we see that Eq. (1.1) admits particular solutions of the form

$$\Psi(\mathbf{u},\mathbf{r},t) = \Phi(\mathbf{u},\mathbf{r}) \exp\left\{-\frac{i}{\hbar} E_{\text{tot}} t\right\} . \tag{1.3}$$

Substituting this expression into the Schrödinger equation, we find that the time-independent wave function $\Phi(\mathbf{u},\mathbf{r})$ satisfies the equation

$$H\Phi(\mathbf{u},\mathbf{r}) = E_{\text{tot}}\Phi(\mathbf{u},\mathbf{r}) . \tag{1.4}$$

Now, for the Hamiltonian H given above, let us try the following as an eigenfunction

$$\Phi(\mathbf{u},\mathbf{r}) = \psi(\mathbf{u},\mathbf{r})\phi(\mathbf{u}) , \tag{1.5}$$

where we make ψ satisfy the Schrödinger equation for the electrons in a static configuration of the nuclei at positions $\mathbf{u}_l$,

$$\left\{\sum_i -\frac{\hbar^2}{2m}\nabla^2_{\mathbf{r}_i} + \sum_{i<j}\frac{e^2}{|\mathbf{r}_i - \mathbf{r}_j|} + V(\mathbf{u},\mathbf{r})\right\}\psi(\mathbf{u},\mathbf{r}) = \mathcal{E}_e(\mathbf{u})\psi(\mathbf{u},\mathbf{r}) . \tag{1.6}$$

We assume we can find the eigenfunctions and eigenvalues for this equation, but these will be functions of $\mathbf{u}_l$.

Now we apply the operator H to this wave function:

$$H\Phi \;=\; -\sum_l \frac{\hbar^2}{2M}\nabla^2_{\mathbf{u}_l}\Phi + \mathcal{E}_e(\mathbf{u})\Phi + G(\mathbf{u})\Phi$$

$$= \psi(\mathbf{u},\mathbf{r})\left\{-\sum_l \frac{\hbar^2}{2M}\nabla^2_{\mathbf{u}_l} + \mathcal{E}_e(\mathbf{u}) + G(\mathbf{u})\right\}\phi(\mathbf{u})$$
$$-\sum_l \frac{\hbar^2}{2M}\left\{2\nabla_{\mathbf{u}_l}\phi\cdot\nabla_{\mathbf{u}_l}\psi + \phi\nabla^2_{\mathbf{u}_l}\psi\right\} . \qquad (1.7)$$

If now the second line of this expression can be ignored, we can solve our complete eigenvalue problem $H\Phi = \mathcal{E}\Phi$ by making $\phi(\mathbf{u})$ satisfy a Schrödinger-type equation

$$\left\{-\sum_l \frac{\hbar^2}{2M}\nabla^2_{\mathbf{u}_l} + \mathcal{E}_e(\mathbf{u}) + G(\mathbf{u})\right\}\phi(\mathbf{u}) = \mathcal{E}\phi(\mathbf{u}) . \qquad (1.8)$$

This is an equation for the wave function of the nuclei alone, where we add to the interaction of the nuclei $G(\mathbf{u})$ the total energy of the electron system as a function of the position of the nuclei.

It is still necessary to demonstrate that the non-adiabatic terms in (1.7) can be ignored. It is easy to prove that they contribute almost nothing to the expectation value of the energy of the system in the state Φ, *i.e.* $E_{\text{tot}} = \langle\Phi|H|\Phi\rangle/\langle\Phi|\Phi\rangle$. The first such term vanishes: it would produce integrals like

$$\int d^3r\,\psi^*\nabla_{\mathbf{u}_l}\psi = \frac{1}{2}\nabla_{\mathbf{u}_l}\int d^3r\,\psi^*\psi$$
$$= \frac{1}{2}\nabla_{\mathbf{u}_l} n_e , \qquad (1.9)$$

where n_e is the total number of electrons. The second term includes diagonal and off-diagonal contributions: the diagonal ones are already taking into account in $\mathcal{E}_e(\mathbf{u})$. The off-diagonal terms are small [18] because, at worst, the electrons would be tightly bound to their nuclei, *i.e.*

$$\psi(\mathbf{u}_l,\mathbf{r}_i) = \psi(\mathbf{u}_l - \mathbf{r}_i) , \qquad (1.10)$$

which would give a contribution like

$$
\begin{aligned}
-\int d^3r\,\psi^* \frac{\hbar^2}{2M}\nabla^2_{\mathbf{u}_l}\psi &= -\int d^3r\,\psi^* \frac{\hbar^2}{2M}\nabla^2_{\mathbf{r}_i}\psi \\
&= -\frac{m}{M}\int d^3r\,\psi^* \frac{\hbar^2}{2m}\nabla^2_{\mathbf{r}_i}\psi\ . \qquad (1.11)
\end{aligned}
$$

This is just m/M times the kinetic energy of the electrons: we can neglect that term since $m/M \sim 10^{-4}$ or 10^{-5}. Of course, this is a very sketchy demonstration. A more rigourous proof is given in Hirschfelder, Curtiss and Bird [17].

Thus, the fact that the mass of the electrons is much smaller than that of the nuclei give rise to a significant simplification: the *Born-Oppenheimer approximation.* It follows from it that one can, in a first approximation, study the motions of the electrons and the nuclei separately. One begins by determining the motion of the electrons for a fixed value of the distance R between the two nuclei; thus one obtains a series of stationary states for the electronic system, of energies $E_1(R)$, $E_2(R)$ ... Then one considers the ground state, of energy $E_1(R)$, of the electronic system; when R varies because of the motion of the nuclei, the electronic system always remains in the ground state, for all R. This means that the system wave function adapts itself instantaneously to any change in R: the electrons, which are very mobile, are said to follow *adiabatically* the motion of the nuclei.

So, by adding the electronic energy to the potential energy of the nuclei, we form the molecular potential $V(\mathbf{u}) = \mathcal{E}_e(\mathbf{u}) + G(\mathbf{u})$, and we get a Schrödinger equation to solve for the motion of the nuclei

$$
\left\{-\sum_l \frac{\hbar^2}{2M}\nabla^2_{\mathbf{u}_l} + V(\mathbf{u})\right\}\phi(\mathbf{u}) = \mathcal{E}\phi(\mathbf{u})\ . \qquad (1.12)
$$

1.1.2 The stationary wave function

We are interested in the non-relativistic collision of two particles A and B, with masses m_A and m_B and coordinates $\mathbf{r}_A$ and $\mathbf{r}_B$ measured from some fixed origin $\mathcal{O}$. Using the Born-Oppenheimer approximation, we assume that these particles interact through a real potential $V(\mathbf{r}_A - \mathbf{r}_B)$ which depends only upon the relative coordinate $\mathbf{r}_A - \mathbf{r}_B$.

The Hamiltonian for the two nuclei is simply

$$H = -\frac{\hbar^2}{2m_A}\nabla^2_{\mathbf{r}_A} - \frac{\hbar^2}{2m_B}\nabla^2_{\mathbf{r}_B} + V(\mathbf{r}_A - \mathbf{r}_B) \ , \tag{1.13}$$

and we need to solve the Schrödinger equation

$$H\Phi(\mathbf{r}_A, \mathbf{r}_B) = E_{\text{tot}}\Phi(\mathbf{r}_A, \mathbf{r}_B) \ . \tag{1.14}$$

We can simplify this problem by using the center of mass coordinates. We introduce the two following vectors

$$\mathbf{r} = \mathbf{r}_A - \mathbf{r}_B \ , \tag{1.15}$$

$$\mathbf{R} = (m_A\mathbf{r}_A + m_B\mathbf{r}_B)/(m_A + m_B) \ , \tag{1.16}$$

where $\mathbf{r}$ is the relative coordinate and $\mathbf{R}$ determines the center of mass of the system. Defining the total mass M and the reduced mass μ of the system by

$$M = m_A + m_B \ , \tag{1.17}$$

$$\mu = m_A m_B/(m_A + m_B) \ , \tag{1.18}$$

we can then rewrite our problem in the new coordinates $(\mathbf{r}, \mathbf{R})$ as

$$\left(-\frac{\hbar^2}{2M}\nabla^2_{\mathbf{R}} - \frac{\hbar^2}{2\mu}\nabla^2_{\mathbf{r}} + V(\mathbf{r})\right)\Phi(\mathbf{r}, \mathbf{R}) = E_{\text{tot}}\Phi(\mathbf{r}, \mathbf{R}) \ . \tag{1.19}$$

Since the potential only depends on $\mathbf{r}$, a separation of the wave function $\Phi(\mathbf{r},\mathbf{R})$ can be made into a product of functions of the relative coordinates and the center of mass coordinates

$$\Phi(\mathbf{r},\mathbf{R}) = \phi(\mathbf{R})\psi(\mathbf{r}) \ , \tag{1.20}$$

where the functions $\phi(\mathbf{R})$ and $\psi(\mathbf{r})$ satisfy respectively the equations

$$-\frac{\hbar^2}{2M}\nabla^2_{\mathbf{R}}\phi(\mathbf{R}) = E_{C.M.}\phi(\mathbf{R}) \ , \tag{1.21}$$

$$\left(-\frac{\hbar^2}{2\mu}\nabla^2_{\mathbf{r}} + V(\mathbf{r})\right)\psi(\mathbf{r}) = E\psi(\mathbf{r}) \ , \tag{1.22}$$

$$E_{\text{tot}} = E_{C.M.} + E \ . \tag{1.23}$$

If we elect to work in the center of mass coordinate system, as we shall do in the remaining of this work, we need not to be concerned by the motion of the center of mass (C.M.), whose coordinates are thus eliminated. The problem of the scattering of two particles interacting through a potential $V(\mathbf{r})$ which depends only on their relative coordinate $\mathbf{r}$ is therefore entirely equivalent, in the C.M. system, to the scattering of a particle of reduced mass μ by the potential $V(\mathbf{r})$.

Now, if E is the energy of the reduced particle, then when $V(\mathbf{r})$ tends to zero asymptotically, we must have

$$E = \frac{p^2}{2\mu} = \frac{\hbar^2 k^2}{2\mu} \ , \tag{1.24}$$

and the initial momentum $\mathbf{p}$ and wave number $\mathbf{k}$ are given by

$$\mathbf{p} = \hbar\mathbf{k} \ . \tag{1.25}$$

Introducing the *reduced potential*

$$U(\mathbf{r}) = \frac{2\mu}{\hbar^2}V(\mathbf{r}) \ . \tag{1.26}$$

the Schrödinger equation to solve becomes

$$\left[\nabla_{\mathbf{r}}^2 + k^2 - U(\mathbf{r})\right] \psi(\mathbf{r}) = 0 \ . \tag{1.27}$$

We shall assume that the potential $V(\mathbf{r})$ tends to zero faster than r^{-1} as $r \to \infty$ (we are not considering the scattering by a Coulomb potential). We can then find a particular solution of Eq. (1.27) which we shall call the stationary scattering wave function and denote by $\psi_{\mathbf{k}}^{(+)}(\mathbf{r})$. This function satisfies the asymptotic boundary condition

$$\psi_{\mathbf{k}}^{(+)}(\mathbf{r}) \to A \left\{ \exp(i\mathbf{k} \cdot \mathbf{r}) + f(k, \theta, \phi) \frac{\exp(ikr)}{r} \right\} \ . \tag{1.28}$$

Here A is independent of $\mathbf{r}$, and θ and ϕ are the usual spherical angles, with our choice of polar z-axis along the direction of the incident wave vector $\mathbf{k}$. The origin $\mathcal{O}$ coincides with that of the vector $\mathbf{r}$. We may easily verify that for any function $f(k, \theta, \phi)$ the asymptotic wave function $\psi_{\mathbf{k}}^{(+)}(\mathbf{r})$ satisfies our Schrödinger equation through terms of order $1/r$ in the region where $V(\mathbf{r})$ can be neglected, provided that the potential vanishes faster than r^{-1} as $r \to \infty$ (see C.J. Joachain [19]).

Let us now investigate the physical meaning of $\psi_{\mathbf{k}}^{(+)}(\mathbf{r})$. We see that for large distances it is the superposition of a *plane wave* of wave number $\mathbf{k}$ and an *outgoing spherical wave* with an amplitude depending on θ and ϕ and inversely proportional to r. That the spherical wave is an outgoing one can be checked by returning to the time-dependent formulation and noting that the expression

$$\frac{1}{r} \exp\{i(kr - \omega t)\} \tag{1.29}$$

indeed describes a spherical wave with *positive phase velocity*

$$\frac{dr}{dt} = \frac{\omega}{k} \ . \tag{1.30}$$

The physical interpretation of the quantities A and f will be given in the next section.

1.1.3 Cross section and the optical theorem

The quantity

$$\sigma(\Omega)d\Omega = \frac{d\sigma}{d\Omega}d\Omega \tag{1.31}$$

is the number of particles emitted per unit time and unit incident flux within the solid angle $d\Omega$ about the direction $\Omega(\theta, \phi)$. It is therefore equal to the outgoing flux of particles scattered through the spherical surface $r^2 d\Omega$ (for $r \to \infty$), divided by the incident flux.

In order to obtain these quantities, let us consider the probability current density associated with the Schrödinger equation, namely

$$\begin{aligned} \mathbf{j}(\mathbf{r}) &= \frac{\hbar}{2\mu i}\{\psi^*(\mathbf{r})[\nabla_{\mathbf{r}}\psi(\mathbf{r})] - [\nabla_{\mathbf{r}}\psi^*(\mathbf{r})]\psi(\mathbf{r})\} \ , \\ &= \mathrm{Re}\left\{\frac{\hbar}{\mu i}\psi^*(\mathbf{r})\nabla_{\mathbf{r}}\psi(\mathbf{r})\right\} \ . \end{aligned} \tag{1.32}$$

It satisfies the continuity equation

$$\nabla_{\mathbf{r}} \cdot \mathbf{j} + \frac{\partial \rho}{\partial t} = 0 \ , \tag{1.33}$$

where $\rho = |\psi|^2$ is the *probability density.* Since we are in a stationary problem, this reduces to

$$\nabla_{\mathbf{r}} \cdot \mathbf{j} = 0 \ . \tag{1.34}$$

Since we want the flux in the outgoing direction, we must use the spherical coordinates for $\nabla_{\mathbf{r}}$. After some manipulations [19], we find that the outgoing flux of particles passing through a spherical surface element $r^2 d\Omega$ for very large r is then given by

$$A^* A \frac{\hbar k}{\mu} |f(k,\Omega)|^2 d\Omega \ , \tag{1.35}$$

and the incident flux is simply

$$A^* A \frac{\hbar k}{\mu} \ . \tag{1.36}$$

So dividing the outgoing flux by the incident one and by $d\Omega$, we obtain the *differential cross section*

$$\frac{d\sigma}{d\Omega} = |f(k,\Omega)|^2 \ , \tag{1.37}$$

while the *total cross section* is given by

$$\sigma_{tot} = \int d\Omega \frac{d\sigma}{d\Omega} \ . \tag{1.38}$$

The quantity $f(k,\Omega)$ is called the *scattering amplitude.* It is worth noting that the cross sections are independent of the *normalization coefficient* A. We may therefore choose this quantity as we please. For example, if $A = 1$ the incident plane wave has unit density in $\mathbf{r}$ space, while the choice $A = (\hbar k/\mu)^{-1/2}$ corresponds to a wave function *normalized* to unit incident flux.

Finally, one can relate the total cross section to the scattering amplitude with $\theta = 0$. As we will show in the next section, one can obtain

$$\sigma_{tot} = \frac{4\pi}{k} \mathrm{Im}[f(k,\theta = 0,\phi)] \ . \tag{1.39}$$

This is the *optical theorem*, also known as the Bohr-Peierls-Placzeck relation.

1.2 Method of partial waves

In this section, we shall learn how to obtain explicitly the scattering amplitude and cross section when the potential is *central*, *i.e.* depends only on the magnitude of r of the vector $\mathbf{r}$. In this case, the solutions of the Schrödinger equation may be separated in spherical coordinates, and a simple connection between the radial solutions and the asymptotic form of the stationary scattering wave function may be found.

1.2.1 The partial wave analysis

We consider here a spinless particle of mass m in the presence of a real central potential $V(r)$. We adopt a spherical coordinate system with the z-axis along the incident direction, while the origin $\mathcal{O}$ coincides with that of the vector $\mathbf{r}$.

The Hamitonian operator $H = -(\hbar^2/2m)\nabla_{\mathbf{r}}^2 + V$ now reads in spherical coordintes

$$H = -\frac{\hbar^2}{2m}\left[\frac{1}{r^2}\frac{\partial}{\partial r}\left(r^2\frac{\partial}{\partial r}\right) + \frac{1}{r^2\sin\theta}\frac{\partial}{\partial\theta}\left(\sin\theta\frac{\partial}{\partial\theta}\right) + \frac{1}{r^2\sin^2\theta}\frac{\partial^2}{\partial\phi^2}\right] + V(r)\ . \quad (1.40)$$

Introducing the orbital angular momentum operator

$$\mathbf{L} = \mathbf{r}\times\mathbf{p}\ . \quad (1.41)$$

where $\mathbf{p}$ is the momentum of the particle and is given by $-i\hbar\nabla_{\mathbf{r}}$, one finds

$$L^2 = L_x^2 + L_y^2 + L_z^2 = -\hbar^2\left[\frac{1}{\sin\theta}\frac{\partial}{\partial\theta}\left(\sin\theta\frac{\partial}{\partial\theta}\right) + \frac{1}{\sin^2\theta}\frac{\partial^2}{\partial\phi^2}\right]\ . \quad (1.42)$$

One can verify that the components of L satisfy the following commutation rules

$$[L_x, L_y] = i\hbar L_z\ , \quad (1.43)$$

with cyclic permutation on x, y, z components, and

$$[L^2, L_x] = [L^2, L_y] = [L^2, L_z] = 0 \ . \tag{1.44}$$

From these relations we deduce that one can find eigenfunctions which are common to the operators L^2 and one of the components of $\mathbf{L}$. Selecting the z component, the desired functions are given by the spherical harmonics $Y_{lm}(\theta, \phi)$

$$L^2 Y_{lm}(\theta, \phi) = l(l+1)\hbar^2 Y_{lm}(\theta, \phi) \ , \tag{1.45}$$

$$L_z Y_{lm}(\theta, \phi) = m\hbar Y_{lm}(\theta, \phi) \ , \tag{1.46}$$

where l and m are respectively called the *orbital angular momentum number* and the *magnetic quantum number.*

Now, we can rewrite the Hamiltonian in a simpler way

$$H = -\frac{\hbar^2}{2m}\left[\frac{1}{r^2}\frac{\partial}{\partial r}\left(r^2\frac{\partial}{\partial r}\right) - \frac{L^2}{\hbar^2 r^2}\right] + V(r) \ , \tag{1.47}$$

so that

$$[H, L^2] = [H, L_z] = 0 \ . \tag{1.48}$$

Because the three operators H, L^2 and L_z all commute, we can look for common eigenfunctions. We can therefore expand $\psi_{\mathbf{k}}^{(+)}(k, \mathbf{r})$ in partial waves corresponding to given values of the quantum numbers l and m as

$$\psi_{\mathbf{k}}^{(+)}(k, \mathbf{r}) = \sum_{l=0}^{\infty} \sum_{m=-l}^{+l} c_{lm}(k) R_{lm}(k, r) Y_{lm}(\theta, \phi) \ . \tag{1.49}$$

Using this expansion in the Schrödinger equation and using the above relations, we obtain for every radial function the equation

$$-\frac{\hbar^2}{2m}\left[\frac{1}{r^2}\frac{d}{dr}\left(r^2\frac{d}{dr}\right) - \frac{l(l+1)}{r^2}\right] R_l(k, r) + V(r) R_l(k, r) = E R_l(k, r) \ . \tag{1.50}$$

Here we have written $R_l(k,r)$ instead of $R_{lm}(k,r)$ since there is no dependence on the magnetic quantum number m in the Hamiltonian. It is convenient to use the new function

$$u_l(k,r) = rR_l(k,r) \ . \tag{1.51}$$

The new radial equation is then

$$\left[\frac{d^2}{dr^2} + k^2 - \frac{l(l+1)}{r^2} - U(r)\right] u_l(k,r) = 0 \ . \tag{1.52}$$

where $k = \sqrt{2mE/\hbar^2}$ and $U = 2mV/\hbar^2$. It is worth noting that there is no loss of generality in assuming that $u_l(k,r)$ is real, since both the real and the imaginary parts of a complex u_l would separately satisfy Eq. (1.52).

Let us look at the solution of Eq. (1.52) in the case of a free particle, *i.e.* when $U = 0$. The differential equation reduces to

$$\left[\frac{d^2}{dr^2} + k^2 - \frac{l(l+1)}{r^2}\right] y_l(k,r) = 0 \ . \tag{1.53}$$

Now, changing variables to $\rho = kr$ and defining the function

$$f_l(\rho) = \frac{y_l}{\rho} \ , \tag{1.54}$$

our equation becomes

$$\left[\frac{d^2}{d\rho^2} + \frac{2}{\rho}\frac{d}{d\rho} + \left(1 - \frac{l(l+1)}{\rho^2}\right)\right] f_l(\rho) = 0 \ . \tag{1.55}$$

This is the *spherical Bessel differential equation.* The general solution is then given by

$$y_l(k,r) = kr\left[C_l^{(1)}(k) j_l(kr) + C_l^{(2)}(k) n_l(kr)\right] \ , \tag{1.56}$$

where $j_l(kr)$ and $n_l(kr)$ are respectively the spherical Bessel and Neumann functions. For a free particle, the solution must be regular at the origin $r = 0$. Thus only the spherical Bessel functions can survive and one must have $C_l^{(2)}(k) = 0$.

Returning to our problem of solving Eq. (1.52) for a real potential, we must look at the boundary conditions to be imposed upon $u_l(k,r)$. It can be shown [19] that if the potential satisfies the condition

$$\lim_{r\to\infty} |U(r)| < \frac{M}{r^{1+\epsilon}} , \tag{1.57}$$

where M is some constant and ϵ is greater than zero, the solution $u_l(k,r)$ will asymptotically be given by

$$u_l(k,r) \sim kr \left[C_l^{(1)}(k) j_l(kr) + C_l^{(2)}(k) n_l(kr)\right] . \tag{1.58}$$

Now, using the expression of the spherical Bessel and Neumann functions for large r

$$j_l(x) \rightarrow \frac{1}{x} \sin\left(x - \frac{1}{2} l\pi\right) , \tag{1.59}$$

$$n_l(x) \rightarrow -\frac{1}{x} \cos\left(x - \frac{1}{2} l\pi\right) , \tag{1.60}$$

we can rewrite the asymptotic from of $u_l(k,r)$ like

$$u_l(k,r) \rightarrow A_l(k) \sin\left(kr - \frac{1}{2} l\pi + \delta_l(k)\right) , \tag{1.61}$$

with

$$A_l(k) = \left\{\left[C_l^{(1)}(k)\right]^2 + \left[C_l^{(2)}(k)\right]^2\right\}^{1/2} , \tag{1.62}$$

$$\tan\delta_l(k) = -\frac{C_l^{(2)}(k)}{C_l^{(1)}(k)} . \tag{1.63}$$

Let us now examine the boundary condition which must be satisfied by $u_l(k,r)$ at the origin $r = 0$. Let us assume that near the origin the interaction has the form

$$U(r) = r^p(a_0 + a_1 r + \cdots) \ , \tag{1.64}$$

where p is an integer such that $p \geq -1$. We then expand u_l in the vicinity of $r = 0$ as

$$u_l = r^s(c_0 + c_1 r + \cdots), \qquad c_0 \neq 0 \ . \tag{1.65}$$

Substituting those two equations into Eq. (1.52) we find by looking at the coefficient of the lowest power of r, *i.e.* r^{s-2}, that the quantity s must satisfy the indicial equation

$$s(s-1) - l(l+1) = 0 \ , \tag{1.66}$$

so that $s = l + 1$ or $s = -l$. The choice $s = -l$ gives an irregular solution and must therefore be discarded. The other choice $s = l + 1$ corresponds to a regular solution which is physically allowed. Then, we have the following condition near the origin

$$u_l(k,0) = 0 \quad \text{and} \quad u_l(k,r) \sim r^{l+1} \quad \text{as} \quad r \to 0 \ . \tag{1.67}$$

The case where the potential is more singular than r^{-1} at the origin is irrelevant here, since the molecular potentials are repulsive at small r (see C.J. Joachain [19]).

We now turn to the determination of the scattering amplitude. We recall the asymptotic form of the scattering wave function $\psi_{\mathbf{k}}^{(+)}(k,\mathbf{r})$ is given by

$$\psi_{\mathbf{k}}^{(+)}(k,\mathbf{r}) \to A(k)\left\{\exp(i\mathbf{k}\cdot\mathbf{r}) + f(k,\theta,\phi)\frac{\exp(ikr)}{r}\right\} \ . \tag{1.68}$$

Noting that the partial wave expansion of the plane wave is given by

$$\exp(i\mathbf{k}\cdot\mathbf{r}) \equiv \exp(ikz) = \sum_{l=0}^{\infty}(2l+1)i^l j_l(kr)P_l(\cos\theta) \ , \tag{1.69}$$

where $P_l(\cos\theta)$ are the Legendre polynomials

$$P_l(\cos\theta) = \sqrt{\frac{4\pi}{2l+1}} Y_{l,0}(\theta,\phi) = \frac{4\pi}{2l+1} \sum_{m=-l}^{l} Y^*_{lm}(\hat{\mathbf{k}}) Y_{lm}(\hat{\mathbf{r}}) \ , \tag{1.70}$$

we can write the asymptotic form of $\psi^{(+)}_{\mathbf{k}}(k,\mathbf{r})$. Notice here that the last equation above is valid for any choice of z-axis. So, using the asymptotic expression for $j_l(kr)$, we get

$$\begin{aligned} \psi^{(+)}_{\mathbf{k}}(k,\mathbf{r}) \ &\rightarrow \ A(k) \left\{ \sum_{l=0}^{\infty} (2l+1) i^l \frac{\sin(kr - l\pi/2)}{kr} P_l(\cos\theta) + f(k,\theta,\phi) \frac{\exp(ikr)}{r} \right\} \ , \\ &\rightarrow \ A(k) \left\{ \sum_{l=0}^{\infty} \sum_{m=-l}^{+l} \sqrt{\frac{4\pi}{2l+1}} i^l \frac{\exp\{i(kr - l\pi/2)\} - \exp\{-i(kr - l\pi/2)\}}{2ikr} \right. \\ &\qquad \left. \times \ Y_{l,0}(\theta,\phi)\delta_{m,0} + f(k,\theta,\phi) \frac{\exp(ikr)}{r} \right\} \ . \end{aligned} \tag{1.71}$$

On the other hand, we may also consider the partial wave expansion

$$\psi^{(+)}_{\mathbf{k}}(k,\mathbf{r}) = \sum_{l=0}^{\infty} \sum_{m=-l}^{+l} c_{lm}(k) R_{lm}(k,r) Y_{lm}(\theta,\phi) \ , \tag{1.72}$$

and using the asymptotic form for $R_{lm}(k,r) \equiv R_l(k,r) = r^{-1} u_l(k,r)$ we can write

$$\begin{aligned} \psi^{(+)}_{\mathbf{k}}(k,\mathbf{r}) \ \rightarrow \ \sum_{l=0}^{\infty} \sum_{m=-l}^{+l} c_{lm}(k) A_l(k) \frac{1}{2ikr} \left[\exp\{i(kr - l\pi/2 + \delta_l)\} \right. \\ \left. - \exp\{-i(kr - l\pi/2 + \delta_l)\} \right] Y_{l,m}(\theta,\phi) \ . \end{aligned} \tag{1.73}$$

Upon comparison of the coefficients of the incoming spherical waves, we have

$$c_{lm}(k) = \frac{A(k)}{kA_l(k)} \sqrt{\frac{4\pi}{2l+1}} i^l \exp(i\delta_l) \delta_{m,0} \ . \tag{1.74}$$

The wave function can then be written as

$$\psi^{(+)}_{\mathbf{k}}(k,\mathbf{r}) = A(k) \sum_{l=0}^{\infty} \frac{(2l+1)}{kA_l(k)} i^l \exp(i\delta_l) R_l(k,r) P_l(\cos\theta) \ . \tag{1.75}$$

Next, by matching the coefficients of the outgoing spherical waves, we find that the scattering amplitude is independent of ϕ and is given by

$$\begin{aligned} f(k,\theta) &= \frac{1}{2ik}\sum_{l=0}^{\infty}(2l+1)\left[\exp\{2i\delta_l(k)\}-1\right]P_l(\cos\theta)\ , \\ &= \frac{1}{k}\sum_{l=0}^{\infty}(2l+1)a_l(k)P_l(\cos\theta)\ , \end{aligned} \tag{1.76}$$

where the *partial wave amplitude* $a_l(k)$ is given by

$$a_l(k) = \exp\{i\delta_l(k)\}\sin\delta_l(k)\ . \tag{1.77}$$

Then, according to the fundamental relation, the differential scattering cross section is given by

$$\begin{aligned} \frac{d\sigma}{d\Omega}(k,\theta) = |f(k,\theta)|^2 &= \frac{1}{k^2}\sum_{l=0}^{\infty}\sum_{l'=0}^{\infty}(2l+1)(2l'+1)\exp\{i[\delta_l(k)-\delta_{l'}(k)]\} \\ &\quad\times\sin\delta_l(k)\sin\delta_{l'}(k)P_l(\cos\theta)P_{l'}(\cos\theta)\ . \end{aligned} \tag{1.78}$$

The total cross section is then obtained as

$$\sigma_{tot}(k) = 2\pi\int_0^{\pi}\frac{d\sigma}{d\Omega}(k,\theta)\sin\theta d\theta\ , \tag{1.79}$$

and using the orthogonality relation for Legendre polynomials

$$\int_{-1}^{+1}dx P_l(x)P_{l'}(x) = \frac{2}{2l+1}\delta_{ll'}\ , \tag{1.80}$$

we finally get

$$\sigma_{tot}(k) = \frac{4\pi}{k^2}\sum_{l=0}^{\infty}(2l+1)\sin^2\delta_l(k) = \sum_{l=0}^{\infty}\sigma_l(k)\ , \tag{1.81}$$

where each partial wave cross section $\sigma_l(k)$ is given by

$$\sigma_l(k) = \frac{4\pi}{k^2}(2l+1)\sin^2\delta_l(k)\ . \tag{1.82}$$

From these last equations, it is easy to get back the optical theorem. Indeed, we have

$$f(k,\theta=0)=\frac{1}{k}\sum_{l=0}^{\infty}(2l+1)\exp\{i\delta_l(k)\}\sin\delta_l(k)\ , \tag{1.83}$$

so that

$$\mathrm{Im}[f(k,\theta=0)]=\frac{1}{k}\sum_{l=0}^{\infty}(2l+1)\sin^2\delta_l(k)\ . \tag{1.84}$$

Hence, upon comparison with the previous result, we find that

$$\sigma_{tot}(k)=\frac{4\pi}{k}\mathrm{Im}[f(k,\theta=0)]\ . \tag{1.85}$$

Finally, let us have a last look at the normalization issue of the radial wave functions $u_l(k,r)$. Since they are not square integrable, they cannot be assigned a finite norm. A natural prescription for normalizing unbound states is to require that their scalar product be proportional to a delta function. This can be done in different ways. For the radial wave functions $u_l(k,r)$, we have asymptotically

$$u_l(k,r)\to A_l(k)\sin(kr-l\pi/2+\delta_l(k))\ , \tag{1.86}$$

so that

$$\int_0^{\infty}dr\,u_l(k,r)u_l(k',r)=A_l^2(k)\frac{\pi}{2}\delta(k-k')\ , \tag{1.87}$$

assuming that both k and k' are positive. If we want the scalar product to be a delta function, we must take $A_l(k)=\sqrt{2/\pi}$. However, in many applications we want the wave functions to be *energy normalized*, which means

$$\int_0^{\infty}dr\,u_l(E,r)u_l(E',r)=\delta(E-E')\ . \tag{1.88}$$

For $E = \hbar^2 k^2/2m$ we have

$$\delta(k - k') = \frac{dE}{dk}\delta(E - E') = \frac{\hbar^2 k}{m}\delta(E - E') \ . \tag{1.89}$$

Hence energy normalized wave function are obtained by choosing $A_l(k) = \sqrt{2m/\pi\hbar^2 k}$, so that the asymptotic from is now

$$u_l(E, r) \rightarrow \sqrt{\frac{2m}{\pi\hbar^2 k}} \sin(kr - l\pi/2 + \delta_l(k)) \ . \tag{1.90}$$

This last form will be used in the last chapter of this work, when we will calculate some absorption probabilities.

1.2.2 The phase shift

As we have seen in the previous section, all the physical information for an elastic scattering problem is included in the scattering phase shift. Therefore, a better understanding of this quantity is imperative.

Let us first establish some general relationships between the phase shift and the interaction potential. We consider the scattering by two reduced potentials $U(r)$ and $\overline{U}(r)$, with respective radial equations

$$\left[\frac{d^2}{dr^2} + k^2 - \frac{l(l+1)}{r^2} - U(r)\right] u_l(r) = 0 \ , \tag{1.91}$$

$$\left[\frac{d^2}{dr^2} + k^2 - \frac{l(l+1)}{r^2} - \overline{U}(r)\right] \overline{u}_l(r) = 0 \ . \tag{1.92}$$

Assuming that both functions are normalized asymptotically like

$$u_l(r) \rightarrow \sin(kr - l\pi/2 + \delta_l) \ , \tag{1.93}$$

$$\overline{u}_l(r) \rightarrow \sin(kr - l\pi/2 + \overline{\delta}_l) \ , \tag{1.94}$$

and defining the Wronskian of the two solutions by

$$W(u_l, \overline{u}_l) = u_l \overline{u}_l' - u_l' \overline{u}_l \ , \tag{1.95}$$

where the prime denotes a derivative with respect to r, we find, after multiplying the first D.E. by $\overline{u}_l$ and the second by u_l and substracting term by term, the identity

$$\overline{u}_l u_l'' - u_l \overline{u}_l'' - (U - \overline{U}) u_l \overline{u}_l = 0 \tag{1.96}$$

or

$$\frac{d}{dr} W(u_l, \overline{u}_l) = -(U - \overline{U}) u_l \overline{u}_l \ . \tag{1.97}$$

Upon integration over r in the interval (a, b), we get

$$W(u_l, \overline{u}_l)\Big|_a^b = -\int_a^b dr\, \overline{u}_l(r)[U(r) - \overline{U}(r)] u_l(r) \ . \tag{1.98}$$

Choosing $a = 0$ and $b = \infty$ and remembering that $u_l(0) = \overline{u}_l(0)$ we find with the help of the asymptotic form of the wave functions

$$k \left[\sin \delta_l \cos \overline{\delta}_l - \cos \delta_l \sin \overline{\delta}_l\right] = -\int_0^\infty dr\, \overline{u}_l(r)[U(r) - \overline{U}(r)] u_l(r) \ , \tag{1.99}$$

provided that both potentials tend to zero faster than r^{-1} for large r and that they are repulsive or less singular than r^{-2} at the origin (for attractive potential). These conditions are always met in the case of molecular potentials (the Coulomb case not being studied here). Now setting $\overline{U} = 0$, *i.e.* $\overline{\delta}_l = 0$, we obtain

$$k \sin \delta_l = -\int_0^\infty dr\, kr j_l(kr) U(r) u_l(r) \ . \tag{1.100}$$

Let us define the following functions

$$s_l(x) \equiv x j_l(x) \qquad \text{and} \qquad c_l(x) \equiv -x n_l(x) \ . \tag{1.101}$$

We then obtain the simple integral expression for the phase shift

$$\sin\delta_l = -\frac{1}{k}\int_0^\infty dr\, s_l(kr)U(r)u_l(r)\ . \tag{1.102}$$

Very often, another asymptotic form for $u_l(r)$ is selected, namely

$$\begin{aligned}\tilde{u}_l(r) &\rightarrow s_l(kr) + c_l(kr)\tan\delta_l\ , \\ &\rightarrow \sin(kr - l\pi/2) + \cos(kr - l\pi/2)\tan\delta_l\ , \\ &\rightarrow \frac{1}{\cos\delta_l}\sin(kr - l\pi/2 + \delta_l)\ ,\end{aligned} \tag{1.103}$$

for which the integral representation for the phase shift becomes

$$\tan\delta_l = -\frac{1}{k}\int_0^\infty dr\, s_l(kr)U(r)\tilde{u}_l(r)\ . \tag{1.104}$$

The physical interpretation of the phase shift can be understood by comparing the free solution to the scattered radial solution. Indeed, we first note that the free solution $v_l(r)$ has nodes at

$$r = \frac{1}{k}(n\pi + l\pi/2)\ , \tag{1.105}$$

while the corresponding nodes of the radial function $u_l(r)$ occur in the asymptotic region at

$$r = \frac{1}{k}(n\pi + l\pi/2 - \delta_l)\ . \tag{1.106}$$

For a repulsive potential we expect that $u_l(r)$ should be "pushed out" with respect to $v_l(r)$. Thus the zeroes given by Eq. (1.106) should be displaced with respect to those of Eq. (1.105) by a *positive* amount $(-\delta_l/k)$, hence $\delta_l < 0$ in this case. By the same reasoning we see that for an attractive potential $u_l(r)$ is "pulled in" with respect to

$v_l(r)$ so that $\delta_l > 0$. A more rigourous analysis can be performed using the expression (1.99) and parametrizing the potentials by some quantity λ and $\overline{\lambda}$ [19].

We now turn to the actual computation of the phase shift. It is obtained by solving the radial equation (1.52) with the appropriate boundary conditions. If the potential has a strict finite range, *i.e.* $V = 0$ for $r \geq a$, one can divide the domain of r into an internal region ($r < a$) and an external region ($r > a$). At the boundary $r = a$, we must have both u_l and du_l/dr continuous, or equivalently the logarithmic derivative $u_l^{-1} du_l/dr$ has to be continuous. So, the exterior solution is given by

$$u_l(r) = A_l(k)[s_l(kr) + c_l(kr)\tan\delta_l] \; . \tag{1.107}$$

Thus, if we denote the value of the logarithmic derivative of the inside solution at $r = a$ by

$$\gamma_l(k) = \left.\frac{1}{u_l(r)}\frac{d}{dr}u_l(r)\right|_{r=a} \; , \tag{1.108}$$

we then find

$$\gamma_l(k) = \frac{k[s_l'(ka) + c_l'(ka)\tan\delta_l]}{s_l(ka) + c_l(ka)\tan\delta_l} \; , \tag{1.109}$$

where we have

$$s_l'(ka) = \left.\frac{d}{dx}s_l(x)\right|_{x=ka} \quad \text{and} \quad c_l'(ka) = \left.\frac{d}{dx}c_l(x)\right|_{x=ka} \; . \tag{1.110}$$

Hence, we get

$$\tan\delta_l = -\frac{ks_l'(ka) - \gamma_l(k)s_l(ka)}{kc_l'(ka) - \gamma_l(k)c_l(ka)} \; . \tag{1.111}$$

If the potential does not vanish identically beyond a certain value of r, but has nevertheless a "range" a, one choose a distance $d \gtrsim a$ at which the influence of the

potential is negligible. We then match both logarithmic derivatives at $r = d$ and get

$$\tan \delta_l = -\frac{k s_l'(kd) - \gamma_l(k) s_l(kd)}{k c_l'(kd) - \gamma_l(k) c_l(kd)} \ . \tag{1.112}$$

In performing calculations of this type, one must check that the phase shift obtained is insensitive to any increase of d (within the accuracy required).

In our case, we will solve Eq. (1.52) numerically, using the Numerov method, with automatic step-size ajustment (see Appendix A for more details). We consider the values $r_n = r_0 + n\Delta r$, so this algorithm gives by recurrence the values of

$$Q_{l,n} = \frac{u_l(r_n)}{u_l(r_{n-1})} \ . \tag{1.113}$$

Using the asymptotic form for $u_l(r)$, we can write

$$Q_{l,n} \sim \frac{s_l(kr_n) + c_l(kr_n) \tan \delta_l}{s_l(kr_{n-1}) + c_l(kr_{n-1}) \tan \delta_l} \quad \text{for} \quad n \to \infty \ , \tag{1.114}$$

with the result

$$\tan \delta_l \sim -\frac{s_l(kr_n) - Q_{l,n} s_l(kr_{n-1})}{c_l(kr_n) - Q_{l,n} c_l(kr_{n-1})} \quad \text{for} \quad n \to \infty \ . \tag{1.115}$$

So, for large enough n, we can find the limit of this quantity and then the value of δ_l modulo π with the desired precision.

Although this numerical scheme is independent of the normalization $A_l(k)$, it is sensitive to the automatic step-size selection, as shown in Appendix A (see also R. Côté and M.J. Jamieson [20]). Therefore special care has to be taken to insure a good numerical result. On the other hand, it can be shown that the integral expression is more stable under automatic step-size selection (Appendix A), but then one has to

be careful about the normalization. We present results of both methods in Appendix A, together with an expression from the Schwinger variational method [see §1.5.3].

Let us now look at the behaviour of δ_l at low energies, *i.e.* for $k \to 0$. If the potential has a "range" a and if we take $d \gtrsim a$, it can be shown using Eq. (1.112) and the behaviour of the spherical Bessel and Neumann functions for $kd \ll 1$ that [19]

$$\tan \delta_l \to \frac{(kd)^{2l+1}}{D_l} \frac{l - \hat{\gamma}_l d}{l + 1 + \hat{\gamma}_l d} , \tag{1.116}$$

where the quantities D_l and $\hat{\gamma}_l$ are defined by

$$\begin{aligned} D_l &= (2l+1)!!(2l-1)!! \quad , \quad l > 0 , \\ D_0 &= 1 , \\ \hat{\gamma}_l &= \lim_{k \to 0} \gamma_l(k) . \end{aligned} \tag{1.117}$$

For the moment, we assume that $\hat{\gamma}_l d \neq -(l+1)$. We then conclude that $\tan \delta_l$ tends to zero (modulo π) as k^{2l+1}. The partial wave amplitude $a_l(k)$ [see Eq. (1.77)] exhibits the low energy behaviour

$$a_l(k) \to \bar{c}_l k^{2l} , \tag{1.118}$$

where $\bar{c}_l$ are real numbers. Except for the s-wave ($l = 0$) contribution, all partial cross sections σ_l ($l \geq 1$) vanish as k^{4l}. The cross section is then isotropic at low energies and given by $\sigma_{tot} = \sigma_0$. Defining the *scattering length* α by

$$\alpha = - \lim_{k \to 0} \frac{\tan \delta_0(k)}{k} , \tag{1.119}$$

we then have

$$f \to -\alpha \quad , \quad \frac{d\sigma}{d\Omega} \to \alpha^2 \ \text{ and } \ \sigma_{tot} \to 4\pi\alpha^2 . \tag{1.120}$$

If by accident

$$\hat{\gamma}_l d = -(l+1) \ , \tag{1.121}$$

the above conclusions are modified depending of the value of l. If $l > 0$, we get the following behaviour

$$a_l(k) \to \bar{d}_l k^{2l-2} \quad , \quad l > 0 \ , \tag{1.122}$$

where $\bar{d}_l$ are real numbers. Then, if $l = 1$, the scattering amplitude takes the form

$$f \to -\alpha + \beta \cos\theta \ , \tag{1.123}$$

where α is the scattering length and β a constant. Hence the differential cross section is never isotropic in this case. If $l \geq 2$ we see that Eq. (1.122) implies that the results in (1.120) are unchanged. For $l = 0$, one finds that the partial wave amplitudes and thus the scattering cross section are divergent [19]. Indeed, we then have

$$a_0(k) \to i/k \ \text{ and } \ \sigma_{tot} \to \infty \quad \text{as} \quad k^{-2}(\text{or } E^{-1}) \ . \tag{1.124}$$

This singular case is often called a *zero-energy resonance* and corresponds to the presence of a bound state at $E = 0$. We will come back to this topic in a later section.

We can also look at the behaviour of δ_l for large l. For a potential with a finite "range", one can show that if $l \gg kd$, we have the following relation

$$\tan\delta_l \to \frac{(kd)^{2l+1}}{D_l} \frac{l - \gamma_l(k)d}{l + 1 + \gamma_l(k)d} \ . \tag{1.125}$$

This expression may be used to analyse the convergence of the partial wave series. It also shows that the higher partial waves contribute less, *i.e.* that δ_l will tend to zero

as $l \to \infty$. We can also use the *first Born approximation* $B1$ of $\tan\delta_l$ to study the same regime. In fact, for $l \gg kd$, the radial wave function will differ by little from the free wave $s_l(kr)$. Hence, using the integral form for $\tan\delta_l$ we can write

$$\tan\delta_l \simeq (\tan\delta_l)_{B1} = -\frac{1}{k}\int_0^\infty dr\,[s_l(kr)]^2 U(r)\ . \tag{1.126}$$

If the potential has a strict finite range $d = a$, we can use the expansion for $s_l(kr)$ to write

$$\tan\delta_l \simeq -\frac{k^{2l-1}}{[(2l+1)!!]^2}\int_0^a dr\, r^{2l+2} U(r)\ . \tag{1.127}$$

Finally, we can also investigate the behaviour of δ_l for a fixed l when the energy tends to infinity ($k \to \infty$). Again, we expect that the potential will have a small effect on the wave function and that $u_l(r) \simeq s_l(kr)$. Thus using the Born approximation above, and with the help of the asymptotic expression for $s_l(kr)$

$$s_l(x) \to \sin(x - l\pi/2) \quad \text{as} \quad x \to \infty\ , \tag{1.128}$$

we deduce that

$$\tan\delta_l \to -\frac{1}{2k}\int_0^\infty dr\, U(r) + \mathcal{O}(k^{-2})\ . \tag{1.129}$$

Hence we seen that $\delta_l(k)$ tends to zero (modulo π) as $k \to \infty$. This suggests that a reasonable *absolute* definition of the phase shifts may be given by requiring that

$$\lim_{k\to\infty} \delta_l(k) = 0\ . \tag{1.130}$$

This is physically satisfactory, since we expect that the particle becomes basically free at high energies, and that we require $\delta_l(k) = 0$ for a free particle.

1.3 Resonances

In this section, we will focus our attention on the phenomenon known as *shape resonance*. Although the so-called *Feshbach resonances* are also of interest, we will not discuss them here. They require at least two coupled channels, and we will not treat such problem in this work.

1.3.1 Preliminaries

In general the phase shifts, and therefore the cross sections, are slowly varying functions of the incident energy and the strength of the potential. However, under certain circumstances it may happen that a phase shift $\delta_l(k)$ suffers a rapid variation for a given potential strength and in a certain energy interval. The corresponding partial wave amplitude a_l and cross section σ_l will then change dramatically in that energy range.

If we consider a finite ranged potential and suppose that it is attractive, then the *effective potential* given by

$$U_{\text{eff}}(r) = U(r) + \frac{l(l+1)}{r^2} \,, \tag{1.131}$$

might have an attractive well followed by a repulsive barrier at larger r (from the centrifugal contribution). If $l = 0$, then the barrier must come from the potential $U(r)$ itself. Now, within the attractive well, a particle can be trapped but not forever. In fact, such a trapped state has a finite lifetime due to quantum-mechanical tunneling. We call those states *quasi-bound states* because they would be real bound states if

the barrier would not disappear at larger distances.

According to our previous study of $\delta_l(k)$, the phase shift must go as k^{2l} when $k \to 0$, and $\delta_l(k) > 0$ for an attractive potential. So, the phase shift corresponding to the partial wave with a resonance will rise from zero through the value $\pi/2$ as the incident energy rises through that of the quasi-bound state, and at the same time the corresponding partial cross section σ_l will pass through its possible maximum value $4\pi(2l+1)/k^2$.

1.3.2 The Breit-Wigner formula

Let us see how the scattering amplitude varies in the vicinity of the resonance energy. If we are to have any connection between σ_l being large and the quasi-bound state, $\delta_l(k)$ must go through $\pi/2$ (or $3\pi/2, \ldots$) from below, as we just mentioned. In other words, $\cot\delta_l$ must go through zero from above. Assuming that $\cot\delta_l$ is smoothly varying near the resonance, that is

$$E \simeq E_R \ , \tag{1.132}$$

we may expand $\cot\delta_l$ as follows

$$\cot\delta_l = \cot\delta_l\Big|_{E=E_R} - c(E-E_R) + \mathcal{O}\left[(E-E_R)^2\right] \ , \tag{1.133}$$

where $\cot\delta_l|_{E=E_R} = 0$ and $c > 0$. Noting that we have

$$a_l(k) = \frac{1}{k}\exp(i\delta_l)\sin\delta_l = \frac{1}{k\cot\delta_l - ik} \ , \tag{1.134}$$

the previous expansion leads to

$$a_l(k) \ = \ \frac{1}{k\cot\delta_l - ik} = \frac{1}{k}\frac{1}{[-c(E-E_R)-i]} \ ,$$

$$= -\frac{\Gamma/2}{k\left[(E-E_R)-i\Gamma/2\right]} \quad \text{for} \quad E \simeq E_R \ , \tag{1.135}$$

where we have defined the *width* Γ by

$$\left.\frac{d(\cot\delta_l)}{dE}\right|_{E=E_R} = -c = -\frac{2}{\Gamma} \ . \tag{1.136}$$

If a simple resonance dominates the l^{th} partial wave cross section, we obtain a one level resonance formula, known as the *Breit-Wigner formula*

$$\sigma_l = \frac{4\pi}{k^2}\frac{(2l+1)(\Gamma/2)^2}{(E-E_R)^2+\Gamma^2/4} \ . \tag{1.137}$$

It has the characteristic *Lorentz shape*. So it is legitimate to regard Γ as the full width at half-maximum, provided the resonance is reasonably narrow so that the variation in $1/k^2$ can be ignored.

It is obvious from the above discussion that a pure Breit-Wigner resonance represents an idealization. In particular, the width Γ is not strictly constant. Moreover, we have neglected a "background" contribution which consists of the scattering contributed by other partial waves ($l' \neq l$) and the "hard sphere" scattering in the partial wave l. As can be shown in a more rigourous treatment of the problem [19], the phase shift can actually be expressed as a sum of two components with different physical interpretation

$$\delta_l = \xi_l + \rho_l \ . \tag{1.138}$$

The first term corresponds to the scattering of a "hard sphere" of range d,

$$\xi_l = \tan^{-1}\left(\frac{j_l(kd)}{n_l(kd)}\right) \ . \tag{1.139}$$

The definition of the second term is more complicated, but one can show that in the vicinity of the resonance it becomes

$$\rho_l \simeq \delta_l^r = \tan^{-1}\left(\frac{\Gamma}{2(E-E_R)}\right) . \tag{1.140}$$

If one includes this "hard sphere" component, the partial cross section becomes

$$\begin{aligned}\sigma_l &= \frac{4\pi(2l+1)}{k^2}\left[\sin^2\xi_l + \frac{\Gamma^2}{4(E-E_R)^2+\Gamma^2}\right. \\ &\qquad \left. + 2\mathrm{Re}\left(\exp(i\xi_l)\sin\xi_l \frac{\Gamma}{2(E_R-E)+i\Gamma}\right)\right] . \end{aligned} \tag{1.141}$$

The first term accounts for pure hard sphere scattering, the second for a pure resonance contribution, and the third is an interference term. A more exhaustive treatment can be found in many textbooks.

1.3.3 Resonances and time delays

As we mentioned before, in the presence of a quasi-bound state, the particle almost gets trapped, and therefore we expect a time delay: the particle spends more time in the interaction region then in a "normal" case. In other words, near the resonance energy E_R the probability of finding the particle within the well becomes very large. From a time-dependent point of view, we should therefore expect that a resonance corresponds to a *metastable state*, whose lifetime τ is much longer than a typical collision time. Using Heisenberg's uncertainty relation $\Delta E \Delta t \simeq \hbar$, with $\Delta E \simeq \Gamma$ and $\Delta t \simeq \tau$, we have

$$\tau \simeq \hbar/\Gamma . \tag{1.142}$$

In a more general way, we have already shown that for a repulsive (positive) interaction potential, the radial wave function is "pushed out" in comparison with the free radial wave function and that δ_l is negative. On the contrary, for an attractive potential δ_l is positive and the radial wave function is "pulled in" with respect to the free case. Now, it is clear that "pushing-out" $u_l(r)$ corresponds to an *advance in time*, while the "pulling-in" induces a *retardation.* In the former case the scattered wave emerges from the scattering region *ahead* of the unscattered wave, while in the latter instance the scattered wave is *delayed* with respect to the free wave. We are interested only in the last case here.

Now, one can give a more accurate description of the time delay than the crude approximation above by using a time-dependent approach. From the expression (1.135) for the scattering amplitude $a_l(k)$ near the resonance, one can write

$$\begin{aligned} a_l(k) &= -\frac{\Gamma/2}{k\left[(E-E_R)+i\Gamma/2\right]}\ , \\ &= -\frac{1}{k}\frac{\Gamma/2}{\sqrt{(E-E_R)^2+(\Gamma/2)^2}}\exp(i\phi(E))\ , \end{aligned} \tag{1.143}$$

where

$$\phi(E) = \tan^{-1}\left[\frac{\Gamma/2}{E_R-E}\right]\ . \tag{1.144}$$

Then, it can be shown that the time delay is given by [19]

$$\Delta t = \hbar\frac{d}{dE}\phi(E) = \hbar\frac{\Gamma/2}{(E-E_R)^2+(\Gamma/2)^2}\ , \tag{1.145}$$

and that it reaches its maximum at $E = E_R$.

1.4 The Levinson theorem

The Levinson theorem makes a link between the phase shift and the number of bound states that a potential can support. Although its derivation is quite complex, it can be illustrated quite adequately by a simple example, namely the scattering by a square well. This example will also illustrate some of the properties of the scattering amplitude mentioned earlier.

1.4.1 The square well

We consider an attractive square well such that

$$U(r) = \begin{cases} -U_0, & r < a \\ 0, & r > a \end{cases} \tag{1.146}$$

where $U_0 > 0$. Defining $\kappa = \sqrt{k^2 + U_0}$, the radial equation (1.52) for $r < a$ becomes

$$\left[\frac{d^2}{dr^2} + \kappa^2 - \frac{l(l+1)}{r^2}\right] u_l(r) = 0 \ . \tag{1.147}$$

The interior radial wave function $R_l(r) = u_l(r)/r$ is given by the regular solution

$$R_l(r) = C_l j_l(\kappa r), \qquad r < a \ , \tag{1.148}$$

where C_l is independent of r. The exterior solution is simply

$$R_l(r) = j_l(kr) - n_l(kr) \tan \delta_l, \qquad r > a \ , \tag{1.149}$$

and by matching the logarithmic derivatives at $r = a$, $\tan \delta_l$ is given by Eq. (1.111)

$$\tan \delta_l = \frac{k j_l'(ka) - \gamma_l(k) j_l(ka)}{k n_l'(ka) - \gamma_l(k) n_l(ka)} \ , \tag{1.150}$$

with

$$\gamma_l(k) = \frac{\kappa j_l'(\kappa a)}{j_l(\kappa a)} \ . \tag{1.151}$$

Now, let us consider the s-wave scattering, *i.e.* $l = 0$. Using the fact that $j_0(x) = (\sin x)/x$ and $n_0(x) = -(\cos x)/x$, we deduce

$$\tan \delta_0 = \frac{k \tan(\kappa a) - \kappa \tan(ka)}{\kappa + k \tan(\kappa a) \tan(ka)} \ , \tag{1.152}$$

or

$$\delta_0 = -ka + \tan^{-1}\left[\frac{k}{\kappa} \tan(\kappa a)\right] \ . \tag{1.153}$$

Let us examine the behaviour of δ_0 at low energies ($ka \ll 1$). First we assume that the potential is weak, *i.e.* $U_0 a^2 \ll 1$. From the definition of κ we also have $\kappa a \ll 1$. Hence, if we require that $\delta_0 \to 0$ when $U_0 \to 0$ (according to the absolute definition of phase shift), we infer from Eq. (1.153) that $\delta_0 \to 0$ as $k \to 0$. For finite values of k such that ($ka \ll 1$) we have approximately

$$\delta_0 \simeq ka \left[\frac{\tan \kappa a}{\kappa a} - 1\right] \ . \tag{1.154}$$

We also note that the scattering length is given by

$$\alpha = \left[1 - \frac{\tan \lambda_0 a}{\lambda_0 a}\right] a \ , \tag{1.155}$$

with $\lambda_0 = \sqrt{U_0}$. Therefore, since $\lambda_0 a \ll 1$ for a weak interaction, α is negative while the s-wave cross section is finite and given by $\sigma_0 = 4\pi\alpha^2$.

While we remain at low energies, let us increase the coupling strength U_0 so that κa also becomes bigger. As κa increases from zero to $\pi/2$, δ_0 grows from zero to

about $\pi/2$. In particular, at zero energy, we have $\kappa a = \lambda_0 a$ and we find that when $\lambda_0 a = \pi/2$ (or $U_0 a^2 = \pi^2/4$) the zero-energy phase shift is given by

$$\lim_{k \to 0} \delta_0 = \frac{1}{2}\pi \ . \tag{1.156}$$

In this case the scattering length becomes infinite and the s-wave cross section σ_0 diverges like k^{-2} at $k = 0$: this is a "zero-energy resonance" described earlier.

This can be explained by looking at the bound states supported by the potential. In fact, one can show that for a square well, if the interaction is weak *i.e.* $\lambda_0 a < \pi/2$, the potential cannot support a bound state. We have seen that $\delta_0 \to 0$ as $k \to 0$ in this case. Now if

$$\frac{\pi}{2} < \lambda_0 a < \frac{3\pi}{2} \ , \tag{1.157}$$

then the potential supports just one bound state. The critical value $\lambda_0 a = \pi/2$ for which $\delta_0(k = 0) = \pi/2$ corresponds precisely to the transition between the two regimes.

Let us now assume that $\lambda_0 a$ satisfies the condition (1.157). In particular, if $\lambda_0 a$ is just above $\pi/2$, the phase shift δ_0 goes through $\pi/2$ as k decreases and one get

$$\lim_{k \to 0} \delta_0 = \pi \ , \tag{1.158}$$

and we can write

$$\delta_0 \simeq \pi - ka \left[1 - \frac{\tan \kappa a}{\kappa a}\right] \ . \tag{1.159}$$

By repeating the arguments made above, it is possible to show if the potential

can support n bound states, then the zero-energy s-wave phase shift is such that

$$\lim_{k\to 0} \delta_0 = n\pi \ . \tag{1.160}$$

Moreover, when $\lambda_0 a = (2n+1)\pi/2$ so that the potential is about to support its $(n+1)^{th}$ bound s-state, we have

$$\lim_{k\to 0} \delta_0 = (n+1/2)\pi \ . \tag{1.161}$$

Those results are in fact true for more general potentials than the square well. They are an example of the *Levinson theorem.* Notice finally that if $l > 0$ one can show in the case of the square well that

$$\lim_{k\to 0} \delta_l = n_l\pi \ , \tag{1.162}$$

and that the anomalous behaviour cannot occur.

1.4.2 General potentials

We will give here a summary of the proof of the Levinson theorem, since it requires the knowledge of the analytical properties of the Jost functions.

It can be shown that the number of bound states supported by a potential is given by [19]

$$n_l = \frac{1}{2\pi i} \oint_C d\log\left[\mathcal{J}_l(-k)\right] \ , \tag{1.163}$$

where $\mathcal{J}$ is known as the Jost function. It is related to the S-matrix through

$$S_l(k) \equiv \exp[2i\delta_l(k)] = \frac{\mathcal{J}_l(k)}{\mathcal{J}_l(-k)} \ . \tag{1.164}$$

Then using the fact that $\delta_l(\infty) = 0$ we obtain the following results

$$\delta_0(0) = \begin{cases} (n_0 + 1/2)\pi & \text{if} \quad \mathcal{J}_0(0) = 0 \\ n_0\pi & \text{if} \quad \mathcal{J}_0(0) \neq 0 \end{cases} . \tag{1.165}$$

Here, the case $\mathcal{J}_0(0) = 0$ corresponds to the appearance of a bound state a zero-energy.

For $l \geq 1$, one obtains

$$\delta_l(0) = n_l\pi \ , \tag{1.166}$$

where n_l denotes the total number of bound states in the partial wave l, including the zero-energy if it exits.

1.5 The effective range expansion

In this section, we want to complete our analysis of potential scattering at low energies. We will outline the derivation of the so-called effective range expansion, *i.e.* that the quantity $k^{2l+1} \cot \delta_l(k)$ may be expanded for small k as a power series in k^2. The complete proof can be found in Goldberger and Watson [21] for example.

1.5.1 Derivation

From the definition of the scattering amplitude and the S-matrix for the partial wave l, we can write

$$a_l^{-1}(k) = \frac{2ik}{S_l(k) - 1} = k \cot \delta_l(k) - ik = 2ik \frac{\mathcal{J}_l(-k)}{\mathcal{J}_l(k) - \mathcal{J}_l(-k)} \ , \tag{1.167}$$

where we used the relation between $S_l(k)$ and the Jost function $\mathcal{J}_l(k)$ given before. Imposing the following condition on the potential

$$\int_0^\infty dr\, e^{\mu r}|U(r)| < \infty \ , \tag{1.168}$$

i.e. that the potential is a short range potential, one has that the Jost function $\mathcal{J}_l(k)$ is analytic for $\mathrm{Im}(k) < \mu/2$ and $a_l(k)$ may be continued off the real axis into the complex k-plane [21].

Then using the analytical properties of $\mathcal{J}_l(k)$, one obtains the expansion

$$k^{2l+1}\cot\delta_l(k) = c_0 + c_1k^2 + c_2k^4 + \cdots \tag{1.169}$$

for $|E| < \hbar^2\mu^2/8m$, provided that there is no zero-energy resonance, *i.e.* $\mathcal{J}_l(0) \neq 0$, and that the potential satisfies the condition (1.168).

1.5.2 Determination of the coefficients

Let us now determine the first coefficients of the expansion (1.169). We start from the radial equation

$$\left[\frac{d^2}{dr^2} + k^2 - \frac{l(l+1)}{r^2} - U(r)\right] u_l(k,r) = 0 \ , \tag{1.170}$$

and shall only analyze in detail the s-wave case ($l = 0$). For the zero-energy wave function, we write

$$u^0(r) \equiv \lim_{k\to 0} u_0(k,r) \ , \tag{1.171}$$

which satisfies the following equation

$$\left[\frac{d^2}{dr^2} - U(r)\right] u^0(r) = 0 \ . \tag{1.172}$$

In the region $r \gg a$, where the potential can be neglected, we have

$$\frac{d^2}{dr^2} u^0(r) \simeq 0 \ , \tag{1.173}$$

and therefore

$$u^0(r) \simeq Br + C \qquad , \qquad r \gg a \ . \tag{1.174}$$

On the other hand, from Eq. (1.61) we deduce that

$$u^0(r) \simeq A[r - \alpha] \qquad \text{where} \qquad \alpha = -\lim_{k \to 0} \frac{\tan \delta_0(k)}{k} \ . \tag{1.175}$$

Returning to the expansion (1.169), we note from the above definition of the scattering length α that

$$\lim_{k \to 0} k \cot \delta_0(k) = -\frac{1}{\alpha} \ , \tag{1.176}$$

so that the first coefficient c_0 is given (for $l = 0$) by $c_0 = -\alpha^{-1}$.

To determine the second coefficient (again for $l = 0$), we consider the same radial equation at two different energies

$$E_1 = \frac{\hbar^2 k_1^2}{2m} \qquad \text{and} \qquad E_2 = \frac{\hbar^2 k_2^2}{2m} \ , \tag{1.177}$$

and we define

$$u^1(r) \equiv u_0(k_1, r) \qquad \text{and} \qquad u^2(r) \equiv u_0(k_2, r) \ . \tag{1.178}$$

Hence

$$\left[\frac{d^2}{dr^2} + k_1^2 - U(r)\right] u^1(r) = 0 \qquad \text{and} \qquad \left[\frac{d^2}{dr^2} + k_2^2 - U(r)\right] u^2(r) = 0 \ . \tag{1.179}$$

If we multiply the first equation by $u^2(r)$ and the second by $u^1(r)$ and substract, we get

$$\frac{d}{dr}(u^1u^{2\prime} - u^2u^{1\prime}) = (k_1^2 - k_2^2)u^1u^2 \ , \tag{1.180}$$

where the prime denotes differentiation with respect to r. Let us define two function v^1 and v^2, solutions of the radial equation without the potential,

$$\left[\frac{d^2}{dr^2} + k_1^2\right] v^1(r) = 0 \qquad \text{and} \qquad \left[\frac{d^2}{dr^2} + k_2^2\right] v^2(r) = 0 \ , \tag{1.181}$$

so that one has

$$\lim_{r\to\infty} u^i(r) = v^i(r) \ . \tag{1.182}$$

Then we obtain the relation

$$\frac{d}{dr}(v^1v^{2\prime} - v^2v^{1\prime}) = (k_1^2 - k_2^2)v^1v^2 \ . \tag{1.183}$$

Substracting (1.183) from (1.180) and integrating on r from 0 to ∞, we obtain

$$\left[u^1u^{2\prime} - u^2u^{1\prime} - v^1v^{2\prime} + v^2v^{1\prime}\right]_0^\infty = (k_1^2 - k_2^2)\int_0^\infty dr\,(u^1u^2 - v^1v^2) \ . \tag{1.184}$$

Now, let us choose our "normalization" such that $v^i(0) = 1$ $(i = 1, 2)$, *i.e.*

$$v^i(r) = \frac{\sin(k_ir + \delta_0)}{\sin\delta_0} \ . \tag{1.185}$$

So, taking into account this normalization and the boundary conditions, we have

$$k_1\cot\delta_0(k_1) - k_2\cot\delta_0(k_2) = (k_1^2 - k_2^2)\int_0^\infty dr\,(v^1v^2 - u^1u^2) \ , \tag{1.186}$$

and for the particular case $k_1 = k$ and $k_2 \to 0$, this equation becomes

$$k\cot\delta_0(k) = -\frac{1}{\alpha} + k^2\int_0^\infty dr\,(v^kv^0 - u^ku^0) \ , \tag{1.187}$$

with $v^k \equiv v^1$, $u^k \equiv u^1$ for $k_1 = k$, and

$$v^0(r) = 1 - \frac{r}{\alpha} \ . \tag{1.188}$$

If we define the quantity

$$b(k) = 2\int_0^\infty dr \left(v^k v^0 - u^k u^0\right) \ , \tag{1.189}$$

we may rewrite our expression as

$$k \cot \delta_0(k) = -\frac{1}{\alpha} + \frac{1}{2} b(k) k^2 \ , \tag{1.190}$$

which is known as the *Bethe formula.* As we will explore later, the potential must tend to zero fast enough so that the integral exist.

If we take the limit $k \to 0$, we finally can write

$$k \cot \delta_0(k) = -\frac{1}{\alpha} + \frac{1}{2} r_e k^2 + \cdots \ , \tag{1.191}$$

where the *effective range* r_e is defined by

$$r_e = 2\int_0^\infty dr \left[(v^0)^2 - (u^0)^2\right] \ . \tag{1.192}$$

The factor of two in front of the integral has been chosen in such a way that for a square well potential of range a one has $r_e = a$.

1.5.3 Schwinger variational principle

Using the integral formulation of $\tan \delta_l$, one can express $k \cot \delta_l(k)$ in a variational formulation. To be more precise, one gets the *Schwinger variational expression*

$$k \cot \delta_l(k) = \frac{\displaystyle\int_0^\infty dr \int_0^\infty dr' u_l(r) U(r) G_l(r,r') U(r') u_l(r') r r' - \int_0^\infty dr U(r) u_l^2(r)}{\left[\displaystyle\int_0^\infty dr j_l(kr) U(r) u_l(r) r\right]^2} \ , \tag{1.193}$$

where $G_l(r,r') = kj_l(kr_<)n_l(kr_>)$ with $r_<$ standing for the smaller one of r and r', and $r_>$ for the larger one of r and r'. One can consider the wave function $u_l(r)$ as a trial function and treat the whole problem as a variational one.

Now, looking at the $l = 0$ case only, and taking $u^0(r)$ defined by Eq. (1.171) as a trial function, one gets (see Blatt and Jackson [22]) the same two first terms in the expansion. Following Blatt and Jackson, we can get the third one ($\mathcal{V}_e k^4$) by taking a trial function with a k dependence as

$$u_0(k,r) = u^0(r) + k^2 v(r) + \mathcal{O}(k^3) \ . \tag{1.194}$$

Noting that we can rewrite $u^0(r)$ in terms of its asymptotic form together with another function, *i.e.*

$$u^0(r) \equiv 1 - r/\alpha - g(r) \qquad \text{for all} \qquad r \ , \tag{1.195}$$

where $g(0) = 1$ and $g(\infty) \to 0$ so that $u^0(r)$ satisfies the right boundary conditions. We can then define a new function $w(r)$ as

$$w(r) \equiv g(r) + U(r)v(r) \ , \tag{1.196}$$

in terms of which the third coefficient of Eq. (1.169) becomes [22]

$$\begin{aligned} \mathcal{V}_e \ = \ & \int_0^\infty \int_0^\infty dr dr' w(r) r_< w(r') + \int_0^\infty dr\, U(r) v^2(r) - \int_0^\infty dr\, r(r_e - r) w(r) \\ & - \frac{1}{3\alpha} \int_0^\infty dr\, r^3 w(r) - \frac{1}{\alpha} \left[\int_0^\infty dr\, r w(r) \right]^2 \ . \end{aligned} \tag{1.197}$$

Substituting $u_0(k,r)$ into the differential equation, one gets to first order in k^2 the differential equation for $v(r)$, namely

$$\left[\frac{d^2}{dr^2} - U(r) \right] v(r) = -u^0(r) \ , \tag{1.198}$$

with the boundary condition $v(0) = 0$. So, one can show that $v(r)$ takes the form

$$v(r) \simeq \frac{1}{2} r(r_e - r) + \frac{1}{6\alpha} r^3 + \frac{r}{\alpha} \int_0^\infty dr'\, r' g(r') - \int_0^\infty dr'\, r_< g(r') \ , \tag{1.199}$$

and the *effective volume* $\mathcal{V}_e$ can be expressed as

$$\mathcal{V}_e = \int_0^\infty dr \left\{ \left[\frac{G}{\alpha} - \frac{r}{2}(r_e - r) - \frac{r^3}{6\alpha} \right] w(r) - v(r) g(r) \right\} - \frac{1}{\alpha} \left[\int_0^\infty dr\, r w(r) \right]^2 \ , \tag{1.200}$$

where

$$G \equiv \int_0^\infty dr\, r g(r) \ . \tag{1.201}$$

As one can easily see, this parameter is well-defined for a potential that tends to zero faster than r^{-7}, *i.e.* a rather short range potential. The expansion then takes the form

$$k \cot \delta_0 = -\frac{1}{\alpha} + \frac{1}{2} r_e k^2 - \mathcal{V}_e k^4 + \cdots \ . \tag{1.202}$$

In the next section, we will give the range of validity of the effective range expansion, together with alternate expansions valid for different potentials.

1.5.4 Form of the expansion and the potentials

As mentioned earlier, the derivation of the effective range expansion is highly dependent on the long-range form of the potential. In fact, the expression (1.169) if valid only for short range potentials that fall to zero exponentially at large distances.

For a potential decreasing like r^{-n}, we obtain very different expansions. For example, if $n < 3$, the scattering length is not well-defined. Moreover, one can show

(see O'Malley, Spruch and Rosenberg [23]) the following behaviours:

$$\left.\begin{aligned} k^{2l+1}\cot\delta_l &\rightarrow -\frac{1}{\alpha \ln k} \quad \text{for} \quad n = 2l+3 \\ k^{2l+1}\cot\delta_l &\rightarrow -\frac{1}{\alpha} \qquad \text{for} \quad n > 2l+3 \end{aligned}\right\} . \tag{1.203}$$

At low kinetic energy, we are interested mostly in the s-wave ($l = 0$) case. It can be shown that the effective range defined by the integral form (1.192) is well defined for $n > 5$, *i.e.* it does not exist for $n = 4$ or 5. Even more, the effective volume $\mathcal{V}_e$ is defined for $n > 7$, as we mentioned before.

In the case of atomic collisions, the most important type of potentials are of the form r^{-3}, r^{-4}, r^{-6}, or r^{-7}. The first one occurs in interactions with excited molecules (or walls), and the expansion is given by (1.203) with $l = 0$. The second one corresponds to a *polarization potential* (see §2.1) which occurs in the scattering of a charged particle of charge Q with a neutral atom of polarizability $\overline{\alpha}$

$$V(r) = -\frac{\overline{\alpha}Q^2}{2\left(r^2+d^2\right)^2} . \tag{1.204}$$

Here d is a parameter having the dimension of length. For large r, this potential behaves like r^{-4} and the expansion takes the form

$$\begin{aligned} k\cot\delta_0 \;=\; & -\frac{1}{\alpha} + \frac{\pi P^2}{3\alpha^2}k + \frac{4P^2}{3\alpha}k^2 \ln\left(\frac{Pk}{4}\right) + \left[\frac{1}{2}r_{0p} + \frac{\pi P}{3} + \frac{20P^2}{9\alpha}\right. \\ & \left. - \frac{8\alpha}{3\alpha}\psi(3/2) - \frac{\pi P^2}{3\alpha^2} - \frac{\pi^2 P^4}{9\alpha^3}\right] k^2 + \cdots , \end{aligned} \tag{1.205}$$

where $P^2 = \overline{\alpha}mQ^2/\hbar^2$, $\psi(3/2) = \Gamma'(\frac{3}{2})/\Gamma(\frac{3}{2}) = 0.0365$ and r_{0p} is given by

$$r_{0p} = 2\int_0^\infty dr \left(v_{0p}^2 - [u^{(0)}]^2\right) , \tag{1.206}$$

with v_{0p} defined as

$$v_{0p} = j_l(P/r) - B_0 n_l(P/r), \qquad \text{with} \qquad l = 0 \ , \tag{1.207}$$

where B_0 is the relative amplitude of the two independent Mathieu solution of the differential equation (see O'Malley, Spruch and Rosenberg [23]).

For the scattering of two neutral atoms with no permanent electric multipoles, the potential has dispersion terms only and behaves like r^{-6} at large distances

$$V(r) = -\frac{C_6}{r^6} \ , \tag{1.208}$$

in which case the expansion takes the form (see Hinckelmann and Spruch [24])

$$k \cot \delta_0 = -\frac{1}{\alpha} + \frac{1}{2} r_e k^2 - \frac{2\pi}{15\alpha^2} \frac{\mu C_6}{\hbar^2} k^3 - \frac{8}{15\alpha} \frac{\mu C_6}{\hbar^2} k^4 \ln k + \mathcal{O}(k^4) \ . \tag{1.209}$$

Finally, when the distance becomes very large, the vacuum fluctuations change the r^{-6} dependence to a r^{-7} dependence for atoms in their ground state, in which case our previous expansion is modified as

$$k \cot \delta_0 = -\frac{1}{\alpha} + \frac{1}{2} r_e k^2 + \frac{4}{15\alpha^2} \frac{\mu C_7}{\hbar^2} k^4 \ln k + \mathcal{O}(k^4) \ . \tag{1.210}$$

As we can see, the power law of the long-range potential has an important effect on the scattering at very low energies (see also M.J. Jamieson, A. Dalgarno, and M. Kimura [25]).

1.5.5 Link with bound states

The effective range expansion also permits one to establish a relationship between the effective range and scattering length and the $l = 0$ bound states, if they exist.

Indeed, following Blatt and Jackson [22], one can show that we have a bound state if and only if the scattering matrix $S = \exp(2i\delta)$ vanishes when $k = -i\nu$. We therefore obtain the condition for the energy $E = -\hbar^2\nu^2/2m$ of a bound state

$$S(-i\nu) = 0 \qquad , \qquad \nu > 0 \ . \tag{1.211}$$

From the definition of S, this condition can be rewritten as

$$\cot \delta_0 = -i \qquad \text{for} \qquad k = -i\nu \ . \tag{1.212}$$

Substituting in the effective expansion (and assuming that the first two terms of the expansion exist), one gets

$$\nu \simeq \frac{1}{\alpha} + \frac{1}{2} r_e \nu^2 + \cdots \ , \tag{1.213}$$

which is valid for small binding energy ($\nu \to 0$) (Joachain [19]).

This can be used to find the last bound state if it is close to zero, as in the case of He-He [25]. Let us now have a look at how these various equations explain the results of the scattering of two lithium atoms and of two sodium atoms.

Chapter 2

Lithium and Sodium cases

In this chapter, we will use the different theoretical tools developed in the previous pages in order to calculate and explain the elastic and spin-change scattering of two lithium atoms and two sodium atoms in the ultralow temperature regime. First, we will explain how we generated the interaction potential curves needed for the calculations. Then, we will analyze the results obtained in the Li and Na cases, and for Na explore the changes due to the Casimir corrections. Finally, we will also examine the temperature dependence of the different quantities.

2.1 Interaction potentials

In this section, we will give some general features of molecular potentials, more precisely of diatomic molecules. We will then explain briefly how those potentials are obtained and give the prescription we followed in order to construct the ones used in the present work. We finally will show how to extrapolate the theoretical (or experimental) data points with analytical continuation to smaller and larger internu-

clear distances r. A general discussion of the molecular classification is presented in Appendix B.

2.1.1 General features of molecular potentials

We will focus our attention on the ground state of molecules, although most of what we will say is applicable to excited states as well. The intermolecular forces are electromagnetic by nature, so that the sources of the interaction can be seen to be due to the charged particles, electrons and protons, which make up the atoms and molecules.

The intermolecular forces are repulsive at short distances and (usually) attractive at large distances. For neutral molecules, the best known empirical intermolecular potential function exhibitting those properties is certainly the Lennard-Jones (6-12) potential, which can be written as

$$V(r) = \frac{a}{r^{12}} - \frac{b}{r^6} , \tag{2.1}$$

where the choice of 12 for the repulsive power is primary one of mathematical convenience. Many other models exist, but we will not use any one of them in this work.

The short-range repulsive forces are easy to explain: when the electron clouds of two molecules (or atoms) approach each other sufficiently closely that they overlap, the Pauli exclusion principle prohibits some electrons from occupying the overlap region and so reduces the electron density in this region. The positively charged

nuclei of the molecules are thus incompletely shielded from each other and therefore exert a repulsive force on each other (see Maitland *et al.* [26]). Such short-range forces are referred to as overlap forces and vary exponentially with the separation (see Hirschfelder *et al.* [17]). The true form of the potential is complicated and depends on the specific type of interaction being considered. It is customary in a number of applications to approximate the short-range contribution by the oversimplified form

$$V_{S-R}(r) = be^{-a(r/a_0)} \ , \tag{2.2}$$

in which a and b are constants. The constant a may be approximated by

$$a = \sqrt{\frac{2a_0}{e^2}} \left[\sqrt{E_I(1)} + \sqrt{E_I(2)}\right] \ , \tag{2.3}$$

in which $E_I(1)$ and $E_I(2)$ are the ionization potentials of the two molecules (or atoms), and a_0 and e are the Bohr radius and the electron charge respectively.

The various contributions to the (attractive) long-range forces vary inversely as powers of the intermolecular separation. It is convenient to divide those contributions into three physically different parts: the *electrostatic contributions*, the *induction contributions*, and the *dispersion contributions.* The first two types can be explained by straightforward electrostatic considerations, and the third (dispersion) by means of quantum mechanics. Finally, for two identical particles (atoms or molecules), one has a supplementary interaction called the *exchange term.* Let us examine each of them in more details.

A. Electrostatic contributions

The electrostatic contributions to the intermolecular potential energy result from

the interactions of the various multipole moments in the molecules: charges (q), dipole moments (μ), quadrupole moments (Q), etc. For the purpose of indicating the analytical form of the various types of electrostatic interactions, we use the variables defined in Fig. 2.1. A direct application of electrostatic laws gives the following formulae for the various types of interaction between molecules a and b:

$$V_{ab}^{q,q} = +\frac{q_a q_b}{r} , \tag{2.4}$$

$$V_{ab}^{q,\mu} = -\frac{q_a \mu_b}{r^2} \cos\theta_b , \tag{2.5}$$

$$V_{ab}^{q,Q} = +\frac{q_a Q_b}{4r^3}(3\cos^2\theta_b - 1) , \tag{2.6}$$

$$V_{ab}^{\mu,\mu} = -\frac{\mu_a \mu_b}{r^3}[2\cos\theta_a \cos\theta_b - \sin\theta_a \sin\theta_b \cos(\phi_a - \phi_b)] , \tag{2.7}$$

$$V_{ab}^{\mu,Q} = +\frac{3\mu_a Q_b}{4r^4}\left[\cos\theta_a(3\cos^2\theta_b - 1) - 2\sin\theta_a \sin\theta_b \cos\theta_b \cos(\phi_a - \phi_b)\right] , \tag{2.8}$$

$$V_{ab}^{Q,Q} = +\frac{3Q_a Q_b}{16r^5}\Big[1 - 5\cos^2\theta_a - 5\cos^2\theta_b - 15\cos^2\theta_a \cos^2\theta_b + 2\{\sin\theta_a \sin\theta_b \cos(\phi_a - \phi_b) - 4\cos\theta_a \cos\theta_b\}^2\Big] . \tag{2.9}$$

The angular dependence of the above expressions is somewhat complicated. We can average this angular dependence by taking into account that different orientations are equivalent to different energies. Thus, one can take a Boltzmann weighting factor and obtain (see Hirschfelder *et al.* [17])

$$\left.\begin{aligned}
\langle V_{ab}^{q,q}\rangle_T &= +\frac{q_a q_b}{r} , & \langle V_{ab}^{\mu,\mu}\rangle_T &= -\frac{2}{3k_B T}\frac{\mu_a^2 \mu_b^2}{r^6} , \\
\langle V_{ab}^{q,\mu}\rangle_T &= -\frac{1}{3k_B T}\frac{q_a^2 \mu_b^2}{r^4} , & \langle V_{ab}^{\mu,Q}\rangle_T &= -\frac{1}{k_B T}\frac{\mu_a^2 Q_b^2}{r^8} , \\
\langle V_{ab}^{q,Q}\rangle_T &= -\frac{1}{20k_B T}\frac{q_a^2 Q_b^2}{r^6} , & \langle V_{ab}^{Q,Q}\rangle_T &= -\frac{7}{40k_B T}\frac{Q_a^2 Q_b^2}{r^{10}} ,
\end{aligned}\right\} \tag{2.10}$$

where k_B is the Boltzmann constant and T the temperature. It should be noted that these averaged potential functions are dependent on the temperature, except $\langle V_{ab}^{q,q}\rangle_T$.

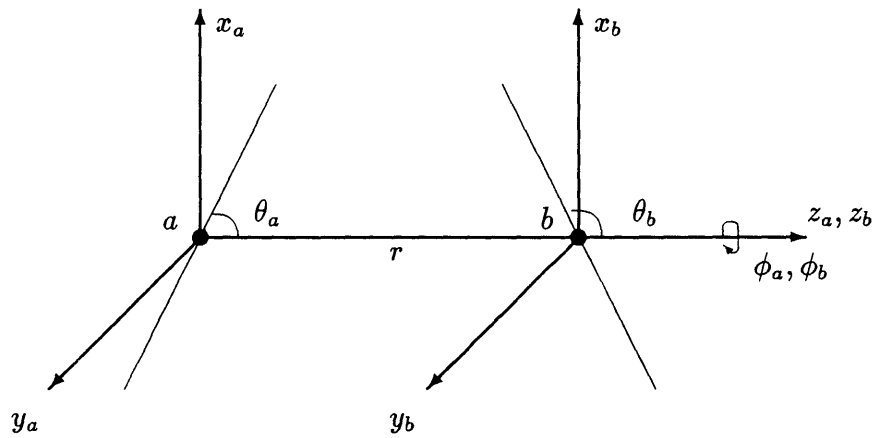

Figure 2.1: Definition of the electrostatic interaction coordinates.

B. Induction contributions

When a charged particle a interacts with a neutral molecule b, it induces in the neutral molecule a dipole moment. If the polarizability of the molecule b is α_b, the dipole moment induced in b is $q_a\alpha_b/r^2$, and the energy of interaction is

$$V_{ab}^{q,\mathrm{ind}\mu} = -\frac{q_a^2\alpha_b}{2r^4} \,. \tag{2.11}$$

Similarly, it can be shown that a permanent dipole moment would induce a dipole moment in the neutral molecule and give an interaction energy of

$$V_{ab}^{\mu,\mathrm{ind}\mu} = -\frac{\mu_a^2\alpha_b(3\cos^2\theta_a + 1)}{2r^6} \,. \tag{2.12}$$

We can average as before to get

$$\langle V_{ab}^{q,ind\mu}\rangle_T = -\frac{q_a^2\alpha_b}{2r^4} \,, \tag{2.13}$$

$$\tag{2.14}$$

$$\langle V_{ab}^{\mu,ind\mu}\rangle_T = -\frac{\mu_a^2\alpha_b}{r^6} \,. \tag{2.15}$$

C. Dispersion contributions

If we consider the interaction of two neutral molecules neither of which has a permanent dipole moment, the source of an attractive energy is more difficult to discern. Although a molecule may possess no permanent dipole moment, its electrons are in a continuous motion so that the electron density in a molecule oscillates continuously in space and time. Thus at any instant any molecule possesses an instantaneous electric dipole which fluctuates as the electron density fluctuates. This instantaneous dipole in one molecule induces an instantaneous dipole in the second molecule. The induced dipole in the second molecule and the inducing dipole in the first interact to produce an attractive energy called *dispersion energy*. In other words, the dispersion energy is a result of the correlations between the density fluctuations in the two molecules. London developed this notion on a quantum mechanical basis and found this interaction to be given approximately by

$$V^{\text{disp},6} = -\frac{3}{2}\left(\frac{h\nu_a h\nu_b}{h\nu_a + h\nu_b}\right)\frac{\alpha_a \alpha_b}{r^6}\,, \tag{2.16}$$

in which $h\nu_a$ and $h\nu_b$ are characteristic energies of the two molecules approximately equal to their ionization potentials. It may be shown that there are further terms in the dispersion energy varying as r^{-8} (induced-dipole–induced-quadrupole), r^{-10} (induced-quadrupole–induced-quadrupole and induced-dipole–induced-octupole), etc.

D. Exchange terms

In the case where the two particles A and B located at positions 1 and 2 are identical, one can form a symmetric and an antisymmetric wave function to represent

the full system

$$\Psi_+ = A(1)B(2) + A(2)B(1) \qquad \text{and} \qquad \Psi_- = A(1)B(2) - A(2)B(1)\ . \tag{2.17}$$

At very large distances, the overlap of the electron clouds for those two configurations will give an exponentially decaying energy contribution to the long-range potential, with opposite signs according to the configuration

$$V_{exc} = \mp A r^a \exp(-br)\ , \tag{2.18}$$

where the signs are for $\Psi_\pm$ respectively. This form will be discussed in §2.1.3 C.

2.1.2 Experimental and theoretical data available

According to the Born-Oppenheimer approximation, the interaction potential curves are obtained by averaging out the motion of the electrons around the nuclei for a particular internuclear distance r. This problem in itself is quite difficult to solve. If someone starts from first principles, *i.e.* from the Hamiltonian and use a quantum mechanical treatment, one finds the *ab initio* values of the potential $V(r)$ at given distance r.

Another possible procedure, called the *Rydberg-Klein-Rees* (RKR) method, is based on spectroscopic measurement of diatomic molecules. This technique gives a pair of turning points for each vibrational level of the molecule observed experimentally. From these points and the value of the energy, one can construct a function representing the potential $V(r)$ in the interval for which the experimental data are available.

We used both types of data (*ab ibitio* and RKR) to construct our potential-energy curves. Let us summarize the procedure adopted (see also Côté, Dalgarno and Jamieson [11] for Li and Côté and Dalgarno [27] for Na).

For the lithium case, there are two potential curves in the ground state, depending on the electronic configuration, namely a singlet state ($X^1\Sigma_g^+$) and a triplet state ($a^3\Sigma_u^+$). For the singlet state, we followed broadly the recommendations of Zemke and Stwalley [28], though with some modifications. Barakat *et al.* [29] have constructed an empirical RKR potential-energy curve for the $X^1\Sigma_g^+$ state at internuclear distances between $3.4a_0$ and $23.9a_0$. (There are two misprints in the data: in their Table 4, $R_2(v = 25)$ should read 4.890 860, not 4.490 860, and $R_2(v = 31)$ should read 5.680 896, not 5.580 896.) We extended the data of Barakat *et al.* by using *ab initio* values calculated by Konowalow and Olson [30] at $2.75a_0$ and $3.00a_0$, and a value of Schmidt-Mink, Müller, and Meyer [31] at $3.75a_0$. We list these data in Table 2.1

The experimental data on the triplet state ($a^3\Sigma_u^+$) for lithium are available over a less extensive range. We used the RKR values of Linton *et al.* [32] between $6.4a_0$ and $15.7a_0$ and we added theoretical values at $3.00a_0$ from Konowalow, Regan, and Rosenkrantz [33] and between $3.25a_0$ and $6.00a_0$ from Schmidt-Mink, Müller, and Meyer [31]. All the data used are also listed in Table 2.1.

The interaction potentials of two sodium atoms have been discussed by Zemke and Stwalley [34]. They have constructed an empirical RKR potential curve for the $X^1\Sigma_g^+$ state using the spectroscopic constants of Babaky and Hussein [35] for vibrational levels between 0 and 44, and those of Barrow *et al.* [36] for $45 \leq v \leq 62$.

$X^1\Sigma_g^+$			$a^3\Sigma_u^+$		
r (a_0)	E (hartree)	Ref.	r (a_0)	E (hartree)	Ref.
2.75	0.061866	a	3.00	0.104471	a
3.00	0.036411				
			3.25	0.082074	
3.25	0.013546	b	3.50	0.063725	
			4.00	0.036778	
			4.50	0.020006	b
1.823 201 Å			5.00	0.010053	
...	RKR (cm^{-1})	c	5.50	0.004370	
12.639 382 Å			6.00	0.001258	
			3.3792 Å		
			...	RKR (cm^{-1})	d
			8.2978 Å		

a : Konowalow and Olson [30]
b : Schmidt-Mink *et al.* [31]
c : Barakat *et al.* [29]
d : Linton *et al.* [32]

Table 2.1: Data points for the ^{7}Li potentials (in atomic units, unless indicated otherwise).

We extended the Zemke and Stwalley RKR curve with Babaky and Hussein data for $v = -0.5$ and $v = -0.25$ (see Table 3 in [35]). As noted by Zemke and Stwalley, we have to exclude the point at $r = 12.429048$ Å (see Table III in [34]). We then have a RKR energy curve ranging from $4.1a_0$ to $30.0a_0$. We completed the data for small distances by using a value from Konowalow *et al.* [37] at $3.8a_0$. Table 2.2 lists the data described above.

The experimental data on the $a^3\Sigma_u^+$ state of sodium cover a narrower range of r. We used the RKR values of Zemke and Stwalley [34] between $8.07a_0$ and $25a_0$, derived from the spectroscopic constants of Li *et al.* [38]. Here again, we exclude a data point at $r = 11.046804$ Å (see Table V in [34]). We extended this RKR curve in the short-range region with eleven points from Konowalow *et al.* ranging from $3.8a_0$ to $7.5a_0$ (see Table III in [37]). The data for the $a^3\Sigma_u^+$ state of sodium are also given in Table 2.2.

2.1.3 Construction of the potential curves

We can separate the domain of the internuclear distance r into three subregions with different functional behaviour: the short-range region, the medium-range region, and the long-range region. Let us examine these three domains in more detail.

A. Short-range

We consider distances that are smaller than the first data point available in this domain, *i.e.* $r < r_{min}$. The short-range repulsive interaction in atomic species is

$X^1\Sigma_g^+$			$a^3\Sigma_u^+$		
r (a_0)	E (hartree)	Ref.	r (a_0)	E (hartree)	Ref.
3.80	0.022410	a	3.80	0.0783293	
			4.00	0.0663480	
2.187393 Å	5886.0193 cm^{-1}		4.25	0.0539591	
...	...	b	4.50	0.0437298	
2.949398 Å	79.3409 cm^{-1}		4.75	0.0352223	
			5.00	0.0281544	a
2.9864098 Å	39.7003 cm^{-1}		5.50	0.0175203	
3.0795259 Å	0.0000 cm^{-1}	c	6.00	0.0104490	
3.1785334 Å	39.7003 cm^{-1}		6.50	0.0058723	
			7.00	0.0029853	
3.221463 Å			7.50	0.0012173	
...	RKR (cm^{-1})	b			
15.875317 Å			4.268684 Å		
			...	RKR (cm^{-1})	b
			13.229431 Å		

a : Konowalow *et al.* [37]
b : Zemke and Stwalley [34]
c : Babaky and Hussein [35]

Table 2.2: Data points for the ^{23}Na potentials (in atomic units, unless indicated otherwise).

related to the distance r between their nuclei when overlapping of electron shells of the particles take place. The resulting intermolecular forces are of an electrostatic and exchange nature, the interaction potential increasing sharply with decreasing distance between them. This allow one to use a simple approximation formula for the repulsive interaction potential of the particles with an exponential-type dependence

$$V(r) = A\exp(-Br) \qquad \text{for} \qquad r \leq r_{min} \ , \tag{2.19}$$

where the parameters A and B vary insignificantly within the range of internuclear distances considered (see Radzig and Smirnov [39]). Moreover, we choose those two constants in such a way that the potential curve and its first derivative are continuous at r_{min}. Thus

$$A = V(r)\exp(-Br)\Big|_{r_{min}} \qquad \text{and} \qquad B = -\frac{\partial}{\partial r}\ln V(r)\Big|_{r_{min}} \ , \tag{2.20}$$

where $\partial V/\partial r|_{r_{min}}$ is evaluated from the cubic spline fitting of the data points for $V(r)$ in the medium-range region (see next section). The different values for A, B and r_{min} for the lithium singlet and triplet, and for the sodium singlet and triplet states are given in Table 2.3.

B. Medium-range

For this region, we used the data described in the previous section, and interpolated it to find the potential as a function of r. More precisely, we selected a cubic spline fitting numerical scheme, which is appropriate for data where the curvature change sign (as is the case here).

One has to be careful with the data. In fact, for each potential curve, we basi-

cally have two sets of data: the *ab initio* points (in a.u.), and the RKR points, in spectroscopic units (*i.e.* in Å and cm^{-1}). So, we have to convert all of the RKR points into atomic units, and therefore the knowledge of the dissociation energy is of first importance. Instead of taking the value published by different authors, we calculate it by requiring that the last RKR point that we take has to coincide with the theoretical value from the long-range region. We will see the explicit form of the long-range region in the next section. Thus, since the RKR data have the minimum of the well at 0 cm^{-1} (usually), we must have

$$V_{RKR}(r_{max}) - D_e = V_{L-R}(r_{max}) \ , \tag{2.21}$$

where the RKR data (and the dissociation energy D_e) have been transformed into a.u. This gives us the D_e to be used for all the other RKR points, and we can then put all the available data (*i.e. ab initio* and RKR) in the same unit system and proceed with the cubic spline fitting. The different sets of data used for the spline fitting are given in Appendix C: they are in atomic units, and the dissociation energy has been subtracted. We also force the fitting to have a continuous derivative at the last point (r_{max}), where we use the analytical form of the long-range region to fix the derivative

$$\frac{\partial}{\partial r} V_{RKR}(r)\bigg|_{r_{max}} = \frac{\partial}{\partial r} V_{L-R}(r)\bigg|_{r_{max}} \ , \tag{2.22}$$

where once again the data are in the same unit system.

C. Long-range

The systems we consider here are made of identical particles, more precisely two neutral atoms without permanent electric multipoles. Thus, the long-range potential

will be made of a dispersion and an exchange term

$$V_{L-R}(r) = V_{\rm disp}(r) \pm V_{\rm exc}(r) \ . \tag{2.23}$$

More precisely, the states we are interested in are the ground states of the systems, for which there are two possible multiplets, namely a singlet (gerade: $X^1\Sigma_g^+$) and a triplet (ungerade: $a^3\Sigma_u^+$) state. We will write those potentials as $V_g(r)$ and $V_u(r)$ respectively. The dispersion component of $V_{g,u}(r)$ is given by the first three Van der Waals coefficients, *i.e.*

$$V_{g,u}(r) = -\left(\frac{C_6}{r^6} + \frac{C_8}{r^8} + \frac{C_{10}}{r^{10}} \pm V_{\rm exc}(r\right) \ . \tag{2.24}$$

For C_6, C_8 and C_{10} we used the values of Marinescu *et al.* [40]. We give them in Table 2.4 and compare their values with other estimates. The values we adopted are a recent theoretical prediction and should be more reliable.

The exchange term $V_{\rm exc}(r)$ is very important to the determination of the spin-change cross section and special care is needed if correct cross sections are to be obtained at low temperatures. Zemke and Stwalley found the form $C\exp(-\beta r)$ to be a good approximation between 11 a_0 and 19 a_0 in the case of lithium [28], and between 10 a_0 and 21 a_0 for sodium [34], but it must become inadequate beyond this range, and Smirnov and Chibisov [41] have shown that the exchange interaction has the asymptotic form

$$V_{exc}(r) = \frac{1}{2}[V_u(r) - V_g(r)] = Cr^\alpha \exp(-\beta r) \ . \tag{2.25}$$

More precisely, for two atoms A and B with ionization potentials $\rho_A^2/2$ and $\rho_B^2/2$

respectively, one has

$$V_u(r) - V_g(r) = r^\alpha \exp(-\beta r) J(\rho_A, \rho_B, r) \ . \tag{2.26}$$

Here, we have two identical atoms ($\rho_A = \rho_B = \rho$) so

$$\begin{aligned} \alpha &\equiv \frac{2}{\rho_A} + \frac{2}{\rho_B} - \frac{1}{\rho_A + \rho_B} - 1 = \frac{7}{2\rho} - 1 \ , \\ \beta &\equiv \rho_A + \rho_B = 2\rho \ , \end{aligned} \tag{2.27}$$

and $J(\rho_A, \rho_B, r) = J(\rho)$ is then r independent [41] and given by

$$J(\rho) = \frac{A^4}{2^{1+1/\rho}} \frac{\Gamma(1/2\rho)}{\rho^{1+1/2\rho}} \int_0^1 dy (1-y)^{3/2\rho} (1+y)^{1/2\rho} \exp[(y-1)/\rho] \ , \tag{2.28}$$

where A is the atomic wavefunction amplitude for large r

$$\phi(r) = A r^{1/\rho - 1} e^{-\rho r} \ . \tag{2.29}$$

For Li, we determine C by fitting Eq. (2.25) to $V_{\rm exc}(r)$, matching $V_g(r)$ and $V_u(r)$ at the largest values of r for which they are reliably determined by experimental data. In the case of Na, this was not possible. Indeed, as we can see from Fig. 2.2, there are too many oscillations in the data. So, we used Eq. (2.28) where the value of A has been determined by using a pseudo-potential model and found to be 0.75116 which compares well with Smirnov and Chibisov's value of 0.751 [41]. The constant C in $V_{\rm exc}(r)$ is simply given by

$$C = J(\rho)/2 \ . \tag{2.30}$$

The different values for $V_{\rm exc}(r)$ are given in Table 2.5, together with values used in other studies. Finally, the log-log scale on Fig. 2.2 helps to illustrate the better exchange term using Eq. (2.25) than the usual exponential expression $Ce^{-\beta r}$. In fact, the small curvature in the *ab initio* data (from [37, 46]) is taken into account.

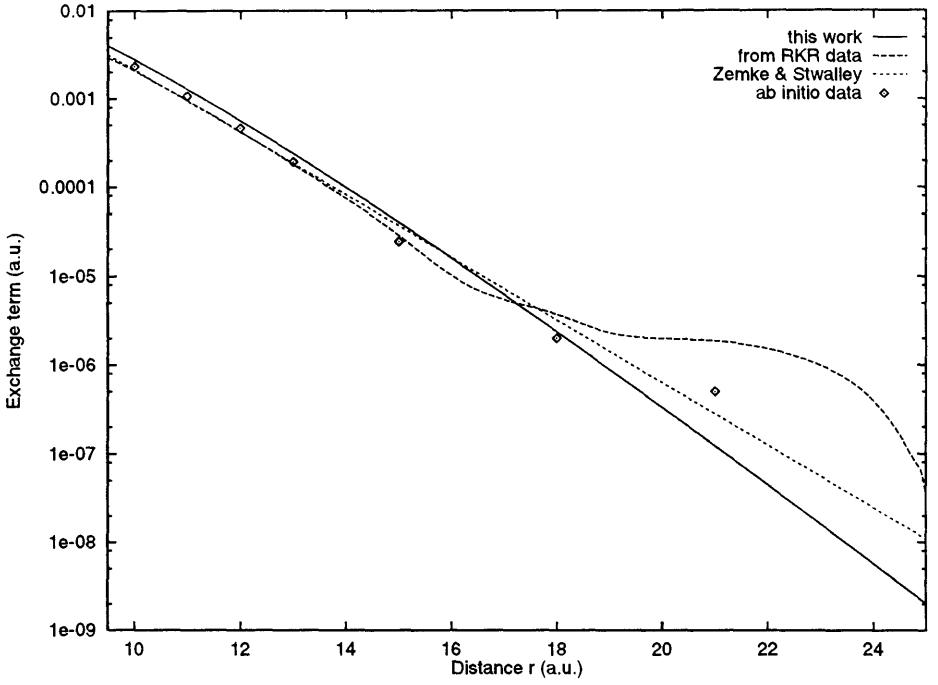

Figure 2.2: Exchange term of Na.

Coefficient	^{7}Li		^{23}Na	
	$X^1\Sigma_g^+$	$a^3\Sigma_u^+$	$X^1\Sigma_g^+$	$a^3\Sigma_u^+$
r_{min}	2.75	3.00	3.80	3.80
$V(r_{min})$	0.061 866	0.104 471	0.022 410	0.078 3293
A	5.109 275	1.773 825	10,018,466	1.863 178
B	1.605 033	0.943 995	5.241 63	0.833 978
$V(0)$*	421.955	30.118	4.479×10^{15}	44.318 404

* $V(0) = Ae^{Br_{min}}$

Table 2.3: Short-range coefficients (a.u.)

^{7}Li

Ref.	C_6 ($e^2a_0^5$)	C_8 ($e^2a_0^7$)	C_{10} ($e^2a_0^9$)
Marinescu *et al.* [40]	1,388	83,230	7,348,000
Zemke and Stwalley [28]	1,381 ±8	82,616 ±2,288	6,425,000 ±514,000
Tang *et al.* [42]	1,390	84,030 ±1,370	7,217,000 ±242,000
Konowalow and Fish [43]	1,390 ±30	120,000	

^{23}Na

Ref.	C_6 ($e^2a_0^5$)	C_8 ($e^2a_0^7$)	C_{10} ($e^2a_0^9$)
Marinescu *et al.* [40]	1,472	111,877	11,065,00
Bussery and Aubert-Frécon [44]	1,698	102,810	6,939,128
Tang *et al.* [42]	1510 ±40	111,400 ±4,400	10,720,000 ±690,000
Maeder and Kutzelnigg [45]	1,540	109,800	10,360,000
Konowalow and Rosenkrantz [46]	1,680	164,000	
Li *et al.* [38]	1,637 ±33	157,000 ±4,700	
Dalgarno and Davison [47]	1,580	107,700	

Table 2.4: Van der Waals coefficients in atomic units. We used the values of Marinescu *et al.*

^{7}Li

Source	ρ	α	β	a
Fitting*	0.6297	4.558	1.259	0.01288
Integral ($A = 0.765$)	0.6297	4.558	1.259	0.01345
Smirnov and Chibisov [41]	0.630	4.56	1.26	0.01355
Konowalow and Fish [43]			0.997	46.5
Zemke and Stwalley [28]			0.945	23.20

^{23}Na

Source	ρ	α	β	a
Integral * ($A = 0.75116$)	0.6148	4.693	1.229	0.0123
Radzig and Smirnov [39]	0.626	4.59	1.252	0.012
Smirnov and Chibisov [41]	0.626	4.59	1.252	0.0125
Zemke and Stwalley [34]			0.81173	7.0896
Li *et al.* [38]			0.7662	4.30
Konowalow and Rosenkrantz [46]			0.649	0.345

* values used in this work. The integral value is obtained from Eq. (2.28) with the indicated value of A.

Table 2.5: The exchange term coefficients in atomic units.

The retardation effects (or Casimir corrections) will become important at large distances. They affect the dynamical part of the potential, *i.e.* the dispersion terms. The exchange term being an overlap of the atomic wave functions, it is not modified by the time delay in the virtual photon travel between the two atoms. The C_n/r^n terms will then become

$$\frac{C_6}{r^6} + \frac{C_8}{r^8} + \frac{C_{10}}{r^{10}} \longrightarrow f_6(r)\frac{C_6}{r^6} + f_8(r)\frac{C_8}{r^8} + f_{10}(r)\frac{C_{10}}{r^{10}} \ . \tag{2.31}$$

The functions $f_n(r)$ are given by (see Marinescu, Babb and Dalgarno [48])

$$\begin{aligned} f_6(r) &\equiv \frac{1}{\pi C_6}\int_0^\infty d\omega A(\omega)\exp(-2\omega\alpha r)P_1(\omega\alpha r) \ , \\ f_8(r) &\equiv \frac{1}{3\pi C_8}\int_0^\infty d\omega B(\omega)\exp(-2\omega\alpha r)P_2(\omega\alpha r) \ , \\ f_{10}(r) &\equiv \frac{1}{18\pi C_{10}}\int_0^\infty d\omega C(\omega)\exp(-2\omega\alpha r)P_3(\omega\alpha r) \ , \end{aligned} \tag{2.32}$$

where

$$\begin{aligned} A(\omega) &\equiv \alpha_1^2(i\omega) \ , \\ B(\omega) &\equiv \alpha_1(i\omega)\alpha_2(i\omega) \ , \\ C(\omega) &\equiv \frac{4}{5}\alpha_1(i\omega)\alpha_3(i\omega) + \alpha_2^2(i\omega) \ , \end{aligned} \tag{2.33}$$

and

$$\begin{aligned} P_1(x) &= x^4 + 2x^3 + 5x^2 + 6x + 3 \ , \\ P_2(x) &= 2x^6 + 6x^5 + 19x^4 + 48x^3 + 84x^2 + 90x + 45 \ , \\ P_3(x) &= 2x^8 + 8x^7 + 32x^6 + 114x^5 + 333x^4 + 750x^3 + 1215x^2 + 1260x + 630 \ . \end{aligned} \tag{2.34}$$

Here $\alpha_N(i\omega)$ are the polarizabilities of the various multipoles [dipole ($N = 1$), quadrupole ($N = 2$), octupole ($N = 3$), *etc.*], ω is a frequency and α is the fine structure constant.

short-range		long-range	
W_4	2.939325(+0)	U_7	4.317877(+3)
W_6	1.647939(+2)	U_9	4.690617(+3)
W_8	7.903911(+5)	U_{11}	5.043503(+3)

Table 2.6: The Casimir coefficients (in a.u.) for ^{23}Na.

For small r, this expression becomes [48]

$$\frac{C_6}{r^6} + \frac{C_8}{r^8} + \frac{C_{10}}{r^{10}} \longrightarrow -\frac{\alpha^2 W_4}{r^4} + \frac{C_6 - \alpha^2 W_6}{r^6} + \frac{C_8 - \alpha^2 W_8}{r^8} + \frac{C_{10}}{r^{10}} \,, \tag{2.35}$$

and very large distances, the expression behaves like

$$\frac{C_6}{r^6} + \frac{C_8}{r^8} + \frac{C_{10}}{r^{10}} \longrightarrow \frac{U_7}{r^7} + \frac{U_9}{r^9} + \frac{U_{11}}{r^{11}} \,. \tag{2.36}$$

We considered the Casimir corrections only for ^{23}Na. As noted by Marinescu *et al.* [48], f_6, f_8 and f_{10} diminish faster in the case of sodium than for any other alkali. The Fig. 2.3 shows this fact in the case of $f_6(r)$, but it is true for f_8 and f_{10} as well. Hence, if any differences arize from the inclusion of the Casimir corrections, they should be the strongest for Na. The different values for W_n and U_n for ^{23}Na are given in Table 2.6 and the $f_n(r)$ are shown in Fig. 2.4.

The adopted hybrid potential curves of the singlet and triplet states of ^{7}Li are illustrated in Fig. 2.5 and for ^{23}Na in Fig. 2.6. In the case of sodium, the differences between the two set of curves *i.e.* with and without Casimir corrections, are too small

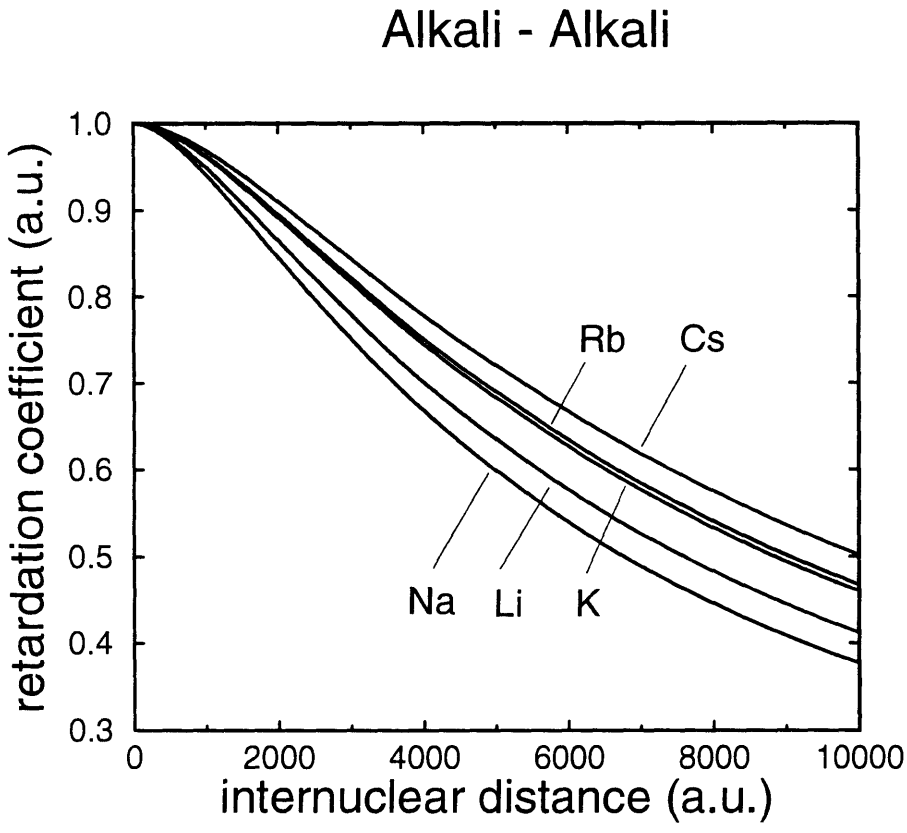

Figure 2.3: Correction function $f_6(r)$ for the alkali atoms.

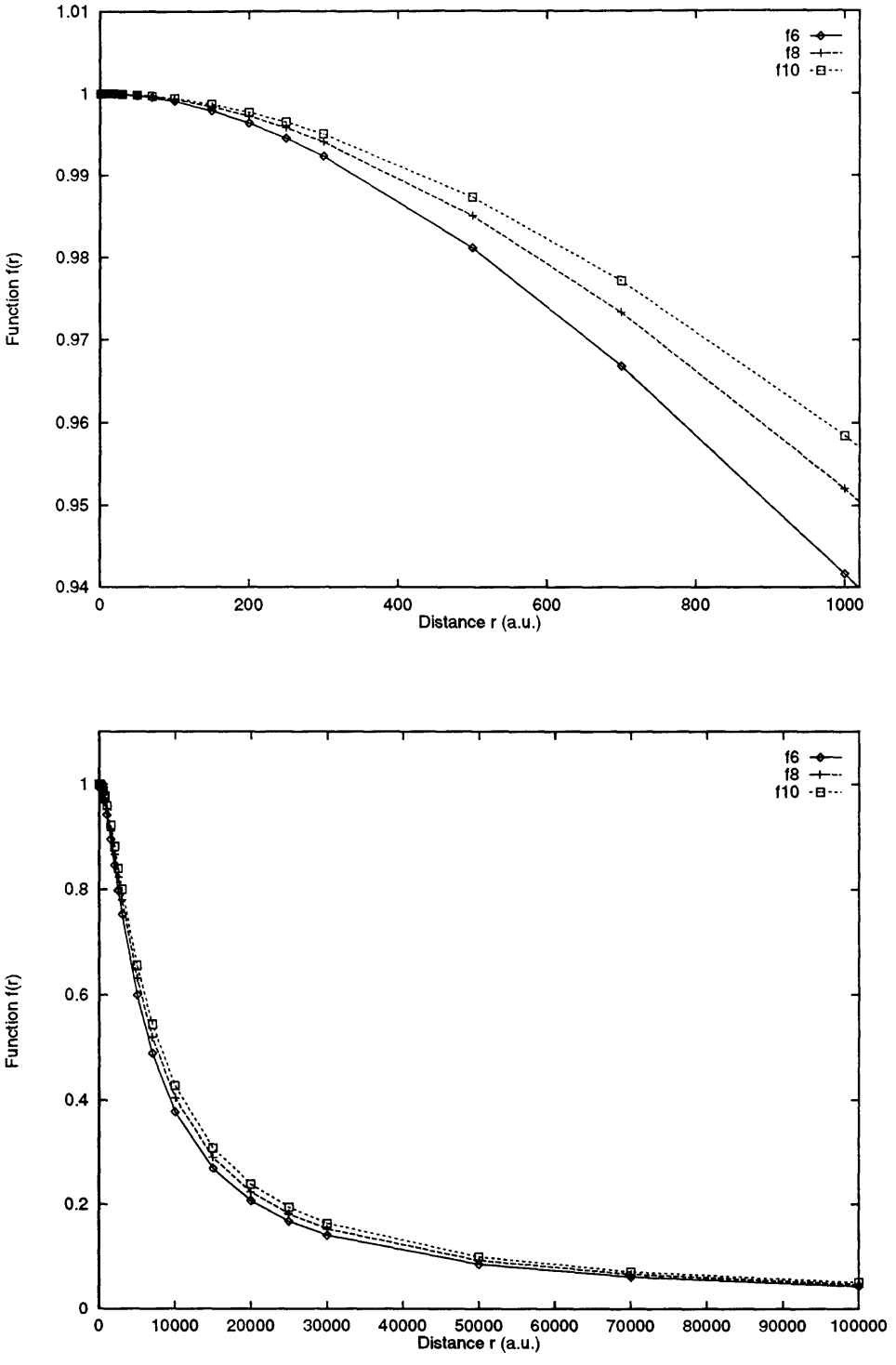

Figure 2.4: Casimir correction functions $f_n(r)$ for ^{23}Na.

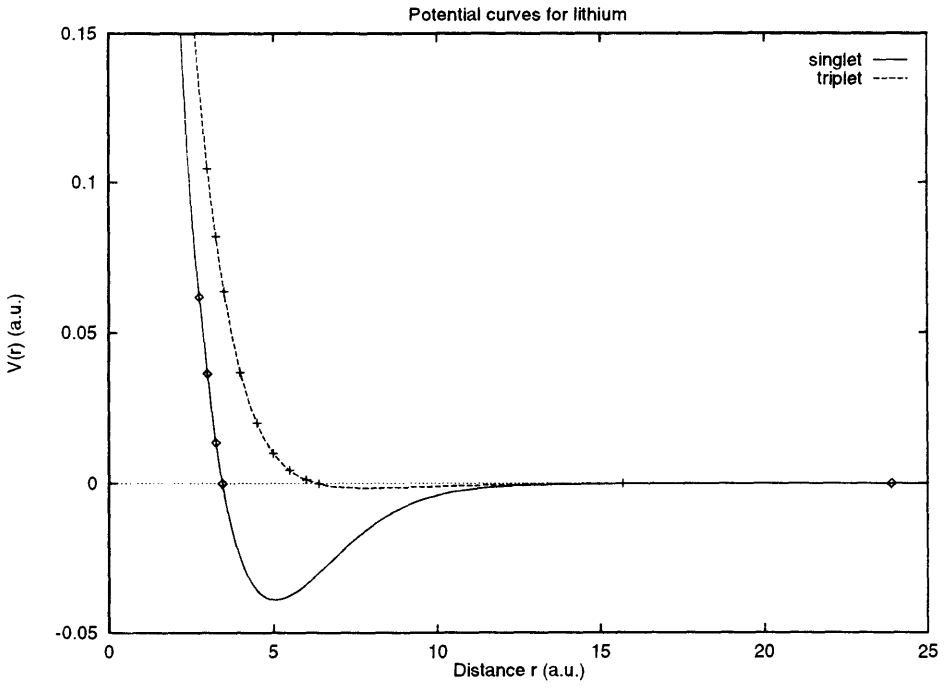

Figure 2.5: Hybrid potential curves for ^{7}Li ground states.

to be shown in Fig. 2.6. We also notice that the two energy curves cross at small r, as expected. In fact, if we collapse the two $_{11}$Na atoms at $r = 0$, we get $_{22}$Ti for which the outer electron configuration $(3d^2 4s^2)$ gives the ground state term $^3F_2$. The lower state at $r = 0$ being a triplet state, the curves must cross. The same is also true for lithium. The two $_3$Li atoms collapse into $_6$C for which the ground state term $^3P_0$ is also a triplet state.

2.2 Scattering results

In this section, we will give and analyze some results for the elastic and spin-change scattering for lithium and sodium at ultralow temperatures. But first, let us derive the expression for the spin-change scattering cross section.

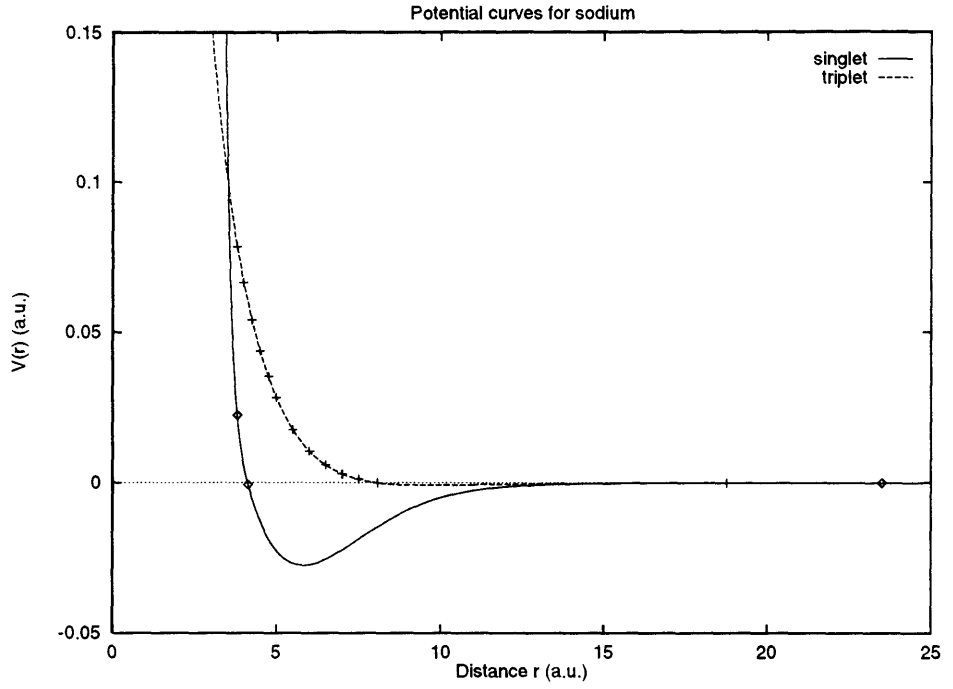

Figure 2.6: Hybrid potential curves for ^{23}Na ground states.

2.2.1 Spin-change expression

Let us give a quick derivation of the spin-change cross section σ_{sc} in the case of two alkali atoms. We are looking at the scattering of two different potentials, a singlet V_S and a triplet V_T, which leads to two functions $f_S(k,\theta)$ and $f_T(k,\theta)$. Calling the two nuclei A and B whose spin wave functions are $\alpha(A)$ and $\chi(B) = \alpha(B)$ or $\beta(B)$, where α and β represents spin up or down respectively, and 1 and 2 the two electrons with spin functions $\alpha(i)$ or $\beta(i)$ for $i = 1$ or 2, the wave functions for each case are

$$\psi_S(r,\theta) \sim \left(e^{i(\mathbf{k}\cdot\mathbf{r})} + f_S(k,\theta)\frac{e^{ikr}}{r}\right)\alpha(A)\chi(B)\bigotimes\frac{1}{\sqrt{2}}\left[\alpha(1)\beta(2) - \beta(1)\alpha(2)\right] ,$$

$$\psi_T(r,\theta) \sim \left(e^{i(\mathbf{k}\cdot\mathbf{r})} + f_T(k,\theta)\frac{e^{ikr}}{r}\right)\alpha(A)\chi(B)\bigotimes\frac{1}{\sqrt{2}}\left[\alpha(1)\beta(2) + \beta(1)\alpha(2)\right] .$$

For the triplet, we do not consider the spin functions $\alpha(1)\alpha(2)$ and $\beta(1)\beta(2)$ which cannot yield a spin exchange. If we consider the initial state so that the spin wave of the atom A is $\alpha(A)\alpha(1)$, then the complete wave function must be

$$\psi = \frac{1}{\sqrt{2}}(\psi_S + \psi_T) \sim \frac{1}{2} e^{i(\mathbf{k}\cdot\mathbf{r})} \alpha(A)\alpha(1)\chi(B)\beta(2) + \frac{e^{ikr}}{r} S \ , \tag{2.37}$$

where

$$\begin{aligned} S &= \frac{1}{2}\left[f_S(k,\theta) + f_T(k,\theta)\right] \alpha(A)\alpha(1)\chi(B)\beta(2) \\ &\quad + \frac{1}{2}\left[f_T(k,\theta) - f_S(k,\theta)\right] \alpha(A)\beta(1)\chi(B)\alpha(2) \ , \end{aligned}$$

whose second term is the only one which corresponds to a spin exchange from the initial state. The spin-change scattering amplitude is then given by

$$\begin{aligned} g(k,\theta) &= \frac{1}{2}\left[f_T(k,\theta) - f_S(k,\theta)\right] \\ &= \frac{1}{2k} \sum_{l=0}^{\infty} \exp\{i(\delta_{S,l} + \delta_{T,l})\} \sin(\delta_{T,l} - \delta_{S,l})(2l+1) P_l(\cos\theta) \ . \end{aligned} \tag{2.38}$$

The spin-change cross section is simply the square of this, *i.e.*

$$\sigma_{sc} = \frac{\pi}{k^2} \sum_{l=0}^{\infty} (2l+1) \sin^2(\delta_{T,l} - \delta_{S,l}) \ . \tag{2.39}$$

We can now examine the numerical results obtained using the potential curves described above.

2.2.2 Dissociation energies

We calculated the dissociation energy D_e using the fitting of the RKR data and the functional form of the long-range potential at the maximum distance possible (r_{max}), as described in §2.1.3 B.

Source	$D_e(X)$	$D_e(a)$
This work*	8,516.617 997	333.395 737
Barakat *et al.* [29]	8,516.78 ± 0.54	
Linton *et al.* [32]		333 ± 1
Zemke and Stwalley [28]	8,516.61 ± 0.08	333.4 ± 0.3

* calculated by fitting the long-range form at the larget turning point available : $R_2 = 12.639382$ Å for $X^1\Sigma_g^+$ and $R_2 = 8.2978$ Å for $a^3\Sigma_u^+$.

Table 2.7: The dissociation energies (cm^{-1}) for ^{7}Li.

In the case of lithium, our adopted potentials yield a value of 8516.618 cm^{-1} for the dissociation energy of the $X^1\Sigma_g^+$ state, which is similar to the values of 8516.78 cm^{-1} of Barakat *et al.* [29] and 8516.61 cm^{-1} of Zemke and Stwalley [28] Similarly, we get 333.396 cm^{-1} for the dissociation energy of the $a^3\Sigma_u^+$ state in close agreement with the values of 333 cm^{-1} of Linton *et al.* [32] and 333.4 cm^{-1} of Zemke and Stwalley [28] Table 2.7 shows these results and dissociation energies published by other groups.

For the sodium case, our adopted potentials yield a value of 6,022.023 cm^{-1} for the dissociation energy of the $X^1\Sigma_g^+$ state in good agreement with the value of 6,022.03 cm^{-1} of Zemke and Stwalley [34] and of $6,022.6 \pm 1.0$ cm^{-1} of Barrow *et al.* [36]. For the $a^3\Sigma_u^+$ state, we obtained 174.083 cm^{-1} for the value of the dissociation energy,

Source	$D_e(X)$	$D_e(a)$
This work*	6,022.023 969	174.082 856
Casimir*	6,022.023 846	174.082 531
Zemke and Stwalley [34]	6,022.03	173.84
Barrow *et al.* [36]	6,022.06 $\pm$1.0	
Verma *et al.* [49]	6,024 $\pm$6	
Li *et al.* [38]		174.45 $\pm$0.36
Friedman-Hill and Field [50]		174.76 $\pm$0.35

* calculated by fitting the long-range form
at the larget turning point available :
$R_2 = 15.875317$ Å for $X^1\Sigma_g^+$ and
$R_2 = 13.229431$ Å for $a^3\Sigma_u^+$.

Table 2.8: The dissociation energies (cm^{-1}) for ^{23}Na.

which compares well with the value of 174.45 ± 0.36 cm^{-1} of Li *et al.* [38] and of 173.84 cm^{-1} using numbers from Zemke and Stwalley [34] The effect of Casimir corrections is negligible as one can see in Table 2.8. Also shown in that same table are dissociation energy results published by other groups.

The close agreement between our numbers and the previously published ones give us confidence in the coefficients used in the long-range form of the potentials. In fact, if the Van der Waals coefficients or the exchange term were off by an appreciable

amount, those dissociation energies would be affected.

2.2.3 Zero-energy limit

We solved the Schrödinger equation

$$\left[\frac{d^2}{dr^2} + k^2 - \frac{l(l+1)}{r^2} - U(r)\right] u_l(k,r) = 0 \tag{2.40}$$

by the Numerov method, with automatic step-size selection. We found that a more stable phase shift is obtained at low energies by substituing the solution into the integral form [20], rather than by fitting to the asymptotic form (see Appendix A for more details). We calculated the scattering lengths and effective ranges using

$$a = -\lim_{k\to 0} \frac{\tan\delta_0}{k} \qquad \text{and} \qquad r_e = 2\int_0^\infty dr \left([v^0(r)]^2 - [u^0(r)]^2\right) . \tag{2.41}$$

We also determined the scattering lengths and effective ranges by fitting the scattering phase shift δ_0 to the effective range expansion

$$k\cot\delta_0 = -\frac{1}{a} + \frac{1}{2} r_e k^2 + \cdots . \tag{2.42}$$

The adopted atomic and reduced masses for the collision of two ^{7}Li atoms and two ^{23}Na atoms are given in Table 2.9. We selected those two isotopes since they are the most abundant in nature (see Table 2.9).

The scattering lengths and effective ranges for the $X^1\Sigma_g^+$ and $a^3\Sigma_u^+$ states are presented in Table 2.10. The close agreement between the calculations of a and of r_e from Eqs. (2.41) and (2.42) confirms the accuracy of the numerical integrations of the partial wave equation (2.40). The size of the scattering lengths and effective

Atom	atomic mass (g/mole)	molecular reduced mass (m_e)	natural abundance (%)	I.P (eV)	spin	$\langle r \rangle$ (a_0)	$\langle r^2 \rangle$ (a_0^2)
^{6}Li	6.015121	5,482.4475	7.5	5.39172	1+	3.874	17.74
^{7}Li	7.016003	6,394.6955	92.5	5.39172	$\frac{3}{2}-$	3.874	17.74
^{23}Na	22.98977	20,953.87958	100.0	5.13908	$\frac{3}{2}+$	4.209	20.70

Table 2.9: The atomic masses and molecular reduced masses.

ranges is closely related to the position of the last vibrational bound states of the energy curves, as can be anticipated by inspection of

$$\frac{1}{a} = \gamma - \frac{1}{2} r_e \gamma^2 \ , \tag{2.43}$$

(see §1.5.5) which, consistent with Levinson's theorem, show that as the binding energy $|E| = \hbar^2\gamma^2/2m$ of the highest levels tends to zero, the scattering length tends to $\pm$ infinity (see also §1.2.2 Eqs. (1.124) or (1.156) about the *zero-energy resonances*). The negative triplet scattering length for lithium suggests the existence of a bound state close to the continuum edge.

Another way to see this is by inspecting the phase shift $\delta_0(k)$. The singlet and triplet δ_0 for ^{7}Li are shown in Fig. 2.7 and those for ^{23}Na in Fig. 2.8. In all the instances for which the scattering length is positive (*i.e.* ^{7}Li $X^1\Sigma_g^+$, ^{23}Na $X^1\Sigma_g^+$ and $a^3\Sigma_u^+$), the phase shift decreases slowly until it reaches $-\pi/2$, at which point it starts up at $+\pi/2$ (δ_0 was obtained by inversing $\tan\delta_0$). However, for ^{7}Li $a^3\Sigma_u^+$ state, δ_0 increases slowly before decreasing like the other cases. This can be interpreted in light of the discussion of the Levinson theorem for the square well (see §1.4.1). In

Atom	state	long-range potential	a		r_e	
			Eq. (2.41)	Eq. (2.42)	Eq. (2.41)	Eq. (2.42)
^{7}Li	$X^1\Sigma_g^+$	no retardation	36.9247	36.9251	66.5	66 ±1
	$a^3\Sigma_u^+$	no retardation	-17.1609	-17.1554	1,014.8	1,012 ±4
^{23}Na	$X^1\Sigma_g^+$	no retardation	34.9352	34.9356	187.5	184 ±1
		with Casimir	34.9945	34.9947	177.5	178 ±1
	$a^3\Sigma_u^+$	no retardation	77.2861	77.2863	62.5	62 ±1
		with Casimir	77.3521	77.3522	60.7	61 ±1

Table 2.10: Scattering lengths and effective ranges in atomic units.

this last case, the potential almost becomes strong enough to support another bound state, but not quite yet. Hence, the phase shift grows but not enough to pass through $\pi/2$ (at which point we would have a zero-energy resonance) or go higher to the next value of π (*i.e.* another bound state in the well).

The effective range depends on the overlap of the wave functions $v^0(r)$ and $u^0(r)$. Fig. 2.9 shows those two wave functions for the singlet and triplet states of ^{7}Li and Fig. 2.10 the wave functions for ^{23}Na. In the case of ^{7}Li, the value of r_e is much bigger for the $a^3\Sigma_u^+$ state than for the $X^1\Sigma_g^+$ state. The reason for this becomes obvious from Fig. 2.9: for $a^3\Sigma_u^+$, $[u^0]^2$ is always smaller than $[v^0]^2$, but for $X^1\Sigma_g^+$ there is a cancellation region where $[v^0]^2 < [u^0]^2$. Moreover, since $a < 0$ for the triplet, this implies that $v^0 = 1 - r/a$ is always greater than one, hence a larger integral than for

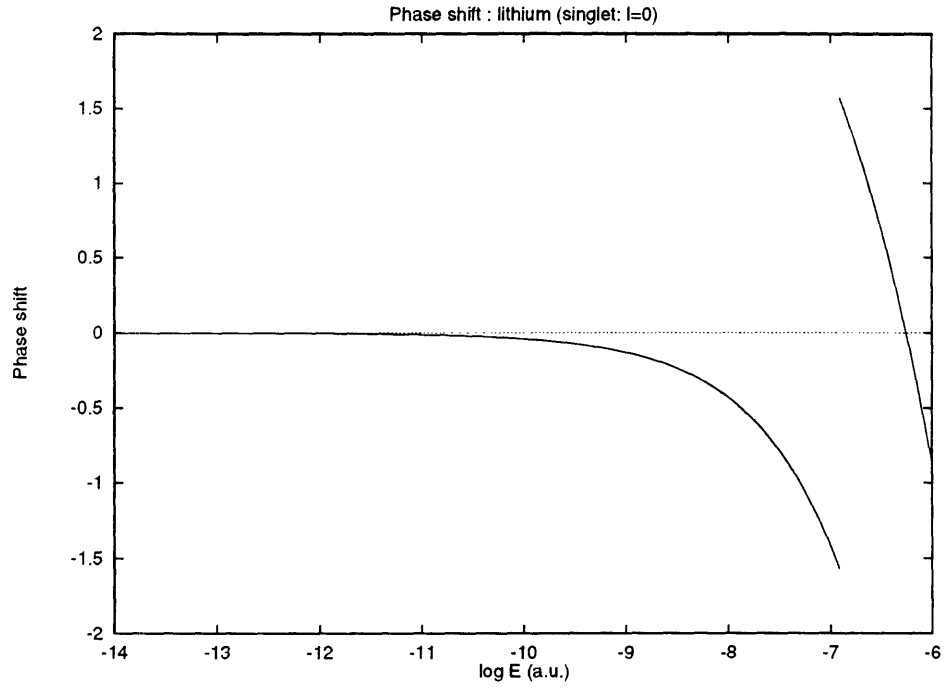

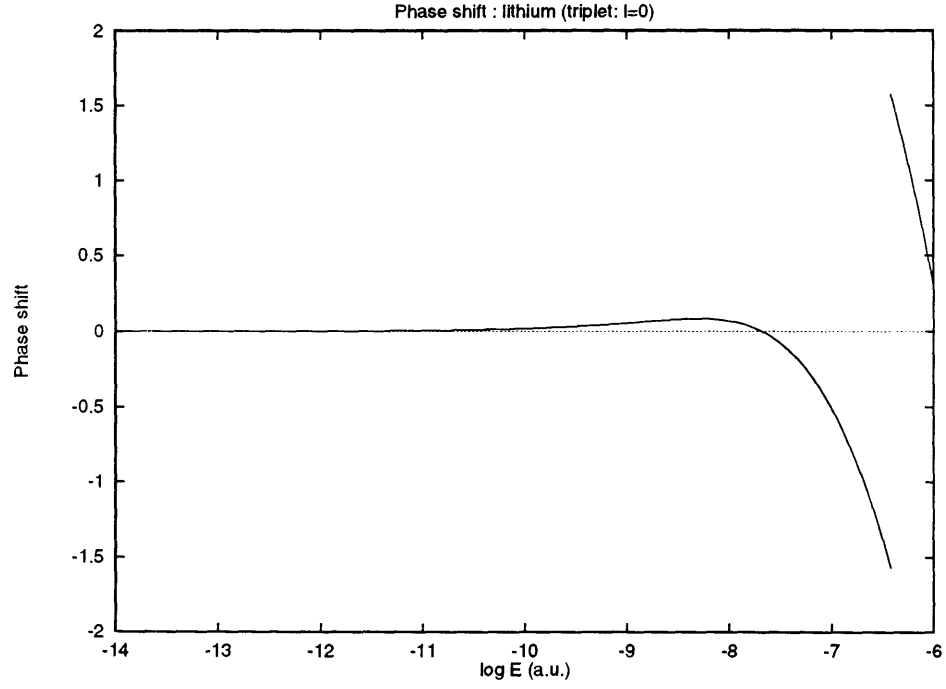

Figure 2.7: The $l = 0$ phase shift for the singlet and triplet cases of ^{7}Li.

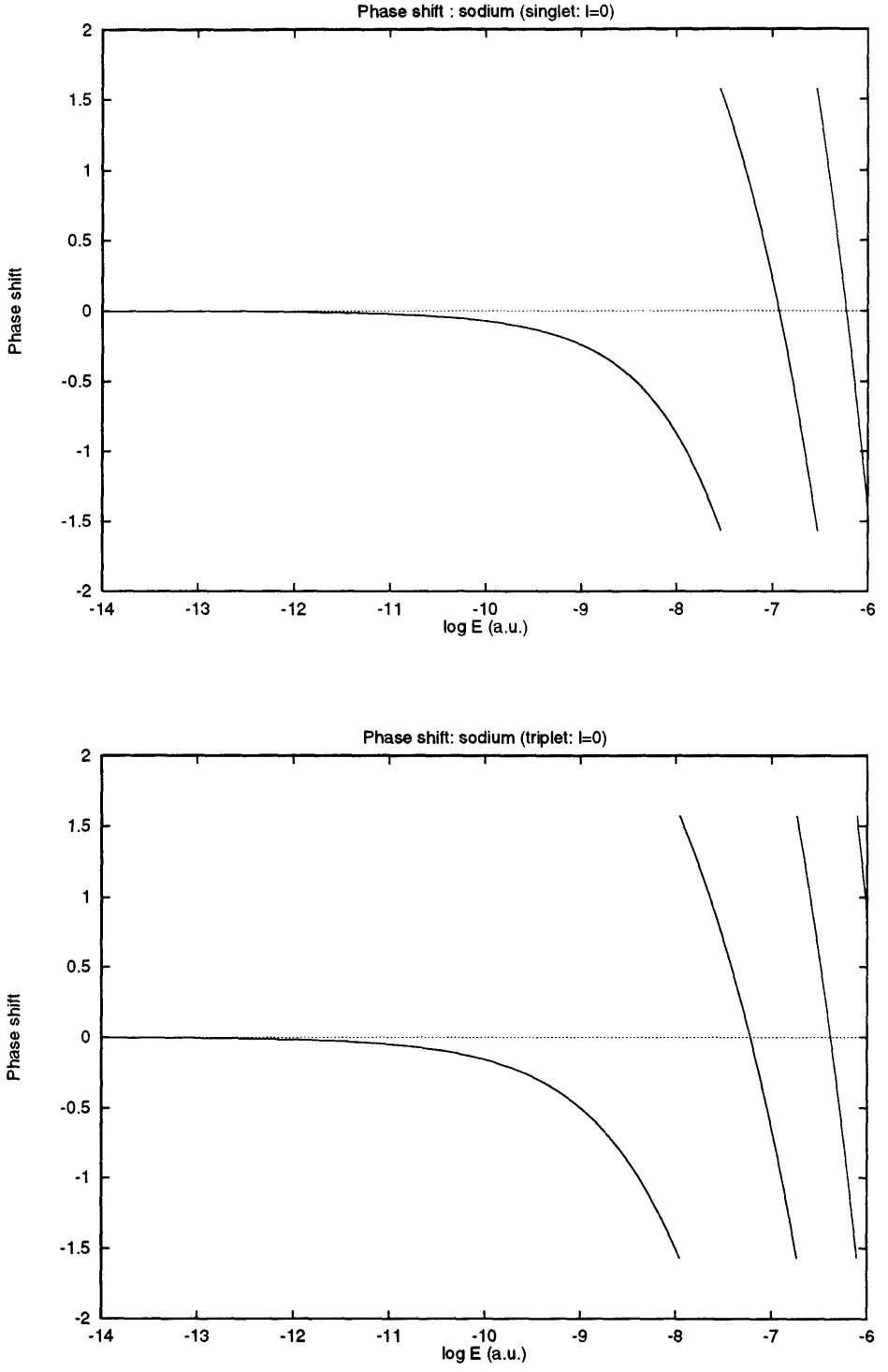

Figure 2.8: The $l = 0$ phase shift for the singlet and triplet cases of ^{23}Na.

the singlet. For $X^1\Sigma_g^+$ $|v^0| < 1$ until $u^0(r)$ almost touch it (at around a distance of $70a_0$). These two effects combine together to give a much bigger effective range for the triplet than for the singlet ^{7}Li case. For ^{23}Na both scattering lengths are positive, and therefore both wave functions $u^0(r)$ have a similar shape. However, the bigger value of r_e for the $X^1\Sigma_g^+$ state comes from the bigger lobe of $u^0(r)$ after $v^0(r)$ crosses the r-axis, when compared to the $a^3\Sigma_u^+$ state (see Fig. 2.10).

From Fig. 2.9-2.10, the geometrical interpretation of a and r_e becomes clearer. The scattering length is nothing else but the point at which the asymptotic form of $u^0(r)$ for large r, namely $v^0(r)$, crosses the r-axis. Since we can write the elastic scattering cross section as $\sigma = 4\pi a^2$ as $k \to 0$, it is also interpreted as the radius at which scattering will occur: the positive sign represents a repulsive interaction, and the negative sign an attractive one. For the effective range, the physical interpretation is directly linked to the actual range of the real potential. In fact, since it is a measurement of the difference between the probability density of the asymptotic (hence *free*) center of mass particle and the one with the potential, it gives the range at which the potential is not felt anymore by the scattering particles.

Calculations of the triplet scattering lengths for ^{7}Li atoms and ^{23}Na atoms have been reported recently. Taking account of uncertainties in the $a^3\Sigma_u^+$ interaction potential, Moerdijk *et al.* [51] concluded that

$$-27.8a_0 < a_T(^7\text{Li}) < -7.1a_0 \tag{2.44}$$

for the scattering length of ^{7}Li, in agreement with our value of $-17.2a_0$. Similarly, Moerdijk and Verhaar [52] computed the scattering length for the $a^3\Sigma_u^+$ state of ^{23}Na.

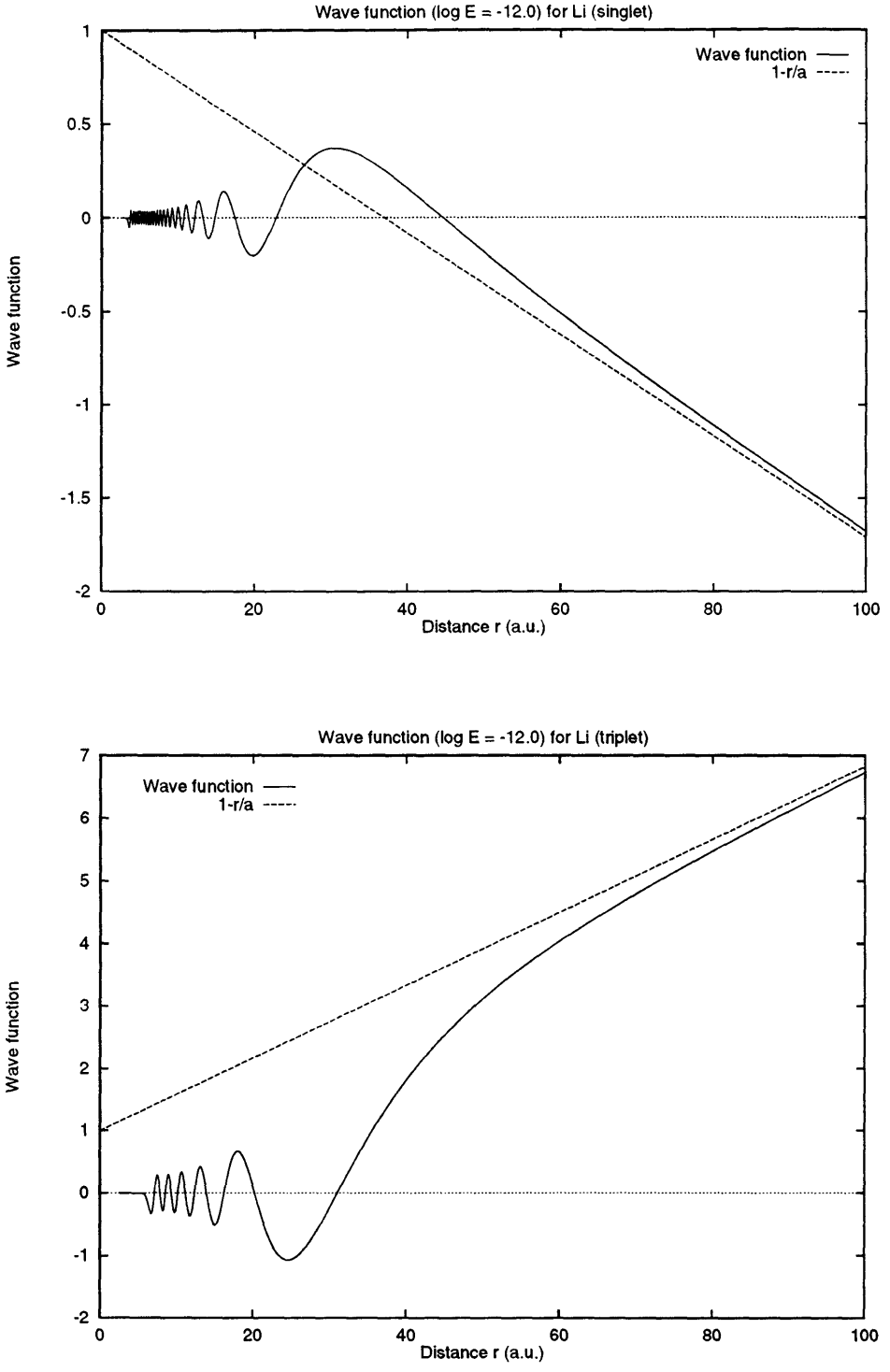

Figure 2.9: The wave functions $v^0(r)$ and $u^0(r)$ for the singlet and triplet cases of ^{7}Li.

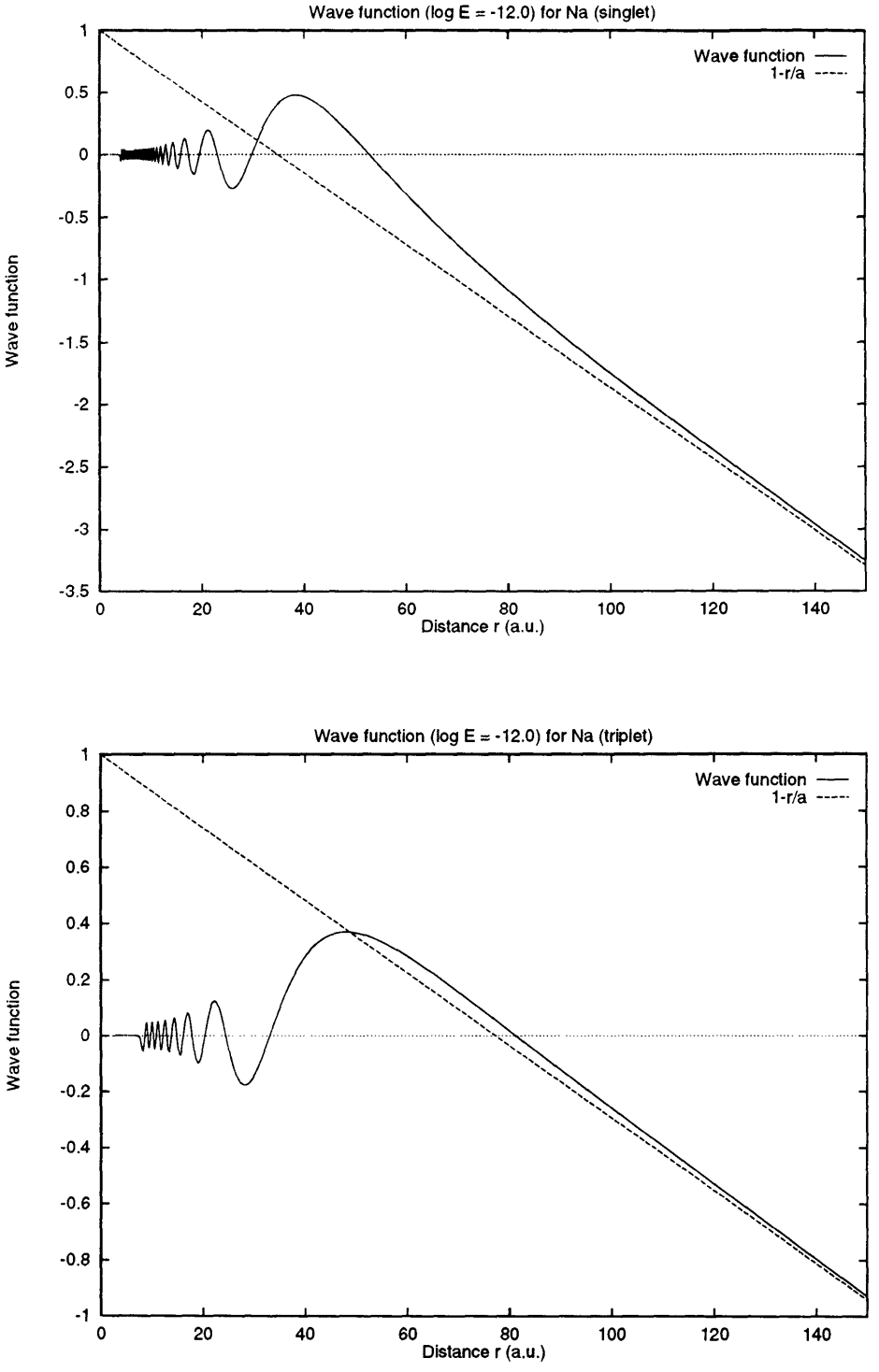

Figure 2.10: The wave functions $v^0(r)$ and $u^0(r)$ for the singlet and triplet cases of ^{23}Na.

They found

$$45a_0 < a_T(^{23}\mathrm{Na}) < 185a_0 \ . \tag{2.45}$$

Our value of $77.3a_0$ lies well inside these bounds.

2.2.4 Bound states

We have obtained the binding energies of the vibrational levels with zero angular momentum for both the $X^1\Sigma_g^+$ and $a^3\Sigma_u^+$ states of ^{7}Li and ^{23}Na, by solving the eigenvalue problem with the potentials described in the previous section (§2.1.2 and 2.1.3) (see Tables 2.11, 2.12, 2.13 and 2.14.

For ^{7}Li, we found 42 bound levels for the $X^1\Sigma_g^+$ state and 11 bound levels for the $a^3\Sigma_u^+$ state. They are listed in Table 2.11 for $X^1\Sigma_g^+$ and Table 2.12 for $a^3\Sigma_u^+$ together with the experimental data [29, 32]. The binding energies ($|E_b| = \hbar^2\gamma^2/2\mu$) of the highest bound levels correspond to values of γ of 0.0667 and 0.149 a.u., respectively, for the singlet and the triplet states. Since neither is within the domain of convergence of Eq. (2.42) one cannot use them to evaluate the scattering length or the effective range from Eq. (2.43) [see also §1.5.5].

For ^{23}Na, we found 66 bound levels for the$X^1\Sigma_g^+$ state and 16 bound levels for the $a^3\Sigma_u^+$ state. They are listed in Table 2.13 and Table 2.14 together with the experimental data [35, 38]. The binding energies of the highest bound levels correspond to values of γ of 0.0824 a.u. and 0.0282 a.u. respectively for the singlet and triplet states. The scattering lengths derived using Eq. (2.43) are not useful estimates because γr_e is large compared to unity and neither value of γ is within the domain of

v	Exp. [29]	Theory	v	Exp. [29]	Theory
0	175.0320	174.9787	21	6246.9482	6246.6143
1	521.2611	521.2205	22	6463.3140	6462.7531
2	862.2642	862.2253	23	6671.3979	6670.9251
3	1197.9974	1197.9469	24	6870.8931	6870.3348
4	1528.4128	1528.3481	25	7061.4199	7060.9622
5	1853.4573	1853.3833	26	7242.5556	7242.1159
6	2173.0721	2172.9640	27	7413.8431	7413.4889
7	2487.1914	2487.0308	28	7574.8736	7574.4980
8	2795.7419	2795.4231	29	7724.9765	7724.7060
9	3090.6412	3097.9413	30	7863.7083	7863.4155
10	3395.7978	3394.5732	31	7990.4162	7990.1590
11	3687.1094	3685.8532	32	8104.4730	8104.2697
12	3972.4624	3971.8652	33	8205.2323	8205.0430
13	4251.7309	4251.1436	34	8292.0294	8291.8688
14	4524.7756	4523.8373	35	8364.3068	8364.1532
15	4791.4274	4791.0078	36	8421.6125	8421.5251
16	5051.5343	5051.1070	37	8463.9645	8463.9218
17	5304.9322	5304.7937	38	8492.0440	8492.0818
18	5551.3992	5551.3130	39	8507.8421	8507.9264
19	5790.7056	5790.2832	40	8514.7777	8514.7986
20	6022.6578	6022.1967	41		8516.5409

Table 2.11: Energies of $X^1\Sigma_g^+$ vibrational levels for ^{7}Li in cm^{-1}.

v	Exp. [32]	Theory	v	Exp. [32]	Theory
0	31.917	31.8235	6	287.779	287.7226
1	90.572	90.4695	7	308.229	308.1986
2	142.637	142.5769	8		322.1335
3	188.358	188.3290	9		330.0006
4	227.803	227.7518	10		333.0137
5	260.968	260.8849			

Table 2.12: Energies of $a^3\Sigma_u^+$ vibrational levels for ^{7}Li in cm^{-1}.

convergence of Eq. (2.42).

2.2.5 Higher partial waves

Let us first look at the ^{7}Li case. With increasing energy, higher angular momentum waves contribute to the scattering. Fig. 2.11 illustrates the variation with energy of the individual partial wave cross sections for the $X^1\Sigma_g^+$ state. The total elastic cross section in units of a_0^2 is also presented in Fig. 2.11. The total cross section is constant at low velocities where only s-wave scattering is significant. For very low energies, the s-wave cross section is constant and then increases slowly before decreasing at higher energies. This behaviour can be explained by the values of a and r_e. Indeed, for $l = 0$, the elastic scattering cross section becomes

$$\sigma_{el} = \frac{4\pi}{k^2}\sin^2\delta_0 = \frac{4\pi}{k^2 + k^2\cot^2\delta_0}\ . \tag{2.46}$$

v	Exp. [35]	Theory (a)	Theory (b)	v	Exp. [35]	Theory (a)	Theory (b)
0	79.3678	79.3329	+1.229(-4)	33	4418.8193	4418.4650	+1.229(-4)
1	237.0455	236.9727	+1.229(-4)	34	4517.4867	4516.9300	+1.229(-4)
2	393.2453	393.1730	+1.229(-4)	35	4613.7454	4613.1759	+1.229(-4)
3	547.9739	547.9142	+1.229(-4)	36	4707.5335	4707.1674	+1.229(-4)
4	701.2267	701.1680	+1.229(-4)	37	4798.7858	4798.1950	+1.229(-4)
5	852.9934	852.9350	+1.229(-4)	38	4887.4339	4887.0951	+1.229(-4)
6	1003.2600	1003.1974	+1.229(-4)	39	4973.4061	4972.8734	+1.229(-4)
7	1152.0113	1151.9439	+1.229(-4)	40	5056.6276	5056.2935	+1.229(-4)
8	1299.2313	1299.1573	+1.229(-4)	41	5137.0199	5136.5454	+1.229(-4)
9	1444.9041	1444.8251	+1.229(-4)	42	5214.5015	5214.1717	+1.229(-4)
10	1589.0133	1588.9307	+1.229(-4)	43	5288.9870	5288.5905	+1.229(-4)
11	1731.5426	1731.4570	+1.229(-4)	44	5360.3878	5360.0572	+1.229(-4)
12	1872.4746	1872.3865	+1.229(-4)	45	5428.6112	5428.3593	+1.229(-4)
13	2011.7915	2011.7005	+1.229(-4)	46	5493.5609	5493.3388	+1.229(-4)
14	2149.4740	2149.3794	+1.229(-4)	47	5555.1368	5555.0003	+1.229(-4)
15	2285.5020	2285.4023	+1.229(-4)	48	5613.2351	5613.0494	+1.229(-4)
16	2419.8534	2419.7471	+1.229(-4)	49	5667.7490	5667.5746	+1.229(-4)
17	2552.5049	2552.3909	+1.229(-4)	50	5718.5693	5718.4347	+1.229(-4)
18	2683.4318	2683.3087	+1.229(-4)	51	5765.5866	5765.4659	+1.229(-4)
19	2812.6075	2812.4742	+1.229(-4)	52	5808.6933	5808.5843	+1.229(-4)
20	2940.0043	2939.8601	+1.229(-4)	53	5847.7876	5847.6878	+1.229(-4)
21	3065.5927	3065.4369	+1.229(-4)	54	5882.7797	5882.7030	+1.229(-4)
22	3189.3422	3189.1731	+1.229(-4)	55	5913.5990	5913.5637	+1.229(-4)
23	3311.2204	3311.0312	+1.229(-4)	56	5940.2058	5940.1880	+1.229(-4)
24	3431.1938	3430.9576	+1.229(-4)	57	5962.6055	5962.5881	+1.229(-4)
25	3549.2271	3548.8673	+1.229(-4)	58	5980.8684	5980.8325	+1.229(-4)
26	3665.2836	3664.6574	+1.229(-4)	59	5995.1549	5995.1109	+1.229(-4)
27	3779.3247	3778.3349	+1.229(-4)	60	6005.7479	6005.7081	+1.229(-4)
28	3891.3098	3890.1847	+1.229(-4)	61	6013.0942	6013.0440	+1.228(-4)
29	4001.1963	4000.4656	+1.229(-4)	62	6017.8555	6017.8067	+1.254(-4)
30	4108.9393	4108.6436	+1.229(-4)	63		6020.4606	+1.185(-4)
31	4214.4913	4213.9245	+1.229(-4)	64		6021.6504	+6.779(-5)
32	4317.8023	4317.0372	+1.229(-4)	65		6022.0011	+7.902(-6)

(a) without retardation (b) retardation correction

Table 2.13: Energies of $X^1\Sigma_g^+$ vibrational levels for ^{23}Na in cm^{-1}.

v	Exp. [38]	Theory (a)	(b)	(c)
0	5859.92	5860.3547	12.1680	+3.248(-4)
1	5883.59	5883.3641	35.1774	+3.248(-4)
2	5904.56	5904.6051	56.4184	+3.248(-4)
3	5924.15	5924.1841	75.9974	+3.248(-4)
4	5941.65	5942.1090	93.9224	+3.247(-4)
5	5958.08	5958.1148	109.9281	+3.247(-4)
6	5972.32	5972.1799	123.9932	+3.247(-4)
7	5984.68	5984.3137	136.1270	+3.246(-4)
8	5994.11	5994.5464	146.3597	+3.239(-4)
9	6003.57	6003.3288	155.1421	+3.225(-4)
10	6010.38	6010.5687	162.3820	+3.251(-4)
11	6016.01	6015.8063	167.6196	+3.086(-4)
12	6019.41	6019.2227	171.0360	+2.363(-4)
13		6021.1887	173.0020	+1.516(-4)
14		6022.0572	173.8705	+6.779(-5)
15		6022.2655	174.0788	+7.902(-6)

(a) without retardation with zero of energy set at the minimum of $X^1\Sigma_g^+$
(b) without retardation with zero of energy set at zero
(c) retardation correction

Table 2.14: Energies of $a^3\Sigma_u^+$ vibrational levels for ^{23}Na in cm^{-1}.

State	l	$\log_{10} E_\Gamma$	Γ ($\times 10^{-8}$ a.u.)	E_Γ ($\times 10^{-8}$ a.u.)	E_R ($\times 10^{-8}$ a.u.)
$X^1\Sigma_g^+$	2	-7.307	1.479	4.932	5.786
$a^3\Sigma_u^+$	4	-6.268	13.13	53.95	55.07

Table 2.15: Resonance energies and widths for ^{7}Li. E_R is the theoretical value.

Using the effective range expansion and keeping only up to order of k^2, we find

$$\sigma_{el} \simeq \frac{4\pi a^2}{(ka)^2 + [1 - \frac{1}{2} r_e a k^2]^2} \simeq 4\pi a^2 \left[1 + ak^2(r_e - a)\right] . \tag{2.47}$$

Since $(r_e - a)$ and a are positive, we obtained the desired behaviour. The s-wave cross section tends to decrease with increasing energy but the decrease is overcome by higher partial waves contributions which initially increase with energy from zero before passing through maxima and decreasing. Oscillations occur through the addition of a small number of partial waves. Sharper structures are due to shape resonances. The most prominent is the d-wave resonance corresponding to a quasi-bound state trapped by the $l = 2$ centrifugal barrier. The d-wave resonance occurs at an energy E_Γ of 4.9×10^{-8} a.u. and has a width (Γ) of 1.5×10^{-8} a.u. (see Table 2.15). The phase shift $\delta_2^S(k)$ is shown in Fig. 2.12. We can see that it goes through $\pi/2$ and then decreases (as described in §1.3.2 and §1.4.1). Notice that the theoretical value for the resonance energy (E_R) is also given in Table 2.15 (see §2.4).

We illustrate in Fig. 2.13 the similar calculations for the $a^3\Sigma_u^+$ state. The same general features are found in this case. The s-wave cross section tends to decrease with

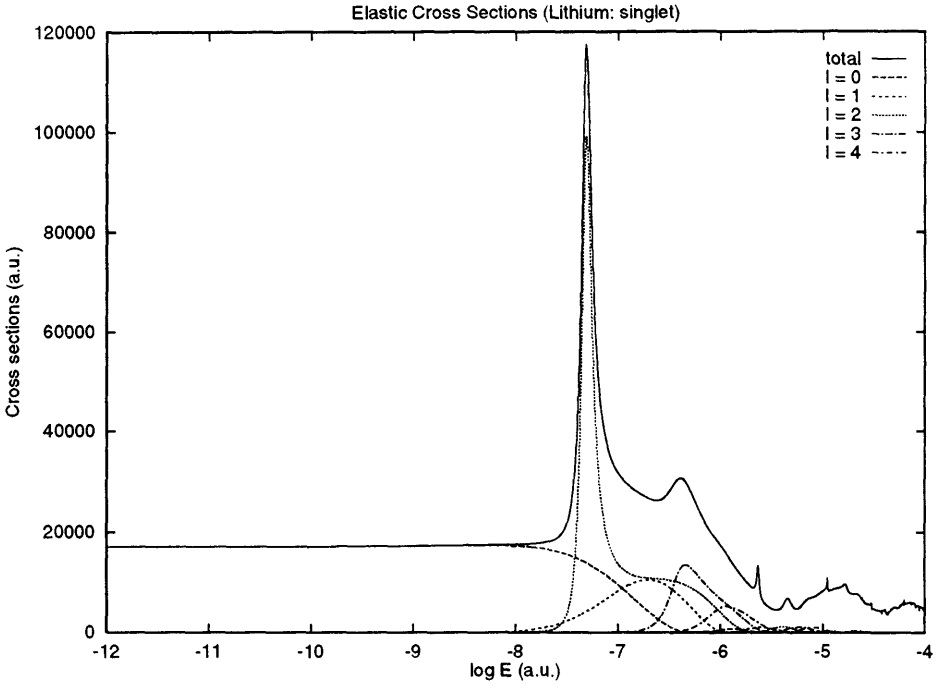

Figure 2.11: Total and partial elastic cross sections for $X^1\Sigma_g^+$ of ^{7}Li.

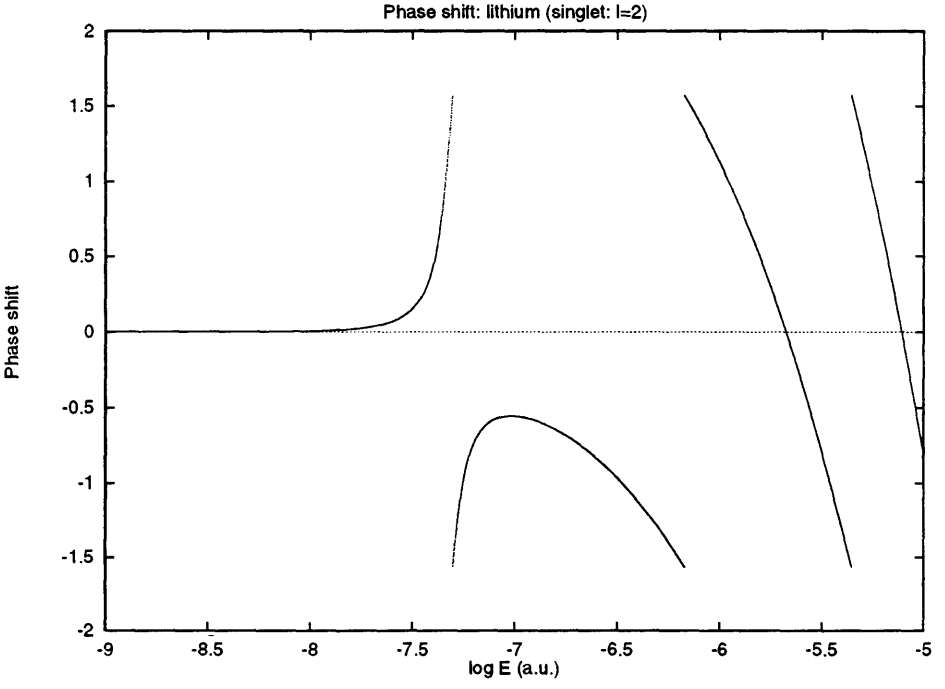

Figure 2.12: Phase shift for the $l = 2$ resonance in $X^1\Sigma_g^+$ of ^{7}Li.

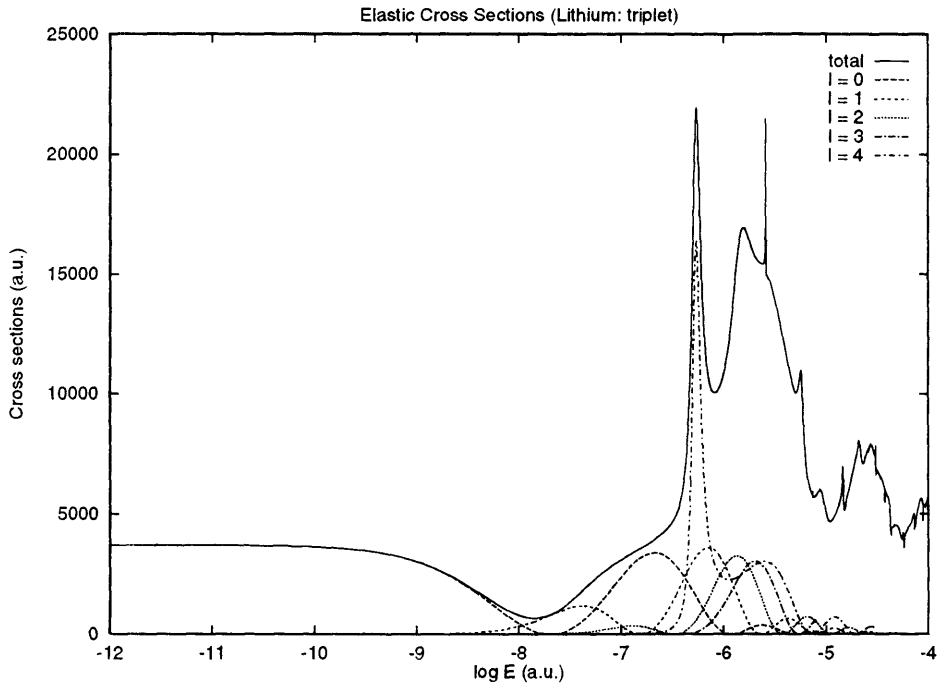

Figure 2.13: Total and partial elastic cross sections for $a^3\Sigma_u^+$ of ^{7}Li.

increasing energy but the decrease is overcome by higher partial wave contributions. We do not observe the small increase in the s-wave cross section before the decrease in this case because $(r_e - a)$ is positive while a is negative. A strong resonance appears in the $l = 4$ partial wave at an energy of 5.5×10^{-7} a.u. with a width of 1.3×10^{-7} a.u. (see Table 2.15 and Fig. 2.13).

The spin-change cross section is shown in Fig. 2.14. The contribution of both the singlet and triplet resonances are visible, and the same general description is valid.

In the case of ^{23}Na, we observe again the same general tendencies. Fig. 2.15 illustrates the variation with energy of the individual partial wave cross sections for the $X^1\Sigma_g^+$ state. For very low energies, the s-wave cross section is constant and then increases slowly before decreasing at higher energies. Since $(r_e - a)$ and

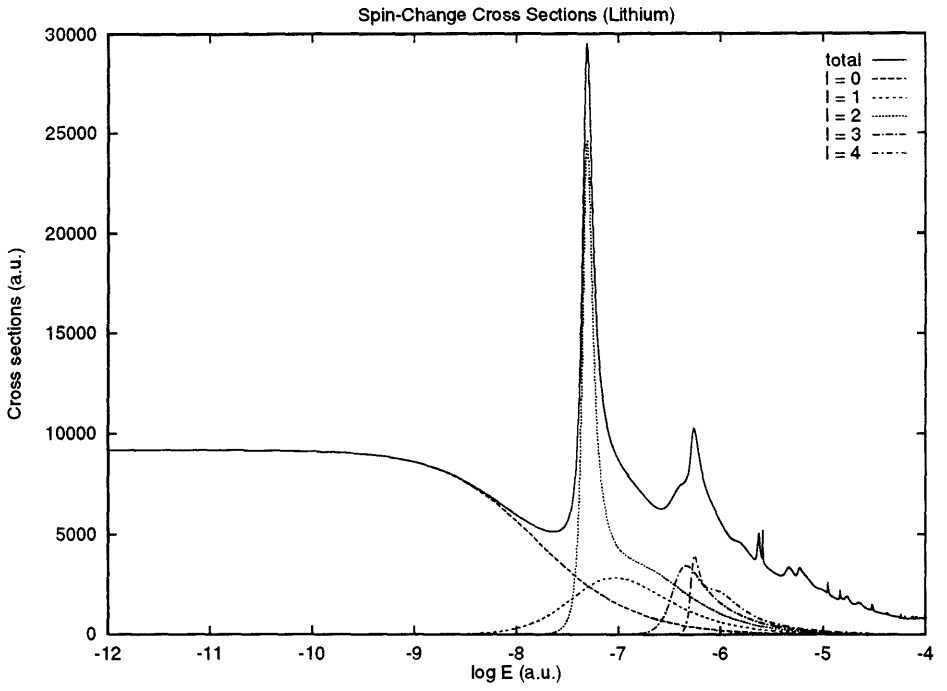

Figure 2.14: Total and partial spin-change cross sections for ^{7}Li.

a are positive, we can explain this behaviour. The s-wave cross section tends to decrease with increasing energy but the decrease is overcome by higher partial waves contributions. Oscillations occur through the addition of a small number of partial waves, and sharper structures are due to shape resonances. The most prominent is the f-wave resonance corresponding to a quasi-bound state trapped by the $l = 3$ centrifugal barrier. A second resonance is found for $l = 7$. Both position in the energy spectrum and width of these resonances are given in Table 2.16. However, the rather big contribution of the partial wave $l = 4$ is due the a quasi shape resonance around $\log_{10} E = -6.7$ as shown in Fig. 2.16. In fact, in this case, $\delta_4^S(k)$ gets very near $\pi/2$ but does not quite go through it: the potential is almost deep enough to get a quasi bound state, but not quite enough.

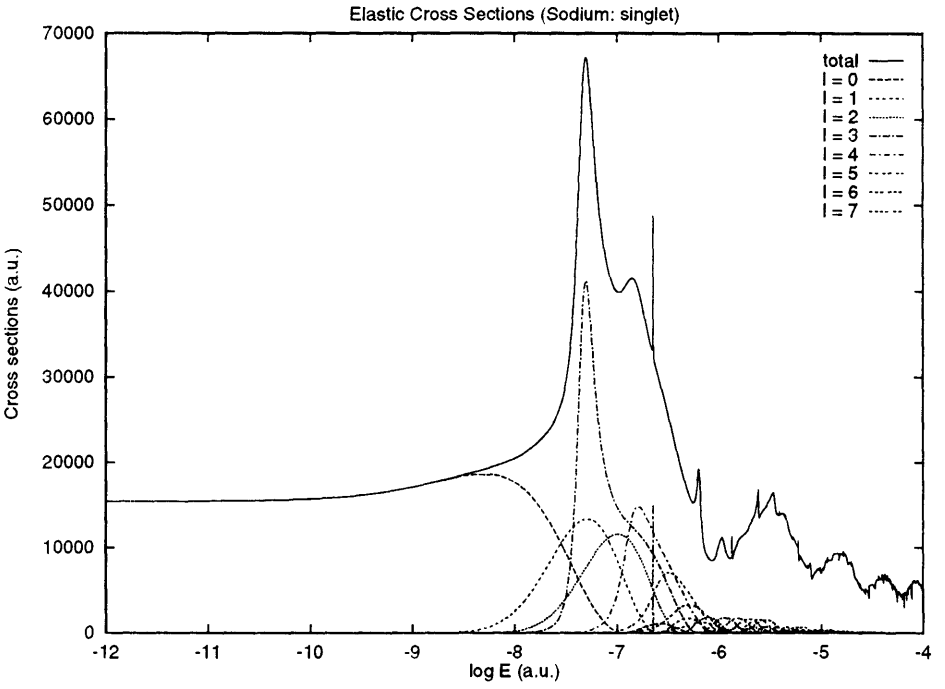

Figure 2.15: Total and partial elastic cross sections for $X^1\Sigma_g^+$ of ^{23}Na.

State	l	long-range potential	$\log_{10} E_\Gamma$	E_Γ ($\times 10^{-9}$ a.u.)	Γ ($\times 10^{-10}$ a.u.)
$X^1\Sigma_g^+$	3	no retardation	-7.303	49.77	161.5
		with Casimir	-7.302	49.89	164.4
	7	no retardation	-6.6454	226.26	3.402
		with Casimir	-6.6450	226.46	3.416
$a^3\Sigma_u^+$	6	no retardation	-6.6571	220.24	54.90
		with Casimir	-6.6568	220.39	55.10

Table 2.16: Resonance energies and widths for ^{23}Na.

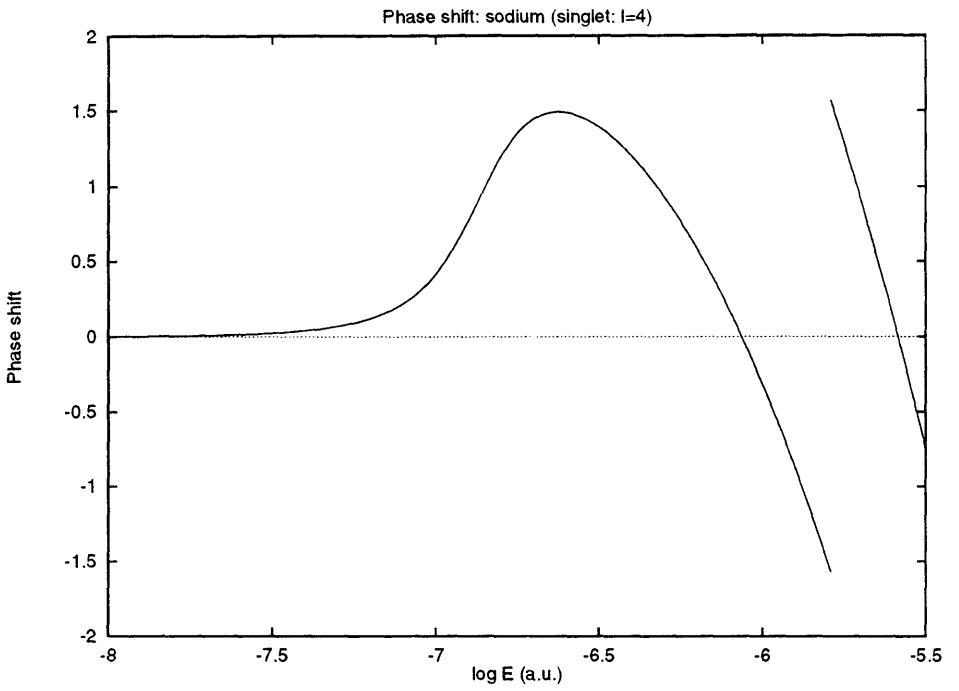

Figure 2.16: Phase shift for the $l = 4$ partial wave for $X^1\Sigma_g^+$ of ^{23}Na.

We illustrate in Fig. 2.17 the similar calculations for the $a^3\Sigma_u^+$ state. The same general features are found in this case, The s-wave cross section tends to decrease with increasing energy but the decrease is overcome by higher partial waves contributions. We do not observe the small increase in the s-wave cross section before the decrease in this case because $(r_e - a)$ is negative while a is positive. A small resonance appears in the $l = 6$ partial wave. Its position and width are given in Table 2.16. Here also, the important contribution from the $l = 2$ partial wave is due to a quasi shape resonance around $\log_{10} E = -7.5$.

The spin-change cross section is shown in Fig. 2.18. The contribution of both the singlet and triplet resonances are visible, and the same general description is valid.

Before analysing the results for the Casimir corrections, we can point out that the

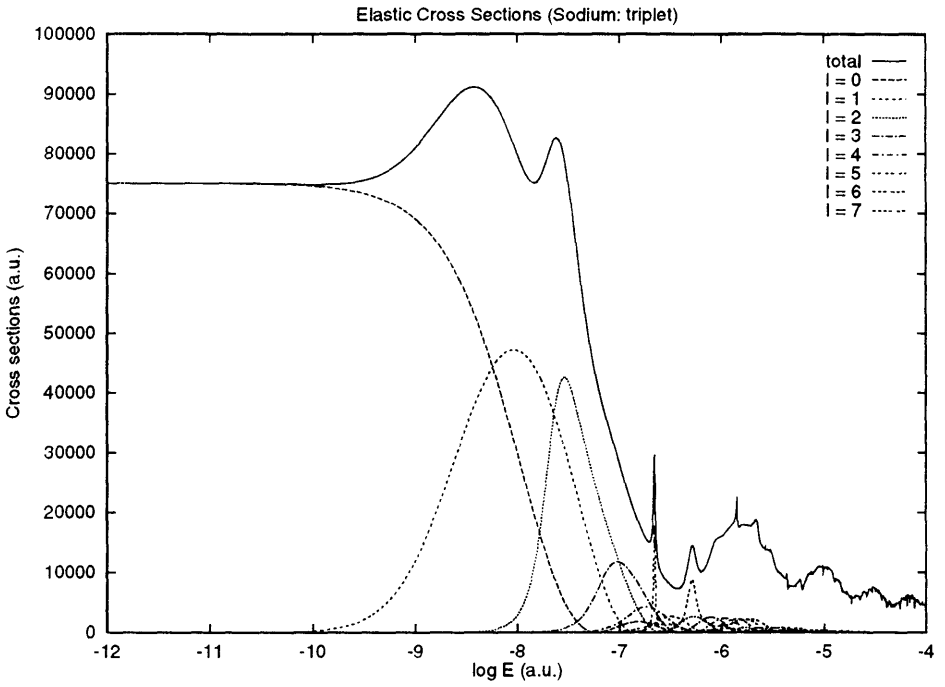

Figure 2.17: Total and partial elastic cross sections for $a^3\Sigma_u^+$ of ^{23}Na.

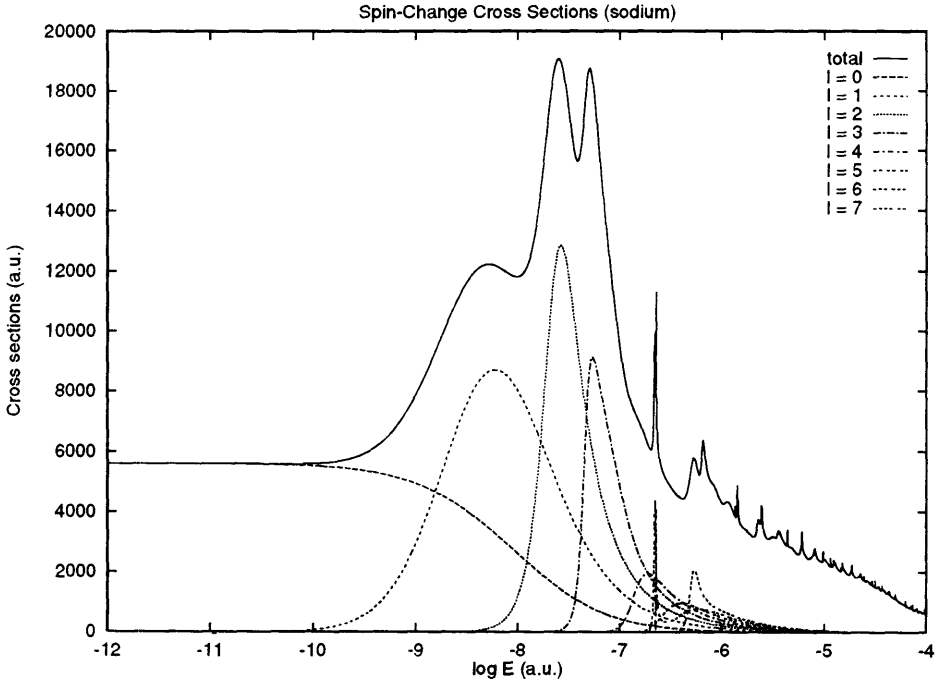

Figure 2.18: Total and partial spin-change cross sections for ^{23}Na.

elastic cross sections $\sigma_{\rm elas}$ are much bigger than what we could expect from a classical argument. In fact, from the expression for the cross section at low energy, we would have semi-classiclally

$$\sigma_{\rm elas} = 4\pi a^2 \rightarrow 4\pi \langle r^2 \rangle \ , \tag{2.48}$$

where $\langle r^2 \rangle$ is the atomic size. From Table 2.9, we can see that a^2 is much bigger than $\langle r^2 \rangle$ for all cases: $\langle r^2 \rangle = 17.74\ a_0^2$ compared to $a^2 = 1363.43$ and $294.50\ a_0^2$ for $X^1\Sigma_g^+$ and $a^3\Sigma_u^+$ of ^{7}Li respectively, and $\langle r^2 \rangle = 20.70\ a_0^2$ compared to $a^2 = 1224.66$ and $5973.14\ a_0^2$ for $X^1\Sigma_g^+$ and $a^3\Sigma_u^+$ of ^{23}Na respectively. These big differences indicate the role played by the long-range interactions in ultra-cold collisions. Indeed, the fact that particles do feel each other from a very large distance due to their relative slow speed can be seen as extending the average radius of the wave function far out. Moreover, those effects are responsible for the large spin-change cross sections calculated, hence the large spin-change rate coefficients computed (see §2.3 and Table 2.17). Also, the much bigger spin-change cross section of ^{7}Li compared to ^{23}Na is due in part to the sign of the triplet scattering length. For ^{7}Li it is negative, and thus the difference between the singlet and triplet scattering lengths $(a_T - a_S)$ is bigger than for ^{23}Na for which both are positive.

Let us now see how the Casimir corrections change the previous results in the case of ^{23}Na.

2.2.6 Effects of Casimir corrections

In this section, we will examine the way the previous results are affected by taking into account the retardation effects. We performed the calculations for the ^{23}Na atom only, because the corrections are stronger than in the case of the ^{7}Li atom.

First, the effect of Casimir corrections over the dissociation energies is negligible as one can see in Table 2.8. In fact, the changes occur on the fourth number after the decimal point, which is far beyond the RKR precision for the potential curves.

The correction to first order in perturbation theory for the bound levels of the $l = 0$ potentials are listed in Table 2.13 for the $X^1\Sigma_g^+$ state, and Table 2.14 for the $a^3\Sigma_u^+$ state. They are obtained simply by defining the Casimir "perturbation" by

$$\Delta \equiv V_{\text{Casimir}} - V_{\text{normal}} \,. \tag{2.49}$$

Then the correction is simply given by

$$\Delta E_v = \frac{\langle \psi_v^{(0)} | \Delta | \psi_v^{(0)} \rangle}{\langle \psi_v^{(0)} | \psi_v^{(0)} \rangle} \,, \tag{2.50}$$

where $\psi_v^{(0)}$ is the wave function of the vibrational level v for the normal potential (*i.e.* without Casimir corrections). As expected, all levels are sligthly shifted upward. We notice that for the lower vibrational levels, there are basically no difference, the correction being 10^{-6} times the energy value. Even for the highest levels, this correction is still small, of the order of one part in a thousand.

As one might suspect, the modification in the values of the scattering lengths and effective ranges due to the Casimir corrections are not very important: 0.17% for a

and 5.3% for r_e for the singlet, and 0.085% for a and 2.88% for r_e for the triplet (see Table 2.10). Even if Eq. (2.43) is not valid here, it is helpful to interpret those results. The Casimir corrections lift the last bound state levels (*i.e.* bring them closer to the dissociation limit), and accordingly, reduce the scattering length. Similarly, by having a potential going to zero at a faster rate, these cause the effective range to become smaller.

Finally, the effect of the Casimir corrections on the shape resonances can also be seen in Table 2.16. They move the resonances by very small amounts and change the width Γ by little. The same heuristic explanation can be used to describe those changes: the energies of the resonances are moved upward (*i.e.* more positive) and the potential decreasing faster at large distances implies a wider centrifugal barrier. This larger barrier means a bigger distance for the particle to tunnel through, hence a longer time delay. This in turn would mean a smaller width Γ. But we observe the inverse effect. This can be explained by the fact that the energy being lifted, it corresponds to a narrower centrifugal barrier which is only partly conterbalanced by the increase due to the faster decrease of the tail of the potential. Of course, those two effects being opposite, the exact analysis is more complicated than this simple picture.

2.3 Temperature dependence

In order to calculate rates which are physically measurable, we must average the previous results over kinetic energies, since the temperature and hence the energy of

the cold collision experiments are distributed over a given range.

We assume the velocity distribution is Maxwellian characterized by a kinetic temperature T, and we define mean elastic and spin-change cross sections by

$$\overline{\sigma}(T) = (k_B T)^2 \int_0^\infty dE\, E\, \sigma(E) \exp(-E/k_B T) \; . \tag{2.51}$$

The corresponding spin-change rate coefficients are given by

$$\mathcal{R} = \left(\frac{8 k_B T}{\pi \mu} \right)^{1/2} \overline{\sigma}_{sc}(T) \; . \tag{2.52}$$

For the ^{7}Li collisions, values of the mean cross sections in units of a_0^2 are shown in Fig. 2.19 for T up to 10 K and values of the spin-change rate coefficient in $cm^3 s^{-1}$ are listed in Table 2.17 also for T up to 10 K. The cross sections are large and basically constant at low temperatures, where only few partial waves are necessary. At higher temperatures where many partial waves contribute, the predictions are more reliable. The influence of higher partial waves begins to become evident at temperature as low as 10 mK.

In the case of ^{23}Na, the same data are presented in Fig. 2.20 for T up to 10 K and values of the spin-change rate coefficient in $cm^3 s^{-1}$ are listed in Table 2.17 also for T up to 10 K. The same general interpretation arizes from those graphs and tables, although the influence of higher partial waves begins to become evident at temperature as low 1 mK for the triplet and 10 mK for the singlet and the spin-change cases, as shown in Fig. 2.20.

Before ending the analysis of the lithium and sodium cold collisions, let us explore

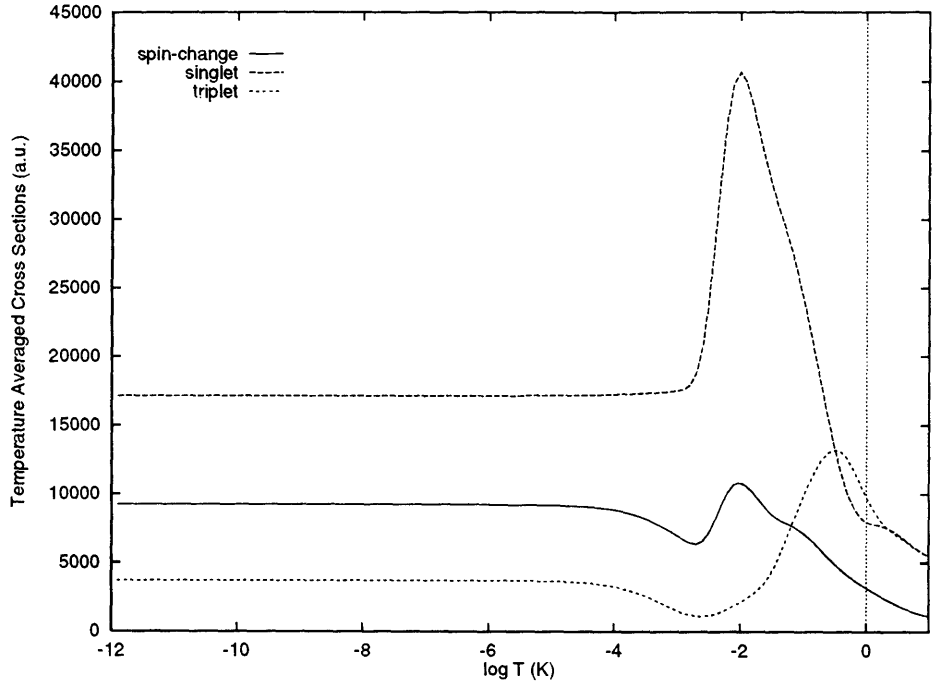

Figure 2.19: Temperature averaged total cross sections for ^{7}Li.

$\log_{10} T(K)$	$\mathcal{R}$ ($\mathrm{cm^3 s^{-1}}$)	
	^{7}Li	^{23}Na
-6	2.0 (-12)	6.7 (-13)
-5	6.3 (-12)	2.1 (-12)
-4	1.9 (-11)	8.2 (-12)
-3	4.8 (-11)	4.4 (-11)
-2	2.4 (-10)	1.7 (-10)
-1	4.9 (-10)	2.1 (-10)
0	6.9 (-10)	3.5 (-10)
1	7.7 (-10)	4.6 (-10)

Table 2.17: Spin-change rate coefficients.

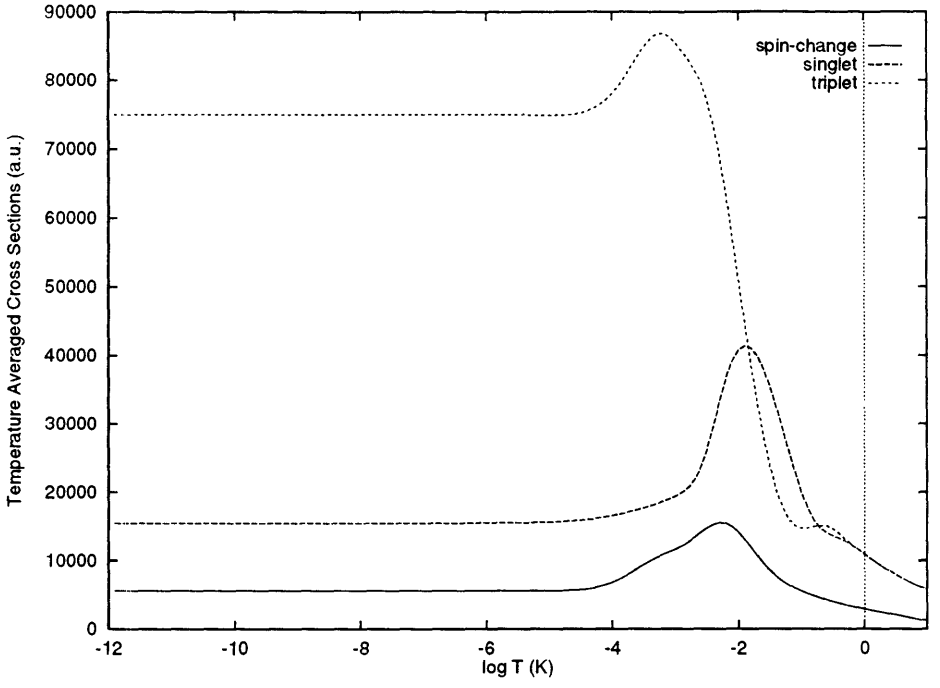

Figure 2.20: Temperature averaged total cross sections for ^{23}Na.

the sensitivity of some of the previous results to the form of the long-range potential, and to the isotopic effect.

2.4 Sensitivity analysis

As we mentioned earlier, the cross sections and the scattering lengths are very sensitive to the location of the last bound state of a potential curve. In order to demonstrate this, we used the same potential data, but a different reduced mass.

More precisely, we took the same potential curves for the $X^1\Sigma_g^+$ and $a^3\Sigma_u^+$ states of ^{7}Li, but used the reduced mass of ^{6}Li (see Table 2.9). As can be seen from Table 2.18, the energy levels are quite affected by this isotopic change. For $X^1\Sigma_g^+$, we find 39 bound levels for ^{6}Li instead of 42 for ^{7}Li, and 10 levels for ^{6}Li instead of 11 for ^{7}Li

in the case of the $a^3\Sigma_u^+$ state (see Table 2.19). Moreover, the position in respect to the dissociation energy is quite different than for ^{7}Li. This should give totally different results according to our previous analysis of the link between bound states and the scattering lengths. Notice that in the case of the $a^3\Sigma_u^+$ state, we also compare our results to the experimental values for ^{6}Li.

We performed the calculations for the $l = 0$ partial wave function and obtained the phase shift δ_0 for both the $X^1\Sigma_g^+$ and $a^3\Sigma_u^+$ states of ^{6}Li. The scattering lengths vary significantly from the ^{7}Li case, as can be seen from Table 2.20. The singlet a is still positive, but a bit bigger ($48.26a_0$ comparatively to $36.92a_0$ for ^{7}Li). The strongest change takes place for the triplet a. We get $-312.2a_0$ instead of the $-17.2a_0$ value obtained for ^{7}Li. This is to be expected from the energy levels. In fact, we can see that the last level for ^{6}Li is deeper than for ^{7}Li, and thus the next level (which would appear if the well was deeper) is closer to the dissociation limit for ^{6}Li than for ^{7}Li.

A second set of potentials was used to demonstrate the sensitivity of the cross sections. For $V_g(r)$ and $V_g(r)$ of ^{7}Li, we used the *ab initio* calculations and the long-range extrapolation of Konowalow and Fish [43], Konowalow and Olson [30], and Konowalow, Regan and Rosenkrantz [33], which has the form

$$V_{g,u}(r) = -\frac{1390}{r^6} - \frac{1.2 \times 10^5}{r^8} \mp 46.5 \exp(-0.997r) \ .$$

The scattering lengths that we computed for ^{7}Li using those potentials are quite different both in magnitude and sign from those obtained using our hybrid potential (see Table 2.20). We found $-0.2a_0$ and $1720a_0$ for the $X^1\Sigma_g^+$ and $a^3\Sigma_u^+$ states of ^{7}Li

v	^{7}Li	^{6}Li	v	^{7}Li	^{6}Li
0	174.9787	188.9222	21	6246.6143	6613.4006
1	521.2205	562.4108	22	6462.7531	6831.2667
2	862.2253	929.7838	23	6670.9251	7038.4630
3	1197.9469	1290.9889	24	6870.3348	7235.1105
4	1528.3481	1645.9687	25	7060.9622	7420.0779
5	1853.3833	1994.6645	26	7242.1159	7593.1134
6	2172.9640	2336.9580	27	7413.4889	7753.3842
7	2487.0308	2672.7413	28	7574.4980	7900.1431
8	2795.4231	3001.7791	29	7724.7060	8032.7646
9	3097.9413	3323.9323	30	7863.4155	8150.3101
10	3394.5732	3639.5817	31	7990.1590	8251.9955
11	3685.8532	3949.1084	32	8104.2697	8337.0286
12	3971.8652	4251.2391	33	8205.0430	8404.8301
13	4251.1436	4545.4026	34	8291.8688	8455.1099
14	4523.8373	4833.0255	35	8364.1532	8488.4931
15	4791.0078	5112.6187	36	8421.5251	8507.0488
16	5051.1070	5384.4034	37	8463.9218	8514.8047
17	5304.7937	5647.8620	38	8492.0818	8516.5729
18	5551.3130	5902.4730	39	8507.9264	
19	5790.2832	6148.8515	40	8514.7986	
20	6022.1967	6385.9805	41	8516.5409	

Table 2.18: Energies of $X^1\Sigma_g^+$ vibrational levels for ^{7}Li and ^{6}Li in cm^{-1}.

v	^{7}Li	^{6}Li		v	^{7}Li	^{6}Li	
	Theory	Theory	Exp. [32]		Theory	Theory	Exp. [32]
0	31.8235	34.3128	34.448	6	287.7226	299.1732	299.224
1	90.4695	97.0759	97.164	7	308.1986	317.3494	317.435
2	142.5769	152.2404	152.293	8	322.1335	328.0802	
3	188.3290	200.0064	200.035	9	330.0006	332.6308	
4	227.7518	240.4121	240.463	10	333.0137		
5	260.8849	273.4800	273.551				

Table 2.19: Energies of $a^3\Sigma_u^+$ vibrational levels for ^{7}Li and ^{6}Li in cm^{-1}.

Atom	potential	$X^1\Sigma_g^+$	$a^3\Sigma_u^+$
^{7}Li	hybrid	36.92	-17.2
^{6}Li	hybrid	48.26	-312.2
^{7}Li	Konowalow	-0.2	1720

Table 2.20: Scattering lengths for different potentials in a_0.

respectively. Once again, this is to be expected when looking at the energy levels listed in Table 2.21 and Table 2.22. The levels are quite different than those from the original potentials (see §2.2.3): for the $X^1\Sigma_g^+$ state we have one less level than previously, and for $a^3\Sigma_u^+$ the last one is quite displaced. Finally, notice that the $l = 2$ and $l = 4$ energy levels for the $X^1\Sigma_g^+$ and $a^3\Sigma_u^+$ states (respectively) are also given in those tables (for our hybrid potential). The last "level" is the resonance energy E_R (see Table 2.15), *i.e.* the bound energy that would exist if the centrifugal barrier would not decrease.

This ends the analysis of the lithium and sodium cold collisions. Let us now look at semi-classical ways to explain some of the features encountered in this section.

v	hybrid ($l=0$)	Konowalow ($l=0$)	hybrid ($l=2$)	v	hybrid ($l=0$)	Konowalow ($l=0$)	hybrid ($l=2$)
0	-3.8007(-2)	-3.7017(-2)	-3.7989(-2)	21	-1.0343(-2)	-9.6743(-3)	-1.0329(-2)
1	-3.6430(-2)	-3.5454(-2)	-3.6412(-2)	22	-9.3581(-3)	-8.7099(-3)	-9.3444(-3)
2	-3.4876(-2)	-3.3915(-2)	-3.4858(-2)	23	-8.4096(-3)	-7.7845(-3)	-8.3962(-3)
3	-3.3346(-2)	-3.2400(-2)	-3.3329(-2)	24	-7.5010(-3)	-6.8998(-3)	-7.4880(-3)
4	-3.1841(-2)	-3.0909(-2)	-3.1823(-2)	25	-6.6325(-3)	-6.0579(-3)	-6.6198(-3)
5	-3.0360(-2)	-2.9442(-2)	-3.0343(-2)	26	-5.8071(-3)	-5.2610(-3)	-5.7948(-3)
6	-2.8904(-2)	-2.8000(-2)	-2.8887(-2)	27	-5.0262(-3)	-4.5109(-3)	-5.0144(-3)
7	-2.7473(-2)	-2.6582(-2)	-2.7456(-2)	28	-4.2926(-3)	-3.8096(-3)	-4.2813(-3)
8	-2.6068(-2)	-2.5190(-2)	-2.6051(-2)	29	-3.6082(-3)	-3.1598(-3)	-3.5974(-3)
9	-2.4689(-2)	-2.3824(-2)	-2.4673(-2)	30	-2.9762(-3)	-2.5643(-3)	-2.9660(-3)
10	-2.3338(-2)	-2.2483(-2)	-2.3321(-2)	31	-2.3987(-3)	-2.0265(-3)	-2.3891(-3)
11	-2.2011(-2)	-2.1170(-2)	-2.1994(-2)	32	-1.8788(-3)	-1.5493(-3)	-1.8698(-3)
12	-2.0707(-2)	-1.9884(-2)	-2.0691(-2)	33	-1.4196(-3)	-1.1349(-3)	-1.4114(-3)
13	-1.9435(-2)	-1.8626(-2)	-1.9419(-2)	34	-1.0240(-3)	-7.8372(-4)	-1.0166(-3)
14	-1.8192(-2)	-1.7397(-2)	-1.8177(-2)	35	-6.9468(-4)	-4.9459(-4)	-6.8816(-4)
15	-1.6975(-2)	-1.6197(-2)	-1.6960(-2)	36	-4.3327(-4)	-2.7483(-4)	-4.2772(-4)
16	-1.5790(-2)	-1.5028(-2)	-1.5775(-2)	37	-2.4010(-4)	-1.3815(-4)	-2.3558(-4)
17	-1.4634(-2)	-1.3891(-2)	-1.4619(-2)	38	-1.1180(-4)	-5.6032(-5)	-1.0837(-4)
18	-1.3511(-2)	-1.2785(-2)	-1.3496(-2)	39	-3.9602(-5)	-1.4796(-5)	-3.7240(-5)
19	-1.2422(-2)	-1.1713(-2)	-1.2408(-2)	40	-8.2897(-6)	-1.4124(-6)	-6.9408(-6)
20	-1.1365(-2)	-1.0676(-2)	-1.1351(-2)	41	-3.5145(-7)		5.7870(-8)

Table 2.21: Energies of $X^1\Sigma_g^+$ vibrational levels for ^{7}Li in Hartree.

v	hybrid ($l=0$)	Konowalow ($l=0$)	hybrid ($l=4$)	v	hybrid ($l=0$)	Konowalow ($l=0$)	hybrid ($l=4$)
0	-1.3741(-3)	-1.4026(-3)	-1.3498(-3)	6	-2.0810(-4)	-2.2489(-4)	-1.9472(-4)
1	-1.1069(-3)	-1.1326(-3)	-1.0843(-3)	7	-1.1481(-4)	-1.2863(-4)	-1.0368(-4)
2	-8.6943(-4)	-8.9364(-4)	-8.4861(-4)	8	-5.1315(-5)	-6.0845(-5)	-4.2809(-5)
3	-6.6097(-4)	-6.8378(-4)	-6.4189(-4)	9	-1.5470(-5)	-2.0264(-5)	-9.8454(-6)
4	-4.8135(-4)	-5.0267(-4)	-4.6406(-4)	10	-1.7405(-6)	-3.0691(-6)	5.5069(-7)
5	-3.3038(-4)	-3.4970(-4)	-3.1498(-4)				

Table 2.22: Energies of $a^3\Sigma_u^+$ vibrational levels for ^{7}Li in Hartree.

Chapter 3

Semi-classical results

In this chapter, we will outline some semi-classical methods and apply them to the previous cases, comparing the exact results to those approximate ones. More precisely, we will explore the Wentzel-Kramers-Brillouin or WKB approximation for the one-dimensional problem. From that starting point, we will summarize the LeRoy and Bernstein [53] method to find the high vibrational energy levels for a molecule. Using the WKB results, we also will follow the treatment of Gribakin and Flambaum [54] and obtain semi-classical expressions for the scattering length and number of bound levels. We then will expand this analysis in order to construct the zero-energy wave function and from there get the effective range (semi-classically). Finally, we will consider the difference in the behaviour of the quantum and classical wave functions as we lower the kinetic energy. This will give rise to a phenomenon called *quantum suppression* (or quantum reflection). Let us begin with the WKB and LeRoy–Bernstein methods.

3.1 WKB approximation and LeRoy–Bernstein method

At first, we will derive the WKB approximation and give its limitations. We then formulate the Bohr-Sommerfeld quantization rule, and from it give some general features regarding the number of bound states in an attractive potential well. Finally, we will elaborate on this question by studying the LeRoy–Bernstein method.

3.1.1 The WKB approximation

We are interested in the solution of the Schrödinger equation in the case of a central potential, which amounts to a one-dimensional problem. Let us look in detail at the s-wave case ($l = 0$), since we are looking at the low-energy regime. In that case, the time-independent Schrödinger equation is

$$\left[\frac{\hbar^2}{2m}\frac{d^2}{dr^2} + E - V(r)\right] u_0(r) = 0 \ , \tag{3.1}$$

where we parametrize the $l = 0$ wave function $u_0(r)$ by

$$u_0(r) \equiv A \exp\left(\frac{i}{\hbar} S(r)\right) \ . \tag{3.2}$$

Our differential equation then becomes

$$\frac{1}{2m}\left(\frac{d}{dr}S\right)^2 - \frac{i\hbar}{2m}\frac{d^2}{dr^2}S - [E - V(r)] = 0 \ . \tag{3.3}$$

Let us now expand the function S as a power series in $\hbar$

$$S = S_0 + \frac{\hbar}{i} S_1 + \frac{\hbar^2}{i^2} S_2 + \cdots \ . \tag{3.4}$$

The classical case corresponds to S_0 only (*i.e.* $\hbar \to 0$), and the WKB method obtains the first two terms in this expansion. Let us first find the classical limit S_0. Dropping the term with $\hbar$ in Eq. (3.3), and keeping only the first term in S, we get

$$\frac{1}{2m}\left(\frac{d}{dr}S_0\right)^2 = E - V(r) \ . \tag{3.5}$$

In this one-dimensional case, we can integrate directly to obtain

$$S_0 = \pm \int dr \sqrt{2m[E - V(r)]} \ , \tag{3.6}$$

in which case the wave function becomes

$$u_0(r) = A \exp\left(\frac{i}{\hbar}S_0(r)\right) = A \exp\left(\pm\frac{i}{\hbar}\int dr\, p(r)\right) \ , \tag{3.7}$$

where

$$p(r) \equiv \sqrt{2m[E - V(r)]} \ , \tag{3.8}$$

is the local momentum.

The omission of the $\hbar$ term in Eq. (3.3) is legitimate only in the case where the second term in Eq. (3.3) is much smaller than the first one, *i.e.*

$$\hbar \left|\frac{S''}{S'^2}\right| = \left|\frac{d}{dr}\left(\frac{\hbar}{S'}\right)\right| \ll 1 \ . \tag{3.9}$$

Since we have $S' = p$ to first order, we can rewrite the above condition in terms of the local wavelength $\lambda\!\!\!^{-}(r)$,

$$\left|\frac{d}{dr}\lambda\!\!\!^{-}(r)\right| \ll 1 \quad \text{where} \quad \lambda\!\!\!^{-}(r) \equiv \frac{\hbar}{p(r)} \ , \ \text{and} \ \ \lambda\!\!\!^{-}(r) = \frac{\lambda}{2\pi} \ , \tag{3.10}$$

provided that

$$\lambda\!\!\!^{-}(r) \neq \infty \ . \tag{3.11}$$

The first condition implies that the potential $V(r)$ must change slowly over a distance comparable to the wavelength. The second condition states that we must stay away from those points r_0 for which $V(r_0) = E$. These are the classical turning points: the velocity of a classical particle vanishes and changes sign at $r = r_0$, so that in classical mechanics the particles never go beyond a turning point.

Let us now find the second term in the expansion, namely S_1. Substituting $S = S_0 + \hbar S_1$ into Eq. (3.3), we obtain the following set of differential equations

$$\left.\begin{aligned} -S_0'^2 + 2m(E-V) &= 0 \\ S_0'' + 2S_0'S_1' &= 0 \end{aligned}\right\} . \tag{3.12}$$

The first of these equations gives the result (3.6) for S_0, while the second equation yields (for $E > V$)

$$S_1' = -\frac{S_0''}{2S_0'} = -\frac{1}{2}\frac{p'}{p} \Longrightarrow S_1 = -\frac{1}{2}\ln p(r) , \tag{3.13}$$

where we dropped the integration constant. Thus, for $E > V$, we find that in the WKB approximation the wave function has the form

$$u_0(r) = \frac{1}{\sqrt{p(r)}}\left\{A\exp\left(\frac{i}{\hbar}\int dr\, p(r)\right) + B\exp\left(-\frac{i}{\hbar}\int dr\, p(r)\right)\right\} . \tag{3.14}$$

The factor $1/\sqrt{p}$ in front of this expression can be interpreted in a simple fashion. In fact, the probability of finding the particle between r and $r + dr$ is given by $|u_0(r)|^2$, *i.e.* it is essentially proportional to $1/p$. This is exactly what one would expect classically: the time spent by a particle in a given interval dr is just the inverse of its speed (or momentum).

For the case $E < V$, (*i.e.* in the classically forbidden region), one obtains

$$u_0(r) = \frac{1}{\sqrt{\kappa(r)}} \left\{ A \exp\left(-\frac{1}{\hbar}\int dr\, \kappa(r)\right) + B \exp\left(\frac{1}{\hbar}\int dr\, \kappa(r)\right)\right\} \ , \tag{3.15}$$

where $\kappa(r) = \sqrt{2m|E - V(r)|}$. It is important to note that both wave functions are valid asymptotically, *i.e.* far from the turning points (in the WKB approximation). Thus, a key element in the WKB method is the connection across the turning point. Before elaborating on that issue, let us look at higher corrections.

In order to understand better the limitations of the WKB approximation, we will derive S_2. The differential equation reads to order $\hbar^2$

$$S_0' S_2' + \frac{1}{2} S_1'^2 + \frac{1}{2} S_1'' = 0 \ , \tag{3.16}$$

where we substitute the expressions for S_0 and S_1 to find

$$S_2' = \frac{p''}{4p^2} - \frac{3p'^2}{8p^3} \ . \tag{3.17}$$

Integrating by parts, we obtain

$$S_2 = \frac{p'}{4p^2} + \frac{1}{8}\int dr\, \frac{p'^2}{p^3} + C_2 \ , \tag{3.18}$$

where C_2 is an integration constant. The wave function can then be written (to first order in $\hbar$ with $\hbar \to 0$) as

$$\begin{aligned} u_0(r) &= \exp\left\{\frac{i}{\hbar} S_0 + S_1\right\}(1 - i\hbar S_2) \\ &= \frac{C}{\sqrt{p}} \left\{1 - \frac{i\hbar}{4}\frac{p'}{p^2} - \frac{i\hbar}{8}\int dr\, \frac{p'^2}{p^3}\right\} \exp\left(\frac{i}{\hbar}\int dr\, p(r)\right) \ . \end{aligned} \tag{3.19}$$

The imaginary correction terms in the factor in front of the exponential are equivalent to a correction (proportional to $\hbar$) in the phase of the wave function. The WKB

method is valid if those two terms are small when compared to unity. The condition for the first of them coincides with the previous condition (3.10). But in the second case, the integral vanishes if p'^2 tends to zero fast enough at distances characteristic of the problem.

Let us now come back to the connection problem between the two regions around the turning point. Since the condition on $\lambda(r)$ is not satisfied, we have to solve the Schrödinger equation near $r = r_0$. Assuming that the potential can be approximated by a linear function near that point, we write

$$E - V(r) = \alpha(r - r_0) \quad \text{for} \quad r \simeq r_0 \ , \tag{3.20}$$

and the Schrödinger equation now reads

$$\frac{d^2}{dy^2} u_0 + \frac{2m\alpha}{\hbar} y u_0 = 0 \ , \tag{3.21}$$

where we have set $y = r - r_0$. This equation may be integrated explicitly and leads to the connection formulae (see Goldberger and Watson [21])

$$A = -i \exp(i\pi/4) D \qquad \text{and} \qquad B = i \exp(-i\pi/4) D \ . \tag{3.22}$$

Hence, for $r > r_0$ the WKB wave function becomes

$$u_0^{WKB}(r) = \frac{2D}{\sqrt{p(r)}} \sin\left\{ \frac{\pi}{4} + \frac{1}{\hbar} \int_{r_0}^{r} dr' p(r') \right\} \ . \tag{3.23}$$

Notice that we can write $p(r) = \hbar\sqrt{k^2 - U(r)}$ where $E = \hbar^2 k^2 / 2m$ and $U = 2mV/\hbar^2$. When comparing this form with the exact asymptotic form (when $r \to \infty$) for u_0, namely

$$u_0^{WKB} \to \frac{2D}{\sqrt{\hbar k}} \sin\left\{ \frac{\pi}{4} + \frac{1}{\hbar} \int_{r_0}^{\infty} dr' [p(r') - \hbar k] + k(r - r_0) \right\} \tag{3.24}$$

and

$$u_0 \to A_0 \sin(kr + \delta_0) \ , \tag{3.25}$$

we conclude that the WKB phase shift is given by

$$\delta_0^{WKB} = \frac{\pi}{4} - kr_0 + \frac{1}{\hbar}\int_{r_0}^{\infty} dr'[p(r') - \hbar k] \ . \tag{3.26}$$

The above results can be generalized for the case $l > 0$. In fact, one then finds (see Joachain [19])

$$u_l^{WKB} = 2D\left(\frac{k^2}{G(r)}\right)^{1/4} \sin\left\{\frac{\pi}{4} + \int_{r_0}^{\infty} dr' G(r')^{1/2}\right\} \ , \tag{3.27}$$

where the function G is given by

$$G(r) \equiv k^2 - U(r) - \frac{(l+1/2)^2}{r^2} \ . \tag{3.28}$$

The phase shift is then

$$\delta_l^{WKB} = (l+1/2)\frac{\pi}{2} - kr_0 + \int_{r_0}^{\infty} dr'[G^{1/2}(r') - k] \ . \tag{3.29}$$

3.1.2 The Bohr-Sommerfeld quantization rule

Let us now assume that we have an attractive potential well with the classically accessible domain $a \leq r \leq b$. In classical mechanics, the particle would make a periodic motion with period T given by

$$T = 2m\int_a^b \frac{dr}{p(r)} \ . \tag{3.30}$$

Now, considering a point to the right of a, we have (from the WKB approximation)

$$\psi = \frac{C_1}{\sqrt{p}} \sin\left\{\frac{\pi}{4} + \frac{1}{\hbar}\int_a^r dr' p(r')\right\} \ , \tag{3.31}$$

and similarly, for a point to the left of b, we get

$$\psi = \frac{C_2}{\sqrt{p}} \sin\left\{\frac{\pi}{4} + \frac{1}{\hbar}\int_r^b dr' p(r')\right\} \ . \tag{3.32}$$

For both functions to be the same in the whole domain of r, the sum of their phases must be a multiple of π

$$\frac{1}{\hbar}\int_a^b dr' p(r') - \frac{\pi}{2} = n\pi \ , \tag{3.33}$$

together with $C_1 = (-1)^n C_2$. Thus, we obtain the *Bohr-Sommerfeld quantization rule*

$$\frac{1}{2\pi\hbar}\oint dr\, p(r) = n + \frac{1}{2} \ , \tag{3.34}$$

where $\oint dr\, p(r) = 2\int_a^b dr\, p(r)$ is taken over a complete period of the classical motion of the particle.

From this equation, one can explore the number of bound states for a given potential. For example, if we consider a potential with an inner repulsive wall and a long-range attractive tail that behaves like a power of r after a certain distance R, *i.e.*

$$V(r) \sim -\frac{\gamma}{r^\alpha} \qquad \text{for} \qquad r > R \quad , \quad (\gamma > 0) \ , \tag{3.35}$$

the outer turning point b near threshold (*i.e.* when $E \to 0$) will tend to ∞, while the inner one a will hardly depend on E

$$b(E) \simeq \left(\frac{\gamma}{|E|}\right)^{1/\alpha} \qquad \text{and} \qquad a(E) \simeq a_0 \ . \tag{3.36}$$

Then from the rule above, we have

$$\begin{aligned} n\pi + \frac{\pi}{2} &= \frac{1}{\hbar}\int_{a(E)}^{b(E)} dr\, p(r) \\ &= \frac{1}{\hbar}\int_{a_0}^{R} dr\, p(r) + \frac{1}{\hbar}\int_R^{b(E)} dr \sqrt{2m\left(\frac{\gamma}{r^\alpha} - |E|\right)} \ . \end{aligned} \tag{3.37}$$

The integral $\int_{a_0}^{R} dr\, p(r)$ converges to a constant for $E \to 0$. The second integral remains finite in the limit $E \to 0$ if the exponent α is greater than 2. Thus we have found a very important fact regarding the number of bound states in an attractive potential, namely that a potential that behaves as a power law at large distance

$$V(r) \to -\frac{\gamma}{r^{\alpha}} \tag{3.38}$$

will support a finite number of bound levels for $\alpha > 2$:

$$\begin{array}{lll} 0 < \alpha \leq 2\ , \quad n \text{ is not defined} & \Rightarrow & \text{support an infinite number of bound states ,} \\ \alpha > 2\ , \quad n \text{ is finite} & \Rightarrow & \text{support a finite number of bound states .} \end{array} \tag{3.39}$$

3.1.3 The LeRoy–Bernstein method

A more rigourous result can be obtained following the LeRoy and Bernstein ideas. For an attractive potential well with a bound level v of energy $E(v)$ whose two classical turning points are written as $R_1(v)$ and $R_2(v)$, the previous quantization rule becomes

$$v + \frac{1}{2} = \frac{\sqrt{2\mu}}{\pi\hbar} \int_{R_1(v)}^{R_2(v)} dr \sqrt{E(v) - V(r)}\ , \tag{3.40}$$

where $E(v) = V[R_1(v)] = V[R_2(v)]$. Although v is an integer, let us consider it as a continuous variable. Differentiation of (3.40) with respect to $E(v)$ yields

$$\frac{dv}{dE(v)} = \frac{\sqrt{\mu/2}}{\pi\hbar} \int_{R_1(v)}^{R_2(v)} \frac{1}{\sqrt{E(v) - V(r)}}\ . \tag{3.41}$$

Using the asymptotic approximation for the potential

$$V(r) = D - \frac{C_n}{r^n}\ , \tag{3.42}$$

where D is the dissociation limit of the potential, C_n is given by

$$E(v) = D - \frac{C_n}{[R_2(v)]^n} \,. \tag{3.43}$$

Changing the variable of integration to $y = R_2(v)/r$, Eq. (3.41) becomes

$$\frac{dv}{dE(v)} = \frac{\sqrt{\mu/2}}{\pi\hbar} \frac{C_n^{1/n}}{[D - E(v)]^{(1/2+1/n)}} \int_1^{R_2/R_1} dy\, y^{-2}(y^n - 1)^{-1/2} \,. \tag{3.44}$$

In the limit $R_2/R_1 \to \infty$ (or $R_1 \to 0$), the integral can be performed. This yields an approximate analytical expression for $dE(v)/dv$ near the dissociation limit

$$\frac{dE(v)}{dv} = K_n[D - E(v)]^{(n+2)/2n} \,, \tag{3.45}$$

where the coefficient K_n is given by

$$K_n = \hbar \left(\frac{2\pi}{\mu}\right)^{1/2} \frac{\Gamma(1 + 1/n)}{\Gamma(1/2 + 1/n)} \frac{n}{C_n^{1/n}} \,. \tag{3.46}$$

Integrating over v (with $n \neq 2$), we finally get the energy level in terms v

$$E(v) = D - [H_n(v_D - v)]^{2n/(n-2)} \,, \tag{3.47}$$

where $H_n = [(n-2)/2n]K_n$ and v_D is an integration constant. Of course, as we mentioned earlier, for $n > 2$ there is a finite number of bound levels and v_D takes on the physical significance of being the effective (noninteger) vibrational index at the dissociation limit, as long as the approximation of the potential by its asymptotic form is valid. The number of bound levels is given by the truncation of $v_D + 1$.

However, depending on how far out is $R_2(v)$, the approximation of the potential might not be good enough. In fact, as we saw before, one should include higher Van der Waals coefficients and write instead

$$V(r) = D - \sum_m \frac{C_m}{r^m} \,, \tag{3.48}$$

and over a short value of r, one can consider the previous expression for $V(r)$ as correct, provided that the n is seen as an "effective" or "local" power corresponding to a weighted average of the different m values [53]

$$n = \frac{\sum_m m(m+1)C_m/[R_2(v)]^{m+1}}{\sum_m mC_m/[R_2(v)]^{m+1}} - 1 \ . \tag{3.49}$$

Usually, applications of the LeRoy–Berstein method are based upon fitting experimental energies $E(v)$ (from RKR data for example) and yield values for the four quantities D, n, C_n and v_D. We applied the method in order to find the number of bound states in the case of the ^{7}Li singlet and triplet states. Since we already knew the Van der Waals coefficients with high precision, and the dissociation energies, we took our energy levels and assumed that the outer turning points $R_2(v)$ were not changed too much from the RKR published values. As a reference point, we selected the last available RKR level for both singlet and triplet and called it v^*. Using $m = 6, 8$ and 10, we calculated the "local" power n. From $R_2(v^*)$ published and $E(v^*)$ already computed, we found the value of the "local" C_n from

$$E(v^*) = D - \frac{C_n}{[R_2(v^*)]^n} \ . \tag{3.50}$$

Then we determined the value of v_D from

$$v_D = v + \frac{[D - E(v)]^{(n-2)/2n}}{H_n} \ . \tag{3.51}$$

If $v > v_D$ the energy would then be complex: this gives us a prescription to find the last bound level. As we can see from Table 3.1, the values of v_D obtained confirm our previous results, *i.e.* that the number of bound levels is 42 in the singlet case, and

State	v^*	$R_2(v^*)$	n	C_n	K_n	H_n	v	v_D
							37	41.726 471
							38	41.638 964
$X^1\Sigma_g^+$	40	23.885	6.333	4,409	0.035 7321	0.012 2238	39	41.551 445
							40	41.494 312
							41	41.506 819
							6	10.073 763
							7	10.300 785
$a^3\Sigma_u^+$	7	15.681	6.839	17,184	0.034 574	0.012 2316	8	10.482 492
							9	10.624 260
							10	10.749 866

Table 3.1: LeRoy–Bernstein method applied to ^{7}Li (all quantities are in a.u.).

11 for the triplet state. In fact, that number is just

$$N_D = [v_D] + 1 \ , \tag{3.52}$$

where $[x]$ means the truncation of x. We can also notice that v_D from the singlet is more stable around v^* than for the triplet case. This is to be expected, since $R_2(v^*)$ is much larger for the singlet than for the triplet, hence a better approximation of the potential by its "local" asymptotic form. This is obvious when comparing the values of n: n should tends to 6 as R_2 increases.

In order to be complete, we also computed the energy levels using v^* as a reference point for v_D, and all the previous variables. The results for the last bound states are given in Table 3.2. As we can observe, the energy levels obtained by the

	$X^1\Sigma_g^+$			$a^3\Sigma_u^+$	
v	exact	LeRoy–Bernstein	v	exact	LeRoy–Bernstein
37	8463.9218	8471.1362	6	287.7226	280.15687
38	8492.0818	8494.8242	7	308.1986	308.19784
39	8507.9264	8508.4830	8	322.1335	324.31090
40	8514.7986	8514.7985	9	330.0006	331.58336
41	8516.5409	8516.5462	10	333.0137	333.36685

Table 3.2: ^{7}Li vibrational energy levels from LeRoy–Bernstein method in cm^{-1}.

LeRoy–Bernstein method are much better in the case of the singlet state than for the triplet. Once again, the reason is linked to the larger value of R_2, although this reflects the limitations of the method on the asymptotic form of the potential.

3.2 Gribakin and Flambaum formulae

Following Gribakin and Flambaum [54], we will find an analytical expression for the scattering length. In order to do so, we solve the Schrödinger equation for zero-energy scattering particle, in which case we have

$$\frac{d^2\psi(r)}{dr^2} - U(r)\psi(r) = 0 \ , \qquad \text{where} \qquad U(r) = \frac{2m}{\hbar^2}V(r) \ , \tag{3.53}$$

with the boundary condition $\psi(0) = 0$. We consider the s-wave case only ($l = 0$). As we already know (see §1.5.2), the scattering length is given by the asymptotic

behaviour of $\psi(r)$

$$\psi(r) \sim C_1 r + C_2 \qquad \text{and} \qquad a = -\frac{C_2}{C_1} \; . \tag{3.54}$$

Now, assuming that the WKB approximation is valid within the potential well, we can write the previous result in the form

$$\psi(r) = \frac{C}{\sqrt{p_0(r)}} \cos\left(\frac{1}{\hbar}\int_{r_0}^{r} dr' p_0(r') - \frac{\pi}{4}\right) \quad \text{, for } \; r > r_0 \; , \tag{3.55}$$

where r_0 is the classical turning point and p_0 is the local zero-energy momentum

$$p_0 = \sqrt{-2mV(r)} \; . \tag{3.56}$$

At large distances, the potential varies as $-\alpha/r^n$ and the condition for the validity of the WKB approximation reads

$$r \ll \left(\frac{2\gamma}{n}\right)^{2/(n-2)} \quad , \qquad \text{where} \qquad \gamma \equiv \frac{1}{\hbar}\sqrt{2m\alpha} \; . \tag{3.57}$$

In the case of lithium, taking $n = 6$ and the value of C_6 from Table 2.4, we get for the right-hand side $37.5a_0$ (^{7}Li: $\gamma = 4213.3$ a.u.) and $36.1a_0$ (^{6}Li: $\gamma = 3901.2$ a.u.), and for sodium, we have $51.2a_0$ (^{23}Na: $\gamma = 7854.2$ a.u.). As the reduced mass increases, this condition is met farther and farther out. In fact, for cesium one gets a value of $117a_0$ ($\gamma = 4.12 \times 10^4$) (see Gribakin and Flambaum [54]). However, one can estimates that the potential curve takes its asymptotic form αr^{-n} at a shorter distance, in which case the differential equation becomes

$$\frac{d^2\psi(r)}{dr^2} + \frac{\gamma^2}{r^n}\psi(r) = 0 \; . \tag{3.58}$$

Hence, for massive systems, we can assume that we always can find a distance r^* for which the WKB approximation will still be valid in the region where the above

equation is also valid. We can then match both solutions at that point r^* and find an expression for the scattering length a.

Let us find the solution of Eq. (3.58). Defining a new function $\psi = \sqrt{r}\phi$ and a new variable x through

$$r = \left(\frac{2\gamma}{(n-2)x}\right)^{2/(n-2)} , \tag{3.59}$$

we can rewrite Eq. (3.58) into a Bessel equation (see O'Malley, Spruch and Rosenberg [23])

$$\frac{d^2\phi(x)}{dx^2} + \frac{1}{x}\frac{d\phi(x)}{dx} + \left[1 - \frac{1}{(n-2)^2x^2}\right]\phi(x) = 0 . \tag{3.60}$$

The general solution is given in terms of a combination of Bessel and Neumann functions. So, for $r > r^*$, the exact solution of the problem is given by

$$\psi_>(r) = \sqrt{r}\left[AJ_\nu(x) - BN_\nu(x)\right] , \tag{3.61}$$

where

$$\nu \equiv \frac{1}{n-2} \qquad \text{and} \qquad x \equiv 2\gamma\nu r^{-\frac{1}{2\nu}} . \tag{3.62}$$

Unless $n = 3$, ν is noninteger, in which case we have

$$N_\nu(x) = \cot(\pi\nu)J_\nu(x) - \frac{1}{\sin(\pi\nu)}J_{-\nu}(x) , \quad \text{for} \quad \nu \neq 0, 1, 2, \ldots . \tag{3.63}$$

For $n = 3$, $\nu = 1$ and we have to take the limit of the above expression

$$N_\nu(x) = \lim_{q\to\nu}\left[\cot(q\pi)J_q(x) - \frac{1}{\sin(q\pi)}J_{-q}(x)\right] , \quad \text{for} \quad \nu = 0, 1, 2, \ldots . \tag{3.64}$$

Assuming that $n > 3$, we can use Eq. (3.63) and the expansion of $J_\nu(x)$ for $r \to \infty$ (or $x \ll 1$)

$$J_{\pm\nu}(x) \simeq \frac{x^{\pm\nu}}{2^{\pm\nu}\Gamma(1 \pm \nu)} , \tag{3.65}$$

to obtain the asymptotic form of $\psi_>(r)$

$$\psi_>(r) = C_1 r + C_2 \ , \tag{3.66}$$

where

$$C_1 = \frac{B}{(\gamma\nu)^\nu} \frac{1}{\sin(\pi\nu)\Gamma(1-\nu)} \ , \tag{3.67}$$

$$C_2 = \frac{(\gamma\nu)^\nu}{\Gamma(1+\nu)}[A - B\cot(\pi\nu)] \ . \tag{3.68}$$

From this form one gets

$$a = -\frac{C_2}{C_1} = \cos(\pi\nu)(\gamma\nu)^{2\nu}\frac{\Gamma(1-\nu)}{\Gamma(1+\nu)}\left[1 - \frac{A}{B}\tan(\pi\nu)\right] \ . \tag{3.69}$$

To determine the constants A and B, we must match the analytical solution to the WKB solution at r^*. Since r^* has been chosen to satisfy the condition (3.57), we can assume that its value is not too large and that $x^* \gg 1$ (from the 2γ term in front of $r^{-\frac{1}{2\nu}}$) in which case we can use the expansion of $J_\nu(x)$ for large x to evaluate $\psi_>(r)$ near r^* (see Butkov [55])

$$J_{\pm\nu}(x) \simeq \sqrt{\frac{2}{\pi x}}\cos\left(x \mp \frac{\pi\nu}{2} - \frac{\pi}{4}\right) + \mathcal{O}\left(\frac{1}{x^{3/2}}\right) \quad \text{for} \quad x \gg 1 \ . \tag{3.70}$$

Then, we get for $r \simeq r^*$ (or $x \simeq x^*$)

$$\psi_>(r) \simeq \frac{r^{n/4}}{\sqrt{\pi\gamma\nu}}\left\{[A - B\cot(\pi\nu)]\cos\left(x - \frac{\pi\nu}{2} - \frac{\pi}{4}\right) + \frac{B}{\sin(\pi\nu)}\cos\left(x + \frac{\pi\nu}{2} - \frac{\pi}{4}\right)\right\} \ , \tag{3.71}$$

where ν and x are defined in terms of n, γ and r by Eq. (3.62). Taking the logarithmic derivative of the above expression, we find

$$\frac{1}{\psi_>(r)}\frac{d\psi_>(r)}{dr} \simeq \frac{n}{4}r^{-1} + \gamma r^{-n/2}\frac{\mathcal{A}\sin f_- + \mathcal{B}\sin f_+}{\mathcal{A}\cos f_- + \mathcal{B}\cos f_+} \ , \tag{3.72}$$

with

$$\left.\begin{array}{ll} \mathcal{A} \equiv A - B\cot(\pi\nu) & f_- \equiv x - \dfrac{\pi\nu}{2} - \dfrac{\pi}{4} \\ \text{and} & \\ \mathcal{B} \equiv \dfrac{B}{\sin(\pi\nu)} & f_+ \equiv x + \dfrac{\pi\nu}{2} - \dfrac{\pi}{4} \end{array}\right\} . \tag{3.73}$$

Doing the same thing for the wave function inside, *i.e.* the WKB approximation for $r \simeq r^*$, and taking into account the fact that we can use $V = -\alpha r^{-n}$ in p and dp/dr, we find

$$\frac{1}{\psi_<(r)}\frac{d\psi_<(r)}{dr} \simeq \frac{n}{4}r^{-1} - \gamma r^{-n/2}\tan[\phi(r) - \pi/4] \; . \tag{3.74}$$

Equating both derivatives at $r = r^*$, we get

$$\tan[\phi(r^*) - \pi/4] = -\frac{\mathcal{A}\sin f_- + \mathcal{B}\sin f_+}{\mathcal{A}\cos f_- + \mathcal{B}\cos f_+} \; . \tag{3.75}$$

Now, we can write

$$\begin{aligned} \phi(r^*) &= \frac{1}{\hbar}\int_{r_0}^{r^*} dr' p(r') \\ &= \frac{1}{\hbar}\int_{r_0}^{\infty} dr' p(r') - \frac{1}{\hbar}\int_{r^*}^{\infty} dr' \sqrt{2m\frac{\alpha}{r^n}} \\ &= \Phi - x^* \; , \end{aligned} \tag{3.76}$$

to finally find

$$\frac{A}{B} = \tan\left(\Phi - \frac{\pi\nu}{2}\right) \; , \qquad \text{with} \qquad \Phi \equiv \frac{1}{\hbar}\int_{r_0}^{\infty} dr' p(r') \; . \tag{3.77}$$

The scattering length is simply given by

$$a = \bar{a} f(\Phi) \; , \tag{3.78}$$

where

$$\bar{a} = \cos(\pi\nu)(\gamma\nu)^{2\nu}\frac{\Gamma(1-\nu)}{\Gamma(1+\nu)} \; , \tag{3.79}$$

$$f(\Phi) = \left[1 - \tan\left(\Phi - \frac{\pi\nu}{2}\right)\tan(\pi\nu)\right] \; . \tag{3.80}$$

From this equation, we can see that if Φ satisfies the condition

$$\Phi - \frac{\pi\nu}{2} = \frac{\pi}{2} + N\pi \ , \qquad \text{with} \qquad N = 1, 2, 3, \dots \ , \tag{3.81}$$

the scattering length becomes infinite. This corresponds to the appearance of the N^{th} bound state in the well. Therefore, the number of bound states in the well is simply given by

$$n_B = \left[\frac{\Phi}{\pi} - \frac{n-1}{2(n-2)}\right] + 1 \equiv [g(\Phi)] + 1 \ , \tag{3.82}$$

where [ ] means the integer part of the expression for $g(\Phi)$. Notice that this expression is very close to the one from LeRoy and Bernstein. In fact, taking $E \to 0$ in Eq. (3.40), which implies $R_1 = r_0$ and $R_2 \to \infty$, we get an expression for v_D in terms of Φ, namely

$$v_D + \frac{1}{2} = \frac{1}{\pi\hbar}\int_{r_0}^{\infty} dr\sqrt{-2\mu V(r)} = \frac{\Phi}{\pi} \ , \tag{3.83}$$

which gives

$$N_D = [v_D + 1] = \left[\frac{\Phi}{\pi} - \frac{1}{2}\right] + 1 \ . \tag{3.84}$$

As we can see, the bigger the power of the inverse distance long-range term (*i.e.* the shorter range the potential), the better is the agreement between the two numbers N_D and n_B. However, the Gribakin and Flambaum expression would not be valid anymore, since a larger n implies a smaller radius where both the WKB and the exact outside solution would have to overlap. Notice that the difference in those two expressions can be traced back to the Bohr-Sommerfeld quantization rule and the use of the WKB approximation. In fact, the LeRoy and Bernstein derivation is based entirely on it, contrary to Gribakin and Flambaum. So, the correction $(n-1)/(n-2)$ is a manifestation of the failure of the WKB approximation in the Bohr-Sommerfeld

State	potential	r_0	Φ	C_6	$f(\Phi)$	$\bar{a}$	a	a_{exact}
	^{7}Li hybrid	3.446	132.151 118 $= 42\pi + 0.204218$	1388	1.191	31.026	36.944	36.92
$X^1\Sigma_g^+$	^{6}Li hybrid	3.446	122.462 440 $= 38\pi + 2.981917$	1388	1.616	29.855	48.257	48.26
	^{7}Li Konowalow	3.480	130.344 837 $= 41\pi + 1.539531$	1390	−1.216	31.037	−37.732	−0.2
	^{7}Li hybrid	6.346	35.946 760 $= 11\pi + 1.389241$	1388	−0.546	31.026	−16.929	−17.2
$a^3\Sigma_u^+$	^{6}Li hybrid	6.346	33.284 115 $= 10\pi + 1.868189$	1388	−9.461	29.855	−282.447	−312.2
	^{7}Li Konowalow	6.278	35.448 723 $= 11\pi + 0.891204$	1390	0.456	31.037	14.142	1720.0
$X^1\Sigma_g^+$	^{23}Na hybrid	4.1183	207.895 737 $= 66\pi + 0.550615$	1472	0.841	42.361	36.616	34.935
$a^3\Sigma_u^+$	^{23}Na hybrid	7.996	49.978 718 $= 15\pi + 2.854827$	1472	1.808	42.361	76.580	77.286

Table 3.3: Gribakin–Flambaum formula applied to previous potentials.

quantization rule around the outer turning point. That is where the Gribakin and Flambaum method uses the exact solution, and therefore should lead to a better result. Notice that more rigorous derivations of the number of bound states exist for various types of potential (*e.g.*, see Dickinson and Bernstein [56]).

Using the formula of Gribakin and Flambaum with $n = 6$, we evaluated the scattering lengths for both the singlet and triplet states, for ^{7}Li–^{7}Li, ^{6}Li–^{6}Li and ^{23}Na–^{23}Na collisions. The results are given in Table 3.3, together with those for ^{6}Li and for the Konowalow potential for ^{7}Li. As we can see, the agreement with the

results of the previous chapter is quite remarkable (except maybe for the Konowalow potential for ^{7}Li). Similarly, the number of bound states predicted by Eq. (3.82) (n_B) confirms the previous results of LeRoy–Bernstein method (N_D) and of the direct calculation of those levels (n_{exact}) (see Table 3.4). The values obtained for the scattering lengths and the number of bound states are determined by the quantity Φ. For the cases considered in the previous chapter, *i.e.* ^{7}Li and ^{23}Na hybrid potentials for the $X^1\Sigma_g^+$ and $a^3\Sigma_u^+$ states, the Gribakin and Flambaum approximation gives results very close to those calculated from the full quantum treatment. For the ^{7}Li hybrid potential, $\Phi = 42\pi + 0.2042$ for the $X^1\Sigma_g^+$ state, which implies that the potential well is just deep enough to contain the last bound level but is far from acquiring another one. Then $\tan(\Phi - \pi/8)$ lies on the negative branch so that $f(\Phi) > 1$ and $a = \bar{a} f(\Phi)$ gives a scattering length larger than the average value $\bar{a} = 31.026 a_0$. For the $a^3\Sigma_u^+$ state, we get $\Phi = 11\pi + 1.3892$ which indicates that the potential well is close to accomodating a new bound state. Here $\tan(\Phi - \pi/8)$ lies on the positive branch, but far out, so that $f(\Phi) < 0$, hence a negative scattering length. In the case of the hybrid ^{23}Na potentials, $\Phi = 66\pi + 0.5506$ for the $X^1\Sigma_g^+$ state which means the the well is not deep enough to acquire a new bound level. Then $\tan(\Phi - \pi/8)$ lies on the positive branch, but not too far so that $f(\Phi) > 0$, hence a positive scattering length smaller than $\bar{a}$. For the $a^3\Sigma_u^+$ state, $\Phi = 15\pi + 2.8548$ which indicates that the potential can almost support a new bound level. Here, $\tan(\Phi - \pi/8)$ is on the negative branch and $f(\Phi) > 1$ which implies a bigger a than $\bar{a}$.

The same reasoning can be applied to the two other cases, namely the ^{6}Li hy-

State	potential	$g(\Phi)$	n_B	$v_D(\Phi)$	v_D	N_D	n_{exact}
	^{7}Li hybrid	41.440 005	42	41.565 005	41.506 819	42	42
$X^1\Sigma_g^+$	^{6}Li hybrid	38.324 174	39				39
	^{7}Li Konowalow	40.865 048	41				41
	^{7}Li hybrid	10.817 209	11	10.942 209	10.749 866	11	11
$a^3\Sigma_u^+$	^{6}Li hybrid	9.960 114	10				10
	^{7}Li Konowalow	10.658 679	11				11
$X^1\Sigma_g^+$	^{23}Na hybrid	65.550 266	66				66
$a^3\Sigma_u^+$	^{23}Na hybrid	15.283 720	16				16

Table 3.4: Gribakin–Flambaum formula and the number of bound states.

brid potentials, and the ^{7}Li Konowalow potentials. However, as is illustrated by the Konowalow potentials, the method fails when we are close to a zero-energy resonance or when the function $f(\Phi) \sim 0$. In fact, to get the values of -0.2 and $1720a_0$ for the $X^1\Sigma_g^+$ and $a^3\Sigma_u^+$ states, we would need

$$\Phi = \begin{cases} 41\pi + 1.1813 & , \text{ singlet} \\ 10\pi + 1.9819 & , \text{ triplet} \end{cases} .$$

In the case of $X^1\Sigma_g^+$, $\tan(\Phi - \pi/8) = \tan(\pi/4 + \Delta)$ is centered around $\pi/4$ with $\Delta = 0.0032$. A small variation of Δ makes a big difference for $f(\Phi)$ and even change its sign. This corresponds to the case where the potential is such that the scattering length is changing sign and therefore any small variation in Φ would have strong consequences. On the other hand, the $a^3\Sigma_u^+$ case corresponds to a zero-energy resonance. In fact, we can write $\tan(\Phi - \pi/8) = \tan(\pi/2 + \Delta)$ is centered around $\pi/2$ with $\Delta = 0.0184$. This is clearly very sensitive to any change in the value of Φ: it could go from $-\infty$ to $+\infty$. These two pathological cases can be summarized by $g(\Phi)$. In fact, we would then need

$$g(\Phi) = \begin{cases} 40.751 & , \text{ singlet} \\ 10.006 & , \text{ singlet} \end{cases} .$$

This in turn gives us the dangerous region where the method fails. In fact, when $g(\Phi) = m + 0.75$ [or $\Phi = \pi(m + 0.75 + 5/8)$] we have $f(\Phi) = 0$ and therefore a small error in Φ would have big consequences. Or when $g(\Phi) = m$ [or $\Phi = \pi(m + 5/8)$] we have a zero-energy resonance, and a small variation of Φ would have an enormous effect. For ^{6}Li, the very good result for $X^1\Sigma_g^+$ implies that we are far from those two cases, but for the $a^3\Sigma_u^+$ state, we are getting closer to a zero-energy resonance, hence a less precise estimate of a.

Although the scattering lengths are close to the ones obtained by calculating the phase shift as we lower the kinetic energy, some caution must be applied regarding this semi-classical formulation. In fact, it is highly dependent on the fact the there exists a substantial region where both the WKB and the exact asymptotic solutions are valid, so that a matching can be made. As one can expect, the greater is the reduced mass of the system, the bigger would be the overlap region. Moreover, as we just saw, if it happens that Φ is such that $f(\Phi) \sim 0$ or we are close to a zero-energy resonance, the method would give unreliable results.

3.3 The zero-energy wave function

In this section, we will expand the treatment of Gribakin and Flambaum, and construct the zero-energy wave function. We then will use it in order to calculate the effective range and compare the results obtained to the actual values found in chapter 2 for the case of sodium.

We consider here the s-wave case with $E = 0$. We already know the exact solution at large distances [see Eqs. (3.61) and (3.68)]. However, we want to normalize $\psi(r)$ in such a way that

$$\psi(r) \simeq C_1 r + C_2 \rightarrow 1 - \frac{r}{a} \,. \tag{3.85}$$

So one must divide the previous result by C_2 and write $\Psi = \psi / C_2$.

Now, we need to match the WKB solution at r^* with that exact one. From Eq.

(3.55) and Eq. (3.71), one must have

$$\Psi_{WKB}(r^*) = \Psi_>(r^*) \qquad \text{or} \qquad \frac{\psi_{WKB}(r^*)}{C_2} = \frac{\psi_>(r^*)}{C_2} \ , \tag{3.86}$$

which gives after some algebra

$$\frac{C}{C_2} = \frac{\sqrt{\hbar}}{\cos(\Phi - x^* - \pi/4)} \left\{ P \cos\left(x^* - \frac{\pi\nu}{2} - \frac{\pi}{4}\right) - \frac{Q}{a} \cos\left(x^* + \frac{\pi\nu}{2} - \frac{\pi}{4}\right) \right\} \ , \tag{3.87}$$

with

$$P \equiv \frac{\Gamma(1+\nu)}{\sqrt{\pi\nu}(\gamma\nu)^\nu} \qquad \text{and} \qquad Q \equiv \frac{\Gamma(1-\nu)(\gamma\nu)^\nu}{\sqrt{\pi\nu}} \ , \tag{3.88}$$

where we used the expressions for a and C_2 from the previous section, and also the fact that $\Phi = \phi(r^*) + x^*$ and $p_0(r^*) = \hbar\gamma[r^*]^{-n/2}$. Notice that the derivatives are already matched: it gave us the relationship between A and B.

The remaining problem to be addressed concerns itself with the region near the classical turning point r_0. As we mentioned before, the WKB approximation fails in that neighbourhood and the problem can be solved by approximating the potential by a linear function [see Eq. (3.20)]. So, by writing

$$\frac{2\mu}{\hbar^2} V(r) \simeq -\zeta(r - r_0) \ , \qquad \text{where} \qquad \zeta > 0 \ , \tag{3.89}$$

the Schrödinger equation near $r \simeq r_0$ takes the form

$$\left[\frac{d^2}{d\xi^2} + \xi\right] \psi(\xi) \ , \qquad \text{with} \qquad \xi \equiv \zeta^{1/3} \left(r - r_0 + \frac{k^2}{\zeta}\right) \ , \tag{3.90}$$

and the general solution can be expressed in terms of the Airy functions Ai and Bi

$$\psi(r) = D_1 \mathrm{Ai}(-\xi) + D_2 \mathrm{Bi}(-\xi) \ . \tag{3.91}$$

In our case, $k = 0$ so $\xi = \zeta^{1/3}(r - r_0)$, and for $r < r_0$, $\xi < 0$. Since we must have $\psi(0) = 0$ and $\mathrm{Bi}(|\xi|)$ grows very fast, we must have $D_2 = 0$. Therefore, near the turning point, we have the solution of the linear potential

$$\Psi_{\mathrm{lin}}(r) = D\mathrm{Ai}(-\xi) \ , \qquad \text{with} \qquad \xi = \zeta^{1/3}(r - r_0) \ . \tag{3.92}$$

The two unknown quantities D and ζ can be found by matching Ψ_{lin} with Ψ_{WKB} at some point r_P where the WKB result is valid. We then obtain

$$\Psi_{\mathrm{lin}}(r_P) = D\mathrm{Ai}(-\xi_P) = \Psi_{WKB}(r_P) \ , \tag{3.93}$$

$$\Psi'_{\mathrm{lin}}(r_P) = -D\zeta^{1/3}\mathrm{Ai}'(-\xi_P) = \Psi'_{WKB}(r_P) \ . \tag{3.94}$$

In principle, we can solve for D and ζ , though we get an implicit equation for ζ. To avoid this problem, we can choose r_P such that $\Psi'_{WKB} = 0$, *i.e.* at an extremum. From the previous matching conditions we then obtain

$$D = \frac{\Psi_{WKB}(r_P^{\mathrm{ext}})}{\mathrm{Ai}(r_P^{\mathrm{ext}})} \qquad \text{and} \qquad \zeta = \left(\frac{-z'_s}{r_P^{\mathrm{ext}} - r_0}\right)^3 \ , \tag{3.95}$$

where r_P^{ext} is the position of the extremum selected, and z'_s is the location of the s^{th} zero of Ai'. By counting the number of nodes of Ψ and knowing the number of bound states, we can determine at which s to make the fitting. We give the values of z'_s and of $\mathrm{Ai}(z'_s)$ for the first three extremum in Table 3.5.

We applied this matching procedure to the sodium case for the singlet and triplet states. The Fig. 3.1 illustrates the results obtained when we match at three different extrema. As we can see, one should not do the matching at the first extremum ($s = 1$), because its location is not very accurate: the WKB approximation fails in this region.

s	z_s	$\mathrm{Ai}'(z_s)$	z'_s	$\mathrm{Ai}(z'_s)$
1	−2.33810 741	+0.70121 082	−1.01879 297	+0.53565 666
2	−4.08794 944	−0.80311 137	−3.24819 758	−0.41901 548
3	−5.52055 983	+0.86520 403	−4.82009 921	+0.38040 794

Table 3.5: Zeroes of $\mathrm{Ai}(x)$ and of $\mathrm{Ai}'(x)$.

	$X^1\Sigma_g^+$	$a^3\Sigma_u^+$
s	$r_P^{\mathrm{ext}}(s)$ (a_0)	$r_P^{\mathrm{ext}}(s)$ (a_0)
1	4.1783	8.226
2	4.3983	8.936
3	4.5383	9.496

Table 3.6: Location of the extrema for ^{23}Na.

However, the results for the second and third are very close and in good agreement with the exact (numerical) wave function. We then selected the second extremum as the best possible case for matching: this corresponds to a smaller r than the third, hence the linear approximation to the potential remains valid. In Table 3.6, we give the location $r_P^{\mathrm{ext}}(s)$ of the s^{th} extremum. The position of the first one for $X^1\Sigma_g^+$ and $a^3\Sigma_u^+$ is not very accurate, as mentioned above.

So, using the second extremum as a matching point, we can construct the full

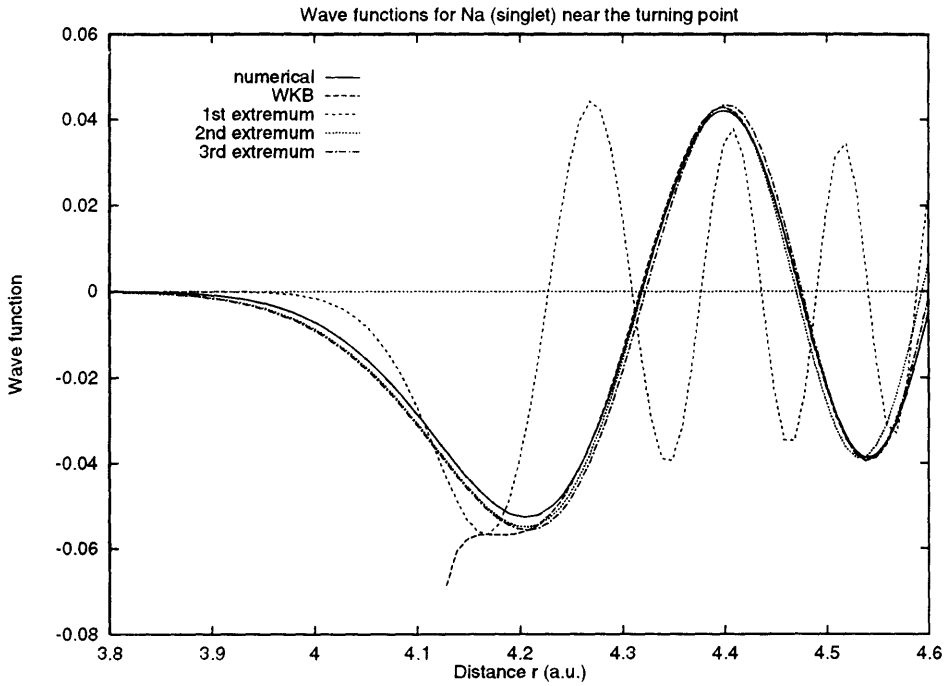

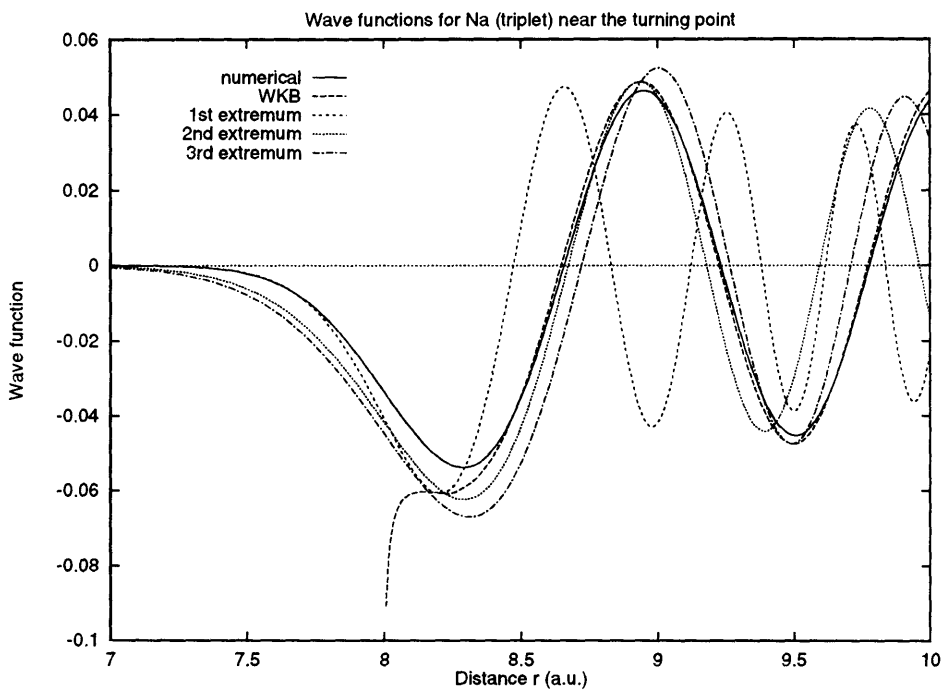

Figure 3.1: Matching at three different r_P^{ext} for both the singlet and then triplet states of ^{23}Na.

zero-energy wave function as

$$\Psi(r) = \begin{cases} \Psi_{\rm lin}(r) & , \quad r \leq r_p^{\rm ext} \\ \Psi_{WKB}(r) & , \quad r_p^{\rm ext} \leq r \leq r^* \\ \Psi_>(r) & , \quad r \geq r^* \end{cases} , \tag{3.96}$$

where the different components are normalized as mentioned above. The full wave functions are compared with the numerical ones for very small kinetic energies. As we can see from Fig. 3.2, the agreement is quite good.

Another way to check the validity of those zero-energy wave functions resides in the calculation of the effective range. In fact, r_e necessitates the wave function at all distances in order to be evaluated by its integral representation. Since we already have $\Psi(r)$ normalized so that its asymptotic form is $1 - r/a$, we can evaluate r_e easily

$$r_e = 2\int_0^\infty dr \left[\left(1 - \frac{r}{a}\right)^2 - \Psi^2(r)\right] . \tag{3.97}$$

In Table 3.7, we give the results obtained using the zero-energy wave function for both the singlet and triplet states of sodium, and compare them with the values obtained in chapter 2. Moreover, we notice that a big contribution comes from the tail of the wave function: as we integrate further out, the results converge slowly to the numerical results obtained in chapter 2. In this table, we stop the integration at $r = r_{\rm max}$ when $|(1 - r/a) - \Psi(r)| \leq \epsilon$. This illustrates well the accuracy of the zero-energy wave functions constructed here. They are exact at large distances, and in very good agreement with the numerical wave functions at distances far from the turning point. Near the turning point, the linear approximation of the potential gives a wave function a bit off the numerical one, but the difference is still small and located around the first lobe of the wave function.

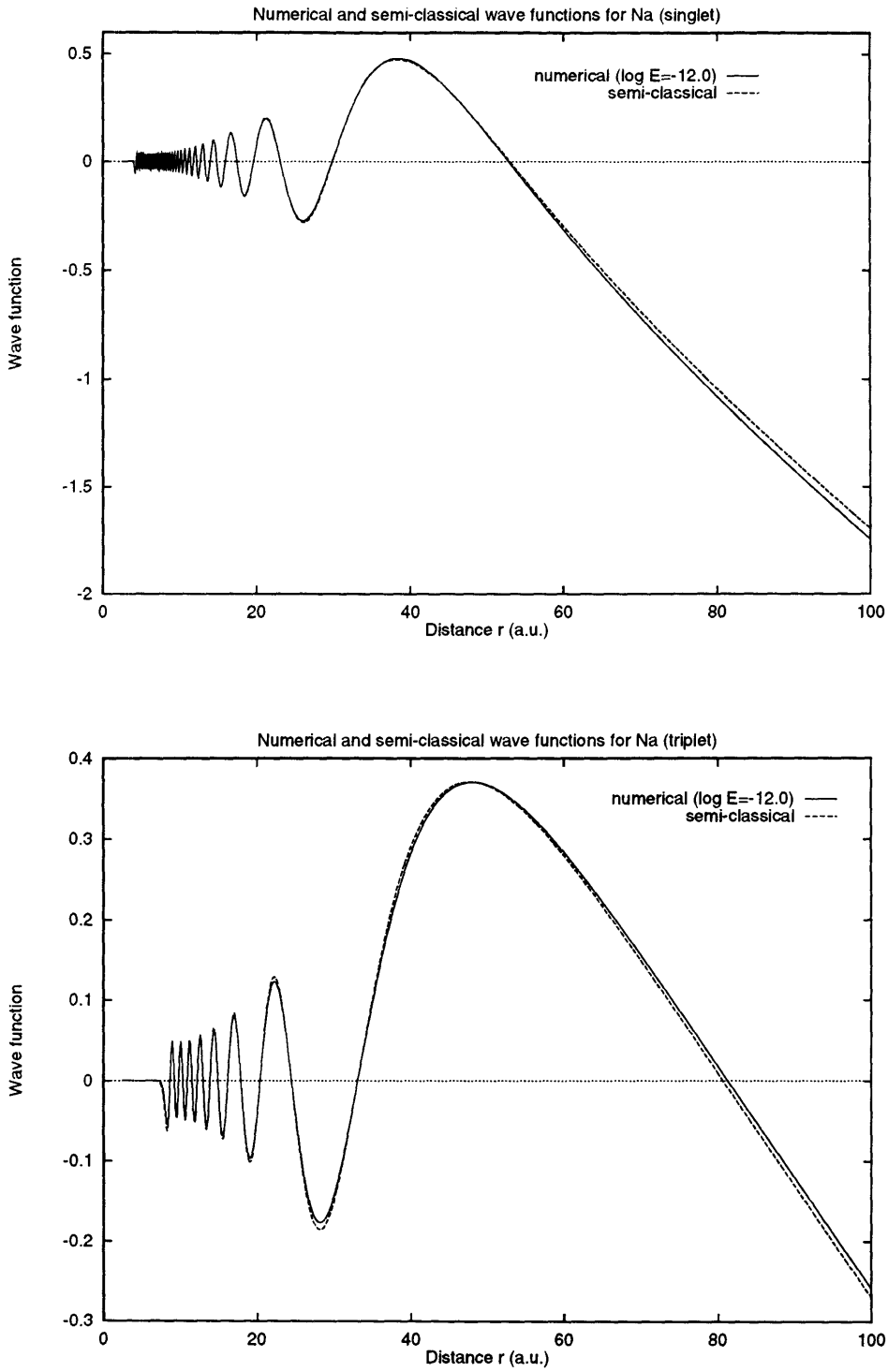

Figure 3.2: The semi-classical ($E = 0$) and numerical ($\log E = -12.0$) wave functions for $X^1\Sigma_g^+$ and $a^3\Sigma_u^+$ of ^{23}Na.

	^{23}Na $X^1\Sigma_g^+$		^{23}Na $a^3\Sigma_u^+$	
$\log_{10}\epsilon$	$r_{\max}$	r_e	$r_{\max}$	r_e
-1	104.3683	63.402	100.006	44.871
-2	235.8683	118.577	169.726	48.444
-3	517.2383	149.659	389.776	54.826
-4	1122.9183	165.231	859.716	58.683
-5	2427.6283	172.704	1870.846	60.663
-6	5238.4583	176.226	4048.716	61.624
-7	11294.1683	177.872	8740.576	62.078
exact		187.5		62.5

Table 3.7: Semi-classical effective ranges for ^{23}Na (in a.u.).

3.4 Quantum suppression

In this section, we will study the amplitude of the wave function as we lower the kinetic energy, for both the semi-classical and the quantum mechanical cases.

3.4.1 Suppression as a function of k

We first consider a particle striking a target in the classical regime. This target could be a rigid wall (surface sticking problem) or another atom (ultracold collision). In both cases, the problem can be reduced to a single particle *falling* in an attractive potential with a repulsive wall at short distances. The ratio of the probability density of being inside of the interaction well to the one of being outside corresponds in a

classical regime to the ratio of time spent in and out of the well (see Clougherty and Kohn [57])

$$K_{\text{class}} = \frac{\rho_{\text{in}}}{\rho_{\text{out}}} = \frac{t_{\text{in}}}{t_{\text{out}}} = \frac{v_\infty}{\overline{v}} = \left(\frac{E}{\overline{E}}\right)^{1/2} = \sqrt{\frac{E}{E+D_e}}\,, \tag{3.98}$$

where the speed at infinity is related to the kinetic energy through $E = \mu v_\infty^2/2$ with μ being the reduce mass (in the case of atom collision) or the particle mass (m) in the case of collision with a wall. Similarly, $\overline{E} \simeq \mu\overline{v}^2/2$ is a typical kinetic energy in the interaction region, chosen to be evaluated at the deepest part of the well (the equilibrium point R_e with value $-D_e$). Notice that this value corresponds to the dissociation energy.

The same result is obtained with a semi-classical treatment. From WKB, the wave function is given by

$$u_{WKB}(r) = \frac{C}{\sqrt{p}}\sin(\phi(r) + \pi/4)\,. \tag{3.99}$$

So, near the equilibrium point R_e of the potential, and far out, we have

$$u^{(\text{in})}_{WKB}(R_e) = \frac{C}{\sqrt{p_e}}\sin(\phi(R_e)+\pi/4) \quad , \quad u^{(\text{out})}_{WKB}(r) = \frac{C}{\sqrt{\hbar k}}\sin(kr+\eta_{WKB})\,. \tag{3.100}$$

We then obtain the semi-classical ratio by taking the amplitude ratio

$$K_{S.C.} = \frac{\rho_{\text{in}}}{\rho_{\text{out}}} = \frac{|u^{(\text{in})}_{WKB}|^2}{|u^{(\text{out})}_{WKB}|^2} = \frac{\hbar k}{p_e} = \sqrt{\frac{E}{E+D_e}} \simeq \frac{\hbar k}{\sqrt{2\mu D_e}}\left[1 - \frac{\hbar^2 k^2}{4\mu D_e} + \cdots\right]\,. \tag{3.101}$$

Let us now consider the same problem in the quantum regime. For an asymptotically vanishing potential, we have at large distances

$$\psi^{\text{out}}(r) \simeq \frac{\sin(kr+\eta)}{\sin(\eta)} \sim 1 - \frac{r}{a}\,. \tag{3.102}$$

Here, the normalization $A = 1/\sin\eta$ is chosen so that the asymptotic form (for $r \to \infty$) is simply $1 - r/a$ and that the effective range expansion is easily obtained. For small energies, one finds that the inside wave function becomes independent of k and goes to a constant $\psi_0^{\rm in}$. The quantum ratio is simply given by:

$$K_{Q.M.t} = \frac{\rho_{\rm in}}{\rho_{\rm out}} = \frac{|\psi^{\rm in}|^2}{|\psi^{\rm out}|^2} = |\psi_k^{\rm in}|^2 \sin^2\eta \ , \tag{3.103}$$

where $|\psi_k^{IN}|$ is evaluated in the vicinity of the equilibrium point R_e. For ultracold collision, only the s-wave ($l = 0$) contributes, and we can use the effective range theory for $k\cot\eta$ as given in §1.5.3 and §1.5.4. Taking the case of two neutral atoms interaction (for which the potential goes as αr^{-n} with $n = 6$), we can rewrite $K_{Q.M.}$ in the limit $k \to 0$ as

$$K_{Q.M.} \simeq |\psi_0^{\rm in}|^2 \sin^2\eta \simeq |\psi_0^{\rm in}|^2 \frac{k^2}{k^2 + \left(\frac{1}{a} - \frac{1}{2}r_e k^2\right)^2} \ , \tag{3.104}$$

$$\simeq a^2 |\psi_0^{\rm in}|^2 k^2 \left[1 + ak^2(r_e - a)\right] + \mathcal{O}(k^5) \ , \tag{3.105}$$

where a and r_e are the scattering length and the effective range respectively. For $n > 3$, the quantity $|\psi_0^{\rm in}|$ can be evaluated from Eq. (3.87). In fact, we have

$$\psi_0^{\rm in} \equiv \frac{1}{\sqrt{p_e}} \frac{C}{C_2} \ . \tag{3.106}$$

Using the expression for a and the equation (3.87) for C/C_2, we can rewrite $\psi_0^{\rm in}$ as

$$\psi_0^{\rm in} \simeq -\frac{\sqrt{\hbar}}{a} \frac{\Gamma(1-\nu)(\gamma\nu)^\nu}{\sqrt{\pi\nu}(2\mu D_e)^{1/4}} \frac{\sin(\pi\nu)}{\cos(\Phi - \pi\nu/2)} \ . \tag{3.107}$$

As mentioned before, the case $n = 3$ is quite peculiar because then $\nu = 1$ and the Gribakin and Flambaum scheme becomes ill-defined.

Comparing both treatments, we conclude that $K_{Q.M.} \ll K_{S.C.}$ as $k \to 0$ which implies that the particles come in the interaction region with a smaller probability quantum mechanically than classically. This quantum suppression effect can best be seen by comparing the two ratios at very low energies

$$\mathcal{R} \equiv \frac{K_{S.C.}}{K_{Q.M.}} \simeq \mathcal{R}_0 \frac{1}{k} \left[1 - k^2 \left(a(r_e - a) + \frac{\hbar^2}{4\mu D_e} \right) \right] , \tag{3.108}$$

with

$$\mathcal{R}_0 = \frac{\pi\nu}{(\gamma\nu)^{2\nu}[\Gamma(1-\nu)]^2} \frac{\cos^2(\Phi - \pi\nu/2)}{\sin^2(\pi\nu)} . \tag{3.109}$$

This relation can also be given in terms of the kinetic energy

$$\mathcal{R} \simeq \frac{\mathcal{R}_0}{\sqrt{2\mu}} \frac{\hbar}{\sqrt{E}} \left[1 - \frac{2\mu}{\hbar^2} \left(a(r_e - a) + \frac{\hbar^2}{4\mu D_e} \right) E \right] . \tag{3.110}$$

This form is valid for $n > 5$, although the leading term is good for $n > 3$. Notice that it compares well with the result of Clougherty and Kohn. Indeed, they found $\mathcal{R} \sim E^{-1/2}$ (see [57]).

Let us look at some realistic cases, namely the cold collisions of neutral alkali atoms in their ground states. More precisely, we consider the ^{7}Li–^{7}Li collision in its two possible ground states ($X^1\Sigma_g^+$ and $a^3\Sigma_u^+$) and similarly for the ^{23}Na–^{23}Na collision. In Table 3.8 we give the phase shift and the inside amplitude evaluated at the deepest point of the potential, *i.e.* the equilibrium point R_e for the four different cases as a function of the kinetic energy. We can compare these amplitudes with those obtained from the analytical expression (see Table 3.9). As one can see, they are in close agreement.

In Fig. 3.3 and Fig. 3.4, we compare the numerical ratio $\mathcal{R}$ with the analytical

	Li_2			
	$X^1\Sigma_g^+$		$a^3\Sigma_u^+$	
$\log_{10} E$	η	$\lvert\psi_E^{\text{in}}\rvert$	η	$\lvert\psi_E^{\text{in}}\rvert$
-9.0	-0.132 945	0.032 457 6	0.055 288	0.310 242 8
-10.0	-0.041 795	0.032 966 9	0.019 194	0.290 084 0
-11.0	-0.013 206	0.033 025 2	0.006 130	0.288 043 1
-12.0	-0.004 176	0.033 031 3	0.001 940	0.287 835 3

	Na_2			
	$X^1\Sigma_g^+$		$a^3\Sigma_u^+$	
$\log_{10} E$	η	$\lvert\psi_E^{\text{in}}\rvert$	η	$\lvert\psi_E^{\text{in}}\rvert$
-9.0	-0.240 411	0.029 065 6	-0.500 465	0.040 283 7
-10.0	-0.072 210	0.032 119 0	-0.158 352	0.044 769 2
-11.0	-0.022 644	0.032 565 3	-0.050 039	0.045 276 0
-12.0	-0.007 153	0.032 615 9	-0.015 822	0.045 329 7

Table 3.8: Phase shift and inner amplitude as a function of the kinetic energy.

	Li_2		Na_2	
	$2\mu = 12798.391$ $\alpha = 1388$ $\gamma = 4213.274$		$2\mu = 41907.7602$ $\alpha = 1472$ $\gamma = 7854.185$	
	$X^1\Sigma_g^+$	$a^3\Sigma_u^+$	$X^1\Sigma_g^+$	$a^3\Sigma_u^+$
a	36.9	-17.2	34.94	77.3
r_e	66.5	1014.8	187.5	62.5
D_e	38.8046×10^{-3}	1.519063×10^{-3}	27.438359×10^{-3}	793.1798×10^{-6}
Φ	$42\pi + 0.204218$	$11\pi + 1.389241$	$66\pi + 0.5506$	$15\pi + 2.8548$
$\lvert\psi_0^{\text{in}}\rvert$	0.03252	0.28852	0.0318	0.0455
$\mathcal{R}_0$	3.11314×10^{-2}	9.2125×10^{-3}	2.190993×10^{-2}	1.28207×10^{-2}

Table 3.9: Inner amplitude for zero-energy ($n = 6, \nu = 1/4$). All quantities are in atomic units.

expression (3.110) for both the lithium and the sodium atoms. The agreement is also quite good. As we can see from that figure, the suppression grows very fast as we lower the energy, being of the order of 100 at energies corresponding to ~ 1 μK. Notice that in those figures, the big values at higher energies (for example at $\log_{10} E = -7.0$ and -4.0 for ^{7}Li singlet and triplet respectively, and $\log_{10} E = -6.0$ and -8.0 for ^{23}Na singlet and triplet respectively) correspond to the an oscillation in the phase shift. In fact, for those values, $\eta \to 0$ but the energy is finite, hence a quantum result tending to zero which gives a big ratio.

3.4.2 Suppression as a function of r

Now, let us examine in detail how the WKB and the quantum wave functions compare to each other as a function of the distance, for a small kinetic energy.

In order to compare similar quantities, we will look at the amplitudes as a function of the distance r. First, the WKB amplitude is simply given by

$$A_{WKB} = \frac{C}{\sqrt{p}} \,. \tag{3.111}$$

Here, we want $A = 1$ at $r \to \infty$, so we must have $C = \sqrt{\hbar k}$. Therefore, the WKB amplitude normalized to unity is

$$A_{WKB} = \sqrt{\frac{\hbar k}{p}} = \left(\frac{k^2}{k^2 - U(r)}\right)^{1/4} \,. \tag{3.112}$$

Following Milne [58], we can write the quantum wave function in the form

$$\psi(r) = A(r)\sin[\phi(r) + \pi/4] \,, \tag{3.113}$$

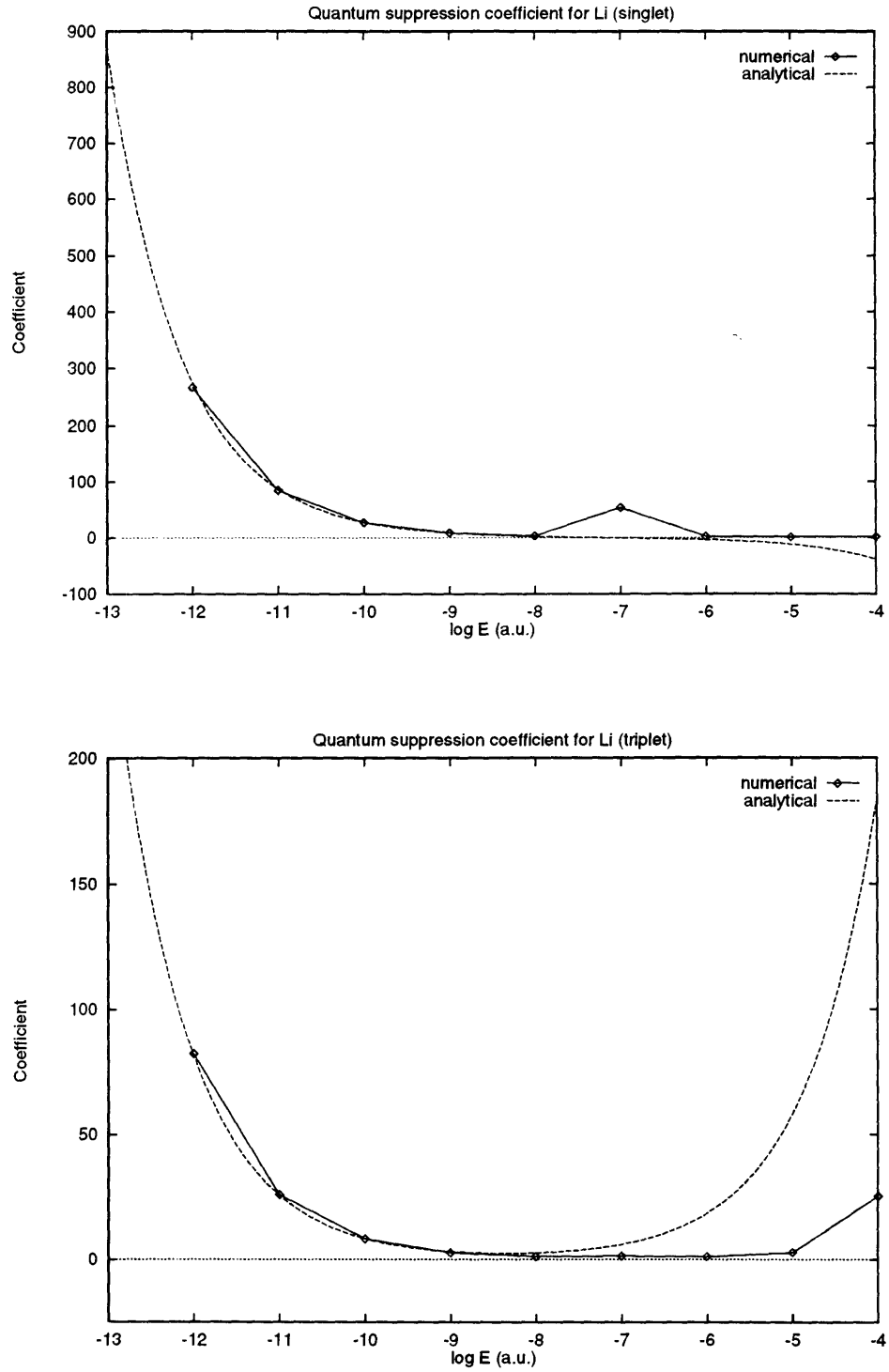

Figure 3.3: Suppression ratio $\mathcal{R}$ for the $X^1\Sigma_g^+$ and $a^3\Sigma_u^+$ states of ^{7}Li.

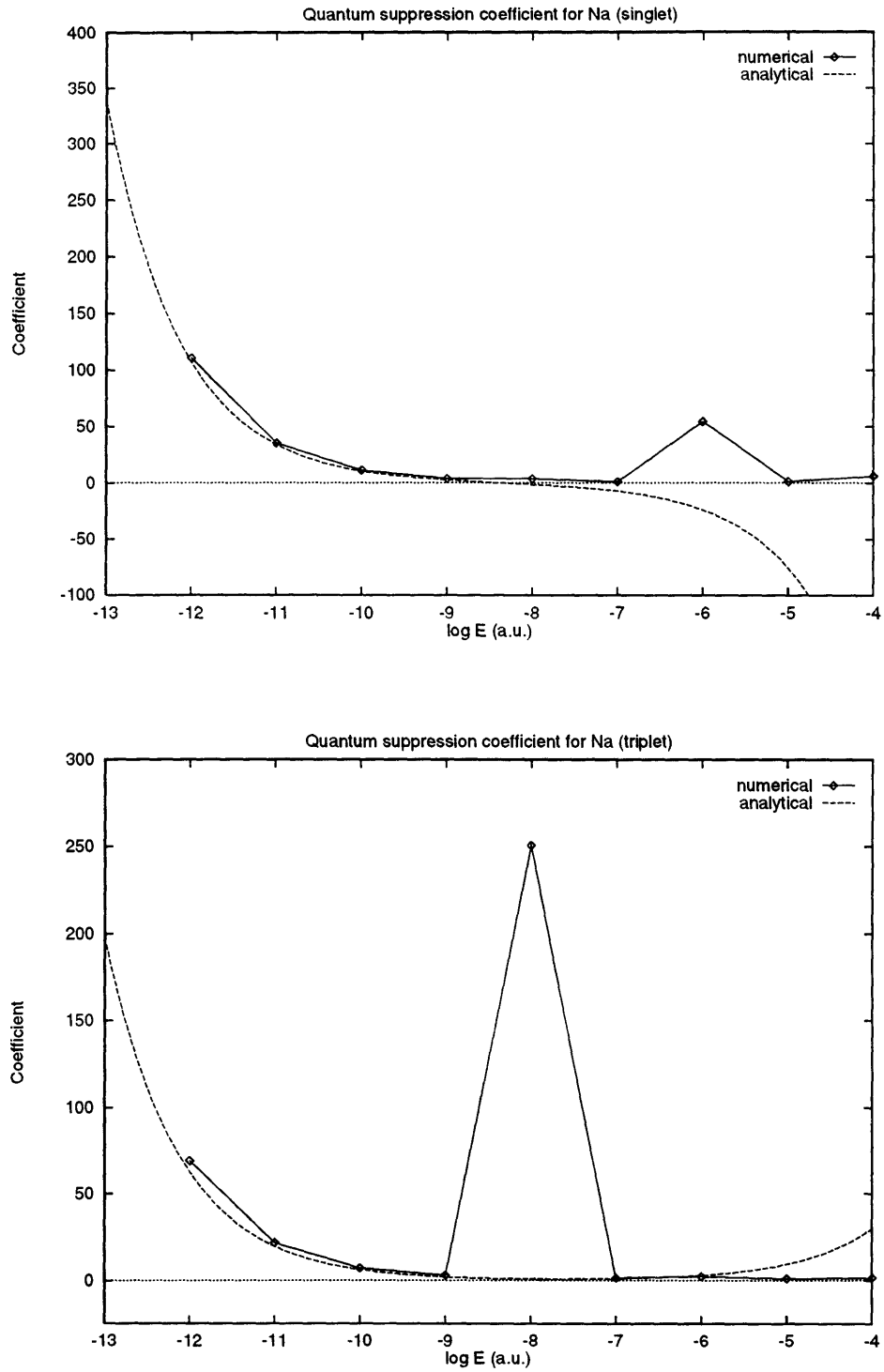

Figure 3.4: Suppression ratio $\mathcal{R}$ for the $X^1\Sigma_g^+$ and $a^3\Sigma_u^+$ states of ^{23}Na.

where the $\pi/4$ in the phase is there to help comparing with the WKB form. Then, substituting in the Schrödinger equation, one can show that the two functions $A(r)$ and $\phi(r)$ must satisfy the two differential equations

$$0 = A''(r) - \phi'^2(r)A(r) + [k^2 - U(r)]A(r) , \tag{3.114}$$

$$0 = \phi''(r) + 2A'(r)\phi'(r) . \tag{3.115}$$

The second equation can be integrated to give

$$\phi'(r) = C_0 A^{-2}(r) . \tag{3.116}$$

Now, from the asymptotic expression for $\psi(r)$, namely

$$\psi(r) = A(r)\sin[\phi(r) + \pi/4] \rightarrow \sin(kr + \eta) , \tag{3.117}$$

where we normalize $\psi(r)$ so that $A = 1$ for large distances, we must have

$$\phi(r) \rightarrow kr + \eta - \pi/4 . \tag{3.118}$$

Then, with $A = 1$ at infinity, we find (for large distance)

$$\phi'(r) = k \implies C_0 = k . \tag{3.119}$$

If we would normalize our wave function so that $A \rightarrow 1/\sqrt{\hbar k}$, then we would have $C_0 = \hbar$. Substituting back in our previous set of equations, we finally get the Milne equations

$$0 = A''(r) - k^2 A^{-3}(r) + [k^2 - U(r)]A(r) , \tag{3.120}$$

$$\phi(r) = k \int dr A^{-2}(r) . \tag{3.121}$$

We notice that this equation is a nonlinear, second-order differential equation, which makes it harder to solve numerically. However, the general solution to Milne's equation can be written in terms of any two particular solutions (y_1, y_2) of the Schrödinger equation

$$y''(r) + [k^2 - U(r)]y(r) = 0 \ , \tag{3.122}$$

as

$$A(r) = \left[\alpha y_1^2(r) + \beta y_2^2(r) + 2\gamma y_1(r) y_2(r)\right]^{1/2} \ , \tag{3.123}$$

where α, β and γ are related to the Wronskian $W(y_1, y_2)$ by (see Yoo and Green [59])

$$\alpha\beta - \gamma^2 = [W(y_1, y_2)]^{-2} \ . \tag{3.124}$$

Before trying to solve Milne's equation, we will describe the physical implications one can extract from it and the results of §3.4.1. We are interested in the behaviour at small energies. Let us first look near the deepest section of the potential interaction curve, *i.e.* the equilibrium point R_e. There, the amplitude will be given by

$$A(R_e) \simeq |\psi_0^{\rm in} \sin\eta| \ . \tag{3.125}$$

Thus, for small k, we can write

$$\begin{aligned} A^{-4} &\simeq \frac{|\psi_0^{\rm in}|^{-4}}{k^4}\left[k^2 + \left(\frac{1}{a} - \frac{1}{2}r_e k^2\right)^2\right]^2 \\ &\simeq \frac{|\psi_0^{\rm in}|^{-4}}{a^4 k^4} + \mathcal{O}(k^{-2}) \\ &\simeq -\frac{2\mu D_e}{\hbar^2}\frac{1}{k^4}\frac{(\pi\nu)^2\cos^4(\Phi - \pi\nu/2)}{[\Gamma(1-\nu)]^4(\gamma\nu)^{4\nu}\sin^4(\pi\nu)} + \mathcal{O}(k^{-2}) \ . \end{aligned} \tag{3.126}$$

Since $|U(R_e)| = 2\mu D_e/\hbar^2$ is the maximum values of $|U(r)|$, then we have (for small

k)

$$k^2 A^{-4} \simeq \frac{2\mu D_e}{\hbar^2}\frac{N}{k^2} \gg |U(r) - k^2| \,, \tag{3.127}$$

where N is the coefficient in (3.126), and Milne's equation gives

$$\begin{aligned} 0 &= A'' - \left[k^2 A^{-4} + U - k^2\right] A \\ &\simeq A'' - k^2 A^{-3} \,. \end{aligned} \tag{3.128}$$

Since A is a positive quantity, we then conclude that the second derivative (*i.e.* the curvature) of A is positive at the bottom of the well.

So, we have that $A_{Q.M.} < A_{S.C.}$ and $A''_{Q.M.} > 0$ at the deepest part of the potential. Since $A_{Q.M.} \to 1$ at large distance, the curvature will have to change sign. This will occur when $A'' = 0$. From Milne's equation, we conclude that

$$A'' = 0 \Longrightarrow A = \left(\frac{k^2}{k^2 - U(r)}\right)^{1/4} \Longrightarrow A_{Q.M.} = A_{S.C.} \,. \tag{3.129}$$

So, when the amplitude $A_{Q.M.}$ crosses the semi-classical curve $A_{S.C.}$, its curvature changes sign. There are many possible behaviours agreeing with this statement, but only one meets our physical requirements. In fact, we demand all oscillations in the wave function to be taken care of by the phase $\phi(r)$, so that the amplitude has to be a slowly varying smooth function. Moreover, we want $A_{Q.M.}$ to be positive and not greater than one. As we can see from Fig. 3.5, if $A'' > 0$ at large r and $A_{Q.M.} > A_{S.C.}$ (case a), the curve for $A_{Q.M.}$ will never cross the semi-classical curve, hence growing to infinity as r decreases. Otherwise, if $A_{Q.M.}$ is below $A_{S.C.}$ but still with a positively vanishing curvature (case b), it will have to cross the semi-classical curve more than

once as we decrease r, giving rise to oscillations in the amplitude, contrary to our physical requirements. So, we need a negative curvature at large r.

However, if $A_{Q.M.} < A_{S.C.}$ at large r with a negative curvature, the amplitude might never cross the semi-classical curve at smaller r and $A_{Q.M.}$ would go to $-\infty$ (case c). Also, it could cross once, and then grow bigger than $A_{S.C.}$ for decreasing r (case d), which the opposite of what we found earlier, *i.e.* that in the well, the quantum mechanical amplitude must be smaller than the semi-classical one. The last possibility is a negative curvature at large r and $A_{Q.M.} > A_{S.C.}$ (cases e and f). Then, as we decrease the distance, the amplitude will cross the semi-classical curve at least once and change sign accordingly. Moreover, we can see that there should be no more than one crossing, otherwise oscillations would appear in the amplitude. So, the quantum mechanical amplitude $A_{Q.M.}$ will be smaller than the semi-classical one in the well, together with a positive curvature. As r increases, it will cross $A_{S.C.}$ only once and tend to unity: it will be bigger than $A_{S.C.}$ at large r (case f).

It turns out to be very difficult to solve Milne's equation numerically for small k. In fact, if we integrate inward from $+\infty$, and fix $A_{Q.M.} = 1$ and $A'_{Q.M.} = 0$ as initial conditions, we pick up the irregular solution as we progress inward, giving rise to oscillations in the amplitude (see Fig. 3.6 for examples). However, we do not have the exact initial conditions to start integrating from inside the well. In fact, taking the approximate values of $A_{Q.M.}$ from our expression, we will have an error amplified by the nonlinearity of the Milne equation. Notice that this problem is due to the fact $A_{Q.M.}$ is very small for very low energies: at bigger values of k, these nonlinear effects

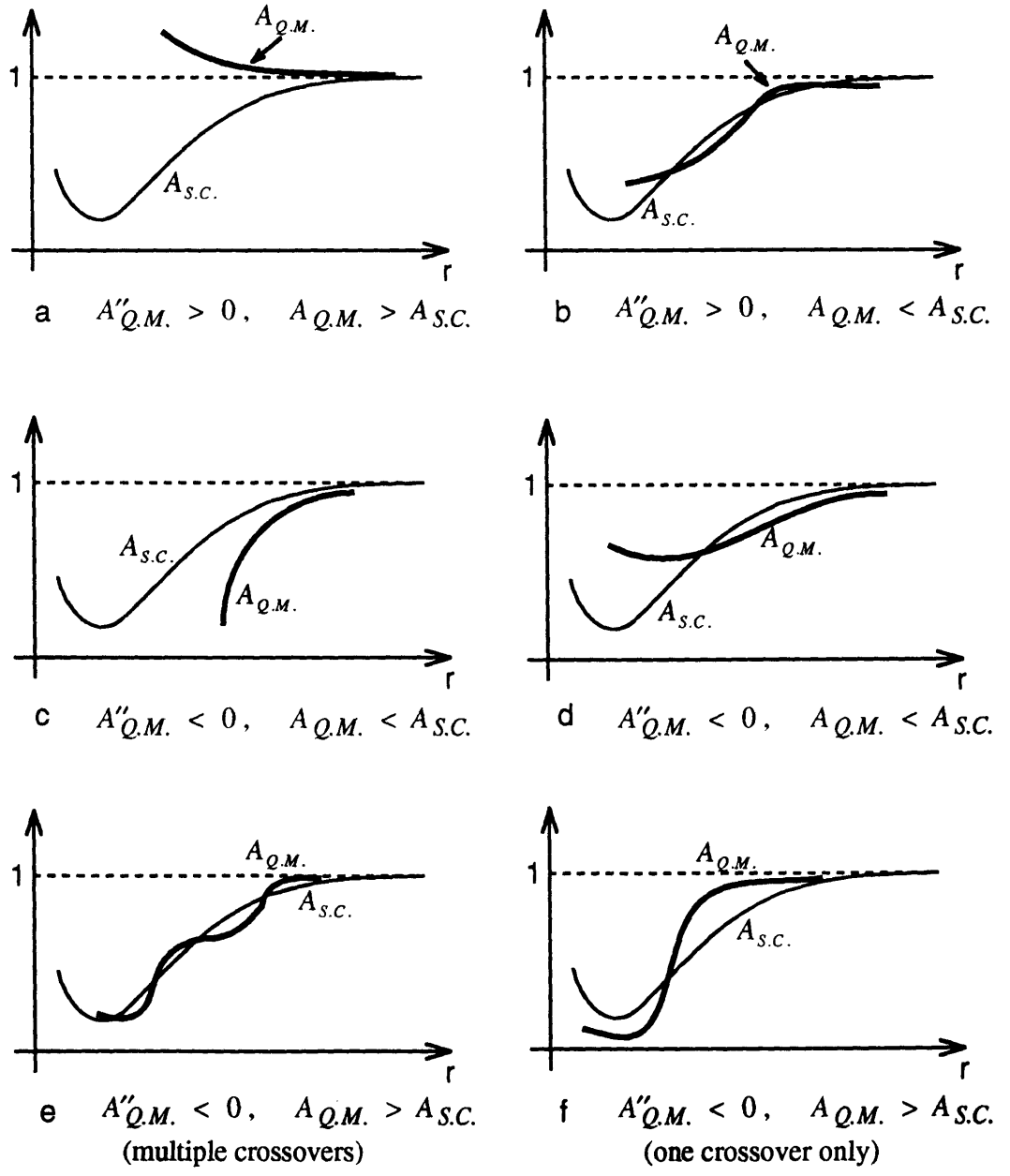

Figure 3.5: Possible behaviours of A according to Milne's equation.

would be diminuished (see Fig. 3.6).

A possible way to solve Milne's equation uses an iterative procedure. Indeed, we can reformulate our problem in a different manner. Defining a new function $z(r)$ as

$$z^{-1/2}(r) \equiv A(r) \ , \tag{3.130}$$

we get (for $A \to 1$ at infinity)

$$z^2(r) = \frac{\lambda(r)}{k^2} + \frac{z^{1/2}(r)}{k^2}\frac{d^2}{dr^2}z^{-1/2}(r) \ , \tag{3.131}$$

where

$$\lambda(r) \equiv k^2 - U(r) - \frac{l(l+1)}{r^2} \ . \tag{3.132}$$

We are interested in the $l = 0$ case. Then, setting $z_0 = 1$, we can solve this equation iteratively

$$z_0 = 1 \ , \tag{3.133}$$

$$z_1 = \sqrt{\frac{\lambda}{k^2}} \ , \tag{3.134}$$

$$z_2 = \sqrt{\frac{\lambda}{k^2} + \frac{5}{16k^2}\left(\frac{\lambda'}{\lambda}\right)^2 - \frac{1}{4k^2}\frac{\lambda''}{\lambda}} \ , \tag{3.135}$$

$$\vdots$$

$$z_n = \sqrt{\frac{\lambda(r)}{k^2} + \frac{z_{n-1}^{1/2}(r)}{k^2}\frac{d^2}{dr^2}z_{n-1}^{-1/2}(r)} \ . \tag{3.136}$$

As we can see, z_1 is just the semi-classical result. Although this method is easy to implement, it fails when the quantity under the square root becomes negative. Then the amplitude has a imaginary component, which is contrary to our construction (A and ϕ are both defined real). This could be seen as a correction to the phase however.

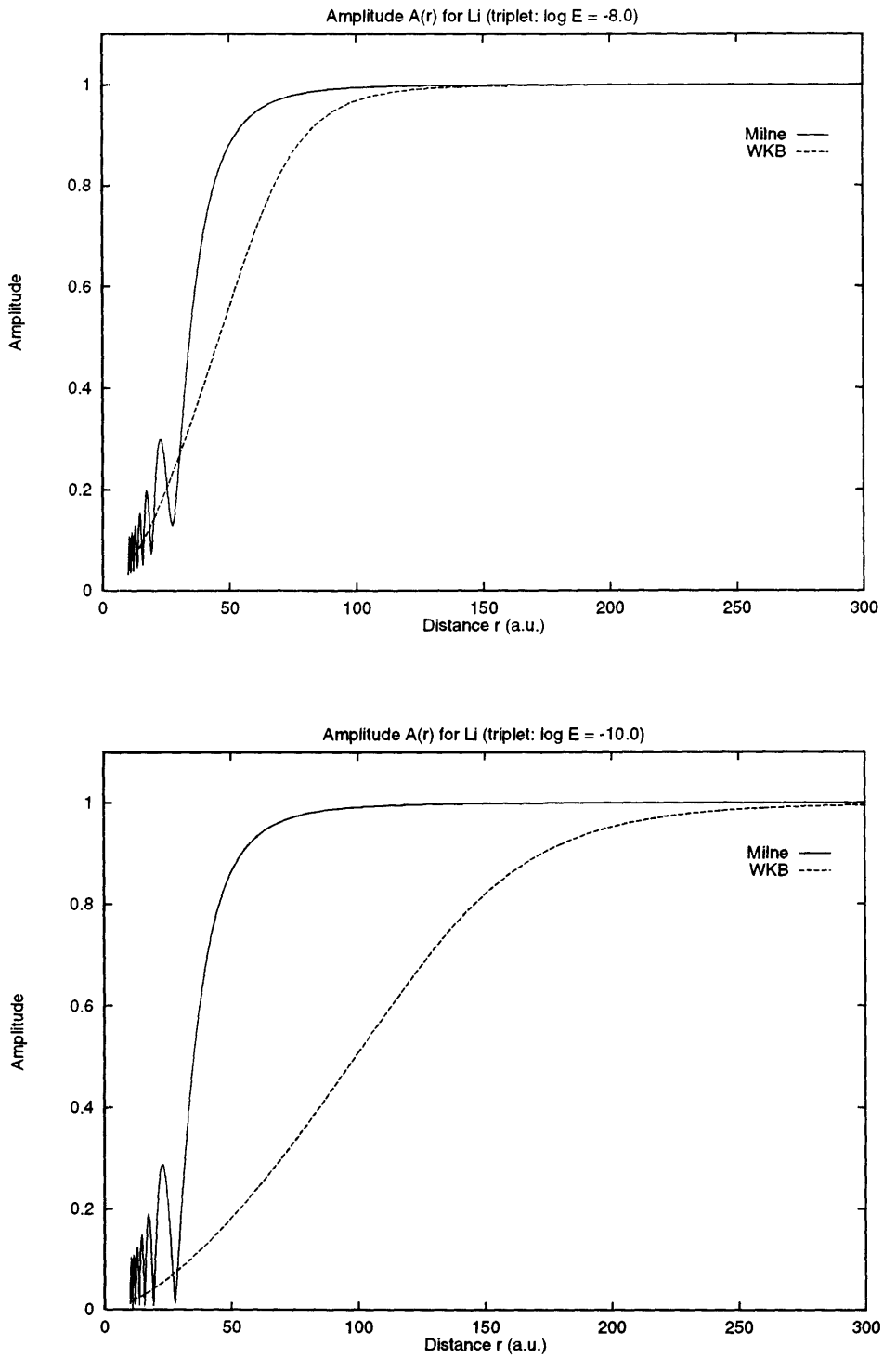

Figure 3.6: Integration of Milne's equation for the $a^3\Sigma_u^+$ state of ^{7}Li, starting from ∞ with different energies.

Another way to explore the behaviour of the amplitude $A(r)$ and the phase $\phi(r)$ resides in the use of higher order WKB approximation. Indeed, by doing so, we will capture more of the physics involved and understand better the limitation of the method. Let us come back to §3.1.1. If we take more terms in the the expression (3.4), then according to the differential equation (3.3), we will have to solve the following set of first-order differential equations

$$S_0'^2 = p^2 \quad , \quad \text{order } \hbar^0 \ , \tag{3.137}$$

$$2S_0'S_1' + S_0'' = 0 \quad , \quad \text{order } \hbar^1 \ , \tag{3.138}$$

$$2S_0'S_2' + S_1'^2 + S_1'' = 0 \quad , \quad \text{order } \hbar^2 \ , \tag{3.139}$$

$$2S_0'S_3' + 2S_1'S_2' + S_2'' = 0 \quad , \quad \text{order } \hbar^3 \ , \tag{3.140}$$

$$2S_0'S_4' + 2S_1'S_3' + S_2'^2 + S_3'' = 0 \quad , \quad \text{order } \hbar^4 \ , \tag{3.141}$$

$$2S_0'S_5' + 2S_1'S_4' + 2S_2'S_3' + S_4'' = 0 \quad , \quad \text{order } \hbar^5 \ , \tag{3.142}$$

$$2S_0'S_6' + 2S_1'S_5' + 2S_2'S_4' + S_3'^2 + S_5'' = 0 \quad , \quad \text{order } \hbar^6 \ , \ldots \ . \tag{3.143}$$

The solution to the first three equations has been given in §3.1.1. Integrating each of these iteratively, we get (after some algebra and integration by parts)

$$S_0' = p \ , \tag{3.144}$$

$$S_1' = -\frac{p'}{2p} \ , \tag{3.145}$$

$$S_2' = \frac{1}{4}\frac{p''}{p^2} - \frac{3}{8}\frac{p'^2}{p^3} \ , \tag{3.146}$$

$$S_3' = -\frac{1}{8}\frac{p'''}{p^3} + \frac{3}{4}\frac{p''p'}{p^4} - \frac{3}{4}\frac{p'^3}{p^5} \ , \tag{3.147}$$

$$S_4' = \frac{1}{16}\frac{p^{iv}}{p^4} - \frac{5}{8}\frac{p'''p'}{p^5} - \frac{13}{32}\frac{p''^2}{p^5} + \frac{99}{32}\frac{p''p'^2}{p^6} - \frac{297}{128}\frac{p'^4}{p^7} \ , \tag{3.148}$$

$$S_5' = -\frac{1}{32}\frac{p^v}{p^5} + \frac{15}{32}\frac{p^{iv}p'}{p^6} + \frac{3}{4}\frac{p'''p''}{p^6} - \frac{111}{32}\frac{p'''p'^2}{p^7} - \frac{9}{2}\frac{p''^2p'}{p^7} + \frac{255}{16}\frac{p''p'^3}{p^8} - \frac{153}{16}\frac{p'^5}{p^9} , \tag{3.149}$$

$$S_6' = \frac{1}{64}\frac{p^{vi}}{p^6} - \frac{21}{64}\frac{p^vp'}{p^7} - \frac{5}{8}\frac{p^{iv}p''}{p^7} - \frac{49}{128}\frac{p'''^2}{p^7} + \frac{435}{128}\frac{p^{iv}p'^2}{p^8} + \frac{347}{32}\frac{p'''p''p'}{p^8} + \frac{301}{128}\frac{p''^2}{p^8} - \frac{1419}{64}\frac{p'''p'^3}{p^9} - \frac{11037}{256}\frac{p''^2p'^2}{p^9} + \frac{50139}{512}\frac{p''p'^4}{p^{10}} - \frac{50139}{1024}\frac{p'^6}{p^{11}} . \tag{3.150}$$

Integrating these, we finally get

$$S_0 = \int dr\, p + C_0 , \tag{3.151}$$

$$S_1 = -\frac{1}{2}\ln p + C_1 , \tag{3.152}$$

$$S_2 = \frac{1}{4}\frac{p'}{p^2} + \frac{1}{8}\int dr \frac{p'^2}{p^3} + C_2 , \tag{3.153}$$

$$S_3 = -\frac{1}{8}\frac{p''}{p^3} + \frac{3}{16}\frac{p'^2}{p^4} + C_3 , \tag{3.154}$$

$$S_4 = \frac{1}{16}\frac{p'''}{p^4} - \frac{3}{8}\frac{p''p'}{p^5} + \frac{13}{32}\frac{p'^3}{p^6} - \frac{1}{32}\int dr \frac{p''^2}{p^5} + \frac{15}{128}\int dr \frac{p'^4}{p^7} + C_4 , \tag{3.155}$$

$$S_5 = -\frac{1}{32}\frac{p^{iv}}{p^5} + \frac{5}{16}\frac{p'''p'}{p^6} + \frac{7}{32}\frac{p''^2}{p^6} - \frac{51}{32}\frac{p''p'^2}{p^7} + \frac{153}{128}\frac{p'^4}{p^8} + C_5 , \tag{3.156}$$

$$S_6 = \frac{1}{64}\frac{p^v}{p^6} - \frac{15}{64}\frac{p^{iv}p'}{p^7} - \frac{25}{64}\frac{p'''p''}{p^7} + \frac{225}{128}\frac{p'''p'^2}{p^8} + \frac{147}{64}\frac{p''^2p'}{p^8}$$

$$-\frac{519}{64}\frac{p''p'^3}{p^9}+\frac{12771}{2560}\frac{p'^5}{p^{10}}+\frac{1}{128}\int dr\frac{p'''^2}{p^7}+\frac{7}{128}\int dr\frac{p'''^3}{p^8}$$

$$-\frac{105}{256}\int dr\frac{p''^2p'^2}{p^9}+\frac{945}{1024}\int dr\frac{p'^6}{p^{11}}+C_6\ . \tag{3.157}$$

Notice here that we took the + sign for S_0: − would change the sign of all the higher S_n.

Now, going back to the wave function, we can write

$$\begin{aligned}\psi(r) &= \exp\left(\frac{i}{\hbar}S\right)\\ &= \exp\left\{S_1-\hbar^2S_3+\hbar^4S_5+\cdots\right\}\\ &\qquad\times\exp\left\{i\left(\frac{1}{\hbar}S_0-\hbar S_2+\hbar^3S_4-\hbar^5S_6+\cdots\right)\right\}\ .\end{aligned} \tag{3.158}$$

From this equation, we conclude that we can rewrite the wave function in the Milne's form, namely

$$\psi(r)=A(r)\sin[\phi(r)+\pi/4]\ , \tag{3.159}$$

where we identify $A(r)$ and $\phi(r)$ from the above expansion

$$A(r) = \frac{C}{\sqrt{p}}\exp\left\{-\hbar^2S_3+\hbar^4S_5+\cdots\right\}\ , \tag{3.160}$$

$$\phi(r) = \frac{1}{\hbar}S_0-\hbar S_2+\hbar^3S_4-\hbar^5S_6+\cdots+C_\phi\ . \tag{3.161}$$

Notice that the constant C and C_ϕ are given by

$$C = \ln(C_1-C_3+C_5+\cdots)\ , \tag{3.162}$$

$$C_\phi = C_0-C_2+C_4-C_6+\cdots-\pi/4\ , \tag{3.163}$$

and that the S_n are redefined without the integration constants.

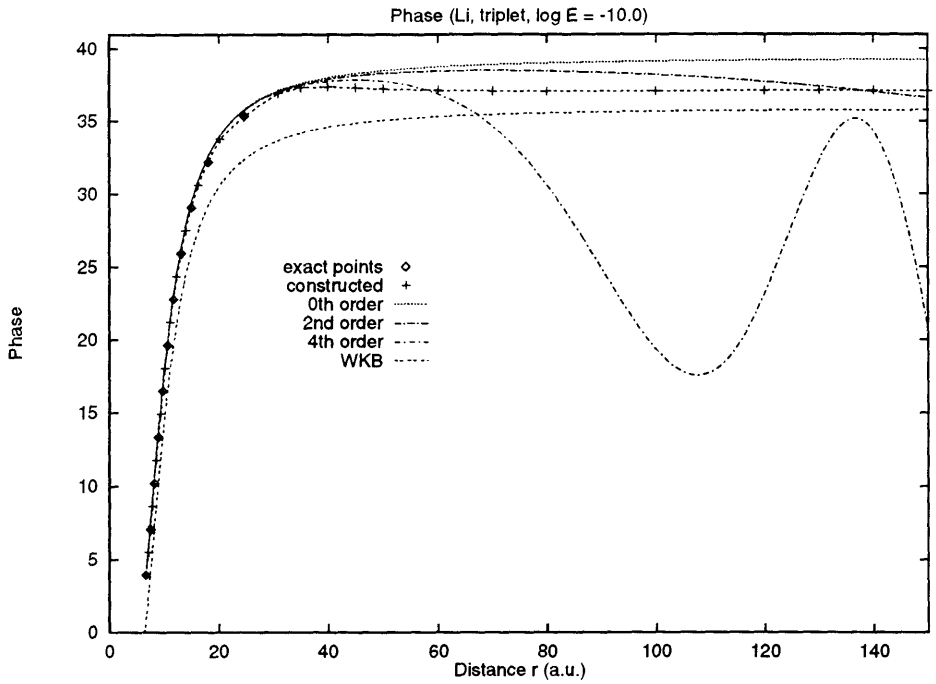

Figure 3.7: Phase $\phi(r)$ for different order of $\hbar$.

In order to study these expressions, let us consider a real case, namely the $^7Li_2$ triplet case at an energy of 10^{-10} hartree. We illustrate the functions $\phi(r)$ and $A(r)$ for different order in $\hbar$ in Fig. 3.7 and Fig. 3.8 respectively. In both figures, the exact points are extracted from the exact numerical solution $\psi(r)$. In fact, when $\psi(r)$ reaches a local minimum or maximum, the amplitude and the phase are then known, and when $\psi(r)$ passes through zero, additional values of $\phi(r)$ are determined. We extract both constants C and C_ϕ from those exact values

In the case of $\phi(r)$, we can see that the first order approximation *i.e.* $\phi(r) = \frac{1}{\hbar}S_0 + C_\phi$ is in very good agreement with the exact points for distances smaller than $30a_0$, but it overshoots after that. In fact, it goes over $(2n_B+3)\pi/2-\pi/4 = 12.5\pi-\pi/4$ (where $n_B = 11$ is the number of bound states in this case) and creates unwanted

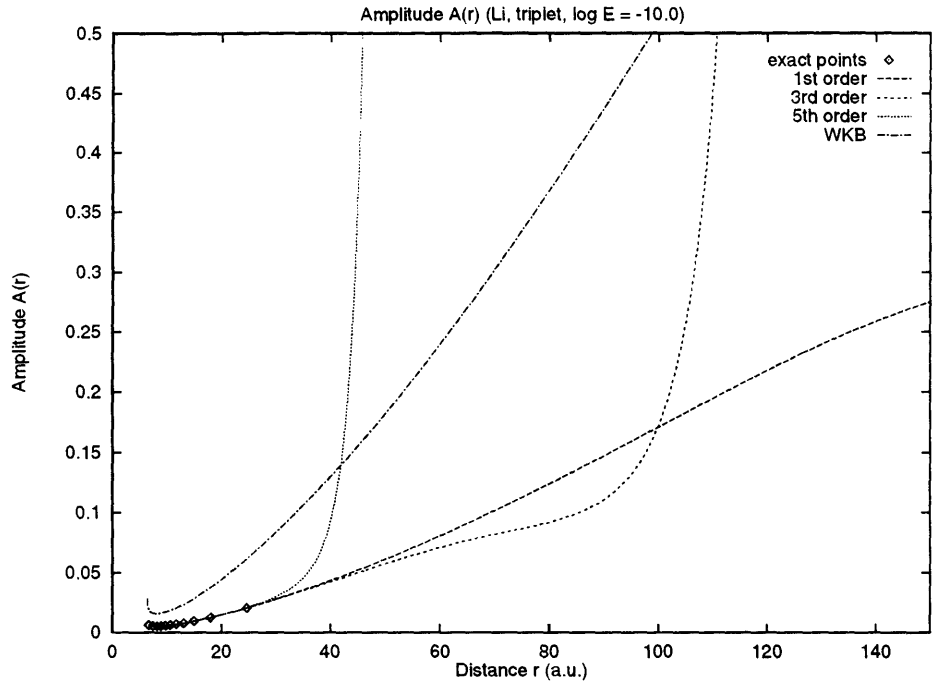

Figure 3.8: Amplitude $A(r)$ for different order of $\hbar$.

oscillations in the wave function when compared to the exact wave function (see Fig. 3.9). We also notice that the higher orders seem to correct this overshooting, but not quite. They overdo it and generate more unwanted oscillations. However, we can expect this behaviour to remain, since we truncate a divergent series. Indeed, as one can see from the expressions for $S_3, \ldots, S_6$, we get a power series for p'/p^2 (and higher derivatives). Although this quantity is well behaved at small or large distances, it is extremely big in the region between 50 and $200a_0$, its maximum being around $100a_0$ (see Figs. 3.9 and 3.10). Therefore, the series is divergent in that neighbourhood and the truncation will give rise to an erroneous behavious. Notice that this is not the only term participating in the divergence, but it is the easiest to follow up. Also on Fig. 3.7 we have the WKB phase, without C_ϕ : it is shifted by a constant equal to π when compared to the exact phase.

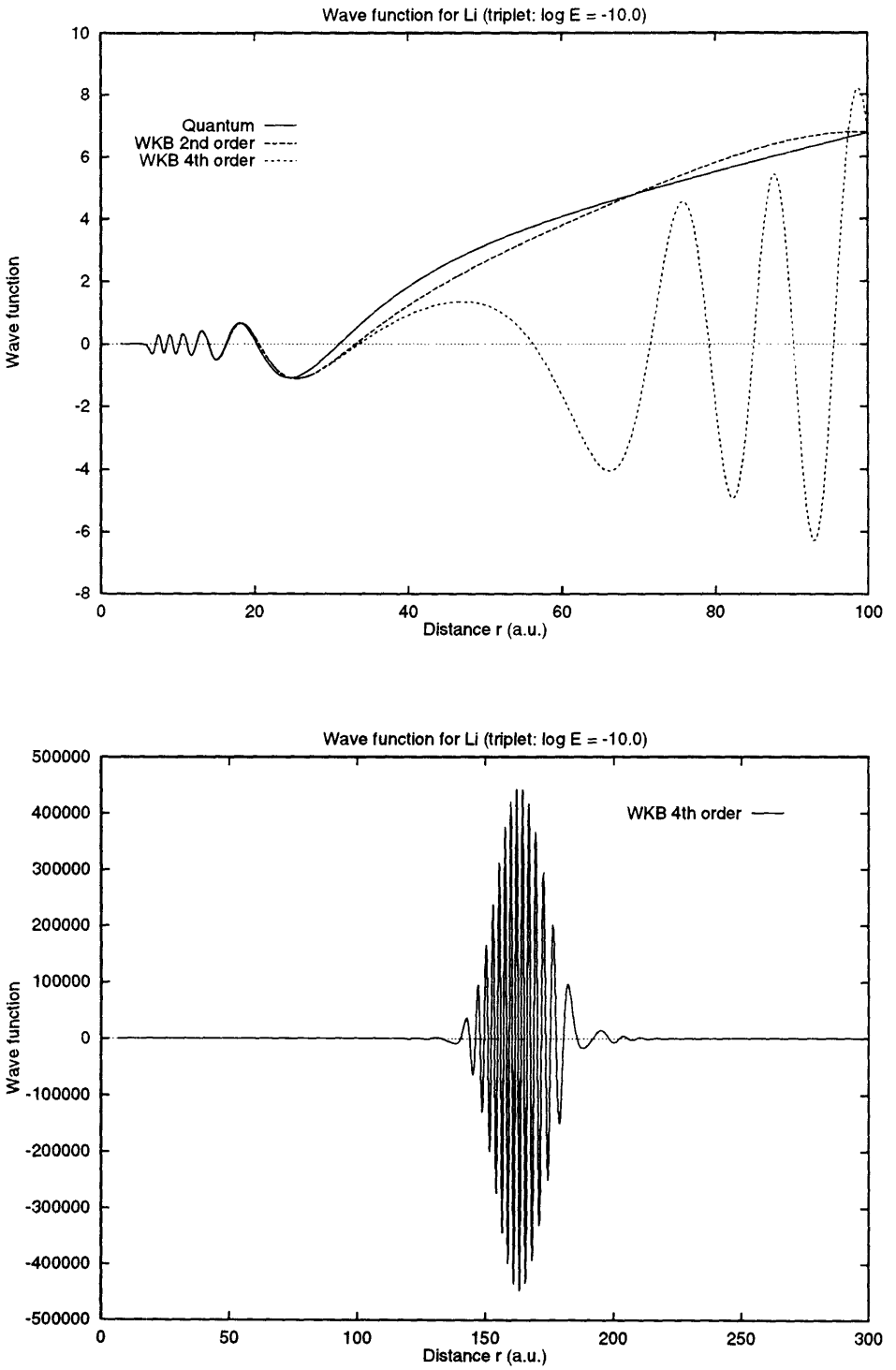

Figure 3.9: Wave function for different order of $\hbar$.

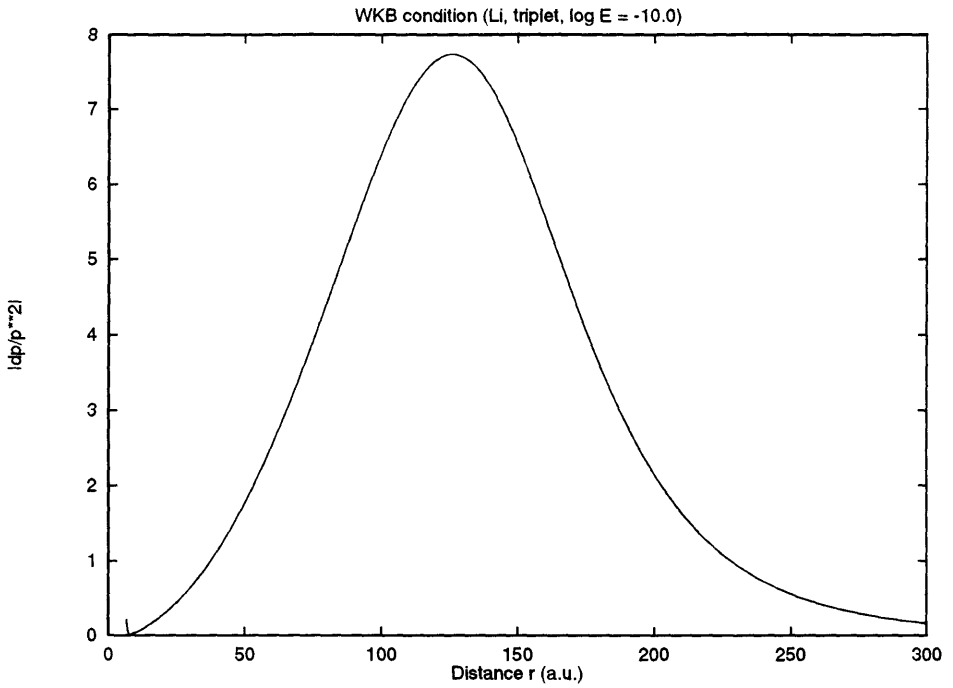

Figure 3.10: The WKB condition $|p'/p^2|$ as a function of r.

The amplitude $A(r)$ suffers from the same truncation problem, as shown in Fig. 3.8. In fact, we can see that the first, second, and third order approximations all coincide with the exact points (below 30 a_0). However, the first order amplitude, although smooth, will never tend to unity, but rather to $C/\sqrt{\hbar k}$ at large r. The second and the third orders grow exponentially in the vicinity of the divergence, as expected from the analysis for the phase above. However, the series being an alternating series, this exponential wall will change position, depending on the order at which we make the truncation. Here again, the Fig. 3.8 illustrates the WKB amplitude, without C. We can see that in all cases, the approximations are well below the WKB values within the potential well.

Now, from the wave function, we know that $\psi(r) \sim \sin(kr + \eta)$ at distance around

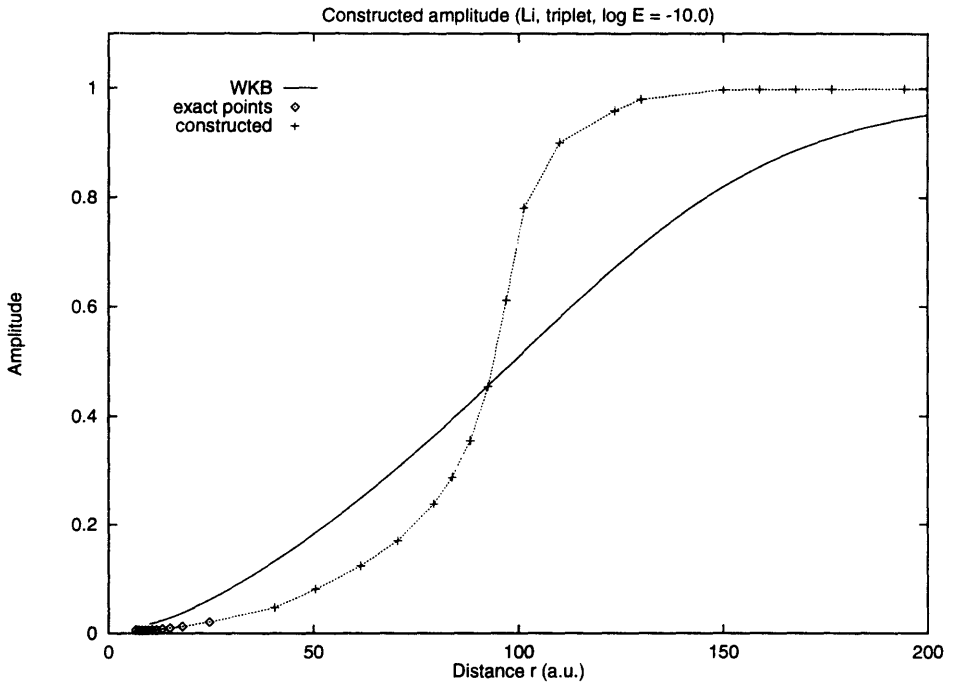

Figure 3.11: The constructed amplitude.

$r = 150\ a_0$. So, from this observation, we conclude that both A and ϕ reached their asymptotic values, namely

$$A \to 1 \qquad \text{and} \qquad \phi(r) \simeq k(r - R) + \phi(R)\ . \tag{3.164}$$

From these facts and the information above, we can try to construct approximate functions for both A and ϕ. Any ϕ that would go through the exact points, not overshooting the next π value, and going smoothly to the asymptotic value mentioned above would be a valid candidate. However, we can expect the position of the exponential wall in A to be roughly located around the maximum divergence in the series, *i.e.* near the maximum value of p'/p^2, around $100a_0$. So, a possible set of functions A and ϕ are shown in Fig. 3.7 and Fig. 3.11 together with the other approximations.

Although not exact, this analysis shows that the amplitude of the quantum prob-

lem is suppressed inside the well when compared to the semi-classical case. Moreover, $A_{Q.M.}$ will grow exponentially and cross $A_{S.C.}$ once before reaching its asymptotic value of one, above the semi-classical amplitude, as we predicted from Milne's equation. Finally, one can look at this strong quantum suppression as a reflection before entering the interaction region of the well (where its depth is significant). In fact, as we lower the energy (or k), the wavelength of the outside wave function grows very large. Now, if we scale our problem in such a way that this wavelength remains constant, we must shrink the r-axis. Then, for an incoming particle, as we lower the energy, the potential resembles more and more a square well with an infinite wall. For extremely small k, the edge of the potential becomes analogous to a sharp elbow (like the square well), and a reflection occurs due to the "discontinuity" in the slope of the potential (see Landau and Lifshitz [60]).

The study of such quantum suppression might be of great help to improve semi-classical treatments at low energies. In fact, one should then rescale the results obtained by WKB with the energy dependent coefficient. Other possible implications of quantum suppression are given in the concluding remarks at the end of this work.

Chapter 4

Photo-absorption of Li_2

In this chapter, we will tackle the problem of the absorption of a photon by a pair of cold lithium atoms. Recent and ongoing studies of ultracold collisions ($T \sim 1$ mK) are revealing a rich variety of new results [1, 10]. Many new features appear because these collisions occur so slowly that the probability of stimulated and spontaneous radiative transitions during a collision are not negligible anymore. The importance of resonances during laser-induced photoassociation has been reported by Thorsheim *et al.* [7] in the case of sodium atoms. More recently, Hulet *et al.* [8, 10] have reported measurements on the fluorescence and photo-absorption of two lithium atoms, for both the ^{6}Li and ^{7}Li isotopes.

Using the tools developed in the previous chapters, we will study here the free-bound and bound-bound transitions for the following systems

$$\mathrm{Li} + \mathrm{Li} + h\nu + E \rightleftharpoons \mathrm{Li}_2^* + E' \,, \tag{4.1}$$

$$\mathrm{Li}_2 + h\nu \rightleftharpoons \mathrm{Li}_2^* \,, \tag{4.2}$$

for both ^{6}Li and ^{7}Li isotopes.

Let us first give a rapid overview of the theory involved to evaluate the photo-absorption transition probability.

4.1 Theory

We assume that the experimental gas density in the optical trap is sufficiently low that only binary collisions occur.

We adopt here the Born-Oppenheimer approximation and write the final state (*i.e.* the excited bound state of Li_2) eigenfunction in the form

$$\begin{aligned} \psi_a(\mathbf{r},\mathbf{R}) &= \phi_a^{v,J,m_J}(\mathbf{R})\chi_a(\mathbf{r},R) \\ &= \frac{1}{R}u_a^{v,J}(R)Y_J^{m_J}(\mathbf{R}/R)\chi_a(\mathbf{r},R) \ , \end{aligned} \tag{4.3}$$

where $\mathbf{R}$ is the vector joining the nuclei, $\mathbf{r}$ denotes the position vectors $\mathbf{r}_i$ of the electrons, v, J and m_J are respectively the nuclear vibrational, rotational and projection quantum numbers and $Y_J^{m_J}$ is the spherical harmonic. The radial function $u_a^{v,J}(R)$ is the well-behaved normalized solution of the equation

$$\left(\frac{d^2}{dR^2} + \frac{2\mu}{\hbar^2}E_a^{v,J} - \frac{2\mu}{\hbar^2}V_a(R) - \frac{J(J+1)}{R^2}\right)u_a^{v,J}(R) = 0 \ , \tag{4.4}$$

where $E_a^{v,J}$ is the eigenvalue, μ is the reduced mass of the two lithium atoms and $V_a(R)$ is the interatomic potential.

For the initial (ground) state eigenfunctions, we write

$$\psi_b(\mathbf{r},\mathbf{R}) = \phi_b^{\mathbf{K}}(\mathbf{R})\chi_b(\mathbf{r},R) \ , \tag{4.5}$$

where $\mathbf{K}$ is the relative momentum of the colliding pair of atoms. The nuclear continuum wavefunction $\phi_b^{\mathbf{K}}(\mathbf{R})$ is expanded in partial waves according to

$$\phi_b^{\mathbf{K}}(\mathbf{R}) = \frac{4\pi}{KR} \sum_l \sum_{m_l} i^l \exp(i\delta_l) u_b^{K,l}(R) Y_l^{m_l}(\mathbf{R}/R) Y_l^{m_l}(\mathbf{K}/K) \ , \tag{4.6}$$

where $\delta_l = \delta_l(K)$ is the elastic scattering phase shift for angular momentum quantum number l and $u_b^{K,l}(R)$ is the regular solution of the partial wave equation

$$\left(\frac{d^2}{dR^2} + K^2 - \frac{2\mu}{\hbar^2} V_b(R) - \frac{l(l+1)}{R^2} \right) u_b^{K,l}(R) = 0 \ , \tag{4.7}$$

$V_b(R)$ being the interatomic potential. We normalized the radial wavefunction with respect to the energy, and $u_b^{K,l}(R)$ has the asymptotic form at large R

$$u_b^{K,l}(R) \sim \left(\frac{2\mu}{\pi\hbar^2 K} \right)^{1/2} \sin \left[KR - \frac{l\pi}{2} + \delta_l(K) \right] \ . \tag{4.8}$$

Notice that for the angular momentum quantum number,we adopted the notation l for the free-ground state, and J for the bound-excited state in order to be consistent with the earlier chapters, contrary to the standard notation for the angular momentum J where J'' and J' represents the value of the initial and final state, respectively.

The electronic transition moment along the internuclear axis (see also §4.2.2) is given by

$$\mathbf{D}_{ab}^Y(R) = \left\langle \chi_a \left| \sum_i e\mathbf{r}_i \right| \chi_b \right\rangle = D_{ab}^Y(R)\hat{\mathbf{R}} \ , \tag{4.9}$$

where Y stands for the molecular state (singlet (s) or triplet (t)), and the sum runs over all electrons. In terms of it, we can write the continuum-bound absorption probability for unit incident photon beam at frequency ν by (see Appendix D)

$$\kappa_{b\to a}^Y(\nu, T) \ = \ \omega_Y \frac{16\pi^3\nu}{3hc} n_{\mathrm{Li}}^2 \frac{h^3}{(2\pi\mu k_B T)^{3/2}} \sum_v \sum_J \pi\hbar\omega_{YJ}$$

State Y	^{6}Li ($I=1$)			^{7}Li ($I=\frac{3}{2}$)		
	ω_Y	ω_{YJ}		ω_Y	ω_{YJ}	
		J even	J odd		J even	J odd
singlet	$\frac{1}{12}$	1	2	$\frac{1}{32}$	5	3
triplet	$\frac{3}{12}$	2	1	$\frac{3}{32}$	3	5

Table 4.1: Statistical weights for the two lithium isotopes.

$$\times \exp\left(-\frac{\hbar^2 K^2}{2\mu k_B T}\right)\left[(J+1)|\langle u_b^{K,J+1}|D_{ab}^Y|u_a^{v,J}\rangle|^2 + J|\langle u_b^{K,J-1}|D_{ab}^Y|u_a^{v,J}\rangle|^2\right] . \quad (4.10)$$

Here $n_{\rm Li}$) is the concentration of lithium atoms. The different weights ω_Y and ω_{YJ} are given in Table 4.1. They also depend upon the nuclear spin I of the isotopes. The total continuum-bound absorption probability can be given as a summation over all vibrational bound levels v, namely

$$\kappa_{b\to a}^Y(\nu,T) = \sum_v \kappa_{b\to a}^Y(v,\nu,T) , \quad (4.11)$$

where the individual vibrational contributions can be written as

$$\kappa_{b\to a}^Y(v,\nu,T) = \omega_Y \frac{\alpha}{3e^2} n_{\rm Li}^2 \frac{(2\pi)^7\hbar^4\nu}{(2\pi\mu k_B T)^{3/2}} \sum_J \omega_{YJ} \times \exp\left(-\frac{\hbar^2 K^2}{2\mu k_B T}\right)\left[(J+1)|\langle u_b^{K,J+1}|D_{ab}^Y|u_a^{v,J}\rangle|^2 + J|\langle u_b^{K,J-1}|D_{ab}^Y|u_a^{v,J}\rangle|^2\right] . \quad (4.12)$$

A similar formula can be obtained for the continuum-continuum absorption probability. One gets (see Sando and Dalgarno [61], and Appendix D)

$$\kappa^Y_{b\to a}(\nu,T) = \int dE_a \kappa^Y_{b\to a}(E_a,\nu,T) \ , \tag{4.13}$$

where $\kappa^Y_{b\to a}(E_a,\nu,T)$ is given by

$$\begin{aligned}\kappa^Y_{b\to a}(E_a,\nu,T) &= \omega_Y \frac{16\pi^3\nu}{3hc} n^2_{\rm Li} \frac{h^3}{(2\pi\mu k_B T)^{3/2}} \sum_J \pi\hbar\omega_{YJ} \\ &\quad \times \exp\left(-\frac{\hbar^2 K_b^2}{2\mu k_B T}\right) \Big[(J+1)|\langle u_b^{K_b,J+1}|D^Y_{ab}|u_a^{K_a,J}\rangle|^2 \\ &\quad + J|\langle u_b^{K_b,J-1}|D^Y_{ab}|u_a^{K_a,J}\rangle|^2\Big] \ , \end{aligned} \tag{4.14}$$

where $E_a = \hbar^2 K_a^2/2\mu$ and $E_b = \hbar^2 K_b^2/2\mu$. The way to handle the asymptotic oscillations for large distance in the case of the continuum-continuum absorption probability is treated in Appendix D, although we will not present any results regarding that regime.

In order to calculate these absorption probabilities, one needs the electronic dipole moments $D^Y_{ab}(R)$ and the potential curves $V_Y(R)$. Let us describe the functions we used.

4.2 Potentials and electronic dipole moments

Let us describe the way we constructed these functions from diverse sources.

4.2.1 Excited potential curves

As mentioned earlier, we are interested in the photo-absorption of ultracold lithium. So, there are only two possible ground states for the 2s-2s limit, namely the $X^1\Sigma_g^+$ and $a^3\Sigma_u^+$ states of Li_2. Those two potential curves are described in detail in §2.1. Now, in the type of transition we consider here, *i.e.*

$$\mathrm{Li} + \mathrm{Li} + h\nu + E \rightleftharpoons \mathrm{Li}_2^* + E' \ , \tag{4.15}$$

there is only one photon involved. Such an interaction does not change the electronic configuration, hence the spin state remains the same. If we started from a singlet state, we must end up in a singlet state, and similarly for the triplet case. The photon changes the parity by one, and in an electric dipole transition (E1), one must then change the parity of the molecular state by one, namely an gerade state (g) will go to an ungerade state (u), and vice-versa.

Fig. 4.1 (from Schmidt-Mink *et al.* [31]) illustrates the lowest lying potential energy curves for the Li_2 molecule. The lowest two, the $X^1\Sigma_g^+$ and $a^3\Sigma_u^+$ states, correspond to the asymptotic singlet and triplet combinations of the atomic configurations $\mathrm{Li}(1s^2 2s) + \mathrm{Li}(1s^2 2s)$ respectively. The next highest asymptotic combination $\mathrm{Li}(1s^2 2s) + \mathrm{Li}(1s^2 2p)$ can be divided up among two sets of four curves shown immediately higher in the figure.

Since we consider photons red-detuned from the $2s+2p$ asymptotic limit, only the potential curves lying below that limit will be possible candidate for the transition. In the case of the singlet transition, the only possibility is the $1^1\Sigma_g^+(X) \rightarrow 1^1\Sigma_u^+(A)$

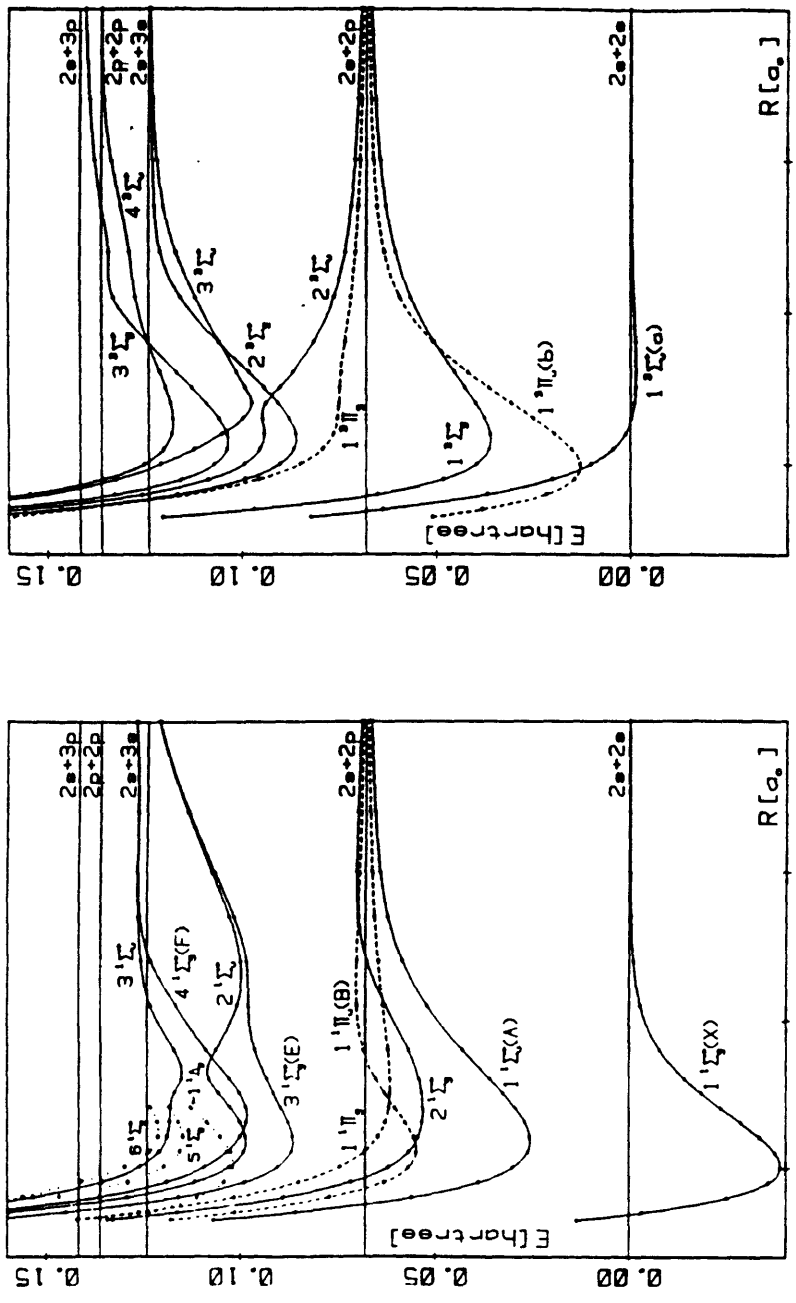

Potential curves of Li_2 singlet states. Energies in atomic units relative to the ground-state asymptote. Solid lines: Σ states: dashed lines: Π states; dotted lines: states that are not further discussed in this paper because the basis set used is insufficient for an accurate description.

Potential curves of Li_2 triplet states. Energies in atomic units relative to the 2s+2s asymptote. Solid lines: Σ states; dashed lines: Π states.

Figure 4.1: Potential curves for Li_2 singlet and triplet states.

transition. In fact, even though the excited state $1^1\Pi_u(B)$ satisfies all the parity and spin constraints, it is repulsive at large distance, hence a red-detuned photon would not have enough energy to make this transition possible. In the case of the triplet transition, the only non-repulsive potential that satisfies the parity and spin configuration conditions is the $1^3\Sigma_g^+$ state, hence the transition $1^3\Sigma_u^+(a) \rightarrow 1^3\Sigma_g^+$.

The two ground state potentials are already described in §2.1. To construct the two excited potentials, we followed a similar procedure, namely we used RKR data when available, and supplement them with *ab initio* values. For $1^1\Sigma_u^+(A)$ we used the RKR data from Kusch and Hessel [62] between $R = 4.13a_0$ and $R = 10.21a_0$. More extended *ab initio* data from Schmidt-Mink, Müller, and Meyer [31] were used for smaller distances (between $R = 3.25$ and $4.00a_0$) and larger distances (between $R = 10.5$ and $30.0a_0$). In the case of $1^3\Sigma_g^+$, we used RKR data from Linton *et al.* [32] between $R = 4.66a_0$ and $R = 7.84a_0$. Once again, we completed these data with *ab initio* values from Schmidt-Mink *et al.* [31] for distances between $R = 3.25$ and $4.50a_0$, and between $R = 8.00$ and $30.0a_0$.

For shorter or longer distances, we completed the potential analytically as described in §2.1.3. However, the *ab initio* data extending far out, we need not to take explicite account of the exchange term. It is already included in the *ab initio* calculations. So, for both excited curves, we used the same expression for the long range form of the potential, namely

$$V_{g,u} \simeq +\frac{C_3}{R^3} - \frac{C_6}{R^6} - \frac{C_8}{R^8} \; . \tag{4.16}$$

The values for the Van der Waals coefficient are listed in Table 4.2, and the two sets

Source	C_3	C_6	C_8
Marinescu and Dalgarno [64]	11.01	2 066	270 500
Vigné-Maeder [65]	10.99	2 025	265 700
Bussery and Aubert-Frécon [66]	11.02	1 927	229 600

Table 4.2: Van der Waals coefficients in atomic units for the Σ 2S-2P excited states of Li_2.

of two potentials are shown in Fig. 4.2. We used the same curves for both ^{6}Li and ^{7}Li. We just changed the reduced mass μ in the Schrödinger equation according to the isotope under study.

As in Chapter 2, we computed the vibrational energy levels for both the singlet and triplet excited Σ states of $^6Li_2$ and $^7Li_2$ molecules. In Table 4.3-4.6, we report the bound state energy levels using $J = 1$. Although this is not the ground angular momentum ($J = 0$), the difference would become sizable for the highest levels: we show later (see Table 4.11) that even then, the difference is small. We also computed the averaged radius $\langle R \rangle$ for each bound state. These are listed in Table 4.3-4.6. Notice here that we used a box extending from 0 to 200 a_0 with 90 001 points. As we can see from the data, the highest vibrational state extends far out, near the border of the box. Therefore, the last few bound states should be used with some caution. In fact, we see that the last two or three levels have a decreasing average radius contrary to the right physical behaviour. A bigger box would be necessary to fix these last levels, but we are interested only in lower levels, where the spin-orbit interaction coupling

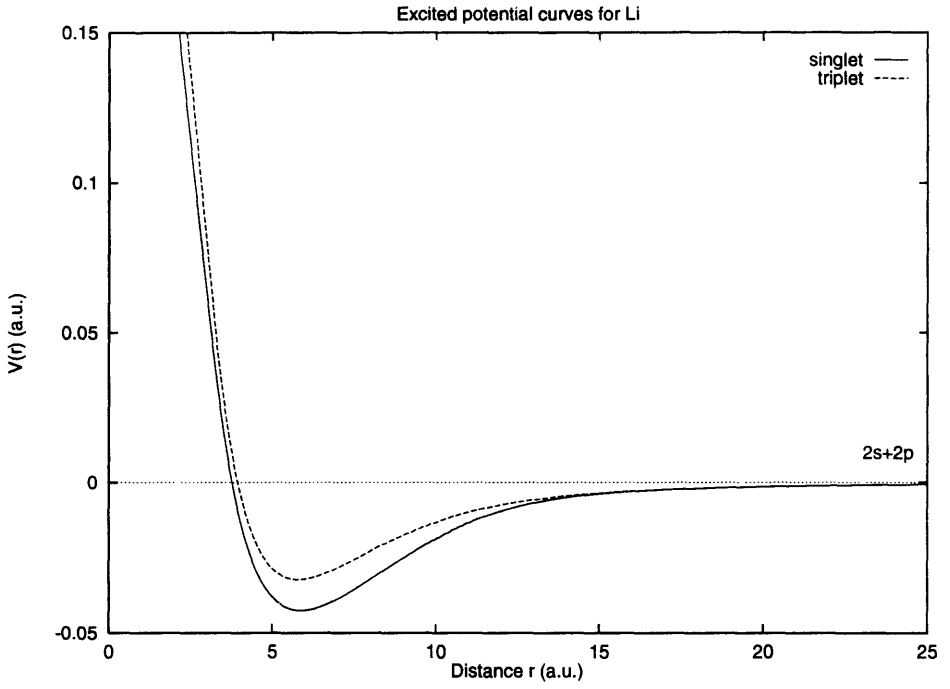

Figure 4.2: The two excited potential curves adopted for Li_2.

can be neglected.

4.2.2 Electronic dipole moments

The transition dipole moment $\mathbf{D}^{Y}_{ab}(R)$ between two electronic states is the matrix element over all electronic coordinates of the dipole operator $\mathbf{d} = -\sum_i e\mathbf{r}_i$ between the inital and final electronic states. Here $\mathbf{r}_i$ is the position vector of the i^{th} electron with the z axis along the line joining the nuclei, e is the electronic charge, and the summation runs over all electrons. For each fixed R, the transition dipole may be written as

$$\mathbf{D}^{Y}_{ab}(R) = D^{\pm Y}_{ab}(R)\hat{\mathbf{R}}_{\pm} \quad \text{and} \quad \mathbf{D}^{Y}_{ab}(R) = D^{Y}_{ab}(R)\hat{\mathbf{R}} \ , \tag{4.17}$$

v	$-E_b(v)$ (hartree)	$\langle r \rangle$ (a_0)	v	$-E_b(v)$ (hartree)	$\langle r \rangle$ (a_0)	v	$-E_b(v)$ (hartree)	$\langle r \rangle$ (a_0)
0	4.20283 (-2)	5.907	34	1.09102 (-2)	8.903	68	4.39833 (-4)	24.061
1	4.08787 (-2)	5.975	35	1.02661 (-2)	9.046	69	3.91522 (-4)	25.194
2	3.97434 (-2)	6.042	36	9.64119 (-3)	9.194	70	3.48162 (-4)	26.213
3	3.86224 (-2)	6.111	37	9.03586 (-3)	9.349	71	3.08423 (-4)	27.229
4	3.75155 (-2)	6.180	38	8.45052 (-3)	9.512	72	2.71939 (-4)	28.282
5	3.64226 (-2)	6.250	39	7.88554 (-3)	9.685	73	2.38427 (-4)	29.398
6	3.53439 (-2)	6.320	40	7.34140 (-3)	9.867	74	2.07839 (-4)	30.627
7	3.42790 (-2)	6.392	41	6.81863 (-3)	10.061	75	1.80262 (-4)	32.045
8	3.32281 (-2)	6.464	42	6.31773 (-3)	10.267	76	1.55888 (-4)	33.693
9	3.21911 (-2)	6.536	43	5.83934 (-3)	10.488	77	1.34561 (-4)	35.415
10	3.11680 (-2)	6.610	44	5.38407 (-3)	10.726	78	1.15722 (-4)	37.217
11	3.01587 (-2)	6.685	45	4.95253 (-3)	10.982	79	9.91744 (-5)	39.183
12	2.91632 (-2)	6.760	46	4.54528 (-3)	11.259	80	8.46477 (-5)	41.300
13	2.81816 (-2)	6.837	47	4.16264 (-3)	11.556	81	7.19544 (-5)	43.581
14	2.72139 (-2)	6.915	48	3.80457 (-3)	11.873	82	6.08954 (-5)	46.066
15	2.62601 (-2)	6.994	49	3.47054 (-3)	12.208	83	5.12928 (-5)	48.771
16	2.53202 (-2)	7.074	50	3.15977 (-3)	12.563	84	4.29896 (-5)	51.716
17	2.43943 (-2)	7.156	51	2.87184 (-3)	12.946	85	3.58410 (-5)	54.936
18	2.34825 (-2)	7.239	52	2.60638 (-3)	13.355	86	2.97137 (-5)	58.467
19	2.25849 (-2)	7.323	53	2.36238 (-3)	13.786	87	2.44866 (-5)	62.351
20	2.17015 (-2)	7.410	54	2.13839 (-3)	14.235	88	2.00501 (-5)	66.638
21	2.08325 (-2)	7.498	55	1.93291 (-3)	14.707	89	1.63052 (-5)	71.382
22	1.99781 (-2)	7.588	56	1.74506 (-3)	15.213	90	1.31627 (-5)	76.653
23	1.91382 (-2)	7.680	57	1.57383 (-3)	15.743	91	1.05422 (-5)	82.531
24	1.83132 (-2)	7.775	58	1.41767 (-3)	16.288	92	8.37177 (-6)	89.112
25	1.75030 (-2)	7.871	59	1.27462 (-3)	16.832	93	6.58734 (-6)	96.514
26	1.67073 (-2)	7.967	60	1.14287 (-3)	17.385	94	5.13183 (-6)	104.879
27	1.59258 (-2)	8.065	61	1.02155 (-3)	17.972	95	3.95480 (-6)	114.383
28	1.51584 (-2)	8.167	62	9.10193 (-4)	18.597	96	3.01186 (-6)	125.238
29	1.44065 (-2)	8.277	63	8.08438 (-4)	19.275	97	2.26325 (-6)	137.481
30	1.36717 (-2)	8.393	64	7.16123 (-4)	20.022	98	1.65225 (-6)	147.416
31	1.29545 (-2)	8.513	65	6.33183 (-4)	20.859	99	1.04572 (-6)	147.737
32	1.22547 (-2)	8.637	66	5.59617 (-4)	21.809	100	3.34329 (-7)	144.017
33	1.15732 (-2)	8.768	67	4.95347 (-4)	22.889			

Table 4.3: Energy levels for the singlet excited state $1^1\Sigma_u^+(A)$ (with $J = 1$) and the averaged radius in atomic units for ^{7}Li.

v	$-E_b(v)$ (hartree)	$\langle r \rangle$ (a_0)	v	$-E_b(v)$ (hartree)	$\langle r \rangle$ (a_0)	v	$-E_b(v)$ (hartree)	$\langle r \rangle$ (a_0)
0	3.17373 (-2)	5.839	31	6.71689 (-3)	9.707	62	3.26590 (-4)	26.594
1	3.06124 (-2)	5.918	32	6.25644 (-3)	9.922	63	2.88852 (-4)	27.630
2	2.95092 (-2)	5.999	33	5.81729 (-3)	10.148	64	2.54154 (-4)	28.707
3	2.84276 (-2)	6.082	34	5.39941 (-3)	10.387	65	2.22346 (-4)	29.876
4	2.73672 (-2)	6.167	35	5.00269 (-3)	10.639	66	1.93441 (-4)	31.189
5	2.63280 (-2)	6.255	36	4.62702 (-3)	10.906	67	1.67604 (-4)	32.724
6	2.53099 (-2)	6.344	37	4.27223 (-3)	11.189	68	1.44918 (-4)	34.434
7	2.43120 (-2)	6.434	38	3.93811 (-3)	11.488	69	1.24951 (-4)	36.166
8	2.33321 (-2)	6.521	39	3.62423 (-3)	11.804	70	1.07320 (-4)	38.065
9	2.23653 (-2)	6.601	40	3.32992 (-3)	12.134	71	9.18350 (-5)	40.084
10	2.14096 (-2)	6.689	41	3.05438 (-3)	12.479	72	7.82640 (-5)	42.287
11	2.04761 (-2)	6.804	42	2.79695 (-3)	12.845	73	6.64059 (-5)	44.668
12	1.95755 (-2)	6.926	43	2.55713 (-3)	13.233	74	5.60886 (-5)	47.249
13	1.87011 (-2)	7.038	44	2.33422 (-3)	13.639	75	4.71456 (-5)	50.063
14	1.78532 (-2)	7.162	45	2.12730 (-3)	14.064	76	3.94242 (-5)	53.140
15	1.70309 (-2)	7.276	46	1.93547 (-3)	14.511	77	3.27868 (-5)	56.507
16	1.62299 (-2)	7.393	47	1.75809 (-3)	14.984	78	2.71082 (-5)	60.203
17	1.54503 (-2)	7.507	48	1.59442 (-3)	15.481	79	2.22743 (-5)	64.273
18	1.46904 (-2)	7.626	49	1.44347 (-3)	15.995	80	1.81814 (-5)	68.770
19	1.39508 (-2)	7.745	50	1.30397 (-3)	16.516	81	1.47355 (-5)	73.756
20	1.32309 (-2)	7.871	51	1.17465 (-3)	17.048	82	1.18520 (-5)	79.305
21	1.25308 (-2)	8.000	52	1.05477 (-3)	17.609	83	9.45488 (-6)	85.505
22	1.18511 (-2)	8.136	53	9.44004 (-4)	18.208	84	7.47614 (-6)	92.462
23	1.11920 (-2)	8.280	54	8.42082 (-4)	18.855	85	5.85519 (-6)	100.304
24	1.05545 (-2)	8.431	55	7.48900 (-4)	19.564	86	4.53827 (-6)	109.189
25	9.93919 (-3)	8.592	56	6.64425 (-4)	20.352	87	3.47795 (-6)	119.310
26	9.34625 (-3)	8.759	57	5.88709 (-4)	21.243	88	2.63249 (-6)	130.882
27	8.77583 (-3)	8.933	58	5.21779 (-4)	22.255	89	1.96028 (-6)	143.043
28	8.22789 (-3)	9.115	59	4.63414 (-4)	23.383	90	1.37200 (-6)	148.670
29	7.70228 (-3)	9.305	60	4.12676 (-4)	24.538	91	7.21862 (-7)	145.978
30	7.19873 (-3)	9.502	61	3.67658 (-4)	25.595			

Table 4.4: Energy levels for the triplet excited state $1^3\Sigma_g^+$ (with $J = 1$) and the averaged radius in atomic units for ^{7}Li.

v	$-E_b(v)$ (hartree)	$\langle r \rangle$ (a_0)	v	$-E_b(v)$ (hartree)	$\langle r \rangle$ (a_0)	v	$-E_b(v)$ (hartree)	$\langle r \rangle$ (a_0)
0	4.19813 (-2)	5.910	31	1.12256 (-2)	8.838	62	4.95229 (-4)	22.890
1	4.07409 (-2)	5.983	32	1.05209 (-2)	8.988	63	4.35610 (-4)	24.155
2	3.95173 (-2)	6.056	33	9.83847 (-3)	9.146	64	3.84188 (-4)	25.366
3	3.83103 (-2)	6.130	34	9.17880 (-3)	9.311	65	3.38224 (-4)	26.456
4	3.71197 (-2)	6.205	35	8.54229 (-3)	9.486	66	2.96326 (-4)	27.564
5	3.59455 (-2)	6.281	36	7.92946 (-3)	9.671	67	2.58112 (-4)	28.720
6	3.47877 (-2)	6.357	37	7.34092 (-3)	9.867	68	2.23314 (-4)	29.974
7	3.36461 (-2)	6.435	38	6.77724 (-3)	10.077	69	1.91955 (-4)	31.395
8	3.25207 (-2)	6.513	39	6.23919 (-3)	10.302	70	1.64235 (-4)	33.078
9	3.14116 (-2)	6.592	40	5.72748 (-3)	10.544	71	1.40205 (-4)	34.941
10	3.03186 (-2)	6.673	41	5.24291 (-3)	10.806	72	1.19260 (-4)	36.842
11	2.92417 (-2)	6.754	42	4.78626 (-3)	11.091	73	1.01004 (-4)	38.951
12	2.81810 (-2)	6.837	43	4.35811 (-3)	11.399	74	8.51547 (-5)	41.210
13	2.71364 (-2)	6.921	44	3.95869 (-3)	11.731	75	7.14517 (-5)	43.682
14	2.61081 (-2)	7.007	45	3.58766 (-3)	12.085	76	5.96404 (-5)	46.388
15	2.50960 (-2)	7.094	46	3.24410 (-3)	12.461	77	4.95067 (-5)	49.347
16	2.41003 (-2)	7.182	47	2.92726 (-3)	12.867	78	4.08548 (-5)	52.595
17	2.31211 (-2)	7.272	48	2.63672 (-3)	13.305	79	3.35045 (-5)	56.177
18	2.21584 (-2)	7.365	49	2.37141 (-3)	13.769	80	2.72926 (-5)	60.140
19	2.12124 (-2)	7.459	50	2.12952 (-3)	14.254	81	2.20726 (-5)	64.539
20	2.02833 (-2)	7.555	51	1.90917 (-3)	14.767	82	1.77132 (-5)	69.440
21	1.93713 (-2)	7.654	52	1.70926 (-3)	15.318	83	1.40967 (-5)	74.921
22	1.84764 (-2)	7.756	53	1.52840 (-3)	15.896	84	1.11179 (-5)	81.079
23	1.75988 (-2)	7.859	54	1.36452 (-3)	16.485	85	8.68338 (-6)	88.030
24	1.67382 (-2)	7.964	55	1.21511 (-3)	17.074	86	6.71041 (-6)	95.915
25	1.58942 (-2)	8.069	56	1.07831 (-3)	17.686	87	5.12608 (-6)	104.911
26	1.50668 (-2)	8.180	57	9.53389 (-4)	18.343	88	3.86653 (-6)	115.238
27	1.42575 (-2)	8.299	58	8.39799 (-4)	19.053	89	2.87610 (-6)	127.158
28	1.34685 (-2)	8.427	59	7.37274 (-4)	19.837	90	2.10332 (-6)	140.290
29	1.27000 (-2)	8.557	60	6.45686 (-4)	20.719	91	1.45545 (-6)	148.056
30	1.19520 (-2)	8.694	61	5.65034 (-4)	21.730	92	7.59127 (-7)	146.025

Table 4.5: Energy levels for the singlet excited state $1^1\Sigma_u^+(A)$ (with $J = 1$) and the averaged radius in atomic units for ^{6}Li.

v	$-E_b(v)$ (hartree)	$\langle r \rangle$ (a_0)	v	$-E_b(v)$ (hartree)	$\langle r \rangle$ (a_0)	v	$-E_b(v)$ (hartree)	$\langle r \rangle$ (a_0)
0	3.16911 (-2)	5.842	29	6.54821 (-3)	9.784	58	3.00506 (-4)	27.296
1	3.04781 (-2)	5.927	30	6.06013 (-3)	10.021	59	2.62153 (-4)	28.444
2	2.92903 (-2)	6.015	31	5.59689 (-3)	10.271	60	2.27182 (-4)	29.684
3	2.81278 (-2)	6.106	32	5.15838 (-3)	10.537	61	1.95594 (-4)	31.079
4	2.69899 (-2)	6.199	33	4.74448 (-3)	10.820	62	1.67556 (-4)	32.725
5	2.58766 (-2)	6.294	34	4.35504 (-3)	11.120	63	1.43176 (-4)	34.575
6	2.47877 (-2)	6.391	35	3.98977 (-3)	11.439	64	1.21936 (-4)	36.460
7	2.37211 (-2)	6.486	36	3.64821 (-3)	11.778	65	1.03380 (-4)	38.543
8	2.26726 (-2)	6.577	37	3.32955 (-3)	12.134	66	8.72581 (-5)	40.772
9	2.16375 (-2)	6.667	38	3.03279 (-3)	12.508	67	7.32963 (-5)	43.218
10	2.06230 (-2)	6.782	39	2.75710 (-3)	12.906	68	6.12459 (-5)	45.888
11	1.96453 (-2)	6.917	40	2.50183 (-3)	13.329	69	5.08963 (-5)	48.804
12	1.87011 (-2)	7.039	41	2.26603 (-3)	13.773	70	4.20498 (-5)	52.006
13	1.77858 (-2)	7.170	42	2.04856 (-3)	14.240	71	3.45246 (-5)	55.538
14	1.69010 (-2)	7.295	43	1.84834 (-3)	14.735	72	2.81569 (-5)	59.442
15	1.60403 (-2)	7.420	44	1.66458 (-3)	15.260	73	2.27996 (-5)	63.773
16	1.52046 (-2)	7.545	45	1.49621 (-3)	15.809	74	1.83201 (-5)	68.594
17	1.43915 (-2)	7.674	46	1.34175 (-3)	16.370	75	1.45994 (-5)	73.982
18	1.36022 (-2)	7.805	47	1.19957 (-3)	16.941	76	1.15310 (-5)	80.031
19	1.28357 (-2)	7.943	48	1.06851 (-3)	17.541	77	9.01989 (-6)	86.854
20	1.20927 (-2)	8.086	49	9.48114 (-4)	18.184	78	6.98198 (-6)	94.588
21	1.13738 (-2)	8.239	50	8.38051 (-4)	18.883	79	5.34306 (-6)	103.403
22	1.06796 (-2)	8.400	51	7.38178 (-4)	19.655	80	4.03802 (-6)	113.515
23	1.00113 (-2)	8.571	52	6.48465 (-4)	20.523	81	3.01006 (-6)	125.179
24	9.36911 (-3)	8.752	53	5.68979 (-4)	21.514	82	2.20811 (-6)	138.308
25	8.75304 (-3)	8.940	54	4.99706 (-4)	22.651	83	1.55196 (-6)	147.607
26	8.16322 (-3)	9.137	55	4.40137 (-4)	23.897	84	8.72860 (-7)	146.593
27	7.59943 (-3)	9.344	56	3.88585 (-4)	25.105	85	6.65353 (-8)	142.765
28	7.06121 (-3)	9.559	57	3.42523 (-4)	26.196			

Table 4.6: Energy levels for the triplet excited state $1^3\Sigma_g^+$ (with $J = 1$) and the averaged radius in atomic units for ^{6}Li.

and $D^Y_{ab}(R)$ in atomic units is given by the appropriate matrix element

$$\langle\psi_a| - \sum_i (x_i \pm iy_i)/\sqrt{2}|\psi_b\rangle \quad \text{and} \quad \langle\psi_a| - \sum_i z_i|\psi_b\rangle \ , \tag{4.18}$$

depending of the symmetries of the states a and b. In our case, both initial and final states are Σ states, and for such a $\Sigma - \Sigma$ transition, only the z_i contributes. So we have here

$$\mathbf{D}^Y_{ab}(R) = D^Y_{ab}(R)\hat{\mathbf{R}} \ , D^Y_{ab}(R) = \langle\psi_a| - \sum_i z_i|\psi_b\rangle \ . \tag{4.19}$$

We used the values calculated by Ratcliff, Fish, and Konowalow [63] for distances ranging from 3.5 to $35.0a_0$ for both singlet and triplet transitions: $1^1\Sigma^+_g(X)$ $\rightarrow$ $1^1\Sigma^+_u(A)$ and $1^3\Sigma^+_u(a) \rightarrow 1^3\Sigma^+_g$. They are listed in Table 4.7, together with the asymtotic value. However, we rescaled all their values by a coefficient. For large distances, the dipole transition moment takes the asymptotic form (see Marinescu and Dalgarno [64])

$$D_{ab}(R) \simeq D^{(0)}_{ab} + \frac{b_{ab}}{R^3} \ . \tag{4.20}$$

We used a better estimate for $D^{(0)}_{ab}$ from Marinescu and Dalgarno [64] and rescaled all the data by the ratio of the two asymptotic values

$$D^{\text{new}}_{ab}(R) = D^{\text{old}}_{ab}(R)\frac{D^{(0),\text{new}}_{ab}}{D^{(0),\text{old}}_{ab}} \ , \tag{4.21}$$

where the *old* values are the original ones from Ratcliff *et al.* [63]. Once the data had been corrected, we used a cubic spline fitting procedure to interpolate between that range of distances.

R (a_0)	$1^1\Sigma_g^+$-$1^1\Sigma_u^+$ singlet	$1^3\Sigma_u^+$-$1^3\Sigma_g^+$ triplet	R (a_0)	$1^1\Sigma_g^+$-$1^1\Sigma_u^+$ singlet	$1^3\Sigma_u^+$-$1^3\Sigma_g^+$ triplet
3.5	2.7013	3.5925	14.0	3.4664	3.4590
4.0	2.8248	3.8247	15.0	3.4377	3.4344
4.5	2.9820	3.9887	16.0	3.4177	3.4163
5.0	3.1615	4.0982	17.0	3.4033	3.4027
5.5	3.3518	4.1601	18.0	3.3925	3.3922
6.0	3.5408	4.1795	19.0	3.3841	3.3840
6.5	3.7153	4.1625	20.0	3.3775	3.3775
7.0	3.8614	4.1177	21.0	3.3723	3.3723
7.5	3.9665	4.0542	22.0	3.3680	3.3680
8.0	4.0222	3.9811	23.0	3.3644	3.3644
8.5	4.0274	3.9055	24.1	3.3612	3.3612
9.0	3.9896	3.8325	25.0	3.3590	3.3590
9.4	3.9377	3.7782	26.0	3.3569	3.3569
10.0	3.8426	3.7056	27.0	3.3551	3.3551
11.0	3.6893	3.6097	29.0	3.3522	3.3522
12.0	3.5791	3.5412	30.0	3.3511	3.3511
13.0	3.5099	3.4930	35.0	3.3471	3.3471
	Li(2s)+Li(2p) Li(2s)+Li(2s)		$D(\infty)$	3.340	

Table 4.7: Electronic transition dipole moments in atomic units.

Source	$D^{(0)}$	b
Marinescu and Dalgarno [64]	3.3175	283.07
Ratcliff *et al.* [63]	3.3400	299.17
Pipin and Bishop [67]	3.3167	

Table 4.8: Asymptotic coefficients of the transition dipole moment in atomic units. We used the values from Marinescu and Dalgarno.

For small distances, we used the Taylor series first term and wrote

$$D_{ab}(R) = D_{ab}(R_{min}) + \left.\frac{dD_{ab}(R)}{dR}\right|_{R_{min}} (R - R_{min}) \; . \tag{4.22}$$

Finally, we selected the value of b_{ab} from Marinescu and Dalgarno [64] and used the expression from Eq. (4.20) for large distances (*i.e.* $R > R_{max}$). Table 4.8 lists the various coefficients used here, and Fig 4.3 shows the two curves.

4.3 Results: total spectrum

In this section, we will give the experimental data obtained by R.G. Hulet and his group at Rice University and compare them with our calculated results using the previous formalism, for both lithium isotopes. We will first present the total spectrum for ^{7}Li which is the most abundant isotope, followed by ^{6}Li.

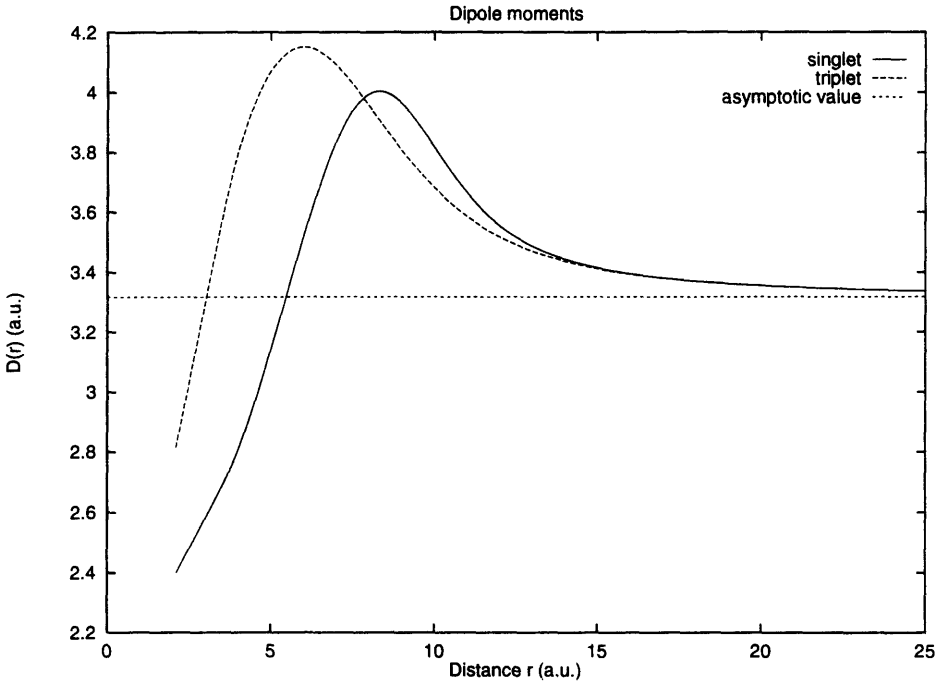

Figure 4.3: Singlet and triplet dipole moments for our transitions.

4.3.1 ^{7}Li

Fig. 4.4 shows the experimental spectrum obtained by R.G. Hulet *et al.* for the photoassociation of ^{7}Li. The frequency ranges from 0 to 2000 GHz red-detuned from the $2S_{1/2} - 2P_{1/2}$ atomic transition limit. As the detuning grows (*i.e.* becomes more negative) we can see two distinct series of sharp peaks. The stronger peaks persist for very large detunings and correspond to a transition between triplet states, as we will show later. The weaker peaks, corresponding to the transition between singlet states, vanish at detuning higher than 400 GHz, while the triplet signal is still quite strong. The experiment was performed at a temperature suggested to be 1 mK. We argue later that the line profiles indicate a temperature near 7 mK.

In order to explain these observations, we computed the photo-absorption spec-

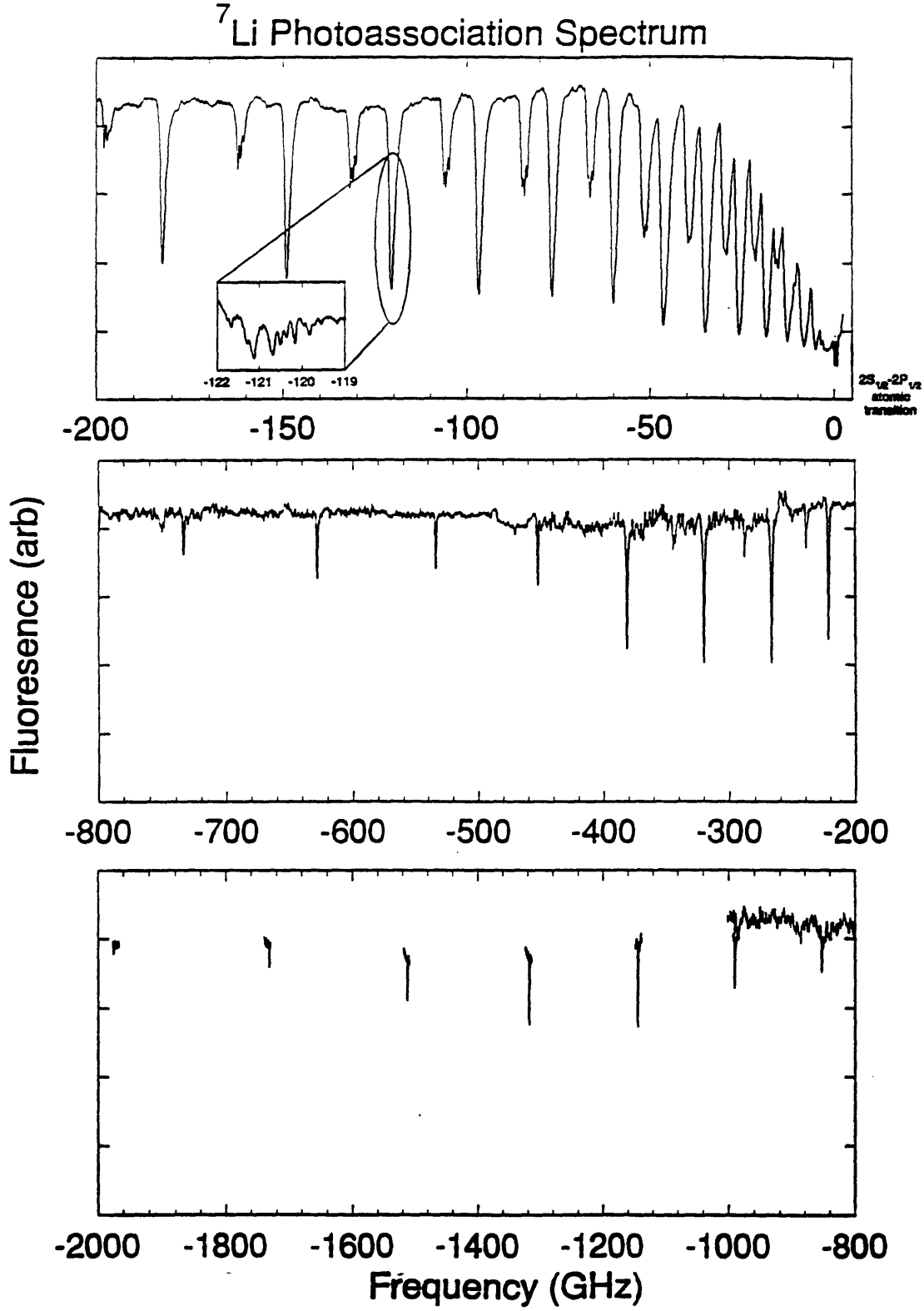

Figure 4.4: Experimental data for ^{7}Li from R.G. Hulet *et al.*

trum using the expression of the previous section. Fig. 4.5 illustrates the results of our calculations for the ^{7}Li case for the same frequency intervals as the experimental data. It is worth noting that the experimental results are the mirror image of the calculations presented in Fig. 4.5. In fact, a peak in the photo-absorption spectrum corresponds to a drop in the fluorescence measured experimentally. Notice here that we included the transition for $l = 0$ in the ground (free) state to $J = 1$ in the excited (bound) state ($l = 0 \rightarrow J = 1$). As we will see later, this is the most important contribution at $T \sim 1$ mK, higher partial waves $l > 0$ being negligible then. Therefore, the equation used to compute the values shown in Fig. 4.5 is a simplification of Eq. (4.10), namely we took $J = 1$ and dropped the $l = J + 1 = 2$ contribution

$$\kappa^Y_{b\rightarrow a}(\nu, T) \simeq \omega_Y \frac{16\pi^3\nu}{3hc} n^2_{\mathrm{Li}} \frac{\pi h^3}{(2\pi\mu k_B T)^{3/2}} \sum_v \omega_{YJ} \times \exp\left(-\frac{\hbar^2 K^2}{2\mu k_B T}\right) \left[J|\langle u_b^{K,J-1}|D^Y_{ab}|u_a^{v,J}\rangle|^2\right] . \quad (4.23)$$

Here also, we find two series of signals, a stronger and a weaker one. The stronger one originates from the triplet transition, namely $1^3\Sigma_u^+ \rightarrow 1^3\Sigma_g^+$, and persists to very large values of detuning. The second weaker series is due to the singlet transition $1^1\Sigma_g^+ \rightarrow 1^1\Sigma_u^+$. It becomes quickly negligible in the 400 GHz range, when compared to the triplet series. The relative intensity between two adjacent triplet and singlet peaks seems to vary between 5 and 10: the triplet peak is five to ten times bigger than the singlet one next to it. This ratio grows with increasing detuning. The line positions agree within 1% but this could be improved by varying the dissociation energy of the excited potential, or by modifying its inner wall slightly. Finally, we notice that the strength of the lines decreases at small detuning (near zero). This is

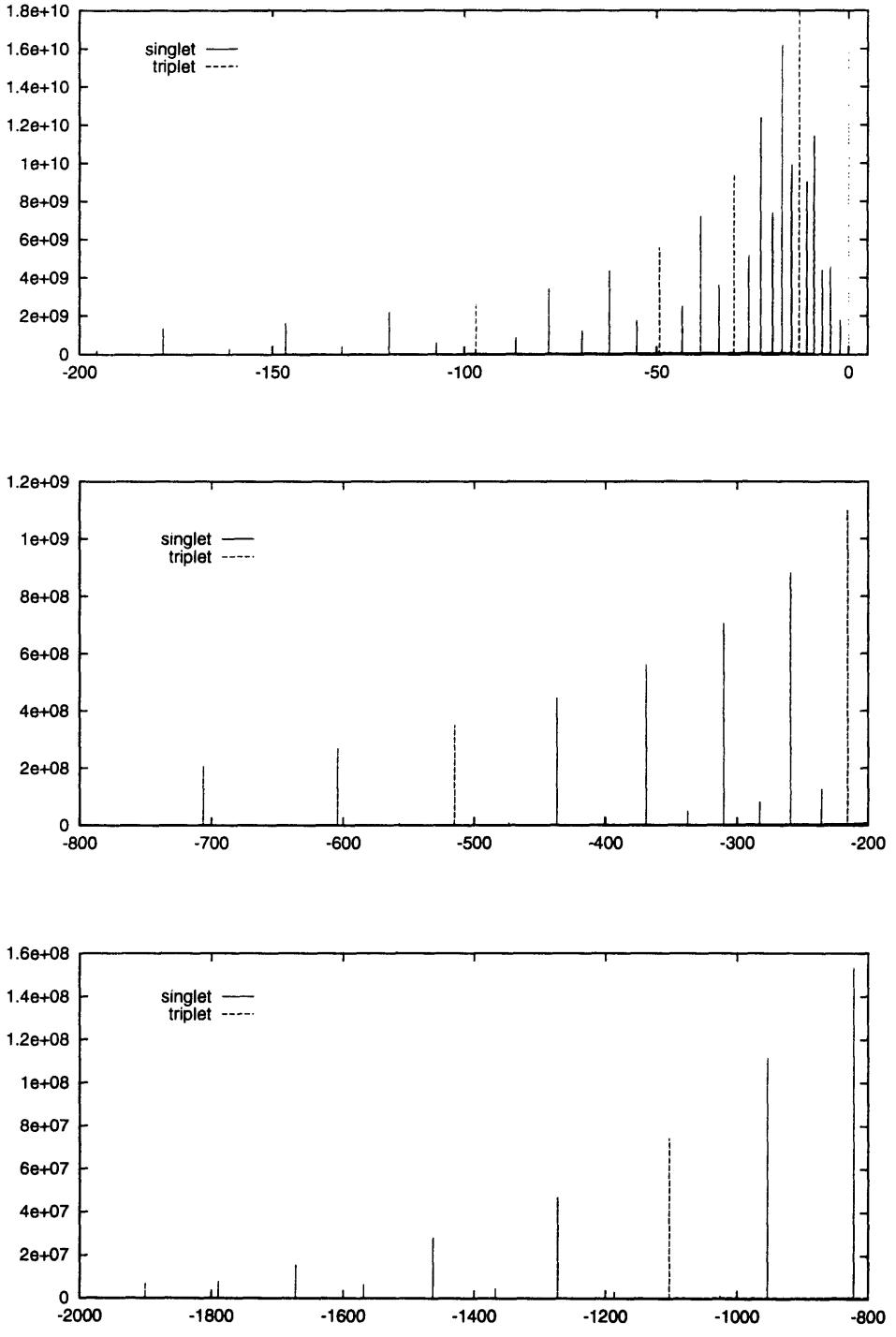

Figure 4.5: Theoretical photo-absorption (in arb. units) for ^{7}Li as a function of the detuning (GHz).

a manifestation of the too small integration box used to compute the excited bound state wave functions for high v (see §4.2.1).

In order to explain these different observations, a closer look at the different elements in the absorption transition probability equation is required. A first candidate for the difference in intensities comes from the statistical weights difference in Eq. (4.23). For the ($l = 0 \rightarrow J = 1$) transition that we considered here, the singlet and triplet signals should have $\omega_Y \omega_{YJ} = 3/32$ and $15/32$ respectively (see Table 4.1 for the ^{7}Li case with J odd). Although this helps in understanding part of the ratio between singlet and triplet intensities, it provides no clues to explain the disappearance of the singlet signal at higher detunings. We must then examine the dipole moment integrals. In order to simplify the notation, let us write

$$|D_v(E)|^2 = |D_{vK}^{J=1,l=0}|^2 \,, \tag{4.24}$$

where

$$D_{vK}^{Jl} \equiv \langle u_a^{v,J}(R)|D_{ab}^Y(R)|u_b^{K,l}(R)\rangle = \int_0^\infty dR\, u_a^{v,J}(R) D_{ab}^Y(R) u_b^{K,l}(R) \,. \tag{4.25}$$

We show a set of ten levels for both the singlet and triplet transitions in Figs. 4.6 and 4.7 respectively. The x-axis is the logarithm of the energy (in base 10), the y-axis the vibrational level of the excited bound state considered. The full range of levels is illustrated in Appendix E, also in this three dimensional representation. We notice some general features: as $E \rightarrow 0$, the singlet values drop faster than the triplet ones. The maximum values for both the singlet and the triplet transitions occur around $\log_{10} E = -7.5$ corresponding to a temperature $T \sim 10$ mK in most

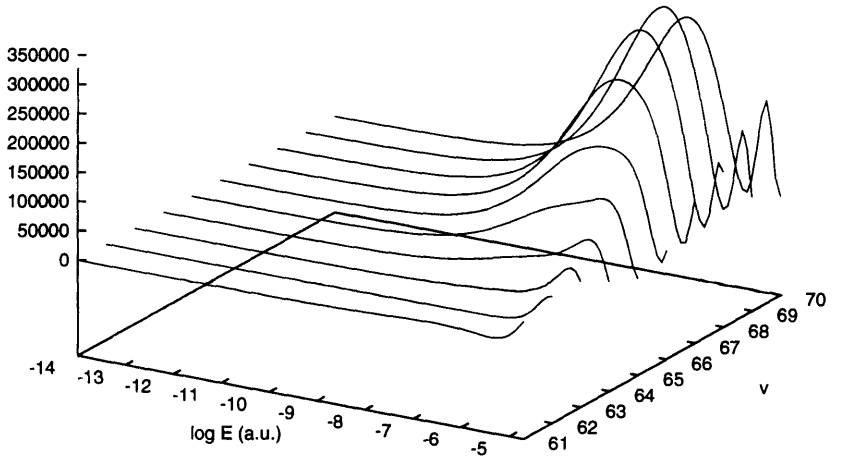

Figure 4.6: Examples of dipole matrix element $|D_v(E)|^2$ for ^{7}Li singlet transitions.

of the vibrational levels. This last result implies that the prefered kinetic energy for a spontaneous dissociation of Li_2^* into two free atoms would be equivalent to a temperature of 10 mK, hence representing a heating mechanism for an optical trap maintained at 1 mK.

On the same graphs, we can see that the triplet values are generally bigger than the singlet ones (except maybe for the extremely low vibrational levels (see Appendix E). One can link this fact to the magnitude of the scattering length, at least for the higher vibrational levels. To illustrate this, let us consider two neighbouring levels, one singlet and one triplet. Let us take the ones near -110 GHz, namely $v_s = 89$ (at $\Delta \sim -107$ GHz) for the singlet transition and $v_t = 80$ (at $\Delta \sim -120$ GHz) for the triplet transition. The bound state wave functions for both levels are shown in Fig.

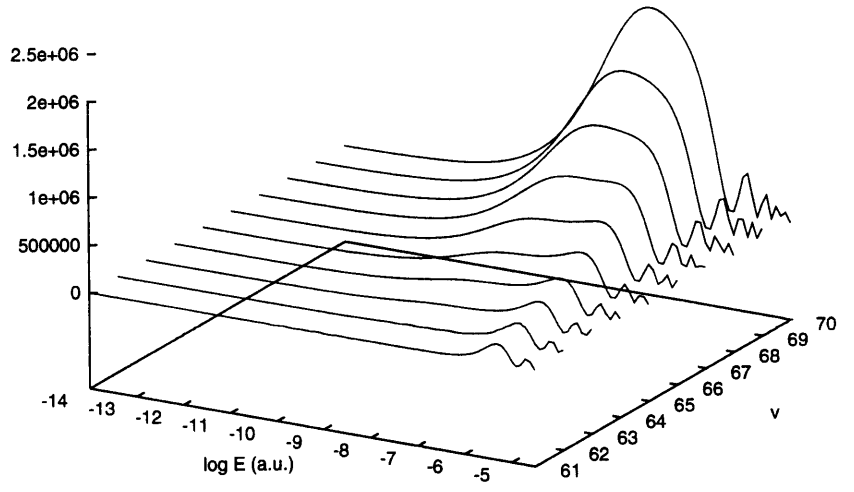

Figure 4.7: Examples of dipole matrix element $|D_v(E)|^2$ for ^{7}Li triplet transitions.

4.8: both are fast oscillating functions with small amplitudes, except for the last lobe centered around 80-85a_0.

Using this fact, we see that for a high vibrational number, most of the contribution to the integral comes from the overlap of this last lobe with the free wave function and the dipole moment. Since $D^Y_{ab}(R)$ for large R is basically a constant $D^Y_{ab}(R) \sim D_0$ for both singlet and triplet transitions, we then have

$$\begin{aligned} |D_v(E)|^2 &= \left| \int_0^\infty dR u_a^{v,J}(R) D^Y_{ab}(R) u_b^{K,l}(R) \right|^2 \\ &\simeq \left| \int_{R_1}^{R_2} dR u_a^{v,J}(R) D^Y_{ab}(R) u_b^{K,l}(R) \right|^2 \\ &\simeq |D_0|^2 \left| \int_{R_1}^{R_2} dR u_a^{v,J}(R) u_b^{K,l}(R) \right|^2 , \end{aligned} \tag{4.26}$$

where R_1 and R_2 define the last lobe. Now, we can assume $E \to 0$. In this case, in

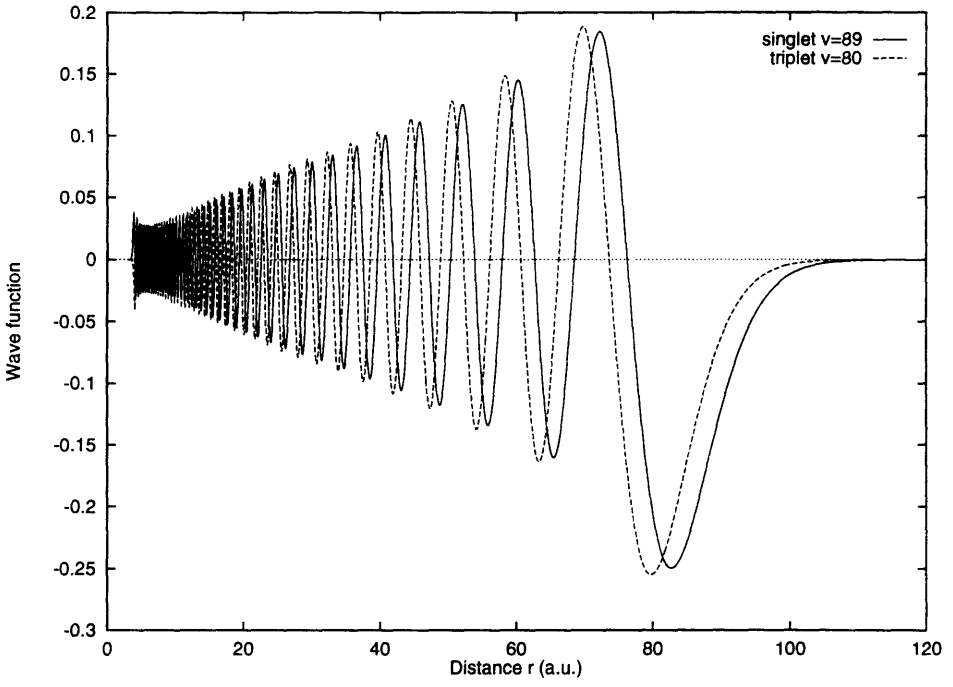

Figure 4.8: Excited wave functions for $^7Li_2$ ($v_s = 89$ and $v_t = 80$).

the vicinity of the lobe, the free wave function takes its asymptotic form (see §1.5.2 and the normalization in §4.1)

$$\begin{aligned} u_b^{K,l}(R) &\simeq \left(\frac{2\mu}{\pi\hbar^2 K}\right)^{1/2} \sin\delta_l(K) \frac{\sin[KR - l\pi/2 + \delta_l(K)]}{\sin\delta_l(K)} \\ &\simeq \left(\frac{2\mu}{\pi\hbar^2 K}\right)^{1/2} \left(1 - \frac{r}{a}\right) \sin\delta_l(K) \ . \end{aligned} \tag{4.27}$$

Substituting in the previous expression, and by the mean value theorem, we get

$$\begin{aligned} |D_v(E)|^2 &\simeq |D_0|^2 \left(\frac{2\mu}{\pi\hbar^2 K}\right) \sin^2\delta_l(K) \left| \int_{R_1}^{R_2} dR \left(1 - \frac{r}{a}\right) u_a^{v,J}(R) \right|^2 \\ &\simeq |D_0|^2 \left(\frac{2\mu}{\pi\hbar^2 K}\right) \left(1 - \frac{\overline{r}}{a}\right)^2 L^2 |u_a^{v,J}(\overline{r})|^2 \sin^2\delta_l(K) \ , \end{aligned} \tag{4.28}$$

where $\overline{r}$ is the position of the center of the lobe and L its dimension. Finally, a further step can be taken by knowing that $\delta_l(K) \to 0$ as $K \to 0$, and using the effective range

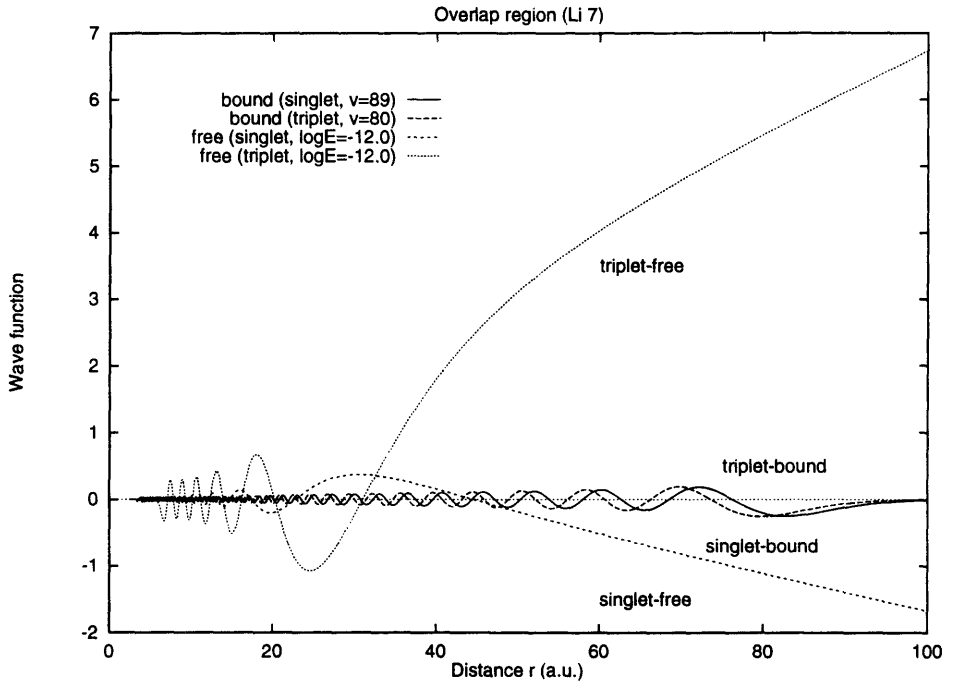

Figure 4.9: Wave functions in the overlap region.

expansion for $l = 0$

$$\sin^2 \delta_0(K) = \frac{K^2}{K^2 + K^2 \cot^2 \delta_0(K)} \simeq a^2 K^2 [1 + aK^2(r_e - a)] + \mathcal{O}(K^5) \ . \qquad (4.29)$$

As we saw in chapter 2, this is valid for energies up to $10^{-9} - 10^{-8}$ a.u. in the case of $l = 0$. Then, we can rewrite $|D_v(E)|^2$ as

$$|D_v(E)|^2 \simeq \left(\frac{2\mu K}{\pi \hbar^2}\right) |D_0|^2 (a - \overline{r})^2 L^2 |u_a^{v,J}(\overline{r})|^2 + \mathcal{O}(K^3) \ . \qquad (4.30)$$

Fig. 4.9 illustrates the wave functions in the overlap region for both the singlet $v_s = 89$ and triplet $v_t = 80$ bound levels, together with the free wave functions.

As we can see from this derivation, the magnitude of $|D_v(E)|^2$ is simply related to the scattering length a. From this relationship, we can explain most of the differences in the amplitudes of the signals. In fact, for two adjacent peaks, like $v_s = 89$ and

$v_t = 80$ considered above, we can assume that the bound state wave functions will behave in a similar way, *i.e.* the position and dimension of the last lobe will be very similar (see Fig. 4.8). Of course, this will cease to be true at lower v, but it is a fair approximation for the higher levels considered here. Therefore, the difference in the amplitude is directly given by the difference in the values of the scattering lengths (as long as the energy is small enough). In the case of ^{7}Li, we have $a = 36.92a_0$ and $-17.16a_0$ for the singlet and triplet respectively. Hence, using both $\bar{r}^t = \bar{r}^s \simeq 80a_0$ the ratio of the two signals should be

$$\frac{|D_v^t(E)|^2}{|D_v^s(E)|^2} \simeq \left(\frac{a^t - \bar{r}^t}{a^s - \bar{r}^s}\right)^2 \simeq 5.1 \ . \tag{4.31}$$

Since the scattering length for the triplet is negative, $|D_v^t(E)|^2$ will always be bigger than $|D_v^s(E)|^2$ for those higher neighbouring vibrational levels. In fact, for the cases mentioned above, we get a good agreement, when we look at the exact results in Fig. 4.10. On that same figure, we also included the curves from the expressions (4.28) and (4.30).

As mentioned before, this approximate expression for $|D_v(E)|^2$ is valid in the low energy limit. However, we can expand the general dependence on the scattering length far beyond $\log_{10} E \simeq -9$. In fact, as we can see in Fig. 4.11 for the two high levels considered before, the free wave function does follow the same qualitative behaviour for energies up to $\log_{10} E \simeq -7.5$ corresponding to a temperature of 10 mK. Of course, the amplitude of the singlet wave function in the overlap region (between 75 and $100a_0$) finally becomes comparable to the triplet one as the energy increases.

Finally, as we lower the vibrational level (or increase the detuning), we can expect

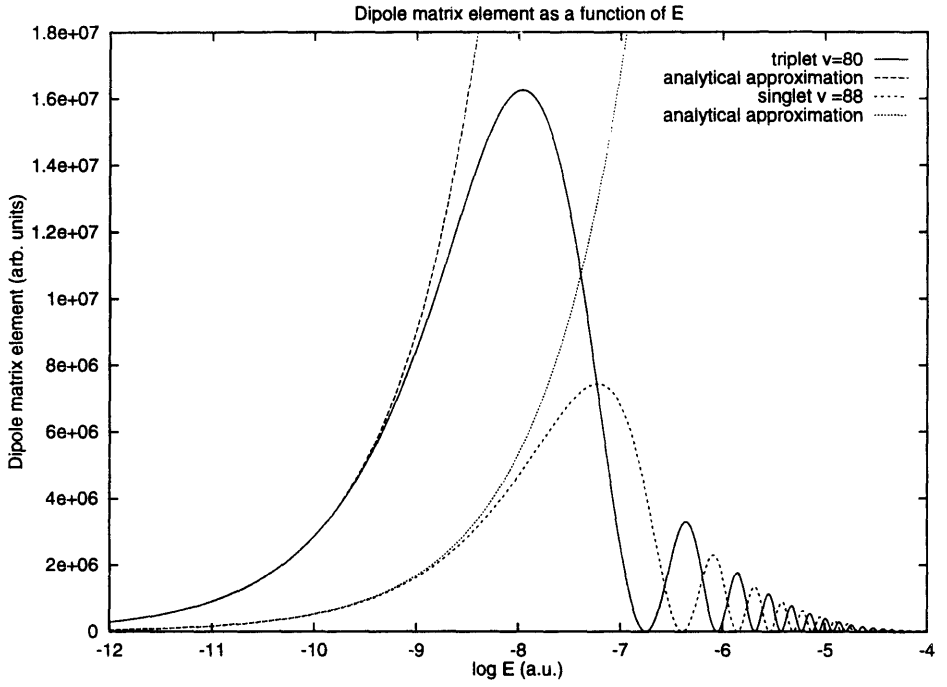

Figure 4.10: Dipole matrix element $|D_v(E)|^2$.

a very different behaviour for the singlet and the triplet signals. In fact, since lowering v implies a smaller value for $\overline{r}$, we conclude that the singlet absorption should decrease faster than the triplet one, due to the difference in the sign of their respective scattering lengths. Moreover, the singlet should go through a minimum for values of $\overline{r}$ near a_s, while the triplet absorption should not be affected. This in fact explain why the singlet signal decreases much faster than the triplet one, and even vanishes.

As we further lower v, the approximation (4.30) is not valid anymore. In fact, when $\overline{r}$ is such that the asymptotic form of the free wave function cannot be used, the overlap integral would become small quite fast. Moreover, one cannot consider $D^Y_{ab}(R)$ constant anymore, and depending on the distance, the singlet or the triplet might have a bigger dipole moment. From the dipole moment curves (see Fig. 4.3),

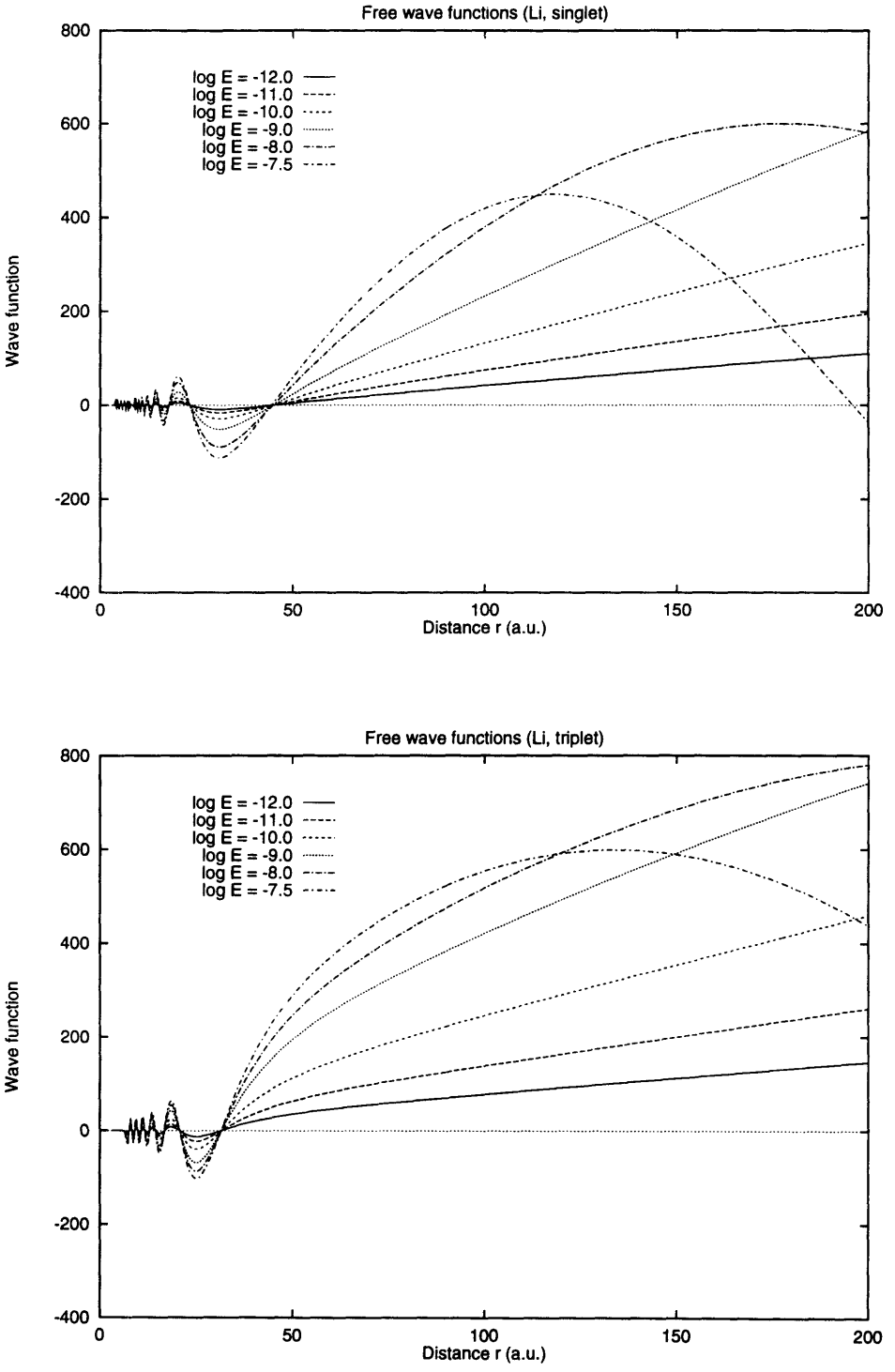

Figure 4.11: Wave functions for the singlet ($v_s = 89$) and triplet ($v_t = 80$) continuous states of ^{7}Li.

we notice that if the overlap region in centered around $\bar{r} < 8a_0$, the triplet signal should be bigger, but if $8 < \bar{r} < 15a_0$, the singlet should be bigger. At distances larger than $15a_0$ th two dipole moments are basically equal, and any difference arises from the overlap of the wave functions only.

Let us summarize the above analysis. The influence of the scattering length will show itself differently depending upon the vibrational bound level of the excited state. In fact, for small v but with $\bar{r}$ large enough so that the asymptotic free wave function can be used, the region of greater overlap will be at a much smaller distance, and the sign of a will be more relevant. As we can see in Fig. 4.11, the amplitude of the free wave function is much bigger in the case of a negative a than for a positive one, unless of course the magnitude of a is so big that the asymptotic behaviour $1 - r/a$ makes no difference in the overlap region. Now, for a higher v where the lobe is far out, the most relevant quantity is the magnitude of a because

$$|u(r)| \sim |1 - r/a| \sim |r/a| \ , \tag{4.32}$$

and only the size of a will really play a role, though a negative a would imply a slightly bigger overlap than a positive one. In our case, $a_t \simeq -a_s/2$, and therefore the triplet signal for high v is roughly 4 times bigger than the singlet one. The effect of the sign would be obvious for smaller v, as we can see in §4.4.

4.3.2 ^{6}Li

We show the experimental spectrum obtained by R.G. Hulet *et al.* for the photoassociation of ^{6}Li in Fig. 4.12. The frequency ranges from 0 to 3000 GHz red-detuned

from the $2S_{1/2} - 2P_{1/2}$ atomic transition limit. Here also we can see two distinct series of sharp peaks as the detuning grows. The stronger peaks corresponding to a transition between triplet states persist for very large detunings, while the weaker peaks (singlet transitions) vanish at detuning higher than 200 GHz. We also notice that the triplet signal is much stronger than the singlet one, and when compare with ^{7}Li, the ratio between intensities of two neighbouring singlet and triplet peaks is bigger here. The experiment was performed at a temperature suggested to be approximately 1 mK.

The results of our calculations are shown in Fig. 4.13 for the same detuning intervals. As we can see, we observe the same general features as described above. The triplet transitions are much bigger than the singlet ones, those last dissappearing around 200 GHz.

The same interpretation is valid here. In fact, one can even argue that this is a better demonstration of the validity of our previous explanation. Since the scattering lengths are so different in this case ($a = 48.3$ and $-312.2a_0$ for the singlet and triplet respectively (see also Table 2.20)), the dependence on the scattering length is more important than in the ^{7}Li case. Again, the decrease near zero detuning is due to the too small integration box for high v (see §4.2.1).

In fact, in the case of the triplet transitions, the intensity of the signal will be mostly dependent on the magnitude of $a/\overline{r}$, due to the large value of a. Moreover, as can be seen from our results (see Fig. 4.13), the relative intensities of the triplet peaks will remain rather constant, except for the very high vibrational levels. This

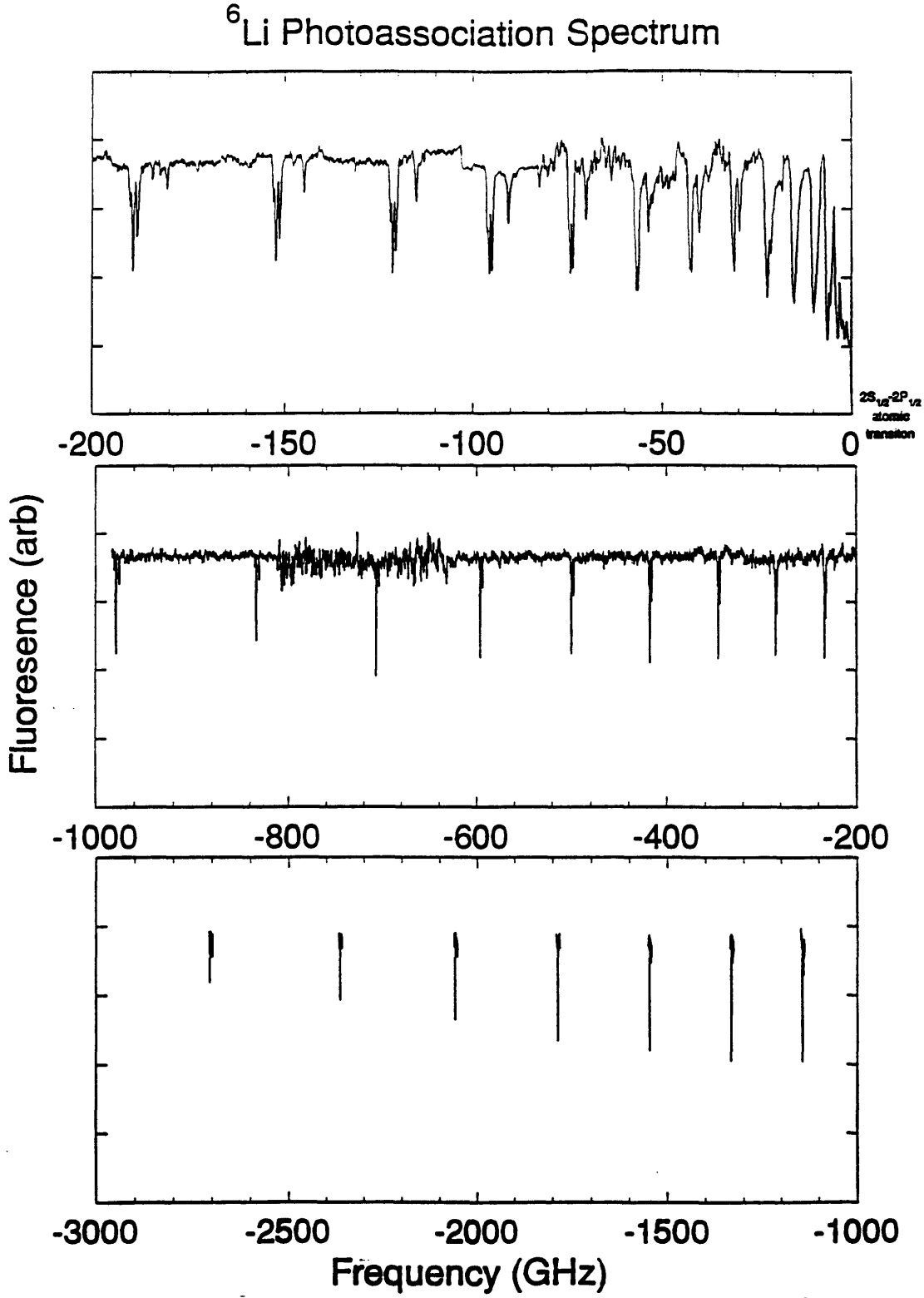

Figure 4.12: Experimental data for ^{6}Li from R.G. Hulet *et al.*

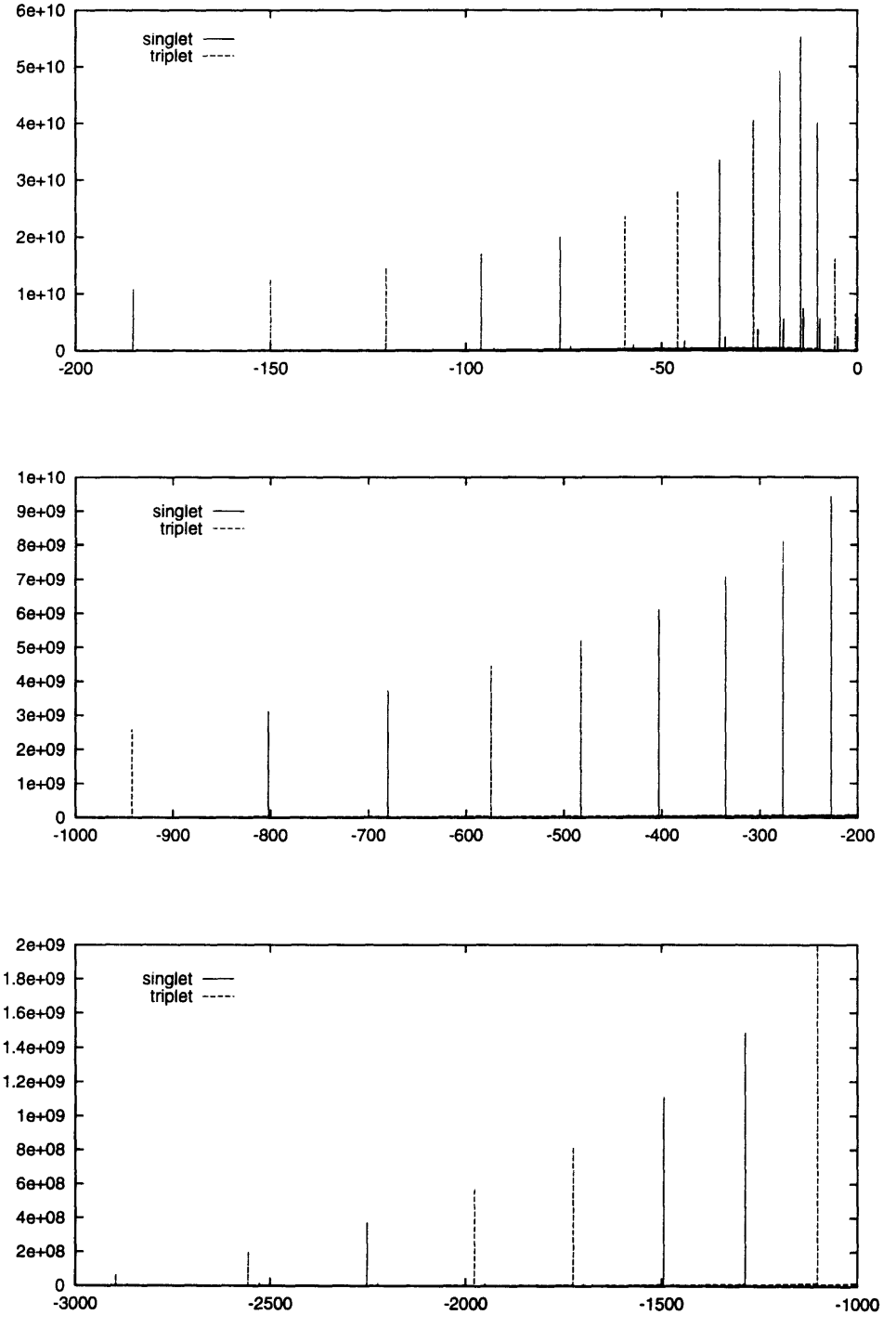

Figure 4.13: Theoretical photo-absorption (in arb. units) for ^{6}Li as a function of the detuning (Ghz).

comes from the fact that $(a - \overline{r}) \sim a$ except for large v, where $\overline{r}$ are sizable.

Let us now examine more accurate experimental results in order to verify our quantitative predictions.

4.4 Intensity ratios

In this section, we will compare a more accurate set of results obtained experimentally by R.G. Hulet *et al.* for a set of levels for the triplet transition for both isotopes. Due to the nature of the measurement, it is very hard to get meaningful values for the intensities of the peaks. In fact, even if the qualitative aspect of the experimental spectrums is adequate, the quantitative values obtained for the intensities of the peaks are not reliable. However, the position of those peaks is well determined by the experiment and give information about the energy levels of the excited states $1^1\Sigma_u^+$ and $1^3\Sigma_g^+$ of both ^{7}Li and ^{6}Li.

Now in order to check our prediction of the dependence of the intensities on the scattering lengths, R.G. Hulet and his group conducted a more precise measurement of the intensities for the triplet transition of both isotopes. They measured the relative strengths of the most deeply bound $1^3\Sigma_g^+$ states of ^{7}Li possible. Since the signal is of trap loss, which is non-linearly related to the rate of photoassociation, they performed the experiment in the following way (R.G. Hulet *et al.*, private communication). They measured the probe laser power necessary to give the same signal for the various vibrational levels. The trap-laser induced fluorescence was diminished by 20% for the

^{7}Li		^{6}Li	
v	P (mW)	v	P (mW)
62	400.0	56	380.0
63	74.0	57	130.0
64	32.0	58	58.0
65	16.0	59	41.0
66	13.1	60	24.0
67	7.5	61	20.0
68	5.5	62	14.5
69	3.7	63	13.1

Table 4.9: Experimental probe laser intensities for triplet transitions.

photoassociation laser powers given in Table 4.9. They repeated the same kind of measurements for the $1^3\Sigma_g^+$ state of ^{6}Li, *i.e.* they measured the intensities to give a constant photoassociation signal. The photoassociation powers needed to give a 8.3% photoassociation signal are given also in Table 4.9. Although the absolute values are not meaningful, the relative powers are.

Using the same vibrational levels, we assume that photo-absorption transition intensities were proportional to the inverse of the laser power, namely

$$\kappa^t_{\Sigma\to\Sigma}(v,\nu,T) \propto h\nu \frac{e^{-E/k_BT}}{T^{3/2}} |D_v(E)|^2 \propto \frac{1}{P} \ , \tag{4.33}$$

where P is the laser power, and $E = \hbar^2K^2/2\mu$ is related to the laser frequency ν and the detuning Δ from the bound level v by

$$h\nu = \Delta + \hbar\omega_p \ , \quad \text{and} \quad \Delta = -(E + |E_b(v)|) \ , \tag{4.34}$$

where $\hbar\omega_p$ is the energy difference between the asymptotes of the potential curves. We considered a temperature of 1 mK. Now, by setting the highest level available to unity, we scaled all the other ones accordingly to obtain the results shown in Fig. 4.14. From our previous analysis of the dependence over the scattering length, we do not expect a great variation of the ratios of the intensities as we vary the scattering length. To demonstrate that fact, we slightly changed the depth D_e of the ground state potential in order to move the scattering length around. The results are also illustrated on the same graph. As we can see, the different theoretical results vary by little, as predicted for a negative scattering length. Moreover, the same trend is observed in the experimental data, although some discrepancies are visible. However, the accuracy of the experimental laser power values was estimated to be around 10% by R.G. Hulet *et al.* Since the most precise data are expected to coincide with the highest levels (because the power does not have to be too strong, hence less trap loss and a more stable temperature, etc.), we can fit all the experimental values by varying our highest values by $\pm 5\%$. This in fact shows that the line strengths are rather insensitive to the exact value of the scattering length, and therefore confirm that the a is probably negative.

The same analysis was performed for ^{6}Li. The results are given in Fig. 4.15 for the same dissociation energies as in the case of ^{7}Li. The scattering lengths vary much more, even becoming positive. This implies that the potential is about to support a new bound state: in fact, in the last case, where the scattering length becomes positive, it does support a supplementary bound state. Since the scattering length

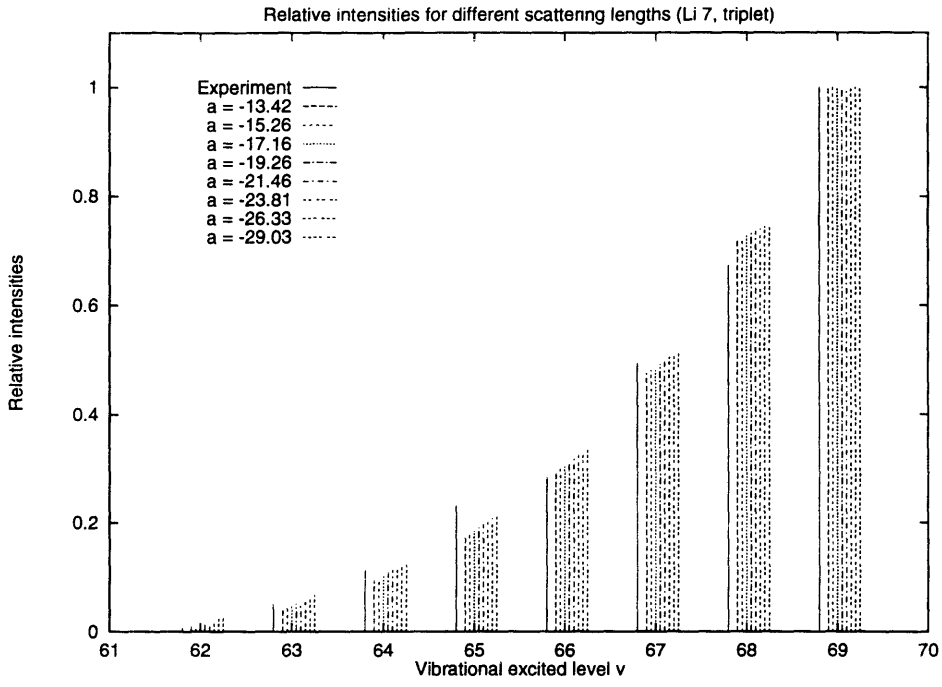

Figure 4.14: Intensity ratios for the triplet transitions of ^{7}Li.

is so large compared to the possible values of $\overline{r}$, the ratio of two subsequent peaks is quite insensitive to variations in a, as can be seen from our calculations. Moreover, the scaling between following peaks will be more dependent on the geometry of the last lobe (size and position) than on the scattering length, according to our approximate derivation (4.30). Finally, we can notice that experimental line strengths are smaller than our theoretical ones for the smaller vibrational number v, but they are bigger for the larger ones. Although these differences seem important, they are within the 10% accuracy of the experimental data. In fact, by reducing the high level intensity ratios by 10% and increasing the low one by the same amount, we get a good agreement. Notice finally that the graph is very dependent upon the level chosen to match to unity: by taking another level than the highest, the figure would look quite different.

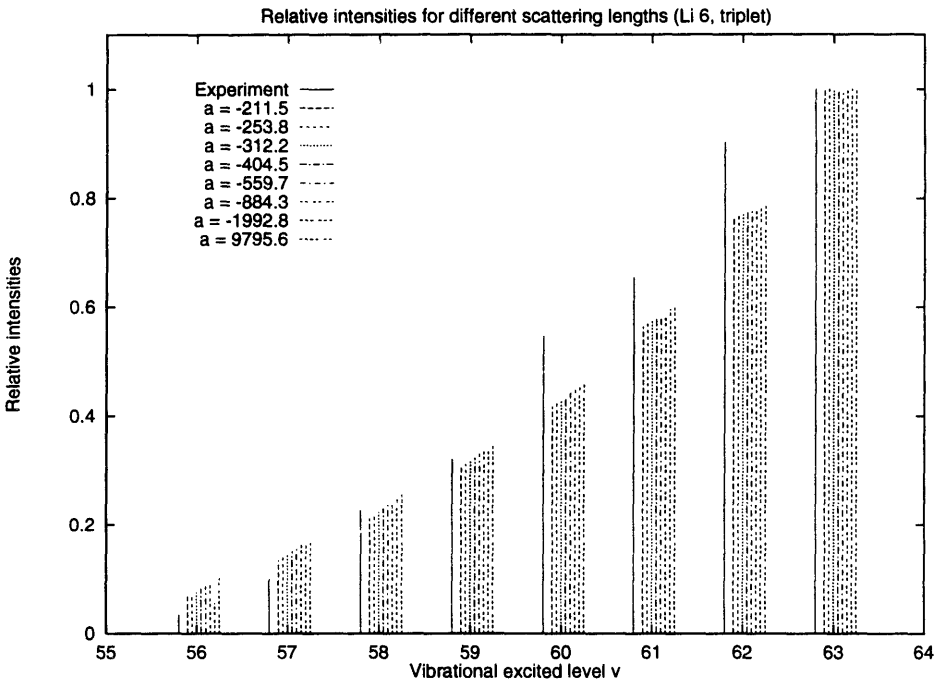

Figure 4.15: Intensity ratios for the triplet transitions of ^{6}Li.

At this point, there are no similar data available for the singlet transitions of ^{6}Li and ^{7}Li. However, since the scattering length is positive in both cases, and of reasonable size, *i.e.* of the order of the outer turning point of higher vibrational state, we predict a rather different behaviour. In fact, based on our previous derivation (4.30), we then should find a detuning region such that the signal would vanish and grow again at higher detunings. This dip in the line strengths should occur at vibrational levels such that $\overline{r}$ is near a. If we take $\overline{r}$ to be the averaged value of R for the excited state, we can predict that the local minimum should be located at $\langle R \rangle \simeq a$. This is an estimate only, since $\langle R \rangle$ is roughly of the same order as $\overline{r}$ for large v. With this in mind, we performed the calculation for both ^{6}Li and ^{7}Li isotopes with three different dissociation energies D_e giving three different scattering lengths a. In Fig. 4.16, we illustrate the results for ^{6}Li, and in Fig. 4.17 those for ^{7}Li. As

	^{7}Li			^{6}Li		
$D_e(X)$ (cm^{-1})	a_s (a_0)	v_{min}	$\langle R \rangle$ (a_0)	a_s (a_0)	v_{min}	$\langle R \rangle$ (a_0)
8515.50	+51.47	82	48.77	+69.36	79	56.18
8516.62	+36.92	78	37.22	+48.26	75	43.68
8518.00	+24.07	74	30.63	+35.00	71	34.94

Table 4.10: Position of the minimum peaks for the singlet transitions.

predicted, the line strength goes to zero as we increase the detuning, but then grows again before vanishing for higher detunings. The location of the minimum is roughly the same as the v level for which $\langle R \rangle \simeq a$. Table 4.10 summarizes the data from Tables 4.3 and 4.5. The agreement is rather good.

Finally, one should remember that this dependence on the scattering length is really a manifestation of the interference pattern in the overlap integral between the free wave function and the bound wave function (the effect of the dipole moment being negligible at such large distances). To better view this, we show in Fig. 4.18 the 3-D plot for the singlet transition in the ^{6}Li and ^{7}Li cases. As one can see, there is a local hill at lower energies as we increase v. However, due to this destructive interference of the free wave function with the bound one, this hill starts to decrease and desappears to be replaced be a new hill, much stronger, that seems to come from higher energies. This "wave" represents the constructive interference occuring

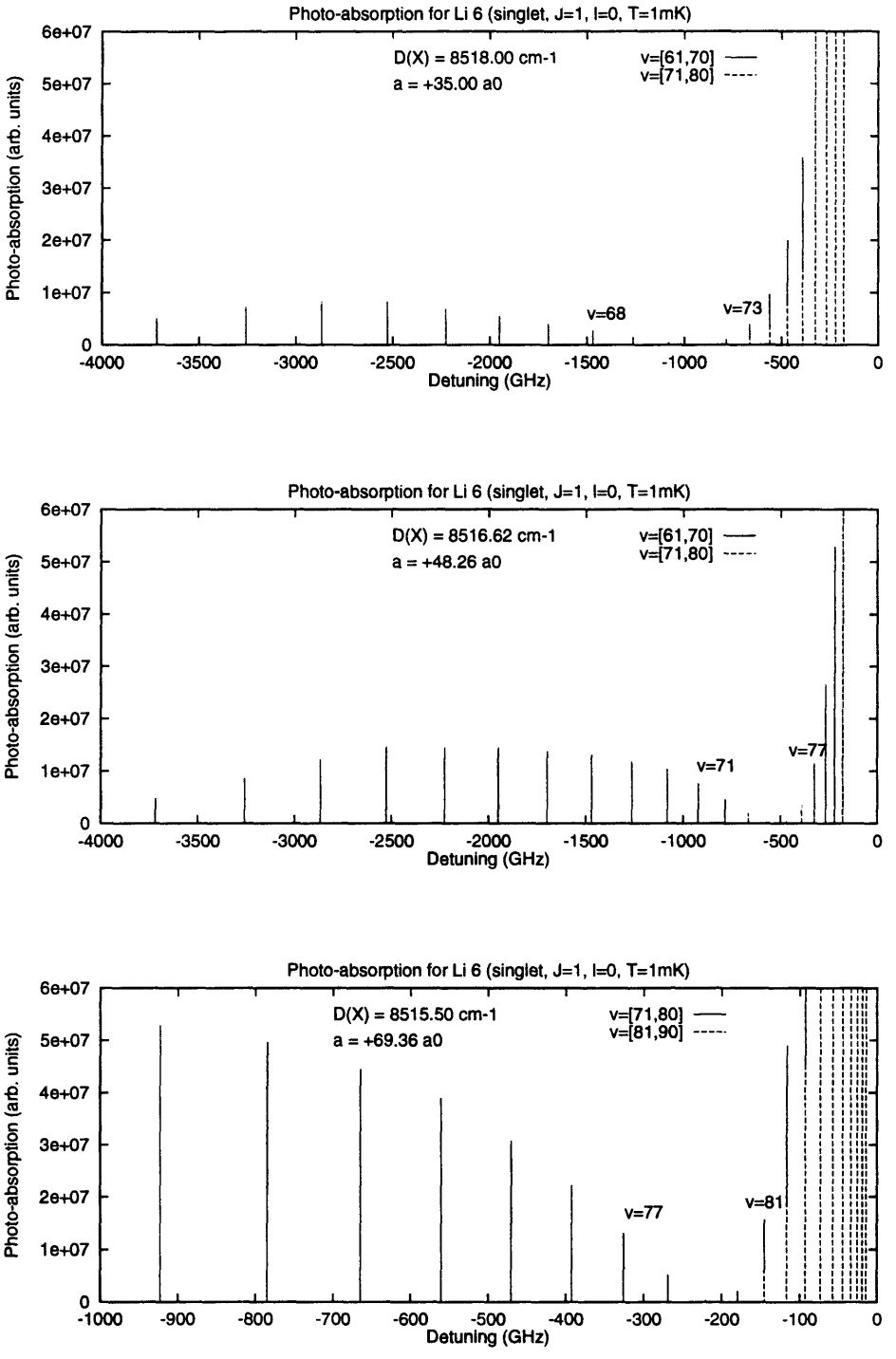

Figure 4.16: Photo-absorption for the singlet transitions of ^{6}Li.

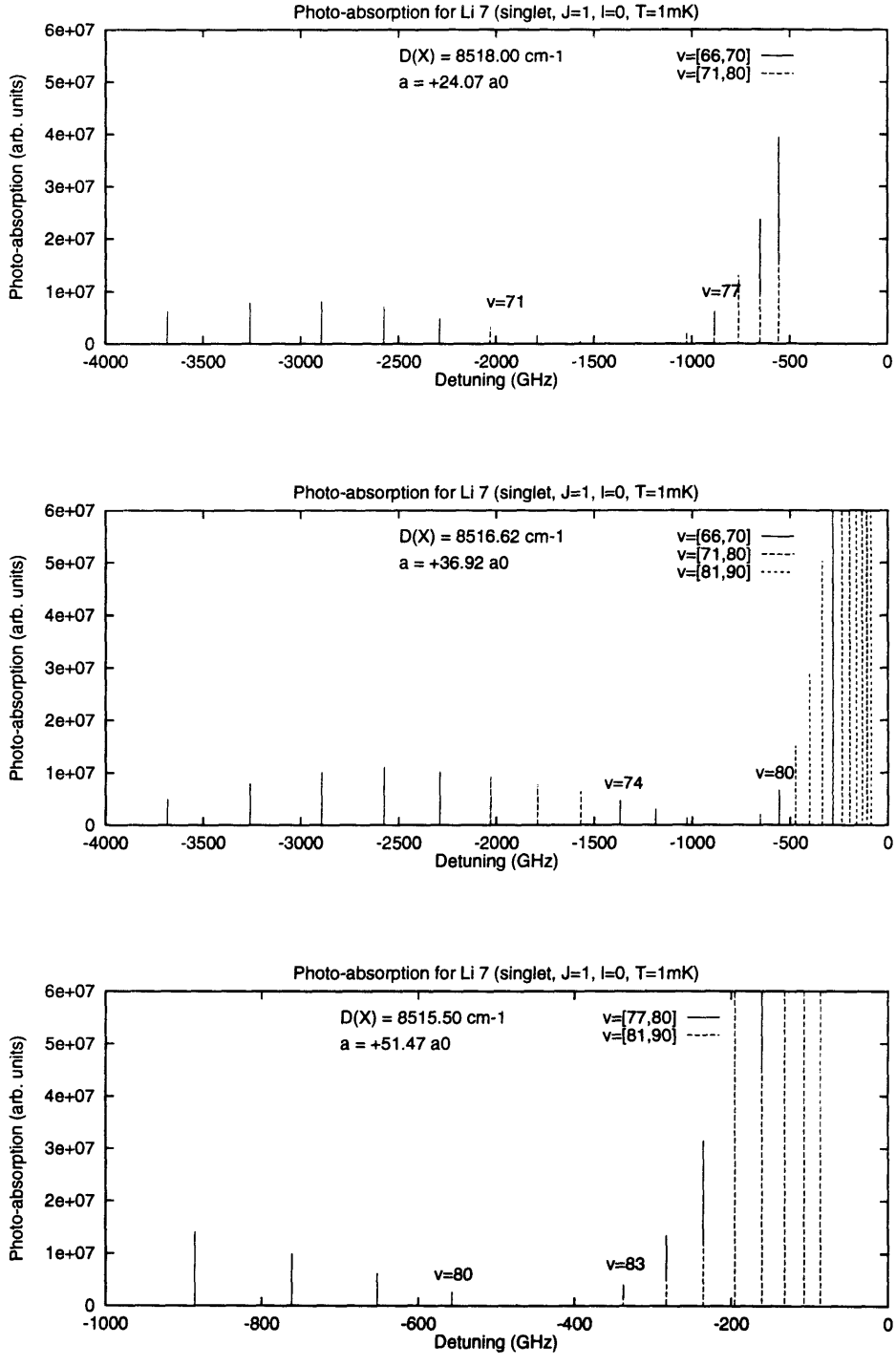

Figure 4.17: Photo-absorption for the singlet transitions of ^{7}Li.

as we increase $\bar{r}$ with higher values of v. Finally, notice that 1 mK corresponds to $\log_{10} E = -8.5$ on these graphs. On the other hand, the maximum of the first hill and the following "wave" are basically located at 10 mK ($\log_{10} E = -7.5$).

4.5 Higher partial waves

In the previous section, we only included the transition $l = 0$ (free wave function, ground state) $\rightarrow J = 1$ (bound level, excited state). Although this is a good approximation when $E < 10^{-9}$ a.u., the higher partial waves might come into play at energies near $10^{-8.5}$ a.u. (or $T \sim 1$ mK).

A look at the partial elastic cross sections for ^{7}Li in chapter 2 is sufficient to illustrate this fact. As we already know, the $l = 0$ partial wave is the major contribution for very low energies (up to $\log E \simeq -8$), but the $l = 1$ partial wave starts to contribute at $\log E \simeq -9$ and $\log E \simeq -8$ for the triplet and singlet states, respectively. In the latter case, the $l = 2$ partial wave dominates at $\log E \simeq -7.3$: it is a shape resonance. All those higher partial waves start to contribute for energies corresponding to 1 mK$< T <$10 mK, and therefore one should take them into account in the calculations.

In order to study the influence of higher partial waves, we conducted calculations including the following set of transitions

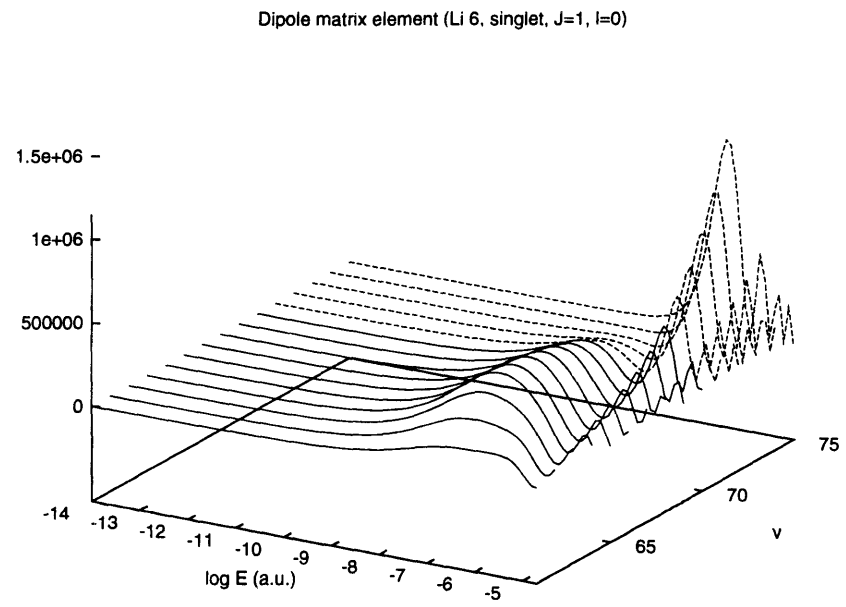

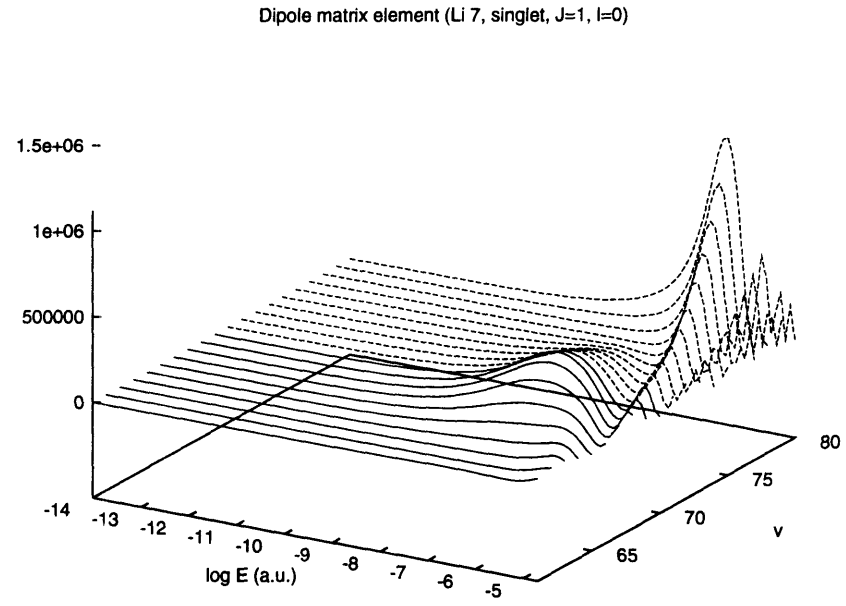

Figure 4.18: Dipole matrix elements near $\overline{r} = a$ for the singlet transitions.

ground (free)		excited (bound)
$l = 0$	$\rightarrow$	$J =$ 1
$l = 1$	$\rightarrow$	$J =$ 0,2
$l = 2$	$\rightarrow$	$J =$ 1,3
$l = 3$	$\rightarrow$	$J =$ 2,4
$l = 4$	$\rightarrow$	$J =$ 3,5
$l = 5$	$\rightarrow$	$J =$ 4,6

As an example, we selected the same two levels as before, namely $v_t = 80$ for the triplet transitions, and $v_s = 89$ for the ^{7}Li singlet transitions. Using Eq. (4.10) for those levels, with the right weights, we obtained the results shown in Fig. 4.19 in the triplet transition case. As we vary the temperature, we span different portions of the energy domain and the contribution from the different partial waves becomes obvious as T increases. At small T, only the $l = 0$ partial wave contributes, but as we increase T, the $l = 1$ contribution begins to grow. However, even at $T = 10$ mK, its height is only a fraction of the main peak ($l = 0$). The higher partial wave $l = 2$ starts to be more appreciable for temperature bigger than 5 mK.

In contrast, the ^{7}Li singlet transition for the vibrational level 89 has a different behaviour (see Fig. 4.20). Although it is similar to the triplet for small T, *i.e.* $l = 0$ is dominant and $l = 1$ grows slowly, the $l = 2$ partial wave contribution increases quite drastically and becomes even dominant at temperatures higher than 5 mK. Of course, as mentioned before, this is due to the shape resonance located at $\log E \simeq -7.3$. On those figures, we notice some little glitches, for example on the side of the second, third and fifth peaks (see Fig. 4.20). Those are due the fact that we are using an interpolation scheme when we add up all the components for a

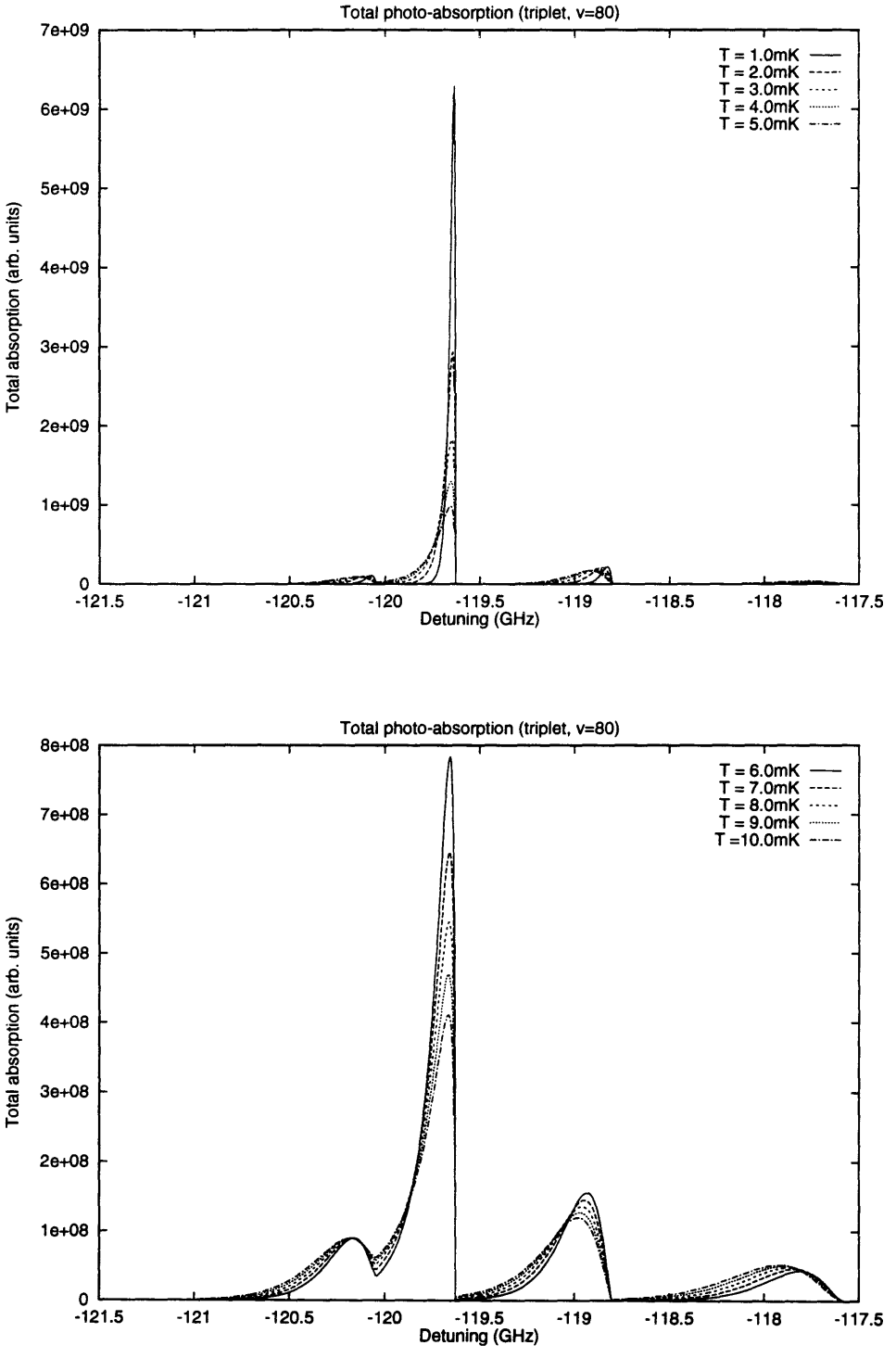

Figure 4.19: Photo-absorption for the $v_t = 80$ triplet transition with higher partial waves.

given detuning. Although $|D_{vK}^{Jl}|^2$ should always be positive, the interpolation gives some small negative values when near a zero of $|D_{vK}^{Jl}|^2$, creating a glitch in the signal calculated.

So, as one can see, for temperature higher than 1 mK, one should take into account the contribution of higher partial waves. Before comparing these last two levels with the experimental results, a more detailed analysis might be useful. As we have shown before, for a given excited level, every J rotational level has two contribution from the ground state $l = J \pm 1$, except for $J = 0$. Since the location of these "sub-peaks" is directly dependent on the energy of the J rotational level, each sub-peak is made of two contributions from the two partial waves. However, the exact location of each component of a sub-peak is also related to the region of higher intensity of $|D_{vK}^{Jl}|^2$. More precisely, the individual contributions are proportional to the following quantities

$$\kappa_{\Sigma\to\Sigma}^{Y}(\nu, T, J, l) \propto h\nu \frac{e^{-E/kT}}{T^{3/2}} |D_{vK}^{Jl}|^2 \ , \tag{4.35}$$

where ν and E are related to the detuning by the relationships

$$h\nu = \Delta + \hbar\omega_p \qquad \text{and} \qquad \Delta = -(E + |E_b(J)|) \ . \tag{4.36}$$

Here, $\hbar\omega_p$ is the energy difference between the limit of the excited and ground states, $|E_b(J)|$ is the energy of the bound level v with excited rotational number J (measured from the 2s+2p limit), and Δ is the detuning (see Fig. 4.21).

So, for a given vibrational energy level with rotational number J, there are two contributions from $l = J \pm 1$. These sub-peaks will be almost located at the same

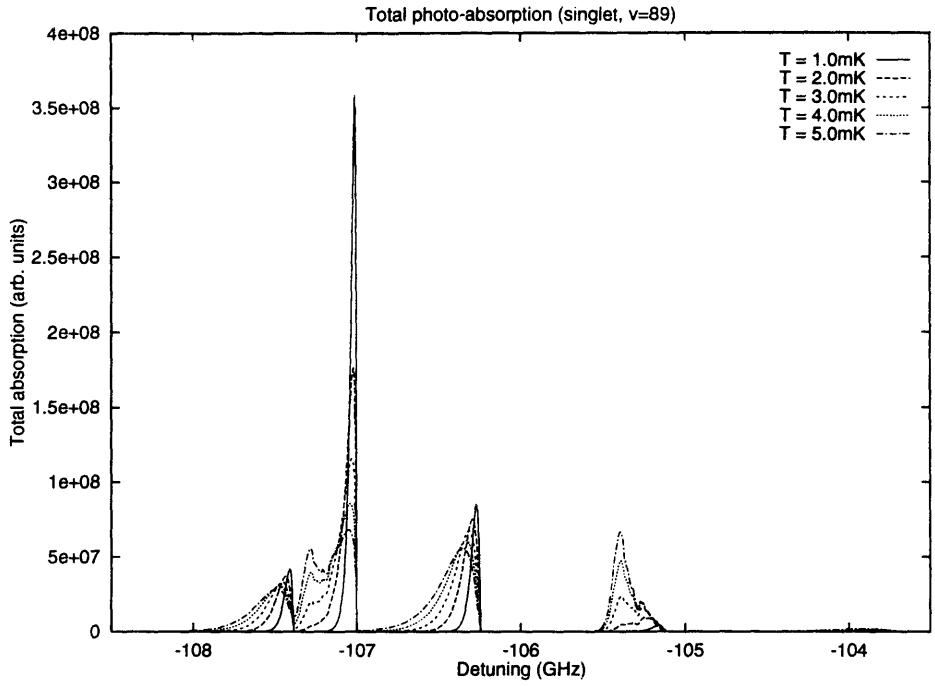

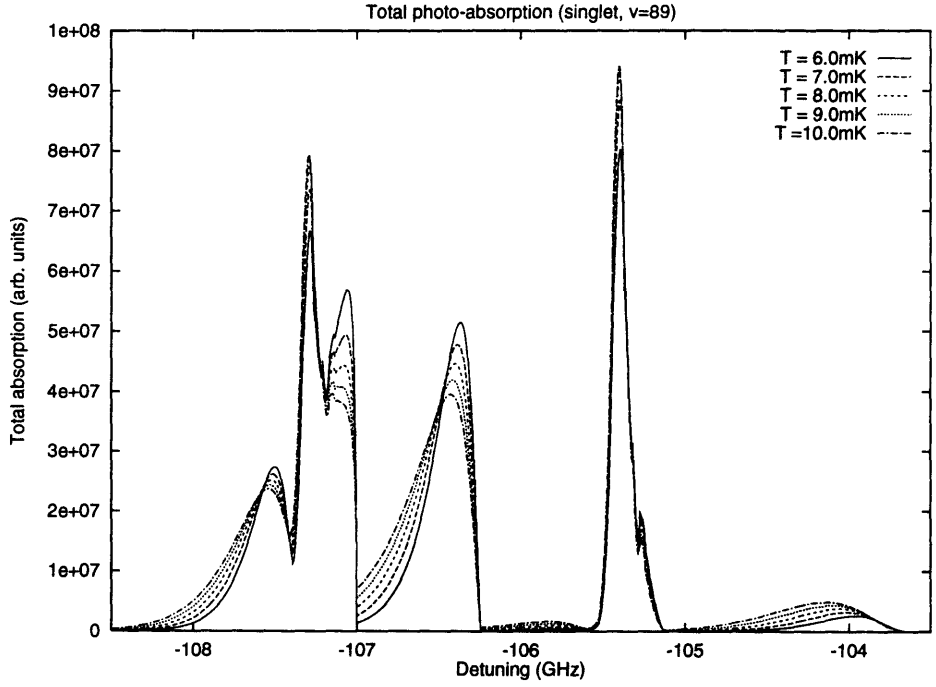

Figure 4.20: Photo-absorption for the $v_s = 89$ singlet transition with higher partial waves.

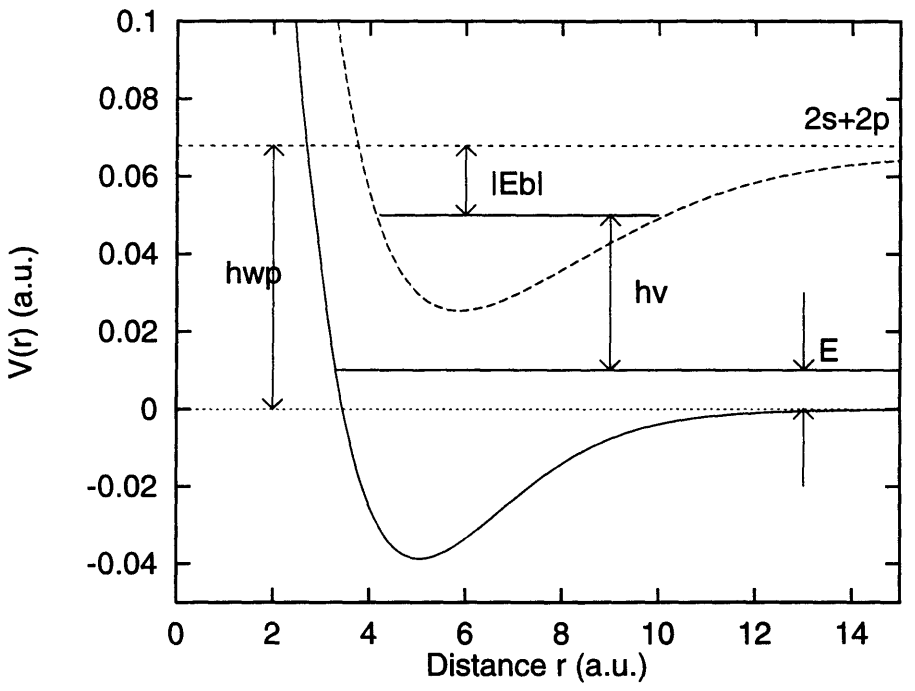

Figure 4.21: Definition of the detuning and other quantities.

detuning value, although the exact location depends on the position of the maximum value of $|D_{vK}^{Jl}|^2$ in question. In fact, $|E_b(J)|$ is usually much larger than the energy corresponding to the maximum of $|D_{vK}^{Jl}|^2$. As an example, we show the first few $|D_{vK}^{Jl}|^2$ in Fig. 4.22 in the case of the singlet transition ($v_s = 89$). For that level, we have the energies given in Table 4.11, together with the location of the maximum of $|D_{vK}^{Jl}|^2$.

Now, the exponential weighting function $e^{-E/kT}$ also influences the location of the sub-peaks. For instance, since $|D_{vK}^{Jl}|^2$ for $(J = 1, l = 0)$ is more important at lower energies, the location of this sub-peak will move from $\Delta \simeq -|E_b(J)|$ to higher values of detuning as we increase the temperature, until it reaches the maximum value of $|D_{vK}^{Jl}|^2$ at $\log E_{max} \simeq -7.3$ (for $v_s = 89$). Notice that the sub-peak will

^{7}Li(singlet, $v = 89$)				^{7}Li(triplet, $v = 80$)			
J	$\|E_b(J)\|$	l	$\log E_{max}$	J	$\|E_b(J)\|$	l	$\log E_{max}$
0	1.632040114 -5	1	-7.0	0	1.824449884 -5	1	-7.3
1	1.626255690 -5	0	-7.3	1	1.818135634 -5	0	-8.0
		2	-7.3			2	-6.9
2	1.614714891 -5	1	-7.0	2	1.805537588 -5	1	-7.3
		3	-6.7			3	-6.6
3	1.597473809 -5	2	-7.3	3	1.786716620 -5	2	-6.9
		4	-6.5			4	-6.5
4	1.574616598 -5	3	-6.7	4	1.761763957 -5	3	-6.6
		5	-6.3			5	-6.3
5	1.546255502 -5	4	-6.5	5	1.730801042 -5	4	-6.5
		6	-6.2			6	-6.2

Table 4.11: Location of the maximum of $|D^{Jl}_{vK}|^2$ for two levels.

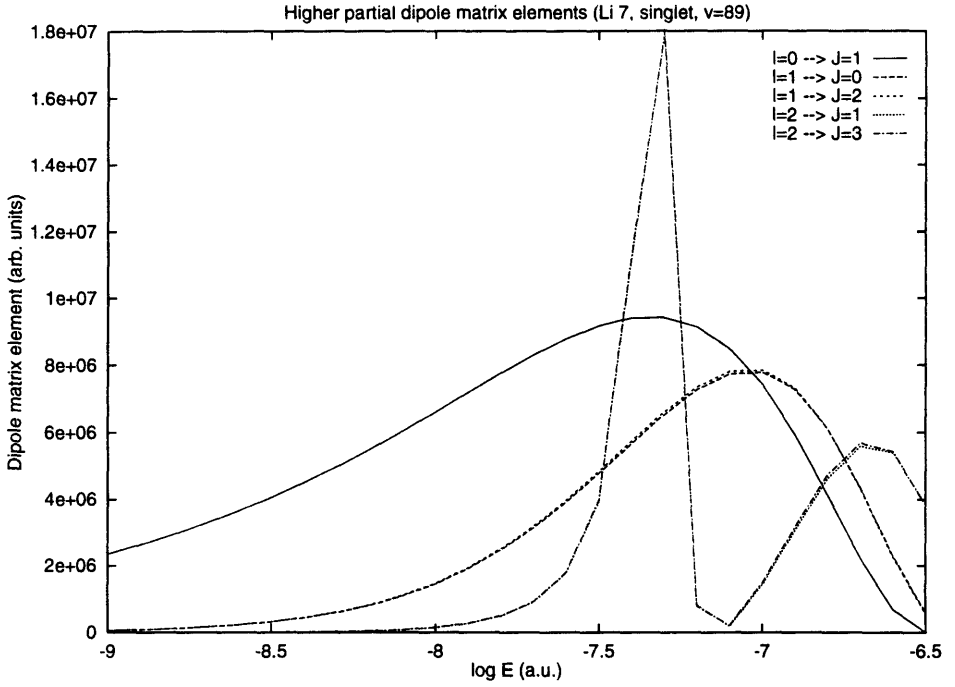

Figure 4.22: $|D_{vK}^{Jl}|^2$ for some partial waves ($v_s = 89$).

become "fatter" as we increase the temperature. At the same time, the resonance for $(J = 1, l = 2)$ will start very small and close to $|E_b(J)|$ and move slowly as we increase T. However, in this case, it will not become fatter, but rather sharper as we approach T of the order of the resonance energy ($\log E_{max} \simeq -7.307$). This sub-peak will stay located around that point, and as we increase T, the two sub-peaks ($l = 0$ and $l = 2$) will be overlapping completely. So, the effect of the resonance is quite drastic in the sense that it "split" the sub-peak into its two components. In Fig. 4.23, we give the $l = 2 \rightarrow J = 1$ dipole matrix element for a set of vibrational levels of the singlet state. As we can see, they are essentially all similar, *i.e.* a major sharp peak centered around $\log E \sim -7.3$, with little more structure at higher energies.

We illustrate the experimental intensity for the same levels in Fig. 4.24 and Fig.

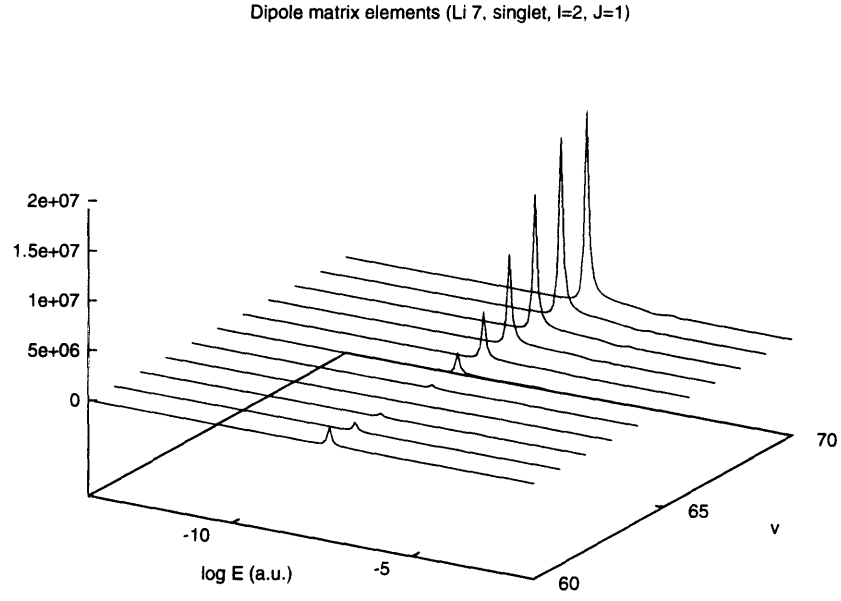

Figure 4.23: The $l = 2, J = 1$ $|D^{Jl}_{vK}(E)|^2$ for the singlet transition of ^{7}Li.

4.25 for the triplet ($v_t = 80$) and singlet ($v_s = 89$), respectively. Also included in these figures are another level for both triplet and singlet transitions for a different detuning region. When compared with our previous partial wave expansion calculations, we notice some similarities, although we do not get the exact same patterns. In the triplet case, the agreement is rather poor: nonetheless, the detuning interval containing the sub-peaks is equivalent in both the experimental and theoretical results. Moreover, if we look at the structure of the other experimental curve (centered at around $\Delta \simeq -991$ GHz), the "agreement" with the theoretical curve is better. Of course, other interactions have to be included in the computation to explain all those sub-peaks, but the higher partial waves should not be neglected, since they are of the same order in intensity and detuning as the experimental results.

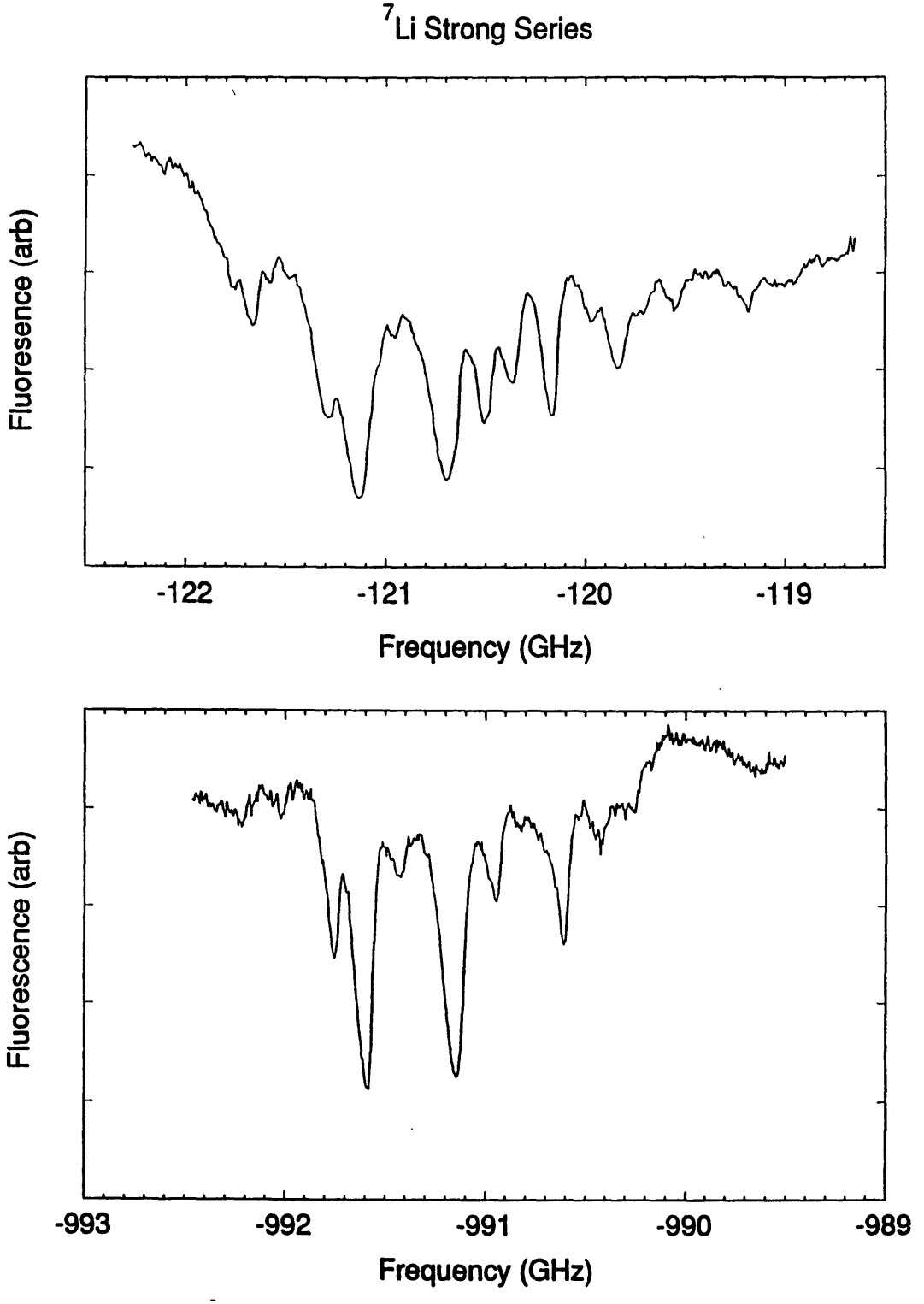

Figure 4.24: Experimental data for triplet transitions of ^{7}Li.

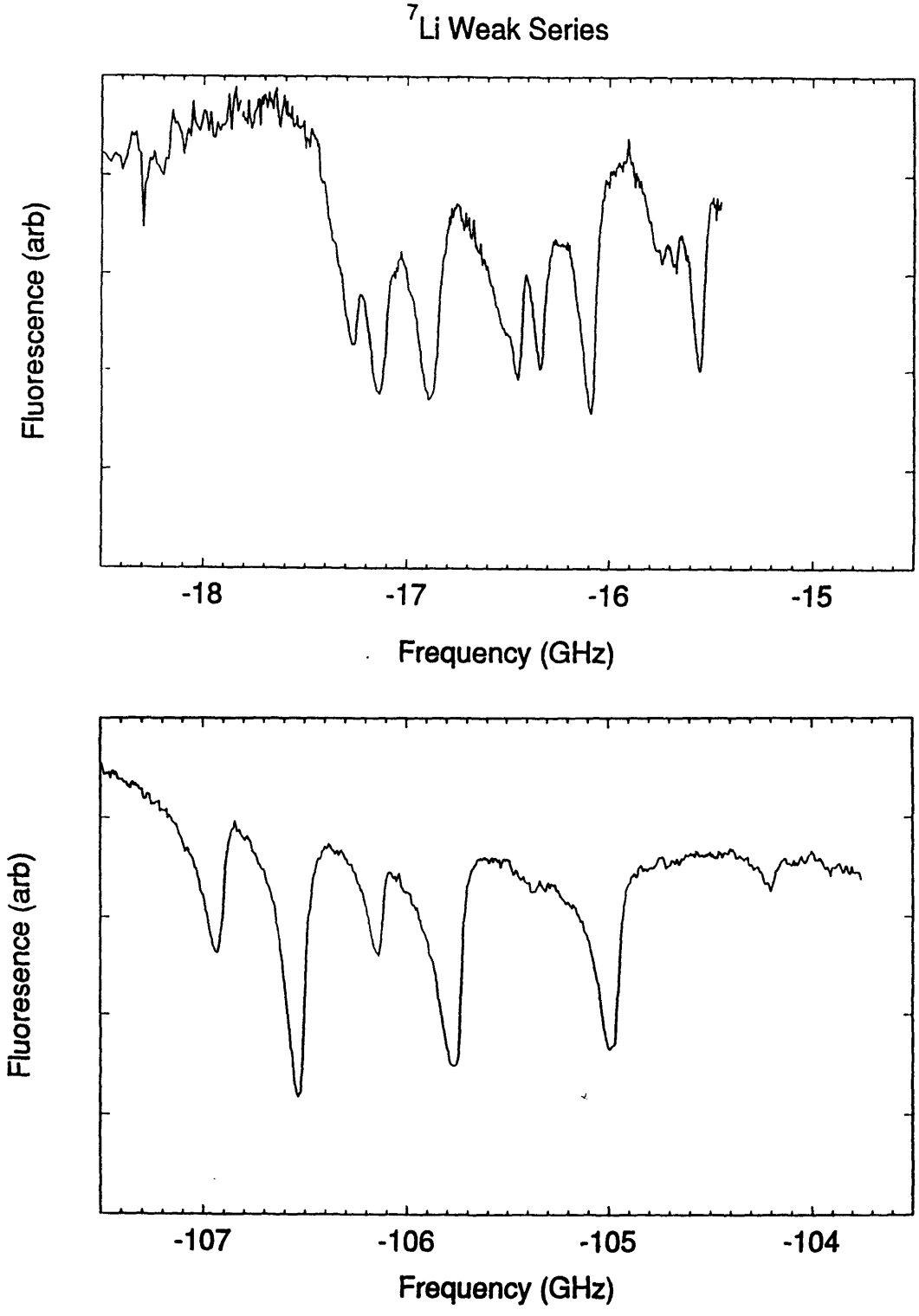

Figure 4.25: Experimental data for singlet transitions of ^{7}Li.

The singlet case is even more striking. The experimental results and the theoretical curve do look alike to a high degree. In fact, the position and relative height of the signals are very close and one could be tempted to explain all the structure through the higher partial waves only. As we will see a bit further in this chapter, this is only part of the explanation.

As a counter example, we also include the results for a singlet level of ^{6}Li ($v_s = 84$ at $\Delta \sim -73$ GHz). It is shown in Fig. 4.26, together with the theretical calculations. In this case, the agreement is rather poor, contrary to one's expectation from the previous ^{7}Li singlet case. As noticed by R. Hulet *et al.* (private communication), the distance between the different sub-peaks corresponds to the hyperfine splitting of the ground state. This is well illustrated in the singlet cases, where the hyperfine splitting is 803.5 MHz for ^{7}Li, and 228.2 MHz for ^{6}Li (see Lin *et al.* [68]). The triplet transitions also exhibit the same behaviour, as can be seen from the experimental data (see Fig. 4.24). Although the hyperfine splittings seem to explain most of the experimental features, it does not do so completely, hence the importance of higher partial waves. Since we did not include the multi-channel treatment required to solve the scattering problem with the hyperfine interactions, we cannot at this point model all the experimental data.

4.6 Line shape and Temperature dependence

In this section, we will explore two different aspects on the previous results, namely the line shape and its temperature dependence, and the position of the shape resonance.

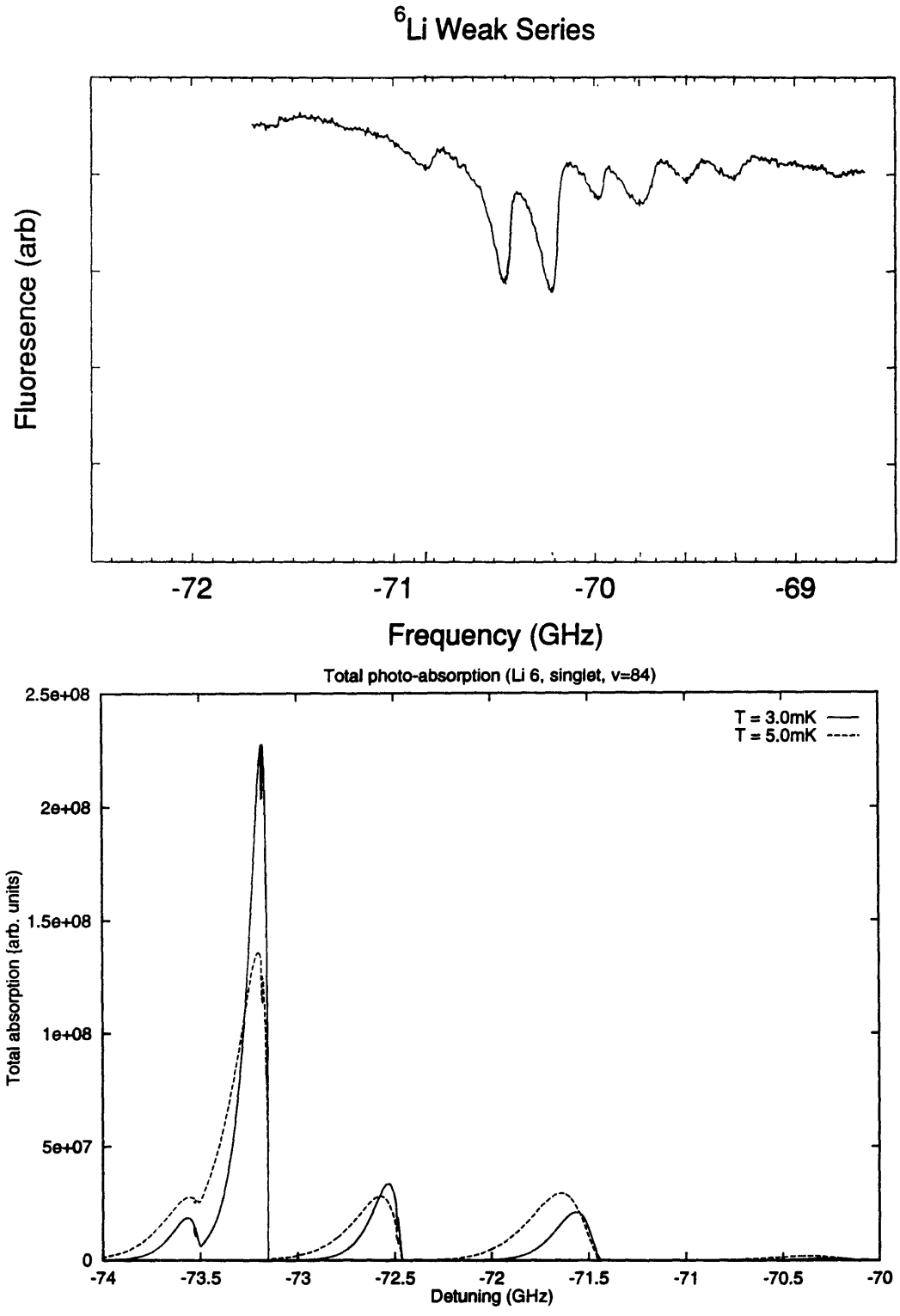

Figure 4.26: Singlet transition for $v_s = 84$ of ^{6}Li.

We will also compute the natural width of specific excited levels and estimate the atomic lifetime from them. Finally, we will give an approximate expression for $|D_{vK}^{Jl}|^2$ at large energy, and estimate the temperature at which the measurements were made.

4.6.1 Line shape

The equation obtained in §4.1 for $\kappa_{a\to b}^{Y}(\nu,T)$ is based on the approximation that the natural line width of the transition is small. In fact, following Napolitano *et al.* [9], one can rewrite $\kappa_{a\to b}^{Y}(\nu,T)$ for a given bound state as

$$K_p(T,\omega) = \left\langle \frac{\pi v}{k^2} \sum_0^\infty (2l+1)|S_p(\varepsilon,l,\omega)|^2 \ , \right\rangle \tag{4.37}$$

where we used the same notation as Napolitano *et al.*. Here, $\langle\cdots\rangle$ implies an average over the distribution of initial velocities v. If a Maxwellian distribution at temperature T is assumed, this expression is reduced to

$$K_p(T,\omega) = \sum_{l=0}^{\infty}(2l+1)\frac{1}{hQ_T}\int_0^\infty d\varepsilon\, e^{-\varepsilon/kT}|S_p(\varepsilon,l,\omega)|^2 \ , \tag{4.38}$$

where $Q_T = (2\pi\mu kT/h^2)^{3/2}$ and ε is the kinetic energy. For a single level, Napolitano *et al.* assume that the square of the S-matrix element $|S_p(\varepsilon,l,\omega)|^2$ can be approximated by

$$|S_p(\varepsilon,l,\omega)|^2 = \frac{\gamma_p\gamma_s(\varepsilon,l)}{(\varepsilon-\Delta_b)^2+(\gamma/2)^2} \ , \tag{4.39}$$

where $\Delta_b = E_b - \hbar\omega$ is the detuning relative to position E_b of the bound state. The total width (in a.u.) is given by

$$\gamma = \gamma_p + \gamma_s(\varepsilon,l) + \gamma_0 \ , \tag{4.40}$$

where $\gamma_p/\hbar$ is the rate of spontaneous decay of the bound state, $\gamma_s(\varepsilon,l)/\hbar$ is the stimulated emission rate back to the ground state, and $\gamma_0/\hbar$ is the decay rate due to any other undetected processes (*e.g.*, molecular predissociation).

The stimulated decay is proportional to the probe laser intensity I and the square of the dipole matrix element (see also §4.7)

$$\gamma_s(\varepsilon,l) = 4\pi^2\frac{I}{c}|\langle\varepsilon,l|d(R)|b\rangle|^2 \ . \tag{4.41}$$

This is given by Fermi's golden rule and is valid for low light intensity. If we neglect γ_0 to first order, and assume I small so that $\gamma_s(\varepsilon,l) \ll \gamma_p$, we find

$$\begin{aligned} |S_p(\varepsilon,l,\omega)|^2 &\simeq \frac{\gamma_p\gamma_s(\varepsilon,l)}{(\varepsilon-\Delta_b)^2+(\gamma_p/2)^2} \\ &\simeq 2\pi\gamma_s(\varepsilon,l)\frac{1}{\pi}\frac{\gamma_p/2}{(\varepsilon-\Delta_b)^2+(\gamma_p/2)^2} \ . \end{aligned} \tag{4.42}$$

Furthermore, if $\gamma_p \to 0$ we can then write

$$|S_p(\varepsilon,l,\omega)|^2 \simeq 2\pi\gamma_s(\varepsilon,l)\delta(\varepsilon-\Delta_b) \ . \tag{4.43}$$

Then substituting back into the expression for $K_p(T,\omega)$, we get

$$K_p(T,\omega) \simeq \sum_{l=0}^{\infty}(2l+1)\frac{h}{(2\pi\mu kT)^{3/2}}e^{-\Delta_b/kT}2\pi\gamma_s(\Delta_b,l) \ . \tag{4.44}$$

So, for a given bound level of the excited state, we finally have

$$K_p(T,\omega) \simeq 8\pi^3\frac{I}{c}\sum_{l=0}^{\infty}(2l+1)\frac{e^{-\Delta_b/kT}}{(2\pi\mu kT)^{3/2}}|\langle\varepsilon,l|d(R)|b\rangle|^2 \ . \tag{4.45}$$

Now, one can see that this is just what we computed in the previous sections. In fact, if we consider this quantity per unit flux of the incident photons, as we did in §4.1, we must divide by

$$F = \frac{|F_0|^2 c}{8\pi h\nu} \ , \tag{4.46}$$

where $|F_0|^2$ is the intensity of the probing laser (see Appendix D). Then we get as before

$$K_p(T,\omega) \propto h\nu \frac{e^{-\Delta_b/kT}}{(2\pi\mu kT)^{3/2}} |D_v(\Delta_b)|^2 \ . \tag{4.47}$$

Notice that the $2l+1$ coefficient is also present in our equation, in the form l and $l+1$ multiplying the different partial wave contributions.

Assuming these conditions on γ to be true, we can examine the line profile of a given transition as a function of the temperature T. We considered the singlet transitions for the level 89 of ^{7}Li. More precisely, we choose the $(J=0, l=1)$, and the $(J=1, l=0,2)$ transitions for three different temperature ($T = 1, 5$ and 10 mK). Fig. 4.27 shows the three set of curves for each transition. For the $l=0$ and $l=1$ cases, the peak is sharp and almost symmetric at low temperature. However, when T is increased, the curve becomes shorter, wider, and less symmetric. From this asymmetry and the width of the signal, one could hope to get an estimate of the temperature at which the experiment was made. According to those two curves, and comparing with the experimental results, one concludes that the temperature is probably somewhere around 5 mK (see §4.6.4).

Now, the $l=2$ peak behaves in a different manner. In fact, instead of raising sharply from zero at smaller detuning and then decreasing slowly (as the previous two cases), the curve becomes higher as you increase T, while remaining more or less symmetric. From this last fact, one could hope to identify which sub-peak are due to a shape resonance. From the experimental curve, we see that the second sub-peak located at ~ -106.5 GHz seems to correspond to such a resonance (see

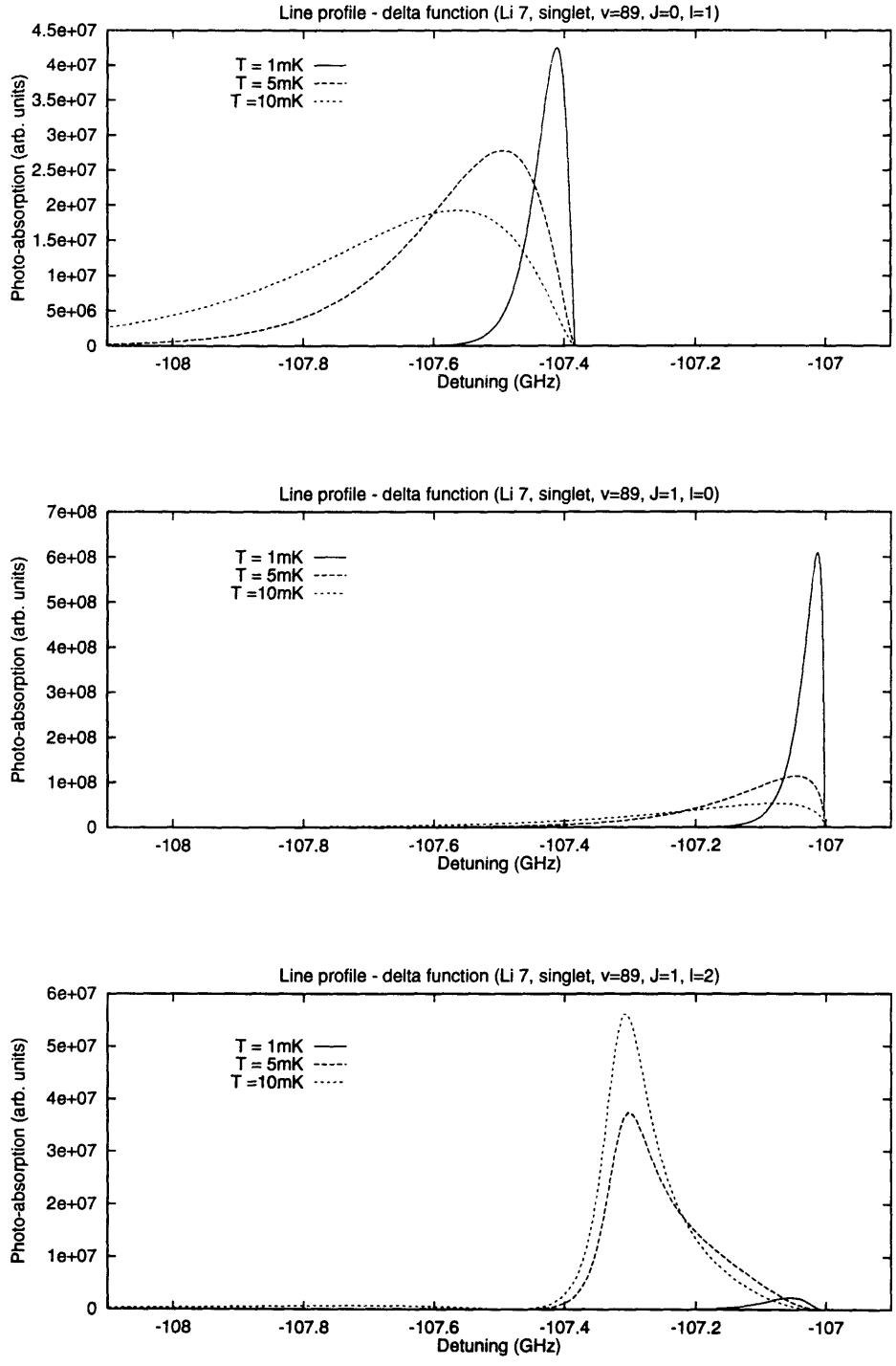

Figure 4.27: Approximated line profile for singlet $v_s = 89$ level of ^{7}Li.

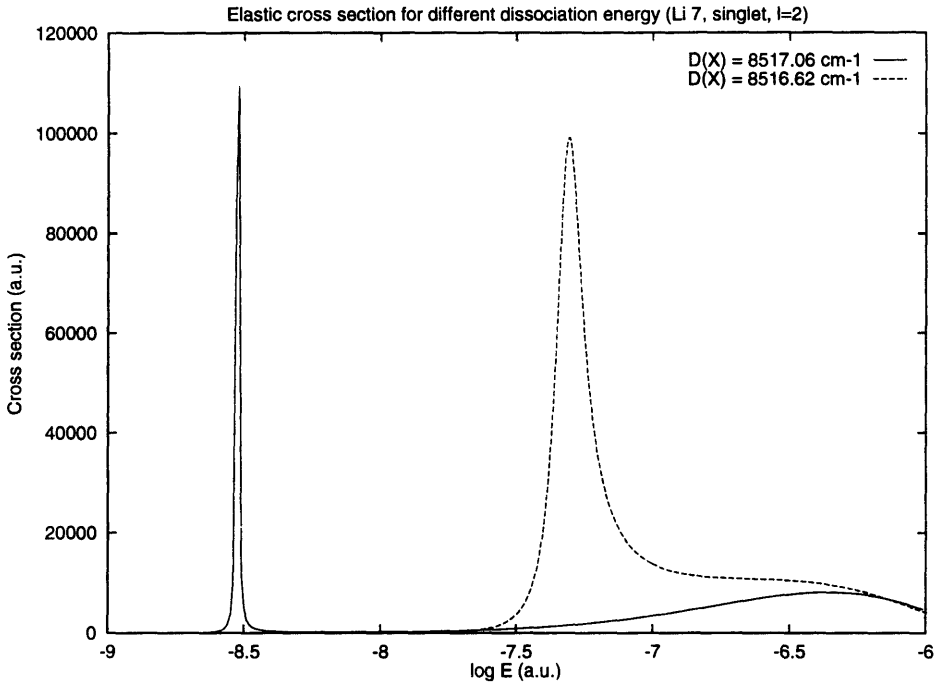

Figure 4.28: Elastic cross sections for different dissociation energies in the singlet $X^1\Sigma_g^+$ state of ^{7}Li. The $l = 2$ shape resonance is moved to lower energies as we increase $D_e(X)$.

Fig. 4.25 and §4.6.4). Having the temperature and which peak is a shape resonance, we can then improve our knowledge of the ground state potential. In fact, one can fine tune the dissociation energy of the ground state to move the resonance at the appropriate regime of kinetic energy. By changing the dissociation energy within the experimental uncertainty for the singlet potential curve, we can translate the resonance to the desired energy. By having the relative height of the resonance signal and the temperature, we can find the location of the resonance. For example, for the level $v_s = 89$ of the ^{7}Li singlet state, we can move the resonance from $\log E_R = -7.3$ to $\log E_R = -8.5$ by changing the dissociation from 8516.62 cm^{-1} to 8517.06 cm^{-1}. This is shown in Fig. 4.28, where we plot the elastic scattering cross section for $l = 2$ partial wave for those two values of $D_e(X)$.

4.6.2 Natural line width γ_p

However, all the above analysis is based on the approximation that $\gamma_p \gg \gamma_s(\varepsilon, l) \gg \gamma_0$, and that $\gamma_p \to 0$. Let us evaluate γ_p for particular levels. To do so, one needs to compute the following expression

$$\gamma_p = \sum_{v'} A_{v'v} + \int_0^\infty d\varepsilon A_v(\varepsilon) \ . \tag{4.48}$$

Here $A_{v'v}$ and $A_v(\varepsilon)$ are the spontaneous emission coefficients from the bound level v into the ground state levels v' and the free state with kinetic energy E, respectively. These are given in terms of the dipole moment integrals

$$A_{v'v} \equiv \frac{4}{3}\alpha^3 \varepsilon_{v'v}^3 |D_{vv'}^{Jl}|^2 \qquad \text{and} \qquad A_v(\varepsilon) \equiv \frac{4}{3}\alpha^3 \varepsilon^3 |D_{vK}^{Jl}|^2 \ , \tag{4.49}$$

where $\varepsilon_{v'v}$ is the energy difference between the bound states and ε between the excited bound state and the free state, and are given by

$$\varepsilon_{v'v} = \hbar\omega_p + E_b(v') - E_b(v) \ \text{ and } \ \varepsilon = \hbar\omega_p + E_b(v') - E \ . \tag{4.50}$$

These expressions give the Einstein spontaneous emission coefficients in atomic units. Dividing them by the atomic unit of time $\tau_0 = 2.4189 \times 10^{-17} s$, we get the coefficients in s^{-1}. Now, depending on the level v considered, the contributions of both the bound-bound and free-bound transitions will vary a lot. We are interested in a high level v, in order to compare with the available experimental results. In this case, one expects the free-bound contribution to be important. We will examine this statement in the next section.

As an example, let us consider $v_t = 80$ for the triplet transition. In principle, the $J = 1$ excited state can decay into both the $l = 0$ and $l = 2$ ground state (free and

bound), and the exact width will be given by

$$\gamma_p = \sum_{v'} [(J+1)A_{v'v}(J, l = J-1) + JA_{v'v}(J, l = J+1)] + \int_0^\infty d\varepsilon \, [(J+1)A_v(\varepsilon, J, l = J-1) + JA_v(\varepsilon, J, l = J+1)] \ , \quad (4.51)$$

where the exact Einstein coefficients are given by

$$A_{v'v}(J,l) \equiv \frac{1}{2J+1}\frac{4}{3}\alpha^3 \varepsilon_{v'v}^3 |D_{vv'}^{Jl}|^2 \qquad \text{and} \qquad A_v(\varepsilon) \equiv \frac{1}{2J+1}\frac{4}{3}\alpha^3 \varepsilon^3 |D_{vK}^{Jl}|^2 \ . \quad (4.52)$$

If we would compute the $(J, l = J)$ transition, we would "average" both contributions. However, we can assume that both $(J, l = J-1)$ and $(J, l = J+1)$ contributions are of the same order, and therefore to a first order, one can approximate γ_p by the $(J, l = J-1)$ contribution only, without the factor of $1/(2J+1)$ in the expression of $A_{v'v}(J, l = J-1)$.

So, in the case ^{7}Li triplet transition, we computed the following results

$$\sum_{v'=0}^{10} A_{v'v=80}(J = 1, l = 0) = 3.47 s^{-1} \ , \quad (4.53)$$

and

$$\int_0^\infty d\varepsilon A_{v=80}(\varepsilon, J = 1, l = 0) = 7.344 \times 10^7 s^{-1} \ . \quad (4.54)$$

The actual bounds of the integral were $\log E = -12.00$ and $\log E = -1.15$. As we can see, the free-bound contribution is by far the most important one. Moreover, the range of energies contributing the most to this free-bound portion are between $-6 < \log E < -4$, as can be seen from Fig. 4.29. From these numbers, we get

$$\gamma_p \simeq 7.344 \times 10^7 s^{-1} \Longrightarrow \gamma_p \simeq 1.776 \times 10^{-9} \text{ a.u.} \ . \quad (4.55)$$

As we can see, in atomic units, γ_p is much smaller than unity. However, when we approach temperature corresponding to energies near $10^{-8.5}$ hartree (*i.e.* $T \simeq 1$ mK), the delta function approximation used before starts to break down. An alternative way to see this is by considering the fact that usually the exponential term and $\gamma_s(\varepsilon, l)$ in the integral vary slowly compared with the rest of the integrand, and therefore one can take them out of the integral

$$\begin{aligned} \int_0^\infty d\varepsilon \frac{e^{-\varepsilon/kT}\gamma_p\gamma_s(\varepsilon,l)}{(\varepsilon-\Delta_b)^2+(\gamma_p/2)^2} &\simeq e^{-\Delta_b/kT}\gamma_s(\Delta_b,l)\int_0^\infty d\varepsilon \frac{\gamma_p}{(\varepsilon-\Delta_b)^2+(\gamma_p/2)^2} \\ &\simeq \pi e^{-\Delta_b/kT}\gamma_s(\Delta_b,l)\ , \end{aligned} \tag{4.56}$$

where we used the fact that $\int_0^\infty dx(x^2+a^2)^{-1} = \pi/2a$. Now, since $\log\gamma_p \simeq -8.75$ and if $T \sim 1$ mK, we cannot take those two terms out of the integral anymore, and the full integral would have to be performed (see §4.6.4).

From the value of γ_p, we can estimate the lifetime of the molecular excited state. In fact, we have

$$\tau_p = \frac{1}{\gamma_p}\ . \tag{4.57}$$

From the previous value for γ_p, we get

$$\tau_p \simeq 1.3617 \times 10^{-8} s = 13.617 ns\ . \tag{4.58}$$

One would expect to recover the atomic lifetime from the molecular one. In fact, for a high level bound state v, the outer turning point is far out and the molecule looks more and more like two separate atoms. If we consider the atomic case as being the molecular limit at large distance that goes to the $2s$-$2p$ limit, we have two possible molecular states. In fact, one can see from Fig. 4.1 that in both cases

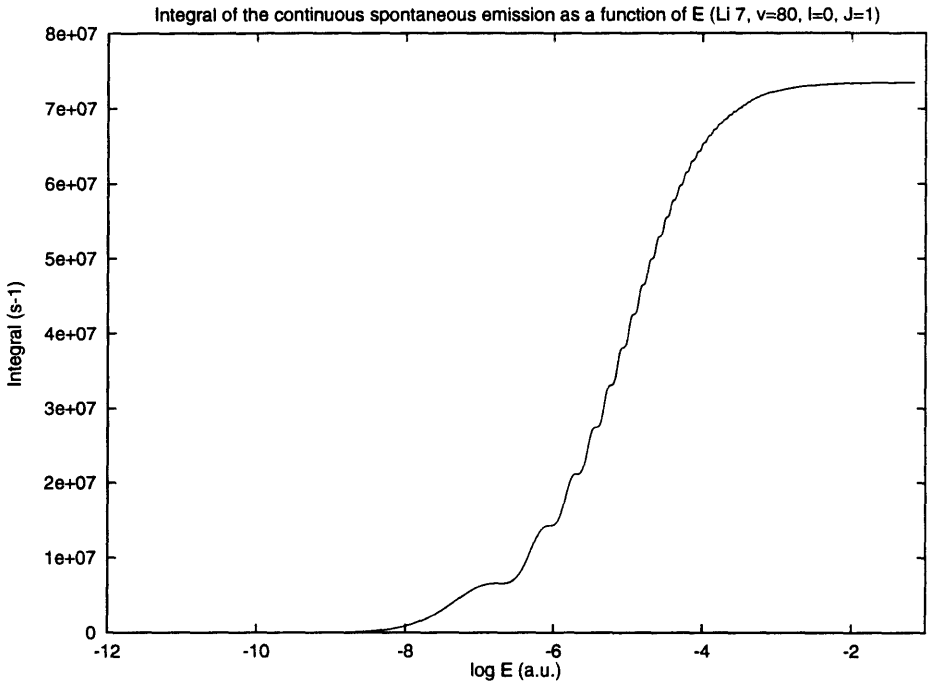

Figure 4.29: Contribution of the free-bound spontaneous emission for the triplet transition from level $v_t = 80$.

(singlet and triplet transitions), there are two Σ states going to the $2s$-$2p$ limit. For the triplet, these are the $1^3\Sigma_g$ and $2^3\Sigma_u$ states, and for the singlet, the $1^1\Sigma_u$ and $2^1\Sigma_g$ states. However, the transitions from the ground state to the excited states are not all allowed (as we have seen before). Therefore, the width corresponding to those forbidden transitions is zero (or an infinite lifetime). Since the atomic limit is equally made of those two Σ states, one must take the average of the molecular widths to get the atomic one. For the case we are interested in, namely the triplet transitions, this gives

$$\begin{aligned} \gamma_{at.} &= \frac{1}{2}\left[\gamma_{mol.}(1^3\Sigma_g) + \gamma_{mol.}(2^3\Sigma_u)\right] \\ &= \frac{1}{2}\left[7.344 \times 10^7 + 0\right] s^{-1} \\ &= 3.672 \times 10^7 s^{-1} \Longrightarrow \tau_{at.} = 27.23ns \ . \end{aligned} \tag{4.59}$$

This is the atomic lifetime measured for both ^{7}Li and ^{6}Li isotopes, namely 27.2 ns (see Lin *et al.* [68]).

As another example, let us compute γ_p for a level of the singlet transitions. We take the level $v_s = 88$ of ^{7}Li. Evaluating the Einstein spontaneous emission coefficient like before, we get

$$\sum_{v'=0}^{41} A_{v'v=88}(J=1,l=0) = 1.31 \times 10^5 s^{-1} \ , \tag{4.60}$$

and

$$\int_0^\infty d\varepsilon A_{v=80}(\varepsilon, J=1,l=0) = 7.3413 \times 10^7 s^{-1} \ . \tag{4.61}$$

Here, the actual bounds of the integral were $\log E = -12.00$ and $\log E = -1.66$. As we can see, the free-bound contribution is the most important one. Moreover, the range of energies contributing the most to this free-bound portion are between $-6 < \log E < -4$, as can be seen from Fig. 4.30. From these numbers, we get

$$\gamma_p \simeq 7.3544 \times 10^7 s^{-1} \Longrightarrow \gamma_p \simeq 1.779 \times 10^{-9} \text{ a.u. .} \tag{4.62}$$

As we can see, in atomic units, γ_p is much smaller than unity. Once again, this gives us the atomic lifetime (for the same reasons as for the triplet case), namely

$$\tau_{at.} \simeq 2\tau_{mol.}(1^1\Sigma_u) = \frac{2}{7.3544 \times 10^7} s = 27.195 ns \ . \tag{4.63}$$

Once again, the agreement with $27.2ns$ [68] is quite good.

4.6.3 Approximate form of $|D_{vK}^{Jl}|^2$ for high energy

Let us spend some more time on the computation of the width. As we just saw, for high bound state levels of the excited state, most of the contribution to the width

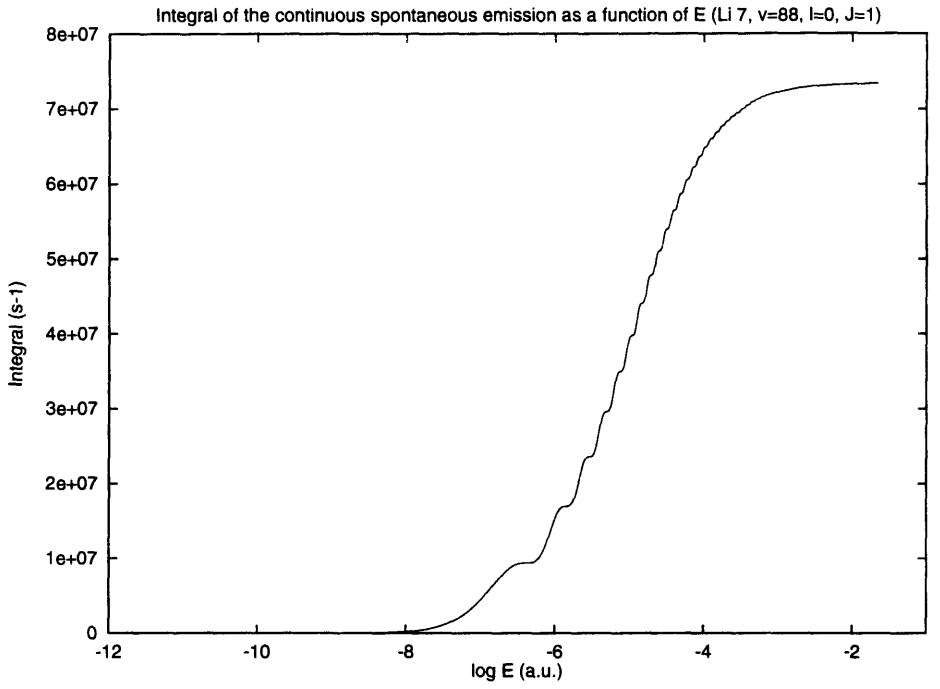

Figure 4.30: Contribution of the free-bound spontaneous emission for the singlet transition from level $v_t = 88$.

comes from the free-bound transitions. However, in order to evaluate the integral to some degree of accuracy, one needs to take high values of kinetic energy. In fact, from the two previous example, we can see that although most of the integral is due to energies between $\log E = -8$ and $\log E = -4$ (see Figs. 4.29 and 4.30), much higher energies have to be reached to insure a well converged value. Indded, we integrated up to $\log E = -1.66$ and $\log E = -1.15$ for the singlet and the triplet, respectively (see previous section). At such high energy, the free wave function oscillates very fast, and a very small step size has to be taken in the numerical integration, hence increasing the amount of computing time. However, we can approximate the expression in a simple manner.

In fact, we want to calculate the following expression

$$I \equiv D_{vK}^{Jl} = \langle u_a^{v,J}(R)|D_{ab}^{Y}(R)|u_b^{K,l}(R)\rangle = \int_0^\infty dR\, u_a^{v,J}(R) D_{ab}^{Y}(R) u_b^{K,l}(R) \ . \qquad (4.64)$$

Now, for high enough energy, *i.e.* for $K^2 \gg |U(R_e)|$ where $|U(R_e)|$ is the deepest part of the potential (at the equilibrium point R_e), the continuous wave function $u_b^{K,l}(R)$ almost does not feel the potential, and can be written as its asymptotic form for most values of R

$$u_b^{K,l}(R) \simeq \left(\frac{2\mu}{\pi\hbar^2 K}\right)^{1/2} \sin\left[KR - \frac{l\pi}{2} + \delta_l(K)\right] \ . \qquad (4.65)$$

This form is valid in the overlapping region with the last lobe of the excited state wave function. Moreover, if we consider the vibrational level v high enough, this overlapping region will be far out, and $D_{ab}^{Y}(R)$ can take its asymptotic form

$$D_{ab}^{Y}(R) = D_0 + \frac{b}{R^3} \simeq D_0 \ , \quad \text{at large } R \quad . \qquad (4.66)$$

As we already have shown in a previous section, $u_a^{v,J}(R)$ is a fast oscillating function, and only the last lobe will define the overlapping region: the rest will basically give a null contribution to the integral. Thus, we can rewrite I as

$$I \simeq \left(\frac{2\mu D_0^2}{\pi\hbar^2 K}\right)^{1/2} \int_{R_1}^{R_2} dR\, u_a^{v,J}(R) \sin\left[KR - \frac{l\pi}{2} + \delta_l(K)\right] \ . \qquad (4.67)$$

Here, R_1 and R_2 define the size and position of the last lobe. If K is big enough, $u_a^{v,J}(R)$ will vary slowly compared to the free wave function, and we can take it out of the integral

$$I \simeq \left(\frac{2\mu D_0^2}{\pi\hbar^2 K}\right)^{1/2} \overline{u}_a^{v,J} \int_{R_1}^{R_2} dR \sin\left[KR - \frac{l\pi}{2} + \delta_l(K)\right] \ , \qquad (4.68)$$

where $\overline{u}_a^{v,J}$ is an average value of $u_a^{v,J}(R)$ in the overlap interval. Then, our expression can easily be integrated to give

$$I \simeq \frac{2}{K}\left(\frac{2\mu D_0^2}{\pi\hbar^2 K}\right)^{1/2} \overline{u}_a^{v,J} \sin\left[K\overline{R} - \frac{l\pi}{2} + \delta_l(K)\right] \sin(KL) \ . \tag{4.69}$$

So, the dipole moment integral squared becomes

$$|D_{vK}^{Jl}|^2 \simeq \frac{8\mu D_0^2}{\pi\hbar^2}\frac{[\overline{u}_a^{v,J}]^2}{K^3} \sin^2\left[K\overline{R} - \frac{l\pi}{2} + \delta_l(K)\right] \sin^2\left(\frac{KL}{2}\right) \ , \tag{4.70}$$

where

$$\overline{R} \equiv \frac{R_2 + R_1}{2} \qquad \text{and} \qquad L \equiv R_2 - R_1 \ . \tag{4.71}$$

Let us check this approximation by comparing with the exact numerical results. In our previous examples, we were interested in the $l = 0$ partial wave. Then, we simply have

$$|D_{vK}^{Jl}|^2 \simeq \frac{8\mu D_0^2}{\pi\hbar^2}\frac{[\overline{u}_a^{v,J}]^2}{K^3} \sin^2\left[K\overline{R} + \delta_l(K)\right] \sin^2(KL) \ . \tag{4.72}$$

Furthermore, for high enough energy, we could use the WKB expression for the phase shift. For $l = 0$, we have from Eq. (3.26)

$$\delta_0(K) \simeq \frac{\pi}{4} - KR_0 + \int_{R_0}^{\infty} dR \left[\sqrt{K^2 - U(R)} - K\right] \ . \tag{4.73}$$

Since we have $K^2 \gg |U(R_e)|$, we can expand the integrand and find to first order in U

$$\int_{R_0}^{\infty} dR \left[\sqrt{K^2 - U(R)} - K\right] \simeq \int_{R_0}^{\infty} dR \left[K\left(1 - \frac{U(R)}{2K^2}\right) - K\right] \ , \tag{4.74}$$

so that the phase shift takes on the simple form

$$\delta_0(K) \simeq \frac{\pi}{4} - KR_0 - \frac{1}{2K}\int_{R_0}^{\infty} dR U(R) \ . \tag{4.75}$$

From this expression, assuming that we have the exact numerical quantum value for δ_0 at some value K_0, we can find $\delta_0(K)$ for higher values of K, namely

$$\delta_0(K) \simeq \delta_0(K_0) - (K - K_0)R_0 - \frac{\mathcal{U}}{2}\left(\frac{1}{K} - \frac{1}{K_0}\right) , \tag{4.76}$$

where the quantity $\mathcal{U}$ is given by

$$\mathcal{U} \equiv \frac{2\mu}{\hbar^2}\int_{R_0}^{\infty} dR\, V(R) . \tag{4.77}$$

For the lithium singlet and triplet ground state potential curves, we find

$$\left.\begin{array}{l} \text{singlet} , \quad R_0 = 3.446a_0 , \quad \displaystyle\int_{R_0}^{\infty} dR\, V(R) = -1.4937 \times 10^{-1} \text{ a.u.} \\ \text{triplet} , \quad R_0 = 6.346a_0 , \quad \displaystyle\int_{R_0}^{\infty} dR\, V(R) = -7.1958 \times 10^{-3} \text{ a.u.} \end{array}\right\} . \tag{4.78}$$

Notice that this approximates the phase shift for $\log E > -3$. In fact, if we consider the deepest point of our ground state potential, namely R_e for the $X^1\Sigma_g^+$ state of ^{7}Li, we have

$$|U(R_e| \simeq 0.04 \text{ a.u.} \ll K^2 \simeq 163.6 \qquad \text{at} \qquad \log E = -3.0 . \tag{4.79}$$

So, in Fig. 4.31, we compare the result of the integration over an energy interval for different choices of L and $\overline{R}$

$$I_\epsilon \equiv \int_a^b d\varepsilon\, |D_{vK}^{Jl}|^2 . \tag{4.80}$$

Instead of evaluating the coefficient in the approximate expression (4.72), which requires an estimate of the quantity $\overline{u}_a^{v,J}$, we match the value of $|D_{vK}^{Jl}|^2$ at some energy. In the case shown in Fig. 4.31, we matched at $\log E = -3.0$. Of course, the value of the coefficient will also depend on the choice of L and $\overline{R}$: if it happens to be a

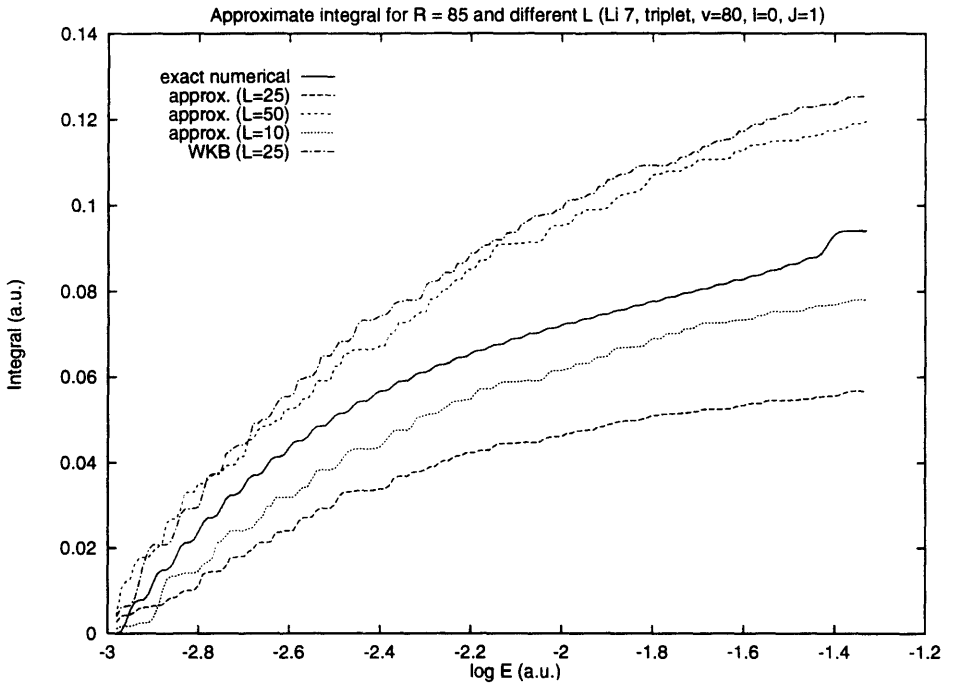

Figure 4.31: Approximate integral $|D_{vK}^{Jl}|^2$ for the continuous spontaneous emission for the triplet $v_t = 80$ of ^{7}Li with $\overline{R} = 85a_0$.

set of parameters such that $\sin^2\left[K\overline{R} + \delta_l(K)\right]\sin^2(KL)$ is near zero, the coefficient would be overestimated. So, in Fig. 4.31, we consider the triplet level $v_t = 80$ of the excited ^{7}Li potential, with $\overline{R} = 85a_0$. We consider three possible values of L, and compare with the exact result. The figure shows the integral as a function of the energy, starting the integration at $\log E = -3.0$. As one can see, for that interval, the approximation behaves in a similar way to the exact result, and its range of values includes the exact one within 30%. However, for the total integral, this last high energy portion does contribute a minor amount, and the error made by the joining the approximated result for $\log E > -3.0$ with the exact result for lower energy reduces itself to less than 0.5%, which is quite acceptable.

For the same level, with the same $\overline{R}$ and $L = 25a_0$, we performed the integral

using the WKB approximated phase shift. The results are given in Fig. 4.31 for the same energy interval. Once again, the approximated integral gives results of the same order as before.

4.6.4 Exact line profile and the temperature

We will use the original form (4.38) for $K_p(T,\nu)$ (see also Napolitano *et al.* [9]). We evaluated the quantity

$$K_p(T,\nu,l) \propto \frac{\nu}{T^{3/2}} \int_0^\infty d\varepsilon\, e^{-\varepsilon/kT} |S_p(\varepsilon,l,\omega)|^2 \ , \tag{4.81}$$

with

$$|S_p(\varepsilon,l,\omega)|^2 \simeq \frac{\gamma_p |D_v(\varepsilon,l)|^2}{(\varepsilon-\Delta_b)^2 + (\gamma_p/2)^2} \ , \tag{4.82}$$

and

$$h\nu = \hbar\omega_p - |E_b(v)| - \Delta_b \ . \tag{4.83}$$

Here, $|E_b(v)|$ is the energy level measured from the 2s+2p limit, and Δ_b is the detuning from this level ($\Delta_b > 0$ for red-detuning in this case [9]). So, we evaluated the function

$$K_p(T,\Delta_b,l) \propto \frac{(\hbar\omega_p - |E_b(v)| - \Delta_b)}{T^{3/2}} \int_0^\infty d\varepsilon\, e^{-\varepsilon/kT} \frac{|D_v(\varepsilon,l)|^2}{(\varepsilon-\Delta_b)^2 + (\gamma_p/2)^2} \ . \tag{4.84}$$

In order to do the integral properly, we took the two previous levels for which an accurate $|D_v(\varepsilon,l)|^2$ was computed on a fine energy grid, and for which γ_p had been calculated.

In Figs. 4.32 and 4.33, we compare the line profiles obtained for the singlet level $v_s = 88$ for the $(l = 0, J = 1)$ transition, at temperatures ranging from 50 μK to

10 mK. Similar data for the triplet level $v_t = 80$ are shown in Figs. 4.34 and 4.35. In both instances, we notice the same behaviour, namely that the profiles are very similar down to temperature near 1 mK, but at lower T, the width of the exact profile is much larger than the one obtained from the delta function approximation. As mentioned earlier, this was to be expected, since $\log \gamma_p \sim -8.75$ in both cases (in a.u.), which is of the order of 1 mK ($\sim 10^{-8.5}$ a.u.). As we decrease T, the profile is more and more symmetric and centered at the bound state energy: the Lorentzian shape becomes the dominant feature. Notice here that the exact profile is given as a function of the detuning from the boung state. For $v_s = 88$, $|E_b| \simeq -2.000 \times 10^{-5}$ a.u. which corresponds to -131.599 GHz, and for $v_t = 80$, $|E_b| \simeq -1.182 \times 10^{-5}$ a.u. which corresponds to -119.624 GHz.

So, the exact profile exhibits the following characteristics: at low temperature, we have a sharp symmetric peak, and as we increase T, the peak becomes smaller, wider and asymmetric. We can use these observations to estimate the temperature from the experimental line profile. We selected the experimental singlet level $v_s = 89$ for this comparison, since detailed data was available. Although we used the $v_s = 88$ level to compare with, the line profile for two very close levels should not vary a lot. A look at $|D_v(E)|^2$ for those two levels confirm this (see Appendix E).

By comparing the experimental profile with the theoretical one for different temperature, we estimate the temperature to be near 7 mK. In fact, in Fig. 4.36, we superposed the two profiles for the experimental sub-peak located at $\Delta \sim -105.8$ GHz. As we can see, the agreement is quite good. Notice that a change of 1 mK is

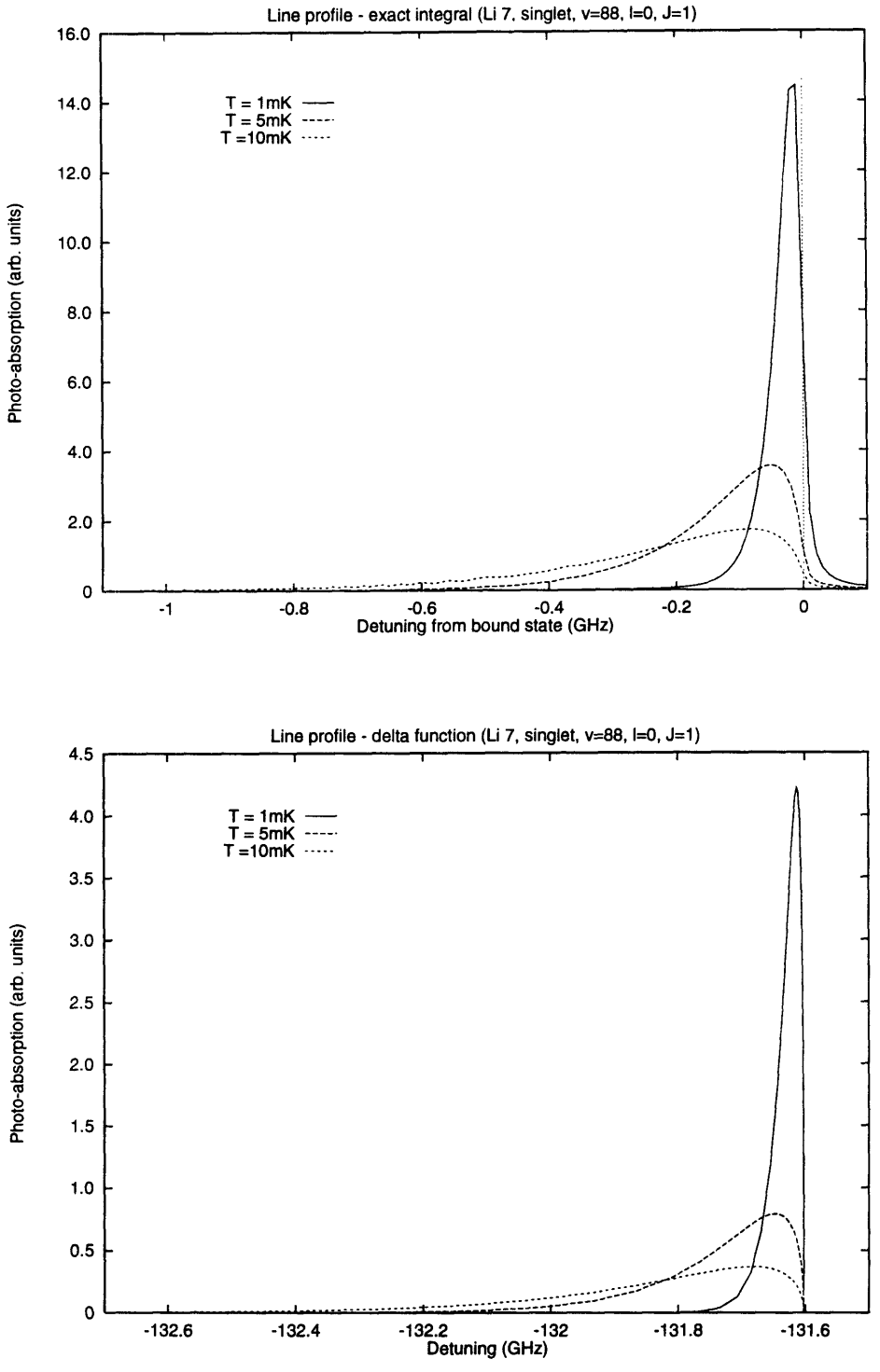

Figure 4.32: Exact (centered at -131.60 GHz) and approximated line profile for the singlet $v_s = 88$ level for $T = 1, 5, 10$ mK.

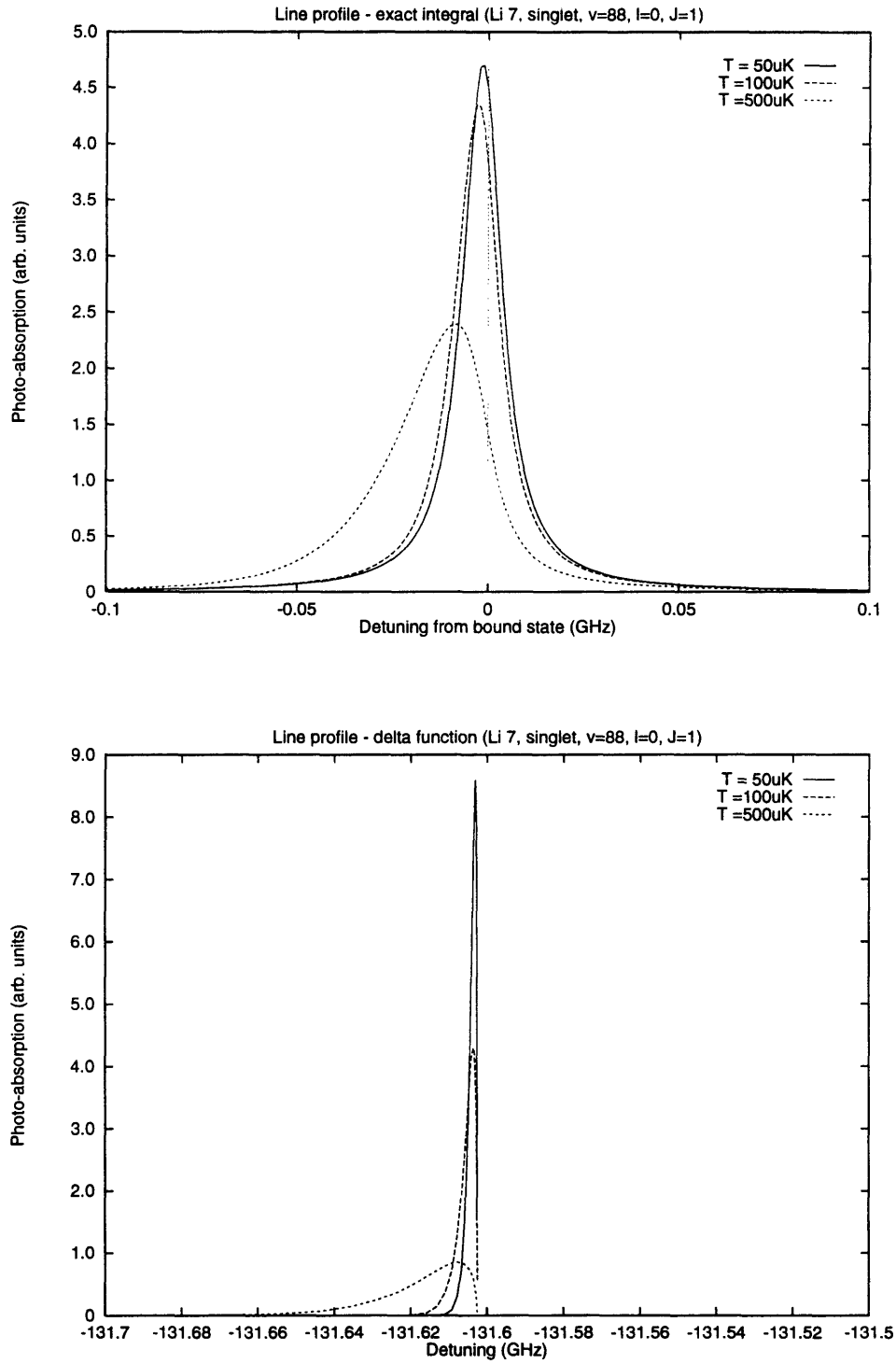

Figure 4.33: Exact (centered at -131.60 GHz) and approximated line profile for the singlet $v_s = 88$ level for $T = 50, 100, 500$ μK.

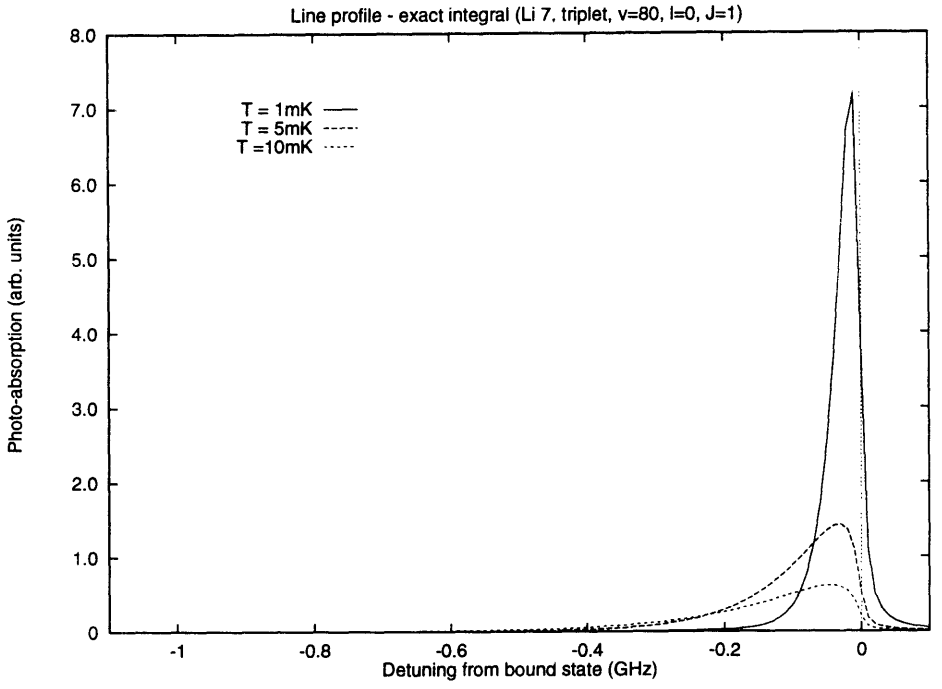

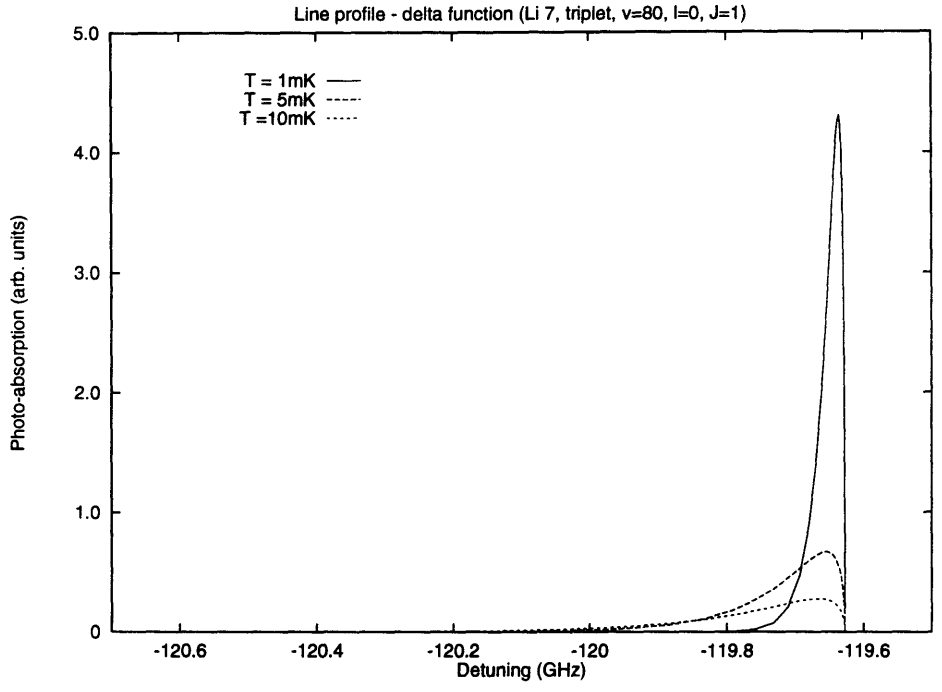

Figure 4.34: Exact (centered at -119.62 GHz) and approximated line profile for the triplet $v_t = 80$ level for $T = 1, 5, 10$ mK.

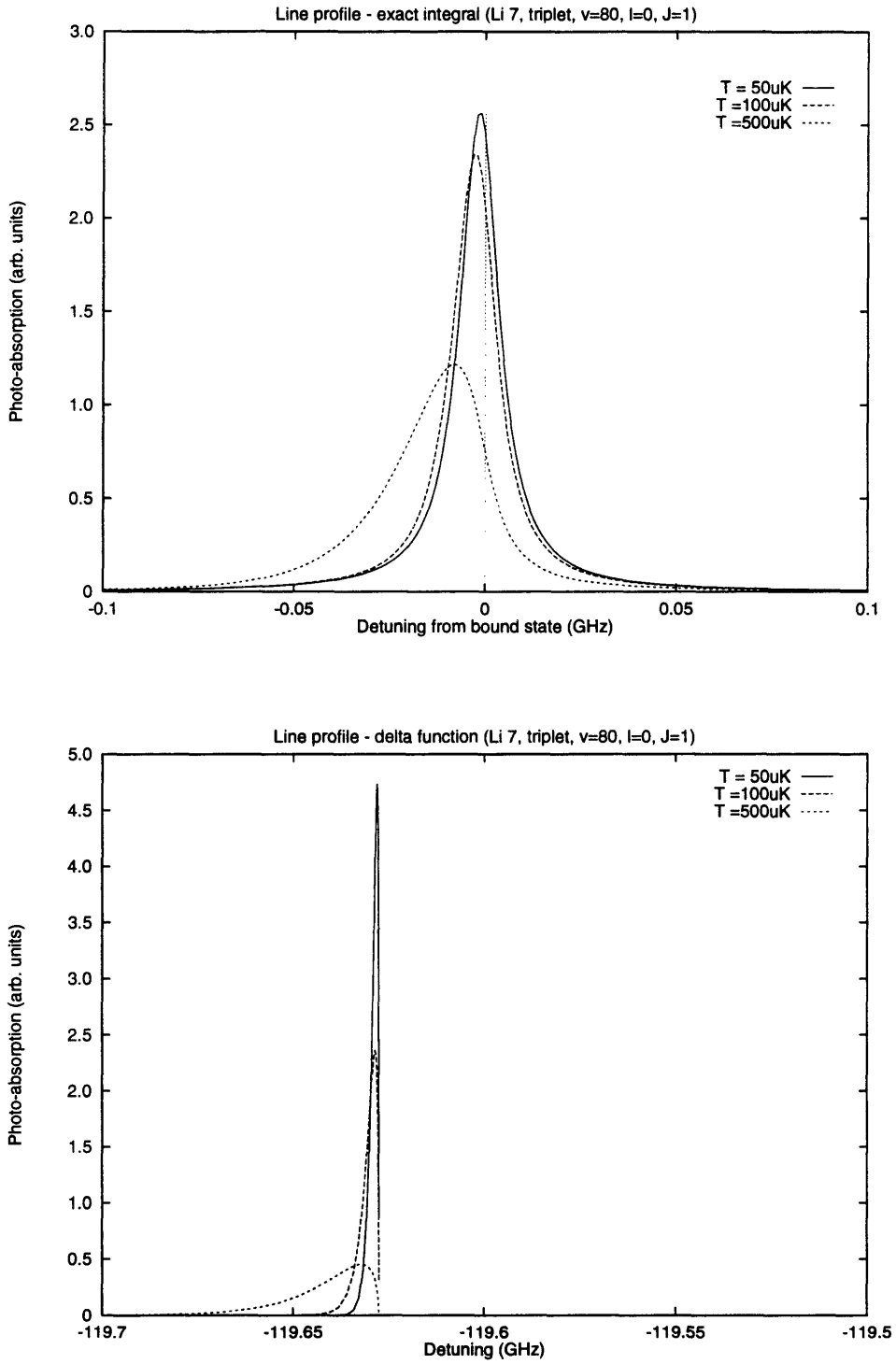

Figure 4.35: Exact (centered at -119.62 GHz) and approximated line profile for the triplet $v_t = 80$ level for $T = 50, 100, 500$ μK.

enough for the two profiles to not well overlap. The same agreement is obtained with all the other sub-peaks of that level, except the one centered at -106.5 GHz. In fact, the overlap is quite bad in that case (see Fig. 4.37). We notice that this sub-peak is more symmetric than the others, and it could be a candidate for a shape resonance (see §4.5 and §4.6.1). In fact, the shape resonance in the $l = 2$ partial wave would contribute at such a temperature. In Fig. 4.38, we compare both the experimental and the $l = 2$ theoretical profiles for $T = 7$ mK. As one can see, the agreement is much better than previously, although not perfect. As mentioned in §4.6.1, one could use the knowledge of T and modify the ground state potential (especially the dissociation energy D_e) and move the resonance to get the best possible fit. This in turn would give very accurate information on the ground state potential.

So, we conclude that $T = 7$ mK, and that the sub-peak located at -106.5 GHz is probably due to a shape resonance in the $l = 2$ partial wave.

4.7 Cold molecules

In this section, we will explore the possibility of producing cold molecules in their ground state. To do so, we will compute the bound-bound transition probabilities and look for levels high enough, so that the probe laser intensity necessary to populate them is small enough and that the trap remain stable, but with a sizable probability to radiate down to the ground state.

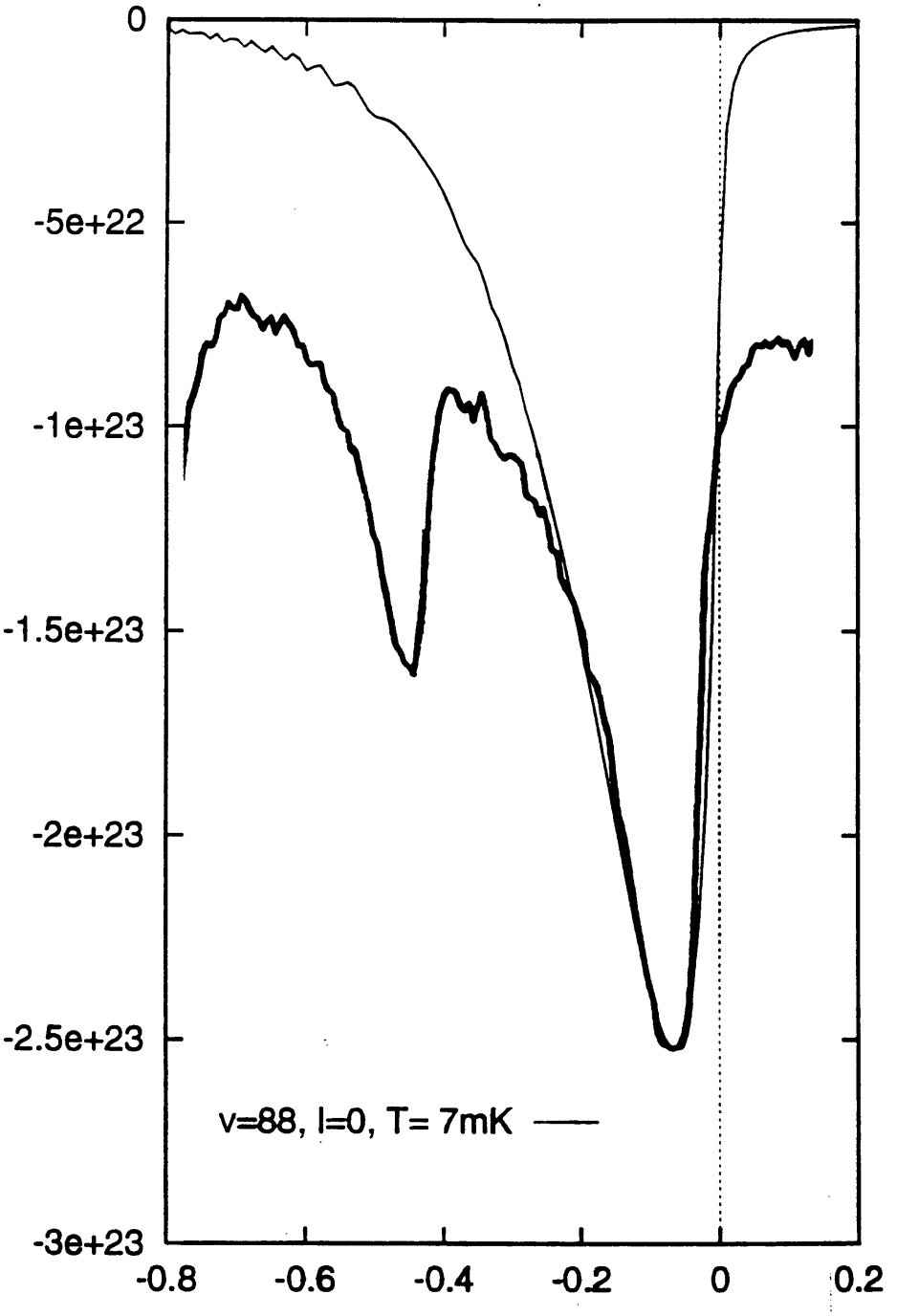

Figure 4.36: Superposition of the experimental and theoretical profiles (in arb. units) for the sub-peak located at -105.8 GHz ($l = 0, J = 1$). The x-axis is the detuning in GHz.

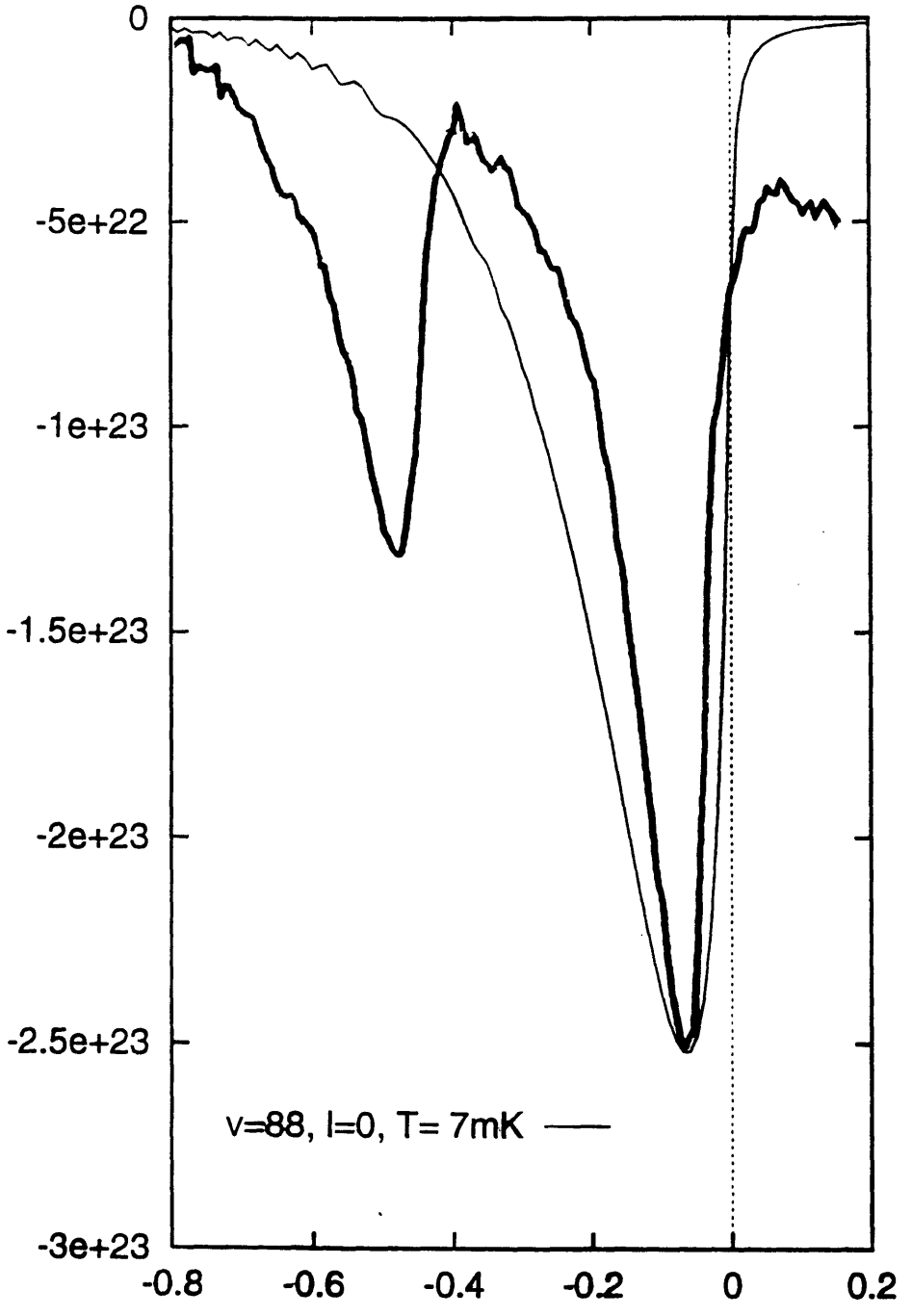

Figure 4.37: Superposition of the experimental and theoretical profiles (in arb. units) for the sub-peak located at -106.5 GHz ($l = 0, J = 1$). The x-axis is the detuning in GHz.

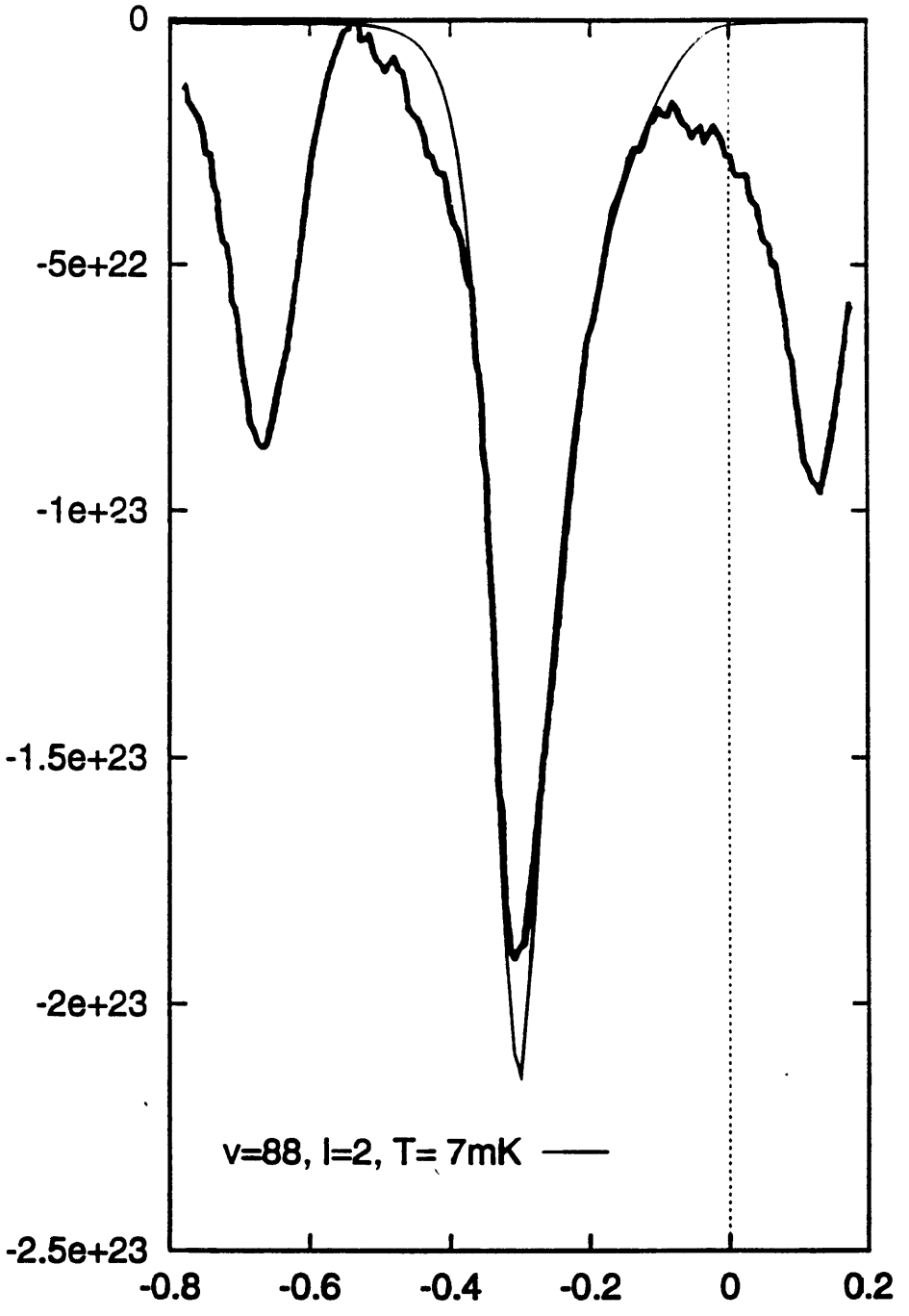

Figure 4.38: Superposition of the experimental and theoretical profiles (in arb. units) for the sub-peak located at -106.5 GHz ($l = 2, J = 1$). The x-axis is the detuning in GHz.

4.7.1 Emission coefficient and oscillator strength

The probability of spontaneous emission (E1) per unit time, A_{ik} from the upper state k to the lower state i is given by

$$A_{ik} = \frac{4}{3}\frac{e^2\omega_{ik}^3}{\hbar c^3}\frac{g}{(2J_k+1)}|\langle i|D|k\rangle|^2 \ , \tag{4.85}$$

where $\omega_{ik} = (E_k - E_i)/\hbar$ is the frequency of the emitted photon, $\langle i|D|k\rangle$ is the matrix element of the molecular dipole moment, and J_k is the angular momentum of the molecule in the state k. Also, g is a statistical weighting factor which depend on the symmetry of the molecular states. For Σ-Σ transitions, g is equal to unity.

As mentioned in the previous section, we consider the excited state with $J = 1$, which can decay into ground states with $l = 0$ or 2. Since both would be of comparable magnitude, we will compute only the $(J = 1, l = 0)$ coefficients without the $2J + 1$ factor, and assume that the result then obtained is an average of the two contributions. So, understanding that we have $(J = 1, l = 0)$, we will drop the reference to those indices, and the spontaneous emission coefficients from an excited level v'' to a ground level v' will simply be written as

$$A_{v'v''} = \frac{4}{3}\alpha^3\varepsilon_{v'v''}^3|D_{v'v''}|^2 \ , \tag{4.86}$$

where all quantities are in atomic units. In our case, since the energies are given from the dissociation limit for both the excited and ground states, we have

$$\varepsilon_{v'v''} = E_b(v'') - E_b(v') + \hbar\omega_p \tag{4.87}$$

where $\hbar\omega_p$ is the separation between the two dissociation limits of the states considered. One has to divide the result by the atomic unit of time to get $A_{v'v''}$ in s^{-1},

namely $\tau_0 = 2.4189 \times 10^{-17} s$.

Similarly, for the absorption oscillator strength $f_{v'v''}$, we will consider the ($J = 1, l = 0$) transition and assume that the result gives the average value into the two possible states ($l = 0, 2$). Then, in atomic units, we will write $f_{v'v''}$ as

$$f_{v'v''} = \frac{2}{3} \varepsilon_{v'v''} |D_{v'v''}|^2 \ . \tag{4.88}$$

Notice that the stimulated emission coefficient $B_{v'v''}$ can be easily found from $f_{v'v''}$ or $A_{v'v''}$

$$B_{v'v''} \equiv \frac{2}{3} \pi \alpha |D_{v'v''}|^2 = \frac{\pi \alpha}{\varepsilon_{v'v''}} f_{v'v''} = \frac{\pi}{2} \frac{1}{\alpha^2 \varepsilon^3_{v'v''}} A_{v'v''} \ . \tag{4.89}$$

In Appendix E, we give all the $A_{v'v''}$ and $f_{v'v''}$ for the singlet and triplet transitions of both the ^{7}Li and ^{6}Li isotopes.

In those tables, we also included the sum over all excited levels, and the sum over all ground levels, namely

$$\sum_{v'} A_{v'v''} \qquad \text{and} \qquad \sum_{v'} f_{v'v''} \ , \text{for a given excited level } v'' \ , \tag{4.90}$$

and

$$\sum_{v''} A_{v'v''} \qquad \text{and} \qquad \sum_{v''} f_{v'v''} \ , \text{for a given ground level } v' \ . \tag{4.91}$$

In Fig. 4.39, we show the total spontaneous emission $\sum_{v'} A_{v'v''}$ for an excited state v'' for both the singlet and triplet transitions, in the two isotopes cases. In the singlet case, the total emission starts at basically $5.5 \times 10^7 s^{-1}$ and decreases slowly into a plateau at $5.2 \times 10^7 s^{-1}$, as the excited vibrational level v'' increases. At $v'' \sim 20$, it drops abruptly until it reaches a first oscillation at $v'' \sim 26$, and oscillates around a

decreasing line until it hits a last plateau near $v'' \sim 80$: it then goes to zero. Both isotopes are behaving the same way, ^{7}Li being shifted to the right of ^{6}Li by few levels.

The shift in v'' is approximately given by scaling relationship of energy levels. In comparing the vibrational quantum number of the two isotopes for the same bound energy, we find that the ratio of the quantum numbers is equal to the ratio of the square root of the reduce masses. This can be shown using the Bohr-Sommerfeld quantization condition (see Eq. (3.40))

$$v + \frac{1}{2} = \frac{\sqrt{2\mu}}{\pi\hbar} \int_{R_1(v)}^{R_2(v)} dR \sqrt{E(v) - V_{\text{eff}}(R)} \; , \tag{4.92}$$

where the potential $V_{\text{eff}}(R)$ includes the centrifugal contribution

$$V_{\text{eff}}(R) = V(R) + \frac{\hbar^2}{2\mu} \frac{J(J+1)}{R^2} \; . \tag{4.93}$$

In our case, $J = 1$ and the centrifugal correction is present. However, since 2μ is of the order of 10^5 a.u., we can neglect the centrifugal correction, to first order. Then, the integral depends on the value of E only, and is independent of the reduce mass. So, for the same energy E, the ratio for the two isotopes gives

$$\frac{v(^7\text{Li}) + 1/2}{v(^6\text{Li}) + 1/2} \simeq \frac{v(^7\text{Li})}{v(^6\text{Li})} \simeq \sqrt{\frac{\mu(^7\text{Li})}{\mu(^6\text{Li})}} \equiv M \; , \tag{4.94}$$

where the omission of $1/2$ is valid for large vibrational quantum numbers. So, this scaling relationship gives a shift approximately equal to

$$v(^7\text{Li}) \simeq M v(^6\text{Li}) + \frac{1}{2}(M - 1) \; . \tag{4.95}$$

In our case, the ratio of reduce masses gives $M = 1.08$, and therefore one can neglect the contribution of 0.04 from the $1/2$ term, and since v is an integer, write

$$v(^7\text{Li}) \simeq [M v(^6\text{Li})] \; , \tag{4.96}$$

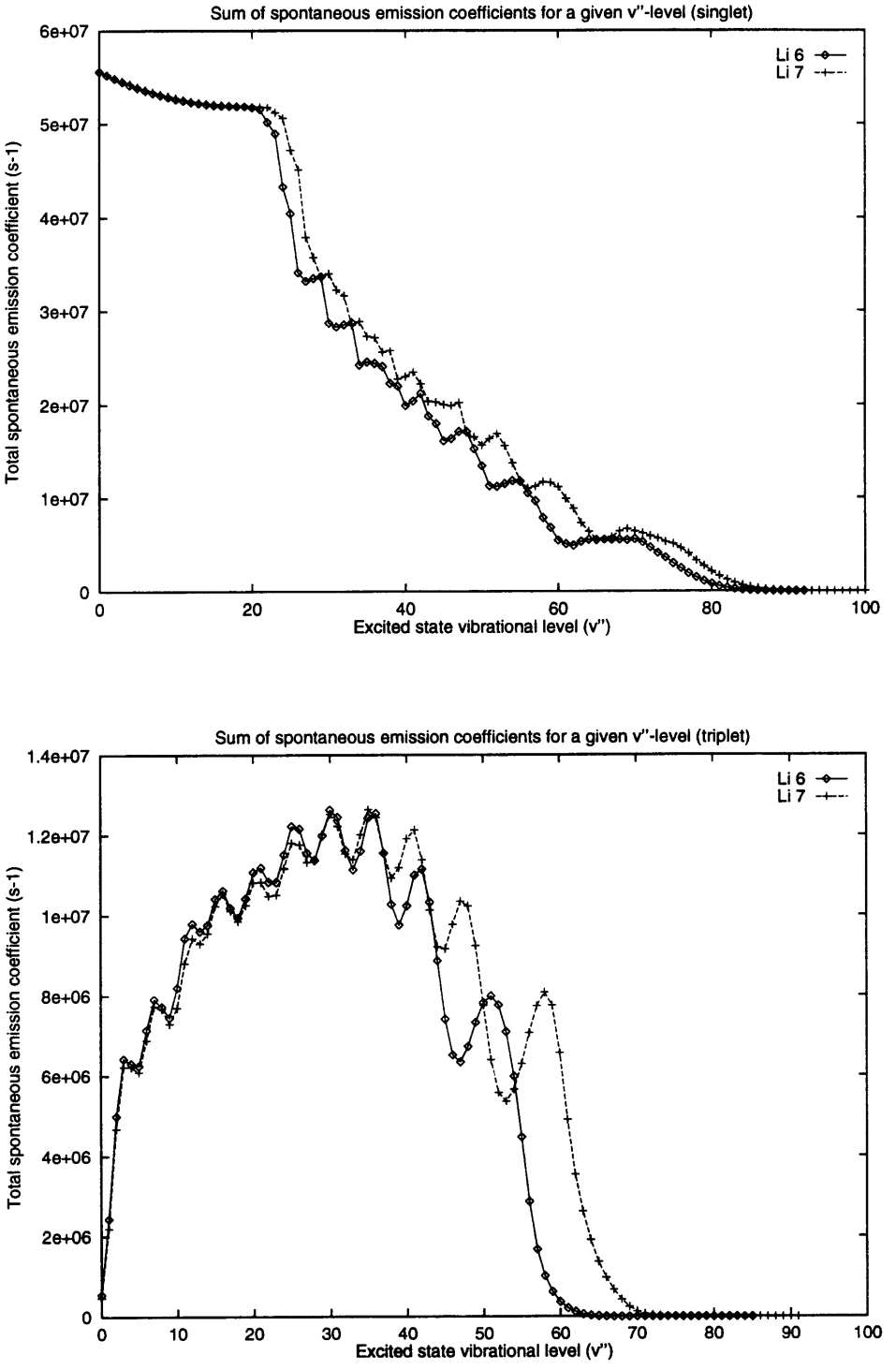

Figure 4.39: Total bound-bound spontaneous emissions from a given excited level v'' into all the ground levels v'.

where [ ] means the integer part of the expression. So, for $v(^6\mathrm{Li})$ around 60, the $^7\mathrm{Li}$ curve would be shifted by 4 to 5 levels to the right, which is in agreement with the results shown in the figure. Notice that this fact can also be traced back to the 2μ dependence of $|D_{v'}(\varepsilon)|^2$ (see Eq. (4.30) for instance).

In the case of the triplet transitions, the total bound-bound emission starts rather low at $\sim 5 \times 10^5 s^{-1}$ and grows, oscillating around an inverse parabola shape, before decreasing to zero. Here again, the shift between the two isotope curves can be linked to the ratio of the reduce masses. However, the main difference with the singlet transitions is in the low vibrational levels. In fact, contrary to the previous case, there is no plateau at low v'', and this would imply a large contribution of the bound-continuous transitions.

This is to be expected, when we compare the overlap of the potential curves in both the singlet and triplet transitions. As can be seen in Fig. 4.40, in the case of the singlet transitions, the two potential curves are basically on top of each other. Hence, the overlap of the low excited v'' with all the ground v' will be very large. Only for higher v'' will the overlap decrease as the last lobe moves out to larger R. But in the case of the triplet transitions, the low excited v'' resides in the portion of the well which overlaps with the repulsive wall of the ground state, giving a poor overlap of the wave functions. As v'' grows, the last lobe centered at the outer turning point of the excited wave function will overlap better and better with the the ground state, giving a more sizable total bound-bound emission. However, this lobe will soon move out of the deepest portion of the ground state well, and the total bound-bound

emission will decrease rapidly.

We can convince ourselves that the difference in the overlap of the wave functions is the major factor to explain those curves, by looking also at the dipole moments as a function of R for both the singlet and triplet transitions. In Fig. 4.3, we can see that the triplet $D(R)$ is larger than the singlet dipole moment at small distances, and that both are of comparable magnitudes at larger R. This would indicate a larger triplet total bound-bound emission than the singlet one, contrary to our results, hence the necessity of the difference in the overlap of the wave functions. In Fig. 4.41, we give the sum of the overlap of the ground state wave functions with a given excited one for level v''. The previous remarks are well illustrated by this figure, namely that the total overlap for the singlet transitions is basically equal to unity for small v'' and the decreases, although the triplet one starts small, increases and the decreases as v'' grows. This also gives a good estimate of the portion of bound-free transitions for a given v'' level: it should be roughly equal to one minus the total bound-bound overlap.

From these two sets of data, the total bound-bound emission and the total bound-bound wave function overlaps, one can estimate the width $\gamma_p(v'')$ and lifetime $\tau_p(v'')$ of a given excited vibrational level v''. In fact, taking the total bound-bound emission and dividing it by the total bound-bound wave function overlap, we compensate for the fraction of bound-free transitions, and we can write

$$\gamma_p(v'') \simeq \frac{\sum_{v'} A_{v'v''}}{\sum_{v'} |\langle v'|v''\rangle|^2} \qquad \text{and} \qquad \tau_p(v'') = \frac{1}{\gamma_p(v'')} \; . \tag{4.97}$$

In Fig. 4.42, we show the results for $\gamma_p(v'')$ in the singlet and triplet transition, for

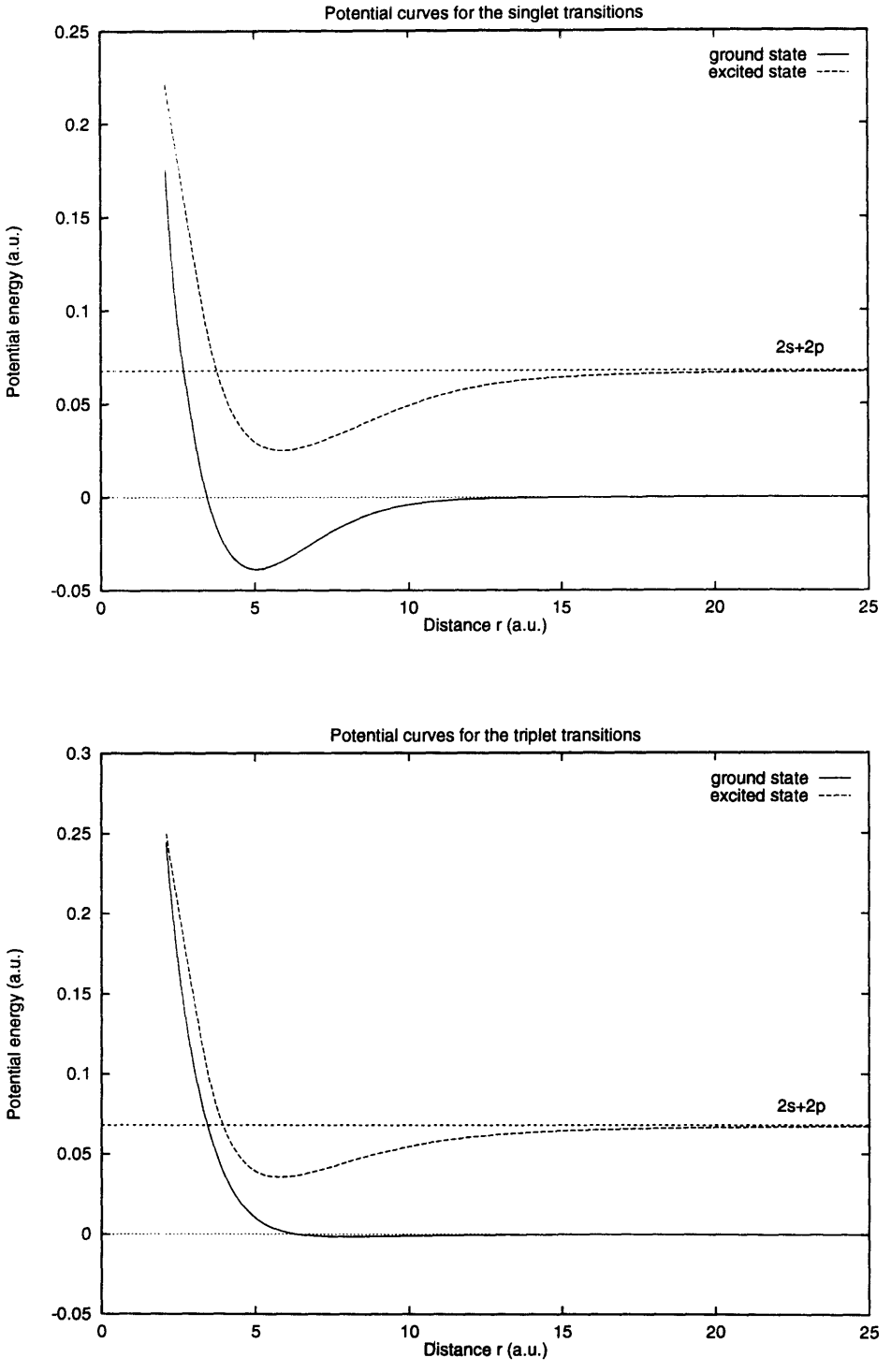

Figure 4.40: Overlap of the excited and ground state potential curves for both the singlet and triplet transitions.

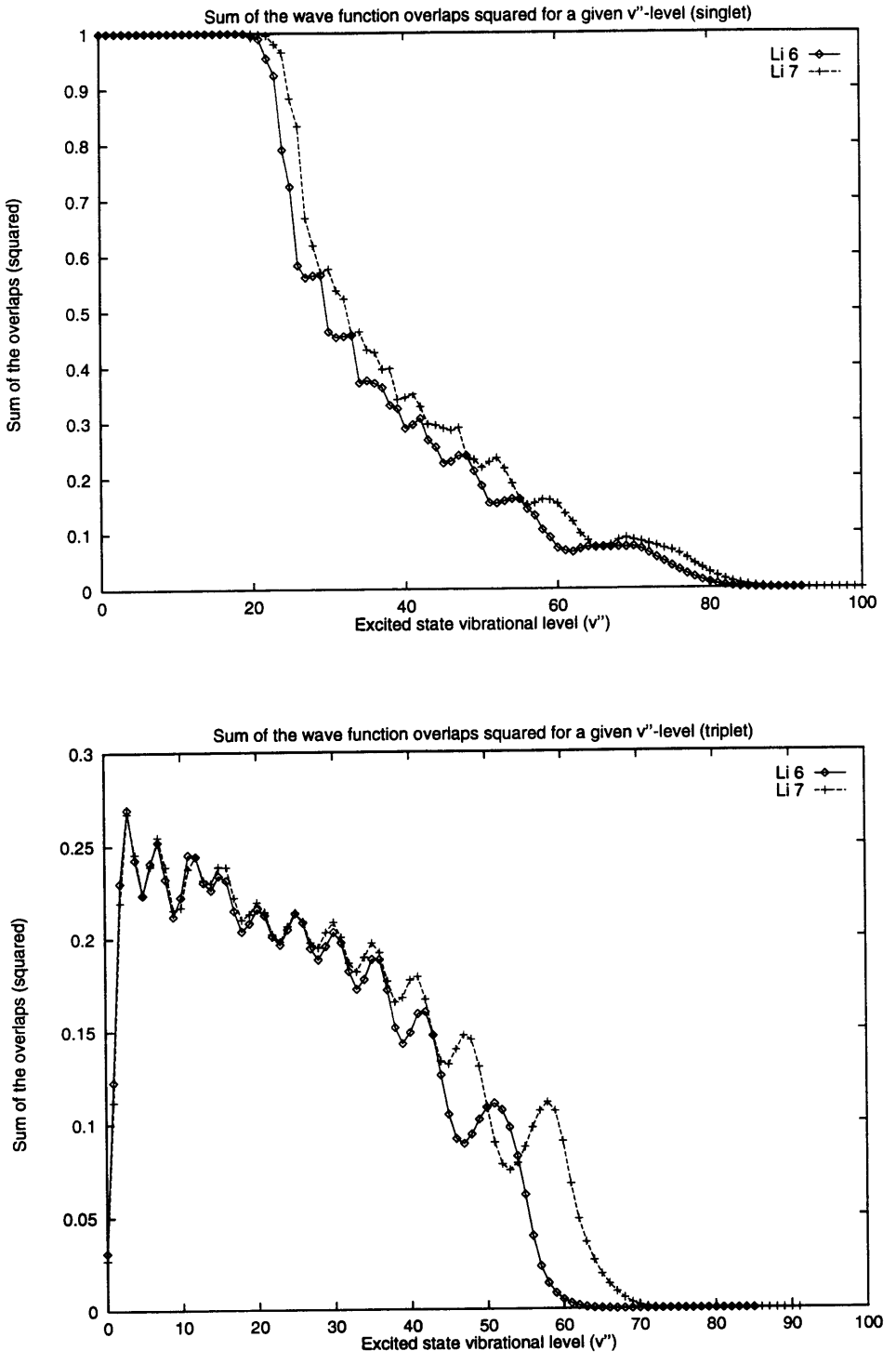

Figure 4.41: Total overlap of the bound-bound wave functions for a given excited level v'' and all the ground levels v'.

both isotopes. In the case of the singlet transitions, $\gamma_p(v'')$ starts from $5.5 \times 10^7 s^{-1}$ and decreases slowly before growing steadily to its asymptotic value of $\sim 7.5 \times 10^7 s^{-1}$. However, we notice that $\gamma_p(v'')$ increases to a new plateau located at $8.5 \times 10^7 s^{-1}$ around $v'' = 80$.

This can be traced back to the procedure used to estimate the width, namely the division by the total bound-bound overlap. As we pointed out in §4.2.1, the box used to compute the energy and wave function of a bound state might not have been large enough, and therefore the last levels might have less accurate wave functions. Since the overlap is already very small, this small effect is amplified by the division we make. To illustrate this, one needs to consider the level we treated in the last section, namely the ^{7}Li singlet $v'' = 88$ level. In that case, we got $\gamma_p = 7.3544 \times 10^7 s^{-1}$, and most of this value was due to the bound-free transition. When we compare with our estimate

$$\gamma_p \simeq \frac{1.306 \times 10^5}{1.654 \times 10^{-3}} s^{-1} = 7.89 \times 10^7 s^{-1} \ , \tag{4.98}$$

we can better appreciate the effect of a small error in the overlap for high level v''. As we already mentioned, those higher vibrational levels should give twice the atomic value, since a large v'' corresponds to a far outer turning point which can be thought of the atomic limit ($R \rightarrow \infty$). So, the last increase in $\gamma_p(v'')$ just represents the imprecision in the total bound-bound overlap of the wave functions. The exact value will be $\gamma_p = 7.35 \times 10^7 s^{-1}$ as we already have shown.

In the case of the triplet transitions, the width is much more regular, starting at $2 \times 10^7 s^{-1}$ and growing to its asymptotic value of $7.35 \times 10^7 s^{-1}$. Here again, the last

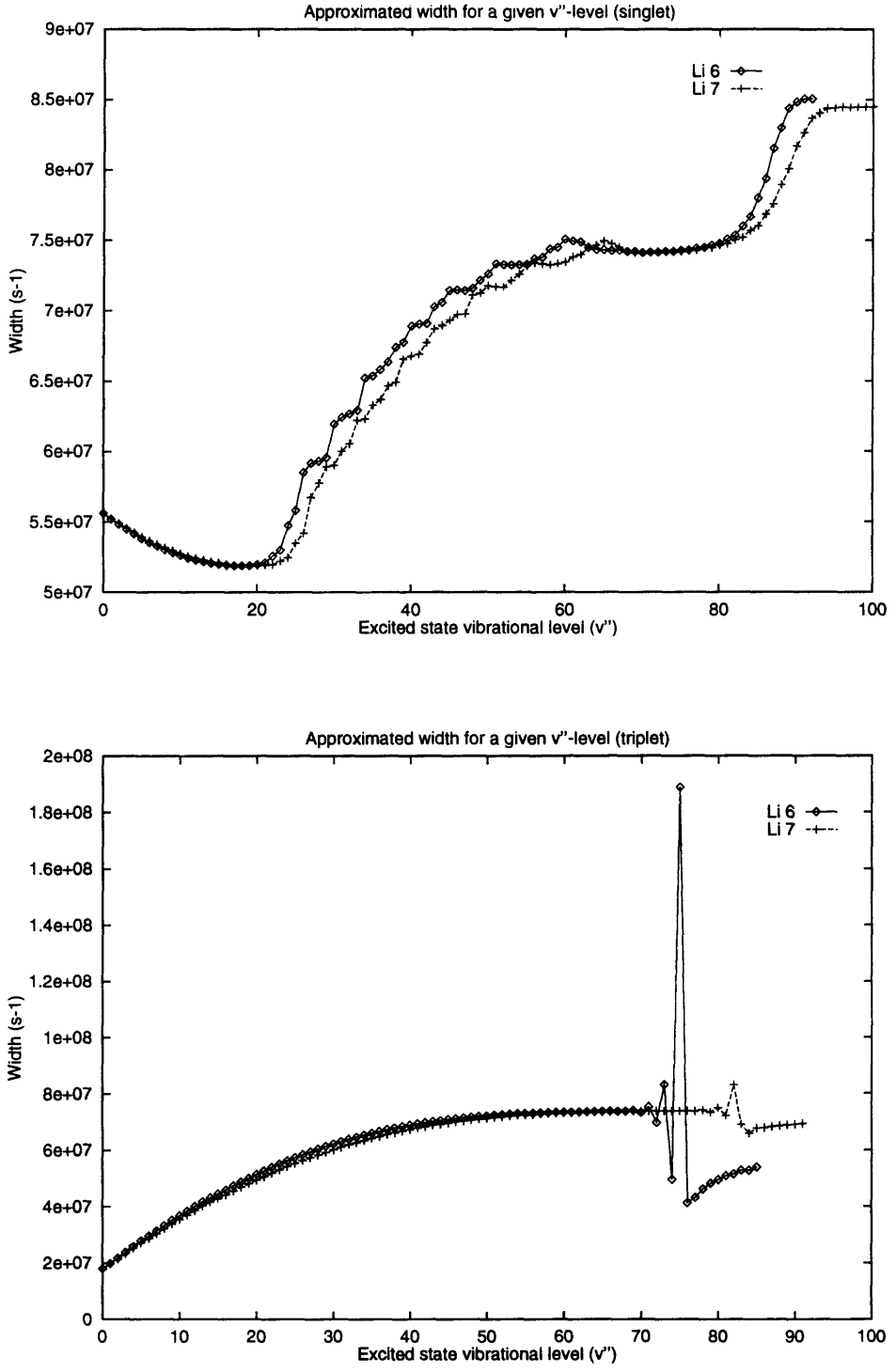

Figure 4.42: Estimated width γ_p (in s^{-1}) for a given v''.

levels exhibit the imprecision due to the quantization box (see the previous section for the evaluation of the level $v'' = 80$ of the ^{7}Li case), although one should notice that this lack of accuracy is amplified by the fact that we divide by a small number.

For sake of completeness, we also give the total spontaneous bound-bound emission for a given ground state v', *i.e.* $\sum_{v''} A_{v'v''}$. They are shown in Fig. 4.43 for both the singlet and triplet cases. As we can see, in the singlet transitions, the curve starts at around $6.7 \times 10^7 s^{-1}$ before decreasing slowly until $v' \sim 10$, then it falls to a plateau between $v' \sim 20$ to $v' \sim 30$ before growing fast to its maximum value of $7.3 \times 10^7 s^{-1}$. Notice that this corresponds to twice the atomic value, which is normal since the last bound state has its outer turning point far out ($R \sim 43\ a_0$). The reason for the shape of this curve is directly related to the dipole moment. In fact, for the small v', the overlap between the wave function is very good, but the overlapping region is situated at small values of R, where $D(R)$ is rather small. As v' increases, the overlap reduces faster than $D(R)$ grows, and the net effect is a sharp decrease in the curve. The two effects balance each other between $v' \sim 20$ and 30, and finally the curve grows again as vibrational quantum number increases. This last behaviour comes from the fact that the overlap with the higher excited states becomes better, and since there are many of them, the total overlap is must larger than at smaller v'.

In the case of the triplet transitions, the curves grow almost linearly from their initial value of $3.5 \times 10^7 s^{-1}$ to the maximum one of $\sim 7.1 \times 10^7 s^{-1}$. This is due to the fact that the ground state potential well is starting farther out at $R_0 \sim 6.3 a_0$, where $D(R)$ is already close to it maximum. Then, as v' increases, we have a better overlap

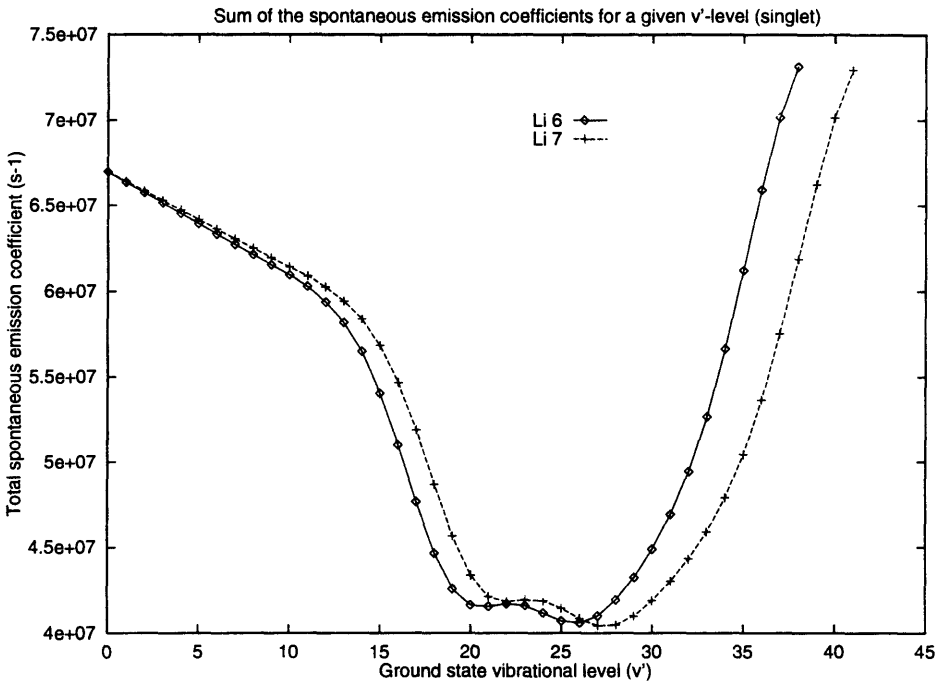

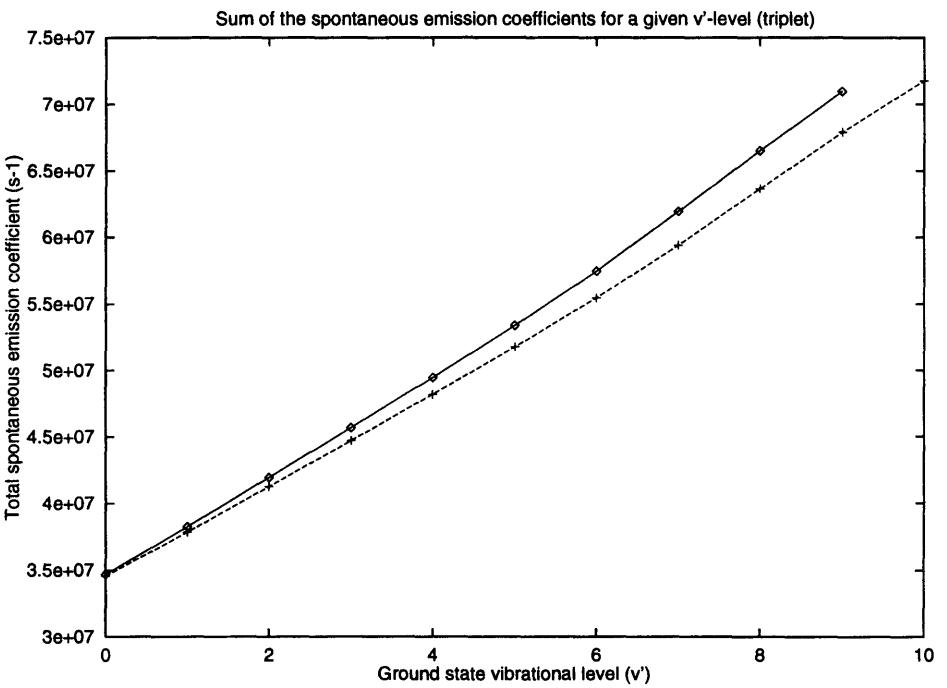

Figure 4.43: Total spontaneous emission coefficient for a given ground level v'.

with the excited states, hence a bigger total spontaneous bound-bound emission.

Finally, we can also look at the fraction of the bound-bound stimulated emission. Since we have

$$\langle v''|D^2(R)|v''\rangle = \sum_{v'} |\langle v'|D(R)|v''\rangle|^2 + \int_0^\infty d\varepsilon |\langle \varepsilon|D(R)|v''\rangle|^2 \ , \tag{4.99}$$

and from the definition of $B_{v'v''}$, we get directly the fraction of the total bound-bound stimulated emission

$$\mathcal{F} \equiv \frac{\sum_{v'} |\langle v'|D(R)|v''\rangle|^2}{\langle v''|D^2(R)|v''\rangle} \ . \tag{4.100}$$

In Fig. 4.44, we give this ratio as a function of the excited vibrational quantum number v''. As we can see, the curves are very similar to the previous one for the total bound-bound spontaneous emission, and the same conclusions are valid.

4.7.2 The cold molecule

From the previous results, one can hope to identify a window of vibrational levels v'' such that the bound-bound transitions have a sizable probability of occurring, but high enough so that the probe laser intensity is still small enough to guarantee a stable trap.

In the case of the singlet transitions, both ^{7}Li and ^{6}Li seems to have a last plateau from $v'' \sim 60$ and higher. However, from the experimental data, the lowest v'' obtained are around $v'' = 83$ at $\Delta \simeq -350$ GHz for ^{7}Li and $v'' = 80$ at $\Delta \simeq -180$ GHz for ^{6}Li. In both cases, the fraction of bound-bound transition is quite small (less than 1%, see Fig. 4.44), but it might still be possible to populate those ground state levels. The

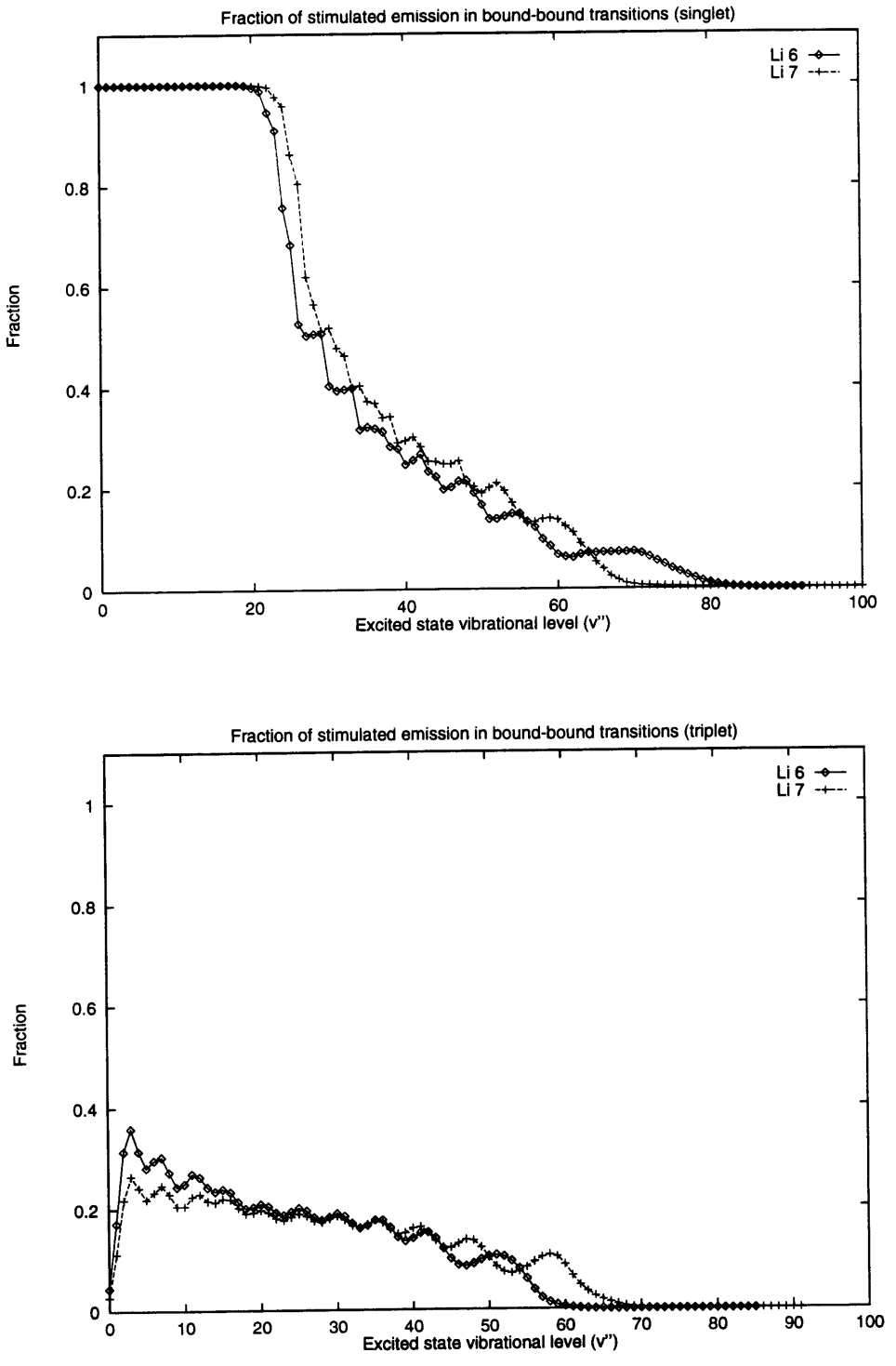

Figure 4.44: Fraction of the stimulated emission into bound-bound transitions for a given excited level v'.

important question is to know which individual ground state levels are being mostly populated. In order to answer that question, one must look at the results listed in Appendix E. For ^{7}Li, one can see that for levels between 80 to about 90, most of the bound-bound transitions go into the last ground state level $v' = 41$, although there is a fair portion distributed in the other high v' levels. This represents between 90% to 30% of the total bound-bound transitions, and therefore one can hope to be able to populate this last state. Notice that for higher levels v'', the bound-bound transitions are more evenly distributed. For ^{6}Li, we observe the same scheme, although it extends from levels 80 to about 86, with branching ratios to the ground level $v' = 38$ varying between 90% and 46% (for higher levels, the total bound-bound transitions are more distributed). Finally, we have to mention that we limited ourselves to the observable levels: for lower levels v'', there are other ground levels v' with a very high branching ratio. In fig. 4.45, we illustrate those upper bound-bound transitions coefficients for v'' between 80 and 92, and 80 and 100, for all the ground state levels v' of both ^{6}Li and ^{7}Li respectively.

To understand better the distribution between the different levels, one can look at the total spectrum of the bound-bound transitions. Figs. 4.46 and 4.47 show this spectrum for ^{7}Li and ^{6}Li, respectively. As one can easily see, there are local maximum branching ratios located along a diagonal in the v'-v'' plane. These "waves" increase, peak, then almost disappear to grow again, along the diagonal. This can easily be explained by the constructive and destructive interferences between the bound state wave functions. The region of maximum overlap move to larger and larger R as v' is

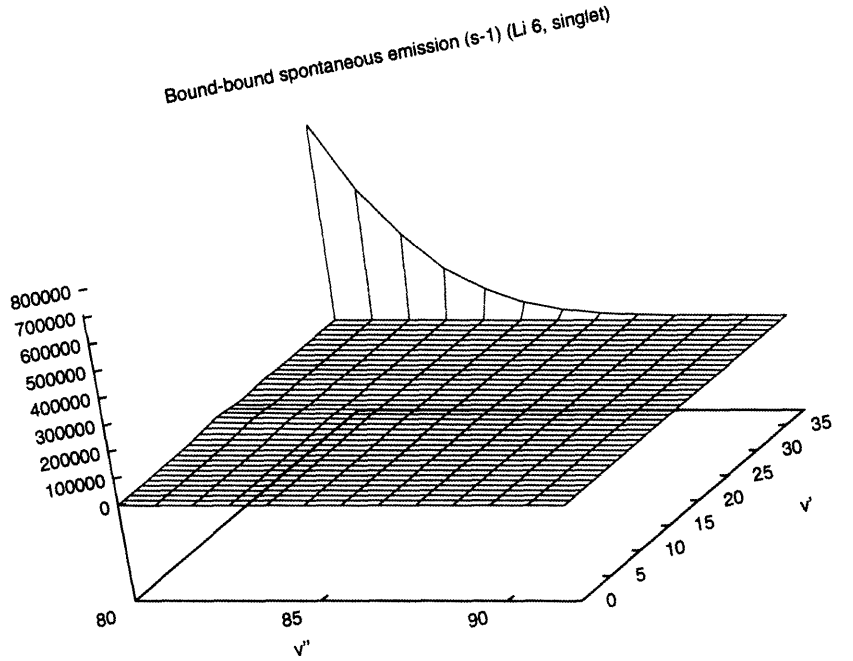

Figure 4.45: Bound-bound transition coefficients for the singlet case of ^{7}Li and ^{6}Li for the upper v'' levels.

increased, and so the maximum branching ratios will move accordingly to the higher v'' levels. Of course, there will be levels such that the interference will be destructive, even if the condition for maximum overlap seems to be met: the wave function will simply be out of phase by $\pi/2$.

Let us now look at the triplet transitions. From Figs. 4.39 and 4.44, we find a sizable bound-bound contribution for v'' higher than 50 for ^{6}Li, and higher than 60 for ^{7}Li. However, from the experimental data, the lowest observed levels are $v'' = 63$ at $\Delta \simeq -2000$ GHz for ^{7}Li, and $v'' = 56$ at $\Delta \simeq -2700$ GHz for ^{6}Li. It seems that the ^{7}Li case would provide a better candidate for cold molecules than ^{6}Li, the fraction of total bound-bound transition representing about 4% (at $v'' = 63$) of the total transitions (see Fig. 4.44). Once again, the individual bound-bound transitions for both ^{7}Li and ^{6}Li are given in Appendix E. For the triplet transitions of ^{7}Li, the branching ratio to the last ground state $v' = 10$ for $v'' = 60$ to about 80 represents basically 100% of the bound-bound transitions for a given v''. For higher v'', this fraction decreases, the transitions being more evenly distributed. In the case of ^{6}Li, for $v'' = 50$ to 73, almost 100% of the bound-bound transitions go into the last ground state level $v' = 9$. At higher v'', the branching ratios are more distributed. So, in the case of the triplet transitions, the level of the ground state that one can hope to populate is basically the last level, in both ^{7}Li and ^{6}Li cases. The individual bound-bound transition coefficients are shown in Fig. 4.48 for $v'' = 51$ to 85 (for ^{6}Li), and $v'' = 61$ to 91 (for ^{7}Li).

Here again, a look at the full spectrum of the bound-bound transitions is instruc-

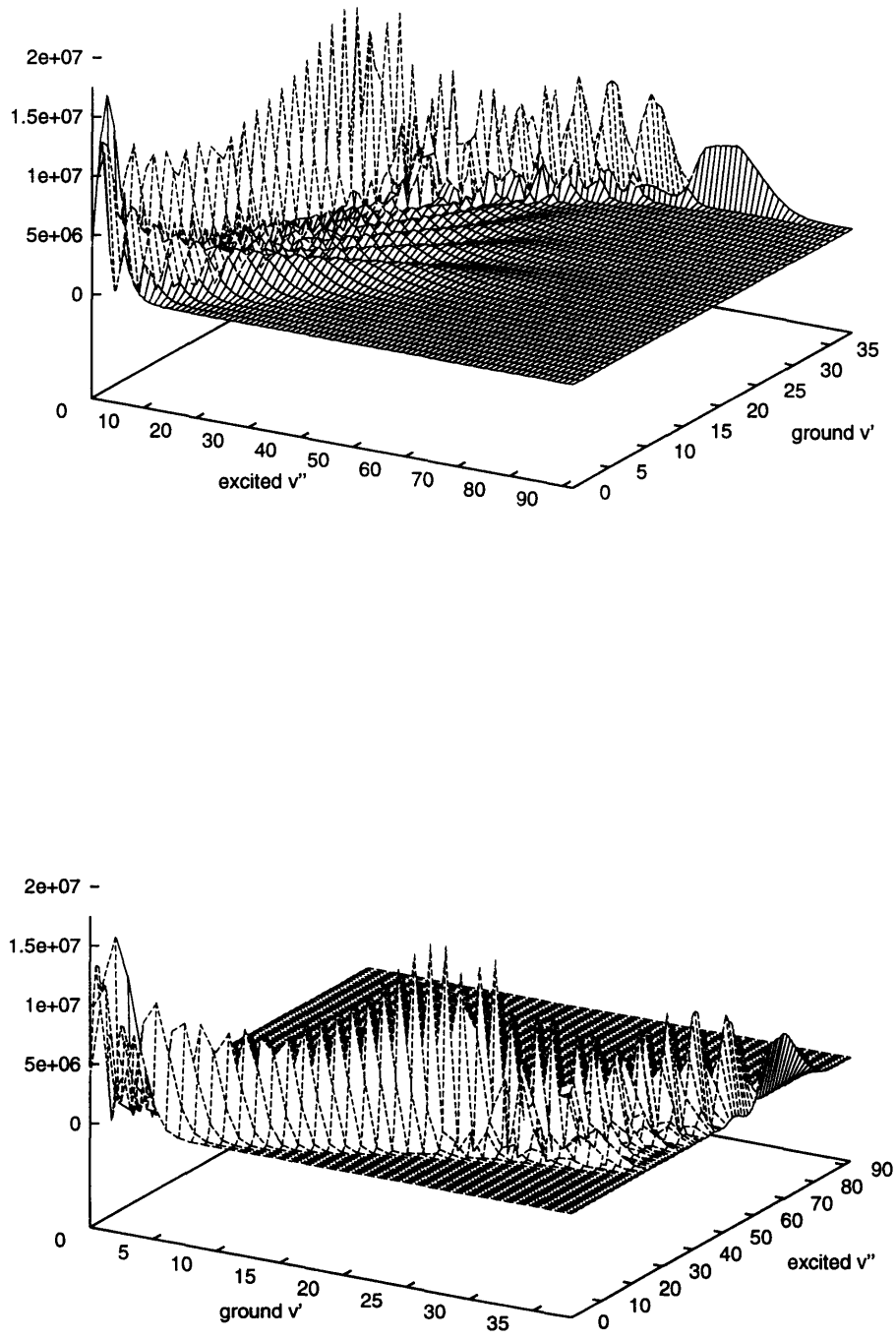

Figure 4.46: Bound-bound transition coefficients for the ^{6}Li singlet case. The bottom plot gives the back of the first one.

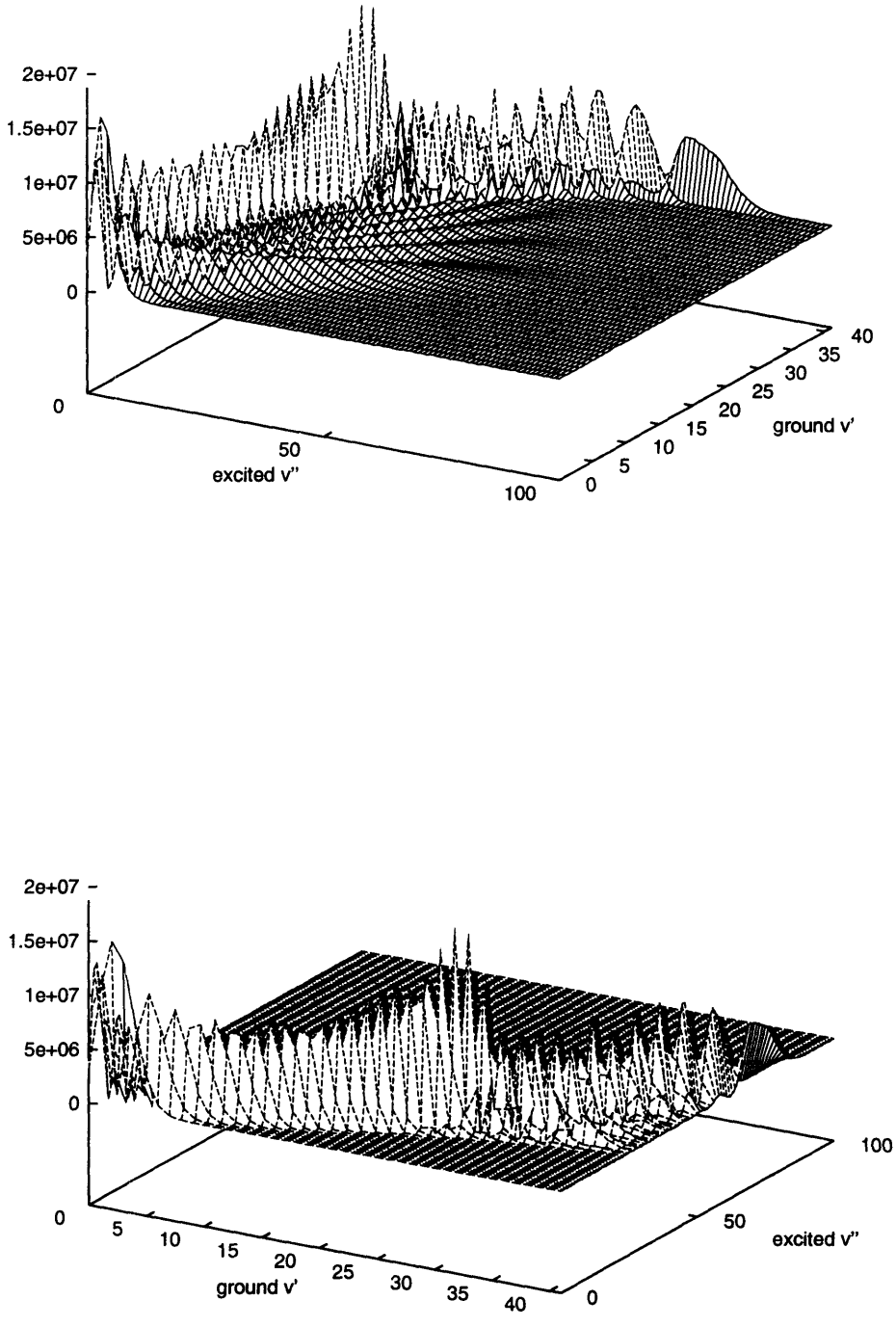

Figure 4.47: Bound-bound transition coefficients for the ^{7}Li singlet case. The bottom plot gives the back of the first one.

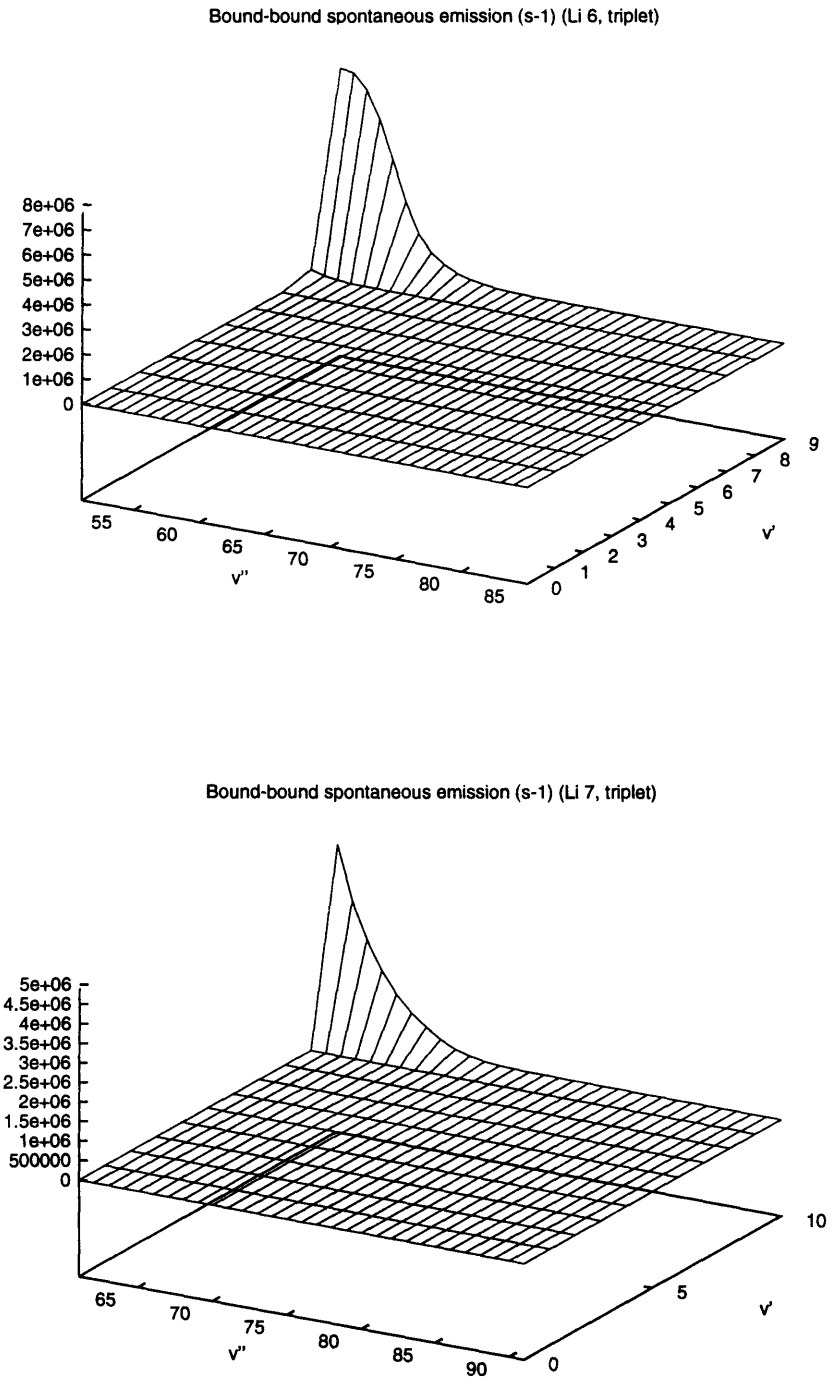

Figure 4.48: Bound-bound transition coefficients for the triplet case of ^{7}Li and ^{6}Li for the upper v'' levels.

tive. In Figs. 4.49 and 4.50, we show it for both ^{7}Li and ^{6}Li, respectively. The same general observations are noted, namely a pulsating local maximum located on a diagonal in the v'-v'' plane. It has the same origin as the singlet cases, *i.e.* it is due to the maximum overlap region being move toward higher v'' as v' increases, and interference pattern in this maximum overlaping region.

Overall, the best candidate to form a cold molecule would be the triplet transition case for ^{7}Li. In fact, the fraction of bound-bound transitions represents up to 4% of the total emission, and most of it occur in the last bound state level of the ^{7}Li molecule. Although the binding energy of this last level is quite small, it nevertheless represents a new window to study cold molecules (see the concluding remarks).

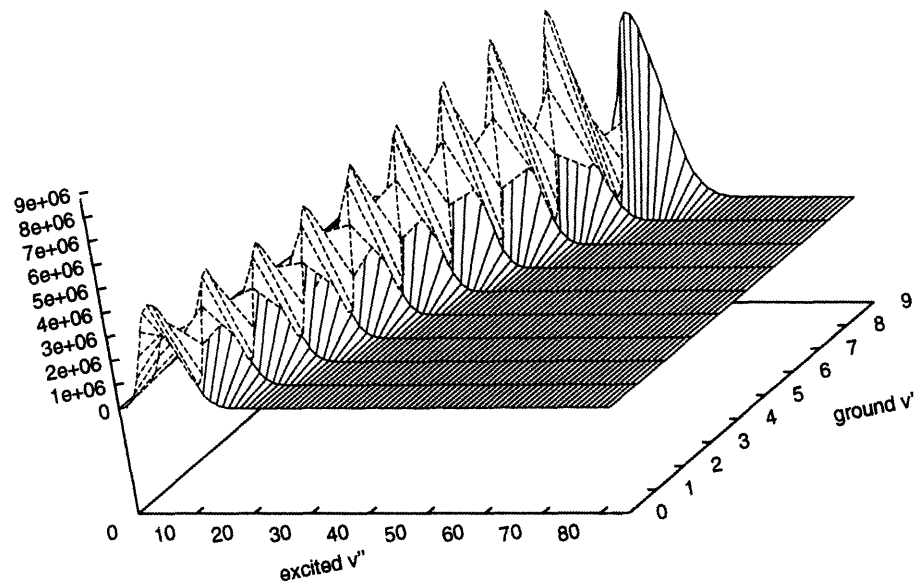

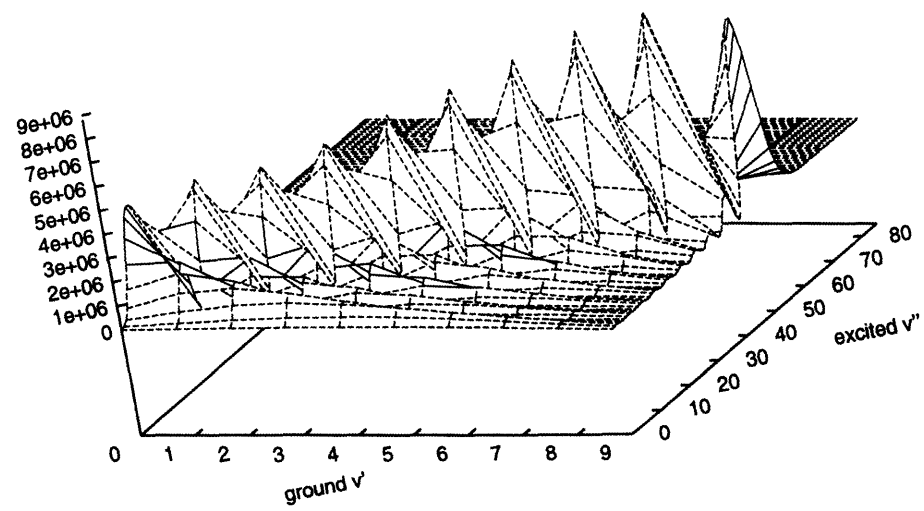

Figure 4.49: Bound-bound transition coefficients for the ^{6}Li triplet case. The bottom plot gives the back of the first one.

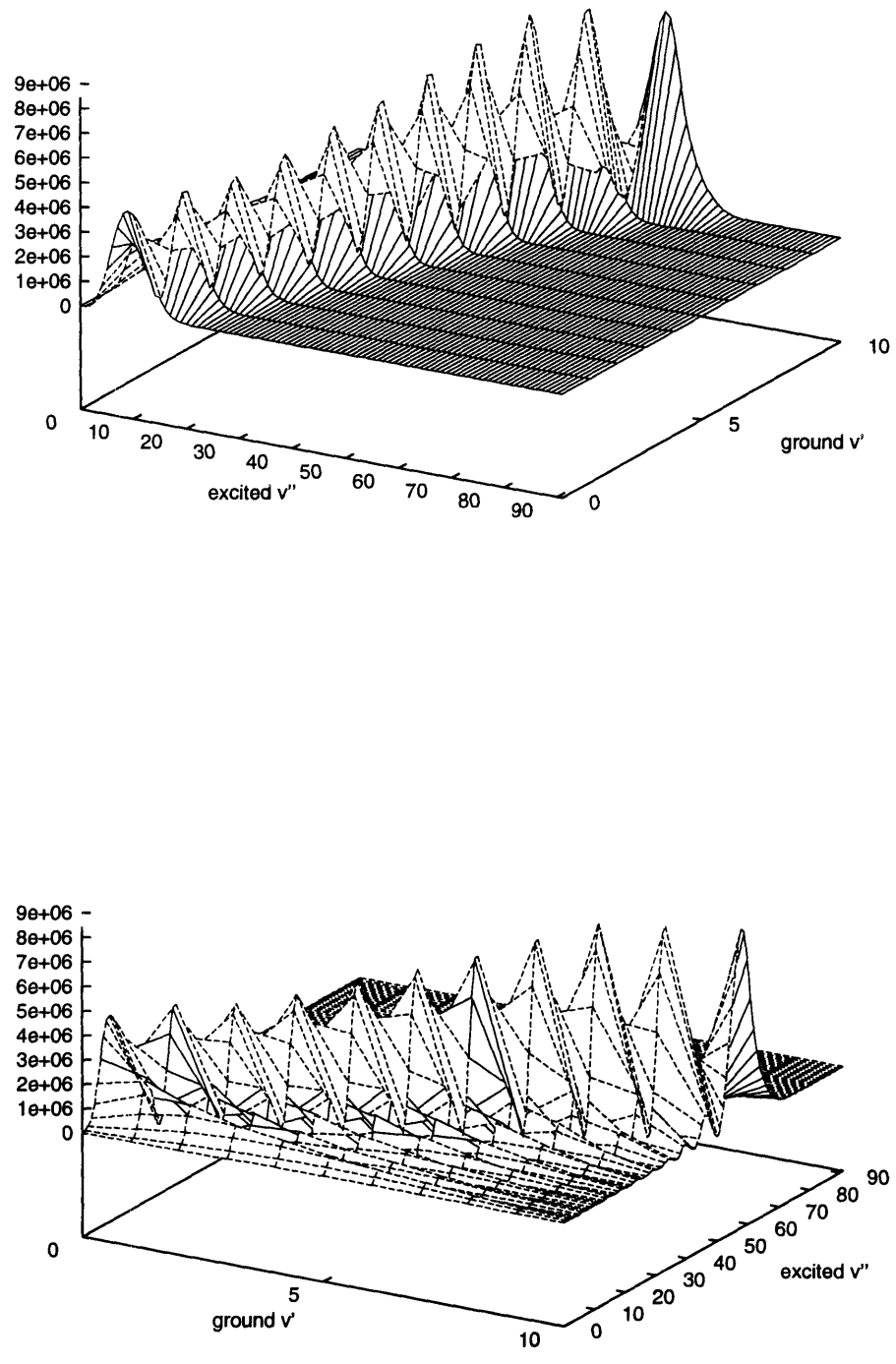

Figure 4.50: Bound-bound transition coefficients for the ^{7}Li triplet case. The bottom plot gives the back of the first one.

Conclusion

In this work, we studied many aspects of ultracold collisions of identical atoms, namely the ^{6}Li, ^{7}Li, and ^{23}Na alkali atoms .

From our calculations of atom collisions along their ground state molecular potentials, we were able to obtain very accurate dissociation energies: our predicted values are within the uncertainty of the most accurate experimental estimates available. In the zero-energy analysis done in §2.2.3, we extracted the scattering lengths and effective ranges for ^{7}Li and ^{23}Na. For ^{7}Li, we found a positive a for the singlet ground state, and a negative a for the triplet ground state. For ^{23}Na, a was found to be positive for both ground state potentials. According to dilute Bose gas theory (see Abrikosov *et al.* [12]), this would imply an unstable Bose condensate for the triplet ^{7}Li potential, though the Bose condensate would be stable in the other cases. We also computed the vibrational bound energy levels for the ground state energy curves: they compare very well with the experimental values. Recently R.G. Hulet and his group [10] were able to measure the last bound state in the $a^3\Sigma_u^+$ state of ^{7}Li. Their value of -12.47 ± 0.03 GHz (corresponding to -0.416 ± 0.001 cm^{-1} from the dissociation limit) is very close to our prediction of -11.45 GHz (corresponding to

-0.382 cm^{-1} from the dissociation limit). By varying the dissociation energy by the difference between these energies (*i.e.* add 0.034 cm^{-1} to our value of $D_e = 333.396$ cm^{-1}), Hulet *et al.* obtained a scattering length of $-26.8 \pm 1.4 a_0$, which is comparable to our value of $-17.2 a_0$.

We also verified that only the s-wave ($l = 0$ partial wave) contributes at low kinetic energy, the higher partial waves starting to be more significant at higher energies. Shape resonances, trapped within the centrifugal barrier, impose sharp structures on the cross sections. The elastic cross sections are very large, of the order of 10^{-13} cm^2. When averaged over the initial velocities, the total cross sections confirm the previous observations regarding the partial waves. Below 1 mK, collisions are dominated by s-wave scattering, but higher order partial waves contribute at higher temperatures. We find a large spin-change cross section for both ^{7}Li and ^{23}Na as $T \to 0$, which in turn give large spin-change rate coefficients. The effect of Casimir corrections on a and r_e is very small: for ^{23}Na, the scattering lengths increase by about 0.1% and the effective ranges decrease by 3.0%. The shape resonances are moved slightly in energy when we consider the retardation effects. We also showed that the elastic scattering at low energy is sensitive to the details of the interaction potentials, especially to the location of the last bound state level.

From the exact quantum treatment, we checked the validity of many semi-classical formulations. For instance, both the LeRoy-Bernstein method and the Gribakin-Flambaum formula gave the same number of bound state levels we found by solving the exact eigenvalue problem, hence confirming their usefulness. Moreover, the

Gribakin-Flambaum formula for the scattering length was very useful to demonstrate the sensitivity of the a to the position of the last bound state. In fact, unless a bound state would be close to the zero-energy limit (a zero-energy resonance), in which case the semi-classical formulation would give wrong results when compared to the exact quantum values, the agreement between the exact quantum and approximate semi-classical values is fairly good. Expanding the Gribakin-Flambaum treatment, we were able to construct the zero-energy wave function and use it to compute a semi-classical effective range. The values of r_e we obtained compare very well with the exact ones. Using this zero-energy wave function, we were able to extract the first coefficients of a series expansion in powers of energy for the suppression of the wave functions. More precisely, the exact quantum probabilities are scaled like $\sqrt{E} \sim \sqrt{T}$ when compared to the semi-classical cases, and the coefficient of proportionality is simply linked to the interaction potential. As a function of r, we found that the suppression is rather sudden, taking place in a small region: it resembles more and more a reflection from a wall located at a given distance, as we lower the energy.

Our simple single-channel approach to the photo-absorption problem has proven to be sufficient to explain many of the features encountered in the experimental data available from R.G. Hulet's group measurements. For both isotopes of lithium, ^{6}Li and ^{7}Li, we found two series of peaks corresponding to singlet and triplet transitions. We were able to link the intensities of those sharp peaks to the sign and magnitude of the scattering length of each ground potential. Precise intensity ratio measurements in the case of triplet transitions for ^{6}Li and ^{7}Li agree with our interpretation. We

predict a more dramatic behaviour for the singlet transitions: they should disappear and grow back before decreasing to zero as we increase the red-detuning. Although no precise data are available at this time, the full spectrum seems to validate this prediction.

For two specific levels of ^{7}Li (singlet $v_s = 88$ and triplet $v_t = 80$), we computed the natural width γ_p and from it, were able to get the atomic lifetime as a check of our values. We estimated the atomic lifetimes to be 27.233ns and 27.195ns for the triplet and the singlet cases, respectively. This is in very good agreement with the accepted value of 27.2ns [68]. From the value of γ_p for the singlet $v_s = 88$ level, we computed the line profile for different temperatures. We estimate the temperature of the experiment to be 7mK by comparing with the experimental profile. At such a temperature, we demonstrated that higher partial waves have to be considered. We showed that the effect of these higher partial waves could be dramatic, especially in the case of ^{7}Li singlet $l = 2$ in the ground state $X^1\Sigma_g^+$. In fact, a shape resonance becomes a dominant feature at these temperatures. Moreover, by comparing the line profile of the $l = 0$ partial wave with the experimental data (where many sub-peaks are present for a single level), we identified a possible candidate for a shape resonance: the profile of this particular peak does not agree with the $l = 0$ partial wave, but agreement is much better with the $l = 2$ resonant partial wave.

Finally, we also looked at the possibility of forming cold translational molecules. Since the intensity of the probe laser has to be as low as possible in order to keep the atoms in the trap, the easiest excited levels to populate are the highest levels. On

the other hand, the levels with the strongest spontaneous emission coefficients into a bound state of the ground molecule are the lowest excited levels. Those two competing effects seem to leave a little window where, while the spontaneous emission is still big enough, the intensity is low enough so the that excited levels can be populated without destroying the trap. We performed this analysis for both singlet and triplet transitions of ^{6}Li and ^{7}Li, and concluded that the best candidate to form a cold translational molecule would be the triplet transitions for the ^{7}Li isotope.

The study of the structure within the individual peaks raised many interesting questions. Although higher partial waves are expected to play an important role in temperature regimes where we concluded the experiment was performed ($\sim$ 7 mK), our treatment does not yet explain every features encountered. For instance, for a given excited level in the case of singlet transitions, there are several sub-peaks, and they seem to be grouped in pairs (R.G. Hulet, private communication). The sub-peaks in each pair are separated by the hyperfine splitting of the atomic ground state (228.2 MHz for ^{6}Li and 803.5 MHz for ^{7}Li [68]). The different pairs might represent a different partial wave for which the degeneracy of the hyperfine level would be lifted. The same would be true for the triplet transitions. Of course, at this point, this is only speculation, but a full multi-channel investigation including the hyperfine interactions should resolve such questions. However, one needs to stress the enormous amount of work necessary to complete such a task, since there would be many hundreds of coupled channels: this last point illustrates well our motivation for choosing a simple single-channel approach to the problem.

The possibility of estimating the temperature and identifying possible shape resonances using the line profiles could also lead to a better understanding of the ground state potential. In fact, the exact location of the energy of the resonance could be inferred more accurately, and this in turn would give a better estimate for the dissociation energy, and possibly the long-range form of the potential. In fact, if D_e is well known from other sources (*e.g.* for the triplet $a^3\Sigma_u^+$ state of ^{7}Li for which the last bound state was measured [10]), the other way to move the resonance is by changing the long-range form of the potential. If one assume the Van der Waals coefficients to be accurate, this would then give information on the exchange term of the ground state of the molecule.

Precise measurements for the very high-lying vibrational states of the excited molecules could also give further information about the long-range form of the excited potential curves. In fact, high levels are quite extended states, the outer turning point (where the last lobe and most of the overlap occurs) being located at large distances. One could then probe the long-range form of the excited potential, and hope to find some indication of the Casimir corrections. In fact, for the excited states, the r^{-3} term is modified by an oscillatory component and takes the form $\sin^2(\rho r)/r^4$ [69]; such effects could translate into oscillations in the intensities of the high levels.

In the case of low excited vibrational levels, one could explore the possibility of using semi-classical techniques in order to evaluate the intensities of the signals. In fact, since those levels are not too extended, the WKB approximation would give a good estimate for the free wave function in the overlapping region. One could then

use the coefficient from the quantum suppression and rescale the values obtained for $|D_v(E)|^2$. This would provide an easy method to compute the intensities for deep levels for ultralow temperatures. One could also use this quantum suppression coefficient to rescale other semi-classical formulation of problems at low temperature (*e.g.*, the Gallagher-Pritchard model [70]). Further studies of the suppression as a function of the distance, for a given small energy, would also give more insights into how this suppression of the WKB wave function takes place. This could lead to a better understanding of the BEC from a semi-classical point of view, and also verify if the sign of the scattering length is really the quantity driving the stability of Bose condensate. In fact, we observed a sharp decrease in the amplitude of the quantum wave function in a rather small interval far out (compared to the magnitude of the scattering length). This is as if the atoms hit a rigid wall far out and are almost completely reflected, which would imply a small probability of being in the region where the negative scattering length could glue the atoms together into a molecule, hence giving a metastable Bose condensate. Of course, this picture is highly speculative at this point, but more attention should be devoted to it.

A last interesting possibility is the creation of ultracold molecules. It would appear possible to create molecules in their ground states for a small set of excited levels. Moreover, the spontaneous emission back into the ground state would populate only the highest vibrational levels, giving a good probability to be realized. Using spectroscopic techniques (*e.g.* Raman scattering), one could then cascade down to any vibational level, especially the lowest $v = 0$ one. By doing so, we could gain a

very accurate knowledge of ground state potentials, but more important maybe, this would open a new window of experiments for the ultracold community. In fact, the possibility of trapping cold molecules could be used to get lower temperatures, the translational energy being transfered to the internal degree of freedom (vibration and rotation). Moreover, these diatomic molecules being composite bosons, some new aspects of BEC could be studied, if one can get the molecule in a single vibro-rotational state (preferably the lowest vibrational level). Finally, one could hope to make precise measurements for a possible T-violation (J.M. Doyle, private communication).

This concludes our study of ultracold collisions of identical atoms.

Appendix A

Numerical Methods

Here, we will give a brief description of the Numerov method used throughout this work to evaluate the free wave scattering problem. At first, we will show a rapid derivation of the numerical scheme and how it was implemented. We also will discuss the step size adjustments necessary for an efficient use of computer capabilities. Finally, we will present the analysis regarding the evaluation of the phase shift from two different approaches: by direct fitting and from an integral equation.

A.1 Derivation

Here, we will give a derivation suitable for our problem, namely the solution of the Schrödinger equation. For more general purposes, others forms based on the same idea might be found in Friedman and Jamieson [71], Allison [72] or Johnson [73]. In here, we follow the steps of Blatt [74].

We are interested in solving the one-dimensional Schrödinger equation in the form

$$\frac{d^2u}{dx^2} + K^2(x)u(x) = 0 \ , \tag{A.1}$$

where the function $K(x)$ is the local momentum which includes the kinetic energy and the potential energy

$$K^2(x) = \frac{2\mu}{\hbar^2}[E - V(x)] \ . \tag{A.2}$$

Here, $V(x)$ might include the centrifugal contribution, if applicable. We start from the Taylor expansion of $u(x+h)$ around the point x

$$u(x+h) = \sum_{n=0}^{\infty} \frac{h^n}{n!} u^{(n)} \ , \tag{A.3}$$

where $u^{(n)}$ is the n^{th} derivative of $u(x)$ evaluated at the point x. From this expression, we obtain

$$\frac{1}{2}[u(x+h) + u(x-h)] = u + \frac{h^2}{2}u^{(2)} + \frac{h^4}{4!}u^{(4)} + \frac{h^6}{6!}u^{(6)} + \cdots \ , \tag{A.4}$$

and, differentiating twice,

$$\frac{1}{2}[u^{(2)}(x+h) + u^{(2)}(x-h)] = u^{(2)} + \frac{h^2}{2}u^{(4)} + \frac{h^4}{4!}u^{(6)} + \cdots \ . \tag{A.5}$$

Multiplying (A.5) by $h^2/12$ and substracting from (A.4), we eliminate $u^{(4)}$. Now, replacing $u^{(2)}$ by $-K^2(x)u(x)$ according to (A.1), we get the Numerov scheme

$$[1+T(x+h)]u(x+h)+[1+T(x-h)]u(x-h) = [2-10T(x)]u(x)-\frac{h^6}{240}u^{(6)}+\cdots \ , \tag{A.6}$$

where we introduced the notation

$$T(x) = \frac{h^2}{12}K^2(x) = \frac{h^2}{12}\frac{2\mu}{\hbar^2}[E - V(x)] \ . \tag{A.7}$$

If $u(x)$ and $u(x-h)$ are known, $u(x+h)$ can be found directly if the error term, proportional to $u^{(6)}$, is ignored. Of course, the values of $T(x)$ are known.

We can rewrite the previous Numerov method in an iterative process

$$(1+T_{n+1})u_{n+1} - 2(1-5T_n)u_n + (1+T_{n-1})u_{n-1} = 0 \ . \tag{A.8}$$

From a programming point of view, the number of arithmetic operations per step can be reduced by means of the substitution (see Allison [72])

$$Y_n = [1+T_n]u_n \ , \tag{A.9}$$

which transforms the Numerov equation in the following way

$$Y_{n+1} = 2Y_n - Y_{n-1} - 12T_n u_n \ . \tag{A.10}$$

Assuming an oscillating solution for $u(x)$ of the form $\sin[K(x)x - b]$ the error can locally be estimated to be

$$\epsilon = \frac{h^6}{240}u^{(6)} \sim \frac{h^6 K^6(x)}{240}u(x) \ , \tag{A.11}$$

where $|u(x)| \leq 1$. So, at most, the error will be given by

$$\epsilon \simeq \frac{h^6 K^6(x)}{240} \ . \tag{A.12}$$

At the start of the integration, we were in the region where the potential is large and repulsive, so we assumed $u_0 = 0$ and $u_1 \sim 10^{-30}$. To select the initial step size, we required the following condition

$$h_{\text{init.}} K_{\text{init.}} = \frac{1}{20} \ , \tag{A.13}$$

which implies an error of

$$\epsilon \simeq \frac{h_{\text{init.}}^6 K_{\text{init.}}^6(x_{\text{init.}})}{240} \sim 6.5 \times 10^{-11} \ . \tag{A.14}$$

This insured a small enough starting step size. Then we propagated the solution to higher values of x.

A.2 Changing the step size

As x increases, $K(x)$ tends to $k = \sqrt{2\mu E/\hbar^2}$. In the limit of small k, the integration will extend on a very large interval before the desired accuracy is reached. However, from the expression for the error ϵ, we can increase h as $K \to k$, as long as the product hK still satisfies the error condition.

So, according to the value of hK, we can double or halve the step size to minimize the amount of computation. More precisely, if we choose two conditions for doubling and halving the step size, namely

$$\frac{h^2K^2}{12} < \epsilon_D \Longrightarrow \text{double} \ , \tag{A.15}$$

$$\frac{h^2K^2}{12} > \epsilon_H \Longrightarrow \text{halve} \ , \tag{A.16}$$

with ϵ_D and ϵ_H small enough (of the order of 10^{-4}), we insure the error condition for the Numerov method to be satisfied. In fact

$$\left(\frac{h^2K^2}{12}\right)^3 = \frac{h^6K^6}{1728} < \frac{h^6K^6}{240} \ . \tag{A.17}$$

Now depending of the condition satisfied, we have to compute the half-way point

before u_n (for halving) or set $u_{n-1} = u_{n-2}$ (for doubling). More precisely, from the Numerov method, we need to do the following operations

Doubling

$$h^{\text{new}} = 2h^{\text{old}} , \tag{A.18}$$

$$T_n^{\text{new}} = 4T_n^{\text{old}} , \tag{A.19}$$

$$Y_n^{\text{new}} = (1 + T_n^{\text{new}})u_n^{\text{old}} , \tag{A.20}$$

$$T_{n-1}^{\text{new}} = 4T_{n-1}^{\text{old}} , \tag{A.21}$$

$$u_{n-1}^{\text{new}} = u_{n-2}^{\text{old}} , \tag{A.22}$$

$$Y_{n-1}^{\text{new}} = (1 + T_{n-1}^{\text{new}})u_{n-1}^{\text{new}} . \tag{A.23}$$

From these new quantities, we can find Y_{n+1}^{new} and then u_{n+1}^{new} from the Numerov method.

Halving

$$h^{\text{new}} = h^{\text{old}}/2 , \tag{A.24}$$

$$T_n^{\text{new}} = T_n^{\text{old}}/4 , \tag{A.25}$$

$$Y_n^{\text{new}} = (1 + T_n^{\text{new}})u_n^{\text{old}} , \tag{A.26}$$

$$u_{n-2}^{\text{new}} = u_{n-1}^{\text{old}} , \tag{A.27}$$

$$T_{n-2}^{\text{new}} = T_{n-1}^{\text{old}}/4 , \tag{A.28}$$

$$Y_{n-2}^{\text{new}} = (1 + T_{n-2}^{\text{new}})u_{n-2}^{\text{new}} , \tag{A.29}$$

$$T_{n-1}^{\text{new}} = [h^{\text{new}}K(x - h^{\text{new}})]^2/12 , \tag{A.30}$$

$$u_{n-1}^{\text{new}} = \frac{Y_{n-2}^{\text{new}} + Y_n^{\text{new}}}{2 - 10T_{n-1}^{\text{new}}} , \tag{A.31}$$

$$Y_{n-1}^{\text{new}} = (1 + T_{n-1}^{\text{new}})u_{n-1}^{\text{new}} . \tag{A.32}$$

From these new quantities, we can find Y_{n+1}^{new} and then u_{n+1}^{new} from the Numerov method.

Finally, the two condition ϵ_D and ϵ_H should be different enough in order to reduce the number of operations. In fact, if $\epsilon_D \sim \epsilon_H$, from one iteration to the next, we might alternate between halving and doubling, hence going through the above procedure many times. This would produce the inverse effect of the desired one, *i.e.* increase the number of arithmetic operations per iteration.

A.3 Phase shift calculations

We want to solve (A.1) in order to find the phase shift η. Our boundary conditions are

$$u(0) = 0 \ , \tag{A.33}$$

and for large R

$$u(R) \rightarrow A \sin(kR + \eta) \ . \tag{A.34}$$

Now, if we denote the exact solution at position R_i by $y(R_i)$, then we may write the numerical solution $u_i(R_i)$ as

$$u_i = y_i + \delta y_i \ , \tag{A.35}$$

where δy_i is the *global* truncation error. Also, the subscripts indicates functions evaluated at $R_i = R_0 + ih$ where h is the step-length and R_0 the initial value at which we start the numerical integration. We can consider δy_i to be the value at R_i of a continuous error $\delta y(R)$ [75, 76] introduced by addition of the perturbation $\frac{\hbar^2}{2\mu}\frac{h^4}{240}\frac{d^6}{dR^6}$ to the potential operator when equation (A.1) is solved by Numerov's method [77];

its leading term is $\mathcal{O}(h^4)$ satisfying the differential equation, derived from equations (A.1) and (A.8), [75, 76]

$$\delta y''(R) + K^2(R)\delta y(R) = \frac{h^4}{240} y^{(vi)}(R). \tag{A.36}$$

The step-length should be chosen to keep the *local relative* truncation error, approximately $\frac{h^6 K_i^6}{240}$ at R_i where K_i is the local wave number, acceptably small [74].

The phase shift can be calculated by fitting the solution $y(R)$ to $\sin(kR)$ and $\cos(kR)$, the asymptotic solutions of equation (A.1). For a s-wave, the phase shift tends to zero as $k \to 0$, and we therefore assume η very small. Let S_i and C_i denote $\sin(kR_i)$ and $\cos(kR_i)$ respectively. Fitting at R_i and R_j we find, for a small phase shift,

$$\eta \approx \tan(\eta) = -\frac{S_i y_j - S_j y_i}{C_i y_j - C_j y_i}. \tag{A.37}$$

From equations (A.35) and (A.37) we find that the relative error, $\frac{\delta\eta}{\eta}$, in the phase shift caused by use of the numerical wave functions u_i and u_j in equation (A.37) is, to $\mathcal{O}(h^4)$,

$$\frac{\delta\eta}{\eta} = -\frac{S_i\delta y_j - S_j\delta y_i}{(C_i y_j - C_j y_i)\eta} - \frac{C_i\delta y_j - C_j\delta y_i}{C_i y_j - C_j y_i}. \tag{A.38}$$

The relative error introduced into a small phase shift by the first term on the right-hand side of equation (A.38) can be large as a consequence of cancellation making the evaluation of expression (A.37) ill-conditioned. Both terms are proportional to the relative errors in the wave function. However even if they are kept small by making the local truncation errors acceptably small (say $\frac{|hK(R)|^6}{240} < 10^{-8}$ or $|hK(R)| < 0.1$) it is still possible for the phase shift to have an unexpectedly large relative error; a small step length might be needed to yield acceptable accuracy. In the special case

where $\frac{\delta y_i}{y_i} = \frac{\delta y_j}{y_j}$ the error given by equation (A.38) vanishes as expected because the relative error, being the same at R_i and R_j, is absorbed into the normalization factor A.

The phase shift is also given by the quadrature [78]

$$\eta \approx \sin(\eta) = -\frac{2\mu}{k\hbar^2 A}\int_0^\infty \sin(kR)V(R)y(R)dR. \tag{A.39}$$

The normalization constant, A, obtained by fitting to the asymptotic expression (A.34) is

$$A^2 = \frac{y_i^2 + y_j^2 - 2y_i y_j \cos[k(R_i - R_j)]}{\sin^2[k(R_i - R_j)]}. \tag{A.40}$$

However its relative error, $\frac{\delta A}{A}$, caused by use of the numerical wave-function and given by

$$\frac{\delta A}{A} = \frac{y_i\delta y_i + y_j\delta y_j - (y_j\delta y_i + y_i\delta y_j)\cos[k(R_i - R_j)]}{y_i^2 + y_j^2 - 2y_i y_j \cos[k(R_i - R_j)]}, \tag{A.41}$$

is well conditioned with respect to the errors in the wave function. The relative error, $\frac{\delta\eta}{\eta}$, in the phase-shift is

$$\frac{\delta\eta}{\eta} = -\frac{\delta A}{A} - \frac{2\mu}{k\hbar^2 A\eta}\int_0^\infty \sin(kR)V(R)\delta y(R)dR\ , \tag{A.42}$$

where $\delta y(R)$ satisfies equation (A.36). In the numerical example described below, quadrature yields more accurate phase-shifts than asymptotic fitting. Unfortunately we cannot *predict* this accuracy because while the first term of expression (A.42) introduces no excessive errors the necessary analysis of the second (integral) term requires knowledge of the solution of the differential equation (A.36). The potential in our numerical example has the form of a steep repulsive core matched to a well which in turn is matched to a slowly varying asymptotic tail. The wave-function

has many oscillations in the well and the subsequent cancellation makes meaningful estimation of the contribution to the integral from the well impossible without a good analytic approximation to $\delta y(R)$. Furthermore although we know a *particular asymptotic* solution to equation (A.36), as $-\frac{h^4k^4}{480}kR\cos(kR+\eta)$, we have insufficient knowledge of $\delta y(R)$ to match the *auxiliary* solution near the well and we cannot estimate the significant contribution of the tail to the integral. The only possible comment is that in the quadrature the error in the numerical wave-function is spread over the range of integration whereas the fitting procedure is sensitive to the errors in the wave-function calculated at two points only.

In a calculation of scattering data at an ultralow energy equation (A.1) must be integrated out to a large internuclear separation where the asymptotic potential is small compared to $\hbar^2k^2/2\mu$ to ensure validity of the asymptotic solutions. In atomic scattering the reduced mass is large causing the value of the step-length necessary for accurate integration at small interatomic distances to be very much smaller than that needed in the asymptotic region for small wave numbers. Typically we should ensure that $|hK(R)|^2 \approx 0.01$ for a local relative truncation error of about 10^{-8}. Ideally the algorithm should incorporate an automatic interval adjustment which increases, say doubles, h if $|hK(R)|^2$ becomes much less than 0.01 and decreases, say halves, h if $|hK(R)|^2$ becomes a little greater than 0.01; when halving an extra intermediate point is needed and the solution can be found at it by solving equation (A.8) once for u_i instead of u_{i+1} [74] (see previous section). The effect of doubling or halving is to introduce discontinuities into the error. These are unimportant if the error is small

but provide a useful diagnostic to check if small phase-shifts calculated by asymptotic fitting are sufficiently accurate. If the step is too large the calculated phase-shift exhibits discontinuities in both the internuclear separation and the energy of relative motion.

We compared asymptotic fitting with quadrature evaluation in a calculation of low energy scattering of two lithium atoms in a potential corresponding to the $X^1\Sigma_g^+$ state of $^7Li_2$. The potential was constructed from *ab initio* values fitted to an exponential short range core and a long range dispersion form [30, 43]; the details are presented in §2.4 (see the Konowalow potential). We incorporated step adjustment. We made separate calculations, at various energies, E, of relative motion, in which the step was doubled when $\frac{|hK(R)|^2}{12}$ became smaller than 10^{-2}, 10^{-3}, 10^{-4} and 10^{-6} (division by twelve was included for computational convenience). With the 10^{-6} criterion greater accuracy was obtained but many steps were required and we took the asymptotically fitted phase-shifts to represent the accurate values for comparison. With the 10^{-2} criterion a relative local truncation error of about 10^{-4} might be expected from fitting but, as seen in Fig. A.1, this was not achieved; furthermore the fitted phase-shifts are discontinuous for both the step doubling criteria shown. The quadrature results are more accurate and have no discontinuities; for the 10^{-4} criterion they have negligible errors. More results of fitting and quadrature are compared on a larger scale in Fig. A.2. The fitted results again exhibit discontinuities. In both figures they occur at intervals of $\log_{10}(4) \approx 0.6$ apart in log-energy. This happens because as the energy is increased the number of step doublings performed in the long asymptotic tail is

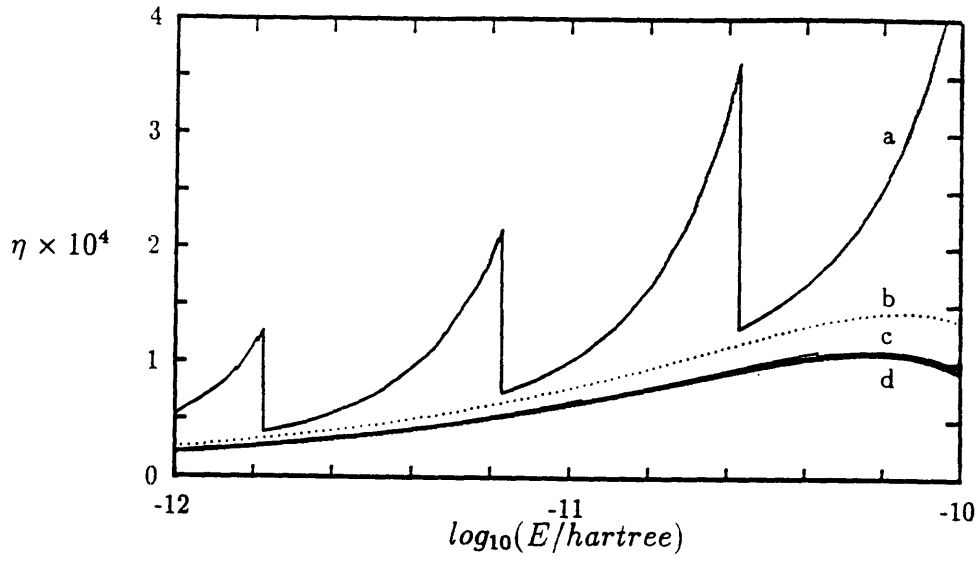

a ... asymptotic fit doubling h when $|hK(R)|^2/12 < 10^{-2}$
b ... quadrature doubling h when $|hK(R)|^2/12 < 10^{-2}$
c ... asymptotic fit doubling h when $|hK(R)|^2/12 < 10^{-4}$
d ... quadrature doubling h when $|hK(R)|^2/12 < 10^{-4}$

Figure A.1: Phase shifts, η for different step-length doubling criteria.

decreased; at a very small energy the step doubling procedure is energy-dependent only in the tail. The error changes discontinuously as a function of R whenever the step is doubled. The doubling criterion depends asymptotically on h^2k^2 or h^2E which changes by a factor of four at each doubling. If we increase the energy by a factor of four we expect one fewer step doubling to be performed leading to a discontinuity in the calculated phase-shift, as a function of E. The intervals between the discontinuities correspond to changes by factors of four in energy or changes of $\log_{10}(4)$ in log-energy. The quadrature is much less sensitive to the number of step doublings because the error is spread over the range of integration.

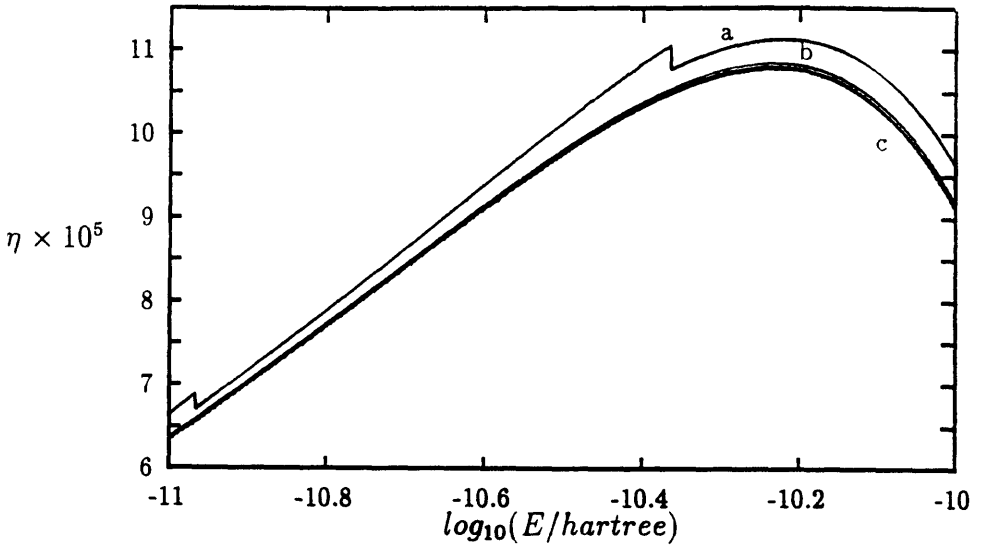

a ... asymptotic fit doubling h when $|hK(R)|^2/12 < 10^{-4}$
b ... quadrature doubling h when $|hK(R)|^2/12 < 10^{-4}$
c ... quadrature doubling h when $|hK(R)|^2/12 < 10^{-6}$

Figure A.2: Phase shifts, η for different step-length doubling criteria.

The Schwinger integral formula for a s-wave [22] (see also §1.5.3),

$$k\cot\eta = \frac{\int_0^\infty dR W(R)y^2(R) - \int_0^\infty dR \int_0^\infty dR' W(r)y(R)G(R,R')W(R')y(R')}{\left[k^{-1}\int_0^\infty dR \sin(kR)W(R)y(R)\right]^2}\ , \tag{A.43}$$

where

$$W(R) = -2mV(R)/\hbar^2\ , \tag{A.44}$$

and

$$G(R,R') = k^{-1}\sin(kR_<)\cos(kR_>)\ , \tag{A.45}$$

with $R_<$ and $R_>$ indicating the smaller and larger of R and R', yields a phase-shift correct to second order in the error of any approximation which may be substituted for the wave-function $y(R)$. It is usually used in variational methods where analytic trial wave-functions are constructed. It should provide a very accurate phase-shift when the *numerical* wave-function, described above, is substituted. However we found that its use is impractical in our example because the oscillation of the wave-function in the potential well introduces severe cancellation in the double integral; an extremely small step is required not by the method used for solving equation (A.8) but by the method used to evaluate the double integral. The time needed for this integration increases as the square of the total number of steps although symmetry does allow a cut by two. Indeed, since the double integral is symmetric, we can rewrite (A.43) in the form

$$k\cot\eta = \frac{-\int_0^\infty dr U(r)y^2(r) - \frac{2}{k}\int_0^\infty dr \cos(kr)U(r)y(r)\int_0^r dr' \sin(kr')U(r')y(r')}{\left[k^{-1}\int_0^\infty dr \sin(kr)U(r)y(r)\right]^2}\ , \tag{A.46}$$

with $U(r) = 2mV(r)/\hbar^2 = -W(r)$. We made many calculations at a log-energy of -10.2: this energy corresponds to the biggest difference between the direct for and the quadrature results (see Fig. A.2). The phase shift obtained was basically 1.076×10^{-4}. Substitution of a numerical wave-function in the Schwinger formula is likely to be unsatisfactory in any low energy atom-atom collision problem because the large reduced mass can introduce many oscillations in any well other than the shallowest; it is probably worse at medium to high energies and better for low energy electron-atom collisions.

Finally, we give the phase shift computed from the three different methods explored here, namely the direct fit, the quadrature form, and the Schwinger variational expression, in Table A.1. They are respectively refered to as 0, 1, and 2, and were computed for different doubling and halving criteria (DBLCON and HAVCON in the table). Those step-adjustment conditions are defined as

$$\frac{h^2K^2}{12} < \text{DBLCON} \Longrightarrow \text{doubling} , \tag{A.47}$$

$$\frac{h^2K^2}{12} > \text{HAVCON} \Longrightarrow \text{halving} . \tag{A.48}$$

In Table A.1, the symbol "x" means that the vectors used in evaluating the integrals exceeded the maximum length set to 250,000, and "–" that the calculation of the double integral would have taken too much time and therefore was not performed. In Table A.2, we give both the length of the vector used, *i.e.* the number of grid points M, and the CPU time T (in sec.) spent to do the full computation. The value of M is based on the convergence of η from the direct fit, and T includes the time for the three processes. Of course, most of T originates from the double integral.

log HAVCON		log DBLCON -2	-3	-4	-5	-6	-7	-8
	0	19 552.954	246.987	133.726	109.496	107.643	107.551	107.559
-2	1	259.476	134.310	132.149	109.246	107.640	107.549	107.549
	2	-5.676	1.309	2.015	30.102	98.361	—	—
	0	250.482	191.966	110.012	108.181	107.643	107.551	107.558
-3	1	143.324	114.112	108.461	107.929	107.640	107.549	107.549
	2	2.163	109.403	51.156	59.232	98.361	107.166	—
	0	133.425	109.711	109.365	108.014	107.556	107.551	107.553
-4	1	132.047	108.350	108.233	107.767	107.553	107.549	107.543
	2	2.012	50.106	112.688	107.511	106.942	—	—
	0	109.430	108.135	107.946	107.805	107.550	107.545	107.552
-5	1	109.221	107.941	107.938	107.667	107.547	107.543	107.543
	2	30.085	67.438	106.786	107.910	107.559	—	—
	0	107.641	107.641	107.554	107.549	107.548	107.546	107.553
-6	1	107.639	107.640	107.552	107.546	107.545	107.543	107.544
	2	98.364	98.364	106.953	107.557	—	—	—
	0	107.551	107.551	107.551	107.545	107.545	107.548	x
-7	1	107.549	107.549	107.549	107.543	107.543	126.281	x
	2	107.166	—	—	107.544	—	—	x
	0	107.557	107.557	107.551	107.551	107.551	x	x
-8	1	107.549	107.549	107.543	107.543	107.543	x	x
	2	107.166	—	—	—	—	x	x

Table A.1: Phase shift $\times 10^{-6}$: 0 is the direct fit, 1 is the integral form, and 2 is the Schwinger variational expression.

log HAVCON		log DBLCON -2	-3	-4	-5	-6	-7	-8
-2	M	651	1,297	3,249	6,621	20,265	68,703	129,841
	T	3.483	11.378	68.501	284.209	2,663.9	—	—
-3	M	1,307	1,995	4,571	7,953	20,265	68,703	129,841
	T	11.542	30.273	135.863	411.074	2,663.4	30,577	—
-4	M	3,265	4,585	6,209	10,687	24,251	69,383	142,965
	T	69.273	136.948	290.453	743.877	3,824.2	—	—
-5	M	6,641	7,969	10,705	17,913	39,637	93,409	165,625
	T	286.296	412.759	746.740	2,422.7	10,229	—	—
-6	M	20,291	20,291	24,275	39,667	61,269	140,147	242,579
	T	2,670.3	2,670.8	3,830.3	10,246	—	—	—
-7	M	68,717	68,717	69,397	93,413	140,157	196,643	x
	T	30,655	—	—	56,661	—	—	x
-8	M	129,857	129,857	142,977	165,641	242,593	x	x
	T	109,312	—	—	—	—	x	x

Table A.2: M is the number of points (M-1 intervals), and T is the total CPU time (in seconds).

As we can see, the best results (for the Schwinger expression) are taking a very long time to calculate. The best one is for log DBLCON = -5 and log HAVCON = -7: other values of those parameters would have given better results, but the time required would have increased drastically. Finally, as mentioned before, the diagonals exhibit the effect of constant doubling and halving when the criteria are set equal. This should be avoided.

In conclusion we recommend that the algorithm used to solve the Schrödinger equation in calculations of ultralow energy scattering should incorporate automatic adjustment of the step-length [74] and that the results of asymptotic fitting and of quadrature A should be made and compared for various step doubling criteria to enable reliable phase-shifts to be determined.

Appendix B

Molecular classification

In this Appendix, we will give a rapid summary of the molecular classification, especially regarding the diatomic molecules.

From the Bohr-Oppenheimer approximation (see §1.1.1), we find that the molecular interaction potentials, or electron terms, of a diatomic molecule are functions of a single parameter, the internuclear distance R.

The classification of atomic terms, since the potentials are centrally symmetric, is based on the conserved values of the total orbital angular momentum L. However, for molecules the electric field of several nuclei is not centrally symmetric, and therefore there exists no law of conservation of the total angular momentum of the electrons.

In diatomic molecules, however, the field has axial symmetry about an axis passing through the two nuclei. Hence, the projection of the orbital angular momentum on this axis is conserved, and a classification of the electron terms of the molecules according to these projections is possible. We denote the absolute value of the pro-

jected orbital angular momentum along the axis of the molecule by Λ. It can take the values 0,1,2 .... Similarly to the atomic terms where we use the Latin letters S, P, D ...for the L values 0,1,2 ..., we denote the different values by the capital Greek letters Σ, Π and Δ ...corresponding to $\Lambda = 0, 1, 2$ ...(higher values of Λ are rarely considered).

Each molecular electron state is also characterized by the total spin S of all the electrons in the molecule. Neglecting the fine structure due to relativistic interactions, there is a degeneracy of degree $2S + 1$. This number is called the *multiplicity* of the term, and is written as an index before the letter for the term. For instance, $^3\Pi$ implies $\Lambda = 1$ and $S = 1$.

The symmetry of a diatomic molecule allows a reflection in any plane passing through the axis. Under such a reflection, the energy of the molecule is unchanged, although the state will not completely remain the same. Indeed, for this type of reflection, the sign of the angular momentum (which is an axial vector) about the axis is changed. So, we conclude that all electron terms with non-zero values of Λ are doubly degenerate: for each value of energy, there are two states which differ in the direction of the projection of the orbital angular momentum on the axis of the molecule. When $\Lambda = 0$, the state of the molecule is not changed under reflection, and therefore the Σ terms are not degenerate. As a result of the reflection, the wave function of a Σ term can only be multiplied by a constant. Since a double reflection is the identity transformation, this constant must be ± 1. So, we must differentiate the Σ terms whose wave functions are unchanged under reflection and those for which

the wave functions change sign. The former are denoted Σ^+ and the latter Σ^-.

In the case of a diatomic molecule with two identical atoms, we can use a new symmetry to characterize further the electron terms. For such a molecule, there is a center of symmetry at the point bisecting the line joining the two nuclei (see Laudau and Lifshitz [60]). Taking this point as origin, the Hamiltonian is invariant with respect to an exchange of the nuclei coordinates in the molecule ($A \leftrightarrow B$). The operator of this transformation also commutes with the orbital angular momentum operator. So, we can classify the terms with a given Λ according to their parity: the wave functions of even (g for gerade) states are unchanged under this nuclei coordinates exchange, while those of odd (u for ungerade) states change sign. The suffixes u, g indicating the parity are written with the letter: for instance Π_g, Π_u and so on.

Finally, the molecular electron terms of the same type are distinguished by letters as follows: the ground state is referred to as X, the excited states of the same multiplicity as $A, B, C, \ldots$, those of different multiplicity as $a, b, c, \ldots$ (see Radzig and Smirnov [39]). For example, $X^1\Sigma_g^+$ relates to the ground singlet even term, $b^3\Pi_u$ relates to an excited triplet state, and so on. A detailed description of the above conventions and notations are given in Herzberg [79], for example.

Appendix C

Data for molecular potentials

In this Appendix, we will give the sets of data used for the cubic spline fitting of the potential curves. All the values are in atomic units, and the dissociation energy has been subtracted to give data which tends to zero as r tends to infinity.

First, we give the data for the ground states of lithium and sodium molecules. Then, we give those of the excited state of lithium used in the photo-absorption problem, namely the $1^1\Sigma_u^+(A)$ and $1^3\Sigma_g^+$ states. In these last two cases, the value of the potential for the last point at $r = 40a_0$ is reset from zero to be equal to the value obtained from the long-range form of the potential

$$V(r) = \frac{C_3}{r^3} - \frac{C_6}{r^6} - \frac{C_8}{r^8} \,. \tag{C.1}$$

By doing so, we get a smooth function by also fitting the derivative at this last point.

Finally, the sources of these data points are given in chapter 2 for the ground states, and chapter 4 for the excited states. One should refer to these chapters for more details on the exact construction of the full potential curves.

r (a_0)	$V(r)$ (hartree)	r (a_0)	$V(r)$ (hartree)	r (a_0)	$V(r)$ (hartree)
2.7500	0.061866000	3.8020	-0.018188171	7.4137	-0.019432255
3.0000	0.036411000	3.8332	-0.019432254	7.5462	-0.018188171
3.2500	0.013546000	3.8665	-0.020704695	7.6801	-0.016973217
3.4454	-0.000008385	3.9022	-0.022004859	7.8142	-0.015788082
3.4458	-0.000039986	3.9406	-0.023332173	7.9546	-0.014633517
3.4470	-0.000111967	3.9820	-0.024722568	8.0963	-0.013510530
3.4490	-0.000239907	4.0269	-0.026066228	8.2418	-0.012420170
3.4520	-0.000432877	4.0761	-0.027472088	8.3917	-0.011363318
3.4562	-0.000693981	4.1303	-0.028903321	8.5469	-0.010341376
3.4614	-0.001023301	4.1909	-0.030359593	8.7087	-0.009355541
3.4674	-0.001418778	4.2597	-0.031840604	8.8775	-0.008407441
3.4749	-0.001877871	4.3396	-0.033346088	9.0548	-0.007498474
3.4836	-0.002397552	4.4363	-0.034875801	9.2424	-0.006630370
3.4934	-0.002974875	4.5615	-0.036429525	9.4421	-0.005805055
3.5043	-0.003606984	4.7568	-0.038007061	9.6562	-0.005024612
3.5162	-0.004290903	5.0517	-0.038804565	9.8880	-0.004290903
3.5289	-0.005024612	5.3837	-0.038007061	10.1417	-0.003606984
3.5431	-0.005805055	5.6542	-0.036429525	10.4214	-0.002974875
3.5581	-0.006630370	5.8560	-0.034875801	10.7353	-0.002397552
3.5742	-0.007498474	6.0304	-0.033346088	11.0927	-0.001877871
3.5914	-0.008407441	6.1896	-0.031840604	11.5082	-0.001418778
3.6097	-0.009355541	6.3392	-0.030359593	12.0042	-0.001023301
3.6288	-0.010341376	6.4821	-0.028903321	12.6143	-0.000693981
3.6494	-0.011363318	6.6204	-0.027472088	13.4000	-0.000432877
3.6712	-0.012420170	6.7556	-0.026066228	14.4700	-0.000239907
3.6944	-0.013510530	6.8886	-0.024722568	16.0543	-0.000111967
3.7189	-0.014633517	7.0203	-0.023332173	18.6399	-0.000039986
3.7449	-0.015788082	7.1513	-0.022004859	23.8850	-0.000008385
3.7726	-0.016973217	7.2822	-0.020704695		

Table C.1: Data for the spline fitting of ground $X^1\Sigma_g^+$ state of Li_2.

r (a_0)	$V(r)$ (hartree)	r (a_0)	$V(r)$ (hartree)	r (a_0)	$V(r)$ (hartree)
3.0000	0.104471000	6.4202	-0.000207845	9.6236	-0.001106386
3.2500	0.082074000	6.4714	-0.000330005	10.4012	-0.000869161
3.5000	0.063725000	6.5373	-0.000481116	11.1919	-0.000660840
4.0000	0.036778000	6.6250	-0.000660840	12.0470	-0.000481116
4.5000	0.020006000	6.7478	-0.000869161	13.0174	-0.000330005
5.0000	0.010053000	6.9321	-0.001106386	14.1797	-0.000207845
5.5000	0.004370000	7.2645	-0.001373638	15.6806	-0.000114668
6.0000	0.001258000	7.8822	-0.001519063		
6.3858	-0.000114668	8.7487	-0.001373638		

Table C.2: Data for the spline fitting of the ground $a^3\Sigma_u^+$ state of Li_2.

r (a_0)	$V(r)$ (hartree)	r (a_0)	$V(r)$ (hartree)	r (a_0)	$V(r)$ (hartree)
3.8000	0.022410000	4.6783	-0.017024935	8.3268	-0.012906812
4.1336	-0.000619683	4.7077	-0.017644724	8.4135	-0.012351492
4.1365	-0.000736004	4.7387	-0.018272057	8.5010	-0.011804843
4.1399	-0.000871715	4.7714	-0.018906840	8.5896	-0.011267029
4.1438	-0.001026599	4.8061	-0.019548983	8.6793	-0.010783781
4.1483	-0.001200316	4.8430	-0.020198400	8.7702	-0.010218590
4.1530	-0.001392450	4.8825	-0.020855012	8.8627	-0.009708331
4.1585	-0.001602497	4.9250	-0.021518742	8.9568	-0.009207640
4.1643	-0.001829987	4.9710	-0.022189517	9.0526	-0.008716725
4.1707	-0.002074407	5.0212	-0.022867269	9.1506	-0.008235803
4.1776	-0.002335224	5.0768	-0.023551934	9.2507	-0.007765104
4.1849	-0.002612017	5.1392	-0.024243447	9.3533	-0.007304868
4.1959	-0.003014892	5.2110	-0.024941752	9.4587	-0.006855349
4.2046	-0.003340286	5.2967	-0.025646791	9.5670	-0.006416811
4.2139	-0.003679716	5.4062	-0.026358509	9.6787	-0.005989532
4.2236	-0.004032776	5.5736	-0.027076855	9.7941	-0.005573806
4.2337	-0.004399078	5.6435	-0.027257471	9.9136	-0.005169938
4.2443	-0.004778249	5.8195	-0.027438359	10.0376	-0.004778249
4.2555	-0.005169938	6.0066	-0.027257471	10.1667	-0.004399078
4.2670	-0.005573806	6.0877	-0.027076855	10.3015	-0.004032776
4.2791	-0.005989532	6.3001	-0.026358509	10.4427	-0.003679716
4.2917	-0.006416811	6.4552	-0.025646791	10.5910	-0.003340286
4.3047	-0.006855349	6.5872	-0.024941752	10.7475	-0.003014892
4.3183	-0.007304868	6.7059	-0.024243447	10.9362	-0.002659875
4.3323	-0.007765104	6.8159	-0.023551934	11.1161	-0.002365289
4.3470	-0.008235803	6.9197	-0.022867269	11.3070	-0.002086120
4.3621	-0.008716725	7.0188	-0.022189517	11.5126	-0.001822942
4.3779	-0.009207640	7.1144	-0.021518742	11.7353	-0.001576210
4.3943	-0.009708331	7.2072	-0.020855012	11.9784	-0.001346436
4.4112	-0.010218590	7.2979	-0.020198400	12.2456	-0.001134112
4.4289	-0.010783781	7.3868	-0.019548983	12.5425	-0.000939735
4.4472	-0.011267029	7.4744	-0.018906840	12.8758	-0.000763755
4.4662	-0.011804843	7.5609	-0.018272057	13.2551	-0.000606602
4.4860	-0.012351492	7.6466	-0.017644724	13.6935	-0.000468600
4.5066	-0.012906812	7.7318	-0.017024935	14.2101	-0.000349946
4.5281	-0.013470651	7.8165	-0.016412790	14.8338	-0.000250664
4.5505	-0.014042864	7.9011	-0.015808396	15.6064	-0.000170348
4.5738	-0.014623312	7.9857	-0.015211864	16.5932	-0.000108149
4.5981	-0.015211864	8.0704	-0.014623312	17.9351	-0.000062659
4.6236	-0.015808396	8.1554	-0.014042864	19.7774	-0.000031824
4.6503	-0.016412790	8.2408	-0.013470651	23.4875	-0.000010202

Table C.3: Data for the spline fitting of the ground $X^1\Sigma_g^+$ state of Na_2.

r (a_0)	$V(r)$ (hartree)	r (a_0)	$V(r)$ (hartree)	r (a_0)	$V(r)$ (hartree)
3.8000	0.078329300	8.0666	-0.000094273	9.6208	-0.000793074
4.0000	0.066348000	8.0666	-0.000094273	10.4016	-0.000731053
4.2500	0.053959100	8.1089	-0.000140707	11.1388	-0.000621892
4.5000	0.043729800	8.1814	-0.000220178	11.7616	-0.000523539
4.7500	0.035222300	8.2360	-0.000269979	12.3559	-0.000432686
5.0000	0.028154400	8.2905	-0.000330018	12.9816	-0.000350170
5.5000	0.017520300	8.3588	-0.000398354	13.6595	-0.000277169
6.0000	0.010449000	8.4460	-0.000475634	14.4084	-0.000212902
6.5000	0.005872300	8.5605	-0.000560441	15.2770	-0.000158905
7.0000	0.002985300	8.7436	-0.000650761	17.2720	-0.000072526
7.5000	0.001217300	9.0761	-0.000747711	18.7615	-0.000041962

Table C.4: Data for the spline fitting of the ground $a^3\Sigma_u^+$ state of Na_2.

r (a_0)	$V(r)$ (hartree)	r (a_0)	$V(r)$ (hartree)	r (a_0)	$V(r)$ (hartree)
3.25000	0.0387460	4.80281	-0.0353492	8.69712	-0.0272183
3.50000	0.0176030	4.87243	-0.0364281	8.83403	-0.0262644
4.00000	-0.0120580	4.95161	-0.0375211	8.97042	-0.0253244
4.12941	-0.0175065	5.04391	-0.0386281	9.10655	-0.0243984
4.15048	-0.0183165	5.15572	-0.0397492	9.24267	-0.0234864
4.17246	-0.0191410	5.30112	-0.0408845	9.37901	-0.0225887
4.19544	-0.0199815	5.52881	-0.0420342	9.51577	-0.0217052
4.21947	-0.0208360	5.87367	-0.0426131	9.65321	-0.0208360
4.24463	-0.0217052	6.26301	-0.0420342	9.79150	-0.0199815
4.27099	-0.0225887	6.58029	-0.0408845	9.93093	-0.0191416
4.29865	-0.0234864	6.81601	-0.0397492	10.07163	-0.0183165
4.32774	-0.0243984	7.01886	-0.0386281	10.21391	-0.0175065
4.35835	-0.0253244	7.20294	-0.0375211	10.50000	-0.0159200
4.39065	-0.0262644	7.37471	-0.0364281	12.00000	-0.0095240
4.42481	-0.0272183	7.53776	-0.0353492	13.50000	-0.0057910
4.46106	-0.0281862	7.69428	-0.0342843	15.00000	-0.0037860
4.49961	-0.0291679	7.84586	-0.0332333	17.00000	-0.0024050
4.54077	-0.0301635	7.99354	-0.0321962	20.00000	-0.0024050
4.58489	-0.0311729	8.13816	-0.0311729	30.00000	-0.0004100
4.63247	-0.0321962	8.28034	-0.0301635	40.00000	0.0*
4.68410	-0.0332333	8.42064	-0.0291679		
4.74053	-0.0342843	8.55944	-0.0281862		

* the potential is reset to the analytical value of the long-range form.
Here, the dissociation energy used is $D_e = 9352.4931\ \text{cm}^{-1}$.

Table C.5: Data for the spline fitting of the excited $1^1\Sigma_u^+(A)$ state of Li_2.

r (a_0)	$V(r)$ (hartree)	r (a_0)	$V(r)$ (hartree)	r (a_0)	$V(r)$ (hartree)
3.25000	0.052244	5.44222	-0.031696	9.000	-0.017525
3.50000	0.028718	5.79768	-0.032312	10.500	-0.011429
4.00000	-0.002836	6.21342	-0.031696	12.000	-0.007454
4.50000	-0.020051	6.55792	-0.030483	13.500	-0.005016
4.66347	-0.023730	6.81964	-0.029296	15.000	-0.003530
4.72243	-0.024793	7.04906	-0.028133	17.000	-0.002352
4.78875	-0.025882	7.26089	-0.026995	20.000	-0.001410
4.86510	-0.026995	7.46196	-0.025882	30.000	-0.000410
4.95505	-0.028133	7.65547	-0.024793	40.000	0.0*
5.06541	-0.029296	7.84425	-0.023730		
5.21092	-0.030483	8.00000	-0.022762		

* the potential is reset to the analytical value of the long-range form. Here, the dissociation energy used is $D_e = 7091.6636\ \text{cm}^{-1}$.

Table C.6: Data for the spline fitting of the excited $1^3\Sigma_g^+$ state of Li_2.

Appendix D

Photo-absorption probability

In this Appendix, we will first give the derivation for the photo-absorption probability used in chapter 4. Then we will deduce the statistical weights found in that expression. Finally, we will show a way to handle the oscillating contribution in the case of a free-free transition.

D.1 Absorption coefficient

Let us derive the equation for the absorption coefficient. We will consider an initial state that lies in the continuum and a final state that is bound. The Hamiltonian has the form

$$H = -\frac{\nabla^2_{\mathbf{R}}}{2\mu} + \frac{Z^2e^2}{R} + \sum_{\substack{j=\text{elec.}\\ i=\text{nuc.}}} \left\{ \frac{-\nabla^2_{j(i)}}{2} - \frac{Ze^2}{r_{j(i)}} + \frac{1}{4} \sum_{\substack{k\neq j\\ l=\text{nuc.}}} \frac{e^2}{|\mathbf{r}_{j(i)} - \mathbf{r}_{k(l)}|} \right\} . \quad \text{(D.1)}$$

The application of a harmonically varying external electric field $\mathbf{E} = \mathrm{Re}[F_0 e^{-2i\pi\nu t}\hat{\mathbf{n}}]$ introduces an additional term to Eq. (D.1),

$$H_{\mathrm{int}} = \mathbf{E} \cdot e\mathbf{r} = \left[\frac{F_0}{2} e^{-2i\pi\nu t} + \frac{F_0^*}{2} e^{2i\pi\nu t}\right] \hat{\mathbf{n}} \cdot e\mathbf{r} \ . \tag{D.2}$$

We will use the variable F_0 to denote the magnitude of the electric field. A variable that characterizes the process of photo-absorption is called the absorption coefficient $\kappa(\nu)$ and is defined by the relation

$$\kappa(\nu, T) = \frac{P(\nu)\mathbf{N}(T)}{F} \ . \tag{D.3}$$

The variable $P(\nu)$ is the absorption probability per molecular state per unit time as a function of the photon energy $h\nu$, F is the flux of photons that are incident on the molecule in units of photons per unit area per unit of time, and $\mathbf{N}(T)$ is the density of molecular states as a function of the temperature T. The flux F is the time averaged real part of the complex Poynting vector (see, for example, J.D. Jackson [80]) divided by the photon energy $h\nu$

$$F = \frac{|F_0|^2 c}{8\pi h\nu} \ . \tag{D.4}$$

Here c denotes the speed of light.

Since the probability $P(\nu)$ and the density $\mathbf{N}(T)$ will be functions of the initial nuclear linear momentum $\mathbf{K}_0$, the product in the numerator of Eq. (D.3) will be rewritten as

$$\kappa(\nu, T) = \frac{\int d\mathbf{K}_0 P(\nu, \mathbf{K}_0)\mathbf{N}(T, \mathbf{K}_0)}{F} \ . \tag{D.5}$$

The application of Fermi's second Golden Rule (see, for example, J.J. Sakurai [81]) for the transition probabilities from the state $|i\rangle$ to the state $|f\rangle$ per unit time

(per unit initial momentum density) gives

$$P_{i\to f}(\nu, \mathbf{K}_0) = \frac{2\pi e^2}{\hbar} \left| \left\langle f \left| \frac{F_0}{2} \hat{\mathbf{n}} \cdot \mathbf{r} \right| i \right\rangle \right|^2 \rho_f(E_f) \ , \tag{D.6}$$

where $|i\rangle$ and $|f\rangle$ are the exact solutions to Eq. (D.1) for the initial and final states of the molecule respectively and are normalized to unity. For a problem that involves the absorption of a single photon, the nucleon that makes the transition from the continuum into a bound level will have an initial momentum that will be denoted $\mathbf{K}_0$. The function $\rho_f(E_f)$ is the density of states function for transitions into bound states from the continuum and is equivalent to a Dirac delta function

$$\rho_f(E_f) = \delta(h\nu + E_i - E_f) \ . \tag{D.7}$$

The variables $E_i = \hbar^2 K_0^2/2\mu$ and $E_{f(J)}$ are the exact eigenvalues of the states $|i(l)\rangle$ and $|f(J)\rangle$ respectively. Here, we explicitly show the angular quantum number J of the excited bound level and l of the ground free state. We will consider incident radiation averaged over all polarizations

$$|\hat{\mathbf{n}} \cdot \mathbf{r}|^2_{\text{ave}} = \frac{1}{3} \sum_i |\hat{\mathbf{n}}_i \cdot \mathbf{r}|^2_{\text{ave}} = \frac{1}{3} |\mathbf{r}|^2 \ . \tag{D.8}$$

Equation (D.5) becomes

$$\begin{aligned} \kappa^Y_{i\to f}(\nu, T) \ &= \ \sum_{l,J} \int d\mathbf{K}_0 \mathbf{N}^Y_l(T, \mathbf{K}_0) \delta(h\nu + E_i - E_f) \\ &\quad \times \frac{8\pi^3 \nu e^2}{3c} |\langle f(J)|\mathbf{r}|i(l)\rangle|^2 \ . \end{aligned} \tag{D.9}$$

Here Y refers to the potential of the initial state V_Y.

The factor $\mathbf{N}^Y_l(T, \mathbf{K}_0)$ can be determined in the following manner. If we denote the number of free atoms by $\mathrm{N_{Li}}$ and the number of initial molecular states (in the

continuum) by N_{Li_2}, then we can write the following equilibrium equation (see, for example, R. Kubo [82])

$$\frac{N_{Li_2}}{N_{Li}^2} = \frac{f_{Li_2}(T)}{[f_{Li}(T)]^2} , \tag{D.10}$$

where f_{Li_2} and f_{Li} are the partition functions of Li_2 and Li, respectively. They are given by

$$f_{Li_2}(T) = \left(\frac{2\pi m_{Li_2} k_B T}{h^2}\right)^{3/2} V j^0_{Li_2} \exp\left(-\frac{E^0_{Li_2}}{k_B T}\right) , \tag{D.11}$$

$$f_{Li}(T) = \left(\frac{2\pi m_{Li} k_B T}{h^2}\right)^{3/2} V j^0_{Li} \exp\left(-\frac{E^0_{Li}}{k_B T}\right) , \tag{D.12}$$

where V is the volume, $j^0_{Li_2}$ and $j^0_{Li_2}$ are the partition functions for the internal degrees of freedom for Li_2 and Li, respectively. Also, $E^0_{Li_2}$ and E^0_{Li} are the energies for Li_2 and Li, the zero point being set at the ground state. Finally, we have $m_{Li_2} = 2m_{Li}$. Substituting in Eq. (D.10), we obtain

$$\frac{N_{Li_2}}{N_{Li}^2} = \frac{1}{V}\left(\frac{h^2}{2\pi\mu k_B T} h^2\right)^{3/2} \frac{j^0_{Li_2}}{[j^0_{Li}]^2} \exp\left(-\frac{(E^0_{Li_2} - 2E^0_{Li})}{k_B T}\right) , \tag{D.13}$$

where the reduce mass is $\mu = m_{Li}/2$. Now, the difference in energy zeroes is simply the kinectic energy, *i.e.* $E^0_{Li_2} - 2E^0_{Li} = \hbar^2 K_0^2/2\mu$.

In terms of the number density of lithium atom $n_{Li} = N_{Li}/V$ and the number density of molecular state $N_l^Y(T, \mathbf{K_0}) = N_{Li_2}/V$, we can rewrite Eq. (D.10) as

$$\frac{N_l^Y(T, \mathbf{K_0})}{n_{Li}^2} = \frac{h^3}{(2\pi\mu k_B T)^{3/2}} \frac{j^0_{Li_2}}{[j^0_{Li}]^2} \exp\left(-\frac{\hbar^2 K_0^2}{2\mu k_B T}\right) . \tag{D.14}$$

Here, $j^0_{Li_2}/[j^0_{Li}]^2$ includes rotation, nuclear and electronic internal degrees of freedom. We will summarize them by the product of the two weights ω_Y and ω_{Yl} since they

will depend on the molecular potential Y and the angular momentum l. Then, we explicitly write $\mathbf{N}_l^Y(T,\mathbf{K}_0)$ as

$$\mathbf{N}_l^Y(T,\mathbf{K}_0) = \omega_Y \omega_{Yl} \frac{n_{\mathrm{Li}}^2 \hbar^3}{(2\pi\mu k_B T)^{3/2}} \exp\left(-\frac{\hbar^2 K_0^2}{2\mu k_B T}\right) . \tag{D.15}$$

Notice that some factors of 2π have been also absorbed in $\omega_Y \omega_{YN}$ (see also Sando and Dalgarno [61]).

Substituting $\mathbf{N}_l^Y(T,\mathbf{K}_0)$ into Eq. (D.9), we obtain

$$\begin{aligned} \kappa_{i\to f}^Y(\nu,T) &= \sum_{l,J} \int d\mathbf{K}_0 \omega_Y \omega_{Yl} \frac{n_{\mathrm{Li}}^2 \hbar^3}{(2\pi\mu k_B T)^{3/2}} \exp\left(-\frac{\hbar^2 K_0^2}{2\mu k_B T}\right) \\ &\quad \times \frac{8\pi^3 \nu e^2}{3c} \delta(h\nu + E_i - E_f) |\langle f(J)|\mathbf{r}|i(l)\rangle|^2 . \end{aligned} \tag{D.16}$$

Here, the wave functions for the lithium atoms going from the $(2s2s)$ state to the $(2s2p)$ state are expanded according to

$$|i(l)\rangle = \sum_{m_l} 4\pi i^l e^{i\delta_l} Y_{lm_l}(\hat{\mathbf{R}}) Y_{lm_l}^*(\hat{\mathbf{K}}_0) \frac{u_Y(K_0,l,R)}{K_0 R} \psi_{\mathrm{elec}}^{(1)}(2s) \psi_{\mathrm{elec}}^{(2)}(2s) , \tag{D.17}$$

and

$$|f(J)\rangle = \sum_{m_J} \frac{R_{f(J)}(R)}{R} Y_{Jm_J}(\hat{\mathbf{R}}) \psi_{\mathrm{elec}}^{(1)}(2s) \psi_{\mathrm{elec}}^{(2)}(2p) . \tag{D.18}$$

Those wave functions are for specific angular momenta l and J. Furthermore, the free wave function is normalized so that

$$\lim_{R\to\infty} u_Y(K_0,l,R) \sim \sin\left(K_0 R - \frac{l\pi}{2} + \delta_l\right) . \tag{D.19}$$

Now, evaluating the integral in Eq. (D.16), we obtain

$$\begin{aligned} \kappa_{i\to f}^Y(\nu,T) &= \sum_{l,J} \omega_Y \omega_{Yl} \frac{2\pi K_0 n_{\mathrm{Li}}^2 \hbar^3}{(2\pi\mu k_B T)^{3/2}} (2\pi\mu k_B T)^{3/2} \exp\left(-\frac{\hbar^2 K_0^2}{2\mu k_B T}\right) \\ &\quad \times \frac{8\pi^3 \nu e^2}{3c} \frac{2\mu}{\hbar^2} |\langle f(J)|\mathbf{r}|i(l)\rangle|^2 , \end{aligned} \tag{D.20}$$

with

$$K_0 = \sqrt{\frac{2\mu}{\hbar^2}(E_f - h\nu)} \; . \tag{D.21}$$

In order to evaluate the dipole moment $\langle f(J)|\mathbf{r}|i(l)\rangle$, we make the identification

$$e\langle \psi^{(1)}_{\rm elec}(2s)\psi^{(2)}_{\rm elec}(2p)|\mathbf{r}|\psi^{(1)}_{\rm elec}(2s)\psi^{(2)}_{\rm elec}(2s)\rangle = \mathbf{D}^Y_{fi}(R) = D^Y_{fi}(R)\hat{\mathbf{R}} \; . \tag{D.22}$$

We then have

$$\begin{aligned} e\langle f(J)|\mathbf{r}|i(l)\rangle &= \sum_{m_l m_J} 4\pi i^l e^{i\delta_l} \int_0^{2\pi} d\varphi \int_0^{\pi} d\theta \sin\theta Y_{lm_l}(\hat{\mathbf{R}}) Y_{Jm_J}(\hat{\mathbf{R}})\hat{\mathbf{R}} \\ &\quad \times \int_0^{\infty} dR\, u_Y(K_0, l_N, R) D^Y_{fi}(R) R_{f(J)}(R) Y^*_{lm_l}(\hat{\mathbf{K}}_0) \; . \end{aligned} \tag{D.23}$$

The square of this term reduces to

$$\begin{aligned} e^2|\langle f(J)|\mathbf{r}|i(l)\rangle|^2 &= \frac{4\pi}{K_0^2}\left|\int_0^{\infty} dR\, u_Y(K_0, l, R) D^Y_{fi}(R) R_{f(J)}(R)\right|^2 \\ &\quad \times [J\delta(J, l+1) + (J+1)\delta(J, l-1)] \; . \end{aligned} \tag{D.24}$$

Substituting the above expression into Eq. (D.20), we obtain

$$\begin{aligned} \kappa^Y_{i\to f}(\nu, T) &= \sum_{l,J} \omega_Y \omega_{Yl} \frac{n_{\rm Li}^2 h^3}{(2\pi\mu k_B T)^{3/2}} \exp\left(-\frac{(E_f - h\nu)}{k_B T}\right) \\ &\quad \times \frac{16\pi^3\nu}{3hc}\left(\frac{2\mu}{E_f - h\nu}\right)^{1/2} \Theta(E_f - h\nu) \\ &\quad \times \left|\int_0^{\infty} dR u_Y(K_0, l, R) D^Y_{fi}(R) R_{f(J)}(R)\right|^2 \\ &\quad \times [J\delta(J, l+1) + (J+1)\delta(J, l-1)] \; . \end{aligned} \tag{D.25}$$

Here $\Theta(E_f - h\nu)$ is a step function which insures that the absorption coefficient remains real, which is the case for a red-detuned photon. In our case, we normalized the free wave function in respect to the energy (see §4.1), in which case we have

to multiply the right-hand side of the above expression by $\pi\hbar^2 K_0/2\mu$ (see also Eq. (4.10)). Finally, one can perform the sum over l to get Eq. (4.12) for a single bound level v: summing this last result over all v gives Eq. (4.10).

D.2 Statistical weights

We will derive the statistical weights used in this work, for the two lithium isotopes.

$^6Li_2$

Here, the nuclear spins of the two ^{6}Li atoms are $I_1 = I_2 = 1$, so that the total nuclear spin will have values

$$I = 2, 1, 0 \ . \tag{D.26}$$

The weights of each value are given by $(2I+1)/\sum_I(2I+1)$. So, we have

$$w_2(I=2) = \frac{5}{9} \ , \ w_1(I=1) = \frac{3}{9} \ , \ w_0(I=0) = \frac{1}{9} \ . \tag{D.27}$$

Now, according to the value of I, we need a combination of molecular states that will conserve the symmetry properties of the wave functions for the ground molecular state. For instance, Σ_g will be even or odd for an even or odd value of l, respectively, but Σ_u will be even or odd for an odd or even value of l. From this and the fact that there is one wave function for a singlet state and three for a triplet state, and since the spatial nuclear wave function is even for an even I and odd for an odd I, we have the following cases

$$I = 0 \text{ even} \ , \ \frac{1}{4}{}^1\Sigma_g(\text{even } l) + \frac{3}{4}{}^3\Sigma_u(\text{odd } l) \ , \tag{D.28}$$

$$I = 1 \text{ odd} \quad , \quad \frac{1}{4}{}^1\Sigma_g(\text{odd } l) + \frac{3}{4}{}^3\Sigma_u(\text{even } l) \; , \tag{D.29}$$

$$I = 2 \text{ even} \quad , \quad \frac{1}{4}{}^1\Sigma_g(\text{even } l) + \frac{3}{4}{}^3\Sigma_u(\text{odd } l) \; . \tag{D.30}$$

Then, summing over all possible molecular states of the excited molecule of ^{6}Li, we obtain

$$\begin{aligned} \sum_{\text{all states}} &= \frac{1}{9}\left\{\frac{1}{4}\left[{}^1\Sigma_g(\text{even } l) + 3^3\Sigma_u(\text{odd } l)\right] + \frac{3}{4}\left[{}^1\Sigma_g(\text{odd } l) + 3^3\Sigma_u(\text{even } l)\right]\right. \\ &\qquad \left. + \frac{5}{4}\left[{}^1\Sigma_g(\text{even } l) + 3^3\Sigma_u(\text{odd } l)\right]\right\} \\ &= \frac{1}{12}\left\{2^1\Sigma_g(\text{even } l) + 6^3\Sigma_u(\text{odd } l) + {}^1\Sigma_g(\text{odd } l) + 3^3\Sigma_u(\text{even } l)\right\} \end{aligned} \tag{D.31}$$

Grouping the even and odd l terms, we get

$$l \text{ even} \quad , \quad \frac{2l+1}{12}\left\{2^1\Sigma_g(\text{even } l) + 3^3\Sigma_u(\text{even } l)\right\} \; , \tag{D.32}$$

$$l \text{ odd} \quad , \quad \frac{2l+1}{12}\left\{{}^1\Sigma_g(\text{odd } l) + 6^3\Sigma_u(\text{odd } l)\right\} \; . \tag{D.33}$$

From these, we get the statistical weights listed below

$$\left.\begin{array}{llll} V_Y \text{ is singlet:} & \omega_Y = \frac{1}{12} & \text{even } l & \omega_{NY} = 2 \\ & & \text{odd } l & \omega_{NY} = 1 \\ V_Y \text{ is triplet:} & \omega_Y = \frac{3}{12} & \text{even } l & \omega_{NY} = 1 \\ & & \text{odd } l & \omega_{NY} = 2 \end{array}\right\} \; . \tag{D.34}$$

Notice that the coefficient $2l + 1$ is included in our derivation of $\kappa^Y_{i\to f}(\nu, T)$. In fact, it is the l and $l+1$ that will come from the delta functions if we sum over J (see Eq. (D.25)).

Finally, from the dipole transition, we must have J even for an odd value of l, and vice-versa. So, bearing this in mind, those weights give us the ones used in Table 4.1, where they are given in respect to J.

$^7Li_2$

We will go through the same steps as before. The nuclear spins of the two ^{7}Li atoms are $I_1 = I_2 = 3/2$, so that the total nuclear spin will have values

$$I = 3, 2, 1, 0 \ , \tag{D.35}$$

with the weights

$$w_3(I=3) = \frac{7}{16} \ , \ w_2(I=2) = \frac{5}{16} \ , \ w_1(I=1) = \frac{3}{16} \ , \ w_0(I=0) = \frac{1}{16} \ . \tag{D.36}$$

As before, we have

$$I = 0 \text{ even} \ , \ \frac{1}{4}{}^1\Sigma_g(\text{even } l) + \frac{3}{4}{}^3\Sigma_u(\text{odd } l) \ , \tag{D.37}$$

$$I = 1 \text{ odd} \ , \ \frac{1}{4}{}^1\Sigma_g(\text{odd } l) + \frac{3}{4}{}^3\Sigma_u(\text{even } l) \ , \tag{D.38}$$

$$I = 2 \text{ even} \ , \ \frac{1}{4}{}^1\Sigma_g(\text{even } l) + \frac{3}{4}{}^3\Sigma_u(\text{odd } l) \ , \tag{D.39}$$

$$I = 3 \text{ odd} \ , \ \frac{1}{4}{}^1\Sigma_g(\text{odd } l) + \frac{3}{4}{}^3\Sigma_u(\text{even } l) \ . \tag{D.40}$$

Then, summing over all possible molecular states of the excited molecule of ^{7}Li, we obtain

$$\begin{aligned} \sum_{\text{all states}} &= \frac{1}{16}\left\{\frac{1}{4}\left[{}^1\Sigma_g(\text{even } l) + 3{}^3\Sigma_u(\text{odd } l)\right] + \frac{3}{4}\left[{}^1\Sigma_g(\text{odd } l) + 3{}^3\Sigma_u(\text{even } l)\right]\right. \\ &\quad \left. + \frac{5}{4}\left[{}^1\Sigma_g(\text{even } l) + 3{}^3\Sigma_u(\text{odd } l)\right] + \frac{7}{4}\left[{}^1\Sigma_g(\text{odd } l) + 3{}^3\Sigma_u(\text{even } l)\right]\right\} \\ &= \frac{1}{32}\left\{3{}^1\Sigma_g(\text{even } l) + 9{}^3\Sigma_u(\text{odd } l)\right. \\ &\qquad \left. + 5{}^1\Sigma_g(\text{odd } l) + 15{}^3\Sigma_u(\text{even } l)\right\} \ . \end{aligned} \tag{D.41}$$

Grouping the even and odd l terms, we get

$$l \text{ even} \ , \ \frac{2l+1}{32}\left\{3{}^1\Sigma_g(\text{even } l) + 15{}^3\Sigma_u(\text{even } l)\right\} \ , \tag{D.42}$$

$$l \text{ odd} \ , \ \frac{2l+1}{12}\left\{5{}^1\Sigma_g(\text{odd } l) + 9{}^3\Sigma_u(\text{odd } l)\right\} \ . \tag{D.43}$$

From these, we get the statistical weights listed below

$$\left.\begin{array}{lllll} V_Y \text{ is singlet:} & \omega_Y = \frac{1}{32} & \text{even } l & \omega_{NY} & = 3 \\ & & \text{odd } l & \omega_{NY} & = 5 \\ V_Y \text{ is triplet:} & \omega_Y = \frac{3}{32} & \text{even } l & \omega_{NY} & = 5 \\ & & \text{odd } l & \omega_{NY} & = 3 \end{array}\right\} . \tag{D.44}$$

As for ^{6}Li, we get back the weights in Table 4.1 by inversing them according to the symmetry of J and l.

D.3 Continuum-continuum transitions

Let us rewrite the dipole moment matrix element as

$$\mathbf{S}_{fi} = \langle \psi_f(r,R)\phi_f^-(R)|e\mathbf{r}|\psi_i(r,R)\phi_i^+(R)\rangle \ , \tag{D.45}$$

where $\psi_{f,i}$ are the two-electron wave functions of the $(2s2p)$ and $(2s2s)$ configurations orbitals in Li_2, respectively. The functions $\phi_{f,i}^{-,+}$ are the nuclear wavefunctions for the excited and initial state, respectively. The superscripts $-,+$ denote incoming and outgoing boundary conditions.

We are interested in two nuclear free wave functions which will oscillate at large distance, hence offering a problem of convergence. Since $\mathbf{D}_{fi} \sim \mathbf{D}_{fi}^{(0)} + \mathbf{b}_{fi}/R^3$ at large distance, we obtain

$$\begin{aligned} \mathbf{S}_{fi} &= \langle \psi_f(r,R)\phi_f^-(R)|e\mathbf{r}|\psi_i(r,R)\phi_i^+(R)\rangle \\ &= \langle \phi_f^-(R)|\mathbf{D}_{fi}(R)|\phi_i^+(R)\rangle \\ &= \langle \phi_f^-(R)|\mathbf{D}_{fi}(R) - \mathbf{D}_{fi}^{(0)}|\phi_i^+(R)\rangle \\ &\quad + \mathbf{D}_{fi}^{(0)}\langle \phi_f^-(R)|\phi_i^+(R)\rangle \ , \end{aligned} \tag{D.46}$$

where the first term will go to zero as $\mathbf{b}_{fi}/R^3$ for large distance. Then, all the oscillation problem is concentrated in the last term. The functions ϕ_f^- and ϕ_i^+ are solutions of the Schrödinger equation for the two potential V_f and V_i

$$\left(\nabla^2\phi_f^-\right)^\dagger + \frac{2\mu}{\hbar^2}[E_f - V_f(R)]\left(\phi_f^-\right)^\dagger = 0\,, \tag{D.47}$$

$$\nabla^2\phi_i^+ + \frac{2\mu}{\hbar^2}[E_i - V_i(R)]\phi_i^+ = 0\,. \tag{D.48}$$

Multiplying the top equation by ϕ_i^+ from the left and the second one by $\left(\phi_f^-\right)^\dagger$ from the left, we obtain after subtracting both

$$\phi_i^+\left(\phi_f^-\right)^\dagger - \left(\phi_f^-\right)^\dagger\phi_i^+ = \frac{2\mu}{\hbar^2}[E_i - E_f]\left(\phi_f^-\right)^\dagger\phi_i^+ + \frac{2\mu}{\hbar^2}[V_f(R) - V_i(R)]\left(\phi_f^-\right)^\dagger\phi_i^+\,. \tag{D.49}$$

Since the orbital ϕ_f^- represents the excited level, and the orbital ϕ_i^+ the initial level, we have $E_f - E_i = h\nu$. Notice also that the potentials are define to be zero at infinity, thus $V_f(\infty) + \hbar\omega_p - V_i(\infty) = \hbar\omega_p = h\nu - \hbar\Delta$. Here $h\nu$ is the energy of the photon from the laser field, and $\hbar\Delta$ is the amount of detuning from the $2S_{1/2}$-$2P_{1/2}$ atomic transition and $\hbar\omega_p$ is the energy difference between the potential curve asymptotes. We rewrite the above equation as

$$\phi_i^+\left(\phi_f^-\right)^\dagger - \left(\phi_f^-\right)^\dagger\phi_i^+ = -\frac{2\mu\Delta}{\hbar}\left(\phi_f^-\right)^\dagger\phi_i^+ + \frac{2\mu}{\hbar^2}[V_f(R) - V_i(R) - \hbar\omega_p]\left(\phi_f^-\right)^\dagger\phi_i^+\,, \tag{D.50}$$

which gives

$$\begin{aligned}\left(\phi_f^-\right)^\dagger\phi_i^+ &= \frac{\hbar}{2\mu\Delta}\nabla\cdot\left[\left(\phi_f^-\right)^\dagger\nabla\phi_i^+ - \phi_i^+\left(\nabla\phi_f^-\right)^\dagger\right] \\ &\quad + \frac{[V_f(R) - V_i(R) - \hbar\omega_p]}{\hbar\Delta}\left(\phi_f^-\right)^\dagger\phi_i^+\,.\end{aligned} \tag{D.51}$$

Integrating this expression over a volume V of radius R and surface area $\mathbf{S}$, we obtain from Green's theorem

$$\int_V dV\left(\phi_f^-\right)^\dagger\phi_i^+ = \frac{\hbar}{2\mu\Delta}\int_{\mathbf{S}} d\mathbf{S}\cdot\left[\left(\phi_f^-\right)^\dagger\nabla\phi_i^+ - \phi_i^+\left(\nabla\phi_f^-\right)^\dagger\right]$$

$$+\int_V dV \frac{[V_f(R) - V_i(R) - \hbar\omega_p]}{\hbar\Delta} \left(\phi_f^-\right)^\dagger \phi_i^+ \ . \qquad \text{(D.52)}$$

Letting $R \to \infty$, we finally obtain

$$\begin{aligned} \langle \phi_f^- | \phi_i^+ \rangle &= \frac{\hbar}{2\mu\Delta} \int_{\text{Sas } R\to\infty} d\mathbf{S} \cdot \left[\left(\phi_f^-\right)^\dagger \nabla \phi_i^+ - \phi_i^+ \left(\nabla \phi_f^-\right)^\dagger \right] \\ &\quad + \left\langle \phi_f^- \left| \frac{[V_f(R) - V_i(R) - \hbar\omega_p]}{\hbar\Delta} \right| \phi_i^+ \right\rangle \ . \end{aligned} \qquad \text{(D.53)}$$

As $R \to \infty$, the second term on the right-hand side becomes a constant, and the first term is oscillatory. Since R is large and the oscillatory behaviour is confined on the surface of the sphere of radius R, we can drop this surface term as $R \to \infty$. In fact, one can show that this term vanishes if a complex coordinate rotation is applied (see Gao and Starace [83])

$$R \to R_0 + Re^{i\theta} \ . \qquad \text{(D.54)}$$

This rotation is analogous to the introduction of an exponentially decaying function in the integral of the form $e^{-\epsilon R}$ (Dalgarno, private communication). One can then show that this oscillatory term vanishes at infinity for any ϵ, as long as ϵ is not strictly zero.

So, discarding the oscillatory term, we finally get

$$\begin{aligned} \mathbf{S}_{fi}|_{\text{non-osc.}} &= \langle \phi_f^-(R) | \mathbf{D}_{fi}(R) - \mathbf{D}_{fi}^{(0)} | \phi_i^+ \rangle \\ &\quad + \frac{\mathbf{D}_{fi}^{(0)}}{\hbar\Delta} \langle \phi_f^-(R) | [V_f(R) - V_i(R) - \hbar\omega_p] | \phi_i^+ \rangle \ . \end{aligned} \qquad \text{(D.55)}$$

Notice here that the detuning Δ is defined negative, *i.e.* red-detuning $\hbar\Delta < 0$.

Using this expression, we computed the following matrix element for four different

values of detuning

$$|D(\Delta,\varepsilon)|^2 \equiv |\langle u_f^{l=1}(R)|Z_1 + Z_2|u_i^{l=0}(R)\rangle|^2 \ , \tag{D.56}$$

where the functions $Z_1(R)$ and $Z_2(R)$ are defined as

$$Z_1(R) = D_{fi}(R) - D_{fi}^{(0)} \ , \tag{D.57}$$

$$Z_2(R) = \frac{D_{fi}^{(0)}}{\hbar\Delta}[V_f(R) - V_i(R) - \hbar\omega_p] \ . \tag{D.58}$$

We used energy normalization for our wave functions. Notice that ε represent the kinetic energy of the ground state and is therefore directly related to the detuning. In fact, from our above conventions, we have

$$\hbar\omega_p = h\nu - \hbar\Delta \quad , \quad h\nu = E_f - E_i \ , \tag{D.59}$$

$$E_f = \hbar\omega_p + K_f \quad , \quad E_i = K_i = \varepsilon \ , \tag{D.60}$$

$$K_f - K_i = \hbar\Delta \implies K_f = \varepsilon + \hbar\Delta \ . \tag{D.61}$$

So, by maintaining a constant detuning, as we vary the kinetic energy of the ground state ε, we also vary the kinetic energy of the excited state K_f. In Fig. D.1, we show the results obtain from the free-free expression as a function of ε for four different detuning. The values of the detuning were selected to match the values from Ritchie *et al.* [84] , *i.e.* $\Delta = -2.3\Gamma, -2.9\Gamma, -3.5\Gamma$ and -4.1Γ, where $\Gamma = 5.8$ MHz. Here, the free wave functions were energy normalized, which explains the increase in the amplitude of the dipole transition as we lower the kinetic energy. Moreover, we see that the four different cases are fast oscillating curves in phase for higher energy and that they slowly become less in phase as we lower the ε: the bigger the detuning, the more to the left is the dipole transition shifted. Finally, we also observe the the

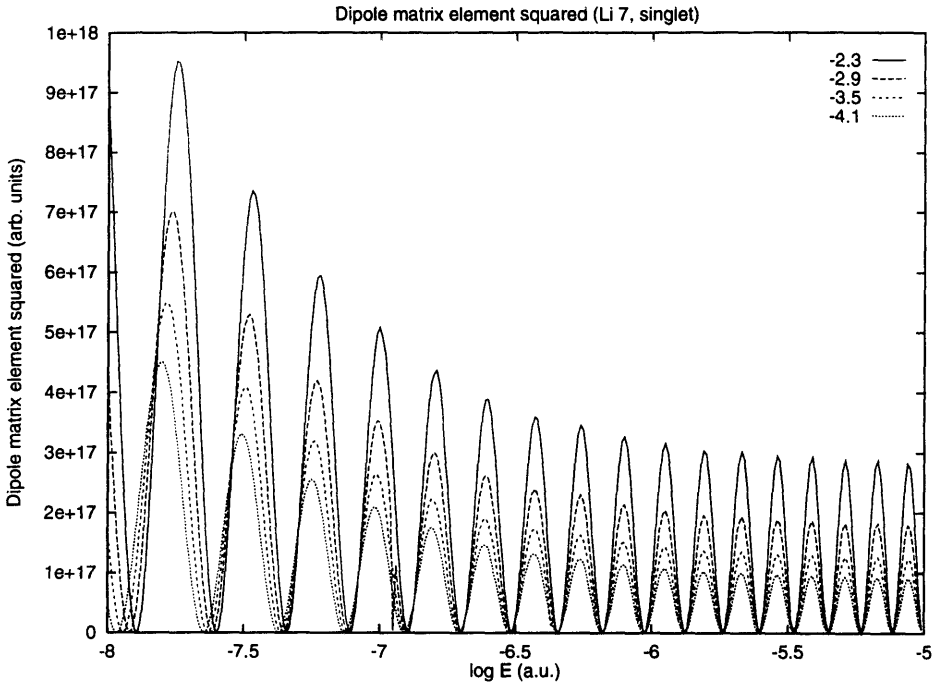

Figure D.1: Free-free dipole matrix element squared $|D(\Delta, \varepsilon)|^2$ as a function of energy, for different values of detunings (Δ) in the ^{7}Li singlet case.

smallest detuning gives the biggest amplitude, while the biggest detuning gives the smallest amplitude. This is due to the energy normalization of our wave functions. When Δ decreases, K_f has to decrease also, for a given $K_i = \varepsilon$ (see Eq. (D.61)), hence a bigger value of $|D(\Delta, \varepsilon)|^2$.

Appendix E

Various data

In this Appendix, we will give the 3-D plots of the square of the dipole matrix element $|D_{v''}(E)|^2$ for each excited vibrational level v'' as a function of energy for the singlet and triplet transitions of ^{6}Li and ^{7}Li.

Then we will also list all the bound-bound spontaneous emission coefficients $A_{v'v''}$ (in s^{-1}) and the oscillator strengths $f_{v'v''}$ (in a.u.) for the same four possibilities. Here, v' refers to the vibrational levels of the ground state, and v'' to the vibrational levels of the excited state.

For more detail concerning these data, one should look at chapter 4.

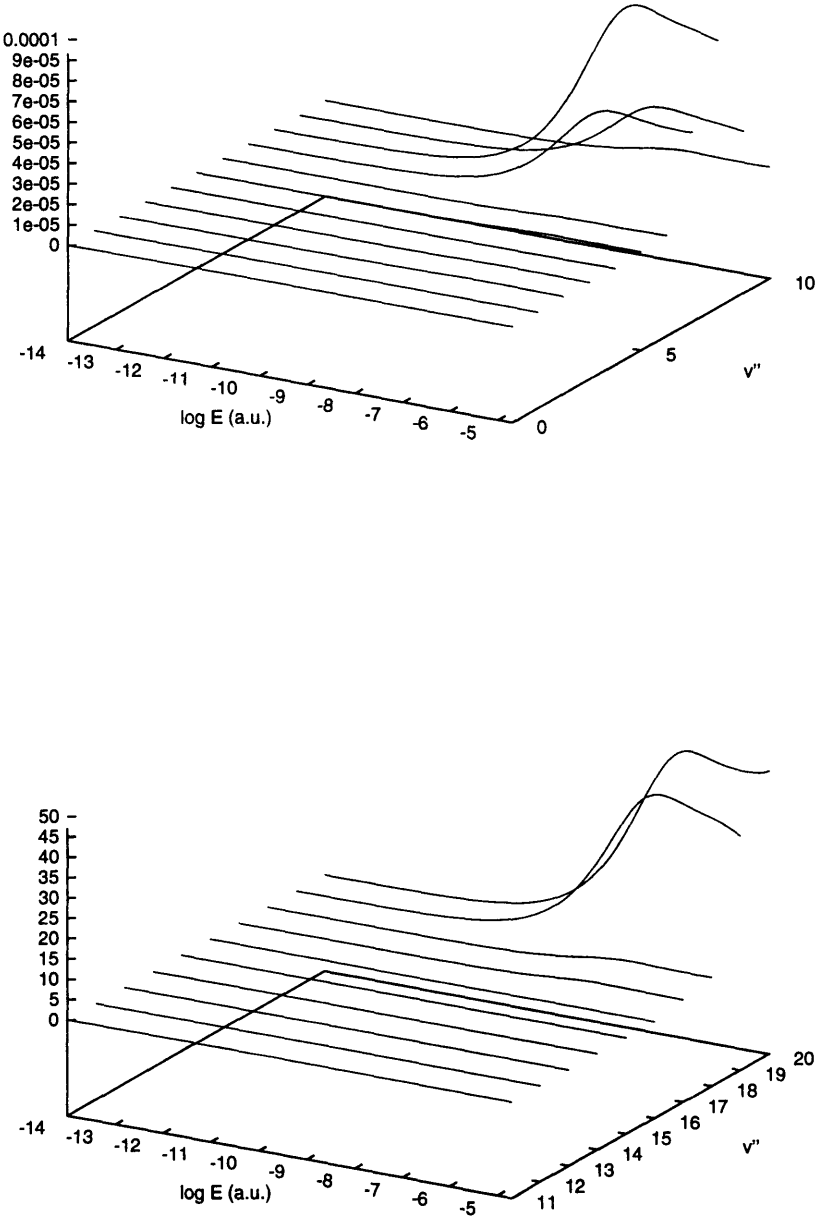

Figure E.1: Dipole matrix element $|D_{v''}(E)|^2$ for ^{6}Li singlet transitions.

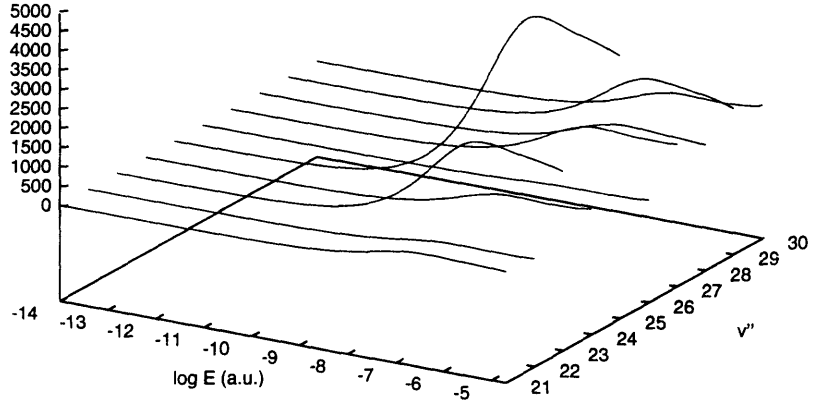

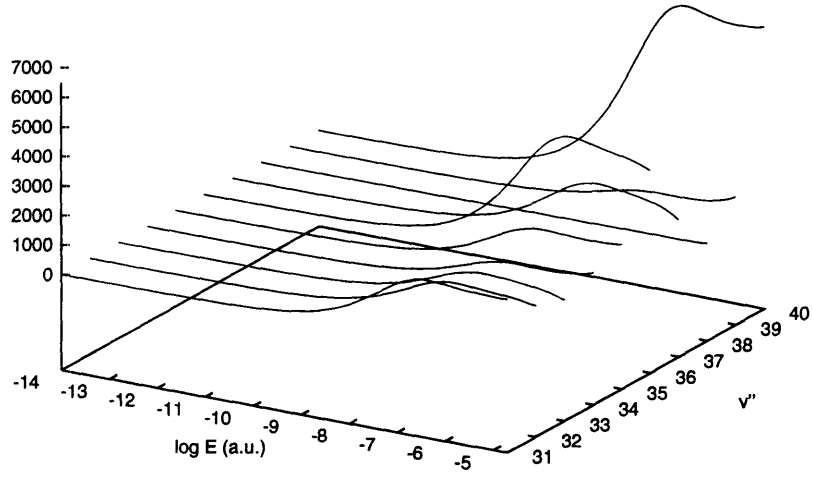

Figure E.2: $|D_{v''}(E)|^2$ for ^{6}Li singlet transitions (continued).

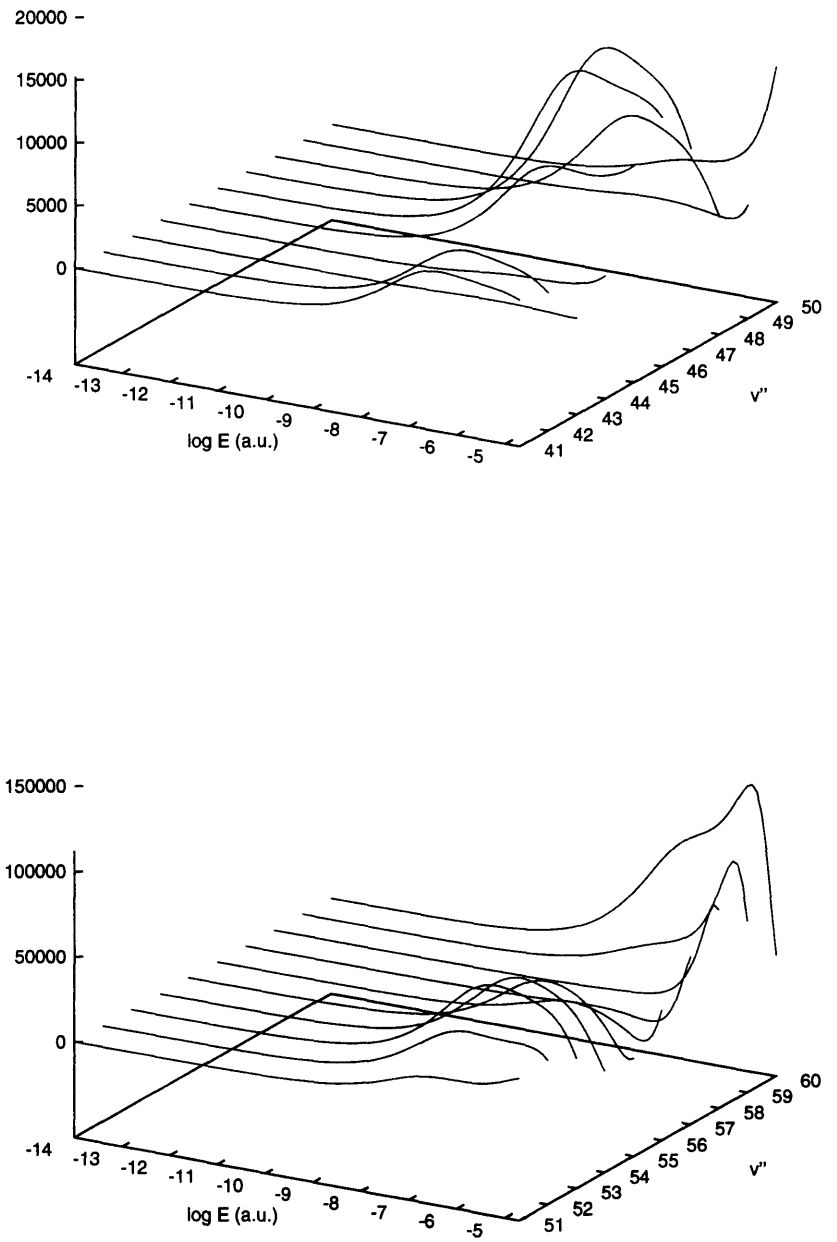

Figure E.3: $|D_{v''}(E)|^2$ for ^{6}Li singlet transitions (continued).

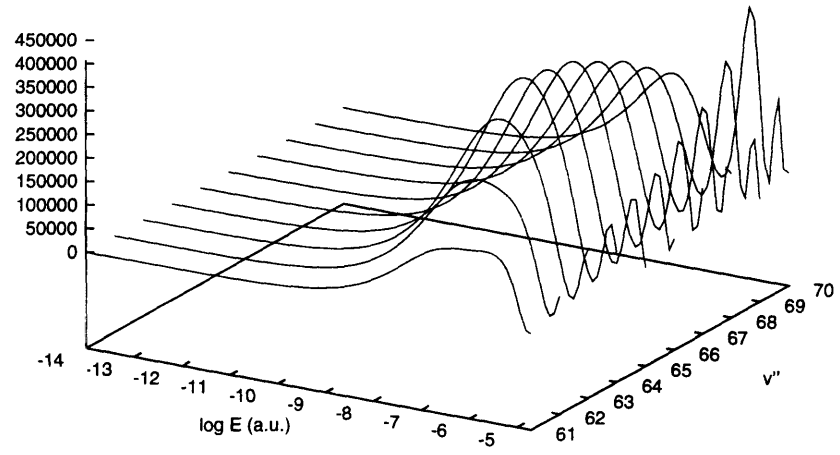

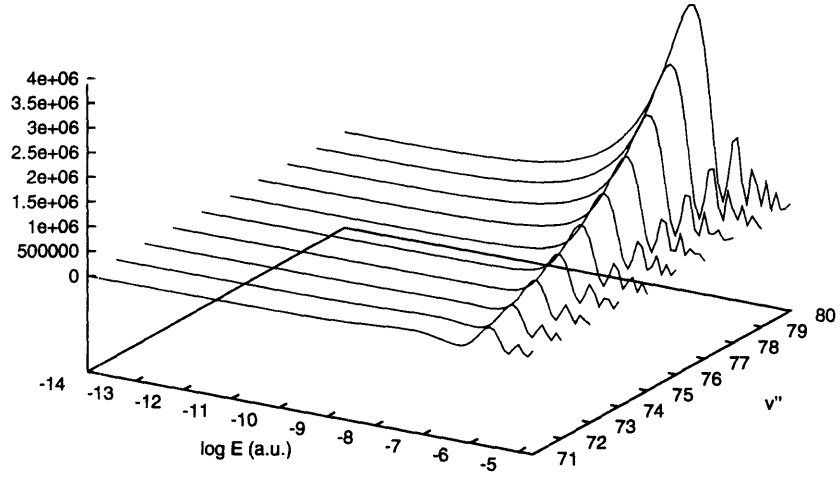

Figure E.4: $|D_{v''}(E)|^2$ for ^{6}Li singlet transitions (continued).

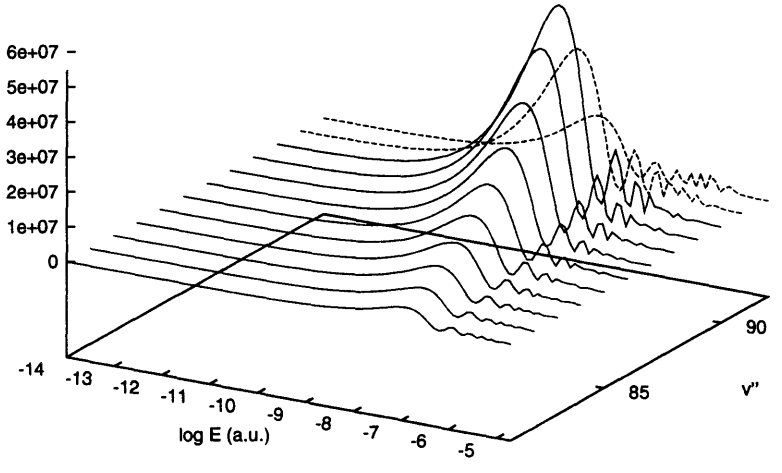

Figure E.5: $|D_{v''}(E)|^2$ for ^{6}Li singlet transitions (continued).

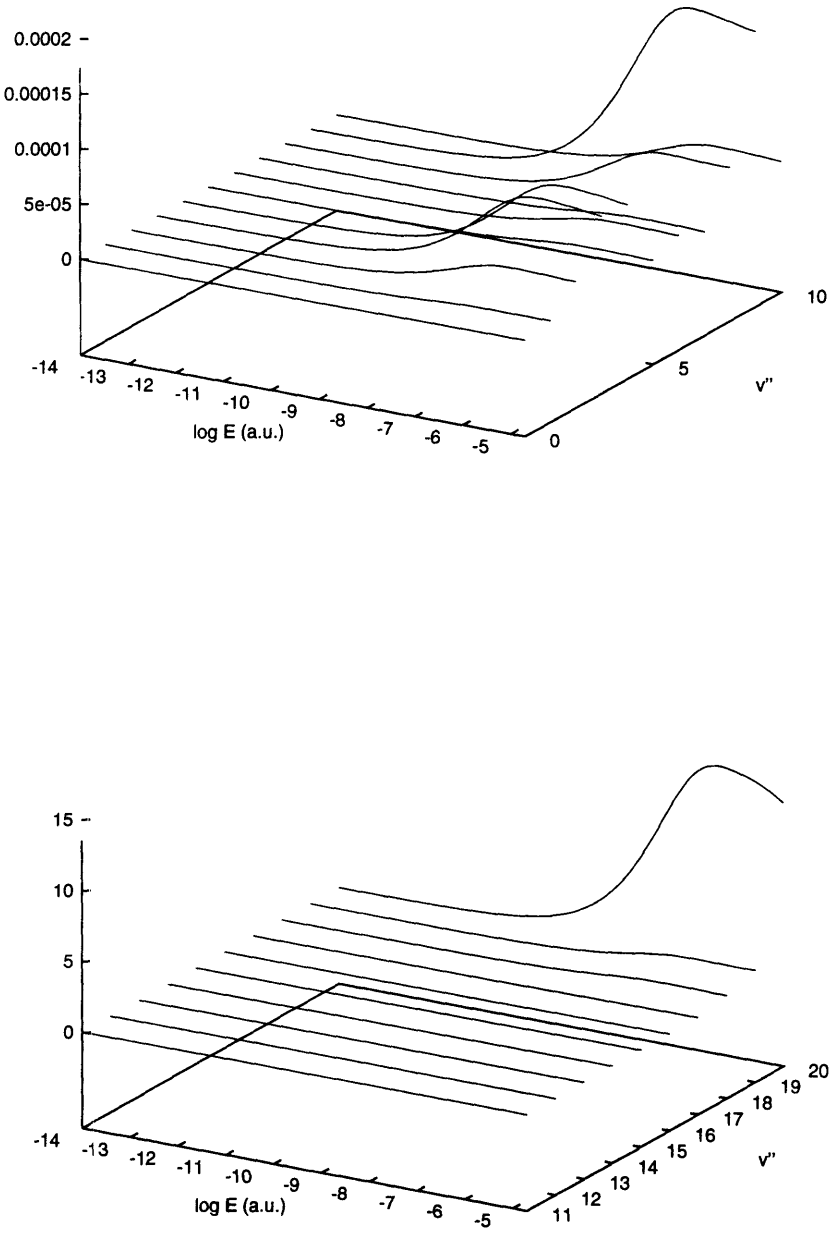

Figure E.6: Dipole matrix element $|D_{v''}(E)|^2$ for ^{7}Li singlet transitions.

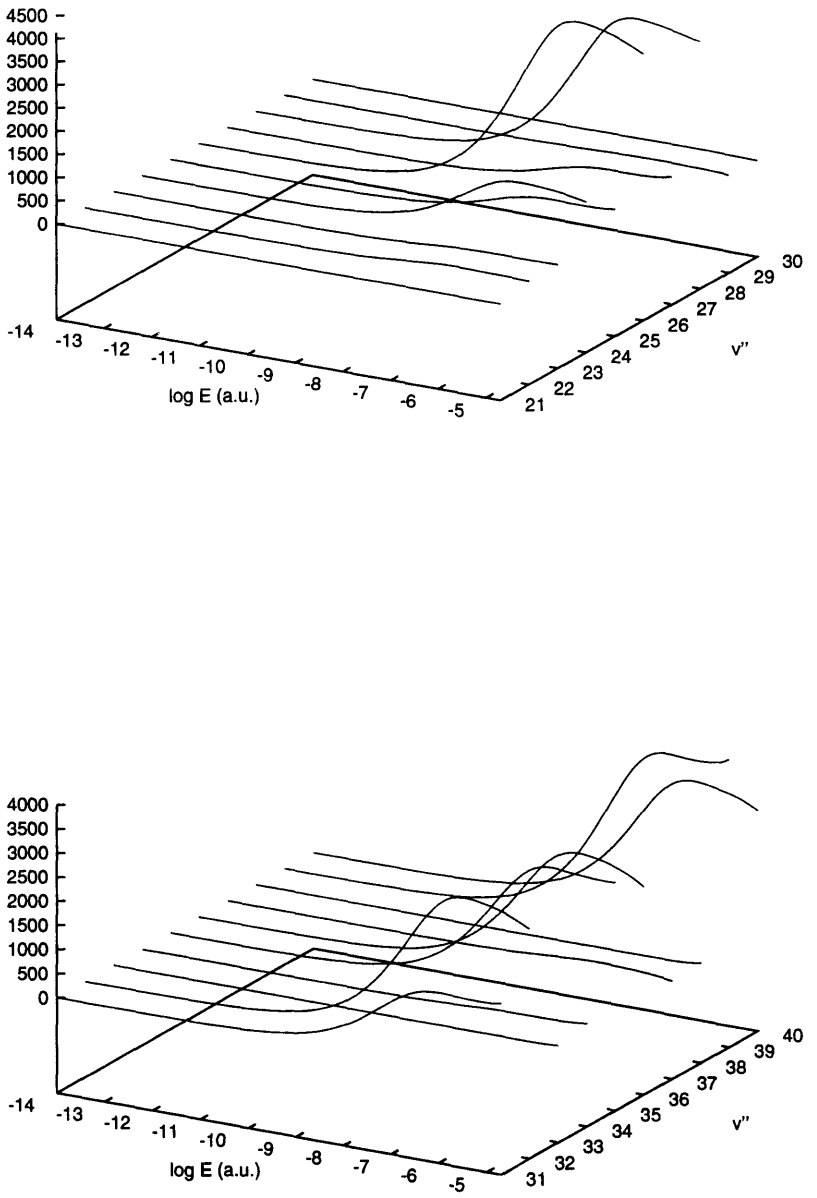

Figure E.7: $|D_{v''}(E)|^2$ for ^{7}Li singlet transitions (continued).

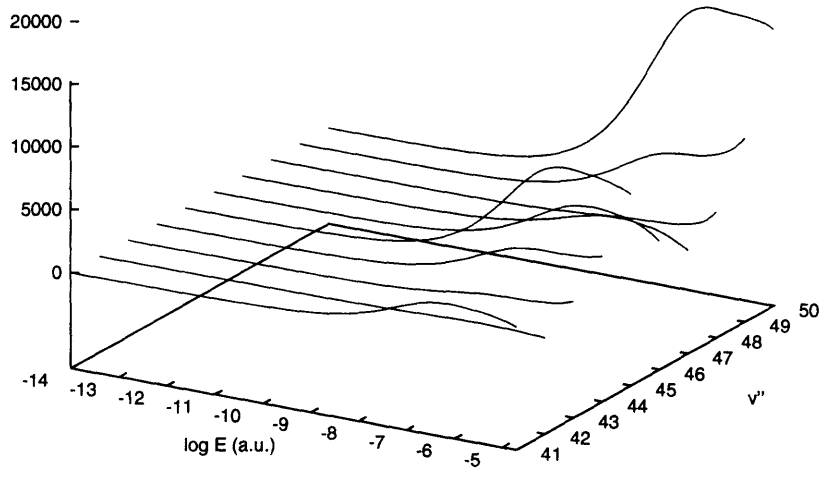

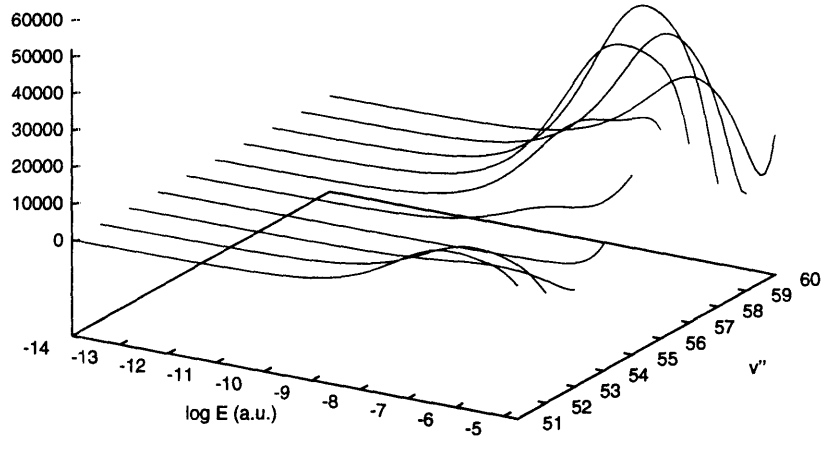

Figure E.8: $|D_{v''}(E)|^2$ for ^{7}Li singlet transitions (continued).

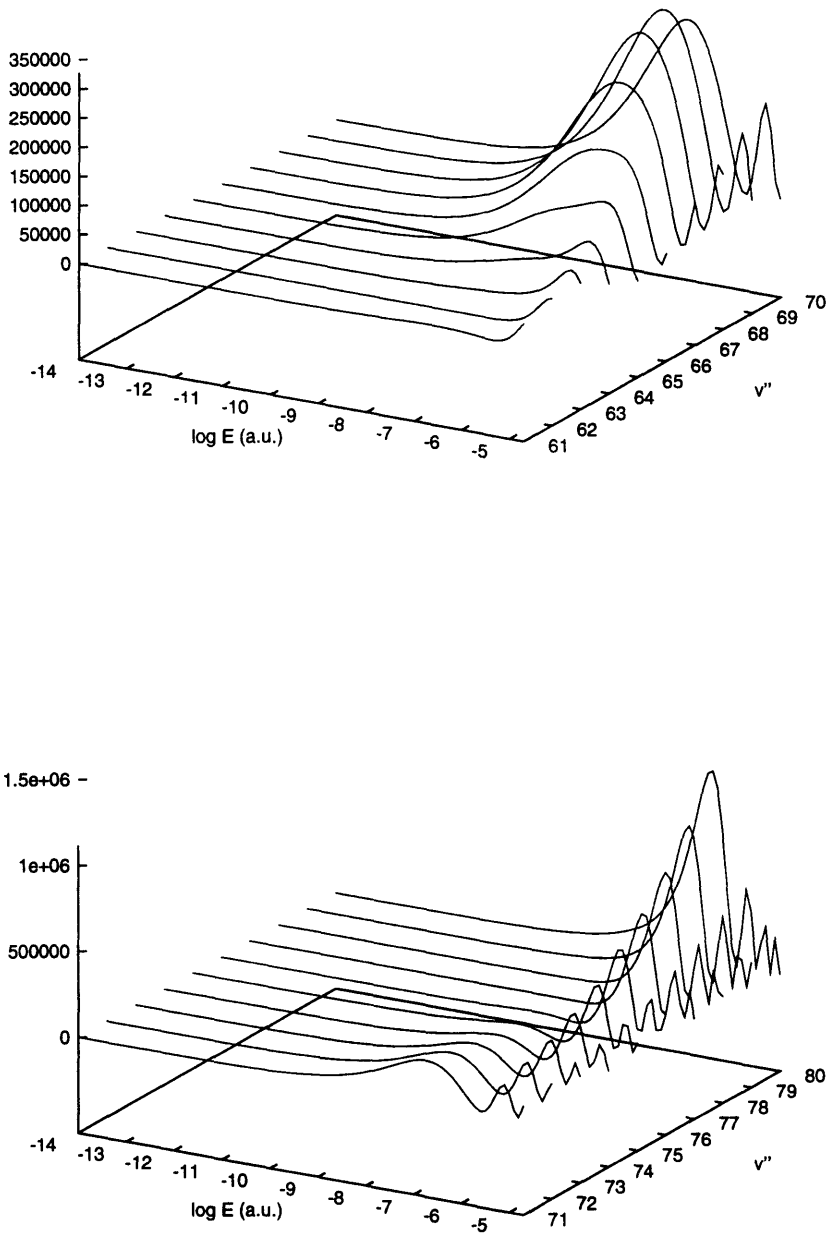

Figure E.9: $|D_{v''}(E)|^2$ for ^{7}Li singlet transitions (continued).

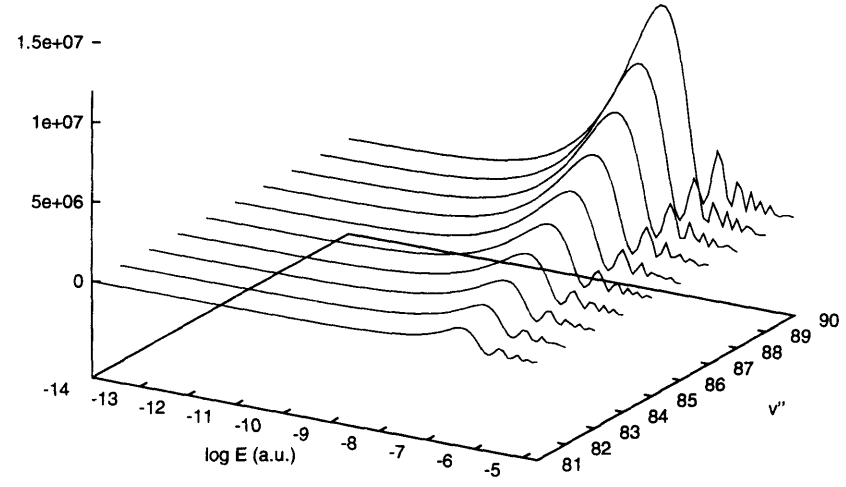

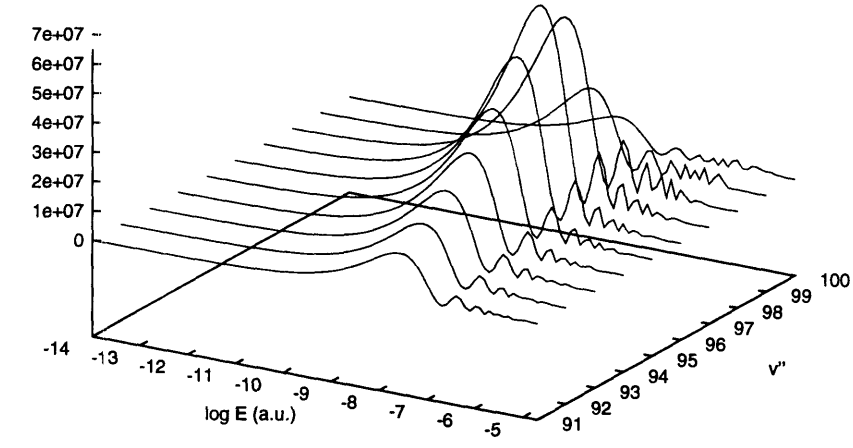

Figure E.10: $|D_{v''}(E)|^2$ for ^{7}Li singlet transitions (continued).

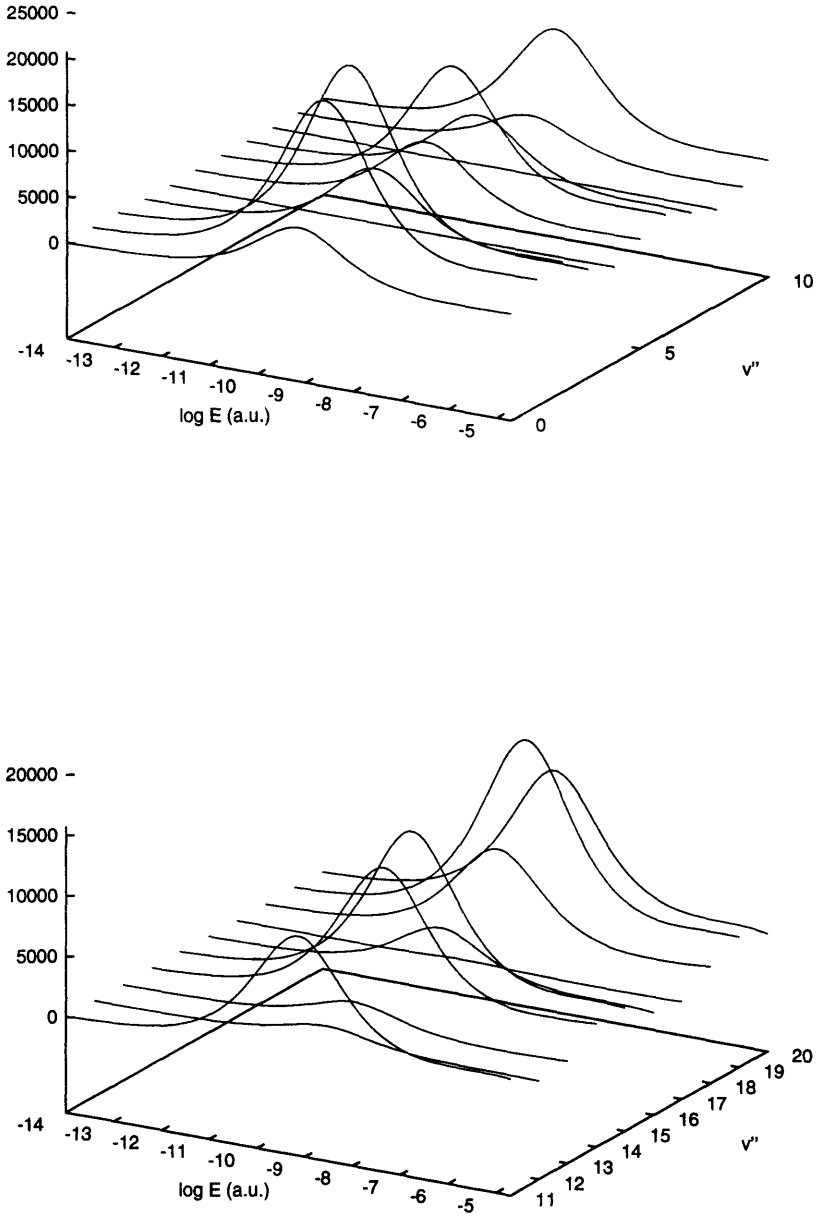

Figure E.11: Dipole matrix element $|D_{v''}(E)|^2$ for ^{6}Li triplet transitions.

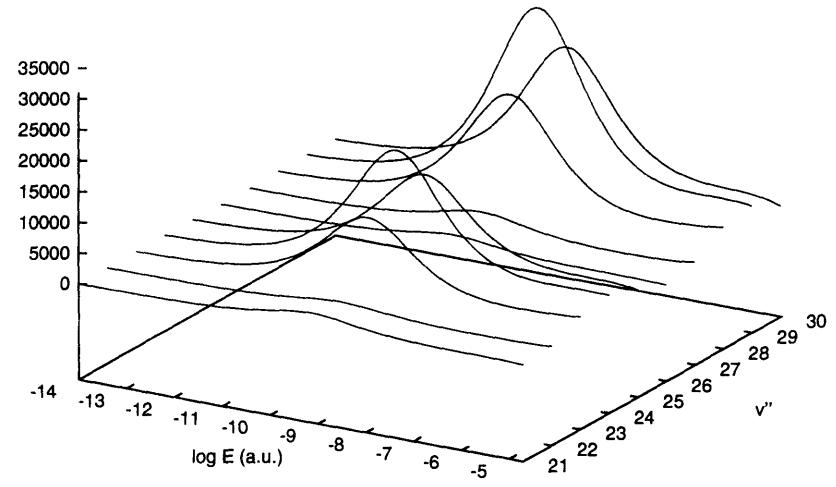

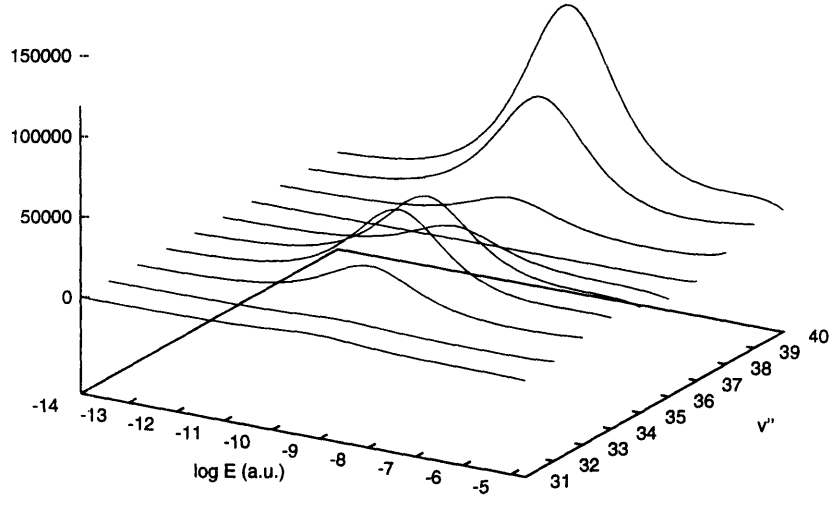

Figure E.12: $|D_{v''}(E)|^2$ for ^{6}Li triplet transitions (continued).

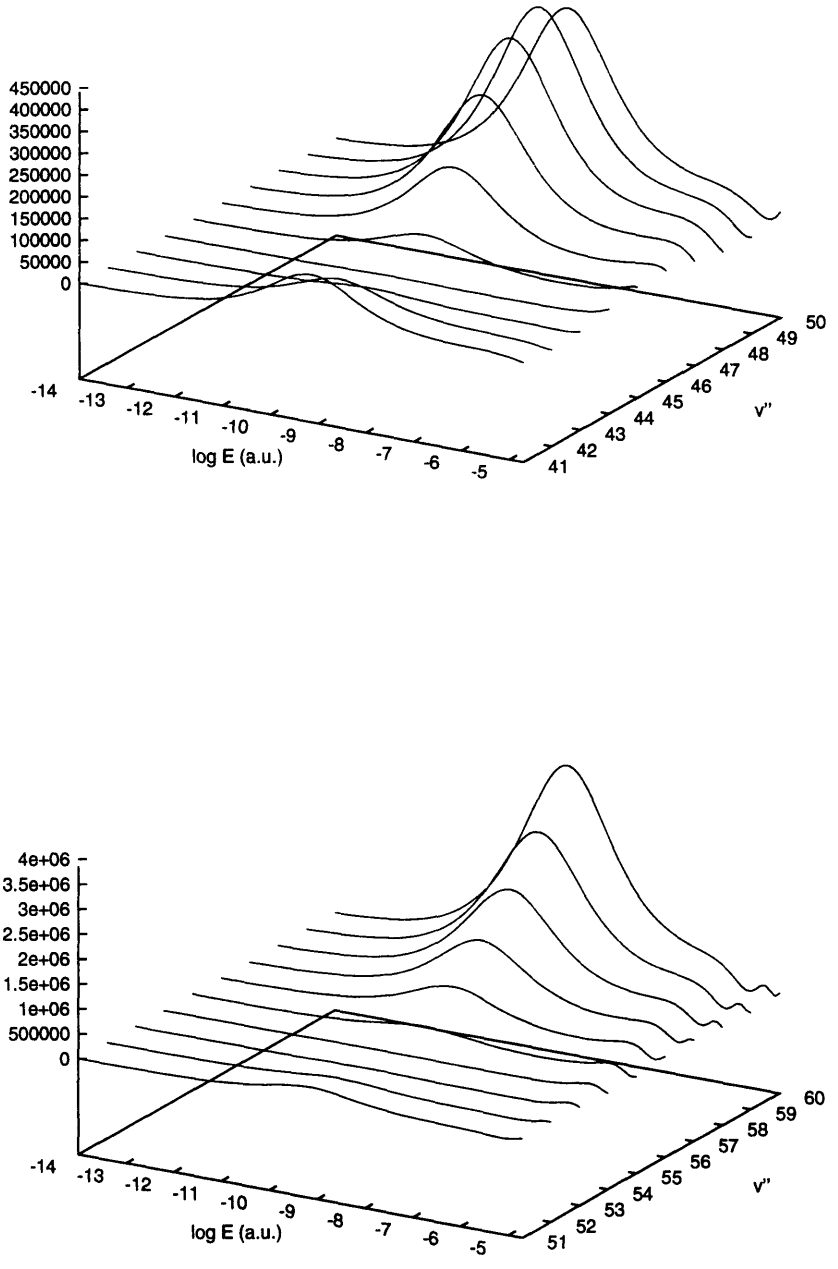

Figure E.13: $|D_{v''}(E)|^2$ for ^{6}Li triplet transitions (continued).

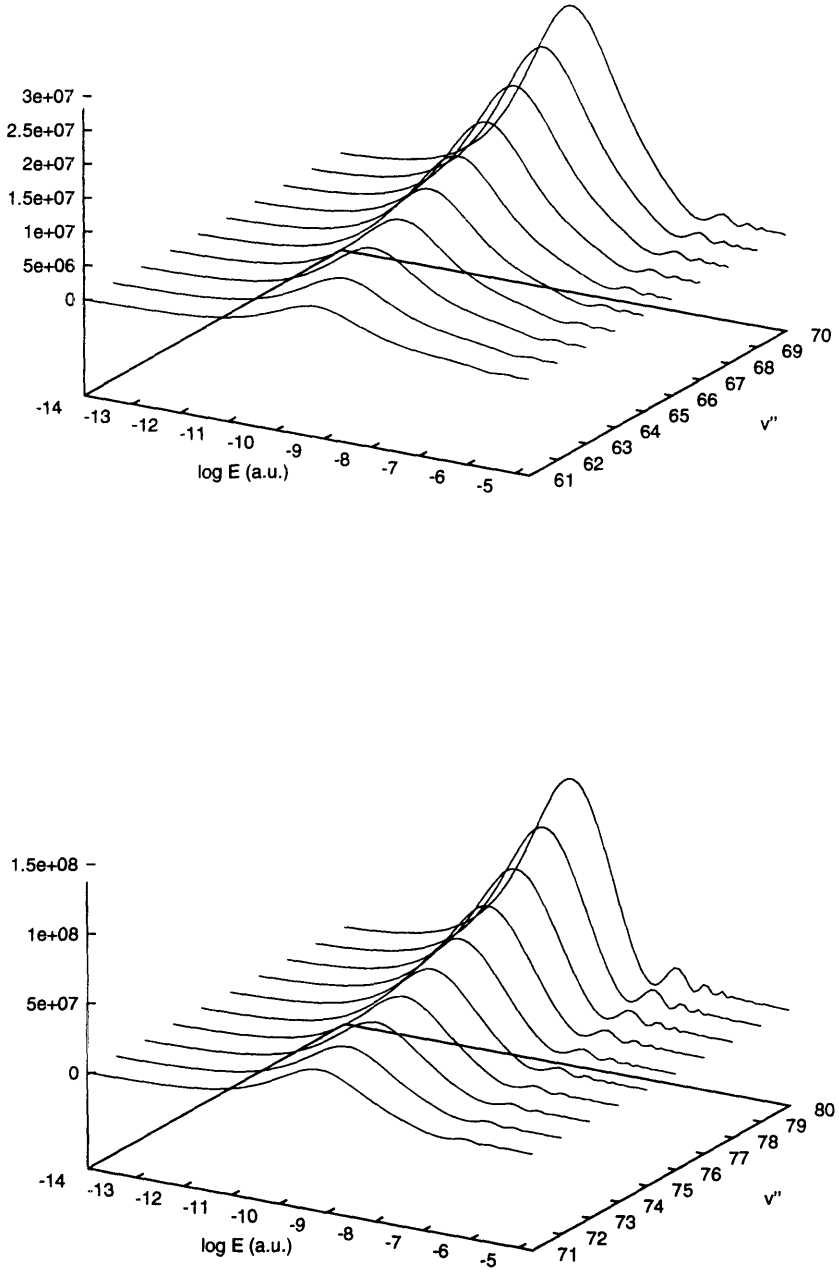

Figure E.14: $|D_{v''}(E)|^2$ for ^{6}Li triplet transitions (continued).

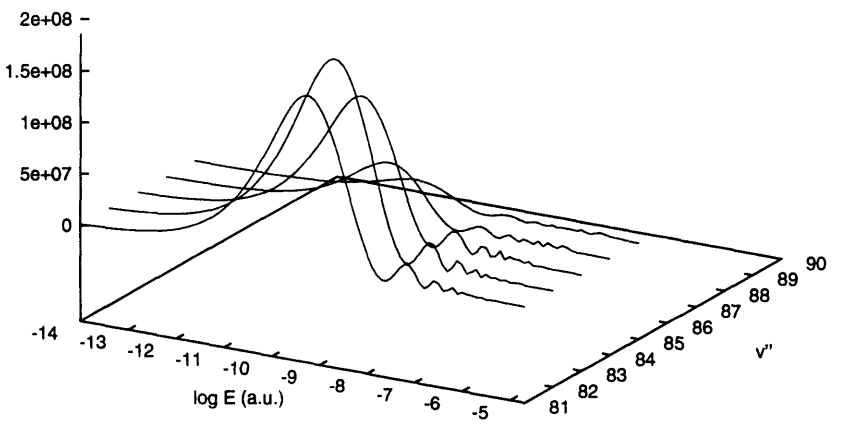

Figure E.15: $|D_{v''}(E)|^2$ for ^{6}Li triplet transitions (continued).

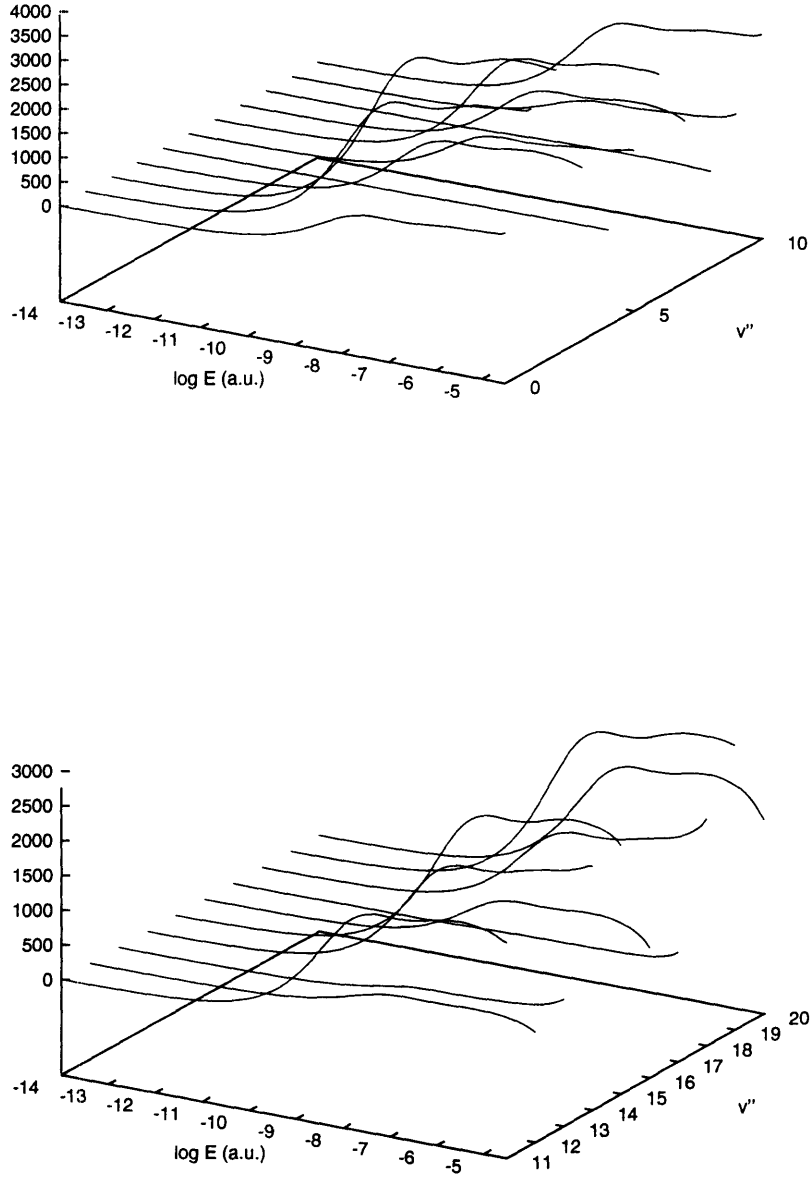

Figure E.16: Dipole matrix element $|D_{v''}(E)|^2$ for ^{7}Li triplet transitions.

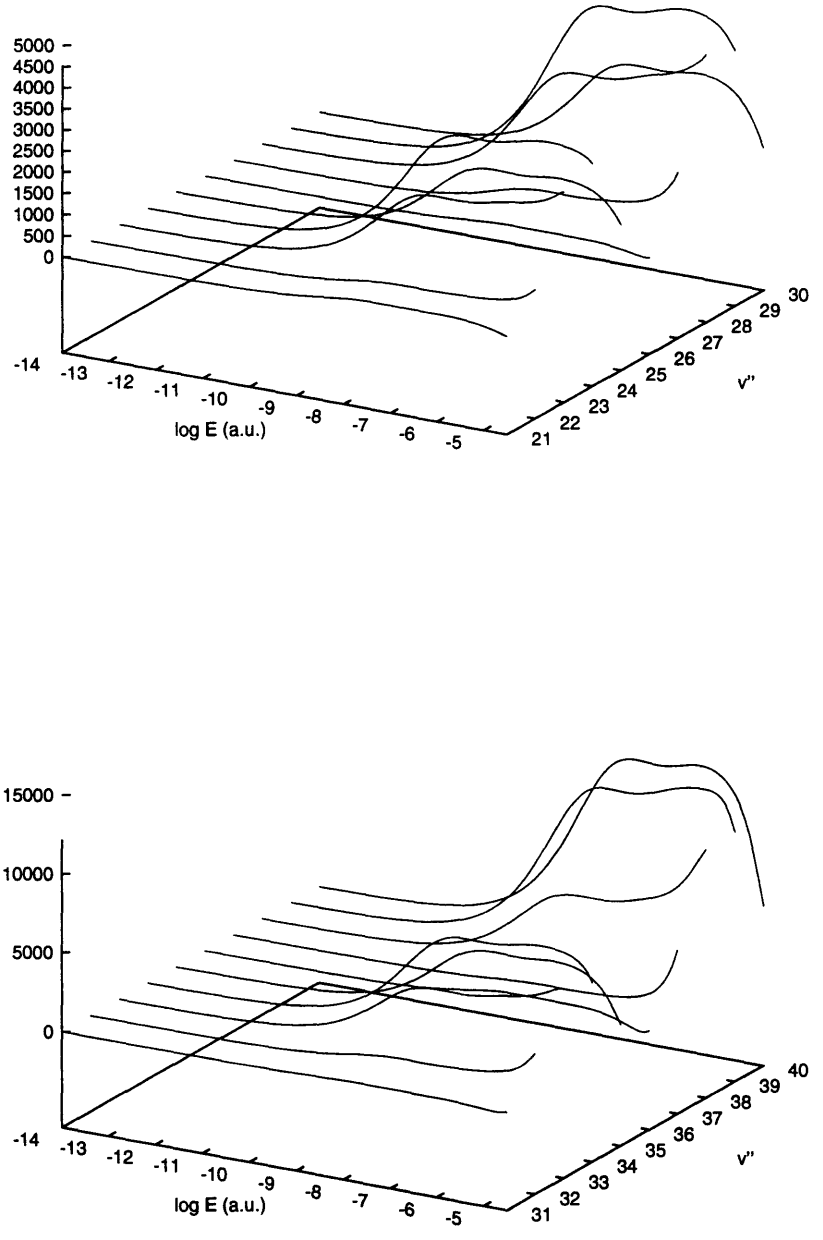

Figure E.17: $|D_{v''}(E)|^2$ for ^{7}Li triplet transitions (continued).

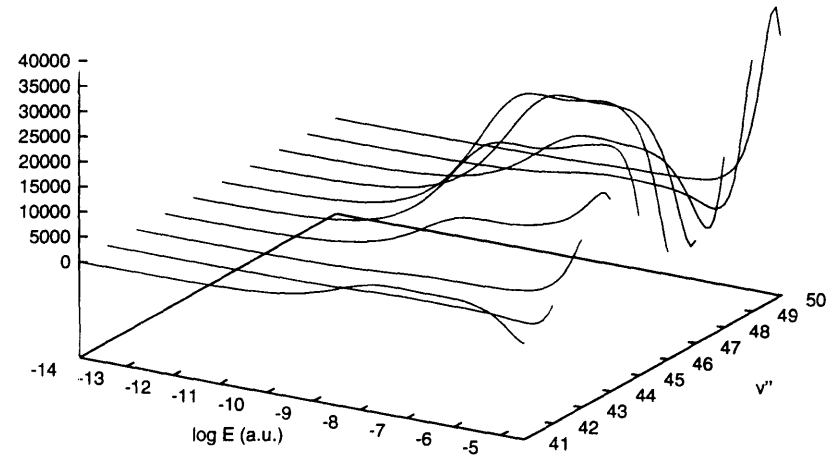

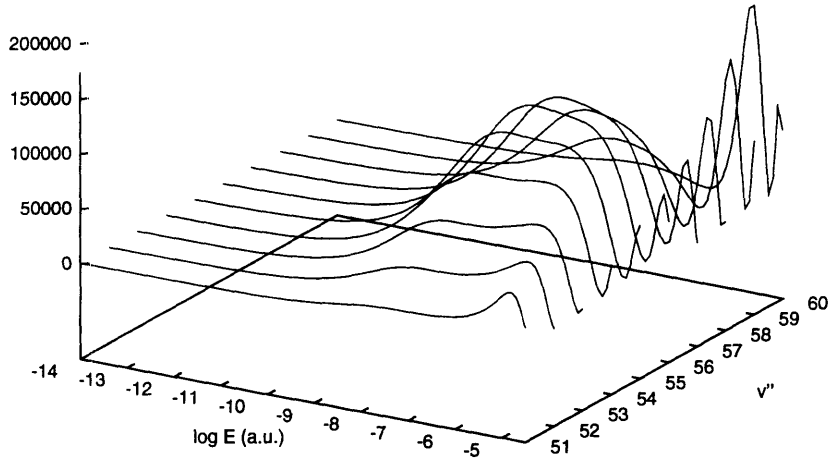

Figure E.18: $|D_{v''}(E)|^2$ for ^{7}Li triplet transitions (continued).

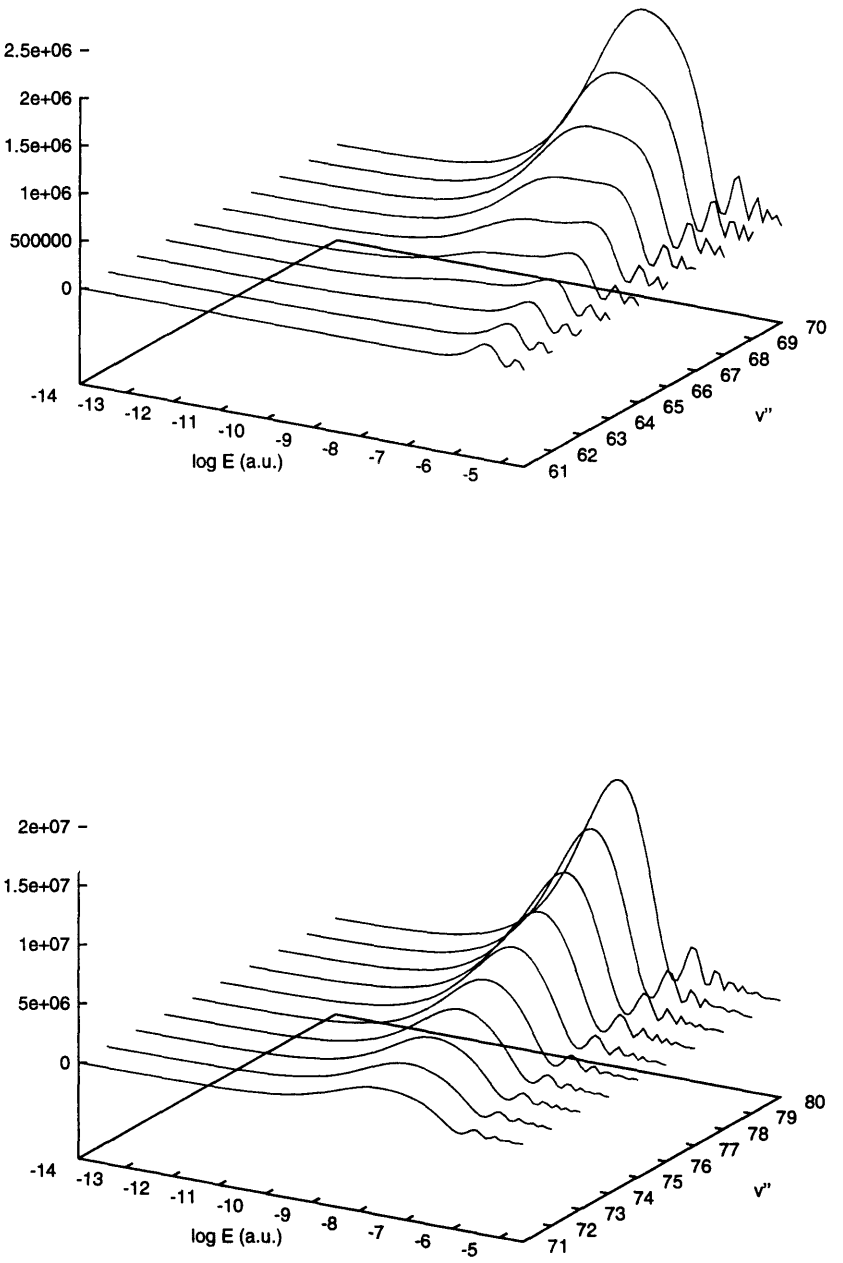

Figure E.19: $|D_{v''}(E)|^2$ for ^{7}Li triplet transitions (continued).

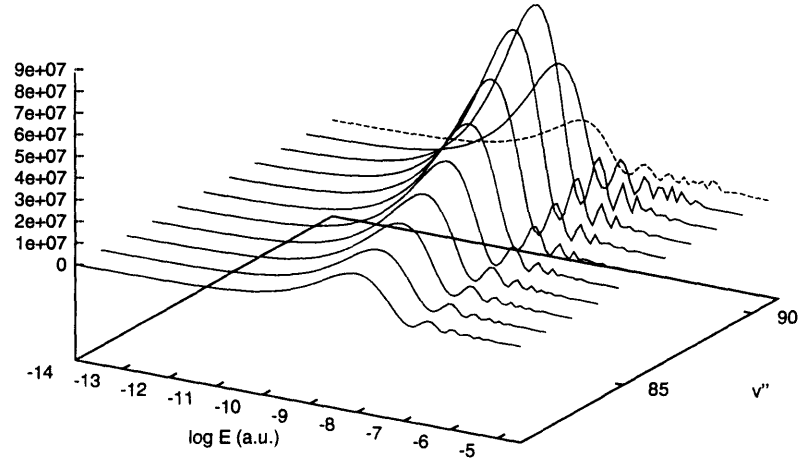

Figure E.20: $|D_{v''}(E)|^2$ for ^{7}Li triplet transitions (continued).

$v'\backslash v''$	0	1	2	3	4	5	6	7
0	3.99 +6	9.72 +6	1.30 +7	1.28 +7	1.02 +7	7.15 +6	4.50 +6	2.63 +6
1	1.19 +7	1.17 +7	3.60 +6	8.81 +2	2.21 +6	5.77 +6	7.60 +6	7.32 +6
2	1.62 +7	2.07 +6	2.03 +6	6.90 +6	4.83 +6	8.42 +5	2.29 +5	2.45 +6
3	1.31 +7	1.57 +6	7.72 +6	1.40 +6	1.01 +6	4.82 +6	4.47 +6	1.44 +6
4	7.02 +6	9.17 +6	1.69 +6	2.90 +6	5.26 +6	7.46 +5	8.55 +5	3.82 +6
5	2.62 +6	1.11 +7	1.61 +6	5.83 +6	4.82 +3	3.66 +6	3.65 +6	3.05 +5
6	6.88 +5	6.75 +6	8.69 +6	2.63 +5	4.87 +6	2.11 +6	5.47 +5	3.78 +6
7	1.27 +5	2.50 +6	9.57 +6	3.73 +6	3.01 +6	1.51 +6	4.15 +6	2.72 +5
8	1.58 +4	5.90 +5	5.07 +6	9.56 +6	4.85 +5	5.02 +6	1.52 +3	3.50 +6
9	1.23 +3	8.78 +4	1.53 +6	7.53 +6	7.25 +6	2.04 +5	4.53 +6	9.49 +5
10	4.82 +1	7.58 +3	2.69 +5	2.90 +6	9.10 +6	4.12 +6	1.78 +6	2.53 +6
11	4.55 -1	3.14 +2	2.62 +4	6.09 +5	4.57 +6	9.48 +6	1.56 +6	3.52 +6
12	4.60 -4	4.38 +0	1.25 +3	6.80 +4	1.15 +6	6.33 +6	8.85 +6	2.32 +5
13	8.45 -3	1.30 -1	2.08 +1	3.22 +3	1.36 +5	1.82 +6	7.85 +6	7.50 +6
14	3.78 -3	1.97 -2	2.22 -2	1.35 +1	5.24 +3	2.22 +5	2.60 +6	9.09 +6
15	3.81 -3	7.53 -2	1.01 +0	1.17 +1	2.51 +0	7.25 +3	3.31 +5	3.46 +6
16	3.32 -3	5.84 -2	4.55 -1	2.59 +0	2.56 +1	4.15 +1	8.21 +3	4.33 +5
17	1.49 -3	2.00 -2	1.62 -1	6.21 -1	6.20 -2	4.05 +1	3.39 +2	6.04 +3
18	1.25 -3	3.11 -2	2.44 -1	7.75 -1	1.17 +0	7.33 -3	1.01 +2	1.28 +3
19	9.05 -4	1.38 -2	1.07 -1	3.17 -1	2.45 -1	2.05 -1	1.16 +0	1.34 +2
20	2.34 -4	1.03 -2	7.65 -2	2.33 -1	2.66 -1	2.65 -2	9.82 -1	5.79 +0
21	5.68 -4	1.54 -2	1.13 -1	3.16 -1	2.63 -1	2.88 -3	4.38 -1	6.45 -1
22	1.43 -6	1.86 -4	1.35 -3	6.36 -3	1.43 -2	2.22 -2	7.01 -3	8.56 -3
23	3.08 -4	1.02 -2	7.17 -2	2.06 -1	1.78 -1	7.19 -4	2.07 -1	6.50 -2
24	1.00 -4	4.18 -3	2.80 -2	7.23 -2	4.37 -2	8.05 -3	1.67 -1	1.19 -1
25	3.89 -5	3.83 -4	3.19 -3	1.12 -2	1.67 -2	5.13 -3	2.35 -3	6.87 -3
26	1.98 -4	4.40 -3	3.14 -2	8.78 -2	7.32 -2	2.27 -5	1.24 -1	1.51 -1
27	1.02 -4	3.11 -3	2.12 -2	5.48 -2	3.58 -2	2.31 -3	8.71 -2	7.10 -2
28	6.76 -7	2.59 -4	1.52 -3	2.96 -3	4.61 -4	2.01 -3	3.26 -3	1.48 -3
29	4.68 -5	3.99 -4	3.17 -3	9.94 -3	1.19 -2	4.86 -4	1.89 -2	5.56 -2
30	9.97 -5	1.40 -3	1.03 -2	2.84 -2	2.51 -2	2.70 -6	4.20 -2	6.31 -2
31	8.64 -5	1.43 -3	1.03 -2	2.68 -2	2.07 -2	1.01 -4	3.13 -2	2.58 -2
32	4.56 -5	8.54 -4	6.05 -3	1.49 -2	1.01 -2	2.14 -4	1.28 -2	3.09 -3
33	1.63 -5	3.53 -4	2.48 -3	5.67 -3	3.15 -3	2.28 -4	3.00 -3	3.05 -4
34	3.93 -6	1.09 -4	7.57 -4	1.54 -3	5.91 -4	1.80 -4	2.76 -4	2.62 -3
35	6.15 -7	2.66 -5	1.84 -4	3.07 -4	4.65 -5	1.14 -4	2.95 -6	3.12 -3
36	6.14 -8	5.84 -6	4.00 -5	5.01 -5	4.06 -9	5.57 -5	4.39 -5	1.95 -3
37	4.77 -9	1.17 -6	7.95 -6	7.68 -6	1.11 -6	1.76 -5	2.45 -5	6.72 -4
38	2.53 -10	9.32 -8	6.34 -7	5.62 -7	1.53 -7	1.58 -6	2.47 -6	6.17 -5
$\sum_{v'} A_{v'v''}$	5.56 +7	5.52 +7	5.48 +7	5.45 +7	5.41 +7	5.38 +7	5.35 +7	5.32 +7

Table E.1: Spontaneous emission coefficient $A_{v'v''}$ for the ^{6}Li singlet case.

$v'\backslash v''$	8	9	10	11	12	13	14	15
0	1.45 +6	7.61 +5	3.86 +5	1.90 +5	9.20 +4	4.37 +4	2.05 +4	9.56 +3
1	5.86 +6	4.14 +6	2.67 +6	1.61 +6	9.24 +5	5.10 +5	2.73 +5	1.42 +5
2	4.87 +6	5.97 +6	5.69 +6	4.63 +6	3.37 +6	2.27 +6	1.43 +6	8.65 +5
3	3.88 +2	1.07 +6	3.11 +6	4.62 +6	5.04 +6	4.57 +6	3.66 +6	2.68 +6
4	3.92 +6	1.64 +6	7.78 +4	4.71 +5	2.03 +6	3.53 +6	4.29 +6	4.25 +6
5	9.01 +5	3.28 +6	3.43 +6	1.64 +6	1.75 +5	2.06 +5	1.36 +6	2.71 +6
6	2.42 +6	7.21 +4	1.01 +6	2.93 +6	3.02 +6	1.55 +6	2.45 +5	8.44 +4
7	1.54 +6	3.40 +6	1.48 +6	3.41 +2	1.12 +6	2.66 +6	2.67 +6	1.44 +6
8	2.01 +6	5.69 +4	2.27 +6	2.77 +6	8.15 +5	3.77 +4	1.22 +6	2.44 +6
9	1.48 +6	3.20 +6	4.79 +5	6.23 +5	2.54 +6	2.06 +6	3.83 +5	1.36 +5
10	2.65 +6	1.26 +5	2.80 +6	1.78 +6	1.07 +3	1.30 +6	2.43 +6	1.42 +6
11	7.02 +5	3.48 +6	2.27 +5	1.45 +6	2.59 +6	5.75 +5	2.34 +5	1.75 +6
12	4.36 +6	5.28 +3	3.05 +6	1.21 +6	3.12 +5	2.32 +6	1.54 +6	3.83 +4
13	4.01 +4	4.17 +6	3.49 +5	1.95 +6	2.17 +6	8.09 +3	1.42 +6	2.10 +6
14	5.92 +6	5.72 +5	3.27 +6	1.21 +6	8.39 +5	2.55 +6	4.23 +5	5.12 +5
15	1.01 +7	4.46 +6	1.37 +6	2.17 +6	2.03 +6	1.67 +5	2.30 +6	1.10 +6
16	4.28 +6	1.08 +7	3.28 +6	2.07 +6	1.21 +6	2.54 +6	4.05 +3	1.69 +6
17	5.10 +5	5.07 +6	1.15 +7	2.48 +6	2.53 +6	5.47 +5	2.65 +6	2.04 +5
18	2.01 +3	5.27 +5	5.67 +6	1.21 +7	2.01 +6	2.72 +6	1.81 +5	2.50 +6
19	3.54 +3	2.93 +2	4.71 +5	6.10 +6	1.29 +7	1.83 +6	2.65 +6	2.51 +4
20	1.42 +2	6.95 +3	1.00 +4	3.44 +5	6.24 +6	1.40 +7	1.98 +6	2.35 +6
21	4.32 +1	1.14 +1	1.02 +4	4.39 +4	1.63 +5	5.96 +6	1.52 +7	2.52 +6
22	2.40 +0	1.24 +2	1.19 +2	1.13 +4	1.12 +5	1.67 +4	5.12 +6	1.65 +7
23	1.40 +0	1.16 +0	1.81 +2	1.17 +3	6.88 +3	2.00 +5	5.47 +4	3.69 +6
24	3.36 -2	3.14 +0	2.03 +1	1.50 +2	4.24 +3	2.48 +2	2.63 +5	4.50 +5
25	5.99 -2	6.70 -1	9.42 -1	7.93 +1	2.92 +0	8.16 +3	1.02 +4	2.21 +5
26	4.11 -3	1.87 -2	2.24 +0	9.08 -1	1.83 +2	5.11 +2	8.22 +3	6.50 +4
27	5.54 -3	8.27 -2	4.77 -1	1.81 +0	3.24 +1	1.12 +2	3.35 +3	1.04 +3
28	8.02 -3	5.10 -3	1.73 -4	1.04 +0	2.74 -4	1.19 +2	4.18 +1	6.90 +3
29	2.79 -2	6.84 -3	7.89 -2	1.71 -1	2.51 +0	1.97 +1	1.32 +2	1.76 +3
30	1.15 -2	6.24 -3	8.85 -2	6.44 -3	1.79 +0	1.94 -1	1.11 +2	4.04 +1
31	2.33 -5	6.12 -6	3.96 -2	1.66 -3	5.67 -1	8.60 -1	3.16 +1	6.14 +1
32	8.12 -3	3.90 -3	8.74 -3	4.42 -3	9.46 -2	1.15 +0	4.15 +0	9.60 +1
33	1.56 -2	7.78 -3	5.17 -4	3.76 -3	3.29 -3	7.44 -1	6.21 -2	5.99 +1
34	1.47 -2	7.04 -3	1.44 -4	2.43 -3	2.72 -3	3.83 -1	1.73 -1	2.80 +1
35	9.54 -3	4.34 -3	5.01 -4	1.36 -3	6.46 -3	1.77 -1	2.87 -1	1.16 +1
36	4.62 -3	2.02 -3	3.93 -4	6.30 -4	4.69 -3	7.22 -2	1.86 -1	4.37 +0
37	1.44 -3	6.18 -4	1.45 -4	1.95 -4	1.69 -3	2.11 -2	6.43 -2	1.23 +0
38	1.30 -4	5.53 -5	1.34 -5	1.75 -5	1.56 -4	1.86 -3	5.91 -3	1.08 -1
$\sum_{v'} A_{v'v''}$	5.30 +7	5.28 +7	5.26 +7	5.24 +7	5.23 +7	5.22 +7	5.20 +7	5.20 +7

Table E.2: $A_{v'v''}$ for ^{6}Li singlet case (continued).

$v'\backslash v''$	16	17	18	19	20	21	22	23
0	4.43 +3	2.05 +3	9.45 +2	4.37 +2	2.03 +2	9.52 +1	4.49 +1	2.14 +1
1	7.32 +4	3.71 +4	1.86 +4	9.30 +3	4.62 +3	2.30 +3	1.14 +3	5.71 +2
2	5.04 +5	2.85 +5	1.58 +5	8.63 +4	4.65 +4	2.48 +4	1.32 +4	6.99 +3
3	1.84 +6	1.20 +6	7.50 +5	4.55 +5	2.70 +5	1.57 +5	9.00 +4	5.11 +4
4	3.68 +6	2.90 +6	2.13 +6	1.48 +6	9.86 +5	6.36 +5	4.00 +5	2.46 +5
5	3.60 +6	3.83 +6	3.55 +6	2.97 +6	2.31 +6	1.70 +6	1.20 +6	8.16 +5
6	9.21 +5	2.08 +6	2.98 +6	3.39 +6	3.32 +6	2.93 +6	2.40 +6	1.86 +6
7	2.89 +5	2.85 +4	6.26 +5	1.59 +6	2.45 +6	2.94 +6	3.03 +6	2.81 +6
8	2.37 +6	1.32 +6	3.16 +5	5.35 +3	4.20 +5	1.21 +6	1.99 +6	2.52 +6
9	1.29 +6	2.25 +6	2.11 +6	1.21 +6	3.33 +5	4.02 +1	2.71 +5	9.05 +5
10	1.38 +5	2.56 +5	1.33 +6	2.07 +6	1.90 +6	1.12 +6	3.49 +5	6.01 +3
11	2.09 +6	9.08 +5	2.69 +4	3.68 +5	1.32 +6	1.90 +6	1.72 +6	1.05 +6
12	7.20 +5	1.90 +6	1.65 +6	5.31 +5	5.94 +1	4.61 +5	1.28 +6	1.73 +6
13	5.71 +5	7.83 +4	1.16 +6	1.82 +6	1.22 +6	2.78 +5	2.14 +4	5.31 +5
14	1.98 +6	1.29 +6	7.59 +4	4.00 +5	1.41 +6	1.59 +6	8.53 +5	1.27 +5
15	4.30 +4	1.37 +6	1.71 +6	5.24 +5	2.04 +4	7.54 +5	1.47 +6	1.29 +6
16	1.67 +6	6.77 +4	6.86 +5	1.68 +6	1.06 +6	9.54 +4	2.19 +5	1.01 +6
17	1.01 +6	1.88 +6	4.05 +5	1.95 +5	1.30 +6	1.37 +6	4.45 +5	3.37 +3
18	5.55 +5	4.78 +5	1.80 +6	8.21 +5	5.25 +3	8.12 +5	1.41 +6	8.33 +5
19	2.21 +6	9.02 +5	1.55 +5	1.51 +6	1.15 +6	6.19 +4	3.86 +5	1.20 +6
20	2.30 +3	1.87 +6	1.15 +6	1.88 +4	1.16 +6	1.31 +6	2.53 +5	1.17 +5
21	1.91 +6	4.17 +4	1.59 +6	1.27 +6	4.15 +3	8.33 +5	1.33 +6	4.65 +5
22	3.64 +6	1.32 +6	1.08 +5	1.40 +6	1.29 +6	4.60 +4	5.76 +5	1.25 +6
23	1.75 +7	5.56 +6	6.70 +5	1.99 +5	1.34 +6	1.20 +6	9.74 +4	4.00 +5
24	1.84 +6	1.74 +7	8.51 +6	1.29 +5	3.52 +5	1.44 +6	1.03 +6	1.38 +5
25	1.24 +6	2.85 +5	1.52 +7	1.23 +7	5.84 +4	6.56 +5	1.83 +6	7.49 +5
26	6.70 +4	2.06 +6	2.73 +5	1.02 +7	1.57 +7	9.34 +5	1.29 +6	2.71 +6
27	1.50 +5	2.51 +4	2.07 +6	2.77 +6	3.77 +6	1.62 +7	2.86 +6	2.44 +6
28	1.01 +4	1.50 +5	5.02 +5	8.30 +5	6.44 +6	2.93 +4	1.16 +7	4.60 +6
29	3.11 +3	7.45 +4	1.51 +4	1.28 +6	4.26 +4	6.77 +6	2.95 +6	3.74 +6
30	5.21 +3	4.57 +3	1.15 +5	1.78 +5	9.81 +5	2.38 +6	2.00 +6	8.16 +6
31	1.90 +3	1.34 +3	5.93 +4	7.74 +3	8.45 +5	3.94 +2	4.56 +6	5.27 +5
32	3.06 +2	3.57 +3	1.21 +4	6.36 +4	2.33 +5	4.75 +5	1.91 +6	1.04 +6
33	1.05 +1	2.55 +3	7.12 +2	5.64 +4	2.12 +4	5.83 +5	2.70 +5	2.35 +6
34	6.17 +0	1.26 +3	1.00 +2	3.05 +4	4.31 +2	3.60 +5	1.92 +2	1.81 +6
35	1.42 +1	5.32 +2	3.92 +2	1.35 +4	5.30 +3	1.69 +5	2.98 +4	9.45 +5
36	9.84 +0	2.01 +2	3.00 +2	5.18 +3	4.63 +3	6.71 +4	3.22 +4	3.92 +5
37	3.47 +0	5.65 +1	1.08 +2	1.46 +3	1.74 +3	1.92 +4	1.28 +4	1.14 +5
38	3.20 -1	4.95 +0	1.01 +1	1.29 +2	1.63 +2	1.69 +3	1.21 +3	1.01 +4
$\sum_{v'} A_{v'v''}$	5.19 +7	5.19 +7	5.19 +7	5.18 +7	5.17 +7	5.16 +7	5.02 +7	4.90 +7

Table E.3: $A_{v'v''}$ for ^{6}Li singlet case (continued).

$v'\backslash v''$	24	25	26	27	28	29	30	31
0	1.03 +1	4.97 +0	2.41 +0	1.17 +0	5.69 -1	2.79 -1	1.39 -1	7.11 -2
1	2.86 +2	1.44 +2	7.33 +1	3.75 +1	1.94 +1	1.02 +1	5.43 +0	2.93 +0
2	3.70 +3	1.97 +3	1.05 +3	5.58 +2	3.00 +2	1.63 +2	8.92 +1	4.95 +1
3	2.88 +4	1.62 +4	9.09 +3	5.09 +3	2.85 +3	1.61 +3	9.17 +2	5.26 +2
4	1.50 +5	9.00 +4	5.36 +4	3.17 +4	1.87 +4	1.11 +4	6.55 +3	3.90 +3
5	5.42 +5	3.52 +5	2.25 +5	1.42 +5	8.87 +4	5.53 +4	3.44 +4	2.14 +4
6	1.38 +6	9.87 +5	6.88 +5	4.68 +5	3.13 +5	2.07 +5	1.36 +5	8.89 +4
7	2.42 +6	1.96 +6	1.52 +6	1.14 +6	8.26 +5	5.88 +5	4.13 +5	2.86 +5
8	2.72 +6	2.64 +6	2.37 +6	2.00 +6	1.62 +6	1.26 +6	9.55 +5	7.09 +5
9	1.60 +6	2.13 +6	2.40 +6	2.42 +6	2.25 +6	1.98 +6	1.66 +6	1.35 +6
10	1.64 +5	6.59 +5	1.26 +6	1.76 +6	2.07 +6	2.17 +6	2.10 +6	1.91 +6
11	3.69 +5	2.14 +4	8.78 +4	4.58 +5	9.48 +5	1.40 +6	1.72 +6	1.88 +6
12	1.55 +6	9.82 +5	3.87 +5	4.39 +4	3.60 +4	2.92 +5	6.78 +5	1.07 +6
13	1.23 +6	1.58 +6	1.41 +6	9.23 +5	4.03 +5	7.39 +4	7.24 +3	1.64 +5
14	6.28 +4	5.72 +5	1.17 +6	1.44 +6	1.29 +6	8.78 +5	4.31 +5	1.15 +5
15	5.66 +5	4.55 +4	1.08 +5	5.85 +5	1.07 +6	1.29 +6	1.17 +6	8.37 +5
16	1.39 +6	1.01 +6	3.59 +5	9.35 +3	1.45 +5	5.69 +5	9.73 +5	1.15 +6
17	4.86 +5	1.13 +6	1.21 +6	7.49 +5	2.15 +5	1.13 +2	1.64 +5	5.25 +5
18	9.31 +4	1.25 +5	7.15 +5	1.13 +6	1.00 +6	5.43 +5	1.28 +5	2.16 +3
19	1.09 +6	3.53 +5	2.94 +2	3.23 +5	8.39 +5	1.03 +6	8.05 +5	3.91 +5
20	8.76 +5	1.15 +6	6.29 +5	7.50 +4	7.64 +4	4.95 +5	8.65 +5	8.99 +5
21	8.87 +3	5.58 +5	1.06 +6	8.18 +5	2.51 +5	2.80 +1	2.14 +5	5.99 +5
22	6.37 +5	1.23 +4	3.09 +5	8.71 +5	8.92 +5	4.38 +5	5.08 +4	4.97 +4
23	1.12 +6	7.37 +5	6.97 +4	1.46 +5	6.63 +5	8.64 +5	5.73 +5	1.62 +5
24	2.94 +5	9.73 +5	7.71 +5	1.36 +5	5.51 +4	4.76 +5	7.70 +5	6.36 +5
25	1.68 +5	2.50 +5	8.41 +5	7.56 +5	1.85 +5	1.52 +4	3.33 +5	6.53 +5
26	3.74 +5	2.10 +5	2.69 +5	7.07 +5	7.13 +5	2.04 +5	2.20 +3	2.32 +5
27	4.50 +6	3.53 +4	3.31 +5	3.98 +5	5.47 +5	6.73 +5	1.89 +5	1.02 +1
28	3.84 +6	7.51 +6	2.26 +5	7.18 +5	8.03 +5	3.19 +5	6.80 +5	1.37 +5
29	3.77 +6	4.02 +6	1.09 +7	1.84 +6	1.83 +6	1.96 +6	4.80 +4	8.57 +5
30	2.73 +3	7.09 +5	1.52 +6	1.08 +7	4.64 +6	4.00 +6	4.80 +6	1.90 +5
31	5.30 +6	2.06 +6	4.42 +5	2.32 +5	4.40 +6	4.67 +6	5.36 +6	9.12 +6
32	5.08 +6	4.93 +4	1.01 +6	1.24 +6	4.42 +6	2.20 +4	5.89 +5	1.97 +6
33	1.31 +6	2.03 +6	1.39 +6	3.19 +5	1.69 +5	2.70 +6	2.35 +6	1.24 +6
34	5.23 +4	2.66 +6	3.69 +5	3.26 +4	2.03 +5	2.76 +6	3.63 +5	5.06 +4
35	3.83 +4	1.75 +6	1.64 +4	2.15 +5	3.06 +5	1.21 +6	1.21 +4	4.90 +5
36	7.23 +4	8.08 +5	3.99 +3	1.77 +5	1.62 +5	4.01 +5	9.18 +4	3.76 +5
37	3.24 +4	2.45 +5	5.21 +3	6.48 +4	4.98 +4	1.02 +5	4.84 +4	1.31 +5
38	3.13 +3	2.18 +4	5.85 +2	6.02 +3	4.44 +3	8.68 +3	4.80 +3	1.20 +4
$\sum_{v'} A_{v'v''}$	4.33 +7	4.04 +7	3.41 +7	3.32 +7	3.35 +7	3.37 +7	2.87 +7	2.83 +7

Table E.4: $A_{v'v''}$ for ^{6}Li singlet case (continued).

$v'\backslash v''$	32	33	34	35	36	37	38	39
0	3.81 -2	2.17 -2	1.34 -2	8.83 -3	6.17 -3	4.45 -3	3.24 -3	2.34 -3
1	1.61 +0	8.99 -1	5.10 -1	2.95 -1	1.74 -1	1.06 -1	6.60 -2	4.26 -2
2	2.79 +1	1.59 +1	9.26 +0	5.49 +0	3.31 +0	2.04 +0	1.28 +0	8.15 -1
3	3.05 +2	1.79 +2	1.06 +2	6.41 +1	3.92 +1	2.43 +1	1.54 +1	9.89 +0
4	2.34 +3	1.41 +3	8.64 +2	5.34 +2	3.34 +2	2.12 +2	1.36 +2	8.83 +1
5	1.33 +4	8.34 +3	5.26 +3	3.34 +3	2.14 +3	1.39 +3	9.08 +2	6.03 +2
6	5.80 +4	3.78 +4	2.48 +4	1.63 +4	1.08 +4	7.17 +3	4.81 +3	3.26 +3
7	1.97 +5	1.35 +5	9.19 +4	6.27 +4	4.29 +4	2.94 +4	2.03 +4	1.42 +4
8	5.19 +5	3.76 +5	2.70 +5	1.93 +5	1.38 +5	9.83 +4	7.01 +4	5.02 +4
9	1.07 +6	8.27 +5	6.30 +5	4.75 +5	3.55 +5	2.64 +5	1.96 +5	1.46 +5
10	1.67 +6	1.41 +6	1.16 +6	9.32 +5	7.39 +5	5.79 +5	4.50 +5	3.47 +5
11	1.89 +6	1.79 +6	1.63 +6	1.42 +6	1.21 +6	1.01 +6	8.32 +5	6.76 +5
12	1.38 +6	1.57 +6	1.64 +6	1.61 +6	1.52 +6	1.37 +6	1.21 +6	1.05 +6
13	4.51 +5	7.71 +5	1.05 +6	1.25 +6	1.37 +6	1.39 +6	1.36 +6	1.27 +6
14	5.40 +2	7.10 +4	2.65 +5	5.10 +5	7.48 +5	9.40 +5	1.07 +6	1.13 +6
15	4.59 +5	1.65 +5	1.72 +4	1.59 +4	1.24 +5	2.92 +5	4.74 +5	6.38 +5
16	1.07 +6	8.08 +5	4.93 +5	2.24 +5	5.67 +4	1.82 +2	3.55 +4	1.31 +5
17	8.56 +5	1.01 +6	9.64 +5	7.72 +5	5.22 +5	2.87 +5	1.15 +5	2.23 +4
18	1.66 +5	4.68 +5	7.40 +5	8.80 +5	8.66 +5	7.34 +5	5.43 +5	3.49 +5
19	7.74 +4	5.73 +3	1.50 +5	3.93 +5	6.16 +5	7.45 +5	7.59 +5	6.81 +5
20	6.34 +5	2.85 +5	5.04 +4	6.78 +3	1.23 +5	3.12 +5	4.91 +5	6.06 +5
21	8.20 +5	7.55 +5	4.97 +5	2.15 +5	3.71 +4	4.88 +3	8.91 +4	2.29 +5
22	3.37 +5	6.31 +5	7.35 +5	6.22 +5	3.94 +5	1.71 +5	3.28 +4	1.63 +3
23	7.70 +1	1.43 +5	4.14 +5	6.09 +5	6.33 +5	5.08 +5	3.18 +5	1.43 +5
24	2.78 +5	2.82 +4	3.51 +4	2.25 +5	4.38 +5	5.51 +5	5.31 +5	4.14 +5
25	6.38 +5	3.63 +5	9.04 +4	6.15 +2	9.75 +4	2.76 +5	4.22 +5	4.76 +5
26	5.35 +5	5.95 +5	4.04 +5	1.52 +5	1.07 +4	2.81 +4	1.50 +5	2.88 +5
27	1.69 +5	4.34 +5	5.31 +5	4.07 +5	1.94 +5	3.78 +4	2.61 +3	6.87 +4
28	3.75 +2	1.37 +5	3.54 +5	4.59 +5	3.81 +5	2.11 +5	6.29 +4	1.17 +3
29	4.69 +4	2.50 +3	1.35 +5	2.88 +5	3.93 +5	3.35 +5	2.05 +5	7.66 +4
30	1.57 +6	1.67 +4	2.65 +4	1.94 +5	2.09 +5	3.48 +5	2.74 +5	1.82 +5
31	1.99 +6	3.77 +6	7.07 +5	2.82 +5	5.02 +5	7.36 +4	3.76 +5	1.83 +5
32	9.12 +6	4.68 +6	7.75 +6	3.90 +6	1.89 +6	2.00 +6	6.40 +4	7.41 +5
33	7.64 +5	1.42 +6	1.95 +6	6.93 +6	7.68 +6	5.85 +6	6.83 +6	1.99 +6
34	5.38 +5	3.90 +6	1.26 +6	1.01 +6	6.77 +4	2.00 +6	3.73 +6	9.13 +6
35	7.70 +5	1.64 +6	3.77 +3	8.80 +4	1.65 +6	2.60 +6	1.46 +6	9.08 +5
36	3.53 +5	4.30 +5	9.88 +4	2.63 +5	1.05 +6	8.22 +5	1.02 +5	1.01 +4
37	9.93 +4	9.24 +4	6.49 +4	1.14 +5	3.23 +5	1.79 +5	1.70 +3	4.46 +4
38	8.64 +3	7.52 +3	6.66 +3	1.08 +4	2.87 +4	1.45 +4	8.52 +0	5.32 +3
$\sum_{v'} A_{v'v''}$	2.86 +7	2.88 +7	2.42 +7	2.46 +7	2.44 +7	2.41 +7	2.23 +7	2.20 +7

Table E.5: $A_{v'v''}$ for ^{6}Li singlet case (continued).

$v'\backslash v''$	40	41	42	43	44	45	46	47
0	1.64 -3	1.11 -3	7.16 -4	4.40 -4	2.56 -4	1.40 -4	7.10 -5	3.26 -5
1	2.85 -2	1.96 -2	1.40 -2	1.01 -2	7.52 -3	5.66 -3	4.30 -3	3.29 -3
2	5.29 -1	3.50 -1	2.36 -1	1.62 -1	1.13 -1	8.10 -2	5.89 -2	4.36 -2
3	6.47 +0	4.31 +0	2.92 +0	2.01 +0	1.41 +0	1.00 +0	7.28 -1	5.35 -1
4	5.82 +1	3.89 +1	2.65 +1	1.83 +1	1.28 +1	9.18 +0	6.68 +0	4.94 +0
5	4.05 +2	2.76 +2	1.90 +2	1.33 +2	9.40 +1	6.76 +1	4.93 +1	3.64 +1
6	2.22 +3	1.53 +3	1.07 +3	7.57 +2	5.43 +2	3.95 +2	2.92 +2	2.18 +2
7	9.92 +3	7.01 +3	5.00 +3	3.60 +3	2.61 +3	1.92 +3	1.43 +3	1.08 +3
8	3.60 +4	2.60 +4	1.89 +4	1.39 +4	1.03 +4	7.67 +3	5.81 +3	4.44 +3
9	1.08 +5	8.05 +4	6.01 +4	4.51 +4	3.40 +4	2.59 +4	1.98 +4	1.53 +4
10	2.67 +5	2.05 +5	1.58 +5	1.21 +5	9.38 +4	7.30 +4	5.72 +4	4.50 +4
11	5.44 +5	4.34 +5	3.46 +5	2.75 +5	2.18 +5	1.74 +5	1.39 +5	1.11 +5
12	8.89 +5	7.45 +5	6.19 +5	5.10 +5	4.19 +5	3.43 +5	2.82 +5	2.31 +5
13	1.16 +6	1.03 +6	9.00 +5	7.77 +5	6.64 +5	5.64 +5	4.77 +5	4.02 +5
14	1.14 +6	1.10 +6	1.04 +6	9.48 +5	8.52 +5	7.57 +5	6.65 +5	5.80 +5
15	7.63 +5	8.42 +5	8.77 +5	8.75 +5	8.44 +5	7.96 +5	7.36 +5	6.71 +5
16	2.52 +5	3.74 +5	4.77 +5	5.53 +5	6.00 +5	6.20 +5	6.19 +5	6.00 +5
17	6.55 +2	3.19 +4	9.39 +4	1.67 +5	2.37 +5	2.96 +5	3.40 +5	3.68 +5
18	1.87 +5	7.62 +4	1.68 +4	4.11 -1	1.26 +4	4.19 +4	7.78 +4	1.13 +5
19	5.47 +5	3.97 +5	2.59 +5	1.49 +5	7.27 +4	2.67 +4	4.90 +3	9.78 +1
20	6.41 +5	6.06 +5	5.23 +5	4.18 +5	3.13 +5	2.20 +5	1.45 +5	8.91 +4
21	3.68 +5	4.66 +5	5.12 +5	5.07 +5	4.65 +5	4.03 +5	3.34 +5	2.66 +5
22	5.43 +4	1.50 +5	2.50 +5	3.29 +5	3.75 +5	3.90 +5	3.79 +5	3.50 +5
23	3.42 +4	3.37 +0	2.48 +4	8.22 +4	1.48 +5	2.05 +5	2.46 +5	2.67 +5
24	2.62 +5	1.28 +5	4.04 +4	2.90 +3	5.56 +3	3.26 +4	6.95 +4	1.06 +5
25	4.37 +5	3.38 +5	2.22 +5	1.21 +5	5.02 +4	1.19 +4	6.14 +1	5.98 +3
26	3.77 +5	3.95 +5	3.53 +5	2.76 +5	1.91 +5	1.17 +5	6.16 +4	2.57 +4
27	1.76 +5	2.70 +5	3.18 +5	3.17 +5	2.80 +5	2.25 +5	1.66 +5	1.13 +5
28	2.54 +4	9.80 +4	1.76 +5	2.32 +5	2.54 +5	2.47 +5	2.19 +5	1.81 +5
29	8.09 +3	6.76 +3	5.01 +4	1.08 +5	1.57 +5	1.86 +5	1.95 +5	1.86 +5
30	7.57 +4	1.39 +4	9.35 +2	2.41 +4	6.28 +4	1.01 +5	1.28 +5	1.41 +5
31	1.59 +5	6.10 +4	1.54 +4	1.08 +1	1.16 +4	3.64 +4	6.28 +4	8.38 +4
32	3.31 +4	1.89 +5	2.68 +4	1.63 +4	5.21 +0	6.04 +3	2.21 +4	3.91 +4
33	2.84 +6	2.92 +5	6.22 +5	1.82 +4	5.33 +4	5.08 +3	1.46 +3	1.71 +4
34	6.50 +6	8.99 +6	4.20 +6	3.84 +6	1.33 +6	7.38 +5	2.49 +5	4.04 +4
35	2.35 +5	1.09 +6	5.80 +6	7.09 +6	1.00 +7	8.26 +6	6.46 +6	4.15 +6
36	1.22 +6	1.49 +6	2.61 +6	9.51 +5	1.71 +5	5.03 +5	2.72 +6	6.12 +6
37	5.21 +5	4.54 +5	5.47 +5	4.84 +4	3.78 +4	6.66 +5	1.37 +6	1.67 +6
38	4.91 +4	3.94 +4	4.33 +4	1.86 +3	7.09 +3	7.02 +4	1.25 +5	1.33 +5
$\sum_{v'} A_{v'v''}$	1.99 +7	2.04 +7	2.12 +7	1.88 +7	1.80 +7	1.62 +7	1.64 +7	1.71 +7

Table E.6: $A_{v'v''}$ for ^{6}Li singlet case (continued).

$v'\backslash v''$	48	49	50	51	52	53	54	55
0	1.29 -5	3.96 -6	6.47 -7	2.92 -9	4.32 -7	1.13 -6	1.77 -6	2.25 -6
1	2.53 -3	1.95 -3	1.52 -3	1.18 -3	9.24 -4	7.27 -4	5.78 -4	4.65 -4
2	3.27 -2	2.50 -2	1.94 -2	1.52 -2	1.21 -2	9.71 -3	7.92 -3	6.57 -3
3	3.99 -1	3.01 -1	2.32 -1	1.80 -1	1.42 -1	1.13 -1	9.15 -2	7.54 -2
4	3.70 +0	2.81 +0	2.17 +0	1.70 +0	1.34 +0	1.07 +0	8.71 -1	7.19 -1
5	2.72 +1	2.07 +1	1.59 +1	1.24 +1	9.79 +0	7.82 +0	6.34 +0	5.23 +0
6	1.65 +2	1.27 +2	9.84 +1	7.75 +1	6.15 +1	4.94 +1	4.02 +1	3.33 +1
7	8.17 +2	6.28 +2	4.90 +2	3.87 +2	3.08 +2	2.48 +2	2.03 +2	1.68 +2
8	3.42 +3	2.67 +3	2.11 +3	1.68 +3	1.35 +3	1.09 +3	8.98 +2	7.49 +2
9	1.19 +4	9.37 +3	7.45 +3	5.98 +3	4.83 +3	3.95 +3	3.26 +3	2.74 +3
10	3.56 +4	2.84 +4	2.29 +4	1.86 +4	1.52 +4	1.25 +4	1.04 +4	8.79 +3
11	8.96 +4	7.25 +4	5.92 +4	4.87 +4	4.01 +4	3.34 +4	2.80 +4	2.39 +4
12	1.90 +5	1.56 +5	1.30 +5	1.08 +5	9.03 +4	7.58 +4	6.43 +4	5.52 +4
13	3.38 +5	2.85 +5	2.41 +5	2.04 +5	1.73 +5	1.47 +5	1.26 +5	1.10 +5
14	5.02 +5	4.34 +5	3.75 +5	3.24 +5	2.79 +5	2.41 +5	2.10 +5	1.84 +5
15	6.03 +5	5.38 +5	4.78 +5	4.24 +5	3.73 +5	3.28 +5	2.91 +5	2.59 +5
16	5.68 +5	5.30 +5	4.89 +5	4.48 +5	4.06 +5	3.66 +5	3.31 +5	3.00 +5
17	3.80 +5	3.80 +5	3.72 +5	3.57 +5	3.37 +5	3.15 +5	2.93 +5	2.74 +5
18	1.43 +5	1.66 +5	1.82 +5	1.91 +5	1.94 +5	1.92 +5	1.88 +5	1.83 +5
19	5.80 +3	1.68 +4	2.96 +4	4.18 +4	5.22 +4	6.02 +4	6.62 +4	7.07 +4
20	5.00 +4	2.50 +4	1.03 +4	2.90 +3	1.98 +2	3.39 +2	2.00 +3	4.39 +3
21	2.04 +5	1.53 +5	1.12 +5	8.03 +4	5.63 +4	3.88 +4	2.63 +4	1.76 +4
22	3.10 +5	2.68 +5	2.27 +5	1.89 +5	1.55 +5	1.26 +5	1.03 +5	8.43 +4
23	2.72 +5	2.64 +5	2.48 +5	2.28 +5	2.04 +5	1.81 +5	1.60 +5	1.41 +5
24	1.35 +5	1.55 +5	1.66 +5	1.69 +5	1.66 +5	1.59 +5	1.50 +5	1.41 +5
25	2.12 +4	3.94 +4	5.66 +4	7.07 +4	8.06 +4	8.66 +4	8.97 +4	9.10 +4
26	6.82 +3	2.65 +2	1.49 +3	6.88 +3	1.38 +4	2.07 +4	2.68 +4	3.19 +4
27	7.08 +4	4.04 +4	2.04 +4	8.50 +3	2.41 +3	1.74 +2	2.62 +2	1.63 +3
28	1.41 +5	1.05 +5	7.46 +4	5.11 +4	3.35 +4	2.10 +4	1.26 +4	7.10 +3
29	1.66 +5	1.41 +5	1.16 +5	9.23 +4	7.16 +4	5.45 +4	4.11 +4	3.08 +4
30	1.43 +5	1.35 +5	1.22 +5	1.07 +5	9.05 +4	7.55 +4	6.24 +4	5.15 +4
31	9.66 +4	1.01 +5	1.00 +5	9.42 +4	8.57 +4	7.61 +4	6.68 +4	5.83 +4
32	5.36 +4	6.33 +4	6.82 +4	6.90 +4	6.66 +4	6.24 +4	5.73 +4	5.22 +4
33	2.39 +4	3.45 +4	4.04 +4	4.40 +4	4.49 +4	4.40 +4	4.20 +4	3.96 +4
34	5.45 +4	4.59 +3	2.91 +4	2.22 +4	2.80 +4	2.71 +4	2.71 +4	2.62 +4
35	1.98 +6	1.14 +6	2.56 +5	2.13 +5	4.91 +3	4.68 +4	6.50 +3	1.99 +4
36	9.25 +6	9.68 +6	9.36 +6	6.42 +6	4.86 +6	2.35 +6	1.51 +6	4.68 +5
37	1.22 +6	2.88 +5	1.96 +4	1.07 +6	2.95 +6	5.87 +6	7.36 +6	8.66 +6
38	7.57 +4	5.61 +3	2.10 +4	1.65 +5	3.29 +5	5.02 +5	4.66 +5	3.68 +5
$\sum_{v'} A_{v'v''}$	1.71 +7	1.53 +7	1.34 +7	1.13 +7	1.12 +7	1.15 +7	1.18 +7	1.18 +7

Table E.7: $A_{v'v''}$ for ^{6}Li singlet case (continued).

$v'\backslash v''$	56	57	58	59	60	61	62	63
0	2.55 -6	2.67 -6	2.65 -6	2.52 -6	2.31 -6	2.05 -6	1.77 -6	1.51 -6
1	3.77 -4	3.06 -4	2.48 -4	2.01 -4	1.62 -4	1.30 -4	1.03 -4	8.22 -5
2	5.50 -3	4.62 -3	3.89 -3	3.26 -3	2.72 -3	2.26 -3	1.85 -3	1.51 -3
3	6.27 -2	5.23 -2	4.38 -2	3.67 -2	3.05 -2	2.52 -2	2.06 -2	1.69 -2
4	5.99 -1	5.01 -1	4.20 -1	3.51 -1	2.92 -1	2.41 -1	1.97 -1	1.61 -1
5	4.36 +0	3.65 +0	3.06 +0	2.56 +0	2.14 +0	1.77 +0	1.45 +0	1.18 +0
6	2.78 +1	2.33 +1	1.96 +1	1.64 +1	1.37 +1	1.13 +1	9.25 +0	7.58 +0
7	1.41 +2	1.19 +2	1.00 +2	8.41 +1	7.04 +1	5.84 +1	4.79 +1	3.93 +1
8	6.30 +2	5.32 +2	4.49 +2	3.78 +2	3.17 +2	2.63 +2	2.16 +2	1.78 +2
9	2.32 +3	1.97 +3	1.67 +3	1.41 +3	1.19 +3	9.92 +2	8.17 +2	6.74 +2
10	7.47 +3	6.37 +3	5.43 +3	4.61 +3	3.89 +3	3.25 +3	2.68 +3	2.22 +3
11	2.05 +4	1.75 +4	1.50 +4	1.29 +4	1.09 +4	9.15 +3	7.59 +3	6.28 +3
12	4.77 +4	4.12 +4	3.55 +4	3.05 +4	2.60 +4	2.19 +4	1.82 +4	1.52 +4
13	9.55 +4	8.31 +4	7.23 +4	6.25 +4	5.36 +4	4.54 +4	3.79 +4	3.16 +4
14	1.62 +5	1.43 +5	1.25 +5	1.09 +5	9.43 +4	8.04 +4	6.75 +4	5.66 +4
15	2.31 +5	2.06 +5	1.82 +5	1.60 +5	1.40 +5	1.20 +5	1.01 +5	8.53 +4
16	2.73 +5	2.46 +5	2.21 +5	1.97 +5	1.73 +5	1.50 +5	1.28 +5	1.08 +5
17	2.54 +5	2.34 +5	2.14 +5	1.94 +5	1.73 +5	1.51 +5	1.30 +5	1.11 +5
18	1.76 +5	1.67 +5	1.57 +5	1.46 +5	1.32 +5	1.18 +5	1.03 +5	8.92 +4
19	7.35 +4	7.45 +4	7.38 +4	7.14 +4	6.75 +4	6.21 +4	5.56 +4	4.92 +4
20	7.01 +3	9.48 +3	1.16 +4	1.31 +4	1.40 +4	1.42 +4	1.37 +4	1.29 +4
21	1.14 +4	7.14 +3	4.24 +3	2.37 +3	1.21 +3	5.47 +2	2.07 +2	5.69 +1
22	6.89 +4	5.60 +4	4.53 +4	3.64 +4	2.90 +4	2.29 +4	1.79 +4	1.40 +4
23	1.24 +5	1.08 +5	9.37 +4	8.05 +4	6.84 +4	5.73 +4	4.73 +4	3.90 +4
24	1.31 +5	1.20 +5	1.09 +5	9.78 +4	8.63 +4	7.48 +4	6.36 +4	5.38 +4
25	9.03 +4	8.77 +4	8.37 +4	7.82 +4	7.16 +4	6.41 +4	5.60 +4	4.85 +4
26	3.59 +4	3.85 +4	3.98 +4	3.98 +4	3.85 +4	3.60 +4	3.27 +4	2.92 +4
27	3.60 +3	5.72 +3	7.67 +3	9.22 +3	1.02 +4	1.07 +4	1.05 +4	9.97 +3
28	3.60 +3	1.54 +3	4.67 +2	4.97 +1	2.16 +1	1.85 +2	3.98 +2	5.87 +2
29	2.28 +4	1.66 +4	1.19 +4	8.35 +3	5.75 +3	3.89 +3	2.59 +3	1.73 +3
30	4.21 +4	3.42 +4	2.75 +4	2.18 +4	1.72 +4	1.34 +4	1.03 +4	7.96 +3
31	5.05 +4	4.32 +4	3.66 +4	3.07 +4	2.55 +4	2.08 +4	1.68 +4	1.35 +4
32	4.70 +4	4.17 +4	3.66 +4	3.17 +4	2.71 +4	2.28 +4	1.88 +4	1.55 +4
33	3.68 +4	3.36 +4	3.02 +4	2.68 +4	2.34 +4	2.00 +4	1.68 +4	1.41 +4
34	2.49 +4	2.32 +4	2.13 +4	1.92 +4	1.70 +4	1.48 +4	1.26 +4	1.06 +4
35	1.26 +4	1.44 +4	1.25 +4	1.17 +4	1.04 +4	9.09 +3	7.79 +3	6.62 +3
36	3.41 +5	5.69 +4	7.39 +4	1.36 +3	1.72 +4	1.33 +3	5.52 +3	2.71 +3
37	7.96 +6	7.71 +6	6.09 +6	5.15 +6	3.48 +6	2.56 +6	1.38 +6	8.11 +5
38	1.60 +5	3.69 +4	1.42 +4	1.77 +5	6.50 +5	1.37 +6	2.54 +6	3.67 +6
$\sum_{v'} A_{v'v''}$	1.05 +7	9.66 +6	7.85 +6	6.82 +6	5.47 +6	5.08 +6	4.91 +6	5.32 +6

Table E.8: $A_{v'v''}$ for ^{6}Li singlet case (continued).

$v'\backslash v''$	64	65	66	67	68	69	70	71
0	1.31 -6	1.18 -6	1.06 -6	9.55 -7	8.54 -7	7.52 -7	6.47 -7	5.52 -7
1	6.79 -5	5.84 -5	5.06 -5	4.41 -5	3.82 -5	3.29 -5	2.77 -5	2.32 -5
2	1.28 -3	1.13 -3	1.00 -3	8.91 -4	7.89 -4	6.91 -4	5.92 -4	5.04 -4
3	1.43 -2	1.26 -2	1.11 -2	9.89 -3	8.75 -3	7.66 -3	6.56 -3	5.58 -3
4	1.37 -1	1.20 -1	1.06 -1	9.44 -2	8.35 -2	7.31 -2	6.25 -2	5.32 -2
5	1.00 +0	8.84 -1	7.83 -1	6.97 -1	6.17 -1	5.40 -1	4.63 -1	3.94 -1
6	6.42 +0	5.65 +0	5.01 +0	4.45 +0	3.94 +0	3.45 +0	2.95 +0	2.51 +0
7	3.34 +1	2.94 +1	2.61 +1	2.33 +1	2.06 +1	1.81 +1	1.55 +1	1.32 +1
8	1.51 +2	1.33 +2	1.18 +2	1.05 +2	9.33 +1	8.18 +1	7.02 +1	5.98 +1
9	5.74 +2	5.07 +2	4.51 +2	4.03 +2	3.58 +2	3.14 +2	2.70 +2	2.30 +2
10	1.89 +3	1.67 +3	1.49 +3	1.33 +3	1.18 +3	1.04 +3	8.95 +2	7.64 +2
11	5.37 +3	4.77 +3	4.26 +3	3.81 +3	3.40 +3	2.99 +3	2.57 +3	2.20 +3
12	1.30 +4	1.16 +4	1.03 +4	9.29 +3	8.29 +3	7.31 +3	6.30 +3	5.39 +3
13	2.72 +4	2.43 +4	2.18 +4	1.96 +4	1.75 +4	1.55 +4	1.34 +4	1.14 +4
14	4.88 +4	4.37 +4	3.93 +4	3.55 +4	3.18 +4	2.82 +4	2.44 +4	2.09 +4
15	7.40 +4	6.65 +4	6.00 +4	5.43 +4	4.88 +4	4.33 +4	3.76 +4	3.23 +4
16	9.44 +4	8.52 +4	7.73 +4	7.02 +4	6.34 +4	5.64 +4	4.91 +4	4.23 +4
17	9.77 +4	8.88 +4	8.10 +4	7.39 +4	6.70 +4	5.99 +4	5.23 +4	4.53 +4
18	7.91 +4	7.25 +4	6.67 +4	6.14 +4	5.60 +4	5.04 +4	4.42 +4	3.84 +4
19	4.44 +4	4.14 +4	3.86 +4	3.59 +4	3.32 +4	3.01 +4	2.67 +4	2.33 +4
20	1.22 +4	1.18 +4	1.14 +4	1.10 +4	1.04 +4	9.68 +3	8.75 +3	7.79 +3
21	5.92 +0	2.62 +0	2.47 +1	5.96 +1	9.85 +1	1.34 +2	1.59 +2	1.74 +2
22	1.14 +4	9.61 +3	8.19 +3	7.00 +3	5.97 +3	5.05 +3	4.18 +3	3.46 +3
23	3.32 +4	2.93 +4	2.60 +4	2.31 +4	2.04 +4	1.79 +4	1.53 +4	1.30 +4
24	4.68 +4	4.21 +4	3.81 +4	3.45 +4	3.10 +4	2.75 +4	2.39 +4	2.05 +4
25	4.30 +4	3.94 +4	3.62 +4	3.33 +4	3.03 +4	2.72 +4	2.39 +4	2.07 +4
26	2.66 +4	2.49 +4	2.33 +4	2.18 +4	2.02 +4	1.84 +4	1.63 +4	1.43 +4
27	9.54 +3	9.33 +3	9.07 +3	8.76 +3	8.34 +3	7.78 +3	7.04 +3	6.29 +3
28	7.47 +2	8.99 +2	1.03 +3	1.13 +3	1.19 +3	1.21 +3	1.17 +3	1.11 +3
29	1.19 +3	8.47 +2	6.00 +2	4.21 +2	2.90 +2	1.96 +2	1.28 +2	8.28 +1
30	6.37 +3	5.31 +3	4.45 +3	3.75 +3	3.15 +3	2.63 +3	2.15 +3	1.75 +3
31	1.13 +4	9.74 +3	8.48 +3	7.40 +3	6.44 +3	5.53 +3	4.66 +3	3.91 +3
32	1.32 +4	1.16 +4	1.03 +4	9.14 +3	8.07 +3	7.05 +3	6.01 +3	5.10 +3
33	1.21 +4	1.08 +4	9.68 +3	8.68 +3	7.74 +3	6.81 +3	5.86 +3	5.00 +3
34	9.22 +3	8.28 +3	7.47 +3	6.74 +3	6.05 +3	5.35 +3	4.63 +3	3.97 +3
35	5.78 +3	5.22 +3	4.73 +3	4.29 +3	3.86 +3	3.43 +3	2.97 +3	2.56 +3
36	2.99 +3	2.52 +3	2.35 +3	2.12 +3	1.92 +3	1.71 +3	1.48 +3	1.28 +3
37	2.90 +5	1.51 +5	4.41 +4	3.31 +4	5.61 +3	7.32 +3	2.59 +2	1.62 +3
38	4.52 +6	4.67 +6	4.88 +6	4.92 +6	5.04 +6	5.05 +6	5.20 +6	4.92 +6
$\sum_{v'} A_{v'v''}$	5.54 +6	5.49 +6	5.53 +6	5.50 +6	5.54 +6	5.50 +6	5.58 +6	5.26 +6

Table E.9: $A_{v'v''}$ for ^{6}Li singlet case (continued).

$v'\backslash v''$	72	73	74	75	76	77	78	79
0	4.78 -7	4.09 -7	3.52 -7	3.01 -7	2.56 -7	2.18 -7	1.84 -7	1.55 -7
1	1.98 -5	1.68 -5	1.42 -5	1.21 -5	1.02 -5	8.62 -6	7.26 -6	6.09 -6
2	4.35 -4	3.73 -4	3.20 -4	2.74 -4	2.33 -4	1.98 -4	1.68 -4	1.42 -4
3	4.82 -3	4.13 -3	3.54 -3	3.03 -3	2.58 -3	2.19 -3	1.86 -3	1.57 -3
4	4.59 -2	3.93 -2	3.37 -2	2.89 -2	2.46 -2	2.09 -2	1.77 -2	1.49 -2
5	3.41 -1	2.92 -1	2.50 -1	2.14 -1	1.83 -1	1.55 -1	1.32 -1	1.11 -1
6	2.17 +0	1.86 +0	1.60 +0	1.36 +0	1.16 +0	9.88 -1	8.37 -1	7.06 -1
7	1.14 +1	9.80 +0	8.42 +0	7.21 +0	6.15 +0	5.23 +0	4.43 +0	3.74 +0
8	5.17 +1	4.43 +1	3.81 +1	3.26 +1	2.78 +1	2.36 +1	2.00 +1	1.69 +1
9	1.99 +2	1.71 +2	1.47 +2	1.26 +2	1.08 +2	9.15 +1	7.76 +1	6.55 +1
10	6.62 +2	5.68 +2	4.89 +2	4.19 +2	3.57 +2	3.04 +2	2.58 +2	2.18 +2
11	1.91 +3	1.64 +3	1.41 +3	1.21 +3	1.03 +3	8.80 +2	7.47 +2	6.31 +2
12	4.68 +3	4.02 +3	3.47 +3	2.98 +3	2.54 +3	2.17 +3	1.84 +3	1.55 +3
13	9.94 +3	8.56 +3	7.38 +3	6.34 +3	5.42 +3	4.62 +3	3.92 +3	3.32 +3
14	1.82 +4	1.57 +4	1.36 +4	1.16 +4	9.97 +3	8.50 +3	7.22 +3	6.11 +3
15	2.82 +4	2.43 +4	2.10 +4	1.81 +4	1.55 +4	1.32 +4	1.13 +4	9.53 +3
16	3.70 +4	3.20 +4	2.77 +4	2.39 +4	2.05 +4	1.75 +4	1.49 +4	1.26 +4
17	3.97 +4	3.44 +4	2.98 +4	2.58 +4	2.21 +4	1.89 +4	1.61 +4	1.37 +4
18	3.38 +4	2.94 +4	2.56 +4	2.21 +4	1.91 +4	1.63 +4	1.39 +4	1.18 +4
19	2.07 +4	1.81 +4	1.58 +4	1.37 +4	1.19 +4	1.02 +4	8.72 +3	7.42 +3
20	7.00 +3	6.20 +3	5.48 +3	4.81 +3	4.18 +3	3.62 +3	3.11 +3	2.66 +3
21	1.83 +2	1.84 +2	1.80 +2	1.71 +2	1.59 +2	1.46 +2	1.31 +2	1.16 +2
22	2.91 +3	2.43 +3	2.04 +3	1.71 +3	1.44 +3	1.20 +3	1.01 +3	8.39 +2
23	1.12 +4	9.59 +3	8.23 +3	7.03 +3	5.98 +3	5.08 +3	4.30 +3	3.62 +3
24	1.79 +4	1.54 +4	1.33 +4	1.15 +4	9.81 +3	8.37 +3	7.11 +3	6.02 +3
25	1.82 +4	1.58 +4	1.37 +4	1.19 +4	1.02 +4	8.73 +3	7.45 +3	6.31 +3
26	1.27 +4	1.11 +4	9.70 +3	8.43 +3	7.28 +3	6.26 +3	5.36 +3	4.56 +3
27	5.65 +3	5.01 +3	4.44 +3	3.89 +3	3.39 +3	2.94 +3	2.53 +3	2.16 +3
28	1.05 +3	9.64 +2	8.81 +2	7.94 +2	7.08 +2	6.24 +2	5.46 +2	4.73 +2
29	5.42 +1	3.50 +1	2.26 +1	1.45 +1	9.23 +0	5.88 +0	3.74 +0	2.38 +0
30	1.46 +3	1.20 +3	1.00 +3	8.33 +2	6.92 +2	5.75 +2	4.78 +2	3.97 +2
31	3.33 +3	2.82 +3	2.39 +3	2.02 +3	1.71 +3	1.44 +3	1.21 +3	1.02 +3
32	4.39 +3	3.75 +3	3.21 +3	2.74 +3	2.32 +3	1.97 +3	1.67 +3	1.40 +3
33	4.33 +3	3.72 +3	3.20 +3	2.74 +3	2.33 +3	1.98 +3	1.68 +3	1.42 +3
34	3.45 +3	2.97 +3	2.56 +3	2.20 +3	1.88 +3	1.60 +3	1.36 +3	1.15 +3
35	2.23 +3	1.92 +3	1.66 +3	1.43 +3	1.22 +3	1.04 +3	8.86 +2	7.50 +2
36	1.11 +3	9.61 +2	8.31 +2	7.15 +2	6.12 +2	5.22 +2	4.44 +2	3.76 +2
37	8.02 +1	4.95 +2	2.00 +2	2.55 +2	1.88 +2	1.71 +2	1.43 +2	1.21 +2
38	4.42 +6	3.86 +6	3.38 +6	2.79 +6	2.30 +6	1.80 +6	1.38 +6	1.00 +6
$\sum_{v'} A_{v'v''}$	4.71 +6	4.12 +6	3.60 +6	2.98 +6	2.46 +6	1.93 +6	1.50 +6	1.10 +6

Table E.10: $A_{v'v''}$ for ^{6}Li singlet case (continued).

$v'\backslash v''$	80	81	82	83	84	85	86	87
0	1.30 -7	1.09 -7	9.00 -8	7.42 -8	6.07 -8	4.93 -8	3.97 -8	3.23 -8
1	5.09 -6	4.23 -6	3.50 -6	2.88 -6	2.35 -6	1.91 -6	1.53 -6	1.22 -6
2	1.19 -4	9.91 -5	8.22 -5	6.78 -5	5.55 -5	4.51 -5	3.63 -5	2.90 -5
3	1.31 -3	1.10 -3	9.10 -4	7.51 -4	6.14 -4	4.99 -4	4.02 -4	3.21 -4
4	1.25 -2	1.04 -2	8.66 -3	7.14 -3	5.85 -3	4.75 -3	3.83 -3	3.05 -3
5	9.31 -2	7.77 -2	6.45 -2	5.31 -2	4.35 -2	3.53 -2	2.85 -2	2.27 -2
6	5.92 -1	4.94 -1	4.10 -1	3.38 -1	2.77 -1	2.25 -1	1.81 -1	1.45 -1
7	3.14 +0	2.62 +0	2.17 +0	1.79 +0	1.47 +0	1.19 +0	9.60 -1	7.66 -1
8	1.42 +1	1.18 +1	9.82 +0	8.10 +0	6.63 +0	5.39 +0	4.34 +0	3.46 +0
9	5.50 +1	4.59 +1	3.81 +1	3.14 +1	2.57 +1	2.09 +1	1.69 +1	1.35 +1
10	1.83 +2	1.53 +2	1.27 +2	1.04 +2	8.56 +1	6.95 +1	5.60 +1	4.47 +1
11	5.30 +2	4.42 +2	3.67 +2	3.03 +2	2.48 +2	2.02 +2	1.63 +2	1.30 +2
12	1.31 +3	1.09 +3	9.06 +2	7.47 +2	6.12 +2	4.98 +2	4.01 +2	3.20 +2
13	2.79 +3	2.33 +3	1.94 +3	1.60 +3	1.31 +3	1.06 +3	8.58 +2	6.85 +2
14	5.14 +3	4.30 +3	3.57 +3	2.95 +3	2.41 +3	1.96 +3	1.58 +3	1.26 +3
15	8.02 +3	6.71 +3	5.57 +3	4.60 +3	3.77 +3	3.07 +3	2.47 +3	1.98 +3
16	1.06 +4	8.88 +3	7.39 +3	6.10 +3	5.00 +3	4.07 +3	3.28 +3	2.62 +3
17	1.15 +4	9.64 +3	8.02 +3	6.63 +3	5.44 +3	4.43 +3	3.57 +3	2.85 +3
18	9.98 +3	8.37 +3	6.97 +3	5.76 +3	4.73 +3	3.85 +3	3.11 +3	2.48 +3
19	6.27 +3	5.26 +3	4.39 +3	3.63 +3	2.98 +3	2.43 +3	1.96 +3	1.57 +3
20	2.26 +3	1.90 +3	1.59 +3	1.32 +3	1.09 +3	8.86 +2	7.16 +2	5.73 +2
21	1.02 +2	8.81 +1	7.52 +1	6.34 +1	5.29 +1	4.37 +1	3.56 +1	2.87 +1
22	6.97 +2	5.77 +2	4.76 +2	3.90 +2	3.18 +2	2.57 +2	2.06 +2	1.64 +2
23	3.04 +3	2.53 +3	2.10 +3	1.73 +3	1.42 +3	1.15 +3	9.26 +2	7.39 +2
24	5.06 +3	4.23 +3	3.52 +3	2.90 +3	2.38 +3	1.93 +3	1.56 +3	1.25 +3
25	5.32 +3	4.46 +3	3.71 +3	3.07 +3	2.52 +3	2.05 +3	1.65 +3	1.32 +3
26	3.85 +3	3.24 +3	2.70 +3	2.23 +3	1.84 +3	1.50 +3	1.21 +3	9.65 +2
27	1.83 +3	1.54 +3	1.29 +3	1.07 +3	8.82 +2	7.20 +2	5.82 +2	4.66 +2
28	4.06 +2	3.45 +2	2.91 +2	2.43 +2	2.01 +2	1.65 +2	1.34 +2	1.07 +2
29	1.51 +0	9.69 -1	6.24 -1	4.05 -1	2.66 -1	1.76 -1	1.19 -1	8.10 -2
30	3.28 +2	2.71 +2	2.22 +2	1.82 +2	1.48 +2	1.19 +2	9.57 +1	7.61 +1
31	8.49 +2	7.06 +2	5.83 +2	4.79 +2	3.91 +2	3.17 +2	2.55 +2	2.03 +2
32	1.18 +3	9.79 +2	8.12 +2	6.68 +2	5.47 +2	4.44 +2	3.57 +2	2.85 +2
33	1.19 +3	9.94 +2	8.25 +2	6.80 +2	5.57 +2	4.53 +2	3.65 +2	2.91 +2
34	9.65 +2	8.06 +2	6.70 +2	5.53 +2	4.53 +2	3.68 +2	2.97 +2	2.37 +2
35	6.30 +2	5.27 +2	4.38 +2	3.61 +2	2.96 +2	2.41 +2	1.94 +2	1.55 +2
36	3.16 +2	2.64 +2	2.20 +2	1.81 +2	1.49 +2	1.21 +2	9.74 +1	7.78 +1
37	1.02 +2	8.52 +1	7.07 +1	5.83 +1	4.78 +1	3.88 +1	3.13 +1	2.50 +1
38	7.10 +5	4.69 +5	3.01 +5	1.75 +5	9.84 +4	4.79 +4	2.26 +4	8.49 +3
$\sum_{v'} A_{v'v''}$	7.95 +5	5.40 +5	3.60 +5	2.24 +5	1.38 +5	8.04 +4	4.88 +4	2.94 +4

Table E.11: $A_{v'v''}$ for ^{6}Li singlet case (continued).

$v'\backslash v''$	88	89	90	91	92	$\sum_{v''} A_{v'v''}$
0	2.59 -8	2.00 -8	1.48 -8	1.35 -8	1.64 -8	6.70 +7
1	9.66 -7	7.54 -7	5.92 -7	5.56 -7	6.55 -7	6.64 +7
2	2.29 -5	1.79 -5	1.41 -5	1.32 -5	1.56 -5	6.57 +7
3	2.54 -4	1.98 -4	1.56 -4	1.46 -4	1.72 -4	6.51 +7
4	2.41 -3	1.88 -3	1.48 -3	1.39 -3	1.64 -3	6.45 +7
5	1.80 -2	1.40 -2	1.10 -2	1.04 -2	1.22 -2	6.39 +7
6	1.14 -1	8.92 -2	7.01 -2	6.58 -2	7.76 -2	6.33 +7
7	6.05 -1	4.73 -1	3.72 -1	3.49 -1	4.12 -1	6.27 +7
8	2.74 +0	2.14 +0	1.68 +0	1.58 +0	1.86 +0	6.21 +7
9	1.06 +1	8.30 +0	6.52 +0	6.13 +0	7.22 +0	6.15 +7
10	3.53 +1	2.76 +1	2.17 +1	2.04 +1	2.40 +1	6.10 +7
11	1.03 +2	8.01 +1	6.30 +1	5.91 +1	6.97 +1	6.03 +7
12	2.53 +2	1.98 +2	1.55 +2	1.46 +2	1.72 +2	5.94 +7
13	5.41 +2	4.23 +2	3.32 +2	3.12 +2	3.68 +2	5.82 +7
14	9.99 +2	7.81 +2	6.13 +2	5.76 +2	6.80 +2	5.65 +7
15	1.56 +3	1.22 +3	9.59 +2	9.01 +2	1.06 +3	5.40 +7
16	2.07 +3	1.62 +3	1.27 +3	1.20 +3	1.41 +3	5.10 +7
17	2.26 +3	1.76 +3	1.39 +3	1.30 +3	1.54 +3	4.76 +7
18	1.96 +3	1.53 +3	1.21 +3	1.13 +3	1.34 +3	4.47 +7
19	1.24 +3	9.71 +2	7.63 +2	7.17 +2	8.46 +2	4.26 +7
20	4.54 +2	3.55 +2	2.79 +2	2.63 +2	3.10 +2	4.16 +7
21	2.29 +1	1.80 +1	1.42 +1	1.34 +1	1.58 +1	4.16 +7
22	1.30 +2	1.01 +2	7.93 +1	7.44 +1	8.76 +1	4.17 +7
23	5.83 +2	4.56 +2	3.58 +2	3.36 +2	3.96 +2	4.16 +7
24	9.84 +2	7.69 +2	6.05 +2	5.68 +2	6.70 +2	4.12 +7
25	1.04 +3	8.17 +2	6.42 +2	6.03 +2	7.11 +2	4.07 +7
26	7.64 +2	5.97 +2	4.70 +2	4.41 +2	5.21 +2	4.06 +7
27	3.69 +2	2.89 +2	2.27 +2	2.13 +2	2.52 +2	4.10 +7
28	8.50 +1	6.67 +1	5.25 +1	4.94 +1	5.84 +1	4.19 +7
29	5.59 -2	3.90 -2	2.80 -2	2.42 -2	2.61 -2	4.32 +7
30	5.99 +1	4.67 +1	3.66 +1	3.44 +1	4.04 +1	4.49 +7
31	1.61 +2	1.25 +2	9.84 +1	9.23 +1	1.09 +2	4.69 +7
32	2.25 +2	1.76 +2	1.38 +2	1.30 +2	1.53 +2	4.94 +7
33	2.30 +2	1.80 +2	1.41 +2	1.33 +2	1.56 +2	5.27 +7
34	1.87 +2	1.46 +2	1.15 +2	1.08 +2	1.27 +2	5.66 +7
35	1.23 +2	9.58 +1	7.52 +1	7.07 +1	8.34 +1	6.12 +7
36	6.15 +1	4.80 +1	3.77 +1	3.55 +1	4.18 +1	6.59 +7
37	1.97 +1	1.54 +1	1.21 +1	1.14 +1	1.34 +1	7.02 +7
38	3.15 +3	7.56 +2	1.91 +2	6.93 +0	3.66 +0	7.31 +7
$\sum_{v'} A_{v'v''}$	1.97 +4	1.37 +4	1.04 +4	9.56 +3	1.13 +4	

Table E.12: $A_{v'v''}$ for ^{6}Li singlet case (continued).

$v'\backslash v''$	0	1	2	3	4	5	6	7
0	3.21 +6	8.43 +6	1.21 +7	1.26 +7	1.07 +7	7.85 +6	5.18 +6	3.15 +6
1	1.04 +7	1.19 +7	4.88 +6	2.12 +5	1.20 +6	4.59 +6	6.99 +6	7.39 +6
2	1.54 +7	3.37 +6	9.14 +5	6.02 +6	5.68 +6	1.75 +6	7.92 +2	1.44 +6
3	1.37 +7	5.33 +5	7.36 +6	2.65 +6	2.31 +5	3.76 +6	4.92 +6	2.44 +6
4	8.19 +6	7.26 +6	3.13 +6	1.42 +6	5.43 +6	1.82 +6	1.51 +5	2.81 +6
5	3.46 +6	1.10 +7	4.07 +5	6.19 +6	4.87 +5	2.27 +6	4.26 +6	1.15 +6
6	1.05 +6	7.98 +6	6.68 +6	1.33 +6	3.33 +6	3.46 +6	9.05 +3	2.83 +6
7	2.31 +5	3.51 +6	9.82 +6	1.60 +6	4.51 +6	2.95 +5	4.18 +6	1.27 +6
8	3.59 +4	1.01 +6	6.49 +6	8.09 +6	1.30 +4	5.00 +6	5.01 +5	2.16 +6
9	3.78 +3	1.93 +5	2.46 +6	8.64 +6	4.58 +6	1.48 +6	2.96 +6	2.43 +6
10	2.43 +2	2.33 +4	5.69 +5	4.37 +6	9.15 +6	1.49 +6	3.60 +6	7.70 +5
11	7.11 +0	1.61 +3	7.88 +4	1.23 +6	6.32 +6	8.04 +6	7.31 +4	4.56 +6
12	2.22 -2	5.04 +1	6.12 +3	1.98 +5	2.19 +6	7.96 +6	5.98 +6	3.24 +5
13	1.34 -4	7.16 -1	2.38 +2	1.74 +4	4.08 +5	3.40 +6	9.02 +6	3.77 +6
14	1.04 -2	1.34 -1	4.71 +0	6.46 +2	3.64 +4	6.96 +5	4.67 +6	9.35 +6
15	9.21 -4	8.13 -3	2.92 -3	4.47 -1	9.04 +2	6.07 +4	1.05 +6	5.96 +6
16	4.36 -3	7.12 -2	7.95 -1	6.81 +0	1.52 +1	1.09 +3	9.30 +4	1.49 +6
17	1.09 -3	3.39 -2	2.92 -1	1.38 +0	9.73 +0	4.08 +1	1.08 +3	1.22 +5
18	1.31 -3	2.11 -2	1.90 -1	7.37 -1	6.66 -1	7.48 +0	1.71 +2	4.36 +2
19	4.56 -4	2.15 -2	1.77 -1	6.46 -1	1.07 +0	2.43 -1	2.16 +1	5.01 +2
20	4.40 -4	1.32 -2	1.08 -1	3.62 -1	4.03 -1	3.85 -3	1.19 +0	1.93 +1
21	1.95 -4	7.68 -3	6.20 -2	2.23 -1	3.20 -1	1.02 -1	2.39 -1	2.67 +0
22	2.88 -4	1.26 -2	9.79 -2	3.21 -1	3.47 -1	1.33 -2	3.86 -1	5.35 -2
23	5.36 -5	2.92 -4	3.03 -3	1.28 -2	3.00 -2	2.95 -2	3.40 -3	1.46 -2
24	3.49 -4	8.58 -3	6.92 -2	2.24 -1	2.60 -1	2.29 -2	1.95 -1	3.83 -1
25	3.57 -5	2.18 -3	1.66 -2	4.73 -2	3.62 -2	7.03 -4	7.98 -2	7.86 -2
26	1.32 -4	1.20 -3	1.01 -2	3.61 -2	5.58 -2	1.50 -2	2.25 -2	1.32 -1
27	2.58 -4	4.20 -3	3.38 -2	1.04 -1	1.16 -1	7.66 -3	9.39 -2	2.04 -1
28	5.57 -5	1.26 -3	1.03 -2	2.73 -2	2.12 -2	3.03 -5	2.18 -2	5.34 -3
29	1.88 -5	1.39 -4	8.95 -4	4.53 -3	1.04 -2	5.74 -3	4.62 -3	6.43 -2
30	1.23 -4	1.63 -3	1.20 -2	3.96 -2	5.03 -2	7.74 -3	2.73 -2	8.48 -2
31	1.22 -4	1.70 -3	1.27 -2	3.78 -2	3.94 -2	2.81 -3	2.01 -2	1.94 -2
32	4.58 -5	6.09 -4	4.67 -3	1.20 -2	9.02 -3	5.40 -6	4.64 -3	7.54 -4
33	2.68 -6	2.03 -5	2.09 -4	1.66 -4	1.20 -4	1.42 -3	8.12 -7	1.45 -2
34	5.06 -6	1.12 -4	6.66 -4	3.13 -3	6.42 -3	3.21 -3	1.54 -3	1.93 -2
35	1.86 -5	3.35 -4	2.15 -3	7.86 -3	1.17 -2	3.33 -3	2.99 -3	1.36 -2
36	2.35 -5	3.99 -4	2.59 -3	8.72 -3	1.13 -2	2.38 -3	2.97 -3	6.88 -3
37	1.98 -5	3.24 -4	2.11 -3	6.78 -3	8.14 -3	1.35 -3	2.19 -3	2.89 -3
38	1.28 -5	2.04 -4	1.33 -3	4.16 -3	4.73 -3	6.62 -4	1.31 -3	1.10 -3
39	6.44 -6	1.01 -4	6.58 -4	2.03 -3	2.24 -3	2.80 -4	6.33 -4	3.90 -4
40	2.17 -6	3.40 -5	2.21 -4	6.75 -4	7.35 -4	8.71 -5	2.10 -4	1.11 -4
41	2.74 -7	4.29 -6	2.78 -5	8.50 -5	9.22 -5	1.08 -5	2.65 -5	1.34 -5
$\sum_{v'} A_{v'v''}$	5.56 +7	5.52 +7	5.49 +7	5.46 +7	5.42 +7	5.39 +7	5.37 +7	5.34 +7

Table E.13: Spontaneous emission coefficient $A_{v'v''}$ for the ^{7}Li singlet case.

$v'\backslash v''$	8	9	10	11	12	13	14	15
0	1.80 +6	9.76 +5	5.10 +5	2.58 +5	1.27 +5	6.17 +4	2.94 +4	1.39 +4
1	6.33 +6	4.72 +6	3.19 +6	2.00 +6	1.18 +6	6.71 +5	3.67 +5	1.96 +5
2	3.92 +6	5.55 +6	5.80 +6	5.05 +6	3.88 +6	2.72 +6	1.78 +6	1.11 +6
3	2.22 +5	3.88 +5	2.16 +6	3.96 +6	4.86 +6	4.78 +6	4.07 +6	3.13 +6
4	4.17 +6	2.56 +6	5.08 +5	7.09 +4	1.21 +6	2.81 +6	3.94 +6	4.29 +6
5	1.79 +5	2.36 +6	3.60 +6	2.47 +6	6.91 +5	1.45 +3	6.78 +5	2.00 +6
6	3.30 +6	6.59 +5	2.52 +5	2.12 +6	3.17 +6	2.31 +6	7.84 +5	1.29 +4
7	4.56 +5	3.02 +6	2.46 +6	3.23 +5	3.49 +5	1.98 +6	2.82 +6	2.13 +6
8	3.11 +6	1.84 +5	1.15 +6	2.90 +6	1.75 +6	1.21 +5	4.54 +5	1.87 +6
9	2.82 +5	3.10 +6	1.57 +6	2.57 +4	1.72 +6	2.56 +6	1.17 +6	2.35 +4
10	3.59 +6	1.78 +5	1.65 +6	2.65 +6	4.64 +5	3.77 +5	2.04 +6	2.12 +6
11	1.62 +3	3.11 +6	1.36 +6	3.09 +5	2.46 +6	1.60 +6	2.37 +4	8.68 +5
12	3.97 +6	6.88 +5	1.67 +6	2.49 +6	4.74 +4	1.36 +6	2.27 +6	6.58 +5
13	1.48 +6	2.57 +6	1.89 +6	4.45 +5	2.70 +6	7.22 +5	3.40 +5	2.00 +6
14	1.92 +6	2.74 +6	1.17 +6	2.78 +6	5.09 +2	2.09 +6	1.61 +6	8.78 +2
15	9.16 +6	7.09 +5	3.58 +6	2.69 +5	2.99 +6	3.01 +5	1.14 +6	2.11 +6
16	7.21 +6	8.64 +6	1.25 +5	3.87 +6	2.02 +1	2.60 +6	9.62 +5	3.75 +5
17	1.91 +6	8.30 +6	7.97 +6	2.65 +3	3.66 +6	2.04 +5	1.89 +6	1.61 +6
18	1.42 +5	2.33 +6	9.35 +6	7.40 +6	1.28 +5	3.17 +6	6.32 +5	1.16 +6
19	2.29 +0	1.41 +5	2.64 +6	1.03 +7	7.01 +6	3.20 +5	2.59 +6	1.08 +6
20	1.19 +3	1.80 +3	1.12 +5	2.82 +6	1.11 +7	6.91 +6	4.68 +5	2.02 +6
21	2.26 +1	2.24 +3	8.92 +3	6.50 +4	2.82 +6	1.19 +7	7.19 +6	4.94 +5
22	9.90 +0	3.21 -1	2.86 +3	2.45 +4	1.57 +4	2.58 +6	1.27 +7	7.97 +6
23	5.16 -1	3.81 +1	9.28 +1	2.67 +3	5.06 +4	4.05 +3	2.04 +6	1.31 +7
24	3.18 -2	2.12 -1	4.89 +1	4.71 +2	1.27 +3	8.05 +4	8.98 +4	1.29 +6
25	1.94 -2	9.40 -1	7.49 +0	2.72 +1	1.36 +3	3.18 +1	9.49 +4	3.26 +5
26	4.88 -2	2.27 -2	5.29 -1	2.20 +1	2.60 -1	2.50 +3	5.03 +3	7.34 +4
27	4.04 -2	2.26 -2	9.47 -1	5.99 -1	4.58 +1	1.46 +2	2.46 +3	2.46 +4
28	2.38 -2	1.19 -2	3.34 -2	3.76 -1	5.39 +0	3.65 +1	8.44 +2	5.02 +2
29	9.77 -2	4.40 -2	7.35 -2	4.18 -1	1.56 -1	2.95 +1	4.17 -1	2.07 +3
30	2.30 -2	6.62 -5	4.84 -2	1.21 -1	6.33 -1	2.89 +0	4.28 +1	2.80 +2
31	9.45 -3	4.91 -2	2.45 -5	6.12 -3	1.92 -1	8.35 -2	1.84 +1	4.12 +0
32	5.31 -2	7.83 -2	1.29 -2	5.39 -3	1.16 -2	6.32 -1	2.04 +0	3.97 +1
33	4.74 -2	3.29 -2	1.02 -2	1.49 -2	1.85 -3	4.70 -1	7.32 -4	2.18 +1
34	1.66 -2	1.20 -3	9.72 -4	1.32 -2	5.14 -3	1.89 -1	2.37 -1	5.57 +0
35	1.27 -3	6.20 -3	9.66 -4	7.94 -3	2.81 -3	4.88 -2	2.71 -1	7.18 -1
36	7.19 -4	1.79 -2	3.89 -3	4.07 -3	8.16 -4	6.92 -3	1.85 -1	1.07 -2
37	2.99 -3	2.00 -2	4.51 -3	1.95 -3	1.47 -4	1.28 -4	1.04 -1	3.23 -2
38	3.25 -3	1.46 -2	3.25 -3	8.93 -4	1.54 -5	2.82 -4	5.27 -2	5.57 -2
39	2.04 -3	7.75 -3	1.69 -3	3.73 -4	6.86 -7	4.33 -4	2.32 -2	3.80 -2
40	7.51 -4	2.67 -3	5.77 -4	1.16 -4	1.14 -9	2.01 -4	7.40 -3	1.42 -2
41	9.68 -5	3.39 -4	7.30 -5	1.44 -5	8.03 -10	2.72 -5	9.23 -4	1.84 -3
$\sum_{v'} A_{v'v''}$	5.32 +7	5.29 +7	5.27 +7	5.26 +7	5.24 +7	5.23 +7	5.22 +7	5.21 +7

Table E.14: $A_{v'v''}$ for ^{7}Li singlet case (continued).

$v'\backslash v''$	16	17	18	19	20	21	22	23
0	6.49 +3	3.02 +3	1.40 +3	6.48 +2	3.00 +2	1.40 +2	6.55 +1	3.09 +1
1	1.02 +5	5.24 +4	2.65 +4	1.33 +4	6.64 +3	3.30 +3	1.64 +3	8.11 +2
2	6.61 +5	3.82 +5	2.15 +5	1.19 +5	6.44 +4	3.45 +4	1.84 +4	9.72 +3
3	2.23 +6	1.50 +6	9.60 +5	5.94 +5	3.57 +5	2.10 +5	1.21 +5	6.91 +4
4	3.97 +6	3.29 +6	2.51 +6	1.80 +6	1.23 +6	8.10 +5	5.16 +5	3.21 +5
5	3.15 +6	3.74 +6	3.72 +6	3.29 +6	2.67 +6	2.03 +6	1.46 +6	1.02 +6
6	3.79 +5	1.43 +6	2.51 +6	3.20 +6	3.39 +6	3.17 +6	2.71 +6	2.17 +6
7	8.22 +5	4.77 +4	2.05 +5	1.02 +6	1.98 +6	2.70 +6	3.02 +6	2.98 +6
8	2.54 +6	1.95 +6	8.29 +5	8.69 +4	1.02 +5	7.17 +5	1.54 +6	2.25 +6
9	5.56 +5	1.78 +6	2.30 +6	1.78 +6	8.18 +5	1.25 +5	4.32 +4	4.94 +5
10	7.30 +5	1.80 +2	6.44 +5	1.69 +6	2.09 +6	1.63 +6	8.00 +5	1.61 +5
11	2.10 +6	1.66 +6	4.23 +5	2.24 +4	7.08 +5	1.60 +6	1.91 +6	1.51 +6
12	7.94 +4	1.27 +6	1.97 +6	1.24 +6	2.22 +5	6.62 +4	7.43 +5	1.50 +6
13	1.51 +6	1.25 +5	3.81 +5	1.51 +6	1.72 +6	8.78 +5	9.82 +4	1.18 +5
14	1.19 +6	1.92 +6	7.33 +5	2.74 +3	7.32 +5	1.58 +6	1.43 +6	6.00 +5
15	3.31 +5	3.93 +5	1.69 +6	1.37 +6	2.19 +5	1.43 +5	1.01 +6	1.52 +6
16	2.03 +6	9.49 +5	1.66 +4	1.07 +6	1.63 +6	7.40 +5	1.14 +4	3.88 +5
17	2.20 +4	1.55 +6	1.47 +6	1.08 +5	4.49 +5	1.44 +6	1.21 +6	2.78 +5
18	1.98 +6	6.98 +4	9.37 +5	1.68 +6	4.79 +5	7.33 +4	9.85 +5	1.37 +6
19	5.99 +5	2.06 +6	3.54 +5	4.25 +5	1.58 +6	8.96 +5	1.08 +4	5.05 +5
20	1.45 +6	2.40 +5	1.91 +6	7.04 +5	1.14 +5	1.27 +6	1.19 +6	1.79 +5
21	1.53 +6	1.69 +6	5.95 +4	1.63 +6	1.00 +6	2.87 +3	8.95 +5	1.30 +6
22	3.87 +5	1.13 +6	1.81 +6	3.14 +3	1.33 +6	1.18 +6	3.20 +4	5.59 +5
23	9.32 +6	1.91 +5	8.08 +5	1.87 +6	5.95 +3	1.05 +6	1.27 +6	1.29 +5
24	1.31 +7	1.13 +7	1.70 +4	5.34 +5	1.91 +6	2.13 +4	8.27 +5	1.26 +6
25	4.77 +5	1.20 +7	1.39 +7	9.36 +4	2.84 +5	2.00 +6	2.27 +4	6.56 +5
26	6.93 +5	7.92 +3	9.74 +6	1.68 +7	7.81 +5	7.36 +4	2.22 +6	5.82 +3
27	1.84 +4	1.02 +6	4.26 +5	6.07 +6	1.87 +7	2.48 +6	7.39 +3	2.69 +6
28	5.43 +4	1.23 +4	1.00 +6	2.06 +6	2.05 +6	1.82 +7	5.27 +6	3.06 +5
29	1.95 +3	6.19 +4	1.97 +5	4.63 +5	4.24 +6	1.26 +3	1.37 +7	8.24 +6
30	1.69 +3	1.97 +4	1.76 +4	5.56 +5	1.86 +2	4.89 +6	2.31 +6	6.06 +6
31	1.34 +3	4.42 +1	4.57 +4	2.37 +4	6.32 +5	9.10 +5	2.46 +6	7.54 +6
32	1.92 +2	1.52 +3	1.06 +4	2.53 +4	2.75 +5	1.21 +5	2.88 +6	3.86 +3
33	5.70 -3	1.17 +3	1.13 +2	3.38 +4	1.26 +4	4.59 +5	3.47 +5	2.38 +6
34	2.24 +1	3.41 +2	7.24 +2	1.25 +4	1.04 +4	2.34 +5	4.93 +4	1.98 +6
35	2.39 +1	4.64 +1	1.01 +3	2.08 +3	2.27 +4	4.98 +4	2.46 +5	5.70 +5
36	1.40 +1	6.32 -1	6.45 +2	6.49 +1	1.66 +4	2.84 +3	2.21 +5	5.29 +4
37	6.64 +0	2.35 +0	3.13 +2	5.79 +1	8.62 +3	6.08 +2	1.25 +5	1.80 +3
38	2.86 +0	3.94 +0	1.35 +2	1.28 +2	3.83 +3	2.16 +3	5.84 +4	1.74 +4
39	1.13 +0	2.67 +0	5.32 +1	9.19 +1	1.53 +3	1.71 +3	2.37 +4	1.58 +4
40	3.43 -1	9.95 -1	1.61 +1	3.50 +1	4.62 +2	6.69 +2	7.24 +3	6.44 +3
41	4.21 -2	1.29 -1	1.97 +0	4.55 +0	5.68 +1	8.75 +1	8.92 +2	8.50 +2
$\sum_{v'} A_{v'v''}$	5.20 +7	5.19 +7	5.19 +7	5.19 +7	5.19 +7	5.18 +7	5.18 +7	5.12 +7

Table E.15: $A_{v'v''}$ for ^{7}Li singlet case (continued).

$v'\backslash v''$	24	25	26	27	28	29	30	31
0	1.46 +1	6.97 +0	3.33 +0	1.59 +0	7.56 -1	3.60 -1	1.74 -1	8.63 -2
1	4.03 +2	2.01 +2	1.01 +2	5.09 +1	2.59 +1	1.32 +1	6.84 +0	3.57 +0
2	5.12 +3	2.70 +3	1.42 +3	7.52 +2	3.98 +2	2.11 +2	1.13 +2	6.11 +1
3	3.90 +4	2.18 +4	1.22 +4	6.78 +3	3.77 +3	2.09 +3	1.17 +3	6.53 +2
4	1.96 +5	1.18 +5	7.04 +4	4.16 +4	2.44 +4	1.42 +4	8.30 +3	4.85 +3
5	6.82 +5	4.47 +5	2.88 +5	1.82 +5	1.14 +5	7.04 +4	4.33 +4	2.65 +4
6	1.65 +6	1.20 +6	8.47 +5	5.83 +5	3.92 +5	2.59 +5	1.69 +5	1.10 +5
7	2.67 +6	2.24 +6	1.78 +6	1.36 +6	1.00 +6	7.18 +5	5.04 +5	3.48 +5
8	2.65 +6	2.73 +6	2.57 +6	2.25 +6	1.87 +6	1.48 +6	1.13 +6	8.46 +5
9	1.19 +6	1.84 +6	2.29 +6	2.47 +6	2.42 +6	2.20 +6	1.89 +6	1.56 +6
10	1.19 +4	3.26 +5	8.97 +5	1.49 +6	1.94 +6	2.18 +6	2.21 +6	2.09 +6
11	7.87 +5	1.99 +5	3.24 +2	2.01 +5	6.56 +5	1.17 +6	1.61 +6	1.88 +6
12	1.75 +6	1.40 +6	7.78 +5	2.38 +5	4.50 +3	1.09 +5	4.50 +5	8.82 +5
13	7.57 +5	1.40 +6	1.59 +6	1.30 +6	7.64 +5	2.74 +5	2.14 +4	4.62 +4
14	3.29 +4	1.67 +5	7.58 +5	1.30 +6	1.46 +6	1.21 +6	7.52 +5	3.13 +5
15	1.14 +6	3.97 +5	5.78 +3	2.05 +5	7.39 +5	1.20 +6	1.33 +6	1.13 +6
16	1.16 +6	1.36 +6	8.81 +5	2.51 +5	1.07 +2	2.32 +5	6.99 +5	1.08 +6
17	3.83 +4	6.26 +5	1.21 +6	1.18 +6	6.68 +5	1.54 +5	5.32 +3	2.40 +5
18	6.97 +5	4.46 +4	1.87 +5	7.99 +5	1.17 +6	9.84 +5	4.92 +5	9.23 +4
19	1.24 +6	1.03 +6	2.99 +5	4.28 +3	3.71 +5	8.96 +5	1.07 +6	8.03 +5
20	1.57 +5	9.16 +5	1.16 +6	6.22 +5	7.14 +4	8.38 +4	5.23 +5	9.09 +5
21	4.44 +5	8.94 +3	5.50 +5	1.07 +6	8.64 +5	2.86 +5	4.56 +2	2.06 +5
22	1.24 +6	6.89 +5	2.83 +4	2.56 +5	8.49 +5	9.54 +5	5.21 +5	8.40 +4
23	3.10 +5	1.09 +6	8.55 +5	1.44 +5	7.62 +4	5.88 +5	9.06 +5	6.95 +5
24	2.35 +5	1.50 +5	8.94 +5	9.24 +5	2.85 +5	5.25 +3	3.54 +5	7.64 +5
25	1.22 +6	3.17 +5	6.36 +4	7.14 +5	9.19 +5	4.06 +5	9.26 +3	1.82 +5
26	5.20 +5	1.15 +6	3.55 +5	2.34 +4	5.64 +5	8.62 +5	4.85 +5	5.06 +4
27	9.57 +3	3.94 +5	1.11 +6	3.45 +5	7.88 +3	4.55 +5	7.81 +5	5.20 +5
28	3.61 +6	1.69 +5	2.44 +5	1.13 +6	2.79 +5	2.61 +3	3.85 +5	6.94 +5
29	1.18 +6	5.19 +6	8.21 +5	6.82 +4	1.31 +6	1.59 +5	4.40 +2	3.57 +5
30	9.08 +6	2.31 +6	7.28 +6	2.56 +6	2.10 +4	1.83 +6	2.22 +4	1.31 +3
31	3.91 +5	5.91 +6	2.38 +6	8.59 +6	5.77 +6	5.93 +5	3.11 +6	8.88 +4
32	8.63 +6	1.63 +6	1.15 +6	6.71 +5	6.53 +6	8.84 +6	2.21 +6	5.60 +6
33	2.93 +6	2.64 +6	5.00 +6	2.14 +5	3.67 +5	1.37 +6	7.37 +6	3.36 +6
34	1.49 +4	5.85 +6	3.59 +5	2.11 +6	8.96 +5	3.16 +6	8.34 +5	1.47 +6
35	1.08 +6	2.68 +6	1.13 +6	3.26 +6	7.66 +4	6.27 +4	1.44 +6	4.42 +6
36	1.33 +6	4.16 +5	2.78 +6	1.14 +6	4.76 +5	3.29 +5	1.90 +6	8.30 +5
37	8.73 +5	3.46 +2	2.37 +6	8.84 +4	1.14 +6	3.23 +5	6.48 +5	1.37 +4
38	4.35 +5	5.24 +4	1.34 +6	1.36 +4	9.58 +5	1.09 +5	1.14 +5	2.34 +5
39	1.83 +5	6.08 +4	5.99 +5	4.80 +4	5.11 +5	2.41 +4	1.36 +4	2.11 +5
40	5.65 +4	2.65 +4	1.89 +5	2.58 +4	1.74 +5	4.51 +3	1.42 +3	8.43 +4
41	6.97 +3	3.55 +3	2.35 +4	3.61 +3	2.19 +4	4.71 +2	1.16 +2	1.11 +4
$\sum_{v'} A_{v'v''}$	5.06 +7	4.72 +7	4.51 +7	3.79 +7	3.57 +7	3.36 +7	3.40 +7	3.23 +7

Table E.16: $A_{v'v''}$ for ^{7}Li singlet case (continued).

$v'\backslash v''$	32	33	34	35	36	37	38	39
0	4.50 -2	2.50 -2	1.50 -2	9.55 -3	6.36 -3	4.30 -3	2.86 -3	1.83 -3
1	1.88 +0	1.00 +0	5.44 -1	3.00 -1	1.70 -1	9.95 -2	6.05 -2	3.83 -2
2	3.33 +1	1.84 +1	1.03 +1	5.87 +0	3.39 +0	1.99 +0	1.19 +0	7.22 -1
3	3.69 +2	2.10 +2	1.21 +2	7.01 +1	4.13 +1	2.47 +1	1.50 +1	9.23 +0
4	2.85 +3	1.68 +3	9.96 +2	5.96 +2	3.60 +2	2.20 +2	1.36 +2	8.47 +1
5	1.62 +4	9.95 +3	6.12 +3	3.78 +3	2.36 +3	1.48 +3	9.38 +2	5.99 +2
6	7.06 +4	4.53 +4	2.91 +4	1.87 +4	1.20 +4	7.77 +3	5.06 +3	3.32 +3
7	2.37 +5	1.61 +5	1.08 +5	7.25 +4	4.86 +4	3.26 +4	2.20 +4	1.48 +4
8	6.20 +5	4.46 +5	3.18 +5	2.24 +5	1.57 +5	1.10 +5	7.67 +4	5.36 +4
9	1.24 +6	9.64 +5	7.34 +5	5.50 +5	4.08 +5	3.00 +5	2.19 +5	1.59 +5
10	1.87 +6	1.60 +6	1.33 +6	1.07 +6	8.44 +5	6.56 +5	5.05 +5	3.85 +5
11	1.99 +6	1.95 +6	1.80 +6	1.60 +6	1.38 +6	1.15 +6	9.43 +5	7.60 +5
12	1.28 +6	1.57 +6	1.73 +6	1.76 +6	1.69 +6	1.55 +6	1.38 +6	1.19 +6
13	2.84 +5	6.26 +5	9.73 +5	1.25 +6	1.44 +6	1.52 +6	1.51 +6	1.44 +6
14	5.04 +4	1.04 +4	1.57 +5	4.13 +5	7.00 +5	9.58 +5	1.15 +6	1.27 +6
15	7.47 +5	3.58 +5	9.30 +4	1.78 +2	6.50 +4	2.37 +5	4.58 +5	6.77 +5
16	1.20 +6	1.05 +6	7.40 +5	4.04 +5	1.47 +5	1.61 +4	1.30 +4	1.08 +5
17	6.42 +5	9.69 +5	1.08 +6	9.81 +5	7.36 +5	4.52 +5	2.11 +5	5.68 +4
18	1.27 +4	2.29 +5	5.68 +5	8.46 +5	9.62 +5	9.03 +5	7.22 +5	4.93 +5
19	3.66 +5	5.70 +4	1.73 +4	2.06 +5	4.88 +5	7.26 +5	8.43 +5	8.24 +5
20	9.39 +5	6.50 +5	2.78 +5	3.87 +4	1.69 +4	1.72 +5	4.00 +5	6.03 +5
21	6.18 +5	8.67 +5	8.08 +5	5.28 +5	2.19 +5	3.06 +4	1.24 +4	1.30 +5
22	3.13 +4	3.18 +5	6.52 +5	7.91 +5	6.85 +5	4.34 +5	1.81 +5	2.85 +4
23	2.51 +5	6.18 +3	1.05 +5	3.96 +5	6.43 +5	7.04 +5	5.82 +5	3.66 +5
24	7.63 +5	4.18 +5	8.50 +4	8.39 +3	1.79 +5	4.31 +5	6.00 +5	6.13 +5
25	5.88 +5	7.42 +5	5.37 +5	2.07 +5	1.26 +4	4.75 +4	2.34 +5	4.33 +5
26	7.64 +4	4.19 +5	6.57 +5	5.87 +5	3.18 +5	7.60 +4	9.78 +2	9.25 +4
27	9.90 +4	2.32 +4	2.82 +5	5.45 +5	5.78 +5	3.93 +5	1.57 +5	1.55 +4
28	5.17 +5	1.36 +5	3.33 +3	1.82 +5	4.33 +5	5.28 +5	4.24 +5	2.24 +5
29	6.07 +5	4.88 +5	1.53 +5	4.81 +1	1.18 +5	3.36 +5	4.59 +5	4.16 +5
30	3.85 +5	5.10 +5	4.48 +5	1.47 +5	1.89 +3	7.90 +4	2.62 +5	3.88 +5
31	3.64 +4	5.32 +5	3.69 +5	4.21 +5	1.18 +5	3.24 +3	5.89 +4	2.06 +5
32	1.05 +6	3.15 +5	1.03 +6	1.50 +5	4.63 +5	6.26 +4	4.21 +3	5.44 +4
33	8.41 +6	3.90 +6	1.53 +6	2.58 +6	7.87 +3	7.61 +5	8.60 +2	1.39 +4
34	1.25 +6	7.14 +6	7.03 +6	4.09 +6	6.26 +6	9.47 +5	2.00 +6	2.42 +5
35	4.99 +5	5.25 +5	9.06 +5	4.15 +6	4.17 +6	9.70 +6	4.17 +6	5.53 +6
36	7.91 +5	7.37 +5	3.37 +6	1.81 +6	1.63 +4	7.29 +4	4.31 +6	4.26 +6
37	1.93 +6	6.23 +5	8.97 +5	3.78 +4	1.53 +6	1.52 +6	3.36 +6	3.66 +5
38	1.34 +6	1.14 +5	5.17 +4	5.60 +5	1.45 +6	5.65 +5	4.68 +5	3.91 +5
39	6.07 +5	5.86 +3	1.48 +3	4.65 +5	6.45 +5	9.66 +4	1.66 +4	6.13 +5
40	1.89 +5	2.28 -3	4.63 +3	1.78 +5	1.92 +5	1.32 +4	1.02 +2	2.68 +5
41	2.33 +4	1.65 +1	7.91 +2	2.30 +4	2.34 +4	1.20 +3	1.20 +2	3.56 +4
$\sum_{v'} A_{v'v''}$	3.16 +7	2.85 +7	2.89 +7	2.73 +7	2.71 +7	2.56 +7	2.58 +7	2.27 +7

Table E.17: $A_{v'v''}$ for ^{7}Li singlet case (continued).

$v'\backslash v''$	40	41	42	43	44	45	46	47
0	1.11 -3	6.17 -4	3.10 -4	1.37 -4	4.95 -5	1.29 -5	1.41 -6	1.10 -7
1	2.52 -2	1.71 -2	1.18 -2	8.29 -3	5.82 -3	4.06 -3	2.80 -3	1.90 -3
2	4.47 -1	2.83 -1	1.82 -1	1.21 -1	8.13 -2	5.61 -2	3.94 -2	2.82 -2
3	5.77 +0	3.67 +0	2.37 +0	1.56 +0	1.04 +0	7.05 -1	4.86 -1	3.42 -1
4	5.37 +1	3.46 +1	2.26 +1	1.50 +1	1.01 +1	6.88 +0	4.77 +0	3.35 +0
5	3.87 +2	2.53 +2	1.67 +2	1.12 +2	7.56 +1	5.20 +1	3.63 +1	2.57 +1
6	2.19 +3	1.47 +3	9.89 +2	6.74 +2	4.64 +2	3.23 +2	2.28 +2	1.62 +2
7	1.01 +4	6.88 +3	4.73 +3	3.28 +3	2.30 +3	1.62 +3	1.16 +3	8.41 +2
8	3.76 +4	2.65 +4	1.87 +4	1.33 +4	9.54 +3	6.87 +3	4.99 +3	3.65 +3
9	1.16 +5	8.39 +4	6.10 +4	4.45 +4	3.26 +4	2.40 +4	1.78 +4	1.33 +4
10	2.92 +5	2.21 +5	1.66 +5	1.25 +5	9.45 +4	7.13 +4	5.40 +4	4.11 +4
11	6.06 +5	4.78 +5	3.75 +5	2.93 +5	2.28 +5	1.78 +5	1.39 +5	1.08 +5
12	1.01 +6	8.46 +5	6.97 +5	5.69 +5	4.61 +5	3.71 +5	2.98 +5	2.39 +5
13	1.33 +6	1.19 +6	1.04 +6	8.96 +5	7.61 +5	6.40 +5	5.34 +5	4.43 +5
14	1.31 +6	1.29 +6	1.23 +6	1.13 +6	1.02 +6	9.04 +5	7.90 +5	6.83 +5
15	8.60 +5	9.91 +5	1.06 +6	1.09 +6	1.06 +6	1.01 +6	9.39 +5	8.54 +5
16	2.59 +5	4.27 +5	5.83 +5	7.08 +5	7.93 +5	8.39 +5	8.49 +5	8.31 +5
17	6.80 +2	2.79 +4	1.12 +5	2.25 +5	3.41 +5	4.45 +5	5.25 +5	5.79 +5
18	2.78 +5	1.17 +5	2.59 +4	5.91 +1	2.49 +4	8.16 +4	1.53 +5	2.24 +5
19	7.01 +5	5.25 +5	3.44 +5	1.90 +5	8.18 +4	2.06 +4	1.97 +2	9.78 +3
20	7.18 +5	7.32 +5	6.61 +5	5.38 +5	3.97 +5	2.64 +5	1.56 +5	7.82 +4
21	3.09 +5	4.78 +5	5.89 +5	6.26 +5	5.97 +5	5.22 +5	4.24 +5	3.21 +5
22	6.28 +3	8.80 +4	2.21 +5	3.55 +5	4.54 +5	5.04 +5	5.06 +5	4.71 +5
23	1.60 +5	3.18 +4	1.18 +3	4.93 +4	1.41 +5	2.40 +5	3.22 +5	3.75 +5
24	4.93 +5	3.14 +5	1.48 +5	3.94 +4	3.85 +2	1.94 +4	7.34 +4	1.40 +5
25	5.41 +5	5.27 +5	4.22 +5	2.78 +5	1.45 +5	5.16 +4	6.47 +3	2.59 +3
26	2.61 +5	4.06 +5	4.71 +5	4.47 +5	3.61 +5	2.50 +5	1.46 +5	6.73 +4
27	1.88 +4	1.26 +5	2.62 +5	3.63 +5	4.00 +5	3.75 +5	3.09 +5	2.27 +5
28	5.94 +4	3.05 +1	4.33 +4	1.42 +5	2.43 +5	3.10 +5	3.30 +5	3.09 +5
29	2.65 +5	1.06 +5	1.39 +4	6.44 +3	6.14 +4	1.40 +5	2.10 +5	2.53 +5
30	3.84 +5	2.77 +5	1.41 +5	3.92 +4	4.73 +2	1.83 +4	6.85 +4	1.25 +5
31	3.23 +5	3.38 +5	2.65 +5	1.56 +5	6.11 +4	9.12 +3	1.99 +3	2.65 +4
32	1.66 +5	2.69 +5	2.88 +5	2.38 +5	1.53 +5	7.27 +4	2.01 +4	4.28 +2
33	7.48 +4	1.27 +5	2.31 +5	2.35 +5	2.03 +5	1.37 +5	7.29 +4	2.67 +4
34	1.28 +5	2.03 +5	5.82 +4	2.32 +5	1.70 +5	1.69 +5	1.10 +5	6.43 +4
35	2.30 +6	1.11 +6	9.92 +5	1.70 +4	4.19 +5	5.87 +4	1.72 +5	6.80 +4
36	8.17 +6	7.05 +6	4.94 +6	4.67 +6	1.27 +6	1.75 +6	9.64 +4	4.30 +5
37	2.14 +4	1.28 +6	4.20 +6	5.89 +6	9.52 +6	6.27 +6	7.34 +6	2.90 +6
38	8.84 +5	2.52 +6	2.20 +6	6.80 +5	5.47 +4	1.34 +6	2.89 +6	8.01 +6
39	6.66 +5	9.86 +5	3.19 +5	1.99 +4	4.24 +5	2.07 +6	1.83 +6	2.02 +6
40	2.24 +5	2.54 +5	3.33 +4	6.22 +4	2.64 +5	7.46 +5	4.33 +5	2.74 +5
41	2.79 +4	2.94 +4	2.65 +3	1.05 +4	3.69 +4	9.33 +4	4.76 +4	2.46 +4
$\sum_{v'} A_{v'v''}$	2.30 +7	2.35 +7	2.22 +7	2.04 +7	2.03 +7	2.00 +7	1.99 +7	2.02 +7

Table E.18: $A_{v'v''}$ for ^{7}Li singlet case (continued).

$v'\backslash v''$	48	49	50	51	52	53	54	55
0	1.37 -6	2.29 -6	2.31 -6	1.71 -6	9.65 -7	3.73 -7	5.63 -8	1.22 -8
1	1.27 -3	8.36 -4	5.42 -4	3.45 -4	2.17 -4	1.35 -4	8.35 -5	5.12 -5
2	2.05 -2	1.52 -2	1.13 -2	8.57 -3	6.52 -3	5.02 -3	3.90 -3	3.06 -3
3	2.44 -1	1.78 -1	1.31 -1	9.85 -2	7.48 -2	5.76 -2	4.50 -2	3.56 -2
4	2.39 +0	1.73 +0	1.27 +0	9.47 -1	7.14 -1	5.46 -1	4.24 -1	3.34 -1
5	1.85 +1	1.35 +1	9.99 +0	7.49 +0	5.69 +0	4.37 +0	3.41 +0	2.69 +0
6	1.17 +2	8.55 +1	6.34 +1	4.75 +1	3.61 +1	2.78 +1	2.17 +1	1.72 +1
7	6.16 +2	4.57 +2	3.44 +2	2.61 +2	2.00 +2	1.55 +2	1.21 +2	9.63 +1
8	2.70 +3	2.02 +3	1.53 +3	1.17 +3	8.99 +2	7.02 +2	5.55 +2	4.44 +2
9	1.01 +4	7.66 +3	5.88 +3	4.55 +3	3.55 +3	2.80 +3	2.23 +3	1.79 +3
10	3.15 +4	2.43 +4	1.89 +4	1.48 +4	1.17 +4	9.33 +3	7.52 +3	6.10 +3
11	8.49 +4	6.69 +4	5.30 +4	4.22 +4	3.38 +4	2.72 +4	2.21 +4	1.81 +4
12	1.92 +5	1.55 +5	1.25 +5	1.02 +5	8.28 +4	6.77 +4	5.59 +4	4.63 +4
13	3.66 +5	3.03 +5	2.51 +5	2.08 +5	1.72 +5	1.43 +5	1.20 +5	1.01 +5
14	5.86 +5	5.01 +5	4.26 +5	3.62 +5	3.07 +5	2.60 +5	2.22 +5	1.89 +5
15	7.67 +5	6.82 +5	6.01 +5	5.26 +5	4.58 +5	3.98 +5	3.46 +5	3.01 +5
16	7.93 +5	7.43 +5	6.85 +5	6.24 +5	5.62 +5	5.03 +5	4.49 +5	3.99 +5
17	6.08 +5	6.16 +5	6.06 +5	5.83 +5	5.50 +5	5.13 +5	4.74 +5	4.35 +5
18	2.86 +5	3.35 +5	3.70 +5	3.89 +5	3.95 +5	3.91 +5	3.80 +5	3.64 +5
19	3.77 +4	7.43 +4	1.12 +5	1.46 +5	1.73 +5	1.93 +5	2.07 +5	2.13 +5
20	2.99 +4	6.00 +3	3.28 +1	5.82 +3	1.81 +4	3.28 +4	4.76 +4	6.08 +4
21	2.29 +5	1.52 +5	9.39 +4	5.25 +4	2.56 +4	9.94 +3	2.31 +3	1.86 +1
22	4.13 +5	3.45 +5	2.77 +5	2.14 +5	1.60 +5	1.17 +5	8.27 +4	5.69 +4
23	3.96 +5	3.90 +5	3.65 +5	3.28 +5	2.85 +5	2.42 +5	2.02 +5	1.66 +5
24	2.00 +5	2.47 +5	2.75 +5	2.85 +5	2.81 +5	2.67 +5	2.47 +5	2.24 +5
25	2.63 +4	6.34 +4	1.03 +5	1.37 +5	1.62 +5	1.78 +5	1.85 +5	1.85 +5
26	2.03 +4	1.35 +3	3.00 +3	1.71 +4	3.66 +4	5.64 +4	7.39 +4	8.76 +4
27	1.48 +5	8.44 +4	3.99 +4	1.36 +4	1.90 +3	3.44 +2	4.91 +3	1.25 +4
28	2.62 +5	2.05 +5	1.48 +5	9.83 +4	6.01 +4	3.31 +4	1.58 +4	5.79 +3
29	2.64 +5	2.50 +5	2.19 +5	1.80 +5	1.41 +5	1.05 +5	7.54 +4	5.19 +4
30	1.71 +5	1.98 +5	2.05 +5	1.96 +5	1.77 +5	1.52 +5	1.27 +5	1.03 +5
31	6.51 +4	1.03 +5	1.32 +5	1.48 +5	1.52 +5	1.47 +5	1.37 +5	1.22 +5
32	7.17 +3	2.91 +4	5.56 +4	7.94 +4	9.64 +4	1.06 +5	1.09 +5	1.07 +5
33	3.79 +3	8.39 +2	1.10 +4	2.71 +4	4.37 +4	5.76 +4	6.74 +4	7.29 +4
34	2.70 +4	6.52 +3	2.69 +1	3.47 +3	1.22 +4	2.26 +4	3.23 +4	3.99 +4
35	5.41 +4	2.13 +4	6.91 +3	4.16 +2	9.70 +2	5.43 +3	1.15 +4	1.75 +4
36	1.45 +3	7.68 +4	6.29 +3	7.65 +3	2.29 +2	2.62 +2	2.71 +3	6.03 +3
37	2.76 +6	6.36 +5	5.52 +5	7.06 +4	5.73 +4	6.27 +3	6.41 +2	3.28 +3
38	7.89 +6	9.84 +6	6.63 +6	5.37 +6	2.74 +6	1.52 +6	6.19 +5	2.17 +5
39	2.62 +5	2.40 +4	1.81 +6	4.30 +6	7.95 +6	9.33 +6	9.37 +6	7.78 +6
40	1.93 +4	3.12 +5	1.30 +6	1.63 +6	1.59 +6	6.69 +5	3.55 +4	3.51 +5
41	7.39 +3	5.32 +4	1.76 +5	1.89 +5	1.51 +5	3.57 +4	4.13 +3	1.21 +5
$\sum_{v'} A_{v'v''}$	1.70 +7	1.65 +7	1.57 +7	1.64 +7	1.69 +7	1.56 +7	1.37 +7	1.19 +7

Table E.19: $A_{v'v''}$ for ^{7}Li singlet case (continued).

$v'\backslash v''$	56	57	58	59	60	61	62	63
0	1.74 -7	4.59 -7	7.94 -7	1.14 -6	1.46 -6	1.73 -6	1.94 -6	2.07 -6
1	3.11 -5	1.89 -5	1.14 -5	6.94 -6	4.20 -6	2.51 -6	1.49 -6	8.74 -7
2	2.41 -3	1.91 -3	1.53 -3	1.25 -3	1.03 -3	8.48 -4	7.02 -4	5.81 -4
3	2.83 -2	2.28 -2	1.86 -2	1.54 -2	1.29 -2	1.08 -2	9.15 -3	7.73 -3
4	2.65 -1	2.13 -1	1.73 -1	1.43 -1	1.20 -1	1.01 -1	8.53 -2	7.21 -2
5	2.13 +0	1.71 +0	1.39 +0	1.15 +0	9.63 -1	8.08 -1	6.81 -1	5.74 -1
6	1.37 +1	1.10 +1	9.02 +0	7.49 +0	6.29 +0	5.31 +0	4.49 +0	3.81 +0
7	7.69 +1	6.20 +1	5.07 +1	4.20 +1	3.52 +1	2.97 +1	2.51 +1	2.12 +1
8	3.57 +2	2.91 +2	2.39 +2	2.00 +2	1.69 +2	1.43 +2	1.22 +2	1.04 +2
9	1.45 +3	1.18 +3	9.72 +2	8.14 +2	6.88 +2	5.84 +2	4.97 +2	4.23 +2
10	4.98 +3	4.10 +3	3.42 +3	2.88 +3	2.45 +3	2.10 +3	1.80 +3	1.54 +3
11	1.49 +4	1.24 +4	1.03 +4	8.77 +3	7.50 +3	6.44 +3	5.54 +3	4.76 +3
12	3.85 +4	3.23 +4	2.72 +4	2.33 +4	2.01 +4	1.73 +4	1.50 +4	1.30 +4
13	8.48 +4	7.18 +4	6.12 +4	5.28 +4	4.59 +4	3.99 +4	3.47 +4	3.02 +4
14	1.61 +5	1.38 +5	1.19 +5	1.04 +5	9.09 +4	7.98 +4	7.00 +4	6.12 +4
15	2.61 +5	2.27 +5	1.99 +5	1.75 +5	1.55 +5	1.37 +5	1.22 +5	1.07 +5
16	3.54 +5	3.13 +5	2.78 +5	2.49 +5	2.23 +5	2.00 +5	1.79 +5	1.59 +5
17	3.95 +5	3.58 +5	3.24 +5	2.95 +5	2.69 +5	2.45 +5	2.22 +5	2.00 +5
18	3.44 +5	3.22 +5	2.99 +5	2.79 +5	2.60 +5	2.41 +5	2.22 +5	2.03 +5
19	2.15 +5	2.11 +5	2.06 +5	1.99 +5	1.92 +5	1.83 +5	1.73 +5	1.62 +5
20	7.15 +4	7.94 +4	8.49 +4	8.89 +4	9.14 +4	9.20 +4	9.11 +4	8.86 +4
21	1.03 +3	3.81 +3	7.36 +3	1.11 +4	1.47 +4	1.79 +4	2.05 +4	2.24 +4
22	3.80 +4	2.45 +4	1.53 +4	9.07 +3	5.01 +3	2.46 +3	9.86 +2	2.54 +2
23	1.34 +5	1.08 +5	8.68 +4	6.98 +4	5.61 +4	4.48 +4	3.57 +4	2.82 +4
24	1.99 +5	1.75 +5	1.53 +5	1.34 +5	1.17 +5	1.02 +5	8.85 +4	7.61 +4
25	1.79 +5	1.70 +5	1.59 +5	1.48 +5	1.38 +5	1.26 +5	1.15 +5	1.03 +5
26	9.67 +4	1.02 +5	1.04 +5	1.04 +5	1.03 +5	9.98 +4	9.54 +4	8.98 +4
27	2.09 +4	2.87 +4	3.53 +4	4.08 +4	4.51 +4	4.79 +4	4.94 +4	4.96 +4
28	1.14 +3	2.88 +0	9.59 +2	3.04 +3	5.63 +3	8.30 +3	1.07 +4	1.27 +4
29	3.42 +4	2.15 +4	1.28 +4	7.12 +3	3.52 +3	1.41 +3	3.61 +2	1.11 +1
30	8.13 +4	6.31 +4	4.83 +4	3.68 +4	2.77 +4	2.05 +4	1.49 +4	1.07 +4
31	1.07 +5	9.11 +4	7.70 +4	6.48 +4	5.43 +4	4.50 +4	3.70 +4	3.02 +4
32	1.00 +5	9.22 +4	8.33 +4	7.47 +4	6.64 +4	5.84 +4	5.09 +4	4.40 +4
33	7.46 +4	7.33 +4	7.02 +4	6.63 +4	6.19 +4	5.69 +4	5.17 +4	4.64 +4
34	4.51 +4	4.78 +4	4.88 +4	4.86 +4	4.75 +4	4.55 +4	4.28 +4	3.97 +4
35	2.27 +4	2.65 +4	2.90 +4	3.06 +4	3.14 +4	3.13 +4	3.05 +4	2.91 +4
36	9.61 +3	1.27 +4	1.52 +4	1.71 +4	1.84 +4	1.91 +4	1.93 +4	1.89 +4
37	2.73 +3	5.79 +3	7.09 +3	8.74 +3	9.85 +3	1.06 +4	1.11 +4	1.12 +4
38	9.92 +4	1.10 +4	1.72 +4	7.90 +2	7.33 +3	4.35 +3	6.20 +3	5.71 +3
39	5.52 +6	3.67 +6	1.88 +6	1.07 +6	3.96 +5	2.47 +5	5.67 +4	5.25 +4
40	1.92 +6	4.17 +6	6.56 +6	7.67 +6	8.26 +6	7.57 +6	6.98 +6	5.50 +6
41	3.61 +5	5.78 +5	6.82 +5	5.50 +5	3.48 +5	1.10 +5	2.86 +3	9.68 +4
$\sum_{v'} A_{v'v''}$	1.10 +7	1.12 +7	1.17 +7	1.16 +7	1.12 +7	9.91 +6	8.86 +6	7.30 +6

Table E.20: $A_{v'v''}$ for ^{7}Li singlet case (continued).

$v'\backslash v''$	64	65	66	67	68	69	70	71
0	2.13 -6	2.11 -6	2.02 -6	1.88 -6	1.71 -6	1.58 -6	1.49 -6	1.42 -6
1	5.07 -7	2.90 -7	1.65 -7	9.38 -8	5.40 -8	3.23 -8	2.00 -8	1.24 -8
2	4.81 -4	3.96 -4	3.24 -4	2.63 -4	2.15 -4	1.80 -4	1.57 -4	1.38 -4
3	6.51 -3	5.46 -3	4.55 -3	3.76 -3	3.11 -3	2.64 -3	2.33 -3	2.07 -3
4	6.09 -2	5.12 -2	4.27 -2	3.54 -2	2.93 -2	2.50 -2	2.20 -2	1.97 -2
5	4.84 -1	4.06 -1	3.38 -1	2.79 -1	2.31 -1	1.96 -1	1.73 -1	1.54 -1
6	3.22 +0	2.72 +0	2.27 +0	1.88 +0	1.56 +0	1.33 +0	1.18 +0	1.05 +0
7	1.79 +1	1.51 +1	1.26 +1	1.04 +1	8.62 +0	7.34 +0	6.48 +0	5.78 +0
8	8.80 +1	7.43 +1	6.23 +1	5.17 +1	4.30 +1	3.67 +1	3.25 +1	2.91 +1
9	3.60 +2	3.04 +2	2.55 +2	2.12 +2	1.76 +2	1.51 +2	1.33 +2	1.19 +2
10	1.31 +3	1.12 +3	9.39 +2	7.82 +2	6.53 +2	5.59 +2	4.96 +2	4.44 +2
11	4.08 +3	3.47 +3	2.93 +3	2.45 +3	2.05 +3	1.75 +3	1.56 +3	1.40 +3
12	1.12 +4	9.54 +3	8.08 +3	6.77 +3	5.68 +3	4.88 +3	4.35 +3	3.91 +3
13	2.61 +4	2.25 +4	1.91 +4	1.61 +4	1.35 +4	1.16 +4	1.04 +4	9.37 +3
14	5.33 +4	4.60 +4	3.93 +4	3.32 +4	2.80 +4	2.42 +4	2.17 +4	1.96 +4
15	9.40 +4	8.17 +4	7.02 +4	5.95 +4	5.04 +4	4.38 +4	3.93 +4	3.56 +4
16	1.41 +5	1.23 +5	1.07 +5	9.09 +4	7.74 +4	6.75 +4	6.08 +4	5.53 +4
17	1.78 +5	1.58 +5	1.37 +5	1.18 +5	1.01 +5	8.86 +4	8.02 +4	7.32 +4
18	1.84 +5	1.65 +5	1.45 +5	1.26 +5	1.09 +5	9.57 +4	8.72 +4	8.00 +4
19	1.50 +5	1.36 +5	1.22 +5	1.07 +5	9.31 +4	8.28 +4	7.60 +4	7.03 +4
20	8.47 +4	7.93 +4	7.27 +4	6.52 +4	5.78 +4	5.22 +4	4.86 +4	4.54 +4
21	2.35 +4	2.37 +4	2.31 +4	2.18 +4	2.01 +4	1.88 +4	1.80 +4	1.73 +4
22	9.54 +0	5.32 +1	2.35 +2	4.47 +2	6.31 +2	7.88 +2	9.37 +2	1.07 +3
23	2.21 +4	1.72 +4	1.33 +4	1.02 +4	7.83 +3	6.22 +3	5.13 +3	4.27 +3
24	6.50 +4	5.50 +4	4.60 +4	3.80 +4	3.14 +4	2.67 +4	2.34 +4	2.08 +4
25	9.21 +4	8.10 +4	7.02 +4	5.99 +4	5.10 +4	4.44 +4	3.99 +4	3.62 +4
26	8.32 +4	7.57 +4	6.76 +4	5.93 +4	5.16 +4	4.57 +4	4.19 +4	3.86 +4
27	4.85 +4	4.62 +4	4.29 +4	3.89 +4	3.47 +4	3.15 +4	2.95 +4	2.76 +4
28	1.42 +4	1.49 +4	1.50 +4	1.45 +4	1.37 +4	1.29 +4	1.25 +4	1.21 +4
29	9.16 +1	3.92 +2	7.54 +2	1.07 +3	1.31 +3	1.49 +3	1.67 +3	1.81 +3
30	7.52 +3	5.18 +3	3.49 +3	2.32 +3	1.54 +3	1.04 +3	7.23 +2	4.98 +2
31	2.44 +4	1.95 +4	1.55 +4	1.21 +4	9.55 +3	7.74 +3	6.50 +3	5.52 +3
32	3.76 +4	3.17 +4	2.64 +4	2.18 +4	1.79 +4	1.51 +4	1.32 +4	1.17 +4
33	4.11 +4	3.59 +4	3.08 +4	2.61 +4	2.20 +4	1.90 +4	1.69 +4	1.52 +4
34	3.61 +4	3.24 +4	2.84 +4	2.46 +4	2.11 +4	1.85 +4	1.67 +4	1.52 +4
35	2.72 +4	2.49 +4	2.24 +4	1.96 +4	1.71 +4	1.52 +4	1.39 +4	1.28 +4
36	1.81 +4	1.70 +4	1.55 +4	1.38 +4	1.22 +4	1.09 +4	1.01 +4	9.35 +3
37	1.09 +4	1.04 +4	9.63 +3	8.69 +3	7.74 +3	7.01 +3	6.52 +3	6.09 +3
38	5.93 +3	5.65 +3	5.32 +3	4.84 +3	4.35 +3	3.96 +3	3.70 +3	3.48 +3
39	2.70 +3	1.18 +4	4.35 +2	3.68 +3	1.60 +3	2.01 +3	1.70 +3	1.67 +3
40	4.47 +6	3.02 +6	2.15 +6	1.16 +6	6.70 +5	2.47 +5	1.26 +5	3.73 +4
41	4.47 +5	1.19 +6	2.21 +6	3.65 +6	4.90 +6	5.69 +6	5.61 +6	5.54 +6
$\sum_{v'} A_{v'v''}$	6.41 +6	5.55 +6	5.52 +6	5.82 +6	6.43 +6	6.70 +6	6.43 +6	6.22 +6

Table E.21: $A_{v'v''}$ for ^{7}Li singlet case (continued).

$v'\backslash v''$	72	73	74	75	76	77	78	79
0	1.34 -6	1.26 -6	1.17 -6	1.06 -6	9.47 -7	8.44 -7	7.53 -7	6.67 -7
1	7.65 -9	4.66 -9	2.78 -9	1.62 -9	9.26 -10	5.31 -10	3.04 -10	1.71 -10
2	1.22 -4	1.08 -4	9.49 -5	8.22 -5	7.00 -5	6.01 -5	5.20 -5	4.48 -5
3	1.85 -3	1.65 -3	1.47 -3	1.28 -3	1.10 -3	9.53 -4	8.28 -4	7.17 -4
4	1.76 -2	1.57 -2	1.40 -2	1.22 -2	1.05 -2	9.10 -3	7.92 -3	6.87 -3
5	1.38 -1	1.23 -1	1.09 -1	9.54 -2	8.20 -2	7.10 -2	6.17 -2	5.35 -2
6	9.40 -1	8.41 -1	7.48 -1	6.55 -1	5.63 -1	4.88 -1	4.25 -1	3.68 -1
7	5.17 +0	4.63 +0	4.11 +0	3.60 +0	3.09 +0	2.68 +0	2.33 +0	2.02 +0
8	2.60 +1	2.33 +1	2.08 +1	1.82 +1	1.57 +1	1.36 +1	1.18 +1	1.03 +1
9	1.07 +2	9.58 +1	8.53 +1	7.48 +1	6.44 +1	5.58 +1	4.87 +1	4.22 +1
10	3.99 +2	3.58 +2	3.19 +2	2.80 +2	2.42 +2	2.10 +2	1.83 +2	1.59 +2
11	1.26 +3	1.13 +3	1.01 +3	8.87 +2	7.66 +2	6.65 +2	5.81 +2	5.05 +2
12	3.52 +3	3.17 +3	2.83 +3	2.49 +3	2.15 +3	1.87 +3	1.64 +3	1.42 +3
13	8.46 +3	7.63 +3	6.83 +3	6.02 +3	5.21 +3	4.53 +3	3.96 +3	3.45 +3
14	1.77 +4	1.60 +4	1.44 +4	1.27 +4	1.10 +4	9.58 +3	8.39 +3	7.31 +3
15	3.23 +4	2.93 +4	2.63 +4	2.33 +4	2.02 +4	1.76 +4	1.54 +4	1.35 +4
16	5.03 +4	4.57 +4	4.12 +4	3.65 +4	3.18 +4	2.78 +4	2.44 +4	2.13 +4
17	6.69 +4	6.09 +4	5.51 +4	4.90 +4	4.27 +4	3.74 +4	3.29 +4	2.88 +4
18	7.34 +4	6.72 +4	6.10 +4	5.44 +4	4.76 +4	4.18 +4	3.69 +4	3.23 +4
19	6.49 +4	5.98 +4	5.46 +4	4.89 +4	4.30 +4	3.79 +4	3.35 +4	2.95 +4
20	4.24 +4	3.94 +4	3.63 +4	3.28 +4	2.90 +4	2.57 +4	2.29 +4	2.02 +4
21	1.65 +4	1.56 +4	1.47 +4	1.35 +4	1.21 +4	1.08 +4	9.73 +3	8.67 +3
22	1.17 +3	1.25 +3	1.29 +3	1.29 +3	1.23 +3	1.17 +3	1.10 +3	1.02 +3
23	3.57 +3	2.99 +3	2.49 +3	2.05 +3	1.67 +3	1.37 +3	1.14 +3	9.43 +2
24	1.85 +4	1.64 +4	1.45 +4	1.26 +4	1.08 +4	9.28 +3	8.04 +3	6.93 +3
25	3.28 +4	2.97 +4	2.67 +4	2.36 +4	2.05 +4	1.78 +4	1.56 +4	1.36 +4
26	3.55 +4	3.26 +4	2.96 +4	2.65 +4	2.32 +4	2.04 +4	1.80 +4	1.58 +4
27	2.59 +4	2.41 +4	2.22 +4	2.01 +4	1.78 +4	1.58 +4	1.41 +4	1.24 +4
28	1.17 +4	1.12 +4	1.05 +4	9.69 +3	8.72 +3	7.85 +3	7.07 +3	6.32 +3
29	1.92 +3	1.99 +3	2.00 +3	1.96 +3	1.85 +3	1.73 +3	1.61 +3	1.48 +3
30	3.38 +2	2.23 +2	1.42 +2	8.59 +1	4.95 +1	2.77 +1	1.47 +1	7.13 +0
31	4.71 +3	4.01 +3	3.40 +3	2.85 +3	2.35 +3	1.96 +3	1.65 +3	1.38 +3
32	1.03 +4	9.12 +3	8.01 +3	6.92 +3	5.89 +3	5.04 +3	4.35 +3	3.74 +3
33	1.37 +4	1.23 +4	1.10 +4	9.62 +3	8.29 +3	7.19 +3	6.26 +3	5.43 +3
34	1.39 +4	1.26 +4	1.13 +4	1.00 +4	8.73 +3	7.62 +3	6.68 +3	5.83 +3
35	1.17 +4	1.08 +4	9.77 +3	8.71 +3	7.62 +3	6.69 +3	5.89 +3	5.16 +3
36	8.67 +3	8.00 +3	7.31 +3	6.56 +3	5.76 +3	5.08 +3	4.50 +3	3.95 +3
37	5.68 +3	5.28 +3	4.85 +3	4.37 +3	3.85 +3	3.41 +3	3.03 +3	2.67 +3
38	3.26 +3	3.04 +3	2.80 +3	2.53 +3	2.24 +3	1.99 +3	1.77 +3	1.56 +3
39	1.54 +3	1.45 +3	1.34 +3	1.22 +3	1.08 +3	9.58 +2	8.53 +2	7.54 +2
40	2.74 +4	4.89 +3	6.22 +3	2.54 +2	1.55 +3	5.21 +1	4.82 +2	1.79 +2
41	5.30 +6	5.12 +6	4.80 +6	4.64 +6	4.27 +6	3.71 +6	2.99 +6	2.46 +6
$\sum_{v'} A_{v'v''}$	5.91 +6	5.66 +6	5.29 +6	5.07 +6	4.65 +6	4.04 +6	3.28 +6	2.72 +6

Table E.22: $A_{v'v''}$ for ^{7}Li singlet case (continued).

$v'\backslash v''$	80	81	82	83	84	85	86	87
0	5.89 -7	5.19 -7	4.54 -7	3.95 -7	3.42 -7	2.95 -7	2.53 -7	2.16 -7
1	9.55 -11	5.24 -11	2.80 -11	1.45 -11	7.21 -12	3.37 -12	1.44 -12	5.32 -13
2	3.85 -5	3.32 -5	2.85 -5	2.44 -5	2.09 -5	1.78 -5	1.51 -5	1.28 -5
3	6.21 -4	5.37 -4	4.63 -4	3.98 -4	3.41 -4	2.91 -4	2.48 -4	2.10 -4
4	5.95 -3	5.15 -3	4.44 -3	3.82 -3	3.27 -3	2.80 -3	2.38 -3	2.02 -3
5	4.63 -2	4.00 -2	3.45 -2	2.97 -2	2.54 -2	2.17 -2	1.85 -2	1.57 -2
6	3.19 -1	2.76 -1	2.38 -1	2.05 -1	1.76 -1	1.50 -1	1.28 -1	1.09 -1
7	1.75 +0	1.52 +0	1.31 +0	1.12 +0	9.64 -1	8.24 -1	7.02 -1	5.95 -1
8	8.90 +0	7.71 +0	6.65 +0	5.72 +0	4.91 +0	4.20 +0	3.58 +0	3.03 +0
9	3.66 +1	3.17 +1	2.74 +1	2.36 +1	2.02 +1	1.73 +1	1.47 +1	1.25 +1
10	1.38 +2	1.19 +2	1.03 +2	8.87 +1	7.62 +1	6.52 +1	5.55 +1	4.71 +1
11	4.38 +2	3.80 +2	3.28 +2	2.83 +2	2.43 +2	2.08 +2	1.77 +2	1.50 +2
12	1.23 +3	1.07 +3	9.26 +2	7.98 +2	6.85 +2	5.87 +2	5.00 +2	4.24 +2
13	3.00 +3	2.60 +3	2.25 +3	1.94 +3	1.67 +3	1.43 +3	1.22 +3	1.03 +3
14	6.36 +3	5.53 +3	4.78 +3	4.12 +3	3.55 +3	3.04 +3	2.59 +3	2.20 +3
15	1.17 +4	1.02 +4	8.84 +3	7.63 +3	6.56 +3	5.63 +3	4.80 +3	4.08 +3
16	1.86 +4	1.62 +4	1.40 +4	1.21 +4	1.04 +4	8.94 +3	7.63 +3	6.48 +3
17	2.51 +4	2.19 +4	1.90 +4	1.64 +4	1.42 +4	1.22 +4	1.04 +4	8.84 +3
18	2.83 +4	2.47 +4	2.15 +4	1.86 +4	1.60 +4	1.38 +4	1.18 +4	1.00 +4
19	2.58 +4	2.26 +4	1.97 +4	1.71 +4	1.47 +4	1.27 +4	1.09 +4	9.24 +3
20	1.78 +4	1.56 +4	1.36 +4	1.18 +4	1.02 +4	8.83 +3	7.57 +3	6.46 +3
21	7.69 +3	6.80 +3	5.97 +3	5.21 +3	4.53 +3	3.92 +3	3.37 +3	2.88 +3
22	9.37 +2	8.52 +2	7.67 +2	6.84 +2	6.05 +2	5.31 +2	4.62 +2	4.00 +2
23	7.84 +2	6.55 +2	5.47 +2	4.57 +2	3.82 +2	3.19 +2	2.67 +2	2.22 +2
24	5.98 +3	5.15 +3	4.43 +3	3.79 +3	3.24 +3	2.77 +3	2.35 +3	1.99 +3
25	1.18 +4	1.03 +4	8.90 +3	7.67 +3	6.60 +3	5.65 +3	4.82 +3	4.09 +3
26	1.38 +4	1.21 +4	1.05 +4	9.08 +3	7.83 +3	6.73 +3	5.76 +3	4.90 +3
27	1.09 +4	9.60 +3	8.38 +3	7.28 +3	6.30 +3	5.43 +3	4.66 +3	3.97 +3
28	5.61 +3	4.97 +3	4.37 +3	3.82 +3	3.32 +3	2.88 +3	2.48 +3	2.12 +3
29	1.35 +3	1.22 +3	1.09 +3	9.68 +2	8.53 +2	7.46 +2	6.48 +2	5.59 +2
30	3.05 +0	1.04 +0	2.06 -1	4.07 -4	9.25 -2	2.91 -1	4.94 -1	6.55 -1
31	1.16 +3	9.82 +2	8.27 +2	6.97 +2	5.87 +2	4.94 +2	4.15 +2	3.47 +2
32	3.21 +3	2.76 +3	2.36 +3	2.02 +3	1.72 +3	1.47 +3	1.24 +3	1.05 +3
33	4.70 +3	4.07 +3	3.51 +3	3.02 +3	2.59 +3	2.21 +3	1.88 +3	1.60 +3
34	5.07 +3	4.41 +3	3.82 +3	3.29 +3	2.83 +3	2.43 +3	2.07 +3	1.76 +3
35	4.51 +3	3.94 +3	3.42 +3	2.95 +3	2.55 +3	2.19 +3	1.87 +3	1.59 +3
36	3.46 +3	3.03 +3	2.64 +3	2.28 +3	1.97 +3	1.70 +3	1.45 +3	1.24 +3
37	2.34 +3	2.05 +3	1.79 +3	1.55 +3	1.34 +3	1.16 +3	9.90 +2	8.43 +2
38	1.37 +3	1.20 +3	1.05 +3	9.13 +2	7.90 +2	6.80 +2	5.83 +2	4.97 +2
39	6.64 +2	5.84 +2	5.10 +2	4.43 +2	3.84 +2	3.31 +2	2.83 +2	2.42 +2
40	2.55 +2	1.84 +2	1.74 +2	1.46 +2	1.28 +2	1.10 +2	9.40 +1	8.01 +1
41	1.91 +6	1.47 +6	1.06 +6	7.64 +5	5.06 +5	3.38 +5	2.01 +5	1.22 +5
$\sum_{v'} A_{v'v''}$	2.14 +6	1.66 +6	1.23 +6	9.11 +5	6.33 +5	4.47 +5	2.95 +5	2.01 +5

Table E.23: $A_{v'v''}$ for ^{7}Li singlet case (continued).

$v'\backslash v''$	88	89	90	91	92	93	94	95
0	1.83 -7	1.55 -7	1.30 -7	1.08 -7	8.90 -8	7.30 -8	5.88 -8	4.80 -8
1	1.48 -13	1.86 -14	1.32 -15	2.40 -14	5.26 -14	7.52 -14	8.40 -14	9.05 -14
2	1.08 -5	9.02 -6	7.51 -6	6.22 -6	5.12 -6	4.19 -6	3.39 -6	2.73 -6
3	1.77 -4	1.49 -4	1.24 -4	1.03 -4	8.47 -5	6.93 -5	5.62 -5	4.52 -5
4	1.70 -3	1.43 -3	1.19 -3	9.90 -4	8.15 -4	6.67 -4	5.41 -4	4.35 -4
5	1.32 -2	1.11 -2	9.26 -3	7.68 -3	6.33 -3	5.17 -3	4.20 -3	3.38 -3
6	9.15 -2	7.68 -2	6.41 -2	5.32 -2	4.38 -2	3.58 -2	2.91 -2	2.34 -2
7	5.02 -1	4.21 -1	3.51 -1	2.91 -1	2.40 -1	1.96 -1	1.59 -1	1.28 -1
8	2.56 +0	2.15 +0	1.79 +0	1.49 +0	1.22 +0	1.00 +0	8.12 -1	6.53 -1
9	1.05 +1	8.85 +0	7.38 +0	6.12 +0	5.05 +0	4.13 +0	3.35 +0	2.69 +0
10	3.97 +1	3.34 +1	2.79 +1	2.31 +1	1.90 +1	1.56 +1	1.26 +1	1.02 +1
11	1.27 +2	1.06 +2	8.88 +1	7.37 +1	6.07 +1	4.97 +1	4.03 +1	3.24 +1
12	3.58 +2	3.01 +2	2.51 +2	2.08 +2	1.72 +2	1.41 +2	1.14 +2	9.17 +1
13	8.73 +2	7.34 +2	6.13 +2	5.08 +2	4.19 +2	3.43 +2	2.78 +2	2.24 +2
14	1.86 +3	1.56 +3	1.30 +3	1.08 +3	8.92 +2	7.30 +2	5.93 +2	4.77 +2
15	3.45 +3	2.90 +3	2.42 +3	2.01 +3	1.66 +3	1.35 +3	1.10 +3	8.85 +2
16	5.48 +3	4.61 +3	3.85 +3	3.20 +3	2.64 +3	2.16 +3	1.75 +3	1.41 +3
17	7.47 +3	6.28 +3	5.25 +3	4.36 +3	3.60 +3	2.94 +3	2.39 +3	1.92 +3
18	8.47 +3	7.13 +3	5.96 +3	4.95 +3	4.08 +3	3.34 +3	2.72 +3	2.19 +3
19	7.83 +3	6.59 +3	5.51 +3	4.58 +3	3.78 +3	3.10 +3	2.52 +3	2.02 +3
20	5.47 +3	4.61 +3	3.86 +3	3.21 +3	2.65 +3	2.17 +3	1.77 +3	1.42 +3
21	2.45 +3	2.07 +3	1.73 +3	1.44 +3	1.19 +3	9.79 +2	7.96 +2	6.41 +2
22	3.43 +2	2.91 +2	2.46 +2	2.06 +2	1.71 +2	1.41 +2	1.15 +2	9.26 +1
23	1.85 +2	1.53 +2	1.26 +2	1.04 +2	8.50 +1	6.91 +1	5.58 +1	4.47 +1
24	1.68 +3	1.40 +3	1.17 +3	9.69 +2	7.98 +2	6.52 +2	5.29 +2	4.25 +2
25	3.46 +3	2.90 +3	2.42 +3	2.01 +3	1.66 +3	1.36 +3	1.10 +3	8.86 +2
26	4.14 +3	3.49 +3	2.91 +3	2.42 +3	2.00 +3	1.64 +3	1.33 +3	1.07 +3
27	3.37 +3	2.84 +3	2.37 +3	1.98 +3	1.63 +3	1.34 +3	1.09 +3	8.74 +2
28	1.80 +3	1.52 +3	1.27 +3	1.06 +3	8.78 +2	7.20 +2	5.86 +2	4.72 +2
29	4.78 +2	4.06 +2	3.42 +2	2.86 +2	2.37 +2	1.95 +2	1.59 +2	1.28 +2
30	7.56 -1	8.01 -1	7.97 -1	7.58 -1	6.94 -1	6.17 -1	5.35 -1	4.53 -1
31	2.90 +2	2.41 +2	2.00 +2	1.65 +2	1.35 +2	1.10 +2	8.89 +1	7.13 +1
32	8.84 +2	7.40 +2	6.16 +2	5.10 +2	4.19 +2	3.43 +2	2.78 +2	2.23 +2
33	1.35 +3	1.13 +3	9.42 +2	7.81 +2	6.43 +2	5.26 +2	4.27 +2	3.43 +2
34	1.49 +3	1.25 +3	1.04 +3	8.65 +2	7.13 +2	5.84 +2	4.74 +2	3.81 +2
35	1.34 +3	1.13 +3	9.44 +2	7.84 +2	6.47 +2	5.30 +2	4.30 +2	3.46 +2
36	1.05 +3	8.80 +2	7.36 +2	6.12 +2	5.05 +2	4.13 +2	3.36 +2	2.70 +2
37	7.14 +2	6.02 +2	5.03 +2	4.19 +2	3.45 +2	2.83 +2	2.30 +2	1.85 +2
38	4.21 +2	3.55 +2	2.97 +2	2.47 +2	2.04 +2	1.67 +2	1.36 +2	1.09 +2
39	2.05 +2	1.73 +2	1.45 +2	1.20 +2	9.92 +1	8.13 +1	6.61 +1	5.32 +1
40	6.79 +1	5.72 +1	4.79 +1	3.99 +1	3.29 +1	2.70 +1	2.19 +1	1.77 +1
41	6.34 +4	3.40 +4	1.47 +4	6.81 +3	2.19 +3	8.76 +2	1.60 +2	6.28 +1
$\sum_{v'} A_{v'v''}$	1.31 +5	9.05 +4	6.19 +4	4.60 +4	3.46 +4	2.74 +4	2.17 +4	1.74 +4

Table E.24: $A_{v'v''}$ for ^{7}Li singlet case (continued).

$v'\backslash v''$	96	97	98	99	100	$\sum_{v''} A_{v'v''}$
0	3.99 -8	2.84 -8	2.40 -8	2.92 -8	3.77 -8	6.70 +7
1	9.36 -14	6.68 -14	5.93 -14	8.83 -14	1.36 -13	6.64 +7
2	2.18 -6	1.71 -6	1.49 -6	1.68 -6	2.00 -6	6.59 +7
3	3.60 -5	2.85 -5	2.49 -5	2.79 -5	3.30 -5	6.53 +7
4	3.47 -4	2.74 -4	2.39 -4	2.69 -4	3.17 -4	6.47 +7
5	2.69 -3	2.13 -3	1.86 -3	2.08 -3	2.46 -3	6.42 +7
6	1.86 -2	1.48 -2	1.29 -2	1.44 -2	1.70 -2	6.36 +7
7	1.02 -1	8.08 -2	7.05 -2	7.91 -2	9.34 -2	6.31 +7
8	5.20 -1	4.12 -1	3.60 -1	4.04 -1	4.77 -1	6.25 +7
9	2.14 +0	1.70 +0	1.48 +0	1.66 +0	1.96 +0	6.20 +7
10	8.09 +0	6.42 +0	5.60 +0	6.28 +0	7.41 +0	6.14 +7
11	2.58 +1	2.05 +1	1.79 +1	2.00 +1	2.37 +1	6.09 +7
12	7.31 +1	5.79 +1	5.05 +1	5.67 +1	6.69 +1	6.03 +7
13	1.78 +2	1.41 +2	1.23 +2	1.38 +2	1.63 +2	5.94 +7
14	3.80 +2	3.01 +2	2.63 +2	2.95 +2	3.48 +2	5.84 +7
15	7.05 +2	5.59 +2	4.88 +2	5.47 +2	6.46 +2	5.69 +7
16	1.12 +3	8.90 +2	7.77 +2	8.72 +2	1.03 +3	5.47 +7
17	1.53 +3	1.22 +3	1.06 +3	1.19 +3	1.41 +3	5.19 +7
18	1.74 +3	1.38 +3	1.21 +3	1.35 +3	1.60 +3	4.87 +7
19	1.61 +3	1.28 +3	1.12 +3	1.25 +3	1.48 +3	4.56 +7
20	1.13 +3	8.99 +2	7.85 +2	8.81 +2	1.04 +3	4.34 +7
21	5.11 +2	4.06 +2	3.54 +2	3.98 +2	4.70 +2	4.21 +7
22	7.40 +1	5.88 +1	5.14 +1	5.78 +1	6.84 +1	4.18 +7
23	3.55 +1	2.80 +1	2.44 +1	2.73 +1	3.22 +1	4.19 +7
24	3.38 +2	2.68 +2	2.34 +2	2.62 +2	3.10 +2	4.19 +7
25	7.06 +2	5.59 +2	4.88 +2	5.48 +2	6.47 +2	4.15 +7
26	8.52 +2	6.76 +2	5.90 +2	6.62 +2	7.82 +2	4.08 +7
27	6.97 +2	5.53 +2	4.83 +2	5.42 +2	6.40 +2	4.04 +7
28	3.76 +2	2.99 +2	2.61 +2	2.93 +2	3.46 +2	4.05 +7
29	1.03 +2	8.14 +1	7.12 +1	8.00 +1	9.47 +1	4.10 +7
30	3.76 -1	3.07 -1	2.75 -1	3.16 -1	3.84 -1	4.19 +7
31	5.66 +1	4.48 +1	3.90 +1	4.37 +1	5.15 +1	4.30 +7
32	1.78 +2	1.41 +2	1.23 +2	1.38 +2	1.62 +2	4.43 +7
33	2.73 +2	2.17 +2	1.89 +2	2.12 +2	2.50 +2	4.59 +7
34	3.04 +2	2.41 +2	2.10 +2	2.36 +2	2.78 +2	4.79 +7
35	2.76 +2	2.19 +2	1.91 +2	2.14 +2	2.53 +2	5.04 +7
36	2.15 +2	1.71 +2	1.49 +2	1.67 +2	1.98 +2	5.36 +7
37	1.48 +2	1.17 +2	1.02 +2	1.15 +2	1.35 +2	5.75 +7
38	8.71 +1	6.91 +1	6.03 +1	6.77 +1	8.00 +1	6.19 +7
39	4.24 +1	3.36 +1	2.94 +1	3.30 +1	3.90 +1	6.62 +7
40	1.41 +1	1.12 +1	9.76 +0	1.10 +1	1.30 +1	7.02 +7
41	9.23 -1	2.31 +0	1.82 +0	8.89 -1	1.74 +0	7.29 +7
$\sum_{v'} A_{v'v''}$	1.38 +4	1.09 +4	9.56 +3	1.07 +4	1.27 +4	

Table E.25: $A_{v'v''}$ for ^{7}Li singlet case (continued).

$v'\backslash v''$	0	1	2	3	4	5	6	7
0	6.18 +3	5.05 +4	2.10 +5	5.93 +5	1.27 +6	2.21 +6	3.21 +6	4.00 +6
1	2.31 +4	1.59 +5	5.45 +5	1.21 +6	1.94 +6	2.30 +6	2.00 +6	1.16 +6
2	4.83 +4	2.85 +5	8.07 +5	1.40 +6	1.60 +6	1.13 +6	3.58 +5	8.86 +2
3	7.45 +4	3.81 +5	8.97 +5	1.21 +6	9.26 +5	2.76 +5	8.35 +3	4.74 +5
4	9.37 +4	4.22 +5	8.36 +5	8.72 +5	4.03 +5	8.55 +3	2.45 +5	8.01 +5
5	1.00 +5	4.03 +5	6.85 +5	5.53 +5	1.30 +5	3.30 +4	4.23 +5	6.93 +5
6	9.12 +4	3.36 +5	5.01 +5	3.18 +5	2.83 +4	9.65 +4	4.12 +5	4.38 +5
7	6.76 +4	2.33 +5	3.15 +5	1.63 +5	2.93 +3	1.06 +5	2.90 +5	2.24 +5
8	3.75 +4	1.24 +5	1.58 +5	7.15 +4	2.60 +1	6.80 +4	1.51 +5	9.50 +4
9	1.11 +4	3.62 +4	4.48 +4	1.91 +4	2.33 +1	2.12 +4	4.32 +4	2.48 +4
$\sum_{v'} A_{v'v''}$	5.53 +5	2.43 +6	5.00 +6	6.42 +6	6.30 +6	6.25 +6	7.14 +6	7.91 +6

$v'\backslash v''$	8	9	10	11	12	13	14	15
0	4.35 +6	4.31 +6	4.09 +6	3.61 +6	2.73 +6	1.81 +6	1.07 +6	5.98 +5
1	3.17 +5	2.05 +3	4.71 +5	1.72 +6	3.30 +6	4.54 +6	4.87 +6	4.35 +6
2	4.31 +5	1.30 +6	1.97 +6	1.89 +6	9.88 +5	1.11 +5	2.07 +5	1.42 +6
3	1.14 +6	1.25 +6	7.24 +5	8.59 +4	1.87 +5	1.20 +6	2.15 +6	2.02 +6
4	9.03 +5	4.28 +5	1.25 +4	2.75 +5	1.06 +6	1.40 +6	7.85 +5	5.68 +4
5	4.22 +5	3.65 +4	1.34 +5	6.74 +5	9.19 +5	4.66 +5	5.61 +3	3.71 +5
6	1.32 +5	1.10 +4	3.01 +5	6.09 +5	4.30 +5	3.94 +4	1.58 +5	7.19 +5
7	2.80 +4	5.04 +4	2.79 +5	3.62 +5	1.39 +5	5.25 +3	2.69 +5	5.39 +5
8	4.28 +3	4.57 +4	1.61 +5	1.63 +5	3.66 +4	2.08 +4	1.86 +5	2.62 +5
9	5.12 +2	1.58 +4	4.78 +4	4.34 +4	7.16 +3	9.41 +3	5.83 +4	7.15 +4
$\sum_{v'} A_{v'v''}$	7.72 +6	7.45 +6	8.19 +6	9.43 +6	9.79 +6	9.60 +6	9.76 +6	1.04 +7

Table E.26: Spontaneous emission coefficient $A_{v'v''}$ for the ^{6}Li triplet case.

$v'\backslash v''$	16	17	18	19	20	21	22	23
0	3.16 +5	1.52 +5	6.79 +4	2.99 +4	1.19 +4	3.99 +3	1.43 +3	4.83 +2
1	3.43 +6	2.45 +6	1.59 +6	9.36 +5	5.08 +5	2.55 +5	1.15 +5	4.73 +4
2	3.07 +6	4.40 +6	4.97 +6	4.73 +6	3.92 +6	2.88 +6	1.89 +6	1.11 +6
3	1.00 +6	1.14 +5	1.84 +5	1.37 +6	3.15 +6	4.73 +6	5.51 +6	5.32 +6
4	2.68 +5	1.30 +6	2.14 +6	2.03 +6	1.05 +6	1.23 +5	2.15 +5	1.62 +6
5	1.16 +6	1.34 +6	7.09 +5	5.39 +4	2.46 +5	1.29 +6	2.24 +6	2.17 +6
6	8.76 +5	3.98 +5	4.08 +3	3.10 +5	1.03 +6	1.33 +6	8.00 +5	9.23 +4
7	3.65 +5	3.68 +4	1.02 +5	5.25 +5	7.53 +5	4.64 +5	4.45 +4	1.48 +5
8	1.15 +5	1.62 +1	1.28 +5	3.32 +5	3.20 +5	1.03 +5	6.32 +3	2.35 +5
9	2.48 +4	1.14 +3	4.70 +4	9.84 +4	7.98 +4	1.67 +4	8.55 +3	8.76 +4
$\sum_{v'} A_{v'v''}$	1.06 +7	1.02 +7	9.94 +6	1.04 +7	1.11 +7	1.12 +7	1.08 +7	1.08 +7

$v'\backslash v''$	24	25	26	27	28	29	30	31
0	8.79 +1	2.88 +1	1.03 +1	2.18 -4	1.00 +0	6.62 -2	2.75 -1	5.29 -1
1	1.77 +4	5.65 +3	1.67 +3	4.68 +2	9.20 +1	2.33 +1	4.45 +0	1.40 -1
2	5.80 +5	2.70 +5	1.12 +5	4.14 +4	1.37 +4	3.96 +3	1.05 +3	2.39 +2
3	4.37 +6	3.10 +6	1.92 +6	1.04 +6	5.04 +5	2.15 +5	8.12 +4	2.76 +4
4	3.76 +6	5.58 +6	6.30 +6	5.78 +6	4.47 +6	2.98 +6	1.73 +6	8.82 +5
5	1.10 +6	8.82 +4	3.70 +5	2.19 +6	4.65 +6	6.49 +6	6.95 +6	6.10 +6
6	2.04 +5	1.30 +6	2.38 +6	2.29 +6	1.09 +6	5.76 +4	5.06 +5	2.61 +6
7	8.01 +5	1.26 +6	9.08 +5	1.75 +5	1.02 +5	1.06 +6	2.20 +6	2.35 +6
8	5.36 +5	5.02 +5	1.57 +5	1.17 +4	3.87 +5	9.13 +5	9.51 +5	4.25 +5
9	1.57 +5	1.16 +5	1.87 +4	2.09 +4	1.57 +5	2.69 +5	2.07 +5	4.58 +4
$\sum_{v'} A_{v'v''}$	1.15 +7	1.22 +7	1.22 +7	1.16 +7	1.14 +7	1.20 +7	1.26 +7	1.24 +7

Table E.27: $A_{v'v''}$ for ^{6}Li triplet case (continued).

$v'\backslash v''$	32	33	34	35	36	37	38	39
0	2.75 -1	4.20 -2	1.45 -2	1.20 -1	2.00 -1	1.91 -1	1.22 -1	5.01 -2
1	5.51 -1	5.25 -2	1.74 -2	1.22 -2	5.60 -2	8.57 -2	7.84 -2	5.08 -2
2	4.67 +1	9.07 +0	7.05 -1	3.24 -1	3.83 -6	1.60 -3	6.94 -3	1.61 -2
3	8.08 +3	2.06 +3	4.61 +2	8.09 +1	1.53 +1	1.19 +0	3.16 -1	1.06 -2
4	3.96 +5	1.55 +5	5.25 +4	1.55 +4	3.86 +3	8.44 +2	1.47 +2	2.56 +1
5	4.52 +6	2.87 +6	1.57 +6	7.43 +5	3.04 +5	1.07 +5	3.27 +4	8.74 +3
6	5.37 +6	7.36 +6	7.76 +6	6.66 +6	4.79 +6	2.93 +6	1.54 +6	7.13 +5
7	1.32 +6	1.56 +5	3.14 +5	2.31 +6	5.29 +6	7.72 +6	8.55 +6	7.74 +6
8	4.45 +3	3.78 +5	1.42 +6	2.19 +6	1.90 +6	7.89 +5	1.24 +4	6.30 +5
9	1.78 +4	2.27 +5	4.90 +5	5.15 +5	2.55 +5	1.12 +4	1.41 +5	6.71 +5
$\sum_{v'} A_{v'v''}$	1.16 +7	1.11 +7	1.16 +7	1.24 +7	1.25 +7	1.16 +7	1.03 +7	9.76 +6

$v'\backslash v''$	40	41	42	43	44	45	46	47
0	8.40 -3	6.85 -4	1.42 -2	3.41 -2	5.01 -2	5.84 -2	5.94 -2	5.50 -2
1	2.29 -2	5.68 -3	5.86 -5	2.20 -3	7.54 -3	1.29 -2	1.67 -2	1.86 -2
2	2.30 -2	2.23 -2	1.74 -2	1.12 -2	5.98 -3	2.50 -3	6.65 -4	2.95 -5
3	3.21 -4	1.50 -2	2.22 -2	2.79 -2	2.78 -2	2.45 -2	1.96 -2	1.43 -2
4	3.08 +0	3.04 -1	7.30 -2	9.13 -3	3.32 -2	3.00 -2	2.81 -2	2.31 -2
5	2.05 +3	4.02 +2	6.57 +1	1.03 +1	1.06 +0	2.01 -1	1.08 -3	3.02 -2
6	2.90 +5	1.02 +5	3.14 +4	8.55 +3	2.07 +3	4.16 +2	7.52 +1	1.19 +1
7	5.94 +6	3.93 +6	2.27 +6	1.16 +6	5.29 +5	2.13 +5	7.63 +4	2.51 +4
8	2.77 +6	5.57 +6	7.85 +6	8.80 +6	8.33 +6	6.83 +6	4.94 +6	3.22 +6
9	1.24 +6	1.40 +6	1.01 +6	3.62 +5	1.63 +3	3.58 +5	1.49 +6	3.09 +6
$\sum_{v'} A_{v'v''}$	1.02 +7	1.10 +7	1.12 +7	1.03 +7	8.86 +6	7.41 +6	6.51 +6	6.34 +6

Table E.28: $A_{v'v''}$ for ^{6}Li triplet case (continued).

$v'\backslash v''$	48	49	50	51	52	53	54	55
0	4.74 -2	3.84 -2	2.95 -2	2.16 -2	1.51 -2	1.01 -2	6.56 -3	4.18 -3
1	1.87 -2	1.75 -2	1.55 -2	1.31 -2	1.07 -2	8.37 -3	6.40 -3	4.85 -3
2	1.22 -4	5.68 -4	1.10 -3	1.57 -3	1.88 -3	2.02 -3	2.01 -3	1.90 -3
3	9.62 -3	5.84 -3	3.14 -3	1.43 -3	4.95 -4	9.25 -5	7.18 -9	5.08 -5
4	1.80 -2	1.32 -2	9.33 -3	6.30 -3	4.06 -3	2.49 -3	1.46 -3	8.28 -4
5	1.83 -2	1.79 -2	1.37 -2	1.03 -2	7.38 -3	5.14 -3	3.49 -3	2.36 -3
6	2.12 +0	1.66 -1	7.35 -2	2.83 -3	1.12 -2	6.19 -3	4.91 -3	3.58 -3
7	7.78 +3	2.24 +3	5.67 +2	1.26 +2	2.30 +1	3.77 +0	2.58 -1	4.95 -2
8	1.97 +6	1.13 +6	6.00 +5	2.93 +5	1.30 +5	5.11 +4	1.68 +4	4.45 +3
9	4.75 +6	6.19 +6	7.21 +6	7.69 +6	7.63 +6	7.04 +6	5.96 +6	4.46 +6
$\sum_{v'} A_{v'v''}$	6.72 +6	7.32 +6	7.81 +6	7.99 +6	7.76 +6	7.09 +6	5.97 +6	4.46 +6

$v'\backslash v''$	56	57	58	59	60	61	62	63
0	2.69 -3	1.75 -3	1.11 -3	6.75 -4	3.86 -4	2.02 -4	9.33 -5	3.64 -5
1	3.76 -3	3.01 -3	2.41 -3	1.94 -3	1.54 -3	1.22 -3	9.41 -4	7.25 -4
2	1.79 -3	1.71 -3	1.62 -3	1.53 -3	1.42 -3	1.29 -3	1.14 -3	9.98 -4
3	1.50 -4	2.65 -4	3.79 -4	4.79 -4	5.58 -4	6.08 -4	6.22 -4	6.07 -4
4	4.62 -4	2.49 -4	1.20 -4	4.74 -5	1.19 -5	3.58 -7	2.71 -6	1.09 -5
5	1.64 -3	1.17 -3	8.34 -4	5.88 -4	4.08 -4	2.77 -4	1.82 -4	1.18 -4
6	2.71 -3	2.11 -3	1.63 -3	1.25 -3	9.50 -4	7.07 -4	5.14 -4	3.72 -4
7	4.42 -4	2.14 -3	6.34 -4	4.68 -4	3.09 -4	2.60 -4	2.41 -4	2.36 -4
8	9.23 +2	1.80 +2	4.38 +1	9.02 +0	2.06 +0	2.40 -1	9.42 -2	1.27 -4
9	2.86 +6	1.67 +6	1.01 +6	6.16 +5	3.64 +5	2.10 +5	1.18 +5	5.77 +4
$\sum_{v'} A_{v'v''}$	2.86 +6	1.67 +6	1.01 +6	6.16 +5	3.64 +5	2.10 +5	1.18 +5	5.77 +4

Table E.29: $A_{v'v''}$ for ^{6}Li triplet case (continued).

$v'\backslash v''$	64	65	66	67	68	69	70	71
0	1.06 -5	1.17 -6	3.21 -7	3.20 -6	7.12 -6	1.07 -5	1.33 -5	1.49 -5
1	5.70 -4	4.47 -4	3.54 -4	2.81 -4	2.24 -4	1.79 -4	1.44 -4	1.16 -4
2	8.79 -4	7.66 -4	6.67 -4	5.76 -4	4.96 -4	4.25 -4	3.62 -4	3.07 -4
3	5.86 -4	5.51 -4	5.11 -4	4.65 -4	4.18 -4	3.71 -4	3.26 -4	2.84 -4
4	2.06 -5	2.92 -5	3.58 -5	3.99 -5	4.17 -5	4.17 -5	4.02 -5	3.76 -5
5	7.76 -5	5.03 -5	3.26 -5	2.10 -5	1.34 -5	8.58 -6	5.48 -6	3.50 -6
6	2.74 -4	2.02 -4	1.51 -4	1.13 -4	8.54 -5	6.51 -5	5.00 -5	3.86 -5
7	2.37 -4	2.34 -4	2.27 -4	2.14 -4	1.97 -4	1.79 -4	1.59 -4	1.39 -4
8	3.10 -3	2.68 -4	1.40 -4	1.08 -5	1.34 -6	1.57 -5	3.01 -5	3.85 -5
9	2.43 +4	9.90 +3	3.78 +3	1.25 +3	3.69 +2	1.06 +2	2.05 +1	5.20 +0
$\sum_{v'} A_{v'v''}$	2.43 +4	9.90 +3	3.78 +3	1.25 +3	3.69 +2	1.06 +2	2.05 +1	5.20 +0

$v'\backslash v''$	72	73	74	75	76	77	78	79
0	1.54 -5	1.51 -5	1.42 -5	1.29 -5	1.15 -5	9.92 -6	8.40 -6	6.95 -6
1	9.30 -5	7.49 -5	6.03 -5	4.85 -5	3.89 -5	3.11 -5	2.47 -5	1.95 -5
2	2.59 -4	2.17 -4	1.81 -4	1.49 -4	1.23 -4	9.99 -5	8.07 -5	6.46 -5
3	2.44 -4	2.08 -4	1.76 -4	1.47 -4	1.22 -4	1.00 -4	8.15 -5	6.55 -5
4	3.43 -5	3.07 -5	2.69 -5	2.32 -5	1.98 -5	1.65 -5	1.37 -5	1.12 -5
5	2.24 -6	1.44 -6	9.28 -7	6.05 -7	3.99 -7	2.66 -7	1.80 -7	1.30 -7
6	3.00 -5	2.34 -5	1.84 -5	1.44 -5	1.13 -5	8.91 -6	6.99 -6	5.38 -6
7	1.20 -4	1.03 -4	8.70 -5	7.28 -5	6.03 -5	4.95 -5	4.02 -5	3.26 -5
8	4.15 -5	4.07 -5	3.76 -5	3.35 -5	2.90 -5	2.45 -5	2.04 -5	1.73 -5
9	5.27 -1	1.26 -1	5.04 -3	4.19 -4	5.37 -4	6.48 -4	9.01 -4	9.34 -4
$\sum_{v'} A_{v'v''}$	5.28 -1	1.27 -1	5.64 -3	9.21 -4	9.53 -4	9.89 -4	1.18 -3	1.16 -3

Table E.30: $A_{v'v''}$ for ^{6}Li triplet case (continued).

$v'\backslash v''$	80	81	82	83	84	85	$\sum_{v''} A_{v'v''}$
0	5.63 -6	4.55 -6	3.60 -6	3.37 -6	3.88 -6	4.74 -6	3.47 +7
1	1.52 -5	1.19 -5	9.19 -6	8.29 -6	9.49 -6	1.12 -5	3.83 +7
2	5.13 -5	4.00 -5	3.13 -5	2.79 -5	3.26 -5	3.83 -5	4.19 +7
3	5.19 -5	4.09 -5	3.20 -5	2.91 -5	3.35 -5	3.99 -5	4.57 +7
4	9.06 -6	7.09 -6	5.62 -6	4.91 -6	5.91 -6	6.88 -6	4.94 +7
5	1.01 -7	6.12 -8	4.79 -8	2.25 -8	3.95 -8	2.87 -8	5.34 +7
6	4.07 -6	3.25 -6	2.46 -6	2.44 -6	2.55 -6	3.19 -6	5.75 +7
7	2.64 -5	2.02 -5	1.60 -5	1.33 -5	1.66 -5	1.87 -5	6.19 +7
8	1.48 -5	1.08 -5	8.93 -6	6.15 -6	9.08 -6	9.15 -6	6.65 +7
9	8.54 -4	7.97 -4	6.59 -4	7.23 -4	7.93 -4	1.08 -3	7.09 +7
$\sum_{v'} A_{v'v''}$	1.03 -3	9.36 -4	7.68 -4	8.18 -4	9.07 -4	1.21 -3	

Table E.31: $A_{v'v''}$ for ^{6}Li triplet case (continued).

$v'\backslash v''$	0	1	2	3	4	5	6	7
0	3.46 +3	3.00 +4	1.33 +5	3.99 +5	9.11 +5	1.68 +6	2.61 +6	3.48 +6
1	1.40 +4	1.04 +5	3.84 +5	9.28 +5	1.63 +6	2.16 +6	2.18 +6	1.61 +6
2	3.14 +4	2.02 +5	6.26 +5	1.21 +6	1.59 +6	1.39 +6	6.95 +5	8.15 +4
3	5.20 +4	2.92 +5	7.62 +5	1.18 +6	1.10 +6	5.28 +5	3.17 +4	1.90 +5
4	7.01 +4	3.47 +5	7.73 +5	9.49 +5	6.00 +5	9.32 +4	7.99 +4	5.98 +5
5	8.07 +4	3.58 +5	6.87 +5	6.71 +5	2.61 +5	2.53 +1	2.75 +5	6.80 +5
6	8.06 +4	3.26 +5	5.49 +5	4.31 +5	9.06 +4	3.66 +4	3.57 +5	5.25 +5
7	6.91 +4	2.60 +5	3.94 +5	2.54 +5	2.38 +4	7.31 +4	3.15 +5	3.24 +5
8	4.76 +4	1.70 +5	2.39 +5	1.32 +5	4.50 +3	6.95 +4	2.09 +5	1.67 +5
9	2.43 +4	8.43 +4	1.13 +5	5.71 +4	6.46 +2	4.04 +4	1.02 +5	7.01 +4
10	6.03 +3	2.07 +4	2.73 +4	1.32 +4	7.35 +1	1.04 +4	2.48 +4	1.60 +4
$\sum_{v'} A_{v'v''}$	4.79 +5	2.19 +6	4.69 +6	6.23 +6	6.21 +6	6.08 +6	6.88 +6	7.74 +6

$v'\backslash v''$	8	9	10	11	12	13	14	15
0	4.04 +6	4.19 +6	4.06 +6	3.81 +6	3.25 +6	2.40 +6	1.57 +6	9.34 +5
1	7.35 +5	1.01 +5	7.53 +4	7.76 +5	2.09 +6	3.52 +6	4.50 +6	4.60 +6
2	1.14 +5	7.85 +5	1.58 +6	1.98 +6	1.58 +6	6.31 +5	1.22 +4	4.17 +5
3	8.47 +5	1.27 +6	1.05 +6	3.99 +5	1.28 +2	4.72 +5	1.56 +6	2.18 +6
4	9.58 +5	6.89 +5	1.55 +5	3.96 +4	6.10 +5	1.29 +6	1.23 +6	4.38 +5
5	6.01 +5	1.64 +5	1.73 +4	4.19 +5	8.99 +5	7.68 +5	1.81 +5	6.14 +4
6	2.62 +5	4.15 +3	1.75 +5	5.62 +5	6.01 +5	1.93 +5	1.78 +4	4.79 +5
7	8.46 +4	1.73 +4	2.50 +5	4.37 +5	2.70 +5	1.08 +4	1.62 +5	5.57 +5
8	2.10 +4	3.78 +4	1.99 +5	2.49 +5	9.39 +4	4.08 +3	1.89 +5	3.66 +5
9	4.47 +3	2.81 +4	1.04 +5	1.09 +5	2.83 +4	9.71 +3	1.13 +5	1.69 +5
10	7.07 +2	7.81 +3	2.60 +4	2.52 +4	5.50 +3	3.40 +3	2.93 +4	3.97 +4
$\sum_{v'} A_{v'v''}$	7.67 +6	7.30 +6	7.69 +6	8.80 +6	9.43 +6	9.30 +6	9.56 +6	1.02 +7

Table E.32: Spontaneous emission coefficient $A_{v'v''}$ for ^{7}Li triplet case.

$v'\backslash v''$	16	17	18	19	20	21	22	23
0	5.27 +5	2.79 +5	1.35 +5	6.19 +4	2.80 +4	1.14 +4	3.98 +3	1.51 +3
1	4.01 +6	3.10 +6	2.20 +6	1.42 +6	8.42 +5	4.63 +5	2.36 +5	1.10 +5
2	1.73 +6	3.25 +6	4.35 +6	4.71 +6	4.37 +6	3.56 +6	2.60 +6	1.72 +6
3	1.72 +6	6.70 +5	1.89 +4	3.62 +5	1.65 +6	3.29 +6	4.60 +6	5.15 +6
4	1.77 +3	5.74 +5	1.62 +6	2.16 +6	1.73 +6	7.09 +5	2.28 +4	3.91 +5
5	7.44 +5	1.37 +6	1.14 +6	3.75 +5	3.13 +3	5.65 +5	1.64 +6	2.26 +6
6	9.44 +5	7.04 +5	1.30 +5	7.42 +4	6.98 +5	1.30 +6	1.17 +6	4.34 +5
7	5.55 +5	1.53 +5	2.27 +4	4.19 +5	8.23 +5	6.91 +5	1.89 +5	2.42 +4
8	2.24 +5	9.92 +3	1.13 +5	4.05 +5	4.61 +5	1.97 +5	1.55 +2	2.09 +5
9	7.38 +4	1.85 +2	9.20 +4	2.15 +5	1.82 +5	4.21 +4	1.38 +4	1.72 +5
10	1.49 +4	4.85 +2	2.59 +4	5.28 +4	3.97 +4	6.49 +3	6.45 +3	4.81 +4
$\sum_{v'} A_{v'v''}$	1.05 +7	1.01 +7	9.85 +6	1.03 +7	1.08 +7	1.08 +7	1.05 +7	1.05 +7

$v'\backslash v''$	24	25	26	27	28	29	30	31
0	5.34 +2	1.12 +2	3.79 +1	1.38 +1	1.75 -1	9.80 -1	2.40 -1	2.89 -1
1	4.70 +4	1.86 +4	6.36 +3	2.02 +3	6.09 +2	1.37 +2	3.57 +1	8.51 +0
2	1.02 +6	5.50 +5	2.67 +5	1.15 +5	4.52 +4	1.60 +4	5.00 +3	1.44 +3
3	4.87 +6	3.97 +6	2.84 +6	1.79 +6	1.00 +6	5.01 +5	2.24 +5	8.91 +4
4	1.85 +6	3.78 +6	5.30 +6	5.82 +6	5.29 +6	4.10 +6	2.76 +6	1.64 +6
5	1.83 +6	7.26 +5	8.71 +3	5.85 +5	2.43 +6	4.63 +6	6.13 +6	6.36 +6
6	1.33 +2	5.50 +5	1.74 +6	2.44 +6	1.91 +6	6.62 +5	3.12 +2	8.63 +5
7	5.43 +5	1.22 +6	1.24 +6	5.29 +5	2.71 +3	5.01 +5	1.73 +6	2.49 +6
8	6.13 +5	6.88 +5	3.08 +5	1.26 +3	3.01 +5	9.65 +5	1.20 +6	6.86 +5
9	3.19 +5	2.45 +5	4.62 +4	3.31 +4	2.95 +5	5.20 +5	3.99 +5	8.38 +4
10	7.68 +4	5.02 +4	5.17 +3	1.57 +4	8.39 +4	1.23 +5	7.60 +4	7.07 +3
$\sum_{v'} A_{v'v''}$	1.12 +7	1.18 +7	1.18 +7	1.13 +7	1.14 +7	1.20 +7	1.25 +7	1.22 +7

Table E.33: $A_{v'v''}$ for ^{7}Li triplet case (continued).

$v'\backslash v''$	32	33	34	35	36	37	38	39
0	4.18 -1	9.58 -2	1.99 -3	1.10 -1	2.04 -1	1.73 -1	7.55 -2	8.74 -3
1	4.59 -1	6.74 -1	1.30 -3	1.50 -3	6.62 -2	7.53 -2	5.80 -2	2.36 -2
2	3.62 +2	7.96 +1	1.87 +1	2.11 +0	5.42 -1	6.86 -2	1.99 -3	2.97 -2
3	3.21 +4	1.03 +4	2.92 +3	7.47 +2	1.51 +2	3.24 +1	4.49 +0	5.41 -1
4	8.56 +5	4.00 +5	1.66 +5	6.07 +4	1.97 +4	5.48 +3	1.37 +3	2.81 +2
5	5.49 +6	4.05 +6	2.60 +6	1.46 +6	7.16 +5	3.09 +5	1.16 +5	3.81 +4
6	3.04 +6	5.43 +6	6.91 +6	6.96 +6	5.82 +6	4.13 +6	2.53 +6	1.34 +6
7	1.99 +6	7.09 +5	2.55 +1	9.03 +5	3.28 +6	5.98 +6	7.66 +6	7.72 +6
8	6.21 +4	2.23 +5	1.26 +6	2.25 +6	2.21 +6	1.12 +6	9.00 +4	3.99 +5
9	3.77 +4	4.30 +5	8.73 +5	8.48 +5	3.56 +5	1.39 +3	3.66 +5	1.31 +6
10	2.51 +4	1.34 +5	2.12 +5	1.59 +5	3.62 +4	1.20 +4	1.69 +5	3.80 +5
$\sum_{v'} A_{v'v''}$	1.15 +7	1.14 +7	1.20 +7	1.26 +7	1.24 +7	1.16 +7	1.09 +7	1.12 +7

$v'\backslash v''$	40	41	42	43	44	45	46	47
0	5.67 -3	4.03 -2	7.38 -2	8.51 -2	7.43 -2	5.20 -2	2.90 -2	1.19 -2
1	2.96 -3	1.28 -3	1.08 -2	2.13 -2	2.66 -2	2.58 -2	2.08 -2	1.43 -2
2	1.99 -2	1.42 -2	6.07 -3	1.40 -3	5.02 -7	8.49 -4	2.64 -3	4.40 -3
3	1.75 -1	1.19 -2	4.72 -2	2.55 -2	1.53 -2	5.50 -3	8.84 -4	5.79 -5
4	4.96 +1	8.78 +0	7.06 -1	2.92 -1	4.40 -3	2.77 -2	9.12 -3	4.64 -3
5	1.08 +4	2.68 +3	5.97 +2	1.10 +2	1.97 +1	1.92 +0	4.58 -1	7.76 -3
6	6.16 +5	2.49 +5	8.92 +4	2.84 +4	7.80 +3	1.88 +3	3.92 +2	7.78 +1
7	6.42 +6	4.55 +6	2.80 +6	1.52 +6	7.29 +5	3.07 +5	1.15 +5	3.89 +4
8	2.39 +6	5.20 +6	7.52 +6	8.45 +6	7.86 +6	6.24 +6	4.34 +6	2.69 +6
9	2.04 +6	1.87 +6	9.28 +5	8.65 +4	2.71 +5	1.80 +6	4.19 +6	6.54 +6
10	4.32 +5	2.59 +5	4.13 +4	3.71 +4	3.49 +5	8.16 +5	1.13 +6	1.08 +6
$\sum_{v'} A_{v'v''}$	1.19 +7	1.21 +7	1.14 +7	1.01 +7	9.22 +6	9.16 +6	9.77 +6	1.03 +7

Table E.34: $A_{v'v''}$ for ^{7}Li triplet case (continued).

$v'\backslash v''$	48	49	50	51	52	53	54	55
0	2.66 -3	1.42 -6	1.65 -3	5.43 -3	9.71 -3	1.34 -2	1.59 -2	1.72 -2
1	8.36 -3	3.96 -3	1.32 -3	1.57 -4	6.15 -5	6.03 -4	1.42 -3	2.23 -3
2	5.58 -3	6.05 -3	5.89 -3	5.29 -3	4.43 -3	3.48 -3	2.57 -3	1.79 -3
3	1.29 -3	3.14 -3	4.80 -3	5.96 -3	6.54 -3	6.63 -3	6.34 -3	5.78 -3
4	9.14 -4	4.15 -6	8.71 -4	2.60 -3	4.44 -3	5.90 -3	6.77 -3	7.05 -3
5	1.08 -2	3.43 -4	1.74 -4	9.71 -5	6.41 -4	1.50 -3	2.36 -3	3.05 -3
6	1.13 +1	1.73 +0	1.79 -1	2.62 -2	2.34 -3	3.94 -5	4.15 -4	5.46 -4
7	1.17 +4	3.03 +3	7.26 +2	1.60 +2	3.34 +1	6.28 +0	9.84 -1	1.41 -1
8	1.49 +6	7.35 +5	3.29 +5	1.37 +5	5.40 +4	1.99 +4	6.65 +3	1.99 +3
9	8.05 +6	8.29 +6	7.42 +6	5.99 +6	4.50 +6	3.17 +6	2.08 +6	1.27 +6
10	6.88 +5	2.13 +5	4.36 +1	2.61 +5	1.01 +6	2.17 +6	3.56 +6	5.01 +6
$\sum_{v'} A_{v'v''}$	1.02 +7	9.24 +6	7.75 +6	6.39 +6	5.57 +6	5.35 +6	5.65 +6	6.29 +6

$v'\backslash v''$	56	57	58	59	60	61	62	63
0	1.72 -2	1.63 -2	1.48 -2	1.30 -2	1.13 -2	1.01 -2	9.05 -3	8.10 -3
1	2.88 -3	3.28 -3	3.43 -3	3.36 -3	3.21 -3	3.09 -3	2.98 -3	2.84 -3
2	1.18 -3	7.25 -4	4.18 -4	2.25 -4	1.14 -4	5.30 -5	1.98 -5	4.15 -6
3	5.08 -3	4.32 -3	3.57 -3	2.89 -3	2.36 -3	1.98 -3	1.68 -3	1.43 -3
4	6.83 -3	6.27 -3	5.51 -3	4.71 -3	4.00 -3	3.49 -3	3.08 -3	2.70 -3
5	3.49 -3	3.65 -3	3.58 -3	3.34 -3	3.07 -3	2.86 -3	2.68 -3	2.49 -3
6	9.31 -4	1.21 -3	1.41 -3	1.51 -3	1.53 -3	1.54 -3	1.54 -3	1.51 -3
7	1.16 -2	3.34 -3	3.37 -4	7.10 -4	5.18 -4	4.25 -4	3.53 -4	3.10 -4
8	5.34 +2	1.20 +2	2.07 +1	2.93 +0	2.45 -1	1.90 -2	5.82 -3	3.63 -4
9	7.24 +5	3.75 +5	1.72 +5	6.79 +4	2.21 +4	6.24 +3	1.85 +3	5.86 +2
10	6.34 +6	7.37 +6	7.90 +6	7.68 +6	6.54 +6	4.90 +6	3.53 +6	2.61 +6
$\sum_{v'} A_{v'v''}$	7.06 +6	7.74 +6	8.07 +6	7.75 +6	6.56 +6	4.90 +6	3.54 +6	2.61 +6

Table E.35: $A_{v'v''}$ for ^{7}Li triplet case (continued).

$v'\backslash v''$	64	65	66	67	68	69	70	71
0	7.23 -3	6.39 -3	5.58 -3	4.77 -3	4.04 -3	3.47 -3	2.96 -3	2.53 -3
1	2.69 -3	2.51 -3	2.30 -3	2.05 -3	1.81 -3	1.61 -3	1.41 -3	1.24 -3
2	6.03 -11	2.95 -6	9.61 -6	1.71 -5	2.37 -5	2.92 -5	3.28 -5	3.51 -5
3	1.21 -3	1.02 -3	8.51 -4	6.97 -4	5.67 -4	4.69 -4	3.87 -4	3.21 -4
4	2.37 -3	2.07 -3	1.78 -3	1.50 -3	1.26 -3	1.07 -3	9.04 -4	7.68 -4
5	2.30 -3	2.10 -3	1.88 -3	1.65 -3	1.43 -3	1.26 -3	1.09 -3	9.50 -4
6	1.45 -3	1.37 -3	1.26 -3	1.13 -3	9.96 -4	8.85 -4	7.77 -4	6.83 -4
7	2.87 -4	2.79 -4	2.76 -4	2.72 -4	2.65 -4	2.60 -4	2.50 -4	2.38 -4
8	2.02 -3	1.47 -3	1.33 -3	9.53 -4	6.70 -4	4.67 -4	3.23 -4	2.27 -4
9	1.77 +2	4.70 +1	1.32 +1	2.99 +0	4.58 -1	8.79 -2	3.38 -3	4.19 -3
10	1.90 +6	1.36 +6	9.67 +5	6.70 +5	4.23 +5	2.40 +5	1.31 +5	6.99 +4
$\sum_{v'} A_{v'v''}$	1.90 +6	1.36 +6	9.67 +5	6.70 +5	4.23 +5	2.40 +5	1.31 +5	6.99 +4

$v'\backslash v''$	72	73	74	75	76	77	78	79
0	2.16 -3	1.84 -3	1.57 -3	1.33 -3	1.13 -3	9.54 -4	8.04 -4	6.75 -4
1	1.08 -3	9.44 -4	8.20 -4	7.08 -4	6.09 -4	5.21 -4	4.44 -4	3.76 -4
2	3.58 -5	3.53 -5	3.40 -5	3.20 -5	2.95 -5	2.68 -5	2.40 -5	2.12 -5
3	2.66 -4	2.21 -4	1.84 -4	1.53 -4	1.27 -4	1.06 -4	8.79 -5	7.30 -5
4	6.51 -4	5.51 -4	4.67 -4	3.95 -4	3.34 -4	2.81 -4	2.36 -4	1.98 -4
5	8.22 -4	7.09 -4	6.11 -4	5.24 -4	4.48 -4	3.81 -4	3.23 -4	2.73 -4
6	5.95 -4	5.17 -4	4.48 -4	3.86 -4	3.31 -4	2.83 -4	2.41 -4	2.04 -4
7	2.23 -4	2.06 -4	1.88 -4	1.70 -4	1.52 -4	1.34 -4	1.17 -4	1.02 -4
8	1.61 -4	1.16 -4	8.53 -5	6.39 -5	4.86 -5	3.76 -5	2.94 -5	2.33 -5
9	3.87 -4	6.84 -4	4.34 -4	4.01 -4	3.64 -4	3.36 -4	3.07 -4	2.75 -4
10	3.40 +4	1.54 +4	6.67 +3	2.50 +3	9.12 +2	2.79 +2	7.84 +1	1.96 +1
$\sum_{v'} A_{v'v''}$	3.40 +4	1.54 +4	6.67 +3	2.50 +3	9.12 +2	2.79 +2	7.84 +1	1.96 +1

Table E.36: $A_{v'v''}$ for ^{7}Li triplet case (continued).

$v'\backslash v''$	80	81	82	83	84	85	86	87
0	5.65 -4	4.71 -4	3.90 -4	3.21 -4	2.63 -4	2.14 -4	1.72 -4	1.38 -4
1	3.17 -4	2.66 -4	2.22 -4	1.83 -4	1.51 -4	1.23 -4	9.93 -5	7.96 -5
2	1.85 -5	1.60 -5	1.36 -5	1.15 -5	9.59 -6	7.92 -6	6.46 -6	5.22 -6
3	6.04 -5	4.99 -5	4.10 -5	3.36 -5	2.73 -5	2.21 -5	1.78 -5	1.42 -5
4	1.65 -4	1.38 -4	1.14 -4	9.37 -5	7.66 -5	6.22 -5	5.02 -5	4.01 -5
5	2.30 -4	1.92 -4	1.60 -4	1.32 -4	1.08 -4	8.81 -5	7.11 -5	5.69 -5
6	1.72 -4	1.44 -4	1.20 -4	9.91 -5	8.14 -5	6.64 -5	5.37 -5	4.30 -5
7	8.73 -5	7.44 -5	6.28 -5	5.25 -5	4.35 -5	3.57 -5	2.90 -5	2.33 -5
8	1.85 -5	1.48 -5	1.19 -5	9.55 -6	7.66 -6	6.14 -6	4.95 -6	3.89 -6
9	2.41 -4	2.09 -4	1.78 -4	1.49 -4	1.24 -4	1.02 -4	8.19 -5	6.60 -5
10	3.46 +0	8.46 -1	3.23 -2	4.04 -2	5.43 -3	8.87 -3	6.06 -3	4.86 -3
$\sum_{v'} A_{v'v''}$	3.47 +0	8.48 -1	3.36 -2	4.15 -2	6.32 -3	9.59 -3	6.65 -3	5.33 -3

$v'\backslash v''$	88	89	90	91	$\sum_{v''} A_{v'v''}$
0	1.09 -4	8.80 -5	8.68 -5	1.03 -4	3.46 +7
1	6.31 -5	5.10 -5	5.03 -5	5.94 -5	3.79 +7
2	4.15 -6	3.37 -6	3.36 -6	4.03 -6	4.12 +7
3	1.12 -5	8.99 -6	8.87 -6	1.05 -5	4.47 +7
4	3.18 -5	2.56 -5	2.52 -5	2.95 -5	4.82 +7
5	4.50 -5	3.64 -5	3.60 -5	4.27 -5	5.17 +7
6	3.42 -5	2.76 -5	2.71 -5	3.17 -5	5.55 +7
7	1.85 -5	1.50 -5	1.49 -5	1.81 -5	5.94 +7
8	3.15 -6	2.52 -6	2.37 -6	2.50 -6	6.37 +7
9	5.15 -5	4.17 -5	4.23 -5	5.32 -5	6.79 +7
10	3.69 -3	2.91 -3	2.86 -3	3.44 -3	7.18 +7
$\sum_{v'} A_{v'v''}$	4.07 -3	3.22 -3	3.16 -3	3.79 -3	

Table E.37: $A_{v'v''}$ for ^{7}Li triplet case (continued).

$v'\backslash v''$	0	1	2	3	4	5	6	7
0	3.05 -02	7.13 -02	9.21 -02	8.71 -02	6.75 -02	4.55 -02	2.78 -02	1.57 -02
1	9.60 -02	9.03 -02	2.68 -02	6.33 -06	1.53 -02	3.86 -02	4.91 -02	4.58 -02
2	1.37 -01	1.69 -02	1.59 -02	5.22 -02	3.52 -02	5.92 -03	1.56 -03	1.61 -02
3	1.18 -01	1.36 -02	6.39 -02	1.11 -02	7.76 -03	3.56 -02	3.19 -02	9.96 -03
4	6.67 -02	8.35 -02	1.48 -02	2.43 -02	4.25 -02	5.80 -03	6.41 -03	2.77 -02
5	2.63 -02	1.07 -01	1.48 -02	5.16 -02	4.10 -05	2.99 -02	2.88 -02	2.32 -03
6	7.32 -03	6.86 -02	8.46 -02	2.46 -03	4.36 -02	1.82 -02	4.54 -03	3.02 -02
7	1.43 -03	2.68 -02	9.84 -02	3.67 -02	2.84 -02	1.37 -02	3.62 -02	2.28 -03
8	1.89 -04	6.71 -03	5.50 -02	9.94 -02	4.83 -03	4.80 -02	1.39 -05	3.09 -02
9	1.55 -05	1.06 -03	1.75 -02	8.26 -02	7.61 -02	2.05 -03	4.37 -02	8.81 -03
10	6.47 -07	9.67 -05	3.26 -03	3.37 -02	1.01 -01	4.36 -02	1.81 -02	2.47 -02
11	6.48 -09	4.24 -06	3.37 -04	7.46 -03	5.35 -02	1.06 -01	1.67 -02	3.61 -02
12	6.96 -12	6.27 -08	1.69 -05	8.80 -04	1.41 -02	7.46 -02	9.97 -02	2.51 -03
13	1.36 -10	1.98 -09	2.99 -07	4.40 -05	1.77 -03	2.26 -02	9.32 -02	8.52 -02
14	6.44 -11	3.17 -10	3.39 -10	1.95 -07	7.21 -05	2.91 -03	3.25 -02	1.09 -01
15	6.91 -11	1.29 -09	1.63 -08	1.79 -07	3.64 -08	1.00 -04	4.36 -03	4.35 -02
16	6.40 -11	1.06 -09	7.79 -09	4.19 -08	3.92 -07	6.04 -07	1.14 -04	5.72 -03
17	3.05 -11	3.84 -10	2.94 -09	1.06 -08	1.00 -09	6.21 -07	4.95 -06	8.40 -05
18	2.71 -11	6.35 -10	4.67 -09	1.40 -08	2.00 -08	1.19 -10	1.55 -06	1.86 -05
19	2.09 -11	2.99 -10	2.17 -09	6.05 -09	4.41 -09	3.49 -09	1.88 -08	2.06 -06
20	5.74 -12	2.37 -10	1.64 -09	4.69 -09	5.06 -09	4.76 -10	1.67 -08	9.33 -08
21	1.48 -11	3.74 -10	2.56 -09	6.71 -09	5.26 -09	5.42 -11	7.81 -09	1.09 -08
22	3.94 -14	4.76 -12	3.23 -11	1.42 -10	3.01 -10	4.39 -10	1.31 -10	1.51 -10
23	9.00 -12	2.76 -10	1.81 -09	4.86 -09	3.94 -09	1.49 -11	4.06 -09	1.20 -09
24	3.09 -12	1.19 -10	7.44 -10	1.79 -09	1.01 -09	1.75 -10	3.43 -09	2.29 -09
25	1.27 -12	1.15 -11	8.91 -11	2.91 -10	4.05 -10	1.17 -10	5.04 -11	1.39 -10
26	6.78 -12	1.39 -10	9.20 -10	2.39 -09	1.86 -09	5.39 -13	2.77 -09	3.17 -09
27	3.68 -12	1.03 -10	6.51 -10	1.56 -09	9.50 -10	5.72 -11	2.03 -09	1.55 -09
28	2.55 -14	8.97 -12	4.86 -11	8.79 -11	1.27 -11	5.16 -11	7.86 -11	3.35 -11
29	1.84 -12	1.44 -11	1.05 -10	3.06 -10	3.40 -10	1.30 -11	4.71 -10	1.30 -09
30	4.08 -12	5.25 -11	3.54 -10	9.06 -10	7.42 -10	7.44 -14	1.08 -09	1.52 -09
31	3.65 -12	5.55 -11	3.65 -10	8.80 -10	6.28 -10	2.85 -12	8.26 -10	6.39 -10
32	1.98 -12	3.40 -11	2.21 -10	5.02 -10	3.13 -10	6.20 -12	3.46 -10	7.81 -11
33	7.24 -13	1.43 -11	9.23 -11	1.95 -10	1.00 -10	6.72 -12	8.25 -11	7.85 -12
34	1.78 -13	4.49 -12	2.87 -11	5.37 -11	1.91 -11	5.38 -12	7.71 -12	6.84 -11
35	2.82 -14	1.11 -12	7.04 -12	1.08 -11	1.51 -12	3.43 -12	8.31 -14	8.21 -11
36	2.83 -15	2.46 -13	1.54 -12	1.77 -12	1.33 -16	1.69 -12	1.24 -12	5.16 -11
37	2.21 -16	4.92 -14	3.07 -13	2.73 -13	3.65 -14	5.35 -13	6.96 -13	1.78 -11
38	1.17 -17	3.93 -15	2.45 -14	2.00 -14	5.02 -15	4.83 -14	7.00 -14	1.64 -12
$\sum_{v'} f_{v'v''}$	4.83 -01	4.85 -01	4.88 -01	4.90 -01	4.91 -01	4.93 -01	4.95 -01	4.96 -01

Table E.38: Oscillator stengths $f_{v'v''}$ for the ^{6}Li singlet case.

$v'\backslash v''$	8	9	10	11	12	13	14	15
0	8.37 -03	4.27 -03	2.10 -03	1.01 -03	4.75 -04	2.20 -04	1.00 -04	4.56 -05
1	3.55 -02	2.43 -02	1.52 -02	8.94 -03	4.98 -03	2.67 -03	1.39 -03	7.10 -04
2	3.10 -02	3.68 -02	3.40 -02	2.69 -02	1.90 -02	1.24 -02	7.65 -03	4.50 -03
3	2.59 -06	6.88 -03	1.95 -02	2.81 -02	2.97 -02	2.62 -02	2.04 -02	1.46 -02
4	2.74 -02	1.11 -02	5.10 -04	3.00 -03	1.25 -02	2.12 -02	2.50 -02	2.41 -02
5	6.62 -03	2.33 -02	2.36 -02	1.09 -02	1.13 -03	1.29 -03	8.27 -03	1.60 -02
6	1.87 -02	5.37 -04	7.26 -03	2.04 -02	2.04 -02	1.02 -02	1.56 -03	5.22 -04
7	1.25 -02	2.66 -02	1.12 -02	2.49 -06	7.95 -03	1.83 -02	1.77 -02	9.30 -03
8	1.71 -02	4.66 -04	1.79 -02	2.12 -02	6.03 -03	2.70 -04	8.50 -03	1.65 -02
9	1.32 -02	2.75 -02	3.98 -03	4.99 -03	1.97 -02	1.54 -02	2.78 -03	9.58 -04
10	2.48 -02	1.14 -03	2.44 -02	1.50 -02	8.71 -06	1.02 -02	1.84 -02	1.04 -02
11	6.92 -03	3.30 -02	2.07 -03	1.27 -02	2.20 -02	4.72 -03	1.86 -03	1.35 -02
12	4.52 -02	5.26 -05	2.92 -02	1.12 -02	2.77 -03	1.99 -02	1.28 -02	3.07 -04
13	4.37 -04	4.35 -02	3.51 -03	1.89 -02	2.02 -02	7.27 -05	1.23 -02	1.76 -02
14	6.77 -02	6.28 -03	3.44 -02	1.22 -02	8.18 -03	2.40 -02	3.84 -03	4.49 -03
15	1.21 -01	5.13 -02	1.51 -02	2.30 -02	2.08 -02	1.64 -03	2.18 -02	1.01 -02
16	5.40 -02	1.30 -01	3.80 -02	2.30 -02	1.29 -02	2.61 -02	4.01 -05	1.61 -02
17	6.76 -03	6.42 -02	1.39 -01	2.89 -02	2.83 -02	5.88 -03	2.74 -02	2.03 -03
18	2.80 -05	7.00 -03	7.20 -02	1.47 -01	2.34 -02	3.05 -02	1.95 -03	2.60 -02
19	5.16 -05	4.08 -06	6.27 -03	7.76 -02	1.58 -01	2.14 -02	2.98 -02	2.72 -04
20	2.18 -06	1.01 -04	1.39 -04	4.58 -03	7.95 -02	1.71 -01	2.32 -02	2.66 -02
21	6.92 -07	1.75 -07	1.48 -04	6.09 -04	2.17 -03	7.59 -02	1.86 -01	2.96 -02
22	4.02 -08	1.98 -06	1.81 -06	1.64 -04	1.54 -03	2.22 -04	6.51 -02	2.02 -01
23	2.45 -08	1.93 -08	2.87 -06	1.77 -05	9.92 -05	2.76 -03	7.23 -04	4.67 -02
24	6.15 -10	5.46 -08	3.35 -07	2.35 -06	6.36 -05	3.55 -06	3.61 -03	5.92 -03
25	1.14 -09	1.21 -08	1.62 -08	1.30 -06	4.55 -08	1.21 -04	1.45 -04	3.01 -03
26	8.15 -11	3.52 -10	3.99 -08	1.54 -08	2.95 -06	7.85 -06	1.21 -04	9.15 -04
27	1.14 -10	1.61 -09	8.80 -09	3.17 -08	5.41 -07	1.78 -06	5.08 -05	1.51 -05
28	1.71 -10	1.03 -10	3.31 -12	1.88 -08	4.71 -12	1.96 -06	6.54 -07	1.03 -04
29	6.15 -10	1.42 -10	1.55 -09	3.19 -09	4.44 -08	3.32 -07	2.13 -06	2.70 -05
30	2.61 -10	1.33 -10	1.79 -09	1.23 -10	3.25 -08	3.35 -09	1.83 -06	6.36 -07
31	5.43 -13	1.34 -13	8.18 -10	3.25 -11	1.05 -08	1.52 -08	5.32 -07	9.87 -07
32	1.93 -10	8.71 -11	1.84 -10	8.82 -11	1.79 -09	2.07 -08	7.10 -08	1.57 -06
33	3.77 -10	1.77 -10	1.11 -11	7.62 -11	6.33 -11	1.36 -08	1.08 -09	9.94 -07
34	3.59 -10	1.62 -10	3.12 -12	4.99 -11	5.29 -11	7.07 -09	3.03 -09	4.69 -07
35	2.35 -10	1.01 -10	1.10 -11	2.82 -11	1.27 -10	3.29 -09	5.09 -09	1.96 -07
36	1.14 -10	4.71 -11	8.63 -12	1.31 -11	9.24 -11	1.35 -09	3.32 -09	7.41 -08
37	3.58 -11	1.44 -11	3.18 -12	4.06 -12	3.33 -11	3.94 -10	1.15 -09	2.08 -08
38	3.22 -12	1.29 -12	2.96 -13	3.64 -13	3.08 -12	3.49 -11	1.05 -10	1.83 -09
$\sum_{v'} f_{v'v''}$	4.97 -01	4.99 -01	5.00 -01	5.01 -01	5.01 -01	5.02 -01	5.03 -01	5.03 -01

Table E.39: $f_{v'v''}$ for ^{6}Li singlet case (continued).

$v'\backslash v''$	16	17	18	19	20	21	22	23
0	2.06 -05	9.31 -06	4.20 -06	1.90 -06	8.65 -07	3.96 -07	1.83 -07	8.54 -08
1	3.55 -04	1.76 -04	8.62 -05	4.21 -05	2.05 -05	9.95 -06	4.85 -06	2.37 -06
2	2.55 -03	1.41 -03	7.63 -04	4.07 -04	2.14 -04	1.12 -04	5.81 -05	3.02 -05
3	9.73 -03	6.18 -03	3.77 -03	2.23 -03	1.29 -03	7.36 -04	4.13 -04	2.30 -04
4	2.03 -02	1.56 -02	1.12 -02	7.57 -03	4.93 -03	3.10 -03	1.91 -03	1.15 -03
5	2.07 -02	2.15 -02	1.94 -02	1.58 -02	1.20 -02	8.64 -03	5.95 -03	3.97 -03
6	5.54 -03	1.22 -02	1.70 -02	1.88 -02	1.80 -02	1.55 -02	1.24 -02	9.40 -03
7	1.82 -03	1.74 -04	3.72 -03	9.23 -03	1.38 -02	1.62 -02	1.63 -02	1.48 -02
8	1.55 -02	8.42 -03	1.96 -03	3.23 -05	2.47 -03	6.95 -03	1.12 -02	1.38 -02
9	8.84 -03	1.49 -02	1.37 -02	7.62 -03	2.04 -03	2.40 -07	1.58 -03	5.15 -03
10	9.85 -04	1.77 -03	8.93 -03	1.36 -02	1.21 -02	6.97 -03	2.11 -03	3.56 -05
11	1.55 -02	6.57 -03	1.89 -04	2.51 -03	8.76 -03	1.23 -02	1.09 -02	6.45 -03
12	5.60 -03	1.44 -02	1.21 -02	3.78 -03	4.11 -07	3.10 -03	8.41 -03	1.10 -02
13	4.64 -03	6.16 -04	8.86 -03	1.35 -02	8.76 -03	1.95 -03	1.46 -04	3.53 -03
14	1.67 -02	1.06 -02	6.04 -04	3.09 -03	1.06 -02	1.16 -02	6.05 -03	8.81 -04
15	3.80 -04	1.17 -02	1.42 -02	4.22 -03	1.59 -04	5.72 -03	1.08 -02	9.30 -03
16	1.54 -02	6.04 -04	5.92 -03	1.40 -02	8.58 -03	7.53 -04	1.68 -03	7.55 -03
17	9.68 -03	1.75 -02	3.65 -03	1.70 -03	1.10 -02	1.13 -02	3.55 -03	2.61 -05
18	5.56 -03	4.63 -03	1.68 -02	7.44 -03	4.61 -05	6.92 -03	1.16 -02	6.70 -03
19	2.30 -02	9.09 -03	1.51 -03	1.43 -02	1.05 -02	5.48 -04	3.31 -03	9.97 -03
20	2.50 -05	1.96 -02	1.16 -02	1.84 -04	1.10 -02	1.20 -02	2.25 -03	1.01 -03
21	2.15 -02	4.54 -04	1.67 -02	1.29 -02	4.07 -05	7.93 -03	1.22 -02	4.16 -03
22	4.27 -02	1.49 -02	1.18 -03	1.47 -02	1.31 -02	4.53 -04	5.49 -03	1.15 -02
23	2.13 -01	6.52 -02	7.57 -03	2.17 -03	1.41 -02	1.23 -02	9.61 -04	3.83 -03
24	2.32 -02	2.11 -01	9.95 -02	1.45 -03	3.83 -03	1.52 -02	1.04 -02	1.37 -03
25	1.61 -02	3.58 -03	1.83 -01	1.43 -01	6.56 -04	7.13 -03	1.92 -02	7.62 -03
26	9.04 -04	2.67 -02	3.41 -03	1.22 -01	1.82 -01	1.05 -02	1.40 -02	2.84 -02
27	2.09 -03	3.36 -04	2.65 -02	3.43 -02	4.49 -02	1.87 -01	3.18 -02	2.63 -02
28	1.45 -04	2.07 -03	6.62 -03	1.05 -02	7.88 -02	3.46 -04	1.32 -01	5.08 -02
29	4.57 -05	1.05 -03	2.05 -04	1.67 -02	5.34 -04	8.19 -02	3.44 -02	4.22 -02
30	7.83 -05	6.59 -05	1.60 -03	2.37 -03	1.26 -02	2.94 -02	2.39 -02	9.40 -02
31	2.91 -05	1.97 -05	8.37 -04	1.05 -04	1.10 -02	4.96 -06	5.53 -02	6.18 -03
32	4.79 -06	5.34 -05	1.74 -04	8.77 -04	3.09 -03	6.07 -03	2.35 -02	1.24 -02
33	1.66 -07	3.87 -05	1.04 -05	7.88 -04	2.85 -04	7.54 -03	3.37 -03	2.84 -02
34	9.87 -08	1.93 -05	1.47 -06	4.30 -04	5.84 -06	4.70 -03	2.42 -06	2.20 -02
35	2.28 -07	8.21 -06	5.80 -06	1.91 -04	7.24 -05	2.23 -03	3.77 -04	1.16 -02
36	1.59 -07	3.12 -06	4.45 -06	7.38 -05	6.35 -05	8.85 -04	4.10 -04	4.82 -03
37	5.62 -08	8.76 -07	1.61 -06	2.09 -05	2.39 -05	2.53 -04	1.63 -04	1.40 -03
38	5.18 -09	7.69 -08	1.50 -07	1.84 -06	2.23 -06	2.23 -05	1.54 -05	1.24 -04
$\sum_{v'} f_{v'v''}$	5.03 -01	5.03 -01	5.03 -01	5.03 -01	5.01 -01	4.98 -01	4.79 -01	4.62 -01

Table E.40: $f_{v'v''}$ for ^{6}Li singlet case (continued).

$v'\backslash v''$	24	25	26	27	28	29	30	31
0	4.02 -08	1.91 -08	9.10 -09	4.34 -09	2.08 -09	1.00 -09	4.91 -10	2.47 -10
1	1.17 -06	5.77 -07	2.88 -07	1.44 -07	7.34 -08	3.79 -08	1.99 -08	1.06 -08
2	1.57 -05	8.16 -06	4.26 -06	2.23 -06	1.18 -06	6.29 -07	3.39 -07	1.85 -07
3	1.27 -04	7.00 -05	3.85 -05	2.11 -05	1.16 -05	6.46 -06	3.61 -06	2.04 -06
4	6.85 -04	4.04 -04	2.36 -04	1.37 -04	7.92 -05	4.60 -05	2.68 -05	1.57 -05
5	2.58 -03	1.64 -03	1.03 -03	6.36 -04	3.90 -04	2.39 -04	1.46 -04	8.91 -05
6	6.82 -03	4.78 -03	3.26 -03	2.18 -03	1.43 -03	9.29 -04	5.99 -04	3.84 -04
7	1.24 -02	9.88 -03	7.50 -03	5.49 -03	3.91 -03	2.73 -03	1.88 -03	1.28 -03
8	1.45 -02	1.38 -02	1.21 -02	1.00 -02	7.94 -03	6.07 -03	4.52 -03	3.30 -03
9	8.87 -03	1.16 -02	1.28 -02	1.26 -02	1.15 -02	9.91 -03	8.17 -03	6.51 -03
10	9.49 -04	3.72 -03	6.94 -03	9.51 -03	1.09 -02	1.12 -02	1.07 -02	9.56 -03
11	2.22 -03	1.25 -04	5.04 -04	2.57 -03	5.21 -03	7.55 -03	9.10 -03	9.75 -03
12	9.69 -03	5.98 -03	2.30 -03	2.56 -04	2.05 -04	1.63 -03	3.71 -03	5.73 -03
13	7.99 -03	1.00 -02	8.75 -03	5.58 -03	2.39 -03	4.28 -04	4.11 -05	9.14 -04
14	4.23 -04	3.76 -03	7.48 -03	9.01 -03	7.90 -03	5.28 -03	2.53 -03	6.64 -04
15	3.96 -03	3.11 -04	7.22 -04	3.81 -03	6.83 -03	8.01 -03	7.13 -03	5.00 -03
16	1.01 -02	7.15 -03	2.48 -03	6.30 -05	9.55 -04	3.67 -03	6.14 -03	7.12 -03
17	3.66 -03	8.29 -03	8.68 -03	5.24 -03	1.47 -03	7.54 -07	1.07 -03	3.36 -03
18	7.28 -04	9.54 -04	5.31 -03	8.16 -03	7.10 -03	3.75 -03	8.62 -04	1.43 -05
19	8.82 -03	2.79 -03	2.26 -06	2.42 -03	6.14 -03	7.39 -03	5.63 -03	2.67 -03
20	7.35 -03	9.41 -03	5.00 -03	5.81 -04	5.78 -04	3.66 -03	6.25 -03	6.35 -03
21	7.71 -05	4.72 -03	8.69 -03	6.56 -03	1.96 -03	2.13 -07	1.60 -03	4.37 -03
22	5.73 -03	1.07 -04	2.62 -03	7.21 -03	7.19 -03	3.45 -03	3.91 -04	3.73 -04
23	1.04 -02	6.65 -03	6.11 -04	1.24 -03	5.51 -03	7.01 -03	4.54 -03	1.26 -03
24	2.81 -03	9.05 -03	6.97 -03	1.20 -03	4.72 -04	3.98 -03	6.28 -03	5.07 -03
25	1.65 -03	2.39 -03	7.82 -03	6.84 -03	1.63 -03	1.30 -04	2.79 -03	5.34 -03
26	3.80 -03	2.07 -03	2.57 -03	6.57 -03	6.45 -03	1.79 -03	1.89 -05	1.94 -03
27	4.69 -02	3.57 -04	3.24 -03	3.79 -03	5.08 -03	6.09 -03	1.67 -03	8.76 -08
28	4.10 -02	7.77 -02	2.28 -03	7.01 -03	7.63 -03	2.95 -03	6.13 -03	1.21 -03
29	4.12 -02	4.26 -02	1.12 -01	1.84 -02	1.77 -02	1.85 -02	4.42 -04	7.69 -03
30	3.04 -05	7.65 -03	1.60 -02	1.10 -01	4.58 -02	3.85 -02	4.50 -02	1.74 -03
31	6.01 -02	2.27 -02	4.70 -03	2.40 -03	4.42 -02	4.57 -02	5.11 -02	8.47 -02
32	5.85 -02	5.49 -04	1.09 -02	1.30 -02	4.51 -02	2.18 -04	5.68 -03	1.85 -02
33	1.53 -02	2.29 -02	1.52 -02	3.39 -03	1.74 -03	2.71 -02	2.29 -02	1.18 -02
34	6.15 -04	3.03 -02	4.08 -03	3.48 -04	2.11 -03	2.79 -02	3.58 -03	4.86 -04
35	4.53 -04	2.00 -02	1.82 -04	2.31 -03	3.20 -03	1.23 -02	1.20 -04	4.73 -03
36	8.58 -04	9.28 -03	4.44 -05	1.91 -03	1.70 -03	4.08 -03	9.11 -04	3.63 -03
37	3.85 -04	2.81 -03	5.80 -05	7.01 -04	5.23 -04	1.04 -03	4.81 -04	1.27 -03
38	3.72 -05	2.51 -04	6.52 -06	6.51 -05	4.67 -05	8.86 -05	4.77 -05	1.16 -04
$\sum_{v'} f_{v'v''}$	3.92 -01	3.57 -01	2.83 -01	2.71 -01	2.73 -01	2.73 -01	2.22 -01	2.17 -01

Table E.41: $f_{v'v''}$ for ^{6}Li singlet case (continued).

$v'\backslash v''$	32	33	34	35	36	37	38	39
0	1.30 -10	7.34 -11	4.45 -11	2.90 -11	2.00 -11	1.43 -11	1.03 -11	7.33 -12
1	5.72 -09	3.15 -09	1.76 -09	1.00 -09	5.86 -10	3.51 -10	2.17 -10	1.38 -10
2	1.03 -07	5.77 -08	3.31 -08	1.94 -08	1.15 -08	7.01 -09	4.34 -09	2.74 -09
3	1.17 -06	6.73 -07	3.94 -07	2.34 -07	1.41 -07	8.66 -08	5.41 -08	3.44 -08
4	9.25 -06	5.51 -06	3.32 -06	2.02 -06	1.25 -06	7.80 -07	4.94 -07	3.18 -07
5	5.47 -05	3.37 -05	2.09 -05	1.31 -05	8.28 -06	5.29 -06	3.42 -06	2.25 -06
6	2.47 -04	1.58 -04	1.02 -04	6.62 -05	4.32 -05	2.84 -05	1.88 -05	1.26 -05
7	8.68 -04	5.84 -04	3.93 -04	2.64 -04	1.78 -04	1.21 -04	8.22 -05	5.65 -05
8	2.37 -03	1.69 -03	1.20 -03	8.42 -04	5.93 -04	4.17 -04	2.93 -04	2.07 -04
9	5.06 -03	3.85 -03	2.89 -03	2.14 -03	1.58 -03	1.16 -03	8.49 -04	6.22 -04
10	8.20 -03	6.80 -03	5.50 -03	4.36 -03	3.41 -03	2.63 -03	2.01 -03	1.53 -03
11	9.64 -03	8.98 -03	8.00 -03	6.89 -03	5.78 -03	4.76 -03	3.86 -03	3.09 -03
12	7.26 -03	8.13 -03	8.36 -03	8.09 -03	7.48 -03	6.69 -03	5.81 -03	4.95 -03
13	2.47 -03	4.14 -03	5.55 -03	6.51 -03	6.98 -03	7.02 -03	6.73 -03	6.22 -03
14	3.05 -06	3.94 -04	1.44 -03	2.74 -03	3.95 -03	4.89 -03	5.48 -03	5.74 -03
15	2.69 -03	9.48 -04	9.72 -05	8.81 -05	6.77 -04	1.57 -03	2.51 -03	3.33 -03
16	6.48 -03	4.81 -03	2.88 -03	1.29 -03	3.20 -04	1.01 -06	1.95 -04	7.04 -04
17	5.37 -03	6.22 -03	5.82 -03	4.58 -03	3.04 -03	1.65 -03	6.53 -04	1.24 -04
18	1.07 -03	2.97 -03	4.62 -03	5.39 -03	5.22 -03	4.35 -03	3.17 -03	2.00 -03
19	5.18 -04	3.76 -05	9.65 -04	2.49 -03	3.83 -03	4.55 -03	4.57 -03	4.03 -03
20	4.38 -03	1.93 -03	3.35 -04	4.42 -05	7.86 -04	1.97 -03	3.05 -03	3.70 -03
21	5.85 -03	5.27 -03	3.40 -03	1.44 -03	2.45 -04	3.17 -05	5.69 -04	1.44 -03
22	2.48 -03	4.55 -03	5.18 -03	4.31 -03	2.68 -03	1.14 -03	2.16 -04	1.05 -05
23	5.83 -07	1.06 -03	3.00 -03	4.34 -03	4.43 -03	3.49 -03	2.15 -03	9.54 -04
24	2.17 -03	2.15 -04	2.62 -04	1.65 -03	3.15 -03	3.89 -03	3.68 -03	2.83 -03
25	5.10 -03	2.84 -03	6.93 -04	4.62 -06	7.19 -04	2.00 -03	3.00 -03	3.33 -03
26	4.39 -03	4.78 -03	3.17 -03	1.17 -03	8.07 -05	2.09 -04	1.09 -03	2.06 -03
27	1.42 -03	3.57 -03	4.27 -03	3.21 -03	1.50 -03	2.87 -04	1.94 -05	5.04 -04
28	3.22 -06	1.15 -03	2.91 -03	3.69 -03	3.01 -03	1.64 -03	4.79 -04	8.79 -06
29	4.11 -04	2.15 -05	1.13 -03	2.36 -03	3.16 -03	2.64 -03	1.59 -03	5.84 -04
30	1.40 -02	1.46 -04	2.26 -04	1.62 -03	1.71 -03	2.80 -03	2.16 -03	1.41 -03
31	1.80 -02	3.34 -02	6.12 -03	2.39 -03	4.17 -03	6.01 -04	3.02 -03	1.44 -03
32	8.38 -02	4.20 -02	6.80 -02	3.35 -02	1.59 -02	1.65 -02	5.19 -04	5.91 -03
33	7.09 -03	1.29 -02	1.73 -02	6.02 -02	6.53 -02	4.88 -02	5.60 -02	1.60 -02
34	5.04 -03	3.56 -02	1.12 -02	8.87 -03	5.81 -04	1.68 -02	3.08 -02	7.40 -02
35	7.24 -03	1.50 -02	3.39 -05	7.73 -04	1.42 -02	2.19 -02	1.21 -02	7.40 -03
36	3.33 -03	3.97 -03	8.90 -04	2.32 -03	9.04 -03	6.97 -03	8.48 -04	8.28 -05
37	9.38 -04	8.53 -04	5.86 -04	1.00 -03	2.80 -03	1.52 -03	1.41 -05	3.65 -04
38	8.17 -05	6.94 -05	6.01 -05	9.54 -05	2.48 -04	1.23 -04	7.10 -08	4.36 -05
$\sum_{v'} f_{v'v''}$	2.18 -01	2.19 -01	1.77 -01	1.79 -01	1.77 -01	1.73 -01	1.58 -01	1.55 -01

Table E.42: $f_{v'v''}$ for ^{6}Li singlet case (continued).

$v'\backslash v''$	40	41	42	43	44	45	46	47
0	5.09 -12	3.41 -12	2.18 -12	1.33 -12	7.68 -13	4.17 -13	2.10 -13	9.57 -14
1	9.15 -11	6.25 -11	4.40 -11	3.17 -11	2.33 -11	1.74 -11	1.32 -11	1.00 -11
2	1.76 -09	1.15 -09	7.70 -10	5.24 -10	3.64 -10	2.58 -10	1.86 -10	1.37 -10
3	2.23 -08	1.47 -08	9.85 -09	6.73 -09	4.67 -09	3.31 -09	2.38 -09	1.74 -09
4	2.07 -07	1.37 -07	9.24 -08	6.32 -08	4.40 -08	3.13 -08	2.26 -08	1.66 -08
5	1.49 -06	1.01 -06	6.86 -07	4.75 -07	3.34 -07	2.38 -07	1.72 -07	1.26 -07
6	8.48 -06	5.79 -06	4.00 -06	2.80 -06	1.99 -06	1.44 -06	1.05 -06	7.83 -07
7	3.92 -05	2.74 -05	1.93 -05	1.38 -05	9.92 -06	7.23 -06	5.34 -06	3.99 -06
8	1.47 -04	1.05 -04	7.55 -05	5.48 -05	4.02 -05	2.99 -05	2.24 -05	1.70 -05
9	4.57 -04	3.36 -04	2.48 -04	1.84 -04	1.38 -04	1.04 -04	7.91 -05	6.07 -05
10	1.17 -03	8.86 -04	6.73 -04	5.13 -04	3.93 -04	3.03 -04	2.36 -04	1.84 -04
11	2.46 -03	1.94 -03	1.53 -03	1.20 -03	9.44 -04	7.46 -04	5.91 -04	4.71 -04
12	4.15 -03	3.44 -03	2.83 -03	2.30 -03	1.87 -03	1.52 -03	1.24 -03	1.01 -03
13	5.59 -03	4.91 -03	4.25 -03	3.63 -03	3.07 -03	2.58 -03	2.17 -03	1.81 -03
14	5.70 -03	5.45 -03	5.05 -03	4.57 -03	4.07 -03	3.58 -03	3.12 -03	2.70 -03
15	3.93 -03	4.29 -03	4.42 -03	4.36 -03	4.16 -03	3.89 -03	3.57 -03	3.22 -03
16	1.34 -03	1.96 -03	2.48 -03	2.84 -03	3.05 -03	3.12 -03	3.09 -03	2.97 -03
17	3.60 -06	1.73 -04	5.03 -04	8.86 -04	1.25 -03	1.54 -03	1.75 -03	1.88 -03
18	1.06 -03	4.26 -04	9.31 -05	2.24 -09	6.83 -05	2.25 -04	4.13 -04	5.95 -04
19	3.20 -03	2.29 -03	1.47 -03	8.40 -04	4.05 -04	1.47 -04	2.68 -05	5.30 -07
20	3.86 -03	3.60 -03	3.07 -03	2.43 -03	1.80 -03	1.25 -03	8.18 -04	4.97 -04
21	2.28 -03	2.85 -03	3.09 -03	3.02 -03	2.75 -03	2.36 -03	1.93 -03	1.52 -03
22	3.47 -04	9.44 -04	1.55 -03	2.02 -03	2.28 -03	2.34 -03	2.25 -03	2.06 -03
23	2.24 -04	2.18 -08	1.58 -04	5.18 -04	9.21 -04	1.26 -03	1.50 -03	1.62 -03
24	1.77 -03	8.52 -04	2.64 -04	1.87 -05	3.55 -05	2.06 -04	4.35 -04	6.56 -04
25	3.01 -03	2.30 -03	1.49 -03	8.02 -04	3.29 -04	7.71 -05	3.94 -07	3.80 -05
26	2.66 -03	2.75 -03	2.42 -03	1.87 -03	1.28 -03	7.77 -04	4.04 -04	1.67 -04
27	1.27 -03	1.92 -03	2.23 -03	2.20 -03	1.92 -03	1.52 -03	1.11 -03	7.50 -04
28	1.87 -04	7.12 -04	1.26 -03	1.64 -03	1.78 -03	1.70 -03	1.50 -03	1.23 -03
29	6.08 -05	5.00 -05	3.65 -04	7.75 -04	1.11 -03	1.31 -03	1.36 -03	1.28 -03
30	5.78 -04	1.05 -04	6.93 -06	1.76 -04	4.54 -04	7.19 -04	9.04 -04	9.91 -04
31	1.23 -03	4.65 -04	1.16 -04	8.01 -08	8.54 -05	2.64 -04	4.51 -04	5.96 -04
32	2.60 -04	1.46 -03	2.04 -04	1.23 -04	3.87 -08	4.43 -05	1.61 -04	2.81 -04
33	2.25 -02	2.28 -03	4.78 -03	1.38 -04	3.99 -04	3.77 -05	1.07 -05	1.24 -04
34	5.18 -02	7.06 -02	3.25 -02	2.93 -02	1.00 -02	5.50 -03	1.84 -03	2.95 -04
35	1.88 -03	8.58 -03	4.51 -02	5.44 -02	7.60 -02	6.19 -02	4.79 -02	3.05 -02
36	9.80 -03	1.18 -02	2.03 -02	7.32 -03	1.30 -03	3.78 -03	2.02 -02	4.51 -02
37	4.20 -03	3.60 -03	4.27 -03	3.73 -04	2.87 -04	5.01 -03	1.02 -02	1.23 -02
38	3.95 -04	3.12 -04	3.38 -04	1.43 -05	5.39 -05	5.28 -04	9.31 -04	9.77 -04
$\sum_{v'} f_{v'v''}$	1.38 -01	1.41 -01	1.47 -01	1.29 -01	1.22 -01	1.08 -01	1.10 -01	1.16 -01

Table E.43: $f_{v'v''}$ for ^{6}Li singlet case (continued).

$v'\backslash v''$	48	49	50	51	52	53	54	55
0	3.77 -14	1.15 -14	1.87 -15	8.42 -18	1.24 -15	3.24 -15	5.06 -15	6.41 -15
1	7.63 -12	5.86 -12	4.53 -12	3.52 -12	2.74 -12	2.15 -12	1.70 -12	1.37 -12
2	1.02 -10	7.75 -11	5.99 -11	4.69 -11	3.70 -11	2.97 -11	2.41 -11	2.00 -11
3	1.29 -09	9.68 -10	7.40 -10	5.74 -10	4.49 -10	3.57 -10	2.88 -10	2.36 -10
4	1.23 -08	9.33 -09	7.17 -09	5.58 -09	4.39 -09	3.50 -09	2.83 -09	2.33 -09
5	9.39 -08	7.09 -08	5.43 -08	4.22 -08	3.31 -08	2.64 -08	2.13 -08	1.75 -08
6	5.88 -07	4.49 -07	3.47 -07	2.72 -07	2.15 -07	1.72 -07	1.40 -07	1.15 -07
7	3.01 -06	2.30 -06	1.79 -06	1.40 -06	1.11 -06	8.92 -07	7.26 -07	6.02 -07
8	1.30 -05	1.01 -05	7.93 -06	6.29 -06	5.03 -06	4.06 -06	3.32 -06	2.77 -06
9	4.69 -05	3.67 -05	2.90 -05	2.32 -05	1.86 -05	1.51 -05	1.25 -05	1.04 -05
10	1.45 -04	1.15 -04	9.21 -05	7.44 -05	6.04 -05	4.95 -05	4.11 -05	3.46 -05
11	3.76 -04	3.03 -04	2.46 -04	2.01 -04	1.65 -04	1.37 -04	1.14 -04	9.70 -05
12	8.23 -04	6.75 -04	5.56 -04	4.61 -04	3.83 -04	3.20 -04	2.71 -04	2.32 -04
13	1.52 -03	1.27 -03	1.07 -03	8.98 -04	7.57 -04	6.42 -04	5.48 -04	4.74 -04
14	2.32 -03	1.99 -03	1.71 -03	1.47 -03	1.26 -03	1.09 -03	9.41 -04	8.24 -04
15	2.88 -03	2.55 -03	2.25 -03	1.98 -03	1.74 -03	1.52 -03	1.34 -03	1.19 -03
16	2.80 -03	2.59 -03	2.38 -03	2.16 -03	1.95 -03	1.75 -03	1.58 -03	1.43 -03
17	1.93 -03	1.91 -03	1.86 -03	1.78 -03	1.67 -03	1.55 -03	1.44 -03	1.34 -03
18	7.46 -04	8.60 -04	9.36 -04	9.78 -04	9.87 -04	9.74 -04	9.49 -04	9.20 -04
19	3.12 -05	8.97 -05	1.57 -04	2.21 -04	2.74 -04	3.15 -04	3.45 -04	3.67 -04
20	2.77 -04	1.37 -04	5.64 -05	1.57 -05	1.07 -06	1.82 -06	1.07 -05	2.34 -05
21	1.16 -03	8.64 -04	6.29 -04	4.48 -04	3.13 -04	2.14 -04	1.45 -04	9.64 -05
22	1.81 -03	1.55 -03	1.31 -03	1.08 -03	8.84 -04	7.17 -04	5.82 -04	4.75 -04
23	1.63 -03	1.57 -03	1.47 -03	1.34 -03	1.19 -03	1.05 -03	9.25 -04	8.13 -04
24	8.30 -04	9.45 -04	1.01 -03	1.02 -03	9.97 -04	9.50 -04	8.93 -04	8.34 -04
25	1.34 -04	2.47 -04	3.52 -04	4.37 -04	4.95 -04	5.29 -04	5.46 -04	5.51 -04
26	4.40 -05	1.69 -06	9.49 -06	4.35 -05	8.68 -05	1.29 -04	1.67 -04	1.98 -04
27	4.66 -04	2.64 -04	1.32 -04	5.48 -05	1.54 -05	1.11 -06	1.66 -06	1.03 -05
28	9.46 -04	6.98 -04	4.94 -04	3.36 -04	2.19 -04	1.37 -04	8.16 -05	4.57 -05
29	1.14 -03	9.58 -04	7.81 -04	6.18 -04	4.76 -04	3.61 -04	2.71 -04	2.02 -04
30	9.90 -04	9.29 -04	8.34 -04	7.24 -04	6.12 -04	5.07 -04	4.18 -04	3.43 -04
31	6.80 -04	7.08 -04	6.93 -04	6.49 -04	5.87 -04	5.19 -04	4.53 -04	3.94 -04
32	3.82 -04	4.47 -04	4.79 -04	4.81 -04	4.62 -04	4.30 -04	3.93 -04	3.56 -04
33	1.72 -04	2.46 -04	2.86 -04	3.10 -04	3.14 -04	3.06 -04	2.91 -04	2.73 -04
34	3.95 -04	3.30 -05	2.07 -04	1.57 -04	1.97 -04	1.90 -04	1.89 -04	1.82 -04
35	1.44 -02	8.26 -03	1.83 -03	1.51 -03	3.47 -05	3.29 -04	4.55 -05	1.38 -04
36	6.75 -02	7.01 -02	6.73 -02	4.58 -02	3.44 -02	1.66 -02	1.06 -02	3.27 -03
37	8.93 -03	2.09 -03	1.41 -04	7.63 -03	2.10 -02	4.14 -02	5.17 -02	6.06 -02
38	5.53 -04	4.07 -05	1.51 -04	1.18 -03	2.34 -03	3.55 -03	3.27 -03	2.58 -03
$\sum_{v'} f_{v'v''}$	1.16 -01	1.02 -01	8.94 -02	7.41 -02	7.39 -02	7.63 -02	7.85 -02	7.83 -02

Table E.44: $f_{v'v''}$ for ^{6}Li singlet case (continued).

$v'\backslash v''$	56	57	58	59	60	61	62	63
0	7.23 -15	7.56 -15	7.49 -15	7.11 -15	6.51 -15	5.76 -15	4.96 -15	4.22 -15
1	1.10 -12	8.94 -13	7.24 -13	5.85 -13	4.71 -13	3.77 -13	2.99 -13	2.38 -13
2	1.66 -11	1.39 -11	1.17 -11	9.81 -12	8.18 -12	6.76 -12	5.53 -12	4.53 -12
3	1.96 -10	1.63 -10	1.36 -10	1.14 -10	9.47 -11	7.80 -11	6.37 -11	5.21 -11
4	1.94 -09	1.61 -09	1.35 -09	1.13 -09	9.36 -10	7.72 -10	6.30 -10	5.15 -10
5	1.46 -08	1.21 -08	1.02 -08	8.50 -09	7.07 -09	5.84 -09	4.77 -09	3.90 -09
6	9.59 -08	8.02 -08	6.72 -08	5.62 -08	4.68 -08	3.86 -08	3.15 -08	2.58 -08
7	5.03 -07	4.22 -07	3.54 -07	2.98 -07	2.48 -07	2.06 -07	1.69 -07	1.38 -07
8	2.32 -06	1.95 -06	1.64 -06	1.38 -06	1.16 -06	9.58 -07	7.86 -07	6.45 -07
9	8.81 -06	7.45 -06	6.31 -06	5.33 -06	4.48 -06	3.73 -06	3.07 -06	2.52 -06
10	2.93 -05	2.49 -05	2.12 -05	1.80 -05	1.51 -05	1.26 -05	1.04 -05	8.58 -06
11	8.29 -05	7.09 -05	6.07 -05	5.17 -05	4.38 -05	3.67 -05	3.03 -05	2.51 -05
12	1.99 -04	1.72 -04	1.48 -04	1.27 -04	1.08 -04	9.07 -05	7.53 -05	6.25 -05
13	4.12 -04	3.58 -04	3.10 -04	2.68 -04	2.29 -04	1.93 -04	1.61 -04	1.34 -04
14	7.23 -04	6.34 -04	5.55 -04	4.82 -04	4.16 -04	3.54 -04	2.96 -04	2.48 -04
15	1.06 -03	9.42 -04	8.32 -04	7.31 -04	6.35 -04	5.44 -04	4.58 -04	3.86 -04
16	1.29 -03	1.16 -03	1.04 -03	9.24 -04	8.11 -04	7.01 -04	5.96 -04	5.04 -04
17	1.24 -03	1.14 -03	1.04 -03	9.37 -04	8.33 -04	7.28 -04	6.25 -04	5.34 -04
18	8.83 -04	8.37 -04	7.84 -04	7.24 -04	6.58 -04	5.85 -04	5.10 -04	4.40 -04
19	3.80 -04	3.83 -04	3.79 -04	3.66 -04	3.45 -04	3.16 -04	2.83 -04	2.50 -04
20	3.72 -05	5.02 -05	6.12 -05	6.92 -05	7.36 -05	7.44 -05	7.17 -05	6.72 -05
21	6.24 -05	3.88 -05	2.30 -05	1.28 -05	6.52 -06	2.95 -06	1.11 -06	3.05 -07
22	3.86 -04	3.13 -04	2.52 -04	2.02 -04	1.61 -04	1.26 -04	9.86 -05	7.71 -05
23	7.12 -04	6.19 -04	5.35 -04	4.59 -04	3.89 -04	3.25 -04	2.68 -04	2.20 -04
24	7.72 -04	7.06 -04	6.39 -04	5.71 -04	5.03 -04	4.35 -04	3.69 -04	3.12 -04
25	5.45 -04	5.27 -04	5.01 -04	4.68 -04	4.27 -04	3.81 -04	3.33 -04	2.88 -04
26	2.21 -04	2.37 -04	2.44 -04	2.43 -04	2.34 -04	2.19 -04	1.98 -04	1.77 -04
27	2.27 -05	3.59 -05	4.80 -05	5.75 -05	6.37 -05	6.61 -05	6.49 -05	6.16 -05
28	2.31 -05	9.83 -06	2.98 -06	3.16 -07	1.37 -07	1.17 -06	2.51 -06	3.70 -06
29	1.49 -04	1.08 -04	7.70 -05	5.40 -05	3.71 -05	2.50 -05	1.66 -05	1.11 -05
30	2.80 -04	2.26 -04	1.81 -04	1.43 -04	1.13 -04	8.74 -05	6.72 -05	5.18 -05
31	3.39 -04	2.89 -04	2.45 -04	2.05 -04	1.69 -04	1.38 -04	1.11 -04	8.92 -05
32	3.19 -04	2.83 -04	2.47 -04	2.14 -04	1.82 -04	1.53 -04	1.26 -04	1.04 -04
33	2.52 -04	2.30 -04	2.06 -04	1.82 -04	1.59 -04	1.35 -04	1.14 -04	9.49 -05
34	1.72 -04	1.60 -04	1.46 -04	1.32 -04	1.16 -04	1.01 -04	8.54 -05	7.20 -05
35	8.77 -05	9.99 -05	8.59 -05	8.04 -05	7.10 -05	6.22 -05	5.31 -05	4.51 -05
36	2.38 -03	3.95 -04	5.11 -04	9.35 -06	1.18 -04	9.15 -06	3.78 -05	1.85 -05
37	5.54 -02	5.35 -02	4.21 -02	3.55 -02	2.40 -02	1.76 -02	9.48 -03	5.54 -03
38	1.12 -03	2.56 -04	9.83 -05	1.22 -03	4.47 -03	9.43 -03	1.74 -02	2.51 -02
$\sum_{v'} f_{v'v''}$	6.96 -02	6.38 -02	5.14 -02	4.45 -02	3.53 -02	3.29 -02	3.19 -02	3.49 -02

Table E.45: $f_{v'v''}$ for ^{6}Li singlet case (continued).

$v'\backslash v''$	64	65	66	67	68	69	70	71
0	3.67 -15	3.29 -15	2.96 -15	2.67 -15	2.38 -15	2.10 -15	1.80 -15	1.54 -15
1	1.96 -13	1.69 -13	1.46 -13	1.27 -13	1.10 -13	9.47 -14	7.97 -14	6.68 -14
2	3.83 -12	3.37 -12	2.99 -12	2.65 -12	2.35 -12	2.05 -12	1.76 -12	1.50 -12
3	4.40 -11	3.87 -11	3.43 -11	3.04 -11	2.69 -11	2.35 -11	2.01 -11	1.71 -11
4	4.35 -10	3.82 -10	3.38 -10	3.00 -10	2.65 -10	2.32 -10	1.98 -10	1.69 -10
5	3.30 -09	2.91 -09	2.57 -09	2.29 -09	2.02 -09	1.77 -09	1.52 -09	1.29 -09
6	2.18 -08	1.92 -08	1.70 -08	1.51 -08	1.33 -08	1.17 -08	9.99 -09	8.50 -09
7	1.17 -07	1.03 -07	9.16 -08	8.15 -08	7.23 -08	6.33 -08	5.43 -08	4.62 -08
8	5.47 -07	4.82 -07	4.28 -07	3.81 -07	3.37 -07	2.95 -07	2.53 -07	2.16 -07
9	2.15 -06	1.90 -06	1.69 -06	1.50 -06	1.34 -06	1.17 -06	1.01 -06	8.58 -07
10	7.30 -06	6.46 -06	5.75 -06	5.13 -06	4.56 -06	4.00 -06	3.44 -06	2.94 -06
11	2.14 -05	1.90 -05	1.70 -05	1.52 -05	1.35 -05	1.19 -05	1.02 -05	8.73 -06
12	5.35 -05	4.75 -05	4.25 -05	3.81 -05	3.40 -05	2.99 -05	2.58 -05	2.21 -05
13	1.15 -04	1.03 -04	9.22 -05	8.29 -05	7.40 -05	6.53 -05	5.64 -05	4.83 -05
14	2.14 -04	1.91 -04	1.72 -04	1.55 -04	1.39 -04	1.23 -04	1.06 -04	9.11 -05
15	3.34 -04	3.00 -04	2.70 -04	2.44 -04	2.20 -04	1.95 -04	1.69 -04	1.45 -04
16	4.39 -04	3.96 -04	3.59 -04	3.26 -04	2.94 -04	2.61 -04	2.27 -04	1.96 -04
17	4.68 -04	4.25 -04	3.87 -04	3.53 -04	3.20 -04	2.86 -04	2.49 -04	2.16 -04
18	3.90 -04	3.57 -04	3.28 -04	3.02 -04	2.75 -04	2.47 -04	2.17 -04	1.88 -04
19	2.25 -04	2.10 -04	1.95 -04	1.82 -04	1.68 -04	1.52 -04	1.35 -04	1.18 -04
20	6.36 -05	6.16 -05	5.95 -05	5.71 -05	5.41 -05	5.03 -05	4.54 -05	4.04 -05
21	3.18 -08	1.40 -08	1.32 -07	3.18 -07	5.26 -07	7.15 -07	8.49 -07	9.28 -07
22	6.26 -05	5.28 -05	4.49 -05	3.84 -05	3.27 -05	2.76 -05	2.29 -05	1.89 -05
23	1.87 -04	1.65 -04	1.46 -04	1.30 -04	1.15 -04	1.00 -04	8.58 -05	7.29 -05
24	2.71 -04	2.43 -04	2.20 -04	1.99 -04	1.79 -04	1.58 -04	1.37 -04	1.18 -04
25	2.55 -04	2.33 -04	2.14 -04	1.96 -04	1.79 -04	1.60 -04	1.40 -04	1.22 -04
26	1.61 -04	1.50 -04	1.41 -04	1.31 -04	1.21 -04	1.11 -04	9.80 -05	8.58 -05
27	5.89 -05	5.75 -05	5.59 -05	5.39 -05	5.12 -05	4.78 -05	4.32 -05	3.85 -05
28	4.70 -06	5.65 -06	6.44 -06	7.06 -06	7.45 -06	7.57 -06	7.35 -06	6.93 -06
29	7.62 -06	5.41 -06	3.83 -06	2.69 -06	1.85 -06	1.25 -06	8.13 -07	5.26 -07
30	4.14 -05	3.45 -05	2.89 -05	2.43 -05	2.04 -05	1.70 -05	1.39 -05	1.13 -05
31	7.42 -05	6.41 -05	5.57 -05	4.86 -05	4.22 -05	3.63 -05	3.05 -05	2.56 -05
32	8.79 -05	7.74 -05	6.84 -05	6.07 -05	5.36 -05	4.67 -05	3.98 -05	3.38 -05
33	8.15 -05	7.26 -05	6.49 -05	5.81 -05	5.18 -05	4.55 -05	3.91 -05	3.34 -05
34	6.24 -05	5.60 -05	5.05 -05	4.55 -05	4.08 -05	3.60 -05	3.11 -05	2.67 -05
35	3.93 -05	3.55 -05	3.21 -05	2.91 -05	2.61 -05	2.32 -05	2.01 -05	1.73 -05
36	2.04 -05	1.71 -05	1.60 -05	1.44 -05	1.30 -05	1.16 -05	1.00 -05	8.64 -06
37	1.98 -03	1.03 -03	3.00 -04	2.25 -04	3.81 -05	4.97 -05	1.76 -06	1.10 -05
38	3.08 -02	3.19 -02	3.32 -02	3.35 -02	3.42 -02	3.42 -02	3.52 -02	3.34 -02
$\sum_{v'} f_{v'v''}$	3.66 -02	3.63 -02	3.66 -02	3.65 -02	3.68 -02	3.66 -02	3.72 -02	3.51 -02

Table E.46: $f_{v'v''}$ for ^{6}Li singlet case (continued).

$v'\backslash v''$	72	73	74	75	76	77	78	79
0	1.33 -15	1.14 -15	9.78 -16	8.37 -16	7.12 -16	6.05 -16	5.12 -16	4.32 -16
1	5.70 -14	4.82 -14	4.09 -14	3.47 -14	2.93 -14	2.47 -14	2.08 -14	1.75 -14
2	1.29 -12	1.11 -12	9.50 -13	8.12 -13	6.92 -13	5.88 -13	4.98 -13	4.20 -13
3	1.48 -11	1.27 -11	1.09 -11	9.29 -12	7.91 -12	6.72 -12	5.69 -12	4.80 -12
4	1.46 -10	1.25 -10	1.07 -10	9.14 -11	7.78 -11	6.61 -11	5.60 -11	4.72 -11
5	1.11 -09	9.54 -10	8.19 -10	7.01 -10	5.97 -10	5.07 -10	4.30 -10	3.63 -10
6	7.34 -09	6.28 -09	5.39 -09	4.61 -09	3.93 -09	3.34 -09	2.83 -09	2.38 -09
7	3.99 -08	3.42 -08	2.94 -08	2.51 -08	2.14 -08	1.82 -08	1.54 -08	1.30 -08
8	1.86 -07	1.60 -07	1.37 -07	1.17 -07	1.00 -07	8.50 -08	7.21 -08	6.08 -08
9	7.42 -07	6.37 -07	5.47 -07	4.69 -07	4.00 -07	3.40 -07	2.88 -07	2.43 -07
10	2.54 -06	2.18 -06	1.88 -06	1.61 -06	1.37 -06	1.17 -06	9.89 -07	8.34 -07
11	7.57 -06	6.50 -06	5.59 -06	4.79 -06	4.09 -06	3.48 -06	2.96 -06	2.50 -06
12	1.91 -05	1.65 -05	1.42 -05	1.22 -05	1.04 -05	8.84 -06	7.51 -06	6.34 -06
13	4.20 -05	3.61 -05	3.11 -05	2.67 -05	2.28 -05	1.95 -05	1.65 -05	1.40 -05
14	7.92 -05	6.83 -05	5.89 -05	5.06 -05	4.33 -05	3.69 -05	3.14 -05	2.65 -05
15	1.26 -04	1.09 -04	9.43 -05	8.12 -05	6.95 -05	5.93 -05	5.04 -05	4.27 -05
16	1.71 -04	1.48 -04	1.28 -04	1.10 -04	9.45 -05	8.07 -05	6.87 -05	5.81 -05
17	1.89 -04	1.64 -04	1.42 -04	1.22 -04	1.05 -04	8.99 -05	7.66 -05	6.49 -05
18	1.66 -04	1.44 -04	1.25 -04	1.08 -04	9.32 -05	7.99 -05	6.82 -05	5.78 -05
19	1.04 -04	9.10 -05	7.96 -05	6.91 -05	5.97 -05	5.13 -05	4.39 -05	3.73 -05
20	3.63 -05	3.21 -05	2.84 -05	2.49 -05	2.16 -05	1.87 -05	1.61 -05	1.38 -05
21	9.76 -07	9.79 -07	9.57 -07	9.11 -07	8.48 -07	7.75 -07	6.98 -07	6.19 -07
22	1.59 -05	1.33 -05	1.11 -05	9.35 -06	7.83 -06	6.56 -06	5.48 -06	4.57 -06
23	6.29 -05	5.37 -05	4.61 -05	3.93 -05	3.34 -05	2.84 -05	2.40 -05	2.02 -05
24	1.03 -04	8.85 -05	7.65 -05	6.57 -05	5.62 -05	4.80 -05	4.08 -05	3.45 -05
25	1.07 -04	9.27 -05	8.05 -05	6.96 -05	5.98 -05	5.12 -05	4.36 -05	3.70 -05
26	7.60 -05	6.65 -05	5.82 -05	5.06 -05	4.37 -05	3.75 -05	3.21 -05	2.73 -05
27	3.46 -05	3.07 -05	2.72 -05	2.38 -05	2.07 -05	1.80 -05	1.55 -05	1.32 -05
28	6.53 -06	6.02 -06	5.50 -06	4.95 -06	4.41 -06	3.89 -06	3.40 -06	2.95 -06
29	3.44 -07	2.22 -07	1.43 -07	9.18 -08	5.86 -08	3.73 -08	2.37 -08	1.51 -08
30	9.39 -06	7.76 -06	6.45 -06	5.36 -06	4.46 -06	3.70 -06	3.08 -06	2.55 -06
31	2.18 -05	1.84 -05	1.56 -05	1.32 -05	1.12 -05	9.41 -06	7.91 -06	6.63 -06
32	2.90 -05	2.48 -05	2.12 -05	1.81 -05	1.53 -05	1.30 -05	1.10 -05	9.25 -06
33	2.89 -05	2.48 -05	2.13 -05	1.82 -05	1.55 -05	1.32 -05	1.12 -05	9.45 -06
34	2.32 -05	1.99 -05	1.72 -05	1.48 -05	1.26 -05	1.07 -05	9.11 -06	7.70 -06
35	1.50 -05	1.30 -05	1.12 -05	9.63 -06	8.23 -06	7.02 -06	5.97 -06	5.05 -06
36	7.53 -06	6.50 -06	5.61 -06	4.83 -06	4.13 -06	3.53 -06	3.00 -06	2.53 -06
37	5.43 -07	3.35 -06	1.35 -06	1.72 -06	1.27 -06	1.16 -06	9.64 -07	8.20 -07
38	2.99 -02	2.62 -02	2.29 -02	1.89 -02	1.55 -02	1.21 -02	9.31 -03	6.76 -03
$\sum_{v'} f_{v'v''}$	3.14 -02	2.75 -02	2.40 -02	1.99 -02	1.64 -02	1.28 -02	9.92 -03	7.27 -03

Table E.47: $f_{v'v''}$ for ^{6}Li singlet case (continued).

$v'\backslash v''$	80	81	82	83	84	85	86	87
0	3.62 -16	3.02 -16	2.50 -16	2.06 -16	1.69 -16	1.37 -16	1.10 -16	8.98 -17
1	1.46 -14	1.21 -14	1.00 -14	8.26 -15	6.75 -15	5.47 -15	4.40 -15	3.51 -15
2	3.52 -13	2.94 -13	2.44 -13	2.01 -13	1.65 -13	1.34 -13	1.08 -13	8.59 -14
3	4.03 -12	3.36 -12	2.79 -12	2.30 -12	1.88 -12	1.53 -12	1.23 -12	9.83 -13
4	3.96 -11	3.30 -11	2.74 -11	2.26 -11	1.85 -11	1.50 -11	1.21 -11	9.65 -12
5	3.04 -10	2.54 -10	2.11 -10	1.74 -10	1.42 -10	1.15 -10	9.30 -11	7.42 -11
6	2.00 -09	1.67 -09	1.38 -09	1.14 -09	9.34 -10	7.58 -10	6.11 -10	4.88 -10
7	1.09 -08	9.12 -09	7.57 -09	6.24 -09	5.11 -09	4.15 -09	3.34 -09	2.67 -09
8	5.10 -08	4.26 -08	3.53 -08	2.91 -08	2.39 -08	1.94 -08	1.56 -08	1.25 -08
9	2.04 -07	1.71 -07	1.42 -07	1.17 -07	9.56 -08	7.77 -08	6.26 -08	4.99 -08
10	7.01 -07	5.85 -07	4.86 -07	4.00 -07	3.28 -07	2.67 -07	2.15 -07	1.71 -07
11	2.10 -06	1.75 -06	1.45 -06	1.20 -06	9.82 -07	7.98 -07	6.43 -07	5.13 -07
12	5.33 -06	4.45 -06	3.70 -06	3.05 -06	2.50 -06	2.03 -06	1.64 -06	1.31 -06
13	1.17 -05	9.81 -06	8.15 -06	6.72 -06	5.51 -06	4.48 -06	3.61 -06	2.88 -06
14	2.23 -05	1.86 -05	1.55 -05	1.28 -05	1.05 -05	8.52 -06	6.87 -06	5.49 -06
15	3.59 -05	3.00 -05	2.49 -05	2.06 -05	1.69 -05	1.37 -05	1.11 -05	8.84 -06
16	4.89 -05	4.10 -05	3.41 -05	2.81 -05	2.31 -05	1.88 -05	1.51 -05	1.21 -05
17	5.47 -05	4.58 -05	3.81 -05	3.15 -05	2.58 -05	2.10 -05	1.70 -05	1.35 -05
18	4.88 -05	4.09 -05	3.40 -05	2.82 -05	2.31 -05	1.88 -05	1.52 -05	1.21 -05
19	3.15 -05	2.65 -05	2.21 -05	1.83 -05	1.50 -05	1.22 -05	9.86 -06	7.89 -06
20	1.17 -05	9.83 -06	8.22 -06	6.82 -06	5.61 -06	4.58 -06	3.70 -06	2.96 -06
21	5.41 -07	4.68 -07	3.99 -07	3.37 -07	2.81 -07	2.32 -07	1.89 -07	1.52 -07
22	3.80 -06	3.15 -06	2.59 -06	2.12 -06	1.73 -06	1.40 -06	1.13 -06	8.96 -07
23	1.70 -05	1.41 -05	1.17 -05	9.67 -06	7.91 -06	6.42 -06	5.17 -06	4.13 -06
24	2.90 -05	2.42 -05	2.01 -05	1.66 -05	1.36 -05	1.11 -05	8.93 -06	7.13 -06
25	3.12 -05	2.61 -05	2.17 -05	1.80 -05	1.47 -05	1.20 -05	9.68 -06	7.74 -06
26	2.31 -05	1.94 -05	1.62 -05	1.34 -05	1.10 -05	8.95 -06	7.23 -06	5.78 -06
27	1.12 -05	9.44 -06	7.89 -06	6.55 -06	5.39 -06	4.40 -06	3.55 -06	2.84 -06
28	2.53 -06	2.15 -06	1.81 -06	1.51 -06	1.25 -06	1.02 -06	8.31 -07	6.67 -07
29	9.60 -09	6.14 -09	3.95 -09	2.56 -09	1.68 -09	1.12 -09	7.52 -10	5.13 -10
30	2.11 -06	1.74 -06	1.43 -06	1.17 -06	9.51 -07	7.68 -07	6.16 -07	4.89 -07
31	5.54 -06	4.60 -06	3.80 -06	3.12 -06	2.55 -06	2.07 -06	1.66 -06	1.33 -06
32	7.75 -06	6.46 -06	5.35 -06	4.41 -06	3.60 -06	2.93 -06	2.36 -06	1.88 -06
33	7.93 -06	6.62 -06	5.49 -06	4.53 -06	3.71 -06	3.01 -06	2.42 -06	1.94 -06
34	6.47 -06	5.40 -06	4.49 -06	3.70 -06	3.03 -06	2.46 -06	1.99 -06	1.59 -06
35	4.24 -06	3.55 -06	2.95 -06	2.43 -06	1.99 -06	1.62 -06	1.31 -06	1.04 -06
36	2.13 -06	1.78 -06	1.48 -06	1.22 -06	1.00 -06	8.14 -07	6.57 -07	5.24 -07
37	6.88 -07	5.75 -07	4.77 -07	3.94 -07	3.22 -07	2.62 -07	2.11 -07	1.69 -07
38	4.80 -03	3.17 -03	2.03 -03	1.18 -03	6.65 -04	3.24 -04	1.53 -04	5.73 -05
$\sum_{v'} f_{v'v''}$	5.23 -03	3.53 -03	2.33 -03	1.43 -03	8.67 -04	4.88 -04	2.85 -04	1.63 -04

Table E.48: $f_{v'v''}$ for ^{6}Li singlet case (continued).

$v'\backslash v''$	88	89	90	91	92	$\sum_{v''} f_{v'v''}$
0	7.20 -17	5.55 -17	4.10 -17	3.76 -17	4.56 -17	4.54 -01
1	2.77 -15	2.16 -15	1.70 -15	1.59 -15	1.88 -15	4.57 -01
2	6.78 -14	5.30 -14	4.17 -14	3.92 -14	4.62 -14	4.59 -01
3	7.76 -13	6.06 -13	4.76 -13	4.47 -13	5.27 -13	4.61 -01
4	7.63 -12	5.96 -12	4.68 -12	4.40 -12	5.18 -12	4.64 -01
5	5.86 -11	4.58 -11	3.60 -11	3.38 -11	3.98 -11	4.66 -01
6	3.85 -10	3.01 -10	2.36 -10	2.22 -10	2.62 -10	4.69 -01
7	2.11 -09	1.65 -09	1.29 -09	1.22 -09	1.43 -09	4.71 -01
8	9.84 -09	7.69 -09	6.04 -09	5.67 -09	6.69 -09	4.74 -01
9	3.95 -08	3.08 -08	2.42 -08	2.27 -08	2.68 -08	4.76 -01
10	1.35 -07	1.06 -07	8.31 -08	7.81 -08	9.21 -08	4.78 -01
11	4.06 -07	3.17 -07	2.49 -07	2.34 -07	2.76 -07	4.80 -01
12	1.03 -06	8.07 -07	6.34 -07	5.95 -07	7.02 -07	4.81 -01
13	2.28 -06	1.78 -06	1.40 -06	1.31 -06	1.55 -06	4.81 -01
14	4.34 -06	3.39 -06	2.66 -06	2.50 -06	2.95 -06	4.78 -01
15	6.99 -06	5.46 -06	4.29 -06	4.03 -06	4.75 -06	4.73 -01
16	9.55 -06	7.47 -06	5.87 -06	5.51 -06	6.50 -06	4.63 -01
17	1.07 -05	8.37 -06	6.58 -06	6.18 -06	7.29 -06	4.53 -01
18	9.59 -06	7.50 -06	5.89 -06	5.54 -06	6.53 -06	4.43 -01
19	6.24 -06	4.88 -06	3.84 -06	3.61 -06	4.25 -06	4.37 -01
20	2.35 -06	1.84 -06	1.44 -06	1.36 -06	1.60 -06	4.37 -01
21	1.21 -07	9.54 -08	7.53 -08	7.10 -08	8.41 -08	4.40 -01
22	7.06 -07	5.51 -07	4.32 -07	4.05 -07	4.77 -07	4.45 -01
23	3.26 -06	2.55 -06	2.00 -06	1.88 -06	2.21 -06	4.48 -01
24	5.63 -06	4.40 -06	3.46 -06	3.25 -06	3.83 -06	4.48 -01
25	6.12 -06	4.78 -06	3.76 -06	3.53 -06	4.17 -06	4.47 -01
26	4.57 -06	3.57 -06	2.81 -06	2.64 -06	3.12 -06	4.47 -01
27	2.25 -06	1.76 -06	1.39 -06	1.30 -06	1.54 -06	4.50 -01
28	5.29 -07	4.15 -07	3.27 -07	3.08 -07	3.64 -07	4.54 -01
29	3.54 -10	2.47 -10	1.77 -10	1.53 -10	1.65 -10	4.59 -01
30	3.85 -07	3.00 -07	2.36 -07	2.21 -07	2.60 -07	4.64 -01
31	1.05 -06	8.17 -07	6.41 -07	6.02 -07	7.09 -07	4.68 -01
32	1.48 -06	1.16 -06	9.10 -07	8.55 -07	1.01 -06	4.73 -01
33	1.53 -06	1.19 -06	9.38 -07	8.81 -07	1.04 -06	4.79 -01
34	1.25 -06	9.79 -07	7.69 -07	7.22 -07	8.52 -07	4.84 -01
35	8.24 -07	6.44 -07	5.06 -07	4.75 -07	5.61 -07	4.90 -01
36	4.14 -07	3.24 -07	2.54 -07	2.39 -07	2.82 -07	4.95 -01
37	1.33 -07	1.04 -07	8.17 -08	7.68 -08	9.05 -08	4.98 -01
38	2.13 -05	5.10 -06	1.29 -06	4.68 -08	2.47 -08	4.98 -01
$\sum_{v'} f_{v'v''}$	1.05 -04	7.07 -05	5.28 -05	4.85 -05	5.72 -05	

Table E.49: $f_{v'v''}$ for ^{6}Li singlet case (continued).

$v'\backslash v''$	0	1	2	3	4	5	6	7
0	2.45 -02	6.20 -02	8.59 -02	8.66 -02	7.11 -02	5.06 -02	3.24 -02	1.91 -02
1	8.33 -02	9.21 -02	3.64 -02	1.53 -03	8.37 -03	3.09 -02	4.57 -02	4.68 -02
2	1.29 -01	2.74 -02	7.16 -03	4.55 -02	4.15 -02	1.24 -02	5.42 -06	9.52 -03
3	1.21 -01	4.55 -03	6.06 -02	2.10 -02	1.77 -03	2.79 -02	3.52 -02	1.69 -02
4	7.65 -02	6.52 -02	2.70 -02	1.18 -02	4.36 -02	1.42 -02	1.13 -03	2.04 -02
5	3.40 -02	1.04 -01	3.70 -03	5.41 -02	4.11 -03	1.84 -02	3.35 -02	8.78 -03
6	1.09 -02	7.94 -02	6.38 -02	1.22 -02	2.95 -02	2.96 -02	7.45 -05	2.25 -02
7	2.52 -03	3.68 -02	9.87 -02	1.55 -02	4.19 -02	2.65 -03	3.61 -02	1.06 -02
8	4.14 -04	1.12 -02	6.87 -02	8.22 -02	1.27 -04	4.70 -02	4.54 -03	1.89 -02
9	4.60 -05	2.24 -03	2.74 -02	9.23 -02	4.69 -02	1.46 -02	2.81 -02	2.22 -02
10	3.12 -06	2.86 -04	6.68 -03	4.91 -02	9.87 -02	1.54 -02	3.59 -02	7.38 -03
11	9.65 -08	2.08 -05	9.74 -04	1.45 -02	7.16 -02	8.74 -02	7.64 -04	4.58 -02
12	3.19 -10	6.89 -07	7.98 -05	2.47 -03	2.61 -02	9.09 -02	6.56 -02	3.42 -03
13	2.03 -12	1.03 -08	3.26 -06	2.28 -04	5.12 -03	4.08 -02	1.04 -01	4.17 -02
14	1.67 -10	2.03 -09	6.83 -08	8.92 -06	4.80 -04	8.77 -03	5.64 -02	1.08 -01
15	1.56 -11	1.31 -10	4.46 -11	6.50 -09	1.25 -05	8.04 -04	1.34 -02	7.24 -02
16	7.81 -11	1.21 -09	1.28 -08	1.04 -07	2.21 -07	1.51 -05	1.24 -03	1.89 -02
17	2.07 -11	6.08 -10	4.96 -09	2.23 -08	1.49 -07	5.97 -07	1.51 -05	1.63 -03
18	2.62 -11	4.00 -10	3.41 -09	1.25 -08	1.08 -08	1.15 -07	2.51 -06	6.11 -06
19	9.67 -12	4.31 -10	3.35 -09	1.16 -08	1.82 -08	3.92 -09	3.32 -07	7.35 -06
20	9.88 -12	2.79 -10	2.15 -09	6.82 -09	7.19 -09	6.53 -11	1.91 -08	2.97 -07
21	4.63 -12	1.71 -10	1.30 -09	4.42 -09	6.01 -09	1.81 -09	4.05 -09	4.30 -08
22	7.21 -12	2.97 -10	2.16 -09	6.68 -09	6.84 -09	2.49 -10	6.83 -09	9.01 -10
23	1.42 -12	7.25 -12	7.04 -11	2.80 -10	6.20 -10	5.77 -10	6.30 -11	2.57 -10
24	9.74 -12	2.24 -10	1.69 -09	5.16 -09	5.63 -09	4.68 -10	3.77 -09	7.05 -09
25	1.05 -12	5.99 -11	4.26 -10	1.14 -09	8.21 -10	1.51 -11	1.62 -09	1.51 -09
26	4.09 -12	3.48 -11	2.74 -10	9.12 -10	1.32 -09	3.37 -10	4.75 -10	2.63 -09
27	8.41 -12	1.27 -10	9.55 -10	2.76 -09	2.87 -09	1.79 -10	2.07 -09	4.25 -09
28	1.90 -12	3.99 -11	3.04 -10	7.53 -10	5.47 -10	7.37 -13	4.99 -10	1.16 -10
29	6.74 -13	4.60 -12	2.76 -11	1.30 -10	2.81 -10	1.45 -10	1.10 -10	1.44 -09
30	4.61 -12	5.64 -11	3.84 -10	1.18 -09	1.40 -09	2.03 -10	6.74 -10	1.97 -09
31	4.75 -12	6.13 -11	4.23 -10	1.17 -09	1.14 -09	7.61 -11	5.12 -10	4.65 -10
32	1.85 -12	2.27 -11	1.61 -10	3.84 -10	2.69 -10	1.51 -13	1.22 -10	1.86 -11
33	1.12 -13	7.79 -13	7.43 -12	5.49 -12	3.68 -12	4.07 -11	2.19 -14	3.67 -10
34	2.17 -13	4.44 -12	2.43 -11	1.06 -10	2.03 -10	9.46 -11	4.25 -11	4.99 -10
35	8.18 -13	1.36 -11	8.02 -11	2.72 -10	3.75 -10	1.00 -10	8.41 -11	3.58 -10
36	1.06 -12	1.65 -11	9.85 -11	3.07 -10	3.71 -10	7.26 -11	8.50 -11	1.85 -10
37	9.05 -13	1.36 -11	8.13 -11	2.42 -10	2.70 -10	4.19 -11	6.33 -11	7.85 -11
38	5.90 -13	8.64 -12	5.17 -11	1.50 -10	1.58 -10	2.06 -11	3.82 -11	3.00 -11
39	2.99 -13	4.31 -12	2.58 -11	7.34 -11	7.53 -11	8.77 -12	1.85 -11	1.07 -11
40	1.01 -13	1.45 -12	8.65 -12	2.45 -11	2.47 -11	2.73 -12	6.16 -12	3.06 -12
41	1.27 -14	1.83 -13	1.09 -12	3.09 -12	3.11 -12	3.39 -13	7.77 -13	3.70 -13
$\sum_{v'} f_{v'v''}$	4.83 -01	4.85 -01	4.87 -01	4.89 -01	4.91 -01	4.92 -01	4.94 -01	4.95 -01

Table E.50: Oscillator strengths $f_{v'v''}$ for the ^{7}Li singlet case.

$v'\backslash v''$	8	9	10	11	12	13	14	15
0	1.06 -02	5.59 -03	2.84 -03	1.40 -03	6.73 -04	3.18 -04	1.48 -04	6.81 -05
1	3.90 -02	2.82 -02	1.85 -02	1.13 -02	6.52 -03	3.60 -03	1.92 -03	9.99 -04
2	2.52 -02	3.47 -02	3.52 -02	2.98 -02	2.23 -02	1.52 -02	9.71 -03	5.89 -03
3	1.49 -03	2.53 -03	1.37 -02	2.44 -02	2.91 -02	2.79 -02	2.31 -02	1.73 -02
4	2.94 -02	1.75 -02	3.36 -03	4.56 -04	7.54 -03	1.71 -02	2.33 -02	2.47 -02
5	1.32 -03	1.68 -02	2.49 -02	1.66 -02	4.50 -03	9.18 -06	4.18 -03	1.20 -02
6	2.54 -02	4.91 -03	1.82 -03	1.49 -02	2.15 -02	1.53 -02	5.04 -03	8.04 -05
7	3.67 -03	2.36 -02	1.86 -02	2.36 -03	2.47 -03	1.36 -02	1.89 -02	1.38 -02
8	2.62 -02	1.50 -03	9.06 -03	2.22 -02	1.29 -02	8.70 -04	3.17 -03	1.27 -02
9	2.49 -03	2.65 -02	1.29 -02	2.05 -04	1.33 -02	1.92 -02	8.49 -03	1.66 -04
10	3.32 -02	1.59 -03	1.43 -02	2.21 -02	3.75 -03	2.95 -03	1.55 -02	1.56 -02
11	1.57 -05	2.91 -02	1.23 -02	2.70 -03	2.08 -02	1.30 -02	1.88 -04	6.67 -03
12	4.03 -02	6.72 -03	1.58 -02	2.27 -02	4.17 -04	1.16 -02	1.87 -02	5.27 -03
13	1.57 -02	2.63 -02	1.86 -02	4.24 -03	2.48 -02	6.42 -03	2.93 -03	1.67 -02
14	2.14 -02	2.93 -02	1.21 -02	2.77 -02	4.89 -06	1.94 -02	1.44 -02	7.63 -06
15	1.07 -01	7.95 -03	3.87 -02	2.80 -03	3.00 -02	2.91 -03	1.07 -02	1.91 -02
16	8.81 -02	1.01 -01	1.41 -03	4.20 -02	2.11 -07	2.62 -02	9.38 -03	3.53 -03
17	2.44 -02	1.02 -01	9.40 -02	3.00 -05	4.00 -02	2.15 -03	1.92 -02	1.58 -02
18	1.91 -03	2.99 -02	1.15 -01	8.77 -02	1.46 -03	3.48 -02	6.69 -03	1.19 -02
19	3.21 -08	1.89 -03	3.40 -02	1.27 -01	8.34 -02	3.67 -03	2.86 -02	1.15 -02
20	1.74 -05	2.53 -05	1.50 -03	3.64 -02	1.38 -01	8.24 -02	5.38 -03	2.24 -02
21	3.47 -07	3.29 -05	1.25 -04	8.75 -04	3.64 -02	1.48 -01	8.59 -02	5.68 -03
22	1.59 -07	4.91 -09	4.19 -05	3.44 -04	2.11 -04	3.33 -02	1.57 -01	9.53 -02
23	8.65 -09	6.09 -07	1.42 -06	3.90 -05	7.08 -04	5.44 -05	2.64 -02	1.63 -01
24	5.56 -10	3.54 -09	7.77 -07	7.16 -06	1.84 -05	1.12 -03	1.20 -03	1.67 -02
25	3.54 -10	1.63 -08	1.24 -07	4.30 -07	2.06 -05	4.60 -07	1.32 -03	4.36 -03
26	9.26 -10	4.10 -10	9.10 -09	3.61 -07	4.07 -09	3.75 -05	7.24 -05	1.01 -03
27	7.98 -10	4.23 -10	1.69 -08	1.02 -08	7.44 -07	2.27 -06	3.66 -05	3.52 -04
28	4.88 -10	2.31 -10	6.18 -10	6.62 -09	9.05 -08	5.86 -07	1.30 -05	7.40 -06
29	2.07 -09	8.86 -10	1.41 -09	7.60 -09	2.70 -09	4.89 -07	6.62 -09	3.15 -05
30	5.05 -10	1.38 -12	9.54 -10	2.28 -09	1.13 -08	4.93 -08	6.98 -07	4.38 -06
31	2.14 -10	1.05 -09	4.98 -13	1.18 -10	3.53 -09	1.46 -09	3.09 -07	6.62 -08
32	1.24 -09	1.72 -09	2.70 -10	1.07 -10	2.18 -10	1.14 -08	3.51 -08	6.51 -07
33	1.13 -09	7.43 -10	2.19 -10	3.02 -10	3.57 -11	8.64 -09	1.29 -11	3.66 -07
34	4.05 -10	2.77 -11	2.12 -11	2.72 -10	1.01 -10	3.55 -09	4.23 -09	9.52 -08
35	3.17 -11	1.46 -10	2.15 -11	1.67 -10	5.62 -11	9.31 -10	4.93 -09	1.25 -08
36	1.81 -11	4.27 -10	8.77 -11	8.69 -11	1.65 -11	1.34 -10	3.40 -09	1.88 -10
37	7.63 -11	4.82 -10	1.03 -10	4.21 -11	3.00 -12	2.50 -12	1.94 -09	5.73 -10
38	8.37 -11	3.54 -10	7.45 -11	1.94 -11	3.17 -13	5.54 -12	9.85 -10	9.94 -10
39	5.28 -11	1.89 -10	3.90 -11	8.14 -12	1.42 -14	8.51 -12	4.36 -10	6.81 -10
40	1.94 -11	6.50 -11	1.33 -11	2.54 -12	2.36 -17	3.95 -12	1.39 -10	2.55 -10
41	2.51 -12	8.26 -12	1.68 -12	3.15 -13	1.66 -17	5.37 -13	1.73 -11	3.31 -11
$\sum_{v'} f_{v'v''}$	4.97 -01	4.98 -01	4.99 -01	5.00 -01	5.01 -01	5.01 -01	5.02 -01	5.03 -01

Table E.51: $f_{v'v''}$ for ^{7}Li singlet case (continued).

$v'\backslash v''$	16	17	18	19	20	21	22	23
0	3.11 -05	1.41 -05	6.40 -06	2.90 -06	1.32 -06	6.02 -07	2.76 -07	1.28 -07
1	5.09 -04	2.55 -04	1.26 -04	6.20 -05	3.03 -05	1.47 -05	7.16 -06	3.48 -06
2	3.43 -03	1.93 -03	1.06 -03	5.74 -04	3.05 -04	1.60 -04	8.34 -05	4.32 -05
3	1.20 -02	7.88 -03	4.94 -03	2.99 -03	1.76 -03	1.01 -03	5.72 -04	3.19 -04
4	2.23 -02	1.80 -02	1.35 -02	9.43 -03	6.29 -03	4.05 -03	2.53 -03	1.54 -03
5	1.85 -02	2.13 -02	2.07 -02	1.79 -02	1.42 -02	1.05 -02	7.43 -03	5.05 -03
6	2.31 -03	8.46 -03	1.45 -02	1.81 -02	1.87 -02	1.71 -02	1.43 -02	1.12 -02
7	5.21 -03	2.94 -04	1.23 -03	5.97 -03	1.13 -02	1.51 -02	1.65 -02	1.59 -02
8	1.68 -02	1.25 -02	5.19 -03	5.30 -04	6.10 -04	4.17 -03	8.77 -03	1.25 -02
9	3.82 -03	1.19 -02	1.50 -02	1.13 -02	5.06 -03	7.55 -04	2.55 -04	2.85 -03
10	5.22 -03	1.25 -06	4.36 -03	1.12 -02	1.34 -02	1.03 -02	4.90 -03	9.65 -04
11	1.57 -02	1.20 -02	2.98 -03	1.54 -04	4.74 -03	1.05 -02	1.22 -02	9.38 -03
12	6.17 -04	9.61 -03	1.44 -02	8.83 -03	1.54 -03	4.48 -04	4.91 -03	9.69 -03
13	1.22 -02	9.85 -04	2.91 -03	1.12 -02	1.24 -02	6.18 -03	6.74 -04	7.89 -04
14	1.01 -02	1.57 -02	5.82 -03	2.12 -05	5.50 -03	1.15 -02	1.02 -02	4.16 -03
15	2.91 -03	3.34 -03	1.40 -02	1.10 -02	1.70 -03	1.08 -03	7.43 -03	1.09 -02
16	1.86 -02	8.40 -03	1.43 -04	8.95 -03	1.32 -02	5.83 -03	8.70 -05	2.89 -03
17	2.10 -04	1.43 -02	1.32 -02	9.35 -04	3.77 -03	1.18 -02	9.58 -03	2.16 -03
18	1.96 -02	6.68 -04	8.69 -03	1.51 -02	4.18 -03	6.22 -04	8.12 -03	1.10 -02
19	6.16 -03	2.04 -02	3.41 -03	3.97 -03	1.43 -02	7.88 -03	9.25 -05	4.19 -03
20	1.55 -02	2.48 -03	1.91 -02	6.81 -03	1.07 -03	1.16 -02	1.05 -02	1.54 -03
21	1.69 -02	1.81 -02	6.17 -04	1.64 -02	9.75 -03	2.71 -05	8.21 -03	1.15 -02
22	4.46 -03	1.26 -02	1.95 -02	3.27 -05	1.34 -02	1.16 -02	3.04 -04	5.15 -03
23	1.11 -01	2.20 -03	9.01 -03	2.02 -02	6.21 -05	1.06 -02	1.24 -02	1.23 -03
24	1.62 -01	1.36 -01	1.96 -04	5.96 -03	2.06 -02	2.23 -04	8.38 -03	1.24 -02
25	6.13 -03	1.49 -01	1.66 -01	1.08 -03	3.16 -03	2.16 -02	2.38 -04	6.66 -03
26	9.21 -03	1.01 -04	1.20 -01	1.99 -01	8.99 -03	8.19 -04	2.39 -02	6.08 -05
27	2.53 -04	1.35 -02	5.43 -03	7.46 -02	2.22 -01	2.84 -02	8.20 -05	2.90 -02
28	7.69 -04	1.68 -04	1.32 -02	2.60 -02	2.50 -02	2.15 -01	6.02 -02	3.39 -03
29	2.85 -05	8.67 -04	2.66 -03	6.02 -03	5.32 -02	1.52 -05	1.60 -01	9.35 -02
30	2.53 -05	2.84 -04	2.44 -04	7.42 -03	2.39 -06	6.08 -02	2.77 -02	7.04 -02
31	2.06 -05	6.53 -07	6.49 -04	3.24 -04	8.33 -03	1.16 -02	3.02 -02	8.96 -02
32	3.03 -06	2.30 -05	1.54 -04	3.54 -04	3.71 -03	1.58 -03	3.61 -02	4.68 -05
33	9.17 -11	1.80 -05	1.67 -06	4.82 -04	1.73 -04	6.07 -03	4.44 -03	2.94 -02
34	3.66 -07	5.35 -06	1.09 -05	1.81 -04	1.45 -04	3.15 -03	6.41 -04	2.48 -02
35	3.98 -07	7.39 -07	1.55 -05	3.06 -05	3.21 -04	6.79 -04	3.24 -03	7.25 -03
36	2.36 -07	1.02 -08	9.98 -06	9.65 -07	2.38 -04	3.91 -05	2.94 -03	6.80 -04
37	1.13 -07	3.82 -08	4.89 -06	8.69 -07	1.24 -04	8.46 -06	1.68 -03	2.34 -05
38	4.88 -08	6.45 -08	2.12 -06	1.92 -06	5.56 -05	3.02 -05	7.87 -04	2.27 -04
39	1.94 -08	4.38 -08	8.38 -07	1.39 -06	2.22 -05	2.39 -05	3.21 -04	2.06 -04
40	5.88 -09	1.63 -08	2.53 -07	5.30 -07	6.73 -06	9.39 -06	9.81 -05	8.42 -05
41	7.23 -10	2.12 -09	3.11 -08	6.89 -08	8.28 -07	1.23 -06	1.21 -05	1.11 -05
$\sum_{v'} f_{v'v''}$	5.03 -01	5.03 -01	5.03 -01	5.03 -01	5.03 -01	5.03 -01	5.01 -01	4.93 -01

Table E.52: $f_{v'v''}$ for ^{7}Li singlet case (continued).

$v'\backslash v''$	24	25	26	27	28	29	30	31
0	5.94 -08	2.78 -08	1.30 -08	6.10 -09	2.86 -09	1.34 -09	6.35 -10	3.11 -10
1	1.70 -06	8.30 -07	4.09 -07	2.03 -07	1.01 -07	5.10 -08	2.59 -08	1.33 -08
2	2.24 -05	1.16 -05	5.98 -06	3.10 -06	1.61 -06	8.43 -07	4.43 -07	2.36 -07
3	1.76 -04	9.69 -05	5.30 -05	2.90 -05	1.58 -05	8.64 -06	4.73 -06	2.61 -06
4	9.22 -04	5.44 -04	3.18 -04	1.84 -04	1.06 -04	6.08 -05	3.49 -05	2.00 -05
5	3.32 -03	2.14 -03	1.35 -03	8.37 -04	5.13 -04	3.12 -04	1.88 -04	1.13 -04
6	8.31 -03	5.93 -03	4.11 -03	2.77 -03	1.83 -03	1.19 -03	7.62 -04	4.85 -04
7	1.40 -02	1.15 -02	8.95 -03	6.69 -03	4.84 -03	3.41 -03	2.35 -03	1.59 -03
8	1.44 -02	1.46 -02	1.34 -02	1.15 -02	9.35 -03	7.27 -03	5.47 -03	4.01 -03
9	6.70 -03	1.02 -02	1.24 -02	1.31 -02	1.25 -02	1.12 -02	9.45 -03	7.65 -03
10	6.94 -05	1.87 -03	5.02 -03	8.18 -03	1.05 -02	1.15 -02	1.15 -02	1.06 -02
11	4.77 -03	1.18 -03	1.88 -06	1.14 -03	3.65 -03	6.41 -03	8.61 -03	9.90 -03
12	1.10 -02	8.64 -03	4.68 -03	1.40 -03	2.60 -05	6.17 -04	2.49 -03	4.80 -03
13	4.95 -03	8.91 -03	9.92 -03	7.94 -03	4.56 -03	1.60 -03	1.23 -04	2.60 -04
14	2.23 -04	1.11 -03	4.90 -03	8.22 -03	9.03 -03	7.34 -03	4.46 -03	1.82 -03
15	8.00 -03	2.72 -03	3.87 -05	1.34 -03	4.73 -03	7.50 -03	8.16 -03	6.80 -03
16	8.44 -03	9.69 -03	6.11 -03	1.70 -03	7.10 -07	1.50 -03	4.43 -03	6.73 -03
17	2.89 -04	4.61 -03	8.68 -03	8.30 -03	4.58 -03	1.03 -03	3.49 -05	1.54 -03
18	5.45 -03	3.40 -04	1.39 -03	5.80 -03	8.27 -03	6.82 -03	3.34 -03	6.13 -04
19	1.00 -02	8.12 -03	2.30 -03	3.21 -05	2.72 -03	6.42 -03	7.47 -03	5.51 -03
20	1.32 -03	7.47 -03	9.18 -03	4.82 -03	5.40 -04	6.20 -04	3.78 -03	6.44 -03
21	3.85 -03	7.54 -05	4.52 -03	8.57 -03	6.76 -03	2.19 -03	3.41 -06	1.50 -03
22	1.11 -02	6.00 -03	2.40 -04	2.11 -03	6.85 -03	7.51 -03	4.01 -03	6.32 -04
23	2.87 -03	9.77 -03	7.49 -03	1.23 -03	6.34 -04	4.77 -03	7.19 -03	5.39 -03
24	2.24 -03	1.40 -03	8.07 -03	8.13 -03	2.45 -03	4.39 -05	2.89 -03	6.10 -03
25	1.20 -02	3.03 -03	5.92 -04	6.46 -03	8.12 -03	3.50 -03	7.78 -05	1.49 -03
26	5.28 -03	1.13 -02	3.40 -03	2.18 -04	5.12 -03	7.62 -03	4.18 -03	4.26 -04
27	9.98 -05	3.99 -03	1.09 -02	3.30 -03	7.35 -05	4.13 -03	6.92 -03	4.50 -03
28	3.87 -02	1.75 -03	2.47 -03	1.11 -02	2.67 -03	2.43 -05	3.50 -03	6.16 -03
29	1.30 -02	5.53 -02	8.50 -03	6.87 -04	1.28 -02	1.52 -03	4.09 -06	3.24 -03
30	1.02 -01	2.52 -02	7.72 -02	2.64 -02	2.11 -04	1.79 -02	2.11 -04	1.21 -05
31	4.50 -03	6.60 -02	2.58 -02	9.04 -02	5.90 -02	5.90 -03	3.02 -02	8.40 -04
32	1.01 -01	1.86 -02	1.27 -02	7.20 -03	6.81 -02	8.97 -02	2.19 -02	5.40 -02
33	3.50 -02	3.06 -02	5.62 -02	2.33 -03	3.89 -03	1.42 -02	7.40 -02	3.29 -02
34	1.81 -04	6.89 -02	4.09 -03	2.34 -02	9.64 -03	3.31 -02	8.50 -03	1.46 -02
35	1.33 -02	3.20 -02	1.31 -02	3.65 -02	8.35 -04	6.65 -04	1.48 -02	4.44 -02
36	1.66 -02	5.00 -03	3.25 -02	1.29 -02	5.23 -03	3.52 -03	1.98 -02	8.42 -03
37	1.09 -02	4.20 -06	2.78 -02	1.01 -03	1.26 -02	3.48 -03	6.79 -03	1.40 -04
38	5.48 -03	6.39 -04	1.59 -02	1.56 -04	1.07 -02	1.18 -03	1.21 -03	2.41 -03
39	2.31 -03	7.43 -04	7.10 -03	5.52 -04	5.71 -03	2.62 -04	1.44 -04	2.17 -03
40	7.14 -04	3.24 -04	2.25 -03	2.97 -04	1.94 -03	4.90 -05	1.51 -05	8.68 -04
41	8.82 -05	4.35 -05	2.80 -04	4.16 -05	2.45 -04	5.12 -06	1.22 -06	1.14 -04
$\sum_{v'} f_{v'v''}$	4.84 -01	4.40 -01	4.14 -01	3.27 -01	3.01 -01	2.76 -01	2.79 -01	2.59 -01

Table E.53: $f_{v'v''}$ for ^{7}Li singlet case (continued).

$v'\backslash v''$	32	33	34	35	36	37	38	39
0	1.60 -10	8.74 -11	5.16 -11	3.25 -11	2.14 -11	1.42 -11	9.37 -12	5.93 -12
1	6.91 -09	3.63 -09	1.94 -09	1.06 -09	5.90 -10	3.41 -10	2.05 -10	1.28 -10
2	1.27 -07	6.89 -08	3.81 -08	2.14 -08	1.22 -08	7.05 -09	4.16 -09	2.49 -09
3	1.45 -06	8.12 -07	4.60 -07	2.64 -07	1.53 -07	9.04 -08	5.41 -08	3.29 -08
4	1.16 -05	6.71 -06	3.93 -06	2.32 -06	1.38 -06	8.30 -07	5.06 -07	3.13 -07
5	6.83 -05	4.12 -05	2.50 -05	1.52 -05	9.34 -06	5.79 -06	3.62 -06	2.28 -06
6	3.07 -04	1.94 -04	1.23 -04	7.76 -05	4.92 -05	3.14 -05	2.02 -05	1.30 -05
7	1.07 -03	7.12 -04	4.71 -04	3.11 -04	2.06 -04	1.36 -04	9.05 -05	6.04 -05
8	2.89 -03	2.05 -03	1.43 -03	9.96 -04	6.88 -04	4.74 -04	3.27 -04	2.25 -04
9	5.99 -03	4.57 -03	3.42 -03	2.53 -03	1.84 -03	1.34 -03	9.63 -04	6.91 -04
10	9.32 -03	7.85 -03	6.39 -03	5.07 -03	3.94 -03	3.02 -03	2.29 -03	1.72 -03
11	1.03 -02	9.87 -03	8.99 -03	7.85 -03	6.64 -03	5.47 -03	4.42 -03	3.52 -03
12	6.84 -03	8.24 -03	8.90 -03	8.90 -03	8.42 -03	7.62 -03	6.68 -03	5.71 -03
13	1.57 -03	3.40 -03	5.19 -03	6.57 -03	7.42 -03	7.72 -03	7.58 -03	7.11 -03
14	2.88 -04	5.83 -05	8.62 -04	2.23 -03	3.73 -03	5.02 -03	5.95 -03	6.45 -03
15	4.41 -03	2.08 -03	5.29 -04	9.94 -07	3.57 -04	1.28 -03	2.44 -03	3.55 -03
16	7.33 -03	6.29 -03	4.35 -03	2.33 -03	8.32 -04	8.97 -05	7.17 -05	5.83 -04
17	4.05 -03	5.99 -03	6.58 -03	5.84 -03	4.31 -03	2.61 -03	1.20 -03	3.17 -04
18	8.24 -05	1.46 -03	3.56 -03	5.20 -03	5.81 -03	5.36 -03	4.22 -03	2.84 -03
19	2.46 -03	3.75 -04	1.12 -04	1.31 -03	3.04 -03	4.45 -03	5.08 -03	4.88 -03
20	6.50 -03	4.41 -03	1.85 -03	2.53 -04	1.09 -04	1.08 -03	2.48 -03	3.68 -03
21	4.41 -03	6.07 -03	5.54 -03	3.56 -03	1.45 -03	1.99 -04	7.93 -05	8.19 -04
22	2.30 -04	2.29 -03	4.61 -03	5.49 -03	4.66 -03	2.90 -03	1.19 -03	1.85 -04
23	1.91 -03	4.59 -05	7.62 -04	2.82 -03	4.50 -03	4.84 -03	3.93 -03	2.43 -03
24	5.96 -03	3.20 -03	6.36 -04	6.15 -05	1.29 -03	3.05 -03	4.16 -03	4.18 -03
25	4.72 -03	5.82 -03	4.13 -03	1.56 -03	9.31 -05	3.45 -04	1.67 -03	3.03 -03
26	6.30 -04	3.37 -03	5.18 -03	4.54 -03	2.41 -03	5.66 -04	7.15 -06	6.65 -04
27	8.37 -04	1.91 -04	2.28 -03	4.32 -03	4.49 -03	3.00 -03	1.17 -03	1.14 -04
28	4.48 -03	1.15 -03	2.76 -05	1.48 -03	3.44 -03	4.12 -03	3.25 -03	1.69 -03
29	5.38 -03	4.22 -03	1.30 -03	3.99 -07	9.57 -04	2.68 -03	3.59 -03	3.20 -03
30	3.48 -03	4.51 -03	3.88 -03	1.25 -03	1.57 -05	6.43 -04	2.09 -03	3.04 -03
31	3.36 -04	4.80 -03	3.26 -03	3.64 -03	9.98 -04	2.69 -05	4.79 -04	1.65 -03
32	9.88 -03	2.89 -03	9.27 -03	1.31 -03	3.99 -03	5.28 -04	3.49 -05	4.41 -04
33	8.04 -02	3.64 -02	1.40 -02	2.30 -02	6.88 -05	6.52 -03	7.22 -06	1.15 -04
34	1.21 -02	6.75 -02	6.50 -02	3.70 -02	5.54 -02	8.22 -03	1.70 -02	2.02 -03
35	4.89 -03	5.02 -03	8.47 -03	3.80 -02	3.74 -02	8.51 -02	3.59 -02	4.67 -02
36	7.82 -03	7.11 -03	3.18 -02	1.67 -02	1.48 -04	6.45 -04	3.74 -02	3.63 -02
37	1.92 -02	6.06 -03	8.53 -03	3.51 -04	1.39 -02	1.36 -02	2.94 -02	3.13 -03
38	1.35 -02	1.11 -03	4.94 -04	5.22 -03	1.32 -02	5.06 -03	4.10 -03	3.36 -03
39	6.10 -03	5.74 -05	1.42 -05	4.35 -03	5.90 -03	8.66 -04	1.46 -04	5.29 -03
40	1.90 -03	2.24 -11	4.44 -05	1.66 -03	1.76 -03	1.18 -04	9.01 -07	2.31 -03
41	2.34 -04	1.62 -07	7.57 -06	2.16 -04	2.14 -04	1.08 -05	1.05 -06	3.08 -04
$\sum_{v'} f_{v'v''}$	2.52 -01	2.19 -01	2.22 -01	2.06 -01	2.04 -01	1.89 -01	1.89 -01	1.62 -01

Table E.54: $f_{v'v''}$ for ^{7}Li singlet case (continued).

$v'\backslash v''$	40	41	42	43	44	45	46	47
0	3.54 -12	1.95 -12	9.74 -13	4.25 -13	1.53 -13	3.93 -14	4.28 -15	3.31 -16
1	8.33 -11	5.59 -11	3.83 -11	2.66 -11	1.85 -11	1.28 -11	8.75 -12	5.89 -12
2	1.53 -09	9.55 -10	6.10 -10	3.99 -10	2.67 -10	1.82 -10	1.27 -10	9.03 -11
3	2.04 -08	1.28 -08	8.18 -09	5.32 -09	3.52 -09	2.36 -09	1.62 -09	1.13 -09
4	1.96 -07	1.25 -07	8.05 -08	5.29 -08	3.52 -08	2.38 -08	1.64 -08	1.14 -08
5	1.46 -06	9.41 -07	6.14 -07	4.07 -07	2.73 -07	1.86 -07	1.28 -07	9.02 -08
6	8.53 -06	5.63 -06	3.76 -06	2.54 -06	1.73 -06	1.19 -06	8.32 -07	5.88 -07
7	4.05 -05	2.73 -05	1.86 -05	1.27 -05	8.82 -06	6.18 -06	4.38 -06	3.14 -06
8	1.56 -04	1.09 -04	7.59 -05	5.34 -05	3.78 -05	2.70 -05	1.94 -05	1.41 -05
9	4.95 -04	3.55 -04	2.55 -04	1.84 -04	1.33 -04	9.74 -05	7.16 -05	5.31 -05
10	1.29 -03	9.63 -04	7.18 -04	5.35 -04	3.99 -04	2.98 -04	2.24 -04	1.69 -04
11	2.76 -03	2.15 -03	1.67 -03	1.29 -03	9.94 -04	7.66 -04	5.92 -04	4.58 -04
12	4.78 -03	3.94 -03	3.20 -03	2.58 -03	2.07 -03	1.65 -03	1.31 -03	1.04 -03
13	6.45 -03	5.70 -03	4.93 -03	4.20 -03	3.53 -03	2.93 -03	2.42 -03	1.99 -03
14	6.57 -03	6.39 -03	5.99 -03	5.46 -03	4.88 -03	4.27 -03	3.70 -03	3.17 -03
15	4.45 -03	5.06 -03	5.37 -03	5.41 -03	5.24 -03	4.93 -03	4.53 -03	4.08 -03
16	1.38 -03	2.25 -03	3.03 -03	3.63 -03	4.02 -03	4.21 -03	4.22 -03	4.09 -03
17	3.74 -06	1.52 -04	6.01 -04	1.19 -03	1.78 -03	2.30 -03	2.69 -03	2.94 -03
18	1.58 -03	6.56 -04	1.43 -04	3.22 -07	1.34 -04	4.34 -04	8.03 -04	1.17 -03
19	4.10 -03	3.02 -03	1.95 -03	1.07 -03	4.53 -04	1.13 -04	1.07 -06	5.25 -05
20	4.32 -03	4.34 -03	3.86 -03	3.10 -03	2.26 -03	1.49 -03	8.69 -04	4.31 -04
21	1.92 -03	2.91 -03	3.54 -03	3.72 -03	3.50 -03	3.03 -03	2.43 -03	1.82 -03
22	4.00 -05	5.52 -04	1.37 -03	2.17 -03	2.74 -03	3.00 -03	2.98 -03	2.74 -03
23	1.04 -03	2.05 -04	7.52 -06	3.09 -04	8.71 -04	1.47 -03	1.95 -03	2.24 -03
24	3.31 -03	2.08 -03	9.65 -04	2.53 -04	2.45 -06	1.21 -04	4.55 -04	8.56 -04
25	3.73 -03	3.58 -03	2.82 -03	1.83 -03	9.43 -04	3.32 -04	4.11 -05	1.63 -05
26	1.84 -03	2.83 -03	3.23 -03	3.02 -03	2.41 -03	1.64 -03	9.47 -04	4.33 -04
27	1.36 -04	8.99 -04	1.84 -03	2.51 -03	2.73 -03	2.53 -03	2.06 -03	1.49 -03
28	4.39 -04	2.22 -07	3.10 -04	1.00 -03	1.69 -03	2.13 -03	2.24 -03	2.08 -03
29	2.00 -03	7.92 -04	1.02 -04	4.64 -05	4.37 -04	9.85 -04	1.46 -03	1.73 -03
30	2.96 -03	2.10 -03	1.05 -03	2.89 -04	3.43 -06	1.31 -04	4.84 -04	8.76 -04
31	2.54 -03	2.61 -03	2.01 -03	1.16 -03	4.51 -04	6.65 -05	1.43 -05	1.89 -04
32	1.32 -03	2.11 -03	2.22 -03	1.81 -03	1.15 -03	5.38 -04	1.47 -04	3.10 -06
33	6.06 -04	1.01 -03	1.81 -03	1.82 -03	1.54 -03	1.03 -03	5.41 -04	1.96 -04
34	1.05 -03	1.63 -03	4.62 -04	1.82 -03	1.31 -03	1.29 -03	8.27 -04	4.77 -04
35	1.90 -02	9.02 -03	7.96 -03	1.34 -04	3.26 -03	4.51 -04	1.30 -03	5.10 -04
36	6.83 -02	5.80 -02	4.00 -02	3.72 -02	9.95 -03	1.35 -02	7.37 -04	3.25 -03
37	1.80 -04	1.06 -02	3.42 -02	4.72 -02	7.52 -02	4.89 -02	5.65 -02	2.21 -02
38	7.48 -03	2.09 -02	1.80 -02	5.47 -03	4.34 -04	1.05 -02	2.24 -02	6.11 -02
39	5.65 -03	8.22 -03	2.62 -03	1.60 -04	3.37 -03	1.62 -02	1.42 -02	1.54 -02
40	1.90 -03	2.11 -03	2.73 -04	5.02 -04	2.10 -03	5.85 -03	3.35 -03	2.10 -03
41	2.37 -04	2.45 -04	2.17 -05	8.50 -05	2.93 -04	7.33 -04	3.69 -04	1.89 -04
$\sum_{v'} f_{v'v''}$	1.64 -01	1.68 -01	1.57 -01	1.41 -01	1.40 -01	1.38 -01	1.37 -01	1.39 -01

Table E.55: $f_{v'v''}$ for ^{7}Li singlet case (continued).

$v'\backslash v''$	48	49	50	51	52	53	54	55
0	4.10 -15	6.80 -15	6.80 -15	5.02 -15	2.81 -15	1.08 -15	1.63 -16	3.53 -17
1	3.91 -12	2.56 -12	1.65 -12	1.04 -12	6.53 -13	4.04 -13	2.49 -13	1.52 -13
2	6.52 -11	4.79 -11	3.56 -11	2.67 -11	2.02 -11	1.55 -11	1.20 -11	9.35 -12
3	8.01 -10	5.79 -10	4.25 -10	3.17 -10	2.39 -10	1.83 -10	1.43 -10	1.12 -10
4	8.08 -09	5.81 -09	4.24 -09	3.14 -09	2.36 -09	1.79 -09	1.39 -09	1.09 -09
5	6.44 -08	4.67 -08	3.44 -08	2.56 -08	1.93 -08	1.48 -08	1.15 -08	9.01 -09
6	4.21 -07	3.05 -07	2.25 -07	1.68 -07	1.27 -07	9.69 -08	7.54 -08	5.93 -08
7	2.29 -06	1.69 -06	1.26 -06	9.47 -07	7.22 -07	5.56 -07	4.35 -07	3.43 -07
8	1.03 -05	7.67 -06	5.76 -06	4.37 -06	3.35 -06	2.60 -06	2.05 -06	1.63 -06
9	3.97 -05	3.00 -05	2.29 -05	1.76 -05	1.36 -05	1.07 -05	8.47 -06	6.77 -06
10	1.28 -04	9.83 -05	7.60 -05	5.91 -05	4.64 -05	3.68 -05	2.95 -05	2.38 -05
11	3.56 -04	2.79 -04	2.19 -04	1.73 -04	1.38 -04	1.11 -04	8.94 -05	7.29 -05
12	8.32 -04	6.66 -04	5.35 -04	4.31 -04	3.48 -04	2.83 -04	2.33 -04	1.92 -04
13	1.63 -03	1.34 -03	1.10 -03	9.06 -04	7.46 -04	6.17 -04	5.14 -04	4.30 -04
14	2.69 -03	2.28 -03	1.93 -03	1.63 -03	1.37 -03	1.15 -03	9.78 -04	8.31 -04
15	3.63 -03	3.20 -03	2.80 -03	2.43 -03	2.11 -03	1.82 -03	1.57 -03	1.36 -03
16	3.87 -03	3.59 -03	3.29 -03	2.97 -03	2.66 -03	2.37 -03	2.10 -03	1.86 -03
17	3.05 -03	3.07 -03	2.99 -03	2.86 -03	2.68 -03	2.48 -03	2.28 -03	2.08 -03
18	1.48 -03	1.72 -03	1.88 -03	1.96 -03	1.98 -03	1.95 -03	1.88 -03	1.79 -03
19	2.01 -04	3.91 -04	5.86 -04	7.57 -04	8.93 -04	9.90 -04	1.05 -03	1.08 -03
20	1.63 -04	3.25 -05	1.76 -07	3.10 -05	9.57 -05	1.73 -04	2.49 -04	3.17 -04
21	1.28 -03	8.47 -04	5.18 -04	2.88 -04	1.39 -04	5.37 -05	1.24 -05	9.93 -08
22	2.38 -03	1.97 -03	1.57 -03	1.21 -03	8.95 -04	6.47 -04	4.56 -04	3.12 -04
23	2.34 -03	2.29 -03	2.12 -03	1.89 -03	1.63 -03	1.38 -03	1.14 -03	9.32 -04
24	1.22 -03	1.48 -03	1.64 -03	1.69 -03	1.65 -03	1.56 -03	1.43 -03	1.29 -03
25	1.63 -04	3.91 -04	6.28 -04	8.30 -04	9.75 -04	1.06 -03	1.10 -03	1.09 -03
26	1.29 -04	8.49 -06	1.88 -05	1.06 -04	2.25 -04	3.45 -04	4.49 -04	5.29 -04
27	9.63 -04	5.44 -04	2.55 -04	8.63 -05	1.20 -05	2.15 -06	3.05 -05	7.71 -05
28	1.75 -03	1.35 -03	9.64 -04	6.37 -04	3.86 -04	2.11 -04	9.99 -05	3.65 -05
29	1.79 -03	1.68 -03	1.46 -03	1.19 -03	9.23 -04	6.84 -04	4.88 -04	3.34 -04
30	1.18 -03	1.35 -03	1.39 -03	1.32 -03	1.18 -03	1.01 -03	8.36 -04	6.74 -04
31	4.58 -04	7.19 -04	9.12 -04	1.01 -03	1.03 -03	9.94 -04	9.15 -04	8.15 -04
32	5.13 -05	2.06 -04	3.90 -04	5.52 -04	6.65 -04	7.25 -04	7.41 -04	7.21 -04
33	2.75 -05	6.02 -06	7.81 -05	1.91 -04	3.06 -04	4.00 -04	4.65 -04	5.00 -04
34	1.98 -04	4.74 -05	1.93 -07	2.47 -05	8.65 -05	1.59 -04	2.25 -04	2.77 -04
35	4.01 -04	1.56 -04	5.02 -05	3.00 -06	6.93 -06	3.85 -05	8.09 -05	1.23 -04
36	1.08 -05	5.68 -04	4.61 -05	5.56 -05	1.65 -06	1.88 -06	1.93 -05	4.26 -05
37	2.07 -02	4.73 -03	4.06 -03	5.16 -04	4.15 -04	4.51 -05	4.58 -06	2.33 -05
38	5.95 -02	7.35 -02	4.90 -02	3.94 -02	1.99 -02	1.10 -02	4.44 -03	1.55 -03
39	1.98 -03	1.79 -04	1.34 -02	3.16 -02	5.79 -02	6.75 -02	6.73 -02	5.55 -02
40	1.46 -04	2.34 -03	9.63 -03	1.20 -02	1.16 -02	4.84 -03	2.55 -04	2.51 -03
41	5.59 -05	3.99 -04	1.30 -03	1.39 -03	1.10 -03	2.59 -04	2.98 -05	8.65 -04
$\sum_{v'} f_{v'v''}$	1.15 -01	1.11 -01	1.05 -01	1.10 -01	1.14 -01	1.05 -01	9.16 -02	7.83 -02

Table E.56: $f_{v'v''}$ for ^{7}Li singlet case (continued).

$v'\backslash v''$	56	57	58	59	60	61	62	63
0	5.00 -16	1.31 -15	2.26 -15	3.23 -15	4.13 -15	4.89 -15	5.46 -15	5.83 -15
1	9.21 -14	5.56 -14	3.36 -14	2.03 -14	1.23 -14	7.33 -15	4.34 -15	2.54 -15
2	7.34 -12	5.81 -12	4.65 -12	3.77 -12	3.09 -12	2.55 -12	2.10 -12	1.74 -12
3	8.91 -11	7.15 -11	5.81 -11	4.80 -11	4.01 -11	3.36 -11	2.83 -11	2.38 -11
4	8.59 -10	6.87 -10	5.58 -10	4.60 -10	3.84 -10	3.22 -10	2.72 -10	2.29 -10
5	7.13 -09	5.71 -09	4.63 -09	3.81 -09	3.18 -09	2.66 -09	2.24 -09	1.88 -09
6	4.71 -08	3.79 -08	3.08 -08	2.55 -08	2.14 -08	1.80 -08	1.52 -08	1.29 -08
7	2.73 -07	2.19 -07	1.79 -07	1.48 -07	1.23 -07	1.04 -07	8.75 -08	7.38 -08
8	1.31 -06	1.06 -06	8.69 -07	7.24 -07	6.10 -07	5.16 -07	4.38 -07	3.72 -07
9	5.45 -06	4.43 -06	3.64 -06	3.04 -06	2.56 -06	2.17 -06	1.84 -06	1.56 -06
10	1.94 -05	1.59 -05	1.32 -05	1.11 -05	9.41 -06	8.02 -06	6.85 -06	5.86 -06
11	5.97 -05	4.93 -05	4.11 -05	3.47 -05	2.96 -05	2.54 -05	2.18 -05	1.86 -05
12	1.59 -04	1.33 -04	1.12 -04	9.51 -05	8.17 -05	7.04 -05	6.07 -05	5.23 -05
13	3.60 -04	3.04 -04	2.58 -04	2.22 -04	1.92 -04	1.67 -04	1.45 -04	1.26 -04
14	7.06 -04	6.02 -04	5.17 -04	4.49 -04	3.92 -04	3.43 -04	3.00 -04	2.62 -04
15	1.18 -03	1.02 -03	8.87 -04	7.79 -04	6.88 -04	6.08 -04	5.37 -04	4.72 -04
16	1.64 -03	1.45 -03	1.28 -03	1.14 -03	1.02 -03	9.10 -04	8.12 -04	7.21 -04
17	1.88 -03	1.70 -03	1.53 -03	1.39 -03	1.26 -03	1.15 -03	1.04 -03	9.30 -04
18	1.69 -03	1.57 -03	1.46 -03	1.35 -03	1.26 -03	1.16 -03	1.07 -03	9.74 -04
19	1.08 -03	1.06 -03	1.03 -03	9.93 -04	9.54 -04	9.07 -04	8.55 -04	7.97 -04
20	3.70 -04	4.09 -04	4.36 -04	4.55 -04	4.66 -04	4.68 -04	4.62 -04	4.48 -04
21	5.46 -06	2.02 -05	3.88 -05	5.84 -05	7.71 -05	9.35 -05	1.07 -04	1.16 -04
22	2.07 -04	1.33 -04	8.25 -05	4.89 -05	2.69 -05	1.32 -05	5.26 -06	1.35 -06
23	7.52 -04	6.03 -04	4.81 -04	3.86 -04	3.09 -04	2.46 -04	1.95 -04	1.54 -04
24	1.14 -03	1.00 -03	8.72 -04	7.60 -04	6.63 -04	5.75 -04	4.96 -04	4.26 -04
25	1.05 -03	9.95 -04	9.28 -04	8.61 -04	7.95 -04	7.26 -04	6.59 -04	5.92 -04
26	5.81 -04	6.09 -04	6.19 -04	6.18 -04	6.08 -04	5.88 -04	5.60 -04	5.26 -04
27	1.28 -04	1.75 -04	2.15 -04	2.47 -04	2.72 -04	2.88 -04	2.96 -04	2.97 -04
28	7.14 -06	1.79 -08	5.96 -06	1.88 -05	3.47 -05	5.10 -05	6.58 -05	7.78 -05
29	2.19 -04	1.37 -04	8.12 -05	4.49 -05	2.21 -05	8.86 -06	2.26 -06	6.88 -08
30	5.29 -04	4.09 -04	3.12 -04	2.36 -04	1.77 -04	1.31 -04	9.50 -05	6.78 -05
31	7.06 -04	6.00 -04	5.05 -04	4.23 -04	3.53 -04	2.92 -04	2.39 -04	1.95 -04
32	6.76 -04	6.17 -04	5.55 -04	4.95 -04	4.39 -04	3.85 -04	3.34 -04	2.88 -04
33	5.08 -04	4.97 -04	4.74 -04	4.46 -04	4.15 -04	3.80 -04	3.44 -04	3.08 -04
34	3.11 -04	3.28 -04	3.33 -04	3.31 -04	3.22 -04	3.07 -04	2.88 -04	2.66 -04
35	1.58 -04	1.83 -04	2.00 -04	2.10 -04	2.15 -04	2.13 -04	2.07 -04	1.97 -04
36	6.75 -05	8.88 -05	1.06 -04	1.18 -04	1.27 -04	1.31 -04	1.32 -04	1.29 -04
37	1.93 -05	4.07 -05	4.95 -05	6.08 -05	6.83 -05	7.36 -05	7.62 -05	7.66 -05
38	7.03 -04	7.78 -05	1.21 -04	5.52 -06	5.10 -05	3.01 -05	4.29 -05	3.93 -05
39	3.92 -02	2.60 -02	1.32 -02	7.46 -03	2.76 -03	1.72 -03	3.93 -04	3.63 -04
40	1.37 -02	2.95 -02	4.62 -02	5.37 -02	5.76 -02	5.26 -02	4.84 -02	3.80 -02
41	2.56 -03	4.09 -03	4.80 -03	3.85 -03	2.43 -03	7.63 -04	1.98 -05	6.69 -04
$\sum_{v'} f_{v'v''}$	7.24 -02	7.43 -02	7.78 -02	7.73 -02	7.41 -02	6.55 -02	5.82 -02	4.76 -02

Table E.57: $f_{v'v''}$ for ^{7}Li singlet case (continued).

$v'\backslash v''$	64	65	66	67	68	69	70	71
0	5.99 -15	5.93 -15	5.67 -15	5.26 -15	4.79 -15	4.41 -15	4.17 -15	3.96 -15
1	1.47 -15	8.41 -16	4.77 -16	2.71 -16	1.56 -16	9.29 -17	5.75 -17	3.57 -17
2	1.44 -12	1.18 -12	9.65 -13	7.83 -13	6.38 -13	5.35 -13	4.66 -13	4.09 -13
3	2.01 -11	1.68 -11	1.40 -11	1.15 -11	9.52 -12	8.08 -12	7.12 -12	6.33 -12
4	1.93 -10	1.62 -10	1.35 -10	1.12 -10	9.25 -11	7.87 -11	6.94 -11	6.19 -11
5	1.58 -09	1.32 -09	1.10 -09	9.08 -10	7.51 -10	6.38 -10	5.62 -10	5.00 -10
6	1.09 -08	9.14 -09	7.62 -09	6.31 -09	5.23 -09	4.45 -09	3.93 -09	3.51 -09
7	6.22 -08	5.22 -08	4.35 -08	3.60 -08	2.98 -08	2.53 -08	2.23 -08	1.99 -08
8	3.15 -07	2.66 -07	2.22 -07	1.84 -07	1.53 -07	1.31 -07	1.15 -07	1.03 -07
9	1.33 -06	1.12 -06	9.37 -07	7.77 -07	6.46 -07	5.51 -07	4.88 -07	4.36 -07
10	4.99 -06	4.23 -06	3.55 -06	2.96 -06	2.46 -06	2.11 -06	1.87 -06	1.67 -06
11	1.59 -05	1.36 -05	1.14 -05	9.53 -06	7.95 -06	6.82 -06	6.05 -06	5.42 -06
12	4.50 -05	3.84 -05	3.24 -05	2.71 -05	2.27 -05	1.95 -05	1.74 -05	1.56 -05
13	1.08 -04	9.30 -05	7.89 -05	6.63 -05	5.57 -05	4.80 -05	4.28 -05	3.85 -05
14	2.28 -04	1.96 -04	1.67 -04	1.41 -04	1.19 -04	1.03 -04	9.18 -05	8.28 -05
15	4.13 -04	3.58 -04	3.07 -04	2.60 -04	2.20 -04	1.91 -04	1.71 -04	1.55 -04
16	6.36 -04	5.56 -04	4.80 -04	4.09 -04	3.48 -04	3.03 -04	2.72 -04	2.47 -04
17	8.29 -04	7.31 -04	6.36 -04	5.46 -04	4.67 -04	4.09 -04	3.69 -04	3.37 -04
18	8.80 -04	7.86 -04	6.91 -04	5.98 -04	5.15 -04	4.54 -04	4.13 -04	3.78 -04
19	7.34 -04	6.67 -04	5.95 -04	5.21 -04	4.54 -04	4.03 -04	3.70 -04	3.41 -04
20	4.27 -04	3.99 -04	3.65 -04	3.27 -04	2.90 -04	2.61 -04	2.43 -04	2.27 -04
21	1.22 -04	1.22 -04	1.19 -04	1.12 -04	1.03 -04	9.65 -05	9.23 -05	8.84 -05
22	5.07 -08	2.82 -07	1.24 -06	2.36 -06	3.33 -06	4.15 -06	4.93 -06	5.61 -06
23	1.20 -04	9.35 -05	7.20 -05	5.51 -05	4.24 -05	3.36 -05	2.76 -05	2.30 -05
24	3.63 -04	3.06 -04	2.55 -04	2.11 -04	1.74 -04	1.47 -04	1.29 -04	1.15 -04
25	5.26 -04	4.62 -04	3.99 -04	3.40 -04	2.89 -04	2.51 -04	2.26 -04	2.04 -04
26	4.86 -04	4.41 -04	3.93 -04	3.44 -04	2.99 -04	2.65 -04	2.42 -04	2.23 -04
27	2.89 -04	2.75 -04	2.55 -04	2.31 -04	2.06 -04	1.87 -04	1.74 -04	1.63 -04
28	8.64 -05	9.08 -05	9.12 -05	8.79 -05	8.26 -05	7.81 -05	7.56 -05	7.31 -05
29	5.69 -07	2.43 -06	4.66 -06	6.62 -06	8.05 -06	9.17 -06	1.02 -05	1.11 -05
30	4.75 -05	3.27 -05	2.20 -05	1.46 -05	9.64 -06	6.52 -06	4.52 -06	3.11 -06
31	1.57 -04	1.25 -04	9.90 -05	7.75 -05	6.09 -05	4.93 -05	4.14 -05	3.51 -05
32	2.45 -04	2.07 -04	1.72 -04	1.41 -04	1.16 -04	9.78 -05	8.54 -05	7.52 -05
33	2.72 -04	2.37 -04	2.03 -04	1.71 -04	1.44 -04	1.24 -04	1.11 -04	9.93 -05
34	2.42 -04	2.16 -04	1.89 -04	1.63 -04	1.40 -04	1.22 -04	1.10 -04	1.00 -04
35	1.84 -04	1.68 -04	1.50 -04	1.32 -04	1.14 -04	1.01 -04	9.27 -05	8.51 -05
36	1.24 -04	1.15 -04	1.05 -04	9.34 -05	8.22 -05	7.36 -05	6.78 -05	6.29 -05
37	7.48 -05	7.10 -05	6.56 -05	5.91 -05	5.26 -05	4.75 -05	4.41 -05	4.12 -05
38	4.08 -05	3.87 -05	3.64 -05	3.30 -05	2.96 -05	2.69 -05	2.52 -05	2.36 -05
39	1.86 -05	8.12 -05	2.98 -06	2.52 -05	1.09 -05	1.37 -05	1.16 -05	1.13 -05
40	3.08 -02	2.08 -02	1.47 -02	7.97 -03	4.58 -03	1.69 -03	8.59 -04	2.54 -04
41	3.08 -03	8.21 -03	1.52 -02	2.50 -02	3.35 -02	3.89 -02	3.83 -02	3.78 -02
$\sum_{v'} f_{v'v''}$	4.16 -02	3.59 -02	3.59 -02	3.81 -02	4.25 -02	4.45 -02	4.27 -02	4.13 -02

Table E.58: $f_{v'v''}$ for ^{7}Li singlet case (continued).

$v'\backslash v''$	72	73	74	75	76	77	78	79
0	3.74 -15	3.51 -15	3.26 -15	2.96 -15	2.63 -15	2.35 -15	2.09 -15	1.86 -15
1	2.20 -17	1.34 -17	7.99 -18	4.66 -18	2.65 -18	1.52 -18	8.70 -19	4.91 -19
2	3.62 -13	3.19 -13	2.81 -13	2.43 -13	2.07 -13	1.78 -13	1.53 -13	1.32 -13
3	5.65 -12	5.05 -12	4.47 -12	3.91 -12	3.35 -12	2.90 -12	2.52 -12	2.18 -12
4	5.53 -11	4.94 -11	4.39 -11	3.84 -11	3.30 -11	2.85 -11	2.48 -11	2.15 -11
5	4.46 -10	3.98 -10	3.53 -10	3.09 -10	2.65 -10	2.29 -10	1.99 -10	1.73 -10
6	3.14 -09	2.81 -09	2.49 -09	2.18 -09	1.88 -09	1.62 -09	1.41 -09	1.23 -09
7	1.78 -08	1.59 -08	1.41 -08	1.24 -08	1.06 -08	9.19 -09	8.00 -09	6.93 -09
8	9.23 -08	8.27 -08	7.35 -08	6.44 -08	5.54 -08	4.80 -08	4.18 -08	3.63 -08
9	3.90 -07	3.50 -07	3.11 -07	2.72 -07	2.35 -07	2.03 -07	1.77 -07	1.54 -07
10	1.50 -06	1.35 -06	1.20 -06	1.05 -06	9.06 -07	7.86 -07	6.85 -07	5.95 -07
11	4.88 -06	4.38 -06	3.91 -06	3.43 -06	2.96 -06	2.57 -06	2.24 -06	1.95 -06
12	1.40 -05	1.26 -05	1.13 -05	9.92 -06	8.56 -06	7.44 -06	6.50 -06	5.65 -06
13	3.47 -05	3.13 -05	2.80 -05	2.47 -05	2.13 -05	1.86 -05	1.62 -05	1.41 -05
14	7.49 -05	6.76 -05	6.06 -05	5.35 -05	4.63 -05	4.04 -05	3.53 -05	3.08 -05
15	1.40 -04	1.27 -04	1.14 -04	1.01 -04	8.75 -05	7.64 -05	6.69 -05	5.83 -05
16	2.25 -04	2.04 -04	1.84 -04	1.63 -04	1.42 -04	1.24 -04	1.09 -04	9.48 -05
17	3.07 -04	2.80 -04	2.53 -04	2.25 -04	1.96 -04	1.72 -04	1.51 -04	1.32 -04
18	3.47 -04	3.17 -04	2.88 -04	2.57 -04	2.24 -04	1.97 -04	1.74 -04	1.52 -04
19	3.15 -04	2.90 -04	2.65 -04	2.37 -04	2.08 -04	1.83 -04	1.62 -04	1.43 -04
20	2.12 -04	1.96 -04	1.81 -04	1.63 -04	1.44 -04	1.28 -04	1.14 -04	1.00 -04
21	8.44 -05	8.00 -05	7.49 -05	6.87 -05	6.16 -05	5.52 -05	4.96 -05	4.42 -05
22	6.16 -06	6.56 -06	6.77 -06	6.73 -06	6.45 -06	6.12 -06	5.76 -06	5.34 -06
23	1.92 -05	1.61 -05	1.34 -05	1.10 -05	8.95 -06	7.35 -06	6.09 -06	5.05 -06
24	1.02 -04	9.05 -05	7.98 -05	6.94 -05	5.93 -05	5.10 -05	4.41 -05	3.80 -05
25	1.85 -04	1.68 -04	1.50 -04	1.33 -04	1.15 -04	1.00 -04	8.78 -05	7.64 -05
26	2.05 -04	1.88 -04	1.71 -04	1.52 -04	1.33 -04	1.17 -04	1.03 -04	9.07 -05
27	1.53 -04	1.42 -04	1.31 -04	1.18 -04	1.05 -04	9.28 -05	8.25 -05	7.28 -05
28	7.03 -05	6.71 -05	6.31 -05	5.82 -05	5.23 -05	4.71 -05	4.24 -05	3.78 -05
29	1.18 -05	1.22 -05	1.23 -05	1.20 -05	1.13 -05	1.06 -05	9.84 -06	9.04 -06
30	2.11 -06	1.39 -06	8.83 -07	5.35 -07	3.08 -07	1.72 -07	9.11 -08	4.43 -08
31	2.99 -05	2.54 -05	2.16 -05	1.80 -05	1.49 -05	1.24 -05	1.04 -05	8.73 -06
32	6.65 -05	5.87 -05	5.15 -05	4.45 -05	3.78 -05	3.24 -05	2.79 -05	2.39 -05
33	8.93 -05	8.02 -05	7.15 -05	6.26 -05	5.39 -05	4.67 -05	4.07 -05	3.53 -05
34	9.15 -05	8.30 -05	7.47 -05	6.61 -05	5.74 -05	5.01 -05	4.39 -05	3.83 -05
35	7.82 -05	7.16 -05	6.50 -05	5.79 -05	5.06 -05	4.44 -05	3.91 -05	3.42 -05
36	5.82 -05	5.37 -05	4.90 -05	4.39 -05	3.86 -05	3.40 -05	3.01 -05	2.64 -05
37	3.84 -05	3.56 -05	3.27 -05	2.94 -05	2.59 -05	2.29 -05	2.04 -05	1.79 -05
38	2.21 -05	2.06 -05	1.90 -05	1.71 -05	1.51 -05	1.34 -05	1.19 -05	1.05 -05
39	1.05 -05	9.86 -06	9.10 -06	8.24 -06	7.30 -06	6.49 -06	5.77 -06	5.10 -06
40	1.87 -04	3.32 -05	4.22 -05	1.72 -06	1.05 -05	3.53 -07	3.26 -06	1.21 -06
41	3.61 -02	3.48 -02	3.26 -02	3.15 -02	2.89 -02	2.51 -02	2.02 -02	1.67 -02
$\sum_{v'} f_{v'v''}$	3.93 -02	3.76 -02	3.51 -02	3.37 -02	3.09 -02	2.68 -02	2.17 -02	1.80 -02

Table E.59: $f_{v'v''}$ for ^{7}Li singlet case (continued).

$v'\backslash v''$	80	81	82	83	84	85	86	87
0	1.64 -15	1.44 -15	1.26 -15	1.10 -15	9.51 -16	8.20 -16	7.04 -16	6.00 -16
1	2.73 -19	1.50 -19	8.01 -20	4.15 -20	2.06 -20	9.64 -21	4.13 -21	1.52 -21
2	1.14 -13	9.80 -14	8.41 -14	7.20 -14	6.15 -14	5.24 -14	4.45 -14	3.77 -14
3	1.89 -12	1.63 -12	1.41 -12	1.21 -12	1.04 -12	8.85 -13	7.53 -13	6.38 -13
4	1.86 -11	1.61 -11	1.39 -11	1.20 -11	1.02 -11	8.76 -12	7.46 -12	6.32 -12
5	1.49 -10	1.29 -10	1.11 -10	9.57 -11	8.21 -11	7.01 -11	5.97 -11	5.06 -11
6	1.06 -09	9.19 -10	7.92 -10	6.81 -10	5.84 -10	5.00 -10	4.25 -10	3.61 -10
7	6.00 -09	5.19 -09	4.48 -09	3.85 -09	3.30 -09	2.82 -09	2.40 -09	2.04 -09
8	3.14 -08	2.72 -08	2.35 -08	2.02 -08	1.73 -08	1.48 -08	1.26 -08	1.07 -08
9	1.33 -07	1.15 -07	9.95 -08	8.56 -08	7.34 -08	6.28 -08	5.35 -08	4.54 -08
10	5.16 -07	4.47 -07	3.86 -07	3.32 -07	2.85 -07	2.44 -07	2.08 -07	1.76 -07
11	1.69 -06	1.46 -06	1.26 -06	1.09 -06	9.35 -07	8.00 -07	6.82 -07	5.78 -07
12	4.90 -06	4.25 -06	3.68 -06	3.17 -06	2.72 -06	2.33 -06	1.98 -06	1.68 -06
13	1.23 -05	1.06 -05	9.20 -06	7.93 -06	6.81 -06	5.83 -06	4.97 -06	4.22 -06
14	2.67 -05	2.32 -05	2.01 -05	1.73 -05	1.49 -05	1.28 -05	1.09 -05	9.24 -06
15	5.08 -05	4.42 -05	3.82 -05	3.30 -05	2.84 -05	2.43 -05	2.08 -05	1.76 -05
16	8.27 -05	7.20 -05	6.23 -05	5.38 -05	4.63 -05	3.97 -05	3.39 -05	2.88 -05
17	1.15 -04	1.00 -04	8.70 -05	7.52 -05	6.48 -05	5.56 -05	4.75 -05	4.04 -05
18	1.33 -04	1.16 -04	1.01 -04	8.73 -05	7.53 -05	6.47 -05	5.53 -05	4.70 -05
19	1.25 -04	1.09 -04	9.51 -05	8.24 -05	7.12 -05	6.12 -05	5.24 -05	4.46 -05
20	8.82 -05	7.74 -05	6.76 -05	5.87 -05	5.08 -05	4.38 -05	3.75 -05	3.20 -05
21	3.92 -05	3.46 -05	3.04 -05	2.65 -05	2.31 -05	1.99 -05	1.72 -05	1.47 -05
22	4.89 -06	4.45 -06	4.00 -06	3.57 -06	3.16 -06	2.77 -06	2.41 -06	2.08 -06
23	4.20 -06	3.51 -06	2.93 -06	2.44 -06	2.04 -06	1.71 -06	1.43 -06	1.19 -06
24	3.28 -05	2.83 -05	2.43 -05	2.08 -05	1.78 -05	1.52 -05	1.29 -05	1.09 -05
25	6.64 -05	5.77 -05	4.99 -05	4.30 -05	3.70 -05	3.17 -05	2.70 -05	2.29 -05
26	7.93 -05	6.93 -05	6.02 -05	5.21 -05	4.49 -05	3.86 -05	3.30 -05	2.81 -05
27	6.41 -05	5.63 -05	4.91 -05	4.27 -05	3.69 -05	3.18 -05	2.73 -05	2.33 -05
28	3.36 -05	2.97 -05	2.61 -05	2.28 -05	1.99 -05	1.72 -05	1.48 -05	1.26 -05
29	8.23 -06	7.43 -06	6.65 -06	5.90 -06	5.20 -06	4.55 -06	3.95 -06	3.40 -06
30	1.90 -08	6.47 -09	1.28 -09	2.52 -12	5.74 -10	1.80 -09	3.06 -09	4.06 -09
31	7.34 -06	6.19 -06	5.22 -06	4.39 -06	3.70 -06	3.11 -06	2.61 -06	2.19 -06
32	2.06 -05	1.77 -05	1.51 -05	1.29 -05	1.10 -05	9.38 -06	7.96 -06	6.72 -06
33	3.05 -05	2.64 -05	2.28 -05	1.96 -05	1.68 -05	1.43 -05	1.22 -05	1.03 -05
34	3.33 -05	2.90 -05	2.51 -05	2.16 -05	1.86 -05	1.59 -05	1.36 -05	1.15 -05
35	2.99 -05	2.61 -05	2.26 -05	1.96 -05	1.69 -05	1.45 -05	1.24 -05	1.05 -05
36	2.31 -05	2.02 -05	1.76 -05	1.52 -05	1.32 -05	1.13 -05	9.68 -06	8.24 -06
37	1.57 -05	1.38 -05	1.20 -05	1.04 -05	9.01 -06	7.76 -06	6.64 -06	5.66 -06
38	9.25 -06	8.12 -06	7.08 -06	6.15 -06	5.32 -06	4.58 -06	3.93 -06	3.35 -06
39	4.49 -06	3.94 -06	3.44 -06	2.99 -06	2.59 -06	2.23 -06	1.91 -06	1.63 -06
40	1.73 -06	1.24 -06	1.18 -06	9.88 -07	8.63 -07	7.40 -07	6.35 -07	5.41 -07
41	1.29 -02	9.91 -03	7.18 -03	5.17 -03	3.42 -03	2.28 -03	1.36 -03	8.23 -04
$\sum_{v'} f_{v'v''}$	1.41 -02	1.09 -02	8.05 -03	5.92 -03	4.07 -03	2.84 -03	1.84 -03	1.23 -03

Table E.60: $f_{v'v''}$ for ^{7}Li singlet case (continued).

$v'\backslash v''$	88	89	90	91	92	93	94	95
0	5.09 -16	4.29 -16	3.60 -16	2.99 -16	2.47 -16	2.02 -16	1.63 -16	1.33 -16
1	4.25 -22	5.33 -23	3.78 -24	6.87 -23	1.50 -22	2.15 -22	2.40 -22	2.59 -22
2	3.17 -14	2.66 -14	2.21 -14	1.83 -14	1.51 -14	1.23 -14	9.99 -15	8.04 -15
3	5.38 -13	4.52 -13	3.77 -13	3.12 -13	2.57 -13	2.10 -13	1.71 -13	1.37 -13
4	5.33 -12	4.47 -12	3.73 -12	3.10 -12	2.55 -12	2.09 -12	1.69 -12	1.36 -12
5	4.27 -11	3.58 -11	2.99 -11	2.48 -11	2.04 -11	1.67 -11	1.35 -11	1.09 -11
6	3.04 -10	2.55 -10	2.13 -10	1.77 -10	1.45 -10	1.19 -10	9.65 -11	7.76 -11
7	1.72 -09	1.44 -09	1.20 -09	9.97 -10	8.21 -10	6.72 -10	5.45 -10	4.38 -10
8	9.02 -09	7.57 -09	6.32 -09	5.24 -09	4.32 -09	3.53 -09	2.86 -09	2.30 -09
9	3.83 -08	3.21 -08	2.68 -08	2.22 -08	1.83 -08	1.50 -08	1.22 -08	9.77 -09
10	1.49 -07	1.25 -07	1.04 -07	8.64 -08	7.12 -08	5.82 -08	4.72 -08	3.80 -08
11	4.88 -07	4.10 -07	3.42 -07	2.84 -07	2.34 -07	1.91 -07	1.55 -07	1.25 -07
12	1.42 -06	1.19 -06	9.96 -07	8.26 -07	6.81 -07	5.57 -07	4.52 -07	3.64 -07
13	3.56 -06	2.99 -06	2.50 -06	2.07 -06	1.71 -06	1.40 -06	1.14 -06	9.13 -07
14	7.81 -06	6.56 -06	5.48 -06	4.55 -06	3.75 -06	3.07 -06	2.49 -06	2.00 -06
15	1.49 -05	1.25 -05	1.05 -05	8.68 -06	7.15 -06	5.85 -06	4.75 -06	3.82 -06
16	2.44 -05	2.05 -05	1.71 -05	1.42 -05	1.17 -05	9.59 -06	7.78 -06	6.26 -06
17	3.41 -05	2.87 -05	2.40 -05	1.99 -05	1.64 -05	1.35 -05	1.09 -05	8.79 -06
18	3.98 -05	3.35 -05	2.80 -05	2.33 -05	1.92 -05	1.57 -05	1.28 -05	1.03 -05
19	3.78 -05	3.18 -05	2.66 -05	2.21 -05	1.82 -05	1.49 -05	1.21 -05	9.77 -06
20	2.71 -05	2.29 -05	1.91 -05	1.59 -05	1.31 -05	1.08 -05	8.75 -06	7.04 -06
21	1.25 -05	1.05 -05	8.81 -06	7.34 -06	6.07 -06	4.98 -06	4.05 -06	3.26 -06
22	1.79 -06	1.52 -06	1.28 -06	1.07 -06	8.91 -07	7.33 -07	5.98 -07	4.83 -07
23	9.88 -07	8.19 -07	6.76 -07	5.56 -07	4.54 -07	3.69 -07	2.98 -07	2.39 -07
24	9.17 -06	7.69 -06	6.41 -06	5.31 -06	4.37 -06	3.57 -06	2.89 -06	2.33 -06
25	1.94 -05	1.63 -05	1.36 -05	1.13 -05	9.29 -06	7.60 -06	6.17 -06	4.96 -06
26	2.37 -05	2.00 -05	1.67 -05	1.39 -05	1.14 -05	9.37 -06	7.61 -06	6.12 -06
27	1.97 -05	1.66 -05	1.39 -05	1.16 -05	9.54 -06	7.82 -06	6.35 -06	5.12 -06
28	1.07 -05	9.08 -06	7.61 -06	6.34 -06	5.24 -06	4.30 -06	3.50 -06	2.82 -06
29	2.91 -06	2.47 -06	2.08 -06	1.74 -06	1.44 -06	1.19 -06	9.68 -07	7.81 -07
30	4.69 -09	4.96 -09	4.94 -09	4.70 -09	4.30 -09	3.82 -09	3.31 -09	2.81 -09
31	1.83 -06	1.52 -06	1.26 -06	1.04 -06	8.50 -07	6.92 -07	5.60 -07	4.49 -07
32	5.65 -06	4.73 -06	3.94 -06	3.26 -06	2.68 -06	2.19 -06	1.77 -06	1.43 -06
33	8.72 -06	7.32 -06	6.10 -06	5.06 -06	4.17 -06	3.41 -06	2.76 -06	2.22 -06
34	9.74 -06	8.18 -06	6.83 -06	5.67 -06	4.67 -06	3.82 -06	3.10 -06	2.50 -06
35	8.89 -06	7.47 -06	6.25 -06	5.19 -06	4.28 -06	3.50 -06	2.84 -06	2.29 -06
36	6.97 -06	5.87 -06	4.91 -06	4.08 -06	3.36 -06	2.75 -06	2.24 -06	1.80 -06
37	4.79 -06	4.03 -06	3.38 -06	2.81 -06	2.32 -06	1.90 -06	1.54 -06	1.24 -06
38	2.83 -06	2.39 -06	2.00 -06	1.66 -06	1.37 -06	1.12 -06	9.13 -07	7.35 -07
39	1.38 -06	1.16 -06	9.75 -07	8.11 -07	6.69 -07	5.48 -07	4.46 -07	3.59 -07
40	4.59 -07	3.86 -07	3.24 -07	2.69 -07	2.22 -07	1.82 -07	1.48 -07	1.19 -07
41	4.28 -04	2.30 -04	9.90 -05	4.60 -05	1.48 -05	5.91 -06	1.08 -06	4.24 -07
$\sum_{v'} f_{v'v''}$	7.72 -04	5.19 -04	3.41 -04	2.47 -04	1.80 -04	1.42 -04	1.11 -04	8.91 -05

Table E.61: $f_{v'v''}$ for ^{7}Li singlet case (continued).

$v'\backslash v''$	96	97	98	99	100	$\sum_{v''} f_{v'v''}$
0	1.11 -16	7.89 -17	6.65 -17	8.12 -17	1.05 -16	4.54 -01
1	2.68 -22	1.91 -22	1.69 -22	2.53 -22	3.88 -22	4.56 -01
2	6.43 -15	5.04 -15	4.38 -15	4.95 -15	5.90 -15	4.59 -01
3	1.09 -13	8.66 -14	7.55 -14	8.47 -14	1.00 -13	4.61 -01
4	1.08 -12	8.58 -13	7.49 -13	8.40 -13	9.93 -13	4.63 -01
5	8.67 -12	6.87 -12	5.99 -12	6.72 -12	7.93 -12	4.65 -01
6	6.18 -11	4.90 -11	4.27 -11	4.79 -11	5.66 -11	4.68 -01
7	3.49 -10	2.77 -10	2.41 -10	2.71 -10	3.20 -10	4.70 -01
8	1.83 -09	1.45 -09	1.27 -09	1.42 -09	1.68 -09	4.72 -01
9	7.79 -09	6.17 -09	5.38 -09	6.04 -09	7.13 -09	4.74 -01
10	3.03 -08	2.40 -08	2.09 -08	2.35 -08	2.77 -08	4.77 -01
11	9.94 -08	7.88 -08	6.88 -08	7.71 -08	9.11 -08	4.79 -01
12	2.90 -07	2.30 -07	2.00 -07	2.25 -07	2.65 -07	4.80 -01
13	7.27 -07	5.77 -07	5.03 -07	5.64 -07	6.67 -07	4.82 -01
14	1.59 -06	1.26 -06	1.10 -06	1.24 -06	1.46 -06	4.81 -01
15	3.04 -06	2.41 -06	2.11 -06	2.36 -06	2.79 -06	4.79 -01
16	4.99 -06	3.96 -06	3.45 -06	3.87 -06	4.57 -06	4.74 -01
17	7.00 -06	5.55 -06	4.85 -06	5.44 -06	6.42 -06	4.66 -01
18	8.18 -06	6.49 -06	5.66 -06	6.35 -06	7.50 -06	4.56 -01
19	7.78 -06	6.17 -06	5.39 -06	6.05 -06	7.14 -06	4.46 -01
20	5.61 -06	4.45 -06	3.89 -06	4.36 -06	5.16 -06	4.39 -01
21	2.60 -06	2.06 -06	1.80 -06	2.02 -06	2.39 -06	4.37 -01
22	3.86 -07	3.07 -07	2.68 -07	3.01 -07	3.57 -07	4.39 -01
23	1.90 -07	1.50 -07	1.31 -07	1.46 -07	1.72 -07	4.43 -01
24	1.85 -06	1.47 -06	1.28 -06	1.44 -06	1.69 -06	4.47 -01
25	3.95 -06	3.13 -06	2.74 -06	3.07 -06	3.62 -06	4.47 -01
26	4.88 -06	3.87 -06	3.38 -06	3.79 -06	4.48 -06	4.46 -01
27	4.08 -06	3.24 -06	2.82 -06	3.17 -06	3.75 -06	4.45 -01
28	2.25 -06	1.78 -06	1.56 -06	1.75 -06	2.07 -06	4.47 -01
29	6.24 -07	4.96 -07	4.33 -07	4.87 -07	5.76 -07	4.50 -01
30	2.33 -09	1.90 -09	1.70 -09	1.96 -09	2.38 -09	4.54 -01
31	3.57 -07	2.82 -07	2.46 -07	2.75 -07	3.25 -07	4.59 -01
32	1.13 -06	8.99 -07	7.84 -07	8.79 -07	1.04 -06	4.63 -01
33	1.77 -06	1.40 -06	1.22 -06	1.37 -06	1.62 -06	4.66 -01
34	1.99 -06	1.58 -06	1.38 -06	1.54 -06	1.82 -06	4.70 -01
35	1.82 -06	1.45 -06	1.26 -06	1.42 -06	1.67 -06	4.74 -01
36	1.44 -06	1.14 -06	9.93 -07	1.11 -06	1.32 -06	4.80 -01
37	9.89 -07	7.84 -07	6.85 -07	7.68 -07	9.08 -07	4.85 -01
38	5.86 -07	4.65 -07	4.06 -07	4.56 -07	5.38 -07	4.91 -01
39	2.86 -07	2.27 -07	1.98 -07	2.22 -07	2.63 -07	4.95 -01
40	9.51 -08	7.54 -08	6.59 -08	7.39 -08	8.74 -08	4.98 -01
41	6.23 -09	1.56 -08	1.23 -08	6.00 -09	1.18 -08	4.98 -01
$\sum_{v'} f_{v'v''}$	7.07 -05	5.60 -05	4.89 -05	5.49 -05	6.48 -05	

Table E.62: $f_{v'v''}$ for ^{7}Li singlet case (continued).

$v'\backslash v''$	0	1	2	3	4	5	6	7
0	1.36 -04	1.04 -03	4.09 -03	1.09 -02	2.21 -02	3.65 -02	5.05 -02	5.99 -02
1	5.16 -04	3.35 -03	1.08 -02	2.26 -02	3.42 -02	3.85 -02	3.19 -02	1.77 -02
2	1.10 -03	6.07 -03	1.61 -02	2.65 -02	2.86 -02	1.92 -02	5.76 -03	1.36 -05
3	1.71 -03	8.21 -03	1.82 -02	2.31 -02	1.67 -02	4.73 -03	1.36 -04	7.35 -03
4	2.17 -03	9.17 -03	1.71 -02	1.68 -02	7.34 -03	1.48 -04	4.03 -03	1.25 -02
5	2.34 -03	8.83 -03	1.41 -02	1.07 -02	2.39 -03	5.73 -04	6.99 -03	1.09 -02
6	2.15 -03	7.41 -03	1.04 -02	6.20 -03	5.21 -04	1.69 -03	6.85 -03	6.93 -03
7	1.60 -03	5.16 -03	6.55 -03	3.20 -03	5.43 -05	1.85 -03	4.83 -03	3.56 -03
8	8.89 -04	2.76 -03	3.29 -03	1.40 -03	4.83 -07	1.20 -03	2.52 -03	1.51 -03
9	2.64 -04	8.05 -04	9.35 -04	3.75 -04	4.32 -07	3.73 -04	7.23 -04	3.95 -04
$\sum_{v'} f_{v'v''}$	1.29 -02	5.28 -02	1.01 -01	1.22 -01	1.12 -01	1.05 -01	1.14 -01	1.21 -01

$v'\backslash v''$	8	9	10	11	12	13	14	15
0	6.23 -02	5.91 -02	5.39 -02	4.56 -02	3.33 -02	2.12 -02	1.21 -02	6.56 -03
1	4.60 -03	2.85 -05	6.26 -03	2.20 -02	4.06 -02	5.39 -02	5.58 -02	4.83 -02
2	6.32 -03	1.82 -02	2.65 -02	2.44 -02	1.23 -02	1.33 -03	2.40 -03	1.59 -02
3	1.68 -02	1.78 -02	9.82 -03	1.12 -03	2.34 -03	1.46 -02	2.51 -02	2.29 -02
4	1.35 -02	6.11 -03	1.71 -04	3.62 -03	1.34 -02	1.70 -02	9.24 -03	6.46 -04
5	6.34 -03	5.25 -04	1.84 -03	8.91 -03	1.17 -02	5.72 -03	6.64 -05	4.25 -03
6	2.00 -03	1.59 -04	4.17 -03	8.09 -03	5.49 -03	4.85 -04	1.88 -03	8.26 -03
7	4.25 -04	7.30 -04	3.88 -03	4.83 -03	1.78 -03	6.48 -05	3.21 -03	6.22 -03
8	6.50 -05	6.63 -04	2.24 -03	2.18 -03	4.70 -04	2.57 -04	2.22 -03	3.03 -03
9	7.79 -06	2.29 -04	6.66 -04	5.80 -04	9.20 -05	1.17 -04	6.97 -04	8.27 -04
$\sum_{v'} f_{v'v''}$	1.12 -01	1.04 -01	1.09 -01	1.21 -01	1.21 -01	1.15 -01	1.13 -01	1.17 -01

Table E.63: Oscillator strength $f_{v'v''}$ for the ^{6}Li triplet case.

$v'\backslash v''$	16	17	18	19	20	21	22	23
0	3.37 -03	1.57 -03	6.82 -04	2.92 -04	1.13 -04	3.70 -05	1.29 -05	4.28 -06
1	3.69 -02	2.56 -02	1.61 -02	9.24 -03	4.89 -03	2.39 -03	1.05 -03	4.23 -04
2	3.33 -02	4.63 -02	5.09 -02	4.71 -02	3.80 -02	2.72 -02	1.75 -02	1.00 -02
3	1.10 -02	1.21 -03	1.90 -03	1.38 -02	3.08 -02	4.51 -02	5.13 -02	4.84 -02
4	2.95 -03	1.39 -02	2.23 -02	2.05 -02	1.04 -02	1.18 -03	2.01 -03	1.48 -02
5	1.29 -02	1.45 -02	7.41 -03	5.48 -04	2.44 -03	1.24 -02	2.11 -02	2.00 -02
6	9.76 -03	4.30 -03	4.28 -05	3.16 -03	1.03 -02	1.29 -02	7.56 -03	8.52 -04
7	4.08 -03	3.99 -04	1.07 -03	5.38 -03	7.51 -03	4.50 -03	4.22 -04	1.37 -03
8	1.29 -03	1.76 -07	1.35 -03	3.40 -03	3.20 -03	9.99 -04	6.00 -05	2.18 -03
9	2.78 -04	1.24 -05	4.96 -04	1.01 -03	7.97 -04	1.62 -04	8.12 -05	8.13 -04
$\sum_{v'} f_{v'v''}$	1.16 -01	1.08 -01	1.02 -01	1.04 -01	1.08 -01	1.07 -01	1.01 -01	9.88 -02

$v'\backslash v''$	24	25	26	27	28	29	30	31
0	7.62 -07	2.45 -07	8.58 -08	1.79 -12	8.05 -09	5.24 -10	2.14 -09	4.06 -09
1	1.55 -04	4.85 -05	1.40 -05	3.86 -06	7.47 -07	1.86 -07	3.49 -08	1.09 -09
2	5.12 -03	2.34 -03	9.46 -04	3.45 -04	1.12 -04	3.19 -05	8.35 -06	1.87 -06
3	3.88 -02	2.70 -02	1.64 -02	8.75 -03	4.15 -03	1.74 -03	6.48 -04	2.17 -04
4	3.36 -02	4.89 -02	5.41 -02	4.88 -02	3.71 -02	2.43 -02	1.39 -02	6.98 -03
5	9.85 -03	7.78 -04	3.20 -03	1.86 -02	3.88 -02	5.32 -02	5.60 -02	4.85 -02
6	1.84 -03	1.15 -02	2.06 -02	1.95 -02	9.09 -03	4.74 -04	4.10 -03	2.09 -02
7	7.26 -03	1.12 -02	7.90 -03	1.50 -03	8.56 -04	8.72 -03	1.78 -02	1.88 -02
8	4.87 -03	4.46 -03	1.36 -03	9.99 -05	3.25 -03	7.54 -03	7.73 -03	3.40 -03
9	1.42 -03	1.03 -03	1.63 -04	1.79 -04	1.32 -03	2.23 -03	1.68 -03	3.67 -04
$\sum_{v'} f_{v'v''}$	1.03 -01	1.07 -01	1.05 -01	9.77 -02	9.46 -02	9.82 -02	1.02 -01	9.91 -02

Table E.64: $f_{v'v''}$ for ^{6}Li triplet case (continued).

$v'\backslash v''$	32	33	34	35	36	37	38	39
0	2.08 -09	3.14 -10	1.07 -10	8.79 -10	1.45 -09	1.36 -09	8.65 -10	3.52 -10
1	4.21 -09	3.96 -10	1.29 -10	8.99 -11	4.08 -10	6.19 -10	5.61 -10	3.60 -10
2	3.60 -07	6.89 -08	5.30 -09	2.41 -09	2.81 -14	1.17 -11	5.01 -11	1.15 -10
3	6.27 -05	1.58 -05	3.49 -06	6.05 -07	1.13 -07	8.71 -09	2.29 -09	7.62 -11
4	3.09 -03	1.19 -03	3.99 -04	1.17 -04	2.87 -05	6.21 -06	1.07 -06	1.85 -07
5	3.54 -02	2.22 -02	1.20 -02	5.61 -03	2.27 -03	7.90 -04	2.40 -04	6.36 -05
6	4.22 -02	5.71 -02	5.95 -02	5.05 -02	3.59 -02	2.17 -02	1.14 -02	5.21 -03
7	1.04 -02	1.21 -03	2.41 -03	1.76 -02	3.98 -02	5.75 -02	6.31 -02	5.66 -02
8	3.51 -05	2.95 -03	1.09 -02	1.67 -02	1.43 -02	5.88 -03	9.19 -05	4.61 -03
9	1.40 -04	1.77 -03	3.77 -03	3.92 -03	1.92 -03	8.36 -05	1.05 -03	4.92 -03
$\sum_{v'} f_{v'v''}$	9.13 -02	8.64 -02	8.90 -02	9.44 -02	9.42 -02	8.60 -02	7.58 -02	7.14 -02

$v'\backslash v''$	40	41	42	43	44	45	46	47
0	5.87 -11	4.75 -12	9.80 -11	2.33 -10	3.41 -10	3.96 -10	4.01 -10	3.70 -10
1	1.61 -10	3.97 -11	4.07 -13	1.52 -11	5.18 -11	8.79 -11	1.13 -10	1.26 -10
2	1.63 -10	1.57 -10	1.22 -10	7.80 -11	4.14 -11	1.72 -11	4.56 -12	2.01 -13
3	2.30 -12	1.06 -10	1.57 -10	1.96 -10	1.94 -10	1.70 -10	1.35 -10	9.85 -11
4	2.21 -08	2.17 -09	5.17 -10	6.43 -11	2.32 -10	2.09 -10	1.95 -10	1.60 -10
5	1.48 -05	2.88 -06	4.68 -07	7.28 -08	7.46 -09	1.41 -09	7.54 -12	2.10 -10
6	2.10 -03	7.37 -04	2.24 -04	6.07 -05	1.46 -05	2.92 -06	5.25 -07	8.30 -08
7	4.32 -02	2.83 -02	1.62 -02	8.25 -03	3.74 -03	1.50 -03	5.35 -04	1.75 -04
8	2.01 -02	4.02 -02	5.63 -02	6.27 -02	5.90 -02	4.82 -02	3.46 -02	2.25 -02
9	9.01 -03	1.01 -02	7.21 -03	2.58 -03	1.16 -05	2.52 -03	1.05 -02	2.16 -02
$\sum_{v'} f_{v'v''}$	7.44 -02	7.94 -02	7.99 -02	7.36 -02	6.28 -02	5.22 -02	4.57 -02	4.43 -02

Table E.65: $f_{v'v''}$ for ^{6}Li triplet case (continued).

$v'\backslash v''$	48	49	50	51	52	53	54	55
0	3.17 -10	2.56 -10	1.96 -10	1.43 -10	9.97 -11	6.68 -11	4.32 -11	2.74 -11
1	1.26 -10	1.18 -10	1.04 -10	8.76 -11	7.10 -11	5.57 -11	4.25 -11	3.21 -11
2	8.33 -13	3.85 -12	7.45 -12	1.06 -11	1.26 -11	1.36 -11	1.34 -11	1.27 -11
3	6.58 -11	3.98 -11	2.13 -11	9.69 -12	3.35 -12	6.23 -13	4.83 -17	3.41 -13
4	1.24 -10	9.07 -11	6.38 -11	4.29 -11	2.76 -11	1.69 -11	9.89 -12	5.59 -12
5	1.26 -10	1.23 -10	9.40 -11	7.05 -11	5.04 -11	3.50 -11	2.37 -11	1.60 -11
6	1.47 -08	1.15 -09	5.07 -10	1.95 -11	7.64 -11	4.23 -11	3.35 -11	2.44 -11
7	5.41 -05	1.55 -05	3.91 -06	8.66 -07	1.58 -07	2.58 -08	1.76 -09	3.38 -10
8	1.37 -02	7.82 -03	4.15 -03	2.02 -03	8.95 -04	3.50 -04	1.15 -04	3.04 -05
9	3.31 -02	4.30 -02	4.99 -02	5.31 -02	5.25 -02	4.83 -02	4.08 -02	3.05 -02
$\sum_{v'} f_{v'v''}$	4.68 -02	5.08 -02	5.40 -02	5.51 -02	5.34 -02	4.86 -02	4.09 -02	3.05 -02

$v'\backslash v''$	56	57	58	59	60	61	62	63
0	1.76 -11	1.15 -11	7.27 -12	4.41 -12	2.52 -12	1.32 -12	6.08 -13	2.37 -13
1	2.49 -11	1.99 -11	1.59 -11	1.28 -11	1.02 -11	8.00 -12	6.19 -12	4.76 -12
2	1.19 -11	1.14 -11	1.08 -11	1.01 -11	9.40 -12	8.55 -12	7.58 -12	6.60 -12
3	1.01 -12	1.78 -12	2.53 -12	3.20 -12	3.73 -12	4.06 -12	4.14 -12	4.04 -12
4	3.11 -12	1.68 -12	8.09 -13	3.19 -13	7.96 -14	2.40 -15	1.81 -14	7.33 -14
5	1.11 -11	7.92 -12	5.63 -12	3.97 -12	2.75 -12	1.86 -12	1.23 -12	7.95 -13
6	1.84 -11	1.43 -11	1.11 -11	8.50 -12	6.43 -12	4.78 -12	3.47 -12	2.51 -12
7	3.01 -12	1.46 -11	4.31 -12	3.18 -12	2.09 -12	1.76 -12	1.63 -12	1.59 -12
8	6.30 -06	1.23 -06	2.98 -07	6.13 -08	1.40 -08	1.63 -09	6.38 -10	8.57 -13
9	1.95 -02	1.14 -02	6.86 -03	4.19 -03	2.47 -03	1.43 -03	7.98 -04	3.91 -04
$\sum_{v'} f_{v'v''}$	1.95 -02	1.14 -02	6.86 -03	4.19 -03	2.47 -03	1.43 -03	7.98 -04	3.91 -04

Table E.66: $f_{v'v''}$ for ^{6}Li triplet case (continued).

$v'\backslash v''$	64	65	66	67	68	69	70	71
0	6.88 -14	7.60 -15	2.09 -15	2.08 -14	4.63 -14	6.95 -14	8.65 -14	9.64 -14
1	3.74 -12	2.93 -12	2.32 -12	1.84 -12	1.47 -12	1.17 -12	9.41 -13	7.56 -13
2	5.81 -12	5.06 -12	4.41 -12	3.81 -12	3.27 -12	2.80 -12	2.39 -12	2.03 -12
3	3.90 -12	3.66 -12	3.39 -12	3.09 -12	2.77 -12	2.47 -12	2.17 -12	1.88 -12
4	1.38 -13	1.95 -13	2.39 -13	2.66 -13	2.78 -13	2.78 -13	2.68 -13	2.51 -13
5	5.22 -13	3.38 -13	2.19 -13	1.41 -13	9.00 -14	5.76 -14	3.67 -14	2.34 -14
6	1.85 -12	1.36 -12	1.02 -12	7.61 -13	5.74 -13	4.38 -13	3.36 -13	2.60 -13
7	1.60 -12	1.58 -12	1.53 -12	1.44 -12	1.33 -12	1.21 -12	1.07 -12	9.39 -13
8	2.10 -11	1.81 -12	9.46 -13	7.32 -14	9.08 -15	1.06 -13	2.03 -13	2.60 -13
9	1.65 -04	6.70 -05	2.55 -05	8.47 -06	2.49 -06	7.15 -07	1.39 -07	3.51 -08
$\sum_{v'} f_{v'v''}$	1.65 -04	6.70 -05	2.55 -05	8.47 -06	2.49 -06	7.15 -07	1.39 -07	3.51 -08

$v'\backslash v''$	72	73	74	75	76	77	78	79
0	9.98 -14	9.79 -14	9.22 -14	8.40 -14	7.44 -14	6.44 -14	5.45 -14	4.51 -14
1	6.09 -13	4.90 -13	3.95 -13	3.17 -13	2.54 -13	2.03 -13	1.62 -13	1.27 -13
2	1.71 -12	1.43 -12	1.19 -12	9.84 -13	8.08 -13	6.58 -13	5.32 -13	4.26 -13
3	1.62 -12	1.38 -12	1.17 -12	9.77 -13	8.10 -13	6.65 -13	5.41 -13	4.34 -13
4	2.29 -13	2.05 -13	1.80 -13	1.55 -13	1.32 -13	1.10 -13	9.11 -14	7.46 -14
5	1.50 -14	9.62 -15	6.22 -15	4.05 -15	2.67 -15	1.78 -15	1.20 -15	8.73 -16
6	2.02 -13	1.57 -13	1.23 -13	9.69 -14	7.62 -14	5.99 -14	4.70 -14	3.61 -14
7	8.12 -13	6.94 -13	5.86 -13	4.90 -13	4.06 -13	3.33 -13	2.71 -13	2.20 -13
8	2.80 -13	2.74 -13	2.54 -13	2.26 -13	1.96 -13	1.66 -13	1.38 -13	1.17 -13
9	3.56 -09	8.52 -10	3.40 -11	2.83 -12	3.62 -12	4.37 -12	6.09 -12	6.30 -12
$\sum_{v'} f_{v'v''}$	3.57 -09	8.57 -10	3.80 -11	6.16 -12	6.38 -12	6.63 -12	7.92 -12	7.78 -12

Table E.67: $f_{v'v''}$ for ^{6}Li triplet case (continued).

$v'\backslash v''$	80	81	82	83	84	85	$\sum_{v''} f_{v'v''}$
0	3.65 -14	2.95 -14	2.34 -14	2.19 -14	2.52 -14	3.07 -14	4.85 -01
1	9.96 -14	7.76 -14	6.01 -14	5.43 -14	6.21 -14	7.32 -14	4.88 -01
2	3.38 -13	2.64 -13	2.06 -13	1.84 -13	2.15 -13	2.52 -13	4.90 -01
3	3.44 -13	2.71 -13	2.12 -13	1.93 -13	2.22 -13	2.65 -13	4.92 -01
4	6.04 -14	4.72 -14	3.75 -14	3.27 -14	3.94 -14	4.59 -14	4.93 -01
5	6.75 -16	4.10 -16	3.21 -16	1.51 -16	2.65 -16	1.92 -16	4.95 -01
6	2.73 -14	2.18 -14	1.65 -14	1.64 -14	1.71 -14	2.14 -14	4.96 -01
7	1.78 -13	1.36 -13	1.08 -13	8.98 -14	1.12 -13	1.26 -13	4.97 -01
8	9.99 -14	7.27 -14	6.02 -14	4.15 -14	6.12 -14	6.17 -14	4.98 -01
9	5.76 -12	5.38 -12	4.45 -12	4.88 -12	5.35 -12	7.27 -12	4.99 -01
$\sum_{v'} f_{v'v''}$	6.95 -12	6.30 -12	5.17 -12	5.51 -12	6.10 -12	8.15 -12	

Table E.68: $f_{v'v''}$ for ^{6}Li triplet case (continued).

$v'\backslash v''$	0	1	2	3	4	5	6	7
0	7.63 -05	6.25 -04	2.62 -03	7.45 -03	1.61 -02	2.84 -02	4.20 -02	5.35 -02
1	3.13 -04	2.19 -03	7.66 -03	1.75 -02	2.92 -02	3.69 -02	3.56 -02	2.50 -02
2	7.13 -04	4.32 -03	1.26 -02	2.32 -02	2.88 -02	2.40 -02	1.15 -02	1.28 -03
3	1.19 -03	6.30 -03	1.55 -02	2.27 -02	2.02 -02	9.21 -03	5.27 -04	3.01 -03
4	1.62 -03	7.57 -03	1.59 -02	1.85 -02	1.11 -02	1.64 -03	1.34 -03	9.58 -03
5	1.88 -03	7.87 -03	1.43 -02	1.32 -02	4.87 -03	4.49 -07	4.65 -03	1.10 -02
6	1.89 -03	7.21 -03	1.15 -02	8.52 -03	1.70 -03	6.53 -04	6.07 -03	8.51 -03
7	1.63 -03	5.78 -03	8.26 -03	5.04 -03	4.49 -04	1.31 -03	5.38 -03	5.28 -03
8	1.13 -03	3.80 -03	5.03 -03	2.64 -03	8.49 -05	1.25 -03	3.57 -03	2.73 -03
9	5.78 -04	1.88 -03	2.39 -03	1.14 -03	1.22 -05	7.26 -04	1.75 -03	1.15 -03
10	1.43 -04	4.62 -04	5.76 -04	2.64 -04	1.39 -06	1.88 -04	4.26 -04	2.63 -04
$\sum_{v'} f_{v'v''}$	1.12 -02	4.80 -02	9.63 -02	1.20 -01	1.13 -01	1.04 -01	1.13 -01	1.21 -01

$v'\backslash v''$	8	9	10	11	12	13	14	15
0	5.96 -02	5.92 -02	5.52 -02	4.98 -02	4.09 -02	2.92 -02	1.85 -02	1.06 -02
1	1.10 -02	1.45 -03	1.03 -03	1.03 -02	2.66 -02	4.33 -02	5.35 -02	5.29 -02
2	1.72 -03	1.13 -02	2.20 -02	2.64 -02	2.03 -02	7.84 -03	1.46 -04	4.85 -03
3	1.29 -02	1.86 -02	1.46 -02	5.37 -03	1.66 -06	5.90 -03	1.89 -02	2.55 -02
4	1.47 -02	1.01 -02	2.19 -03	5.36 -04	7.97 -03	1.63 -02	1.49 -02	5.17 -03
5	9.28 -03	2.42 -03	2.45 -04	5.72 -03	1.18 -02	9.74 -03	2.21 -03	7.29 -04
6	4.06 -03	6.17 -05	2.49 -03	7.71 -03	7.93 -03	2.46 -03	2.20 -04	5.72 -03
7	1.32 -03	2.58 -04	3.58 -03	6.02 -03	3.58 -03	1.38 -04	2.00 -03	6.66 -03
8	3.28 -04	5.67 -04	2.85 -03	3.43 -03	1.25 -03	5.23 -05	2.34 -03	4.39 -03
9	7.00 -05	4.21 -04	1.50 -03	1.50 -03	3.77 -04	1.25 -04	1.41 -03	2.03 -03
10	1.11 -05	1.17 -04	3.74 -04	3.49 -04	7.33 -05	4.38 -05	3.64 -04	4.77 -04
$\sum_{v'} f_{v'v''}$	1.15 -01	1.05 -01	1.06 -01	1.17 -01	1.21 -01	1.15 -01	1.14 -01	1.19 -01

Table E.69: Oscillator strength $f_{v'v''}$ for ^{7}Li triplet case.

$v'\backslash v''$	16	17	18	19	20	21	22	23
0	5.83 -03	3.00 -03	1.41 -03	6.29 -04	2.77 -04	1.10 -04	3.75 -05	1.39 -05
1	4.47 -02	3.37 -02	2.32 -02	1.46 -02	8.42 -03	4.52 -03	2.25 -03	1.02 -03
2	1.95 -02	3.56 -02	4.63 -02	4.88 -02	4.41 -02	3.50 -02	2.50 -02	1.61 -02
3	1.95 -02	7.39 -03	2.02 -04	3.77 -03	1.67 -02	3.26 -02	4.45 -02	4.87 -02
4	2.03 -05	6.37 -03	1.75 -02	2.27 -02	1.77 -02	7.07 -03	2.22 -04	3.72 -03
5	8.57 -03	1.53 -02	1.24 -02	3.96 -03	3.22 -05	5.66 -03	1.61 -02	2.16 -02
6	1.09 -02	7.90 -03	1.42 -03	7.87 -04	7.21 -03	1.31 -02	1.15 -02	4.17 -03
7	6.44 -03	1.72 -03	2.48 -04	4.46 -03	8.54 -03	6.98 -03	1.86 -03	2.33 -04
8	2.61 -03	1.12 -04	1.24 -03	4.32 -03	4.79 -03	2.00 -03	1.53 -06	2.02 -03
9	8.59 -04	2.09 -06	1.01 -03	2.29 -03	1.89 -03	4.27 -04	1.36 -04	1.67 -03
10	1.74 -04	5.49 -06	2.85 -04	5.64 -04	4.13 -04	6.59 -05	6.39 -05	4.65 -04
$\sum_{v'} f_{v'v''}$	1.19 -01	1.11 -01	1.05 -01	1.07 -01	1.10 -01	1.08 -01	1.02 -01	9.97 -02

$v'\backslash v''$	24	25	26	27	28	29	30	31
0	4.81 -06	9.91 -07	3.28 -07	1.17 -07	1.46 -09	8.04 -09	1.94 -09	2.29 -09
1	4.28 -04	1.66 -04	5.56 -05	1.73 -05	5.13 -06	1.13 -06	2.91 -07	6.82 -08
2	9.38 -03	4.95 -03	2.35 -03	9.97 -04	3.84 -04	1.34 -04	4.10 -05	1.17 -05
3	4.50 -02	3.60 -02	2.52 -02	1.56 -02	8.57 -03	4.21 -03	1.85 -03	7.25 -04
4	1.72 -02	3.45 -02	4.73 -02	5.09 -02	4.55 -02	3.46 -02	2.29 -02	1.34 -02
5	1.72 -02	6.65 -03	7.81 -05	5.15 -03	2.10 -02	3.94 -02	5.12 -02	5.23 -02
6	1.25 -06	5.06 -03	1.57 -02	2.15 -02	1.66 -02	5.65 -03	2.62 -06	7.12 -03
7	5.12 -03	1.13 -02	1.12 -02	4.69 -03	2.35 -05	4.29 -03	1.46 -02	2.06 -02
8	5.79 -03	6.36 -03	2.79 -03	1.12 -05	2.62 -03	8.27 -03	1.01 -02	5.70 -03
9	3.02 -03	2.27 -03	4.19 -04	2.94 -04	2.58 -03	4.46 -03	3.37 -03	6.96 -04
10	7.27 -04	4.65 -04	4.69 -05	1.40 -04	7.33 -04	1.06 -03	6.42 -04	5.88 -05
$\sum_{v'} f_{v'v''}$	1.04 -01	1.08 -01	1.05 -01	9.94 -02	9.80 -02	1.02 -01	1.05 -01	1.01 -01

Table E.70: $f_{v'v''}$ for ^{7}Li triplet case (continued).

$v'\backslash v''$	32	33	34	35	36	37	38	39
0	3.27 -09	7.41 -10	1.51 -11	8.31 -10	1.52 -09	1.27 -09	5.50 -10	6.31 -11
1	3.62 -09	5.25 -09	1.00 -11	1.14 -11	4.97 -10	5.59 -10	4.26 -10	1.71 -10
2	2.88 -06	6.25 -07	1.45 -07	1.61 -08	4.10 -09	5.13 -10	1.47 -11	2.18 -10
3	2.57 -04	8.12 -05	2.28 -05	5.75 -06	1.15 -06	2.44 -07	3.35 -08	3.99 -09
4	6.90 -03	3.18 -03	1.30 -03	4.70 -04	1.50 -04	4.15 -05	1.02 -05	2.08 -06
5	4.45 -02	3.24 -02	2.05 -02	1.14 -02	5.51 -03	2.35 -03	8.74 -04	2.84 -04
6	2.47 -02	4.36 -02	5.46 -02	5.44 -02	4.49 -02	3.16 -02	1.91 -02	1.00 -02
7	1.62 -02	5.70 -03	2.03 -07	7.08 -03	2.54 -02	4.58 -02	5.81 -02	5.79 -02
8	5.07 -04	1.80 -03	1.00 -02	1.77 -02	1.72 -02	8.63 -03	6.83 -04	3.00 -03
9	3.09 -04	3.47 -03	6.95 -03	6.67 -03	2.76 -03	1.07 -05	2.78 -03	9.89 -03
10	2.06 -04	1.08 -03	1.69 -03	1.25 -03	2.82 -04	9.23 -05	1.28 -03	2.86 -03
$\sum_{v'} f_{v'v''}$	9.36 -02	9.12 -02	9.51 -02	9.89 -02	9.63 -02	8.85 -02	8.28 -02	8.40 -02

$v'\backslash v''$	40	41	42	43	44	45	46	47
0	4.06 -11	2.86 -10	5.20 -10	5.95 -10	5.16 -10	3.59 -10	1.99 -10	8.14 -11
1	2.14 -11	9.15 -12	7.67 -11	1.50 -10	1.86 -10	1.80 -10	1.44 -10	9.87 -11
2	1.45 -10	1.02 -10	4.34 -11	9.92 -12	3.54 -15	5.95 -12	1.84 -11	3.05 -11
3	1.28 -09	8.64 -11	3.39 -10	1.82 -10	1.08 -10	3.88 -11	6.20 -12	4.03 -13
4	3.65 -07	6.40 -08	5.11 -09	2.10 -09	3.14 -11	1.96 -10	6.43 -11	3.26 -11
5	7.98 -05	1.97 -05	4.34 -06	7.90 -07	1.41 -07	1.37 -08	3.24 -09	5.47 -11
6	4.57 -03	1.83 -03	6.51 -04	2.05 -04	5.61 -05	1.34 -05	2.78 -06	5.50 -07
7	4.77 -02	3.35 -02	2.05 -02	1.11 -02	5.26 -03	2.20 -03	8.21 -04	2.76 -04
8	1.78 -02	3.84 -02	5.51 -02	6.15 -02	5.68 -02	4.48 -02	3.10 -02	1.91 -02
9	1.52 -02	1.38 -02	6.81 -03	6.30 -04	1.96 -03	1.29 -02	2.99 -02	4.65 -02
10	3.22 -03	1.92 -03	3.03 -04	2.71 -04	2.53 -03	5.87 -03	8.09 -03	7.69 -03
$\sum_{v'} f_{v'v''}$	8.86 -02	8.95 -02	8.34 -02	7.37 -02	6.66 -02	6.58 -02	6.98 -02	7.36 -02

Table E.71: $f_{v'v''}$ for ^{7}Li triplet case (continued).

$v'\backslash v''$	48	49	50	51	52	53	54	55
0	1.81 -11	9.61 -15	1.11 -11	3.65 -11	6.49 -11	8.93 -11	1.06 -10	1.14 -10
1	5.73 -11	2.70 -11	8.95 -12	1.06 -12	4.14 -13	4.05 -12	9.48 -12	1.49 -11
2	3.85 -11	4.15 -11	4.03 -11	3.61 -11	3.01 -11	2.35 -11	1.74 -11	1.21 -11
3	8.98 -12	2.17 -11	3.30 -11	4.08 -11	4.47 -11	4.51 -11	4.30 -11	3.91 -11
4	6.38 -12	2.88 -14	6.03 -12	1.79 -11	3.05 -11	4.04 -11	4.62 -11	4.80 -11
5	7.57 -11	2.39 -12	1.21 -12	6.72 -13	4.42 -12	1.03 -11	1.62 -11	2.09 -11
6	7.94 -08	1.21 -08	1.25 -09	1.82 -10	1.62 -11	2.72 -13	2.85 -12	3.75 -12
7	8.23 -05	2.13 -05	5.08 -06	1.11 -06	2.32 -07	4.34 -08	6.79 -09	9.73 -10
8	1.05 -02	5.17 -03	2.30 -03	9.57 -04	3.76 -04	1.38 -04	4.60 -05	1.37 -05
9	5.69 -02	5.84 -02	5.21 -02	4.19 -02	3.13 -02	2.20 -02	1.44 -02	8.79 -03
10	4.87 -03	1.50 -03	3.06 -07	1.82 -03	7.07 -03	1.50 -02	2.46 -02	3.46 -02
$\sum_{v'} f_{v'v''}$	7.24 -02	6.51 -02	5.44 -02	4.46 -02	3.88 -02	3.71 -02	3.91 -02	4.34 -02

$v'\backslash v''$	56	57	58	59	60	61	62	63
0	1.14 -10	1.08 -10	9.74 -11	8.53 -11	7.42 -11	6.59 -11	5.92 -11	5.30 -11
1	1.92 -11	2.18 -11	2.27 -11	2.23 -11	2.12 -11	2.04 -11	1.97 -11	1.87 -11
2	7.89 -12	4.85 -12	2.79 -12	1.50 -12	7.60 -13	3.52 -13	1.32 -13	2.76 -14
3	3.43 -11	2.91 -11	2.40 -11	1.94 -11	1.58 -11	1.32 -11	1.12 -11	9.54 -12
4	4.64 -11	4.25 -11	3.73 -11	3.17 -11	2.70 -11	2.35 -11	2.07 -11	1.81 -11
5	2.38 -11	2.49 -11	2.43 -11	2.26 -11	2.08 -11	1.93 -11	1.81 -11	1.68 -11
6	6.37 -12	8.25 -12	9.61 -12	1.02 -11	1.04 -11	1.05 -11	1.05 -11	1.02 -11
7	7.98 -11	2.29 -11	2.30 -12	4.84 -12	3.52 -12	2.89 -12	2.40 -12	2.10 -12
8	3.67 -06	8.21 -07	1.42 -07	2.00 -08	1.67 -09	1.29 -10	3.96 -11	2.46 -12
9	4.98 -03	2.57 -03	1.18 -03	4.65 -04	1.51 -04	4.26 -05	1.26 -05	3.99 -06
10	4.36 -02	5.06 -02	5.41 -02	5.26 -02	4.47 -02	3.34 -02	2.41 -02	1.78 -02
$\sum_{v'} f_{v'v''}$	4.86 -02	5.32 -02	5.53 -02	5.30 -02	4.48 -02	3.34 -02	2.41 -02	1.78 -02

Table E.72: $f_{v'v''}$ for ^{7}Li triplet case (continued).

$v'\backslash v''$	64	65	66	67	68	69	70	71
0	4.72 -11	4.17 -11	3.64 -11	3.11 -11	2.63 -11	2.26 -11	1.93 -11	1.65 -11
1	1.77 -11	1.65 -11	1.51 -11	1.35 -11	1.19 -11	1.05 -11	9.26 -12	8.14 -12
2	4.00 -19	1.96 -14	6.36 -14	1.13 -13	1.57 -13	1.93 -13	2.17 -13	2.31 -13
3	8.09 -12	6.81 -12	5.67 -12	4.64 -12	3.77 -12	3.12 -12	2.57 -12	2.13 -12
4	1.59 -11	1.38 -11	1.19 -11	1.00 -11	8.40 -12	7.14 -12	6.04 -12	5.13 -12
5	1.55 -11	1.41 -11	1.27 -11	1.11 -11	9.63 -12	8.43 -12	7.32 -12	6.37 -12
6	9.82 -12	9.24 -12	8.51 -12	7.62 -12	6.71 -12	5.96 -12	5.23 -12	4.59 -12
7	1.95 -12	1.89 -12	1.87 -12	1.84 -12	1.79 -12	1.75 -12	1.69 -12	1.60 -12
8	1.37 -11	9.96 -12	8.99 -12	6.45 -12	4.53 -12	3.16 -12	2.19 -12	1.53 -12
9	1.21 -06	3.19 -07	8.97 -08	2.03 -08	3.11 -09	5.95 -10	2.29 -11	2.84 -11
10	1.29 -02	9.25 -03	6.56 -03	4.54 -03	2.87 -03	1.62 -03	8.90 -04	4.73 -04
$\sum_{v'} f_{v'v''}$	1.29 -02	9.25 -03	6.56 -03	4.54 -03	2.87 -03	1.62 -03	8.90 -04	4.73 -04

$v'\backslash v''$	72	73	74	75	76	77	78	79
0	1.40 -11	1.20 -11	1.02 -11	8.65 -12	7.33 -12	6.19 -12	5.22 -12	4.38 -12
1	7.11 -12	6.18 -12	5.36 -12	4.63 -12	3.98 -12	3.41 -12	2.90 -12	2.46 -12
2	2.36 -13	2.33 -13	2.24 -13	2.11 -13	1.95 -13	1.77 -13	1.58 -13	1.40 -13
3	1.76 -12	1.47 -12	1.22 -12	1.01 -12	8.43 -13	7.01 -13	5.83 -13	4.83 -13
4	4.34 -12	3.67 -12	3.11 -12	2.63 -12	2.22 -12	1.87 -12	1.57 -12	1.32 -12
5	5.50 -12	4.75 -12	4.09 -12	3.51 -12	3.00 -12	2.55 -12	2.16 -12	1.83 -12
6	4.00 -12	3.47 -12	3.01 -12	2.59 -12	2.22 -12	1.90 -12	1.62 -12	1.37 -12
7	1.50 -12	1.39 -12	1.27 -12	1.14 -12	1.02 -12	9.02 -13	7.89 -13	6.84 -13
8	1.09 -12	7.83 -13	5.76 -13	4.31 -13	3.28 -13	2.54 -13	1.98 -13	1.57 -13
9	2.62 -12	4.62 -12	2.93 -12	2.71 -12	2.46 -12	2.27 -12	2.07 -12	1.85 -12
10	2.30 -04	1.04 -04	4.51 -05	1.69 -05	6.16 -06	1.89 -06	5.30 -07	1.32 -07
$\sum_{v'} f_{v'v''}$	2.30 -04	1.04 -04	4.51 -05	1.69 -05	6.16 -06	1.89 -06	5.30 -07	1.32 -07

Table E.73: $f_{v'v''}$ for ^{7}Li triplet case (continued).

$v'\backslash v''$	80	81	82	83	84	85	86	87
0	3.67 -12	3.05 -12	2.53 -12	2.08 -12	1.71 -12	1.39 -12	1.12 -12	8.93 -13
1	2.07 -12	1.74 -12	1.45 -12	1.20 -12	9.85 -13	8.03 -13	6.49 -13	5.20 -13
2	1.22 -13	1.05 -13	8.96 -14	7.56 -14	6.31 -14	5.21 -14	4.25 -14	3.43 -14
3	4.00 -13	3.30 -13	2.72 -13	2.22 -13	1.81 -13	1.46 -13	1.18 -13	9.37 -14
4	1.10 -12	9.16 -13	7.58 -13	6.23 -13	5.10 -13	4.14 -13	3.34 -13	2.67 -13
5	1.54 -12	1.28 -12	1.07 -12	8.82 -13	7.24 -13	5.89 -13	4.75 -13	3.80 -13
6	1.15 -12	9.66 -13	8.04 -13	6.65 -13	5.46 -13	4.45 -13	3.60 -13	2.88 -13
7	5.88 -13	5.01 -13	4.23 -13	3.53 -13	2.93 -13	2.40 -13	1.95 -13	1.57 -13
8	1.25 -13	1.00 -13	8.02 -14	6.44 -14	5.16 -14	4.14 -14	3.33 -14	2.62 -14
9	1.63 -12	1.41 -12	1.20 -12	1.01 -12	8.37 -13	6.86 -13	5.52 -13	4.45 -13
10	2.34 -08	5.71 -09	2.18 -10	2.73 -10	3.66 -11	5.98 -11	4.09 -11	3.28 -11
$\sum_{v'} f_{v'v''}$	2.34 -08	5.72 -09	2.27 -10	2.80 -10	4.25 -11	6.46 -11	4.48 -11	3.59 -11

$v'\backslash v''$	88	89	90	91	$\sum_{v''} f_{v'v''}$
0	7.07 -13	5.70 -13	5.63 -13	6.66 -13	4.85 -01
1	4.13 -13	3.33 -13	3.29 -13	3.88 -13	4.87 -01
2	2.73 -14	2.22 -14	2.21 -14	2.65 -14	4.90 -01
3	7.39 -14	5.95 -14	5.87 -14	6.96 -14	4.91 -01
4	2.11 -13	1.70 -13	1.68 -13	1.97 -13	4.93 -01
5	3.01 -13	2.43 -13	2.40 -13	2.85 -13	4.94 -01
6	2.29 -13	1.85 -13	1.82 -13	2.13 -13	4.96 -01
7	1.24 -13	1.01 -13	1.01 -13	1.22 -13	4.97 -01
8	2.12 -14	1.70 -14	1.59 -14	1.69 -14	4.98 -01
9	3.47 -13	2.81 -13	2.86 -13	3.59 -13	4.98 -01
10	2.49 -11	1.97 -11	1.93 -11	2.32 -11	4.99 -01
$\sum_{v'} f_{v'v''}$	2.74 -11	2.17 -11	2.13 -11	2.55 -11	

Table E.74: $f_{v'v''}$ for ^{7}Li triplet case (continued).

Bibliography

[1] C. Salomon, J. Dalibard, W.D. Phillips, A. Clairon and S. Guellati, Europhys. Lett. **12**, 683 (1990).

[2] C. Monroe, W. Swann, H. Robinson and C. Wieman, Phys. Rev. Lett. **65**, 1571 (1990).

[3] J.M Doyle, J.C. Sandberg, I.A. Yu, C.L. Cesar, D. Kleppner and T,J. Greytak, Phys. Rev. Lett. **67**, 603 (1991).

[4] J.D. Miller, R.A. Cline and Heinzen, Phys. Rev. Lett. **71**, 2204 (1993).

[5] P.D.Lett, P.S. Jessen, W.D.Phillips, S.L. Rolston, C.I. Westbrook, and P.L. Gould, Phys. Rev. Lett. **67**, 2139 (1991).

[6] P.S.Julienne and R. Heather, Phys. Rev. Lett. **67**, 2135 (1991).

[7] H.R. Thorsheim, J. Weiner, and P.S. Julienne, Phys. Rev. Lett. **58**, 2420 (1987).

[8] W.I. McAlexander, E.R.I. Abraham, N.W.M. Ritchie, C.J. Williams, H.T.C. Stoof, and R.G. Hulet, (submitted to Phys. Rev. Lett.).

[9] R. Napolitano, J. Weiner, C.J. Williams, and P.S. Julienne, Phys. Rev. Lett. **73**, 1352 (1994).

[10] E.R.I. Abraham, W.I. McAlexander, C.A. Sackett, and R.G. Hulet, (submitted to Phys. Rev. Lett.).

[11] R. Côté, A. Dalgarno, and M.J. Jamieson, Phys. Rev. A **50**, 399 (1994).

[12] A.A. Abrikosov, L.P. Gorkov, and I.E. Dzyaloshinski, *Methods of Quantum Field Theory in Statistical Physics* (Dover, New York 1975).

[13] A.J. Moerdijk and B.J. Verhaar, Phys. Rev. Lett. **73**, 518 (1994).

[14] I.A. Yu, J.M. Doyle, J.C. Sandberg, C.L. Cesar, D. Kleppner, and T.J. Greytak, Phys. Rev. Lett. **71**, 1589 (1993).

[15] C.G. Aminoff, A.M. Steane, P. Bouyer, P. Desbiolles, J. Dalibard, and C. Cohen-Tannoudji, Phys. Rev. Lett. **71**, 3083 (1993).

[16] W.T. Zemke, C.-C. Tsai, and W.C. Stwalley, (submitted to J. Chem. Phys.).

[17] J.O. Hirschfelder, C.F. Curtiss, and R.B. Bird, *Molecular Theory of Gases and Liquids* (John Wiley & Sons, New York 1964).

[18] J.M. Ziman, *Principles of the Theory of Solids* (Cambridge University Press, Cambridge (UK) 1989).

[19] C.J. Joachain, *Quantum Collision Theory* (North-Holland, Amsterdam 1975).

[20] R. Côté and M.J. Jamieson, (submitted to J. Comp. Phys.).

[21] M.L. Goldberger and K.M. Watson, *Collision Theory* (John Wiley & Sons, New York 1964).

[22] J.M. Blatt and J.D. Jackson, Phys. Rev. **26**, 18 (1949).

[23] T.F. O'Malley, L. Spruch, and L. Rosenberg, J. Math. Phys. **2**, 491 (1961).

[24] O. Hinckelmann and L. Spruch, Phys. Rev. A **3**, 642 (1971).

[25] M.J. Jamieson, A. Dalgarno, and M. Kimura, (submitted to Phys. Rev. A).

[26] G.C. Maitland, M. Rigby, E.B. Smith, and W.A. Wakeham, *Intermolecular Forces: their origin and determination* (Clarendon Press, Oxford (UK) 1981).

[27] R. Côté and A. Dalgarno, (to appear in Phys. Rev. A, Dec. 1994).

[28] W.T. Zemke and W.C. Stwalley, J. Phys. Chem. **97**, 2053 (1993).

[29] B. Barakat, R. Bacis, E. Carrot, S. Churrassy, P. Crozet, and F. Martin, Chem. Phys. **102**, 215 (1986).

[30] D.D. Konowalow and M.L. Olson, J. Chem. Phys. **71**, 450 (1979).

[31] I. Schmidt-Mink, W. Müller, and W. Meyer, Chem. Phys. **94**, 263 (1985).

[32] C. Linton, T.L. Murphy, F. Martin, R. Bacis, and J. Verges, J. Chem. Phys. **91**, 6036 (1989).

[33] D.D. Konowalow, R.M. Regan, and M.E. Rosenkrantz, J. Chem. Phys.**81**, 4534 (1984).

[34] W.T. Zemke and W.C. Stwalley, J. Chem. Phys. **100**, 2661 (1994).

[35] O. Babaky and K. Hussein, Can. J. Phys. **67**, 912 (1989).

[36] R.F. Barrow, J. Verges, C. Effantin, K. Hussein, and J. D'Incan, Chem. Phys. Lett. **104**, 179 (1984).

[37] D.D. Konowalow, M.E. Rosenkrantz, and M.L. Olson, J. Chem. Phys. **72**, 2612 (1980).

[38] L. Li, S.F. Rice and R.W. Field, J. Chem. Phys. **82**, 1178 (1985).

[39] A.A. Radzig and B.M. Smirnov, *Reference Data on Atoms, Molecules. and Ions* (Springer-Verlag, Berlin 1985).

[40] M. Marinescu, H.R. Sadeghpour and A. Dalgarno, Phys. Rev. A **49**, 982 (1994).

[41] B.M. Smirnov and M.I. Chibisov, Zh. Eksp. Teor. Fiz. **48**, 939 (1965) [Sov. Phys. JETP **21**, 624 (1965)].

[42] K.T.Tang, J.M. Norbeck, and P.R. Certain, J. Chem. Phys. **64**, 3063 (1976).

[43] D.D. Konowalow and J.L. Fish, Chem. Phys. **77**, 435 (1983).

[44] B. Bussery and M. Aubert-Frécon, Chem. Phys. Lett. **105**, 64 (1984).

[45] F. Maeder and W. Kutzelnigg, Chem. Phys. **42**, 95 (1979).

[46] D.D. Konowalow and M.E. Rosenkrantz, J. Phys. Chem. **86**, 1099 (1982).

[47] A. Dalgarno and W.C. Davison, Adv. At. Mol. Phys. **2**, 1 (1966).

[48] M. Marinescu, J.F. Babb, and A. Dalgarno, Phys. Rev. A **50**, 3096 (1994).

[49] K.K Verma, J.T.Bahns, A.R. Rajaei-Rizi, W.C. Stwalley, and W.T. Zemke, J. Chem. Phys. **78**, 3599 (1983).

[50] E.J. Friedman-Hill and R.W. Field, J. Chem. Phys. **96**, 2444 (1992).

[51] A.J. Moerdijk, W.C. Stwalley, R.G. Hulet, and B.J. Verhaar, Phys. Rev. Lett. **72**, 40 (1994).

[52] A.J. Moerdijk and B.J. Verhaar, Phys. Rev. Lett **73**, 518 (1994).

[53] R.J. LeRoy and R.B. Bernstein, J. Chem. Phys. **52**, 3869 (1070).

[54] G.F. Gribakin and V.V. Flambaum, Phys. Rev. A **48**, 546 (1993).

[55] E. Butkov, *Mathematical Physics* (Addison-Wesley, Reading (Massachusetts) 1968).

[56] A.S. Dickinson and R.B. Bernstein, Mol. Phys. **18**, 305 (1970).

[57] D.P. Clougherty and W. Kohn, Phys. Rev. B **46**, 4921 (1992).

[58] W.E. Milne, Phys. Rev. **35**, 863 (1930).

[59] B. Yoo and C.H. Greene, Phys. Rev. A **34**, 1635 (1986).

[60] L.D. Landau and E.M. Lifshitz, *Quantum Mechanics (Non-relativistic Theory)* (Pergamon Press, Oxford (UK) 1981).

[61] K.M. Sando and A. Dalgarno, Mol. Phys. **20**, 103 (1971).

[62] P. Kusch and M.M. Hessel, J. Chem. Phys. **67**, 586 (1977).

[63] L.B. Ratcliff, J.L. Fish, and D.D. Konowalow, J. Mol. Spectrosc. **122**, 293 (1987).

[64] M. Marinescu and A. Dalgarno (to be submitted to Phys. Rev. A).

[65] F. Vigné-Maeder, Chem. Phys. **85**, 139 (1984).

[66] B. Bussery and M. Aubert-Frécon, J. Chem. Phys. **82**, 3224 (1985).

[67] J. Pipin and D.M. Bishop, Phys. Rev. A **45**, 2736 (1992).

[68] Z. Lin, K. Shimizu, M. Zhan, F. Shimizu, and H. Takuma, Jpn. J. Appl. Phys. **30**, 1324 (1991).

[69] R.R. McLone and E.A. Power, Proc. Roy. Soc. London **286A**, 573 (1965).

[70] A. Gallagher and D.E. Pritchard, Phys. Rev. Lett. **63**, 957 (1989).

[71] R.S. Friedman and M.J. Jamieson, Comput. Phys. Commun. **62**, 53 (1991).

[72] A.C. Allison, J. Comput. Phys. **6**, 378 (1970).

[73] B.R. Johnson, J. Comput. Phys. **13**, 445 (1973),

[74] J.M. Blatt, J. Comput. Phys. **1**, 382 (1967).

[75] L. Fox and D. F. Mayers, *Computing Methods for Scientists and Engineers* (Oxford Univ. Press, Oxford, 1968).

[76] D. F. Mayers, Comput. J. **7**, 54 (1964).

[77] M. J. Jamieson and R. S. Friedman, Comput. Phys. Commun. **70**, 53 (1992).

[78] N. F. Mott and H. S. W. Massey, *The Theory of Atomic Collisions* (Oxford Univ. Press, Oxford, 1965).

[79] G. Herzberg, *Molecular Spectra and Molecular Structure: I. Spectra of Diatomic Molecules* (Van Nostrand Reinhold Co., New York 1950).

[80] J.D. Jackson, *Classical Electrodynamics* (John Wiley & Sons, New York 1975).

[81] J.J. Sakurai, *Modern Quantum Mechanics* (Addison-Wesley, Redwood City (California) 1985).

[82] R. Kubo, *Statistical Mechanics: An Advanced Course with Problems and Solutions* (North Holland, Amsterdam 1965).

[83] B. Gao and A.F. Starace, Computers in Physics, Nov/Dec 70 (1987).

[84] N.W.M. Ritchie, E.R.I. Abraham, Y.Y. Xiao, C.C. Bradley, R.G. Hulet, and P.S. Julienne, (submitted to Phys. Rev. Lett.).